

AD-756 048

EXPANDABLE FLOATING BASES PROGRAM:
MODEL TEST AND ANALYSIS

Glenn W. Quaint

Goodyear Aerospace Corporation

Prepared for:

Office of Naval Research

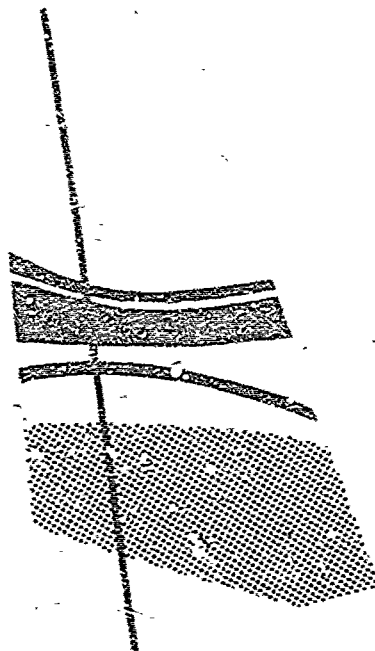
30 January 1973

DISTRIBUTED BY:

NTIS

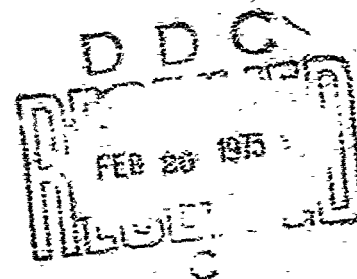
National Technical Information Service
U. S. DEPARTMENT OF COMMERCE
5285 Port Royal Road, Springfield Va. 22151

AD 256048



Final Report - Expandable
Floating Bases Program
Model Test and Analysis

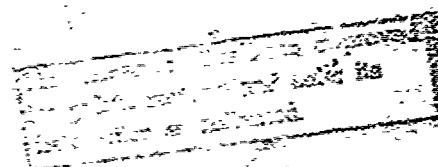
NATIONAL TECHNICAL
INFORMATION SERVICE



GER-15665

30 January 1973

Copy No. 16



GOODYEAR AEROSPACE CORPORATION Akron, Ohio

Ho 3

GOODYEAR AEROSPACE CORPORATION

AKRON, OHIO 44315

FINAL REPORT - EXPANDABLE
FLOATING BASES PROGRAM:
MODEL TEST AND ANALYSIS

GER-15665

30 January 1973

Sponsored by
Advanced Research Projects Agency
ARPA Order No. 1645

This research was supported by the Advanced Research Projects Agency of the Department of Defense and was monitored by the Office of Naval Research under Contract No. N00014-72-C-0477.

The views and conclusions contained in this document are those of the authors and should not be interpreted as necessarily representing the official policies, either expressed or implied, of the Advanced Research Projects Agency of the U. S. Government.



ABSTRACT

This report covers research performed under Contract N00014-72-C-0477 for the Advanced Research Projects Agency, which was monitored by the Office of Naval Research. The effort was directed specifically toward examining and comparing the responses of similarly configured expandable and rigid bodies subject to wave action, to investigation of hydrodynamic problems associated with closely spaced multiple floats in an array, and to an assessment of cost of expandable structures in relation to certain design requirements for a floating base.

Subcontractors were Davidson Laboratory (DL), located at Stevens Institute of Technology, for hydrodynamic testing and analysis of models and Lockheed Underwater Missile Test Facility (LUMF), which provided a test tank for large-scale models of isolated floats. The Davidson Laboratory work comprised a major portion of the program and consisted of the following four parts:

- Part 1 - Exploratory investigation of interaction effects on deck motion
- Part 2 - Comprehensive program on hydrodynamic interaction effects
- Part 3 - Analysis and supporting test work of study of response of deformable floats
- Part 4 - Large-scale model tests of response of deformable floats

The Davidson Laboratory work is reported in Appendixes F, G, H, and I.

TABLE OF CONTENTS

	<u>Page</u>
LIST OF ILLUSTRATIONS	ix
LIST OF TABLES	xi
<u>Section</u>	<u>Title</u>
I	INTRODUCTION 1
II	SUMMARY 3
III	ISOLATED FLOAT STUDY. 5
	1. Background 5
	2. Forces in General 5
	3. Attenuator Features in Regard to Heave Force. 7
	a. General 7
	b. Shoulder Transition. 8
	c. Increased Mass 9
	d. Experimental Verification 12
	4. Hinge Influence 14
	a. General 14
	b. Surge Force 14
	c. Bending Moment 16
	d. Theoretical Results. 17
	e. Experimental Verification 24
	5. Skin Design for 1/8-Scale Model 24
	a. General 24
	b. Test Float Design 28
	6. Natural Frequency Response Measurements 38
	a. Structural Natural Frequency 38
	b. Heaving Natural Frequency 40
	c. Pendular Natural Frequency 41
	d. Frequency Summary 44
	7. Float Force as a Function of Frequency 44
	a. Heave Force 44
	b. Surge Force 46
	c. Bending Moment 50
	d. Force Summary 50
	8. Small-Scale Inflatable Float Tests 52
	9. Heave Motion Response 52

<u>Section</u>	<u>Title</u>	<u>Page</u>
IV	PLATFORM MOTION INVESTIGATIONS.	57
	1. Background	57
	2. Exploratory Investigation of Interaction Effects on Deck Motion	57
	a. Introduction	57
	b. Model Description and Test Plan	58
	c. Measurements	61
	d. Results	64
	3. Hydrodynamic Interaction Effects	68
	a. General	68
	b. Model Description	68
	c. Measurements	69
	d. Results	76
	4. Analytic Investigation of Array Motions	78
	a. Background	78
	b. Model Description	78
	c. Calculations	81
	d. Analysis of Island Motion	101
	e. Results	108
	5. Summary	108
V	COST INVESTIGATIONS.	109
	1. Background	109
	2. Discussion	109
	3. Variables Affecting Platform Costs	111
	4. Materials	112
	a. General	112
	b. Deck	112
	c. Float System	113
	5. Inflatable Float Cost Exercise	117
	LIST OF REFERENCES	121
<u>Appendix</u>		
A	REPORT OF ARPA REVIEW GROUP ON EXPANDABLE FLOATING BASES	123
B	PROPOSAL FOR BARE BONES STABLE EXPANDABLE FLOATING PLATFORM PROGRAM	131
C	SENECA LAKE SURVEY	137
D	PLATFORM SPIN-OFF INVESTIGATIONS	141

<u>Appendix</u>	<u>Title</u>	<u>Page</u>
E	LOCKHEED UNDERWATER MISSILE FACILITY	143
F	HYDRODYNAMIC TESTS AND ANALYSIS PROGRAM FOR EXPANDABLE FLOATING BASES: PART 1 - EXPLOA- TORY INVESTIGATION OF INTERACTION EFFECTS ON DECK MOTION	147
G	HYDRODYNAMIC TESTS AND ANALYSIS PROGRAM FOR EXPANDABLE FLOATING BASES: PART 2 - COMPRE- HENSIVE PROGRAM OF HYDRODYNAMIC INTERATION EFFECTS	203
H	HYDRODYNAMIC TESTS AND ANALYSIS PROGRAM FOR EXPANDABLE FLOATING BASES: PART 3 - ANALYSIS AND SUPPORTING TEST WORK OF STUDY OF RESPONSE OF DEFORMABLE FLOATS	339
I	HYDRODYNAMIC TESTS AND ANALYSIS PROGRAM FOR EXPANDABLE FLOATING BASES: PART 4 - LARGE SCALE MODEL TESTS OF RESPONSE OF DEFORMABLE FLOATS	383

LIST OF ILLUSTRATIONS

<u>Figure</u>	<u>Title</u>	<u>Page</u>
1	Theoretical Heave Force on Fixed Float	10
2	Heave Force Verification on Scale Fixed Float.	13
3	Expressions for Surge Force and Moment on Constant-Diameter Float.	18
4	Expressions for Surge Force and Moment on Stepped-Diameter Float.	19
5	Theoretical Surge Force on Fixed Float.	21
6	Bending Moment versus Frequency	22
7	Compression for Surge Force and Moment on Hinged Float	23
8	Surge Force Verification of Hinged and Unhinged Floats. .	25
9	Surge Force Verification of Constant-Diameter Float. . .	26
10	Surge Force Verification for Slender Float	27
11	Fabric Model Dimensions (1/8 Scale)	33
12	Wood Model Dimensions (1/8 Scale)	34
13	Fabric Model	35
14	Wood Model	36
15	Fabric Hinge	37
16	Fabric Model - Deflated and Folded	37
17	Mounting Platform	39
18	Interface with Force Balance on Mounting Platform . . .	39
19	Heave Force Measurements - 1/8 Scale Floats.	45
20	1/8-Scale Float Models in Regular Waves - Model Surge Force Amplitudes.	47
21	Surge Force Measurements on Upper Float Section and Attenuator Separately	49
22	Surge Force as Sums of Component Measurements	51
23	Bending Response - Wood Model	53
24	Heave Motion Prediction	56
25	Model Island Heave Motion	59
26	Subsequent Model Island Motions	62
27	Heave Force Measured on Model Island	63

Figure	Title	Page
28	Surge Force Measured on Model Island	63
29	Heave Motion and Heave Force Measured Along Length of Array	65
30	Mode Shapes for Deck Stiffness 5	70
31	Mode Shapes for Deck Stiffness 3	73
32	Mode Shapes for Deck Stiffness 2	74
33	Frequency Response Plot	75
34	Vertical Motion at Row 1	84
35	Horizontal Motion of Upper Float Section	84
36	Horizontal Motion of Lower Float Section	85
37	Horizontal Motion of Deck	85
38	Vertical Load Imposed on Deck by Float	87
39	Bending Moment Imposed on Deck by Float	87
40	Deck Profile at Isolated Time Increments	89
41	Model Shape of Analytic Studies as Wave Frequency Changes	89
42	Mode Shape for Analytical Studies as Deck Stiffness Changes	95
43	Concentrated Deck Load versus Floating Base Cost.	110
44	Variation in Cost as Function at Face Sheet Thickness	114
45	Variation in Cost as Function at Core Thickness	114
46	Float Configuration for Cost Study	115

LIST OF TABLES

<u>Table</u>	<u>Title</u>	<u>Page</u>
I	Theoretical Heave Data	11
II	Theoretical Surge Force and Bending Moment Data . .	20
III	Materials Comparison	29
IV	Maximum Design Forces Predicted for Hinged Float . .	30
V	Weight Characteristics of 1/8-Scale Model	32
VI	Structural Natural Frequencies	40
VII	Test Schedule for 1/8-Scale Floats	46
VIII	Exploratory Program Test Summary	60
IX	Wave Elevation Summary	61
X	Comprehensive Test Program Plan	71
XI	Parameters for Array with Large-Diameter Floats . .	82
XII	Array Motion at Isolated Time Increment	83
XIII	Summary of Extreme Values - Run No. 2	88
XIV	Summary of Extreme Values - Run No. 41	90
XV	Summary of Extreme Values - Run No. 16	91
XVI	Summary of Extreme Values - Run No. 15	92
XVII	Summary of Extreme Values - Run No. 14	93
XVIII	Wave Force Data for Wave Frequency Changes	94
XIX	Summary of Extreme Values - Run No. 12	96
XX	Summary of Extreme Values - Run No. 18	97
XXI	Extreme Values with Heave Force Alone Applied - Run No. 3	98

LIST OF TABLESGER-15665

<u>Table</u>	<u>Title</u>	<u>Page</u>
XXII	Extreme Values with Surge Force Alone Applied - Run No. 14	99
XXIII	Factory Costs	118
XXIV	Comparison of Float Reinforcement Fiber Properties .	119

SECTION I - INTRODUCTION

The technical feasibility of creating large expandable structures that can be assembled at sea to form stable platforms of various sizes was investigated by Goodyear Aerospace Corporation (GAC) and a subcontractor for hydrodynamics, Davidson Laboratory, Stevens Institute of Technology, during an 18-month period ending in late 1971. The results of this study, which are reported in GER-15491,^{1, a} indicate with certain qualifications that the concept is feasible.

A group of experts convened by the Advanced Research Projects Agency (ARPA) and the Office of Naval Research (ONR) reviewed the results of the study to determine what additional work would be appropriate to develop a large-scale platform. The full report of the ARPA review group is presented in Appendix A. Briefly, the review group concluded that additional investigations should be made: (1) to verify the assumption that pressurized rubber/fabric structures (built to act as supporting floats for a deck) would respond like rigid bodies under wave action, (2) to examine certain hydrodynamic problems associated with a closely spaced multiple float array (including the cause of test model deck motion amplification), and (3) to assess further the effect of platform design and performance on costs.

The program reported herein, conducted under Contract N00014-72-C-0477, was undertaken to elucidate these issues, and the program plan as well as the format of this report were structured to respond to the three general problem areas cited by the ARPA review panel.

Other work presented includes a minimum-cost proposal in Appendix B; description of the Naval Underwater Systems Center at Seneca Lake, New York, in Appendix C; spin-off investigations in Appendix D and a description of the Lockheed Underwater Missile Facility in Appendix E. Reports prepared by Davidson Laboratory, Stevens Institute of Technology, on hydrodynamic testing and analysis of models are presented in Appendixes F through I.

^aSuperior numbers in the text refer to items in the List of References.

SECTION II - SUMMARY

Analytical studies and model tests were conducted on isolated floats and on arrays of floats connected by simulated deck structures. Regular waves of varying frequencies and forced heave motion were imposed on the models to determine their motion and/or force response.

Significant geometric features of the proposed float configuration include: (1) a hinge separating the upper float section from the attenuator, (2) a transition section where the diameter increases, and (3) an increased mass element in the attenuator.

Analytical expressions for heave force show the advantage of the shoulder design over designs without a shoulder for the particular critical frequency range immediately above resonance. Test results on 1/57.6-scale floats with and without shoulders provide verification of the analytical expression for heave force.

Analytical expressions for a hinged float show the great reduction in surge force transmitted to the float support in comparison with that for an unhinged float. Test results on 1/57.6-scale floats without hinges provide reasonable verification with theory except for non-critical, high-frequency waves where the theory is non-conservative. Theory is shown to be conservative for hinged floats, particularly at low frequencies for floats with both shoulders and hinges.

Flexible floats made of fabric and easily packaged can be filled with water, then air-pressurized to act in a manner similar to rigid floats. A rigid wooden model and a fabric model of 1/8-scale size were comparatively tested. Results show that heave and surge force and bending moment measurements are similar between the model and comparable with theoretical predictions. Pendular and heaving natural frequencies were also shown to be comparable with each other and with theory. Structural natural frequencies were different as expected.

Arrays of unhinged 1/57.6-scale model floats held rigidly in place for force measurements show an increase in heave and surge force values over theoretically predicted values. The increase in heave force is related in part to an increase in wave height noted within the array. The increase in wave height

is related to an interference to wave flow caused by the closely packed array of floats.

Array models constructed with deck structures that permit motion tests show that excessive motions above theoretical predictions occur throughout the array. Parallel linkage models showed excessive stern motion (tail wagging) and excessive bow motion at certain frequencies, over and above those motions at the center. Stiffened deck models show both bow and stern motions to be excessive. Structural interaction is experimentally shown to contribute to excessive motion.

An analytical model of an array supports test data in regard to mode shape of the deck and excessive bow and stern motions. Studies isolating heave and surge force effects show that surge force interaction is responsible for the majority of the deck motion. Evidence available promotes the contention that structural intersection of the deck can be greatly reduced by proper positioning of the hinge.

Cost studies are presented that indicate that unit cost of construction is in the range of \$107 per square foot for full-scale construction of small arrays.

Recommendations for further study in five areas are presented below:

1. Modify existing analytical model to verify experimental arrays more precisely.
2. Examine modifications to construction of the float to reduce surge force interaction on the deck. Shifting the location of the hinge can be easily examined by the analytical model.
3. Consider advantages of the float design extended in this program, including geometry and packageability, to areas of spar buoy interest.
4. Consider rigid float construction in light of geometric advantages extended by the float design of this program.
5. Examine construction techniques for deck edge restraint and their influence on the motions of arrays of floats.

SECTION III - ISOLATED FLOAT STUDY

1. BACKGROUND

The ARPA review group commentary on isolated float data included the suggestion that "the response and behavior of rigid versus expandable buoyant elements" be investigated. The review group recommended that further work be directed to

1. Determine if inflatable floats can be made to act like a rigid structure under wave action
2. Examine the properties of inflatable deformable floats to determine if their elastic properties are useful to performance of a stable floating platform

Doubt was expressed by a number of review group members that a water and air-pressurized rubberized fabric body would react structurally in a manner similar to a non-deforming metal or concrete float of similar configuration. Also, the degree of stiffness that can be achieved in a fiber-reinforced elastomeric structure was questioned.

Two test programs were conceived to examine the problems postulated:

1. Small-scale model test and analysis
2. Large-scale model tests

Analytical effort was also expended to develop mathematical expressions that could be used to evaluate the test measurements as well as to broaden the knowledge of the unique features of the proposed float design.

2. FORCES IN GENERAL

Forces on vertical cylinders caused by waves are well understood. Available technology has provided design capability for both stationary piles, which develop side forces as waves pass, and isolated floats or spar buoys, which respond with dynamic motion to ocean waves.

Before beginning a study of the forces exerted on submerged floats, the pressure field under a passing wave must be examined. Underwater forces result from the motion of a passing wave as well as from the head of water above the point of consideration. From the general energy expression for steady flow (Bernoulli), which considers potential, pressure, and velocity heads, the following dynamic equation for pressure potential can be obtained.²

$$\frac{p}{\rho} = gz - \frac{\partial \phi}{\partial t} - \frac{1}{2} \left[\left(\frac{\partial \phi}{\partial x} \right)^2 + \left(\frac{\partial \phi}{\partial z} \right)^2 \right], \quad (1)$$

where

p = pressure,

ρ = density of incompressible fluid,

ϕ = potential function,

g = acceleration of gravity,

z = vertical dimension measured positive downward from the still water level, and

x = horizontal measurement measured positive in the direction of the wave

The potential function, ϕ , which describes the total energy potential of the orbiting water particles, is given by:³

$$\phi = \zeta V_w \frac{\cosh K(Z + d)}{\sinh Kd} \sin K(x - V_w t), \quad (2)$$

where

ϕ = potential function (ft²/sec),

d = water depth,

ζ = wave amplitude (1/2 wave height),

K = wave number ($2\pi/L_w$),

L_w = wave length, and

V_w = wave velocity.

The "static pressure" component of the total pressure term (that pressure acting in all directions neglecting velocity) is given by the first two terms of the pressure function. The last two terms of the expression deal with $\partial\phi/\partial x$ and $\partial\phi/\partial z$, which are velocities.

For deep-water consideration (large d), the ratio $\cosh K(-Z + d)/\sinh Kh$ approaches e^{-Kz} . Static pressure below a wave field in deep water is consequently

$$\frac{p_s}{\rho} = gz - \frac{\partial\phi}{\partial t}$$

$$p_s = \rho gz \pm \zeta_a \rho g e^{-Kz} \cos(Kx - \omega t). \quad (3)$$

The Smith effect is referred to as the difference in pressure that would be calculated at the instantaneous water level, neglecting wave motion and that is calculated as above. Maximum variation would occur at a wave crest or trough when

$$\cos(Kz - \omega t) = 1.0.$$

The Smith effect would then be:

$$\Delta p = \rho g \zeta_a (1 - e^{-Kz}). \quad (4)$$

Floats considered for the floating base application employ many design features that make response of the floats different from a conventional cylindrical spar buoy. The influence of these features in regard to imposed force is discussed below. Particularly significant design items include the attenuator, hinge, and skin.

3. ATTENUATOR FEATURES IN REGARD TO HEAVE FORCE

a. General

The attenuator is termed such because it houses the elements that reduce the response of the float to a fraction of the wave motion. Specific features of the attenuator are the shoulder transition and its increased mass.

b. Shoulder Transition

Use of this increase in diameter, at a level below the lowest point the wave form is expected to reach, provides a transition area against which imposed wave forces will act in opposition to forces applied at the bottom. Figure 1 depicts the opposing forces described above. Also shown in the figure is a plot of heave force amplitude in pounds per foot of wave amplitude versus wave frequency imposed on a cylinder with and without a shoulder. Significance of the shoulder in regard to heave force is demonstrated by a simple theory that considers only the variation in pressure at depth as the wave passes but disregards inertia and drag effects. Referring to Equation 3, above, and considering force amplitude alone, the equation for heave force is:

$$F_n = \rho g \left[(Z_t A_t - Z_b A_b) \pm \zeta \left(e^{-Kz_t} A_t - e^{KZ_b} A_b \right) \right],$$

where

A = area of the cross section and

t, b = subscripts denoting location of
pressure calculation at transition
or base.

The floats shown have a water plane diameter of six feet, are filled with water, and are capable of carrying the same payload. The table in Figure 1 shows the geometric difference between the floats represented by the curves. Curve A represents the heave force resulting on a constant-diameter float being held fixed in the water. Note that the force amplitude is greater for lower-frequency waves where the wave height has a longer time to affect the bottom of the float. The force shown is in phase with the wave.

Curve B shows the dramatic change that occurs with the addition of a shoulder transition. This float is the same length as that for Curve A, but with an increase in diameter to 12 ft at a depth of 30.23 ft below the water line. Note that a null point occurs at a frequency of 0.104 cps. Heave forces at frequencies above the null are out of phase with the wave. Below the null, heave forces are in phase. The cause of this phasing phenomenon is simply explained by the fact that at higher frequencies the product of pressure times

area at the transition is greater than at the base. More completely, the exponential decay of pressure with depth is greater for the high-frequency short waves than for the low-frequency long waves; this in turn causes the greater force to change from the base to the shoulder as wave frequency increases. To aid in reducing the size of the plot, the lower portion of curve B (the out-of-phase portion) can be flopped over as shown with the dashed curve.

Table I is an example of the computer data from which the plots of Figure 1 were made. The particular case shown is for float B.

c. Increased Mass

An increase in mass of the float is beneficial in reducing the motion of the float due to the forces described above. A significant parameter associated with response is the natural heaving frequency of the float, which is a function of the mass. Water plane frequency, as it is termed, is calculated as:

$$f = \frac{1}{2\pi} \sqrt{\frac{K}{m}} ,$$

where

$K = \rho g A_w$ (lb/ft) spring constant of float as measured
by the weight of water displaced per foot of float
heave

m = mass of the float to be accelerated.

Referring to Figure 1, the constant-diameter float A has a natural frequency of 0.125 cps. This frequency would be undesirable from the viewpoint of a float designed for ocean use, because many waves would contain this same frequency, and a consequent resonance would result, causing excessively large motions. Float B on the other hand has a natural frequency of 0.083 cps. This frequency is lower than the significant waves expected to be encountered in the design considered.

Curve C is provided to show the effect of increasing the length of a constant diameter float A from 52 ft to 117.3 ft, where its mass is equal to that for B. The natural frequency of B and C are consequently the same.

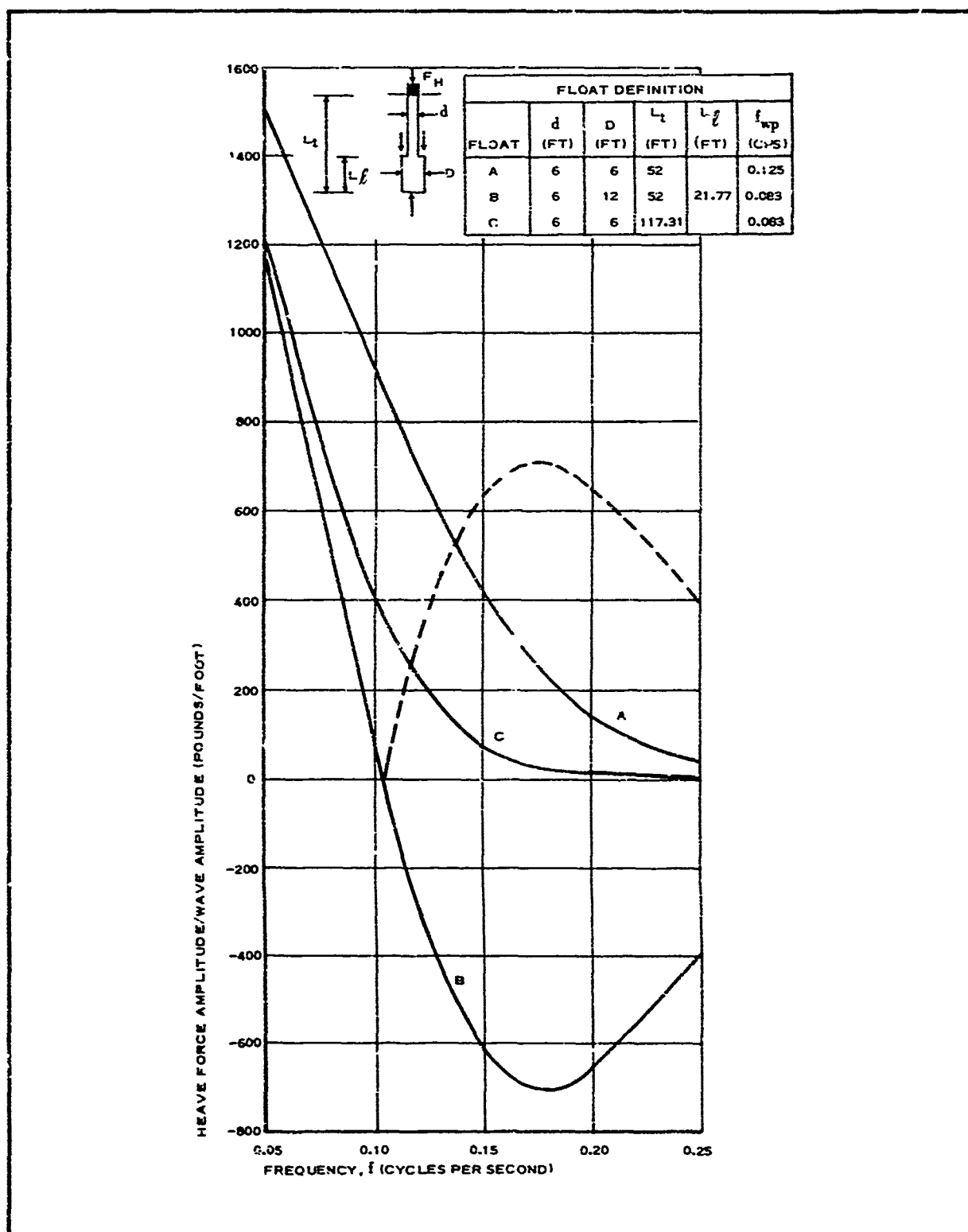


Figure 1 - Theoretical Heave Force on Fixed Float

TABLE I - THEORETICAL HEAVE DATA

77

WFC

HEAVE FORCES ON A SUBMERGED FLCAIT - WFC 10-25-72

15:22:33

12/22/72

INPUT

RAISE = 3.00000
RELOAT = 3.00000
ZBASE = 52.00000
ZTRANS = 10.20000
ZETA = 1.00000
FREQ = 0.01000
SCALE = 57.59999

UNITS
(FT, LB, SEC)

GEOMETRY AND STATIC FORCES

ANASE = 28.274
DELTA = 74.274
ATRAIS = 0.0
FRASE1 = 91744.375
CTRAH1 = 0.0
FAH1 = -91744.375
CVP = 1.000
MCLOAT = 2449.205
AMP = 1766.315
FREQP = 0.125

WAVE FORCES

DATA AT FULL SCALE

WAVE AND FORCE
DATA AT SCALE

SIZE VALUES

HEAVE MOTION DATA

TAU	FREQ	LAMDA	FTRAN2	FBASE2	FMAVE	QO	ZOZETA	TAJS	FRECS	FMAVES	ZOZ
100.00	0.01000	51140.0	0.0	1753.103	-1753.103	0.997	1.000	13.14	0.07589	-0.523	1.006
50.00	0.02000	12795.0	0.0	1717.931	-1717.931	0.987	1.000	6.59	0.15179	-0.518	1.026
33.33	0.03000	5486.7	0.0	1665.931	-1665.931	0.972	1.002	4.39	0.22768	-0.502	1.061
25.00	0.04000	3198.7	0.0	1593.219	-1593.219	0.951	1.006	3.29	0.30358	-0.480	1.114
20.00	0.05000	2047.2	0.0	1504.376	-1504.376	0.924	1.014	2.54	0.37947	-0.453	1.190
16.67	0.06000	1621.7	0.0	1402.938	-1402.938	0.894	1.032	2.23	0.45537	-0.423	1.298
14.29	0.07000	1046.5	0.0	1290.938	-1290.938	0.859	1.064	1.88	0.53126	-0.389	1.454
12.50	0.08000	799.7	0.0	1173.204	-1173.204	0.821	1.123	1.43	0.60716	-0.354	1.689
11.11	0.09000	631.9	0.0	1052.699	-1052.699	0.781	1.234	1.46	0.68305	-0.317	2.088
10.00	0.10000	511.9	0.0	932.604	-932.604	0.739	1.458	1.32	0.75895	-0.281	2.759
9.09	0.11000	423.0	0.0	815.741	-815.741	0.697	2.023	1.20	0.83484	-0.246	3.375
8.33	0.12000	355.4	0.0	704.483	-704.483	0.654	4.873	1.10	0.91074	-0.212	4.203
7.69	0.13000	302.8	0.0	603.690	-603.690	0.612	7.374	1.01	0.98663	-0.181	5.3
7.14	0.14000	261.1	0.0	505.700	-505.700	0.571	1.149	0.94	1.06252	-0.152	6.007
6.67	0.15000	227.5	0.0	423.330	-423.330	0.531	-0.344	0.98	1.13842	-0.127	7.302
6.25	0.16000	199.9	0.0	344.958	-344.958	0.493	-0.309	0.82	1.21431	-0.104	8.582
5.88	0.17000	177.1	0.0	279.509	-279.509	0.457	-0.198	0.78	1.29021	-0.084	1.024
5.56	0.18000	158.0	0.0	223.608	-223.608	0.423	-0.077	0.73	1.36610	-0.067	0.938
5.26	0.19000	141.8	0.0	176.621	-176.621	0.391	-0.077	0.69	1.44200	-0.053	0.748
5.00	0.20000	127.9	0.0	137.740	-137.740	0.362	-0.050	0.66	1.51789	-0.042	0.552
4.76	0.21000	116.1	0.0	106.057	-106.057	0.334	-0.033	0.63	1.59379	-0.032	0.479
4.55	0.22000	105.7	0.0	80.627	-80.627	0.309	-0.022	0.60	1.66969	-0.024	0.421
4.35	0.23000	96.7	0.0	63.519	-63.519	0.286	-0.014	0.57	1.74558	-0.018	0.374
4.17	0.24000	88.9	0.0	44.849	-44.849	0.265	-0.010	0.55	1.82147	-0.014	0.335
4.00	0.25000	81.9	0.0	32.816	-32.816	0.246	-0.006	0.53	1.89737	-0.010	0.335

HEAVE FORCES ON A SUBMERGED FLCAIT - WFC 10-25-72

HEAVE FORCES ON A SUBMERGED FLCAIT - WFC 10-25-72

Advantages of the constant-diameter design are evident by the reduced force imposed on the float over a portion of the frequency range. Referring to Figure 1, float C has a reduced force compared with that shown for float B at frequencies above 0.117 cps. Below 0.117 cps, float B has a reduced response as a result of its null point.

Advantages of the shoulder design result because:

1. Surface area or total fabric area of the increased diameter section is only $\pi \times 12 \times 21.77 = 820$ sq ft as opposed to $\pi \times (6) \times 87.08 = 164.0$ sq ft for housing the same mass in the constant-diameter float. (A ratio of 1 to 2)
2. Bending stress is reduced because the length is shorter and the diameter increased
3. Shoulder depth can be designed so that the null point frequency occurs in range of significant energy of the wave

d. Experimental Verification

References 1 and 4 provide test data on isolated floats built to a scale of 1/57.6, which were tested in an earlier phase of the GAC study of floating bases. Figure 2 provides a plot of heave force versus frequency as measured on the floats depicted on the plot. Results are scaled up to full-scale values by multiplying wave force/foot values by $\lambda^2 = (57.6^2)$, and frequency by $1/\sqrt{2}$. Note that the floats shown are similar to float B discussed above.

The theoretical curve for float B shown in Figure 1 is repeated in Figure 2 for comparison purposes. This curve is termed static force plus Smith correction, because it neglects orbital velocity and acceleration effects of the water particles. The theory shown here has been termed Froude-Krylov or Newman by Mercier in Reference 5.

A modification to this curve to account for acceleration influence of the particles is included. The theory used to obtain this modification follows more readily after the discussion presented in the next section (refer to Appendix C for expressions relating this effect).

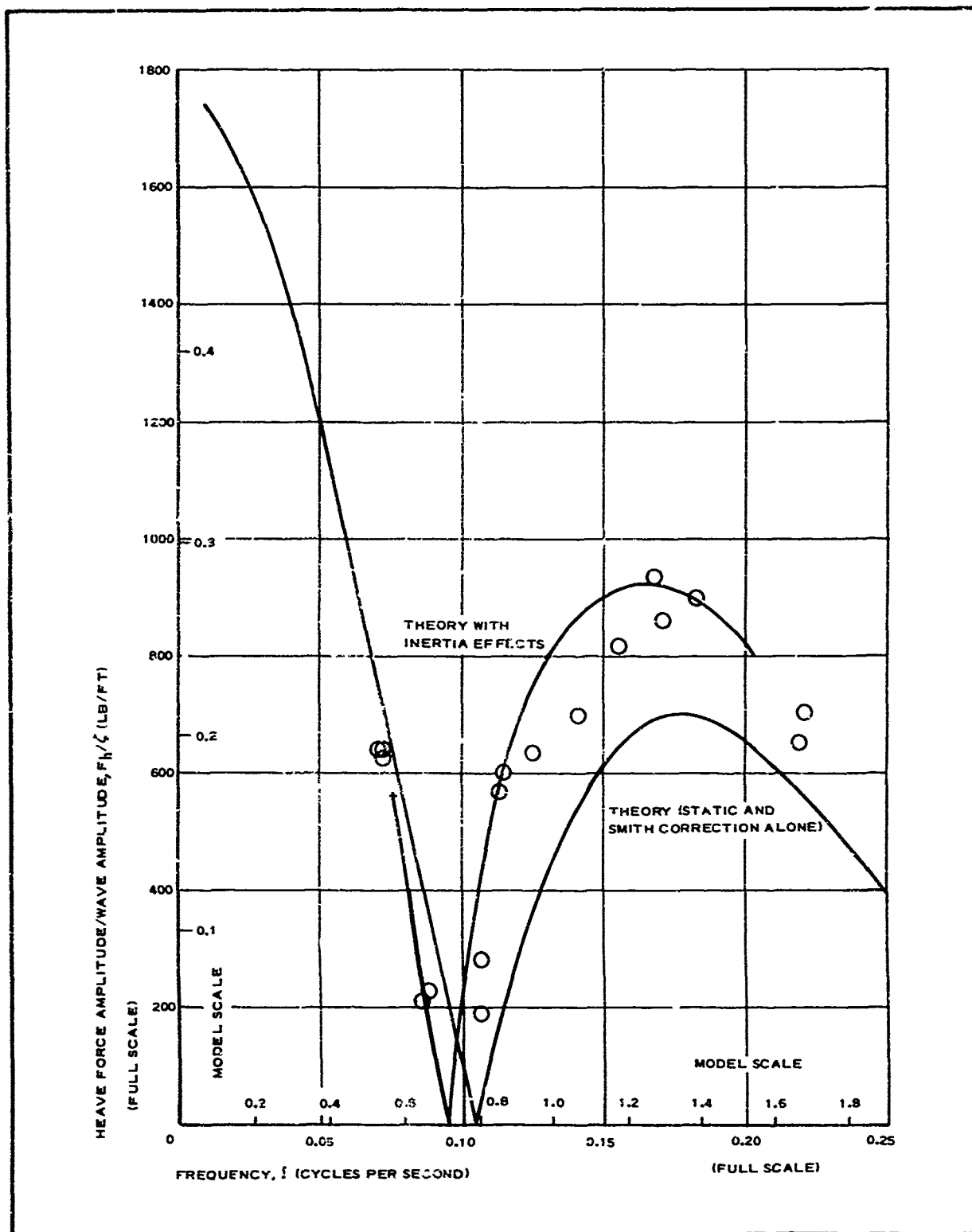


Figure 2 - Heave Force Verification on Scale Fixed Float

This modification for inertia effects appears to match the data more accurately and will consequently be adopted as representative of heave forces.

4. HINGE INFLUENCE

a. General

A hinge is included in the float between the attenuator and the upper section of the float. A function of this hinge is to reduce the shear force and bending moment at the hinge level. The shear, induced by the surge force, reduces when a hinge is installed, because the wave force is partially resisted by the inertial force of the swinging attenuator rather than being transmitted entirely to the hinge.

b. Surge Force

Shear or surge force as a function of time, imposed on a body held fixed as a wave passes, is developed from considerations of unsteady flow.

Equation 1 provides consideration of the velocity component of the orbital motion within the wave. The static force component of Equation 1 is disregarded in consideration of surge forces, because it is balanced by a pressure force, equal in magnitude but opposite in direction, applied to the other side of the float. It is assumed here that the float is slender compared with the wave length.

Unsteady flow considers the additional influence of the acceleration or inertia potential of the orbiting particles of water as the velocity vector changes direction and centrifugal forces are exerted. Reference 2 provides a consideration of both the acceleration and velocity effects of the wave, as shown below:

$$f_s(z) = \left[C_m \rho \left(\frac{\pi D^2}{4} \right) \frac{\partial u}{\partial t} + \frac{1}{2} C_D \rho D |u|u \right] \Delta z,$$

where

$$u = \frac{2\pi \xi}{T} \frac{\cosh \left[\frac{2\pi(-z+d)}{L_w} \right]}{\sinh \left(\frac{2\pi d}{L_w} \right)} \cos 2\pi \left(\frac{x}{L} - \frac{t}{T} \right)$$

and

$$\frac{\partial u}{\partial t} = \frac{4\pi^2 \zeta}{T^2} \frac{\cosh \left[\frac{2\pi (-z + d)}{L_w} \right]}{\sinh \frac{2\pi d}{L_w}} \sin 2\pi \left(\frac{x}{L} - \frac{t}{T} \right) .$$

Consider the body diameter small with respect to the wave length ($x \ll L_w$), then,

$$f_s = -4\pi^2 C_m \rho V \frac{\zeta}{T^2} \frac{\cosh \left[\frac{2\pi (z + d)}{L_w} \right]}{\sinh \left(\frac{2\pi d}{L_w} \right)} \sin \frac{2\pi t}{T} \\ + 2C_D \rho A \pi^2 \frac{\zeta^2}{T^2} \frac{\cosh \frac{2\pi (z + d)}{L_w}}{\sinh \frac{2\pi d}{L_w}} \left| \cos \frac{2\pi t}{T} \right| \cos \frac{2\pi t}{T} ,$$

where

f_s = surge force applied to a small element of volume,

V = volume of element to which F_h is applied,

ζ = wave amplitude of motion (1/2-wave height),

T = wave period

L_w = wave length,

t = time reference,

C_m = coefficient of mass (or inertia), and

C_D = coefficient of drag.

For deep water considerations, where d/L is large, then

$$\frac{\cosh \left[\frac{2\pi (z + d)}{L_w} \right]}{\sinh \left(\frac{2\pi d}{L_w} \right)} \approx e^{-Kz} ,$$

where $K = 2\pi/Lw$, as shown in Reference 3. The contribution of drag to the force is found to be small; consequently, the inertia force may be considered as the important term.

The resulting expression is:

$$f_s = -4\pi^2 C_m \rho V \frac{\xi}{T^2} e^{-Kz} \sin \frac{2\pi t}{T}.$$

Consider a cylindrical segment of a vertical float with a diameter D and length ℓ .

$$V = \frac{\pi D^2 \ell}{4}$$

Pressure acting on this segment is:

$$p = \frac{f_s}{D\ell} = -\pi^3 C_m D \frac{\xi}{T^2} e^{-Kz} \sin \frac{2\pi t}{T}$$

Let

$$\alpha = \pi^3 C_m \rho D^2 \frac{\xi}{T^2}.$$

Then

$$R = -\frac{\alpha}{D} e^{-Kz} \sin \frac{2\pi t}{T}.$$

The total surge force acting on a vertical cylinder of constant diameter can be obtained by integrating the pressure over the projected area of the cylinder considered.

c. Bending Moment

Moment applied to the float by the forces described above can be computed as:

$$\begin{aligned} M_s &= \int_{z_1}^{z_2} Z p dA = \int_{z_1}^{z_2} p D z dz \\ &= \frac{\alpha}{K^2} \left(e^{-Kz_2} - e^{-Kz_1} \right) (Kz + 1) \sin \frac{2\pi t}{T} \end{aligned}$$

d. Theoretical Results

Maximum forces and moments applied to the float are of interest here. Amplitudes of the preceding expressions provide information that become maxima midway between the crest and trough of the wave.

Figure 3 provides expressions for the forces and moments on a constant-diameter float and Figure 4 provides them for a stepped float represented by two constant-diameter cylindrical sections.

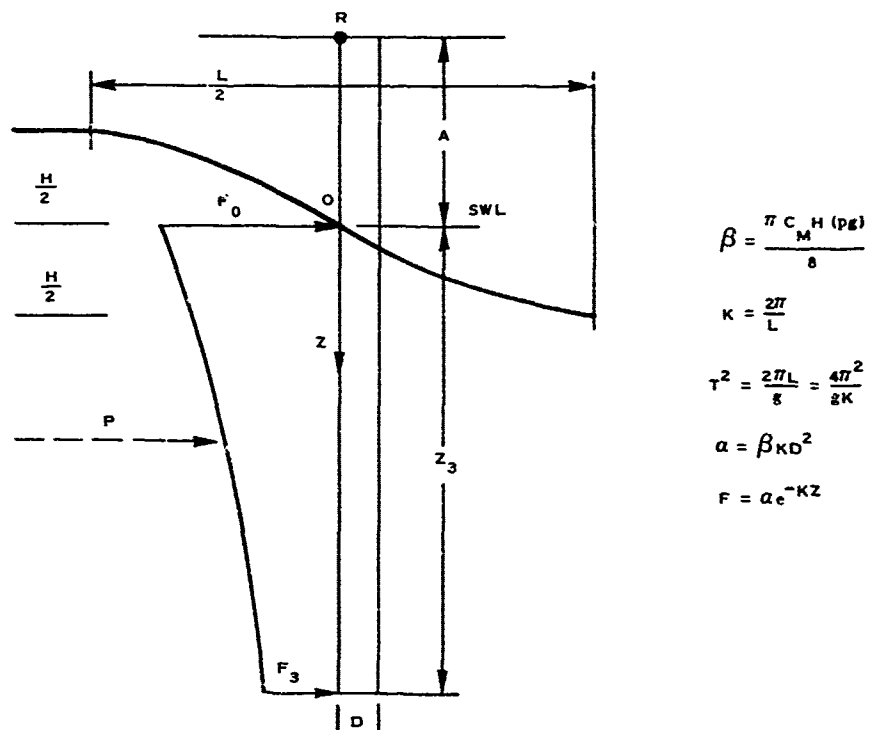
Expressions from Figures 3 and 4 were programmed with typical results provided in Table II and Figure 5 for surge and in Figure 6 for bending moment. Curves A, B, and C of each figure represent float configurations as shown in the sketches provided. Note that these cases are the same as those shown for heave force in Figure 1. As would be expected, the short float A has the least surge force and moment, while the broad float B has the greatest magnitude. The long float C attains intermediate values because much of its projected area occurs at depths where surge forces are reduced.

An exception occurs for float C when low-frequency waves are considered. In this regard, the length of float C coupled with surge force causes the bending moment (Figure 6) to be higher than for floats A and B.

Modifications are made to the preceding expressions to account for the addition of a hinge in the upper cylindrical section of the float. This hinge permits the attenuator to swing; consequently, equilibrium equations for a static-type solution can be maintained by the application of a reversed effective force located at the center of gravity of the attenuator. Magnitude of the force can be calculated from the condition that the sum of the moments about the hinge must be zero.

Figure 7 provides the pertinent geometry and equations that were programmed with the results shown in Figures 5 and 6. Curve D of each figure shows the influence of placing a hinge in float B at a level of 23.0 ft down from the water line.

Note the dramatic decrease in both surge force and bending moment that occur for the hinged float D in comparison with the other floats.



$$F_0 = a e^0 = a$$

$$F_3 = \alpha e^{-KZ_3}$$

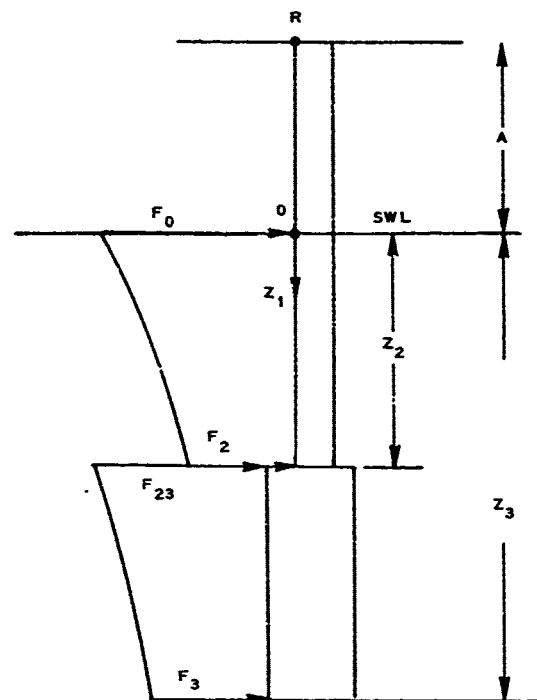
$$P = \int_{z_a}^{z_b} F dz = \beta_D^2 \left(e^{-Kz_a} - e^{-Kz_b} \right) = \beta_D^2 \left(1 - e^{-Kz_3} \right)$$

$$M_0 = \int_{z_a}^{z_b} z F dz = \frac{\beta_D^2}{K} \left[(1 + K z_a) e^{-K z_a} - (1 + K z_b) e^{-K z_b} \right]$$

$$= \frac{\beta_D^2}{\kappa} \left[1 - (1 + \kappa Z_3) e^{-\kappa Z_3} \right]$$

$$M_R = M_0 + AP$$

Figure 3 - Expressions for Surge Force and Moment on Constant-Diameter Float



$$a_{02} = \beta K D_2^2$$

$$a_{23} = \beta K D_3^2$$

$$F_0 = a_{02}$$

$$F_2 = a_{02} e^{-KZ_2}$$

$$F_{23} = a_{23} e^{-KZ_2}$$

$$F_3 = a_{23} e^{-KZ_3}$$

$$P_{02} = \beta D_2^2 (1 - e^{-KZ_2})$$

$$M_{02} = \frac{\beta D_2^2}{K} [1 - (1 + KZ_2) e^{-KZ_2}]$$

$$P_{23} = \beta D_3^2 [e^{-KZ_2} - e^{-KZ_3}]$$

$$M_{023} = \frac{\beta D_3^2}{K} [(1 + KZ_2) e^{-KZ_2} - (1 + KZ_3) e^{-KZ_3}]$$

$$P = P_{02} + P_{23}$$

$$M_0 = M_{02} + M_{023}$$

$$M_R = M_0 + AP$$

Figure 4 - Expressions for Surge Force and Moment on Stepped-Diameter Float

TABLE II - THEORETICAL SURGE FORCE AND BENDING MOMENT DATA

N	PG	HM	CM	DA	DR	7A	ZR	ZC	
2	62.39999	2.00	2.30	6.00	12.00	21.77	52.00	0.0	
F	XLD	XS	POA	XMA	POB	XMB	PO	XMU	
0.01000	51248.	0.	11.	126.	60.	2131.	71.	2257.	
0.02000	12812.	0.	43.	476.	236.	8680.	279.	9157.	
0.03000	5694.	0.	96.	1048.	520.	19123.	616.	20171.	
0.04000	3201.	0.	170.	1836.	896.	32898.	1065.	34733.	
0.05000	2050.	0.	262.	2820.	1344.	49247.	1606.	52067.	
0.06000	1424.	0.	372.	3982.	1842.	67315.	2214.	71297.	
0.07000	1046.	0.	497.	5297.	2365.	86158.	2863.	91455.	
0.08000	801.	0.	637.	6739.	2889.	104851.	3527.	111590.	
0.09000	633.	0.	789.	8279.	3391.	122520.	4180.	130798.	
0.10000	512.	0.	951.	9938.	3849.	133399.	4800.	148287.	
0.11000	424.	0.	1120.	11536.	4247.	151870.	5367.	162406.	
0.12000	356.	0.	1295.	13195.	4571.	162540.	5866.	175675.	
0.13000	303.	0.	1473.	14835.	4812.	169959.	6286.	184794.	
0.14000	261.	0.	1653.	16431.	4957.	174211.	6620.	190642.	
0.15000	228.	0.	1832.	17958.	5036.	175302.	6858.	193260.	
0.16000	200.	0.	2029.	19396.	5023.	173433.	7032.	192829.	
0.17000	177.	0.	2182.	20724.	4934.	158917.	7115.	189641.	
0.18000	158.	0.	2349.	21928.	4779.	162142.	7128.	184070.	
0.19000	142.	0.	2510.	22397.	4568.	153539.	7078.	176537.	
0.20000	128.	0.	2663.	23922.	4314.	143558.	6976.	167480.	
0.21000	116.	0.	2807.	24697.	4027.	132635.	6834.	157333.	
0.22000	106.	0.	2943.	25321.	3718.	121179.	6651.	146500.	
0.23000	97.	0.	3069.	25795.	3398.	109550.	6468.	135345.	
0.24000	89.	0.	3186.	26123.	3076.	93057.	6262.	124180.	
0.25000	82.	0.	3293.	26309.	2759.	86951.	6052.	113260.	

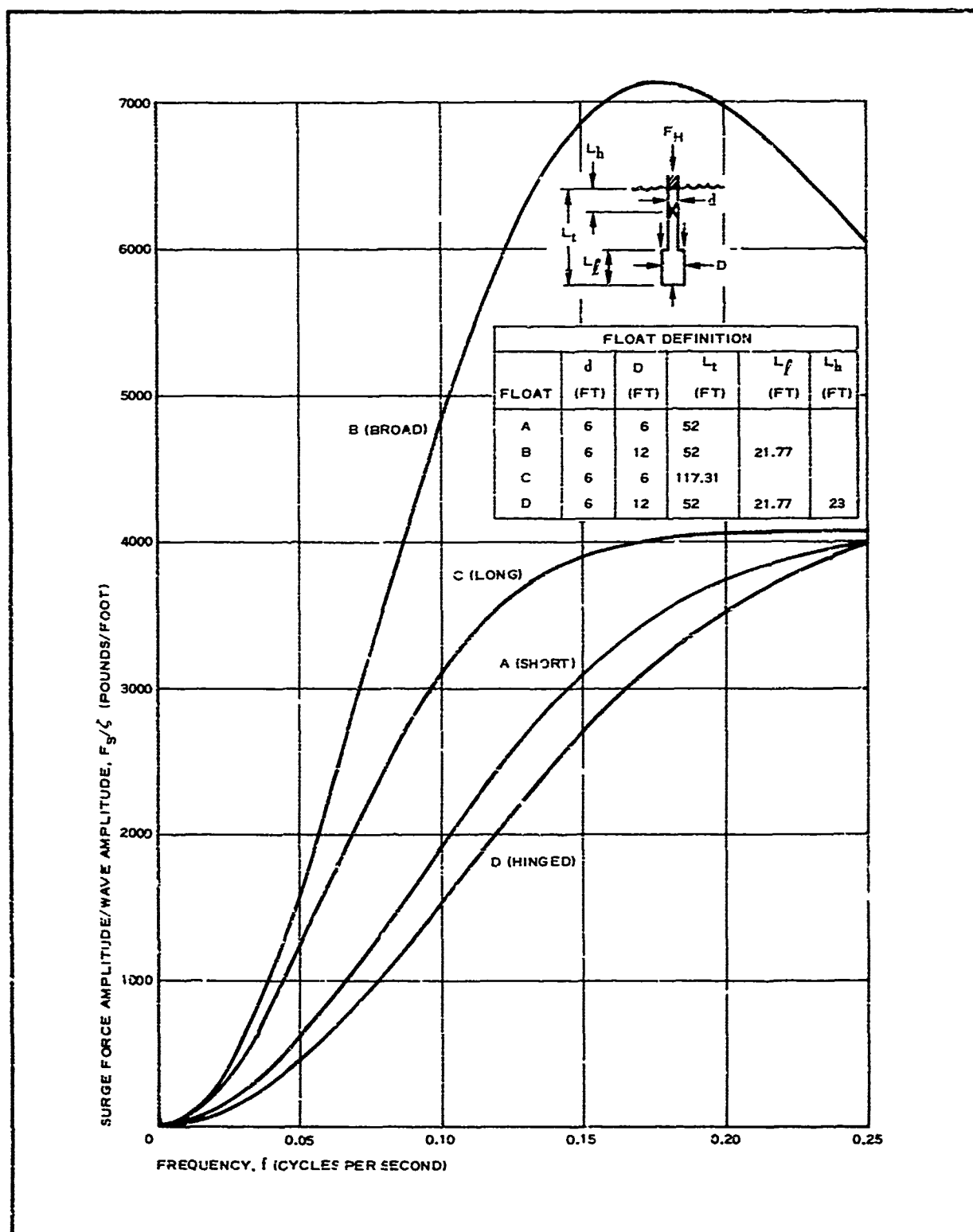


Figure 5 - Theoretical Surge Force on Fixed Float

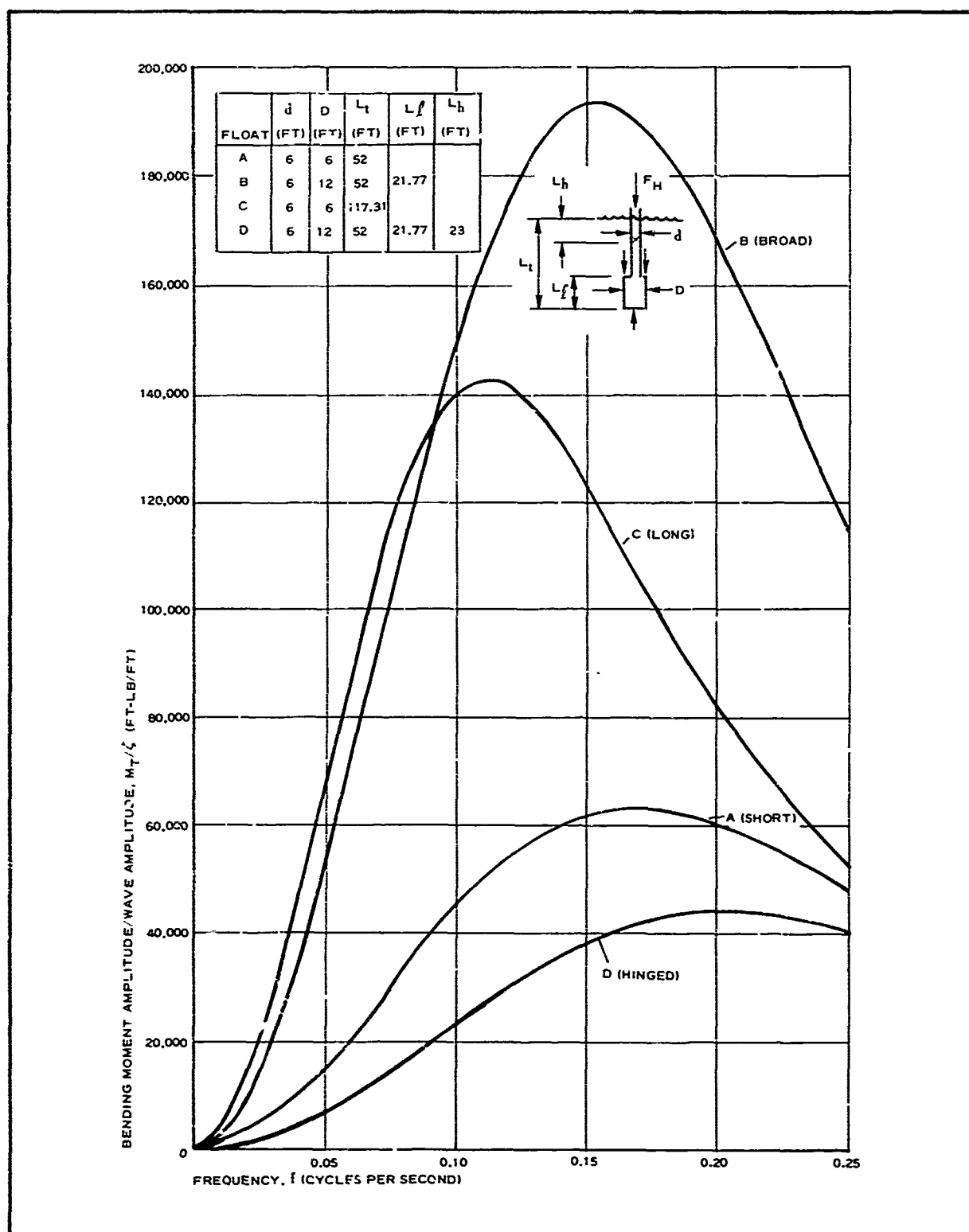


Figure 6 - Bending Moment versus Frequency

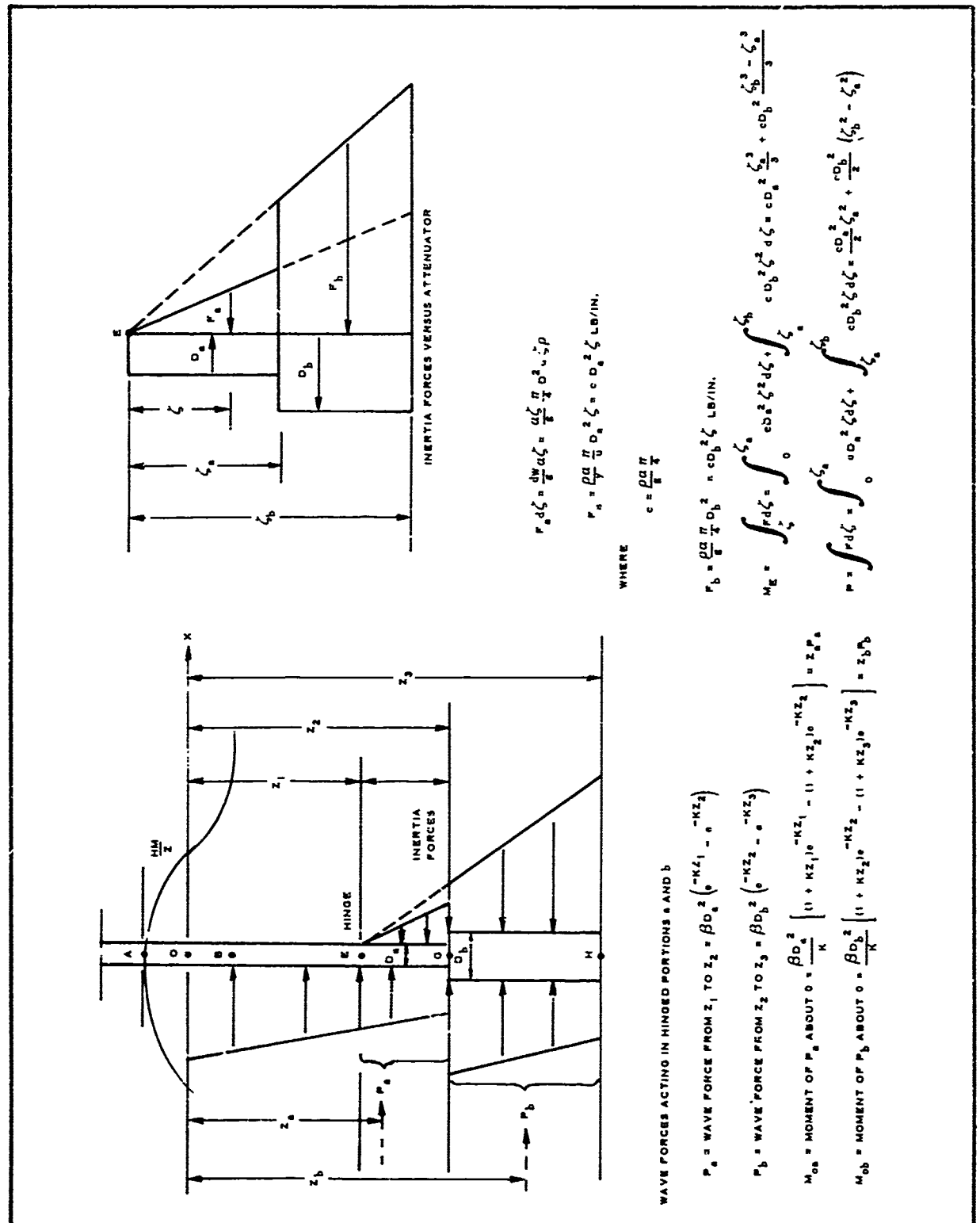


Figure 7 - Compression for Surge Force and Moment on Hinged Float

e. Experimental Verification

Reference 4 provides test data on isolated floats built to a scale of $1/57.6$. Figures 8, 9, and 10 provide plots of surge force per foot of wave height for a range of wave frequencies. Results are scaled up to full-scale equivalents.

Floats B and D discussed previously are depicted in Figure 8. Theoretical results are slightly nonconservative in regard to float B, the unhinged case. Theory is, however, conservative in regard to float D with a hinge.

Tests conducted on floats with no shoulders are presented in Figure 9. Theory and data for the long float (6 ft by 117 ft) show good agreement, except at higher frequencies. When the float was hinged at a level of 23 ft down from the water surface, the forces reduced considerably and theory was slightly conservative. The upper portion of the float (6 ft by 23 ft) was tested alone. Here the theory was slightly non-conservative.

Tests conducted on a float with less-pronounced shoulders are provided in Figure 10. Both hinged and unhinged conditions were examined. Agreement is again good for the rigid float, except at higher frequencies where it is somewhat non-conservative. In the case of the hinged float, the theory is conservative.

5. SKIN DESIGN FOR $1/8$ -SCALE MODEL

a. General

Float geometry is established by matching the preceding load relations to design requirements to obtain an optimum configuration. The above work neglects local and overall bending deformations the structure might attain. If the float were made of a ballasted wood structure or thick-wall concrete or steel structures, where deflection is small, the above work could be utilized without further consideration of structural effects. These cases would be examples of near-rigid structures.

Economy of design, however, dictates that metal structures must be as thin as possible. Membrane theory consequently is utilized in the computation of stresses in such elements. Overall bending and local deformations in these cases do result, and natural frequency of the structure decreases.

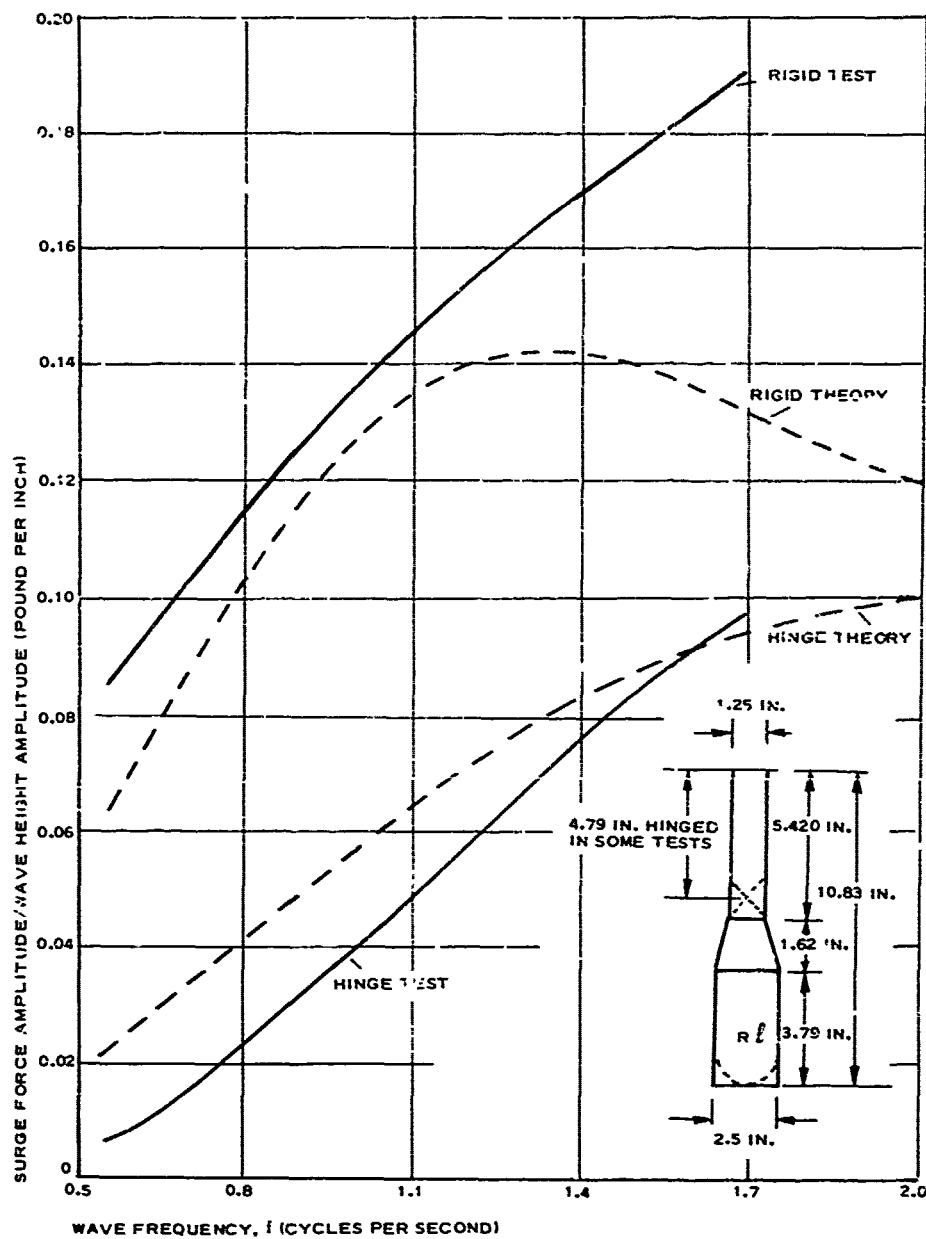


Figure 8 - Surge Force Verification of Hinged and Unhinged Floats

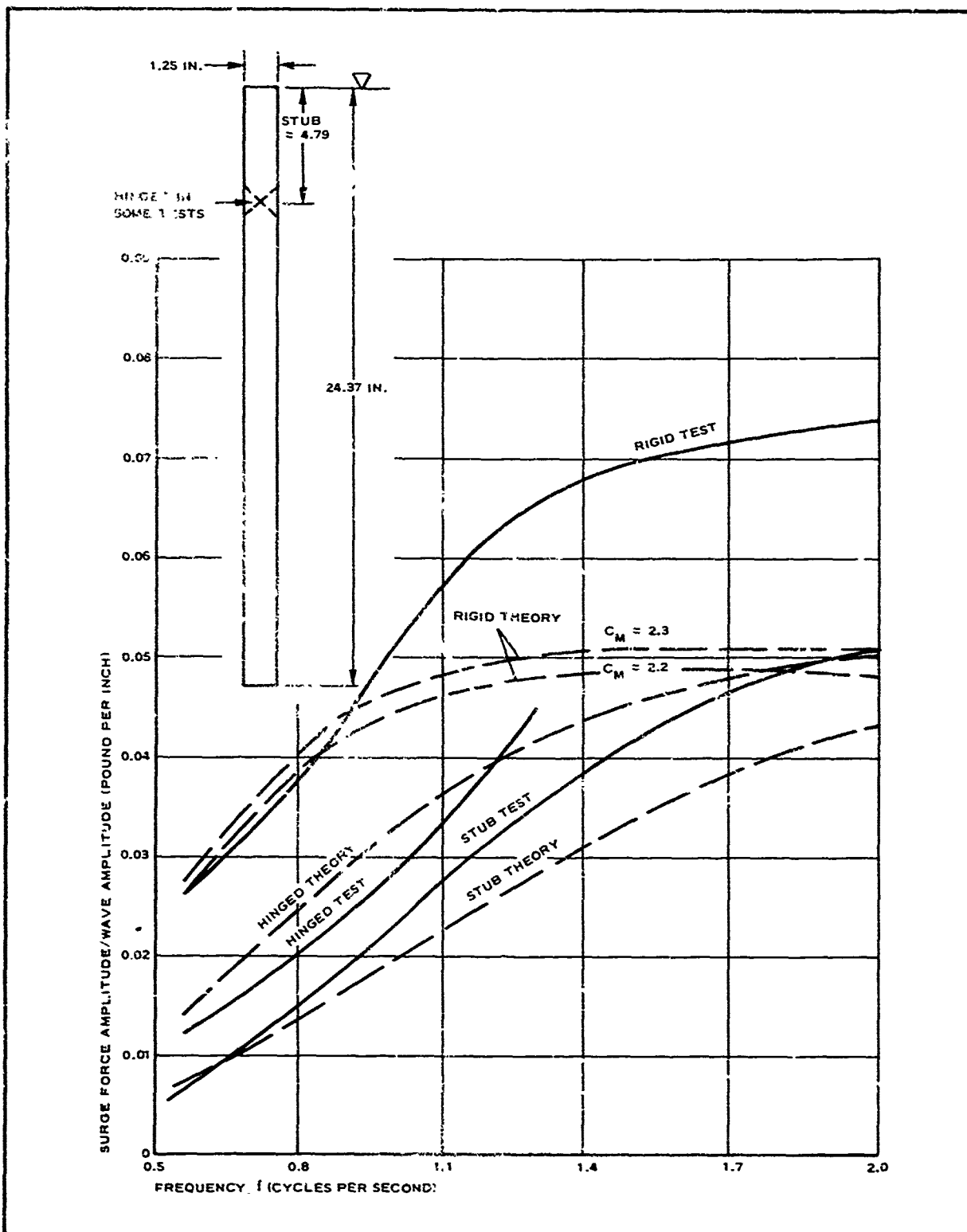


Figure 9 - Surge Force Verification of Constant-Diameter Float

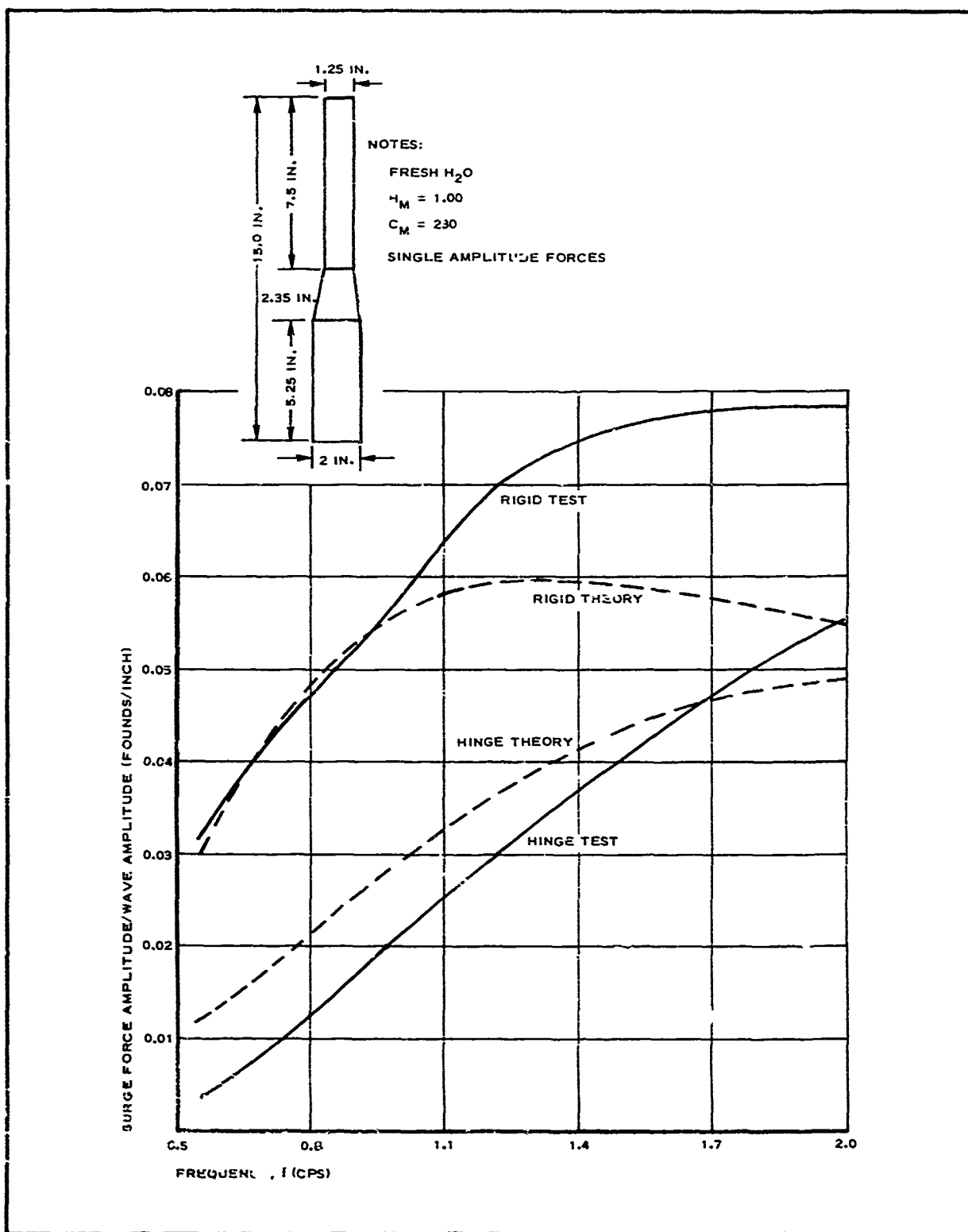


Figure 10 - Surge Force Verification for Slender Float

Evaluation of these parameters must be made before it can be concluded that the preceding theory can be used, without modification, to account for structural effects.

Desire for packageability, transportability, and flexibility at high loads has led to the consideration of expandable float technology. Basically, this consists of the use of pressurized fabric skins in the design of the float.

Technology is well-developed in the area of inflatable fabric structures. Essentially, the pretensioning of the fabric by internal pressure results in a structure that can have considerable stiffness and strength. Specific modulus and strength (that is modulus/density and strength/density ratio) values for some typical materials are included in Table III. Properties for the dacron, nylon, and Fiber B materials are shown as for uncoated cloths. Steel and aluminum materials selected represent the lower strength properties available as common construction materials.

Many fabric structures have been built that practically demonstrate their ability to replace metallic structures. The INFLATOPLANE^a is an example of the use of dacron fabric to make inflatable wings and fuselage parts that can be folded and packaged. A current GAC program on the B-1 airplane utilizes fiber B to make expandable stabilizing fins and spoilers for the crew escape capsule. These components rapidly inflate during the ejection process.

Evaluation of skin-type structures, whether fabric or metal, in relation to rigid structures can be made by observing the structural natural frequency of the item in regard to the frequency of the exciting force. If the natural frequency is high, then the response can be considered similar to a rigid structure, which would have an infinite natural frequency.

b. Test Float Design

Tests were conducted on rigid and flexible models to compare their response. The models were fabricated to 1/8 scale of the following full-size dimensions:

^aTM, Goodyear Aerospace Corporation, Akron, Ohio.

TABLE III - MATERIALS COMPARISON

Property	Dacron	Nylon	Fiber B	Steel	Aluminum
Density γ or γ_t	0.000241 lb/in. ³	0.000350 lb/in. ³	0.000604 lb/in. ³	0.283 lb/in. ²	0.100 lb/in. ²
Elastic modulus E or Et	1250 lb/in. ²	1875 lb/in. ²	30×10^3 lb/in. ²	30×10^6 lb/in.	10.6×10^6 lb/in.
Tensile ultimate or t	250 lb/in. ²	375 lb/in. ²	1500 lb/in. ²	55×10^3 lb/in.	46×10^3 lb/in.
Specific modulus E/ γ or Et/ γ_t (in.)	5.20×10^6	5.36×10^6	49.7×10^6	106×10^6	106×10^6
Specific strength / γ or t/ γ_t (in.)	1.04×10^6	1.071×10^6	2.48×10^6	195×10^3	460×10^3

1. Float length, $L = 110$ ft
2. Diameter ratio, $D_L/D_u = 1.5$
3. Upper diameter, $D_u = 6.0$ ft
4. Aspect ratio, $L/D_u = 18.33$
5. Hinge location, = 23 ft below water line

Measurement of forces transmitted to the float support were deemed to be the most indicative measure of float response. This was accomplished by a rigid mounting of the float to an immovable force balance.

Forces measured in this manner were equivalent for both models; however, they do not include components of force reduction that would result if the force balance mechanism were free to be displaced in heave, surge, and pitch motions.

Design of the 1/8-scale fabric model was accomplished to provide skin thickness, strength, and stiffness as well as internal pressure as scaled down from a prototype design based on data available before testing.

Design of the portion of the float below the hinges was accomplished to establish nearly equal mass distribution characteristics for the two models. Since the fabric model was to be filled with water below the hinge, this entailed

the ballasting of the wood model with metal to render it slightly heavier than a neutrally buoyant condition would require.

Design requirements for the fabric model included the use of a cable truss network to resist lateral forces in the float. For similarity, these cables were incorporated into the wood model as well.

Buoyancy and pressurization forces in the fabric float were created by the incorporation of an air chamber located in its upper section. A diaphragm separated water and air within the float. This diaphragm allowed the pneumatic pressure applied in the top chamber to be transmitted to the water in the lower chamber.

Specific design procedure for the flexible model was based on a conservative determination of wave forces that would be imposed on a full-scale float. Data on forces and locations are obtained from Reference 4. The range of interest in terms of frequency of waves applied to the float lies between 0.06 seconds and 0.224 cps. These values are selected because data on small models are available and because the significant range of waves in the operational condition lie in this region. The maximum forces and moments occur at the higher frequency end of the range. Table IV provides measured force data on small-scale floats, projected to full-scale values as well as 1/8-scale values. Design was set for a full-scale wave of 15-ft peak to peak (7.5-ft amplitude).

TABLE IV - MAXIMUM DESIGN FORCES PREDICTED FOR
HINGED FLOAT*

Force	Full scale	1/8 scale
Surge force for a 7.5-ft wave amplitude	3700 lb/ft [†] 27,800 lb	54.2 lb
Center of pressure (Cp) from calm water level	158.5 in.	19.81 in.
Heave force (F_h) for a 7.5-ft wave amplitude	260 lb/ft [‡] 1951 lb	3.82 lb

* Maximum forces occurring on a hinged float (at $f = 0.224$ cps).

[†] Taken from Figure 16, Ref 4.

[‡] Taken from Figure 13, Ref 4.

Based on the forces shown in Table IV, inflation pressure and fabric strength for a 1/8-scale model are determined below:

$$\text{Surge force } F_s = 54.2 \text{ lb}$$

$$\text{Center of pressure, } Z_{cp} = 19.81 \text{ in.}$$

$$\text{Moment arm, } Z = Z_{cp} - 9 \text{ in.} = 10.81 \text{ in.}$$

$$\text{Bending moment, } M = F_s(Z) = 54.2(10.81) = 585 \text{ in.-lb}$$

$$\text{Bending stress, } N_{\phi_b} = \frac{M}{\pi r^2} = \frac{58.2}{\pi (4.5)^2} = 9.20 \text{ lb/in.}$$

$$\text{Heave force, } F_h = 3.82 \text{ lb}$$

$$\text{Direct stress, } N_{\phi_d} = \frac{F_h}{\pi r^2} = \frac{3.8}{\pi (4.5)^2} = 0.0600 \text{ lb/in.}$$

$$\begin{aligned} \text{Pressure required, } p &= \frac{2(N_{\phi_b} + N_{\phi_d})}{r} \\ &= \frac{2(9.20 + 0.06)}{(4.5)} = 4.11 \text{ psi} \end{aligned}$$

$$\begin{aligned} \text{Max longitudinal stress, } N_{\phi} &= \frac{pr}{2} + N_{\phi_t} + N_{\phi_d} \\ &= \frac{4.11(4.5)}{2} + 9.20 + 0.06 = 18.51 \text{ lb/in.} \end{aligned}$$

$$\text{Max circumferential stress, } N_{\theta} = pr = 4.11(4.5) = 18.52 \text{ lb/in.}$$

Quickbreak strength

$$\begin{aligned} \text{Longitudinal } N_{qb} &= \text{S.F. } N_{\theta} \text{ max} = 4.0(18.5) = 74.0 \text{ lb/in.} \\ (\text{Safety factor} &= 4.0 \text{ for longitudinal fabric}) \end{aligned}$$

$$\begin{aligned} \text{Circumferential } N_{qb} &= \text{S.F. } (N_{\sigma} \text{ max}) \\ &= 5.0(18.5) = 92.5 \text{ lb/in.} \end{aligned}$$

(Safety factor = 5.0 for circumferential fabric)

Fabric strength for attenuator

$$\text{Circumferential - } N_{qb} = 5.0(4.11) \left(\frac{10.8}{2} \right) = 111 \text{ lb/in.}$$

In this consideration, the bending moment was calculated at a point located six feet below the water line where the cable truss will be attached. Bending moment is considered most severe here because of the cantilever effect of the stub extending below this point.

The maximum strength requirement is 111-lb/in. quick break, occurring circumferentially in the attenuator. This value is considered conservative in regard to a full-scale design. Full-scale design would optimize the hinge and truss location to provide for reduced stress on the float fabric. It is noted, additionally, that the geometry of the float considered here does not identically match the model float from which the test data were taken. Differences in the float are judged unimportant in regard to the forces of interest on the basis of extrapolation of other test data.

Dimensions of the two models are provided in Figures 11 and 12. Weight characteristics of the models are provided in Table V.

Figures 13 and 14 are photographs of the fabric and wood floats, respectively. Figure 15 shows a detail of the fabric hinge construction.

Packageability of the fabric float is illustrated by the partially folded model shown in Figure 16.

TABLE V - WEIGHT CHARACTERISTICS OF 1/8-SCALE MODEL

Section	Fabric model	Wood model
Lower section (below hinge)		
Total weight	365.0 lb	355.2 lb
Net weight (in water)	1.8 lb	15.0 lb
cg (from hinge center)	48.90 in.	49.26 in.
Upper section		
Total weight	26.4 lb	86.2 lb
Net weight (in water)	-42.1 lb	11.2 lb
Mounting platform	90.0 lb	90.0 lb

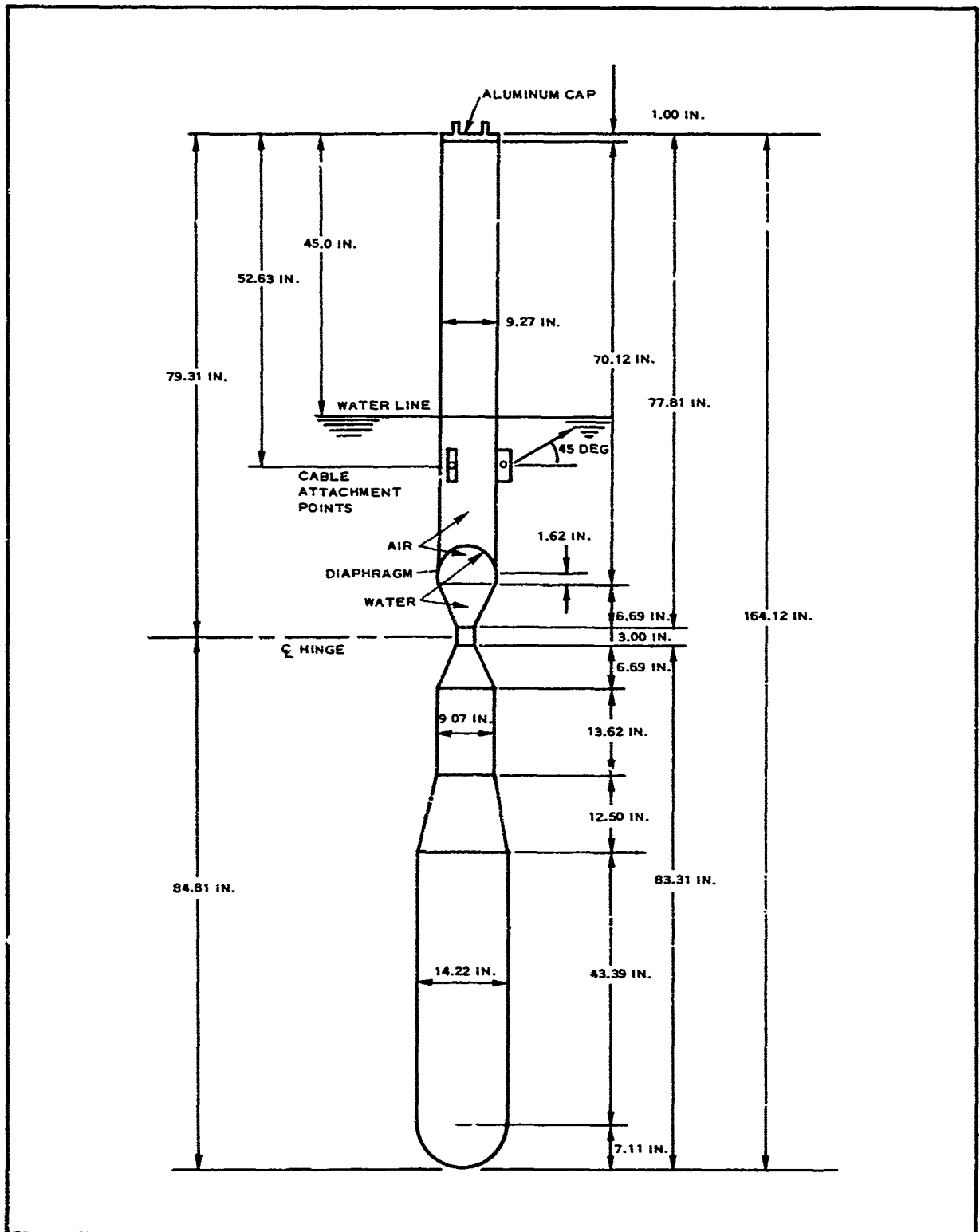


Figure 11 - Fabric Model Dimensions (1/8 Scale)

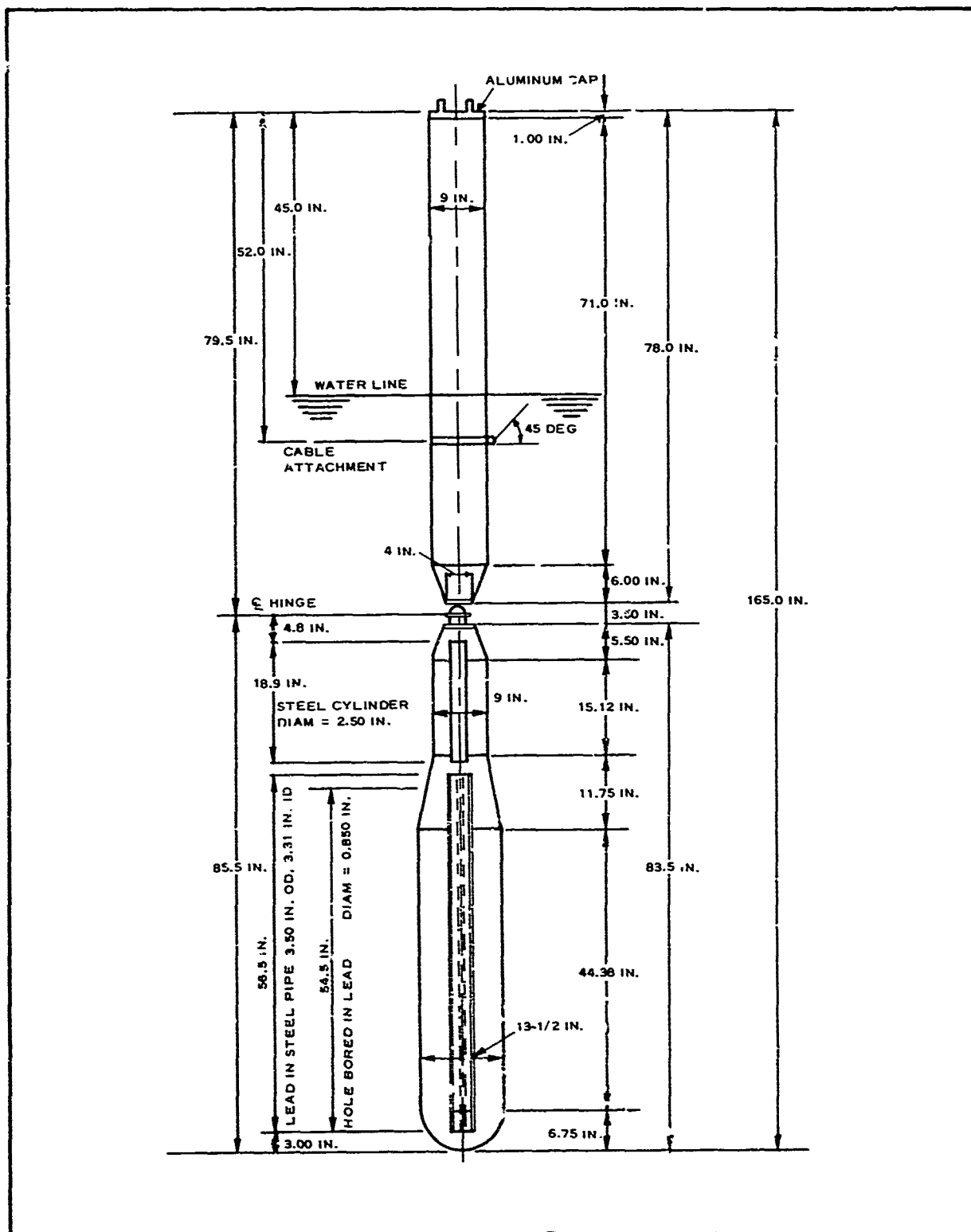


Figure 12 - Wood Model Dimensions (1/8 Scale)

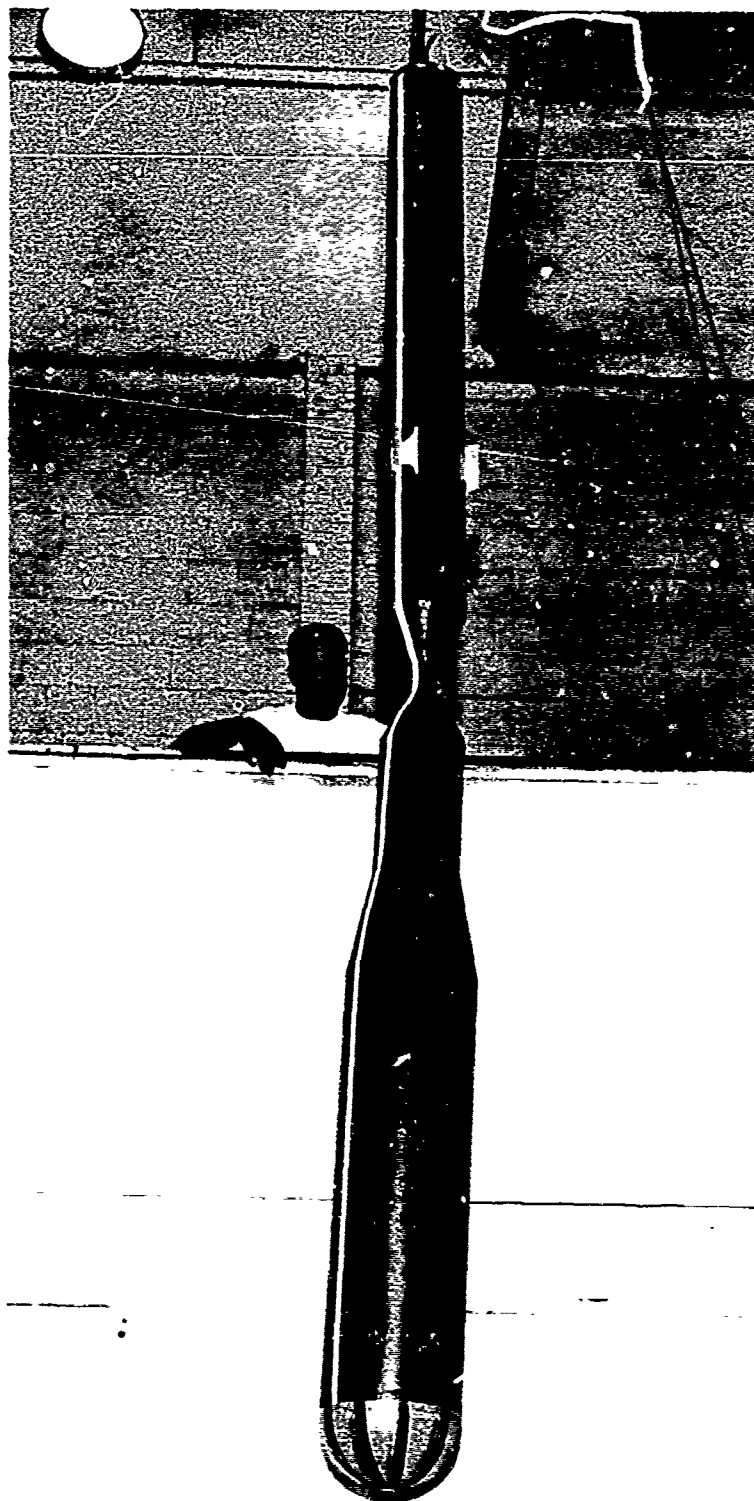


Figure 13 - Fabric Model

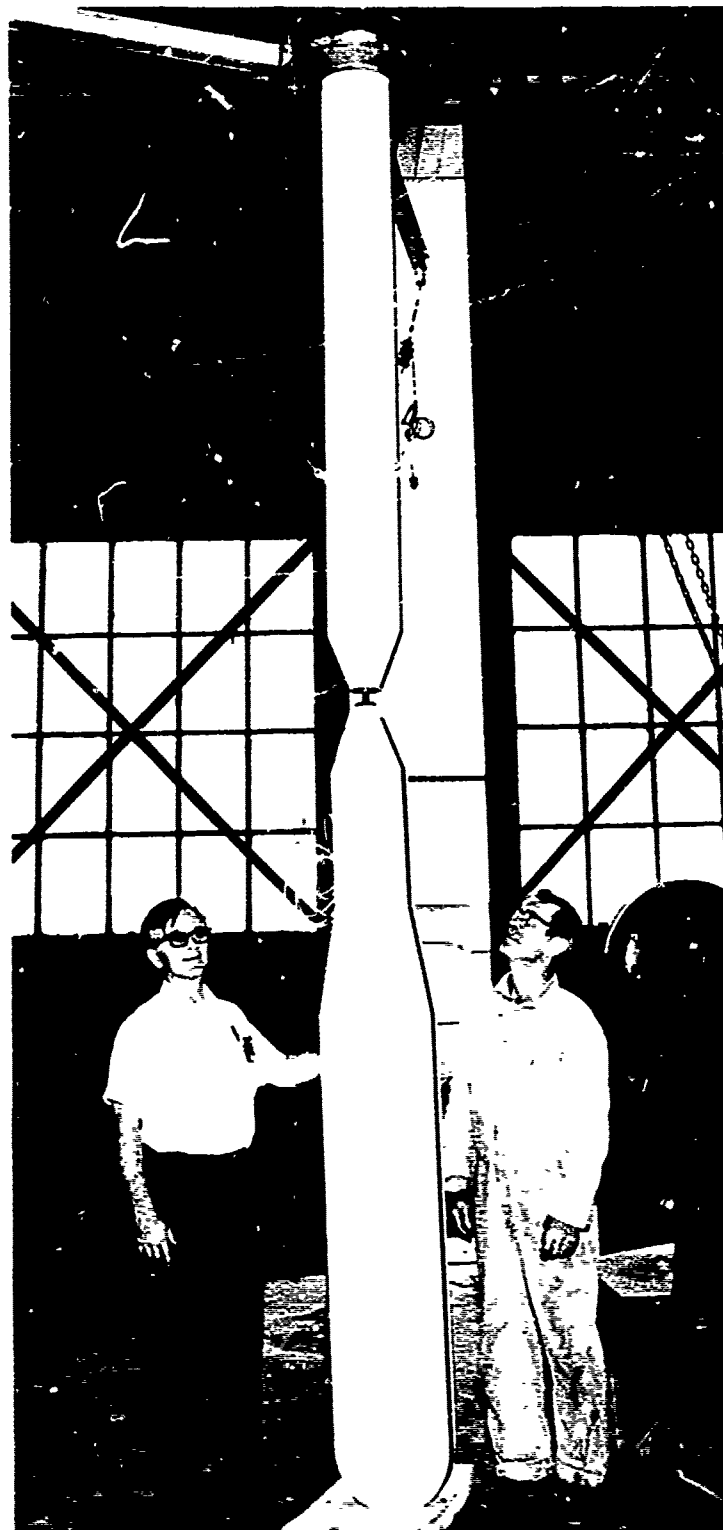


Figure 14 - Wood Model



Figure 15 - Fabric Hinge

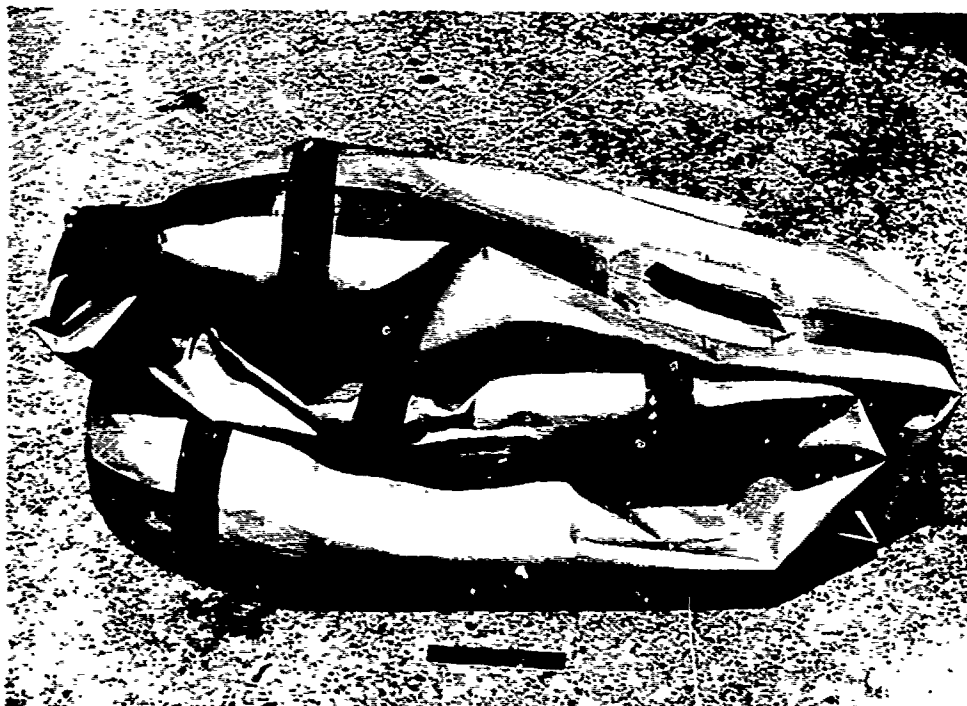


Figure 16 - Fabric Model - Deflated and Folded

The upper mounting platform with outrigger booms for cable truss attachment is shown in Figure 17. This platform was used for both models and was rigidly attached to the force balance by means of the upper angle bracket, as shown in Figure 18.

6. NATURAL FREQUENCY RESPONSE MEASUREMENTS

a. Structural Natural Frequency

Dynamic behavior of the floats can be evaluated by studying the natural frequencies of the floats as mounted on the force balance and situated in the water. A data report on these floats is given in Appendix I.

High-frequency structural modes of heave oscillation, developed by extensional stiffness, were obtained by striking the upper flange of the float in a vertical direction. The frequency of oscillation of the heave force balance was recorded and results are shown in Table VI.

These values are significantly influenced by the natural frequency of the force balance. A complex 2-frequency mode was observed for the fabric model. The lower mode is related to the soft characteristic of the hinge, which allows the attenuator to move relative to the upper float section.

Influence of this 2.5-cps response can be evaluated by comparing it with the frequency of the waves of concern. In full scale, this frequency becomes $F = 2.5 (1/\sqrt{8}) = 0.882$ cps. This frequency is much greater than the 0.112 cps for the significant energy of a Sea State 5 condition. It is concluded from this that the influence of the structural frequency of the fabric float, although different from the infinite value of a rigid float, will have little influence on the heave response of the float in rough sea conditions. It is further noted that a significant increase in the frequency can be attained by a simple design change of the hinge whereby it is stiffened.

Bending natural frequency of the float was excited by imposing a transverse force on the float. Measured values are shown in Table VI. Here again the frequency of the fabric model is less than the wooden model. Hinge design is likewise responsible for the difference. The metal hinge requires transverse motion of the upper float section to be equal to the attenuator at the



Figure 17 - Mounting Platform

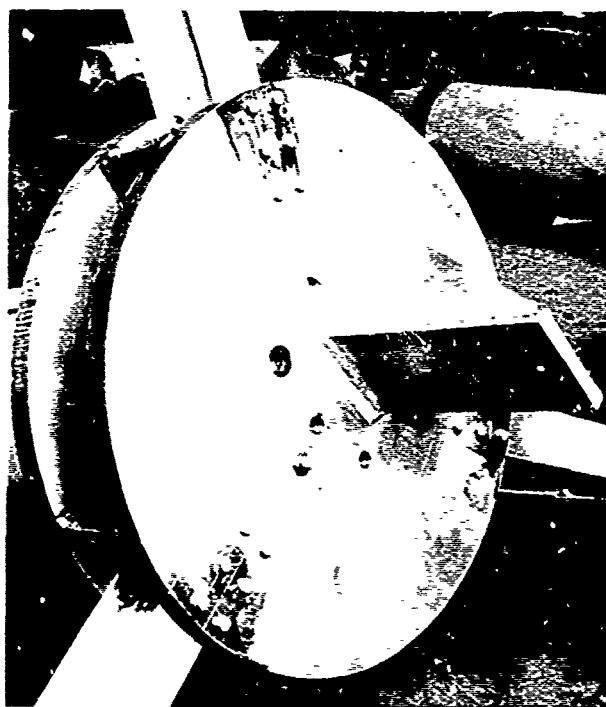


Figure 18 - Interface with Force
Balance on Mounting Platform

TABLE VI - STRUCTURAL NATURAL FREQUENCIES

Frequency			
Frequency measured	Model scale	Full-scale equivalent	Remarks
Extensional mode (heave direction)			
Rigid - wood	4.3	1.52	Model plus balance system
Flexible - fabric (higher mode)	7.7	2.72	Upper float plus balance system
(Lower mode)	2.5	0.882	Attenuator hinge
Bending mode (transverse direction)			
Rigid - wood	1.7	0.600	Model plus balance system
Flexible - fabric	1.0	0.352	Model plus balance system
Water plane heaving frequency			
Rigid - wood	0.263	0.0929	Model detached from balance
Flexible - fabric	0.249	0.0880	Model detached from balance (average of 5 cycles)
Pendular frequency of attenuator			
Rigid - wood	0.0645	0.0228	Pendular motion due to hinge (average of 10 cycles)
Flexible - fabric	0.0671	0.0237	Pendular motion due to hinge (average of 10 cycles)

hinge. In the fabric model, the two motions do not have to be equal, consequently at a frequency of 1.0 cps, this softness will become significant. At full scale this frequency is 0.352 cps. This frequency is again higher than the significant frequency to be encountered in rough seas. As noted above, the control of this frequency is easily managed by a change in the hinge design.

b. Heaving Natural Frequency

Buoyant or water plane frequency of the floats was measured by removing the models from the force balance and allowing them to heave in reaction to

an upward force on the float. Five cycles of motion were recorded and averaged as shown in Table VI.

Theoretical values for this frequency can be calculated as:

$$f = \frac{1}{2\pi} \sqrt{\frac{K}{m}},$$

where

K = spring constant for restoring force
acting on the float and

M = mass of float.

For the wooden (rigid) float,

$$f = \frac{1}{2\pi} \sqrt{\frac{62.4\pi (0.375)^2}{\frac{441.4}{32.2}}}$$
$$= 0.226 \text{ cps}$$

For the fabric float,

$$f = \frac{1}{2\pi} \sqrt{\frac{62.4\pi (0.386)^2}{36532.2}}$$
$$= 0.256 \text{ cps}$$

Natural frequency measured for the fabric float (0.249 cps) is close to the theoretical value (0.256 cps). Measured value for the wooden float (0.263 cps) is different from the theoretical value (0.226 cps). The measured value in this case is considered not accurate, because the value was taken by untrained observers and for only one cycle of motion.

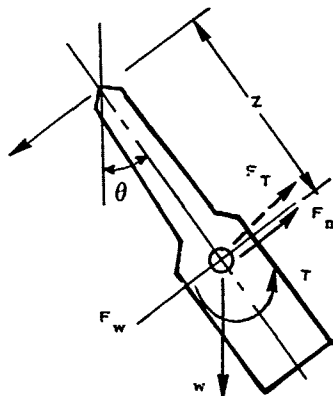
Natural frequency of the fabric float is greater than the wooden float, as expected, because its mass is less and its water plane diameter is greater. Accuracy in the prediction of this frequency is important, because it is a limiting feature in design.

Its value can be controlled to any desired magnitude, specifically to a frequency sufficiently below the wave spectral frequency, to avoid resonant amplification. Data above show that the use of a fabric material in construction does not affect this natural frequency phenomenon and that the body can be considered as a rigid body.

c. Pendular Natural Frequency

Free pendulation of the attenuator about its hinge point was measured by observing its motion after the surface of the wave channel had become relatively calm. Little damping appeared to exist in the motion and 10 cycles were easily observed, with the average value for one cycle reported in Table VI.

Theoretical values for these frequencies can be calculated from the differential equation for pendular motion of a submerged body.



Forces and accelerations acting on the body are:

1. Weight force, $F_W = W \sin \theta$
2. Restoring linear inertia force, $F_m = m\ddot{z}$
3. Restoring rotational inertia couple, $T = J\ddot{\theta}$

This restoring torque can be represented by a couple of magnitude:

$$F_T = \frac{T}{Z} = \frac{J}{Z} \ddot{\theta}$$

$$= \frac{mr^2}{Z} \ddot{\theta}$$

The differential equation of motion becomes

$$m \left(\ddot{z} + \frac{r^2}{Z} \ddot{\theta} \right) = -W \sin \theta ,$$

where

m = mass of the attenuator,

W = net weight of attenuator in water,

r = radius of gyration of attenuator,

J = polar moment of inertia of attenuator, and

θ = angular position.

It is assumed here that the center of gravity and center of buoyancy occur at the same point on the body. Also, a term is included for the effect of rotational inertia in addition to linear inertia in decelerating the pendular motion.

For small angles, $\sin \theta = \theta$, and the following expression for frequency is developed:

$$f = \frac{\omega}{2\pi}$$

$$= \frac{1}{2\pi} \sqrt{\frac{\frac{W}{m}}{\frac{Z}{g} + \frac{r^2}{Z}}}$$

For a single pendulum with a concentrated mass suspended in air, $r = 0$ and $W = mg$, thus,

$$f = \frac{1}{2\pi} \sqrt{\frac{g}{Z}}$$

This is the classical expression for such a problem.

Theoretical value for the wooden float is approximated by reducing its net weight in water (15 lb) by 4 lb to account for a concentrated mass of metal located near the hinge.

$$f_{\text{wood}} = \frac{1}{2\pi} \sqrt{\frac{11 (32.2)}{(4.07 + \left(\frac{4.23}{4.07}\right)(355.2))}} = 0.0706$$

No value is calculated for the fabric floats because the differential equation above doesn't allow for a restoring force at the hinge as exists for this model. Note that the frequency is very sensitive to the net weight value W . When $W = 0$, the natural frequency is zero and the float will follow the wave. Control of the magnitude of W is a simple matter involving ballasting.

The value calculated above is sufficiently close to the measured values of 0.0645 cps for the wood model that confidence in prediction methods is established.

The use of fabric in construction has no influences on this natural frequency mode.

d. Frequency Summary

The frequency responses discussed above indicate that a fabric float can be designed with frequency characteristics that are not detrimental to the functioning of a float in waves. Specifically, the assumed rigid-body motions of heaving and pendulating are accurately predicted for the fabric float using rigid-body theory. Structural natural frequencies of extension and bending of the float are different, as would be expected, with the fabric float lower than the more rigid wooden float. Of primary influence on these structural frequencies is the hinge. Construction as used for the model tested provides a natural frequency sufficiently high so as to make its response only slightly higher than the more rigid float. Low-cost techniques can be employed to change this hinge construction to the point where its frequency can be raised to near that of the more rigid float and consequently eliminate its influence from any concern if desired.

7. FLOAT FORCE AS A FUNCTION OF FREQUENCY

a. Heave Force

Verification of the observations made in the preceding discussion concerning frequency can be made by measuring the forces transmitted through the structure to a support as waves pass by.

Wave tests were conducted on the wood and fabric models as outlined in Table VII. Wave frequency varied from 0.245 to 0.675 cps. In full-scale terms, this range is 0.0865 to 0.238 cps, which is sufficient to examine the comparative response of the floats in a frequency range similar to what would be encountered in ocean waves.

Details of the test setup, recording equipment, and results are provided in Appendix I.

A graphical presentation of the heave force is made in Figure 19. An analytical prediction based on the preceding theory is also shown. Results indicate that the rigid and flexible floats respond similarly throughout the frequency range.

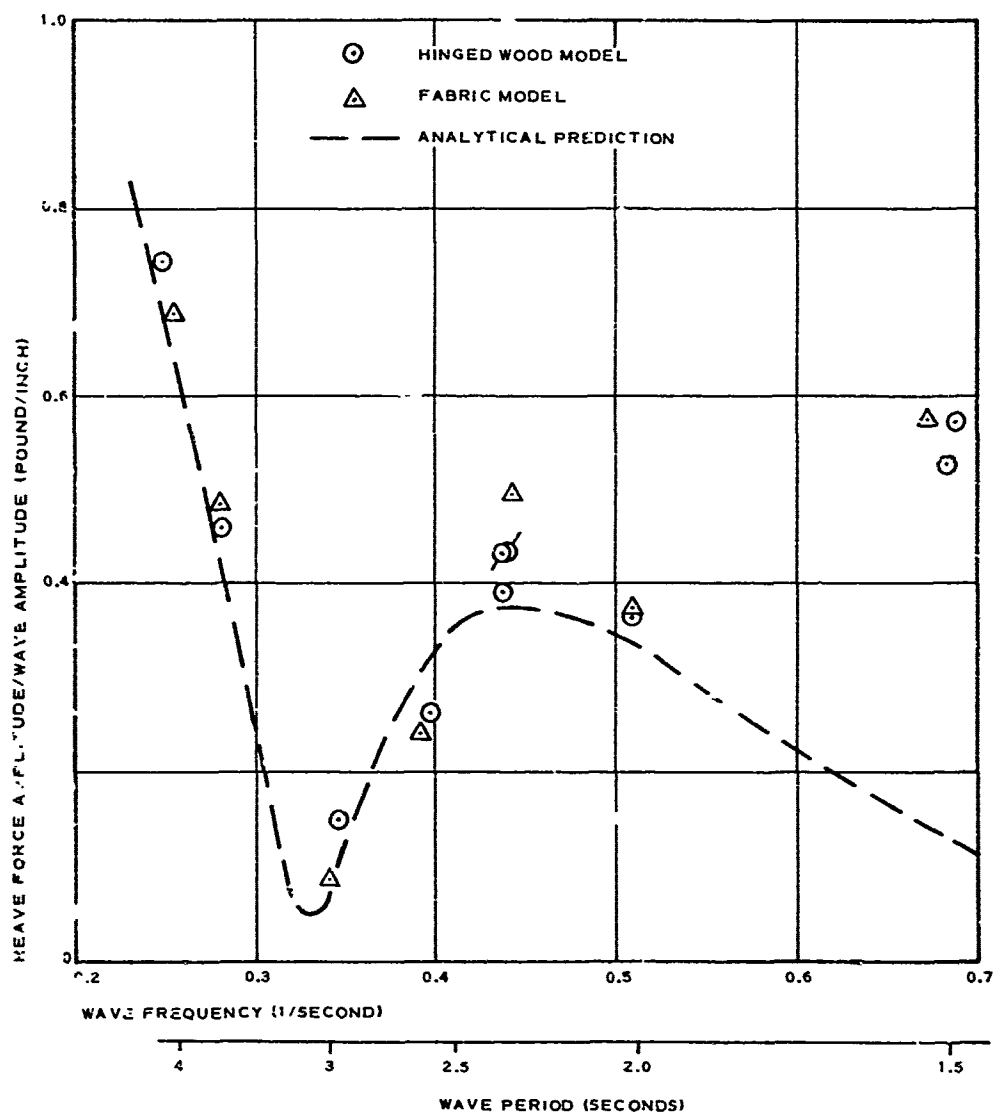


Figure 19 - Heave Force Measurements ~ 1/8-Scale Floats

TABLE VII - TEST SCHEDULE FOR 1/8-SCALE FLOATS

Test series	Model	Wave frequency (cps)	Wave amplitude (nominal) (in.)
1	Wooden model (with hinge)	0.675 0.25 to 0.50	2 4 to 7
2	Wooden model (upper float portion alone)	0.25 to 0.66	4 to 7
3	Wooden model (hinge eliminated by rigid collar)	0.3	2
4	Fabric model (internal pressure = 4.11 psi)	0.66 0.27 - 0.66 0.44	3 4 to 5 6
5	Fabric model (internal pressure = 2.5 psi)	0.25	6

Theoretical prediction of the response is good throughout the range except at the highest frequency tested. This highest frequency wave (0.675 and 0.660 cps for the wood and fabric models, respectively) is sufficiently below the natural frequency in heave (4.3 and 2.5 cps) that significant amplification should not occur. Concern over the above discrepancy is not important, since wave amplitudes imposed on a prototype at this frequency would be small and that the resulting motion would likewise be small. Note that the curves presented earlier for the small-scale floats (1/57.6) did not show this effect. Further work should eventually be conducted to examine more fully this high-frequency range.

b. Surge Force

Surge force results are graphically presented in Figure 20. Theoretical predictions based on expressions shown earlier for rigid structures are also shown, with the fabric model having a slightly higher response than the wood model because of geometric differences.

Experimental response of the wood model in comparison with theory is in reasonably close agreement. The close proximity of the bottom of the tank

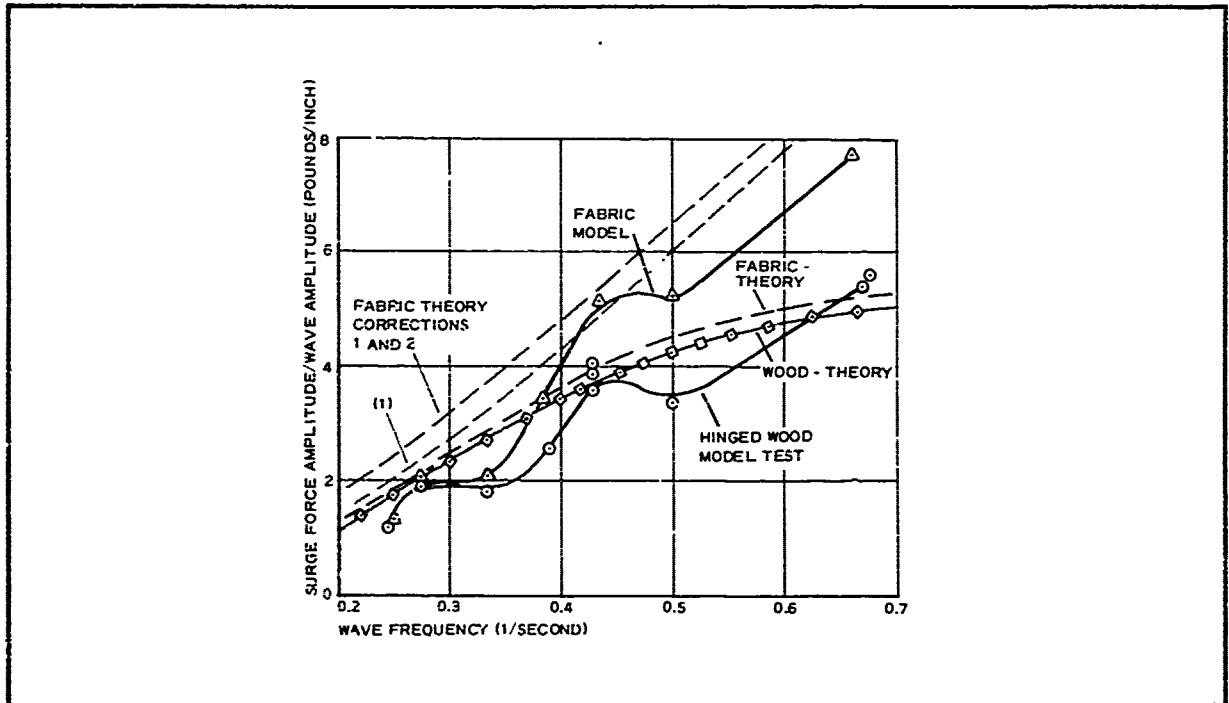


Figure 20 - 1/8-Scale Float Models in Regular Waves - Model Surge Force Amplitudes

to the model would give shallow water effects, particularly for the lower frequency waves. Tank depth (d) is 17 ft while wave lengths range from 10 to 80 ft. Depth-to-wave length ratio d/λ is 1.7 to 0.213. Deep-water theory is generally applicable for $d/\lambda > 0.5$.

The theory plotted did not account for shallow water influence; consequently, the test data might be expected to be greater than shown for the theoretical curve. The data surprisingly is below theory, however. Response of the fabric model is greater than the theory predicts. Two causes are suggested for this action.

1. Force amplification due to the low structural resonance of the model. An expression from Appendix I provides a method for calculating this effect.

$$F_T = \left[\frac{1}{1 - \left(\frac{f}{f_n} \right)^2} \right] F_E ,$$

where

F_T = transmitted force,

F_E = exciting force (taken here to be the predicted force),

f = wave frequency, and

f_n = natural frequency of element

This influence is shown as a modified theoretical plot in Figure 20.

2. A second influence is suggested due to the resisting "stiffness" built into the fabric hinge, which is not present in the metal hinge of the wooden model. The three-inch diameter fabric hinge has a collapsing moment of:

$$\begin{aligned} M &= \frac{1}{2} p \pi r^3 \\ &= \frac{1}{2} (4.11) \pi (1.5)^3 \\ &= 21.8 \text{ in. -lb} \end{aligned}$$

Considering the center of surge force pressure to be acting at a level of four feet from the hinge, a force of $F = 21.8/48 = 0.454$ pounds would have to be applied before hinging action would occur.

An unreported plot shows that pressure within the attenuator varies as the waves pass; consequently, the pressure used in the equation above is actually a variable. Post-buckling behavior of a fabric tube should be considered in a complete analysis of the hinge.

A plot showing the combined effect of the two corrections, based on the simple assumptions shown above, is included in Figure 20.

Tests were run with the upper section of the wooden float alone without the attenuator installed. These results are shown in Figure 21 along with a theoretical prediction that shows good agreement.

The strain link installed between the float and attenuator at the hinge provided valuable information regarding surge forces acting on the attenuator alone. These values are included in Figure 21, also.

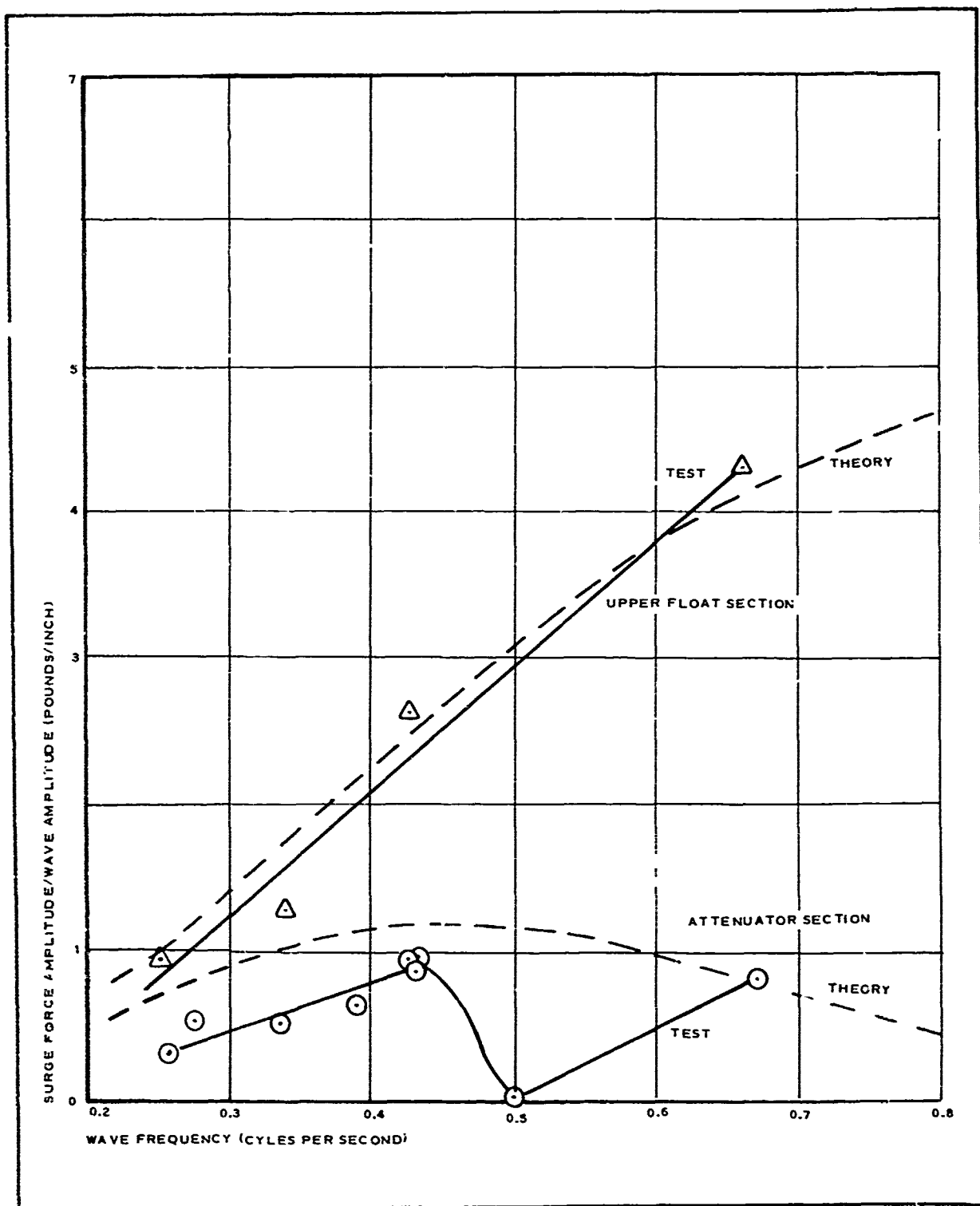


Figure 21 - Surge Force Measurements on Upper Float Section and Attenuator Separately

Figure 22 provides a comparison of these plots. Theory and measured data for the float in total are shown as two of the curves. The third curve shows summation of data for the attenuator and float, as was shown separately in Figure 21.

Good agreement of the curves further establishes confidence in the theory and verifies the assumed phase relation between surge force on the float and the attenuator, namely that they are in phase.

c. Bending Moment

Bending moment as measured at a point on the top surface of the cap of each model is provided in Figure 23. Theoretical predictions for this moment are also included.

In both cases the measured response is less than the predicted value, except for the highest frequency run of the fabric model.

Corrections 1 and 2 for the frequency effect and the resistant moment influence of the hinge, as utilized in the surge force comparison above, are also shown on the plot.

Cause for the conservative values generated by the theory must be related to the distribution of surge force on the side of the float. (Magnitude of the force was shown to be relatively accurate in Figure 12). Further work in this area, whereby the theoretical prediction can be made less conservative, will allow for reductions in the stress requirements for the float construction.

d. Force Summary

Force measurements show that the response of the wood and fabric models to imposed waves are similar. Differences in forces can be essentially attributed to construction details. Corrections for natural frequency differences, associated primarily with the hinge construction, explain much of the response deviation between the models.

Theoretical predictions of the forces are available and agree well with measurements, except in regard to the distribution of surge force on the floats. Theory predicts a conservative bending moment on the float at the deck level.

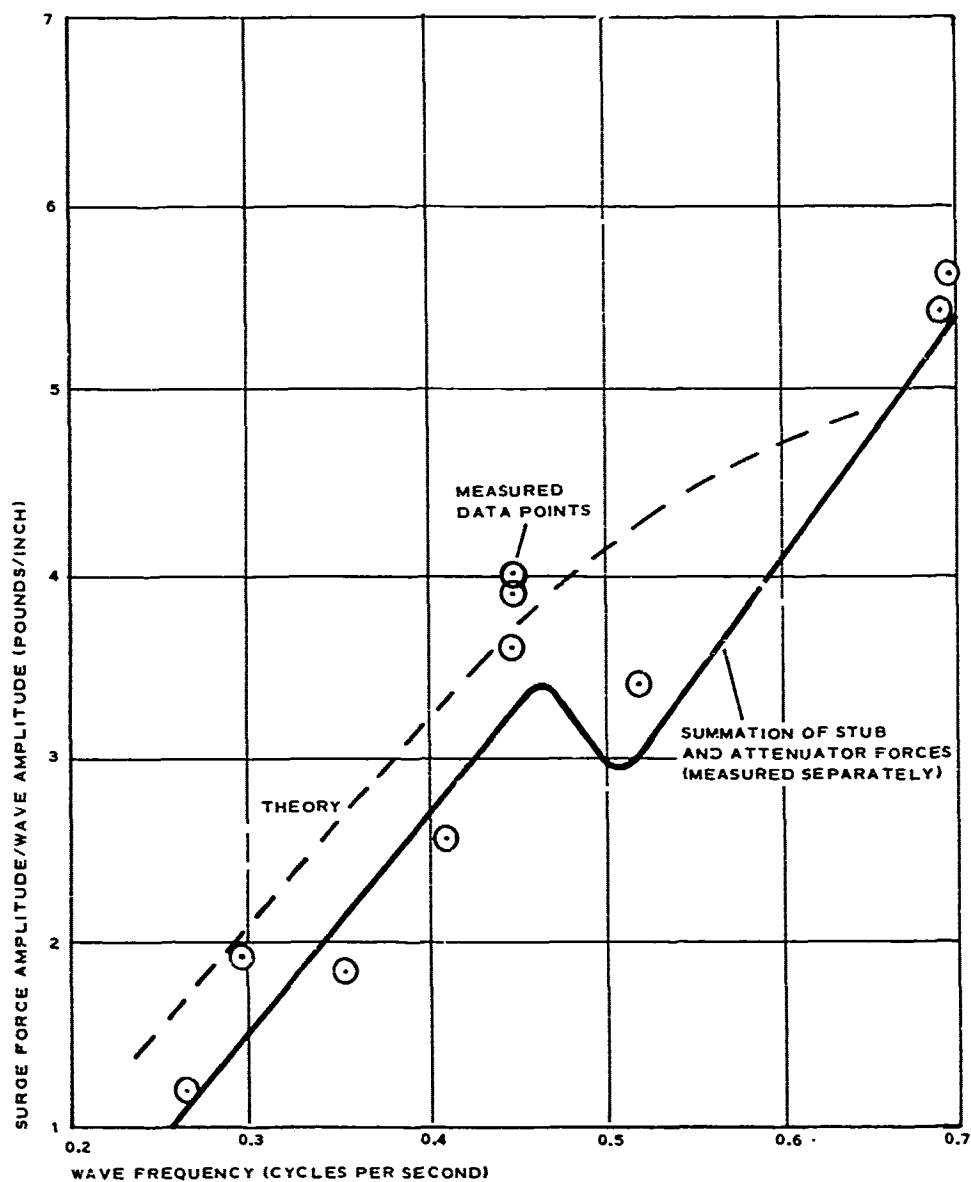


Figure 22 - Surge Force as Sums of Component Measurements

8. SMALL-SCALE INFLATABLE FLOAT TESTS

Tests on small-scale inflatable floats made of an unreinforced flexible vinyl material were to be made as the first step in the program. For expediency, the shape selected was similar to a shape previously tested by Stevens Institute. The shape selected, however, was significantly different than the proposed float design. Information gained here was to be used as an aid in the establishment of the larger scale inflatable model discussed in the preceding.

Requests to complete the program within a short time span demanded that the large-scale models be designed and fabricated in the same calendar period as the small-scale models. Benefit of small-scale test data consequently was not available for large-scale model design.

Test plan, model geometry, and results are presented in Appendix H. No discussion is presented here, because of unresolved problems associated with the test. Unresolved questions include:

1. Deformation magnitudes due to low pressure
2. Influence of creep phenomena associated with vinyl materials in regard to skin stresses

Additional effort could have been expanded to resolve these questions and make use of the data presented. It was concluded, however, that further expenditure was not warranted on the basis that the results of large-scale model tests were available showing good correlation to theory. Further, geometry of the small-scale models does not represent prototype geometry, whereas the large-scale model closely represents such geometry.

9. HEAVE MOTION RESPONSE

Tests of unrestrained floats in waves, to determine their heave motion response, were not made. Motion prediction methods are available, however, from which plots can be made. Newman in Reference 5 presents an expression for heave motion response of an isolated float as developed from slender body theory neglecting damping and added mass. Mercier provides plots in Reference 4, based on Newman's expression, which is:

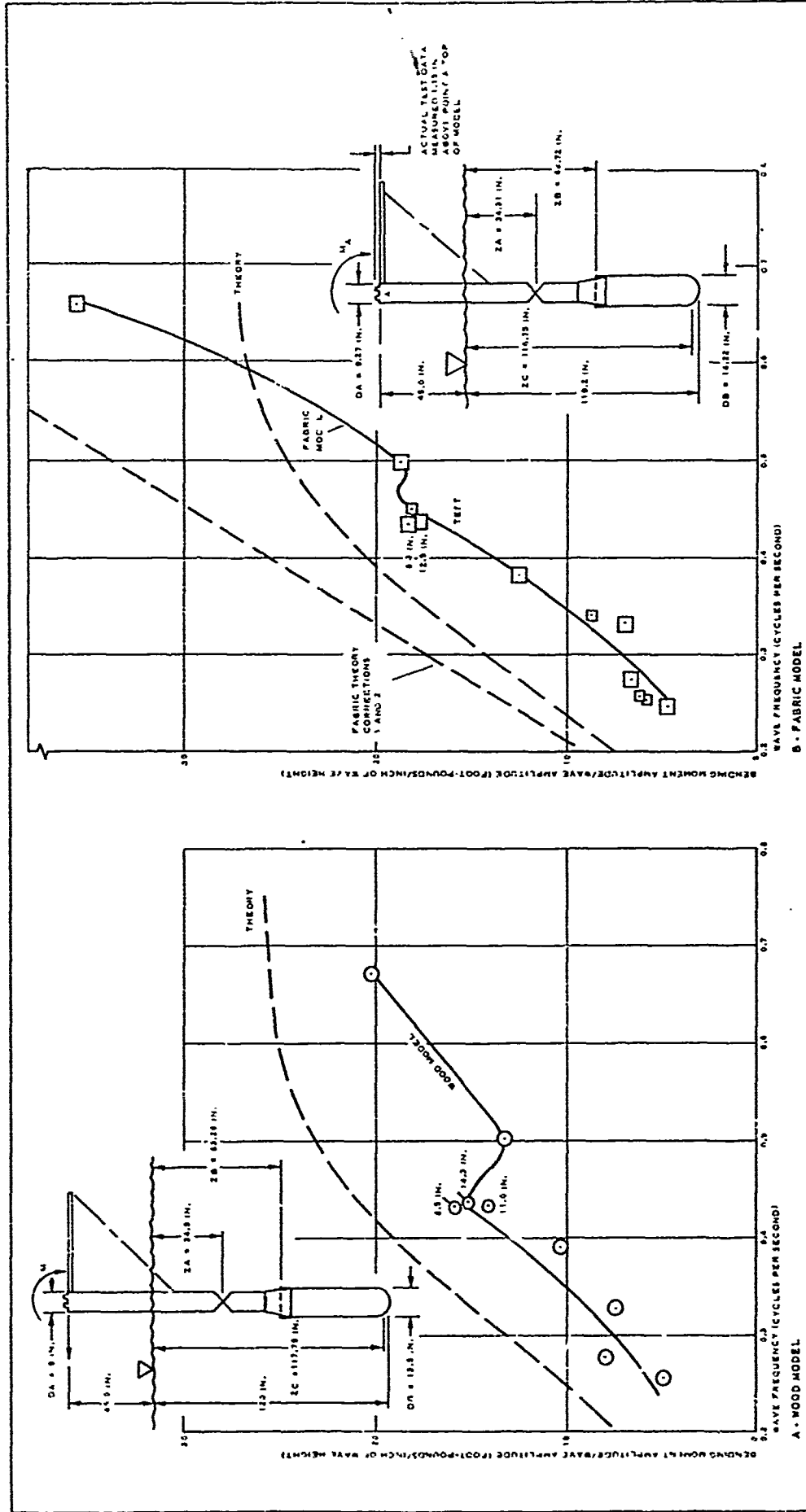


Figure 23 - Bending Response

$$\frac{Z}{\xi} = \frac{1 - C_{VP} Q_o K T}{1 - C_{VP} K T}$$

where

Z = maximum amplitude of motion experienced

ξ = wave amplitude of motion

C_{VP} = vertical prismatic coefficient

∇ = displacement volume of the float

T = draft of float

K = wave number

Q_o = nondimensional volume ratio modified by a factor to account for wave influence decay with depth:

$$Q_o = \frac{1}{\nabla} \int_{-T}^0 e^{Kz} \delta(Z) dZ .$$

These expressions are utilized to generate the data in the 7th and 8th columns of Table I. Figure 24 provides a plot of this predicted heave motion for floats A, B, C, and D discussed in earlier sections of the report.

Although this theory neglects certain terms that should be included for a more complete analysis, it does provide a comparative response not greatly in error from expected motions.

Preceding page blank

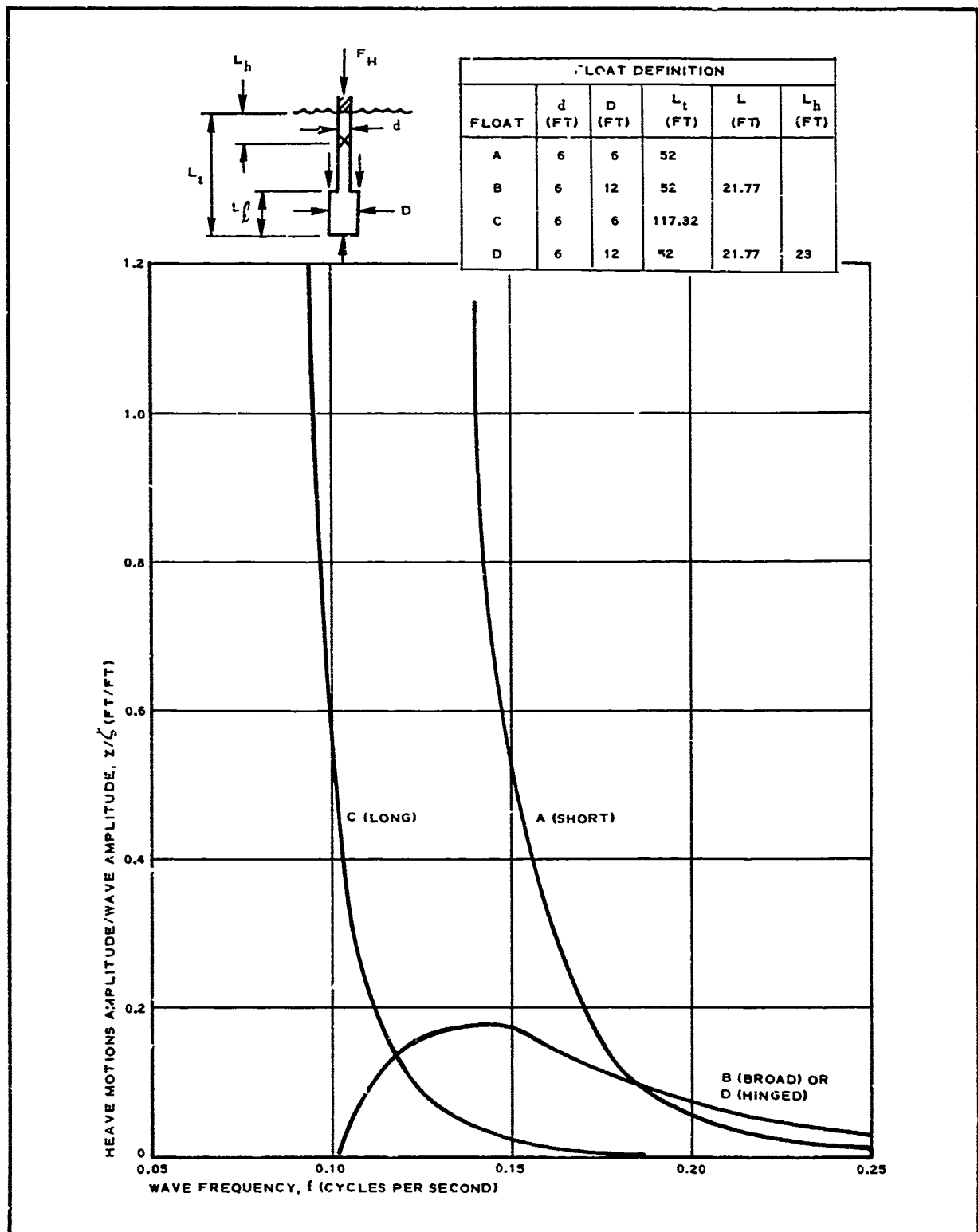


Figure 24 - Heave Motion Prediction

SECTION IV - PLATFORM MOTION INVESTIGATIONS

1. BACKGROUND

The ARPA review group noted that an expandable floating base "has some rather unusual features: the columns are closely spaced ... the ratio of column diameter to that of attenuators is $3/2$; a full structure may have a regular array of hundreds to thousands of such floats; and the deck and truss structure connecting the columns is rather flexible."

Concern was expressed over the effects of interaction in such arrays, about distributed reflection and absorption of wave energy, and about the validity of "scaleability" of model test results. Recommendation was made that further work be assayed on three basic hydrodynamic problems:

1. Interaction of the viscous wake of a float with neighboring floats
2. Distributed wave reflection and absorption
3. Elastic response of the structure to wave-induced forces

Emphasis was suggested on exploration by empirical and analytical means of the stern motion amplification (tail wagging) noted in tank tests of the 6-by-35 float array, which employed a deck with parallel linkage connections offering no restraint to heave forces.

Investigation of these problems was undertaken by Davidson Laboratory through model tests and analysis in two tasks (Appendixes F and G). GAC participation in this effort was to interpret and analyze test results and to attempt to predict platform behavior through mathematical models.

2. EXPLORATORY INVESTIGATION OF INTERACTION EFFECTS ON DECK MOTION

a. Introduction

In this first phase of the test program, an attempt was made to determine the nature of the cause of the motion of the previously tested articulated model.

Figure 25 is a display of the motions of that model as taken from Reference 5. Of primary concern is the observation that motions throughout the model are magnified over that predicted by theory. Also of concern is the observation that at most wave frequencies, motions become amplified as the stern is approached (tail wagging). Near resonance, the bow motion begins to show higher motions. Note that the resonant or heave natural frequency of the various rows appears to occur at a lower frequency than predicted for an isolated float.

Several items considered in establishment of the test program are discussed below. Items that influence motion and scaling are included:

1. Forces induced on individual rows of floats. (If the forces imposed on the floats are greater than theoretical, then the magnification effect can be explained by hydrodynamic causes. Amplification effects, tail wagging, can likewise be explained if force variation is similar).
2. Wave elevation measurements - Magnification and amplification effects may be explained as surface wave elevations.
3. Reynold number effects - Possibility of viscous wake interaction due to vortex shedding, separated flow, etc, may occur. This influence can be examined by changes in the Reynolds number resulting from a change in model scale.
4. Weber's number effect - Surface tension effects on these small-scale tests may be tested by introducing a chemical surfactant.
5. Test tank sidewall effects - This influence could be examined by moving to a larger test tank.

b. Model Description and Test Plan

Tests were programmed as shown in Table VIII, which provides a general description of the models and measurements made. Note that the float used is the same as float B discussed earlier in this report. Details of the

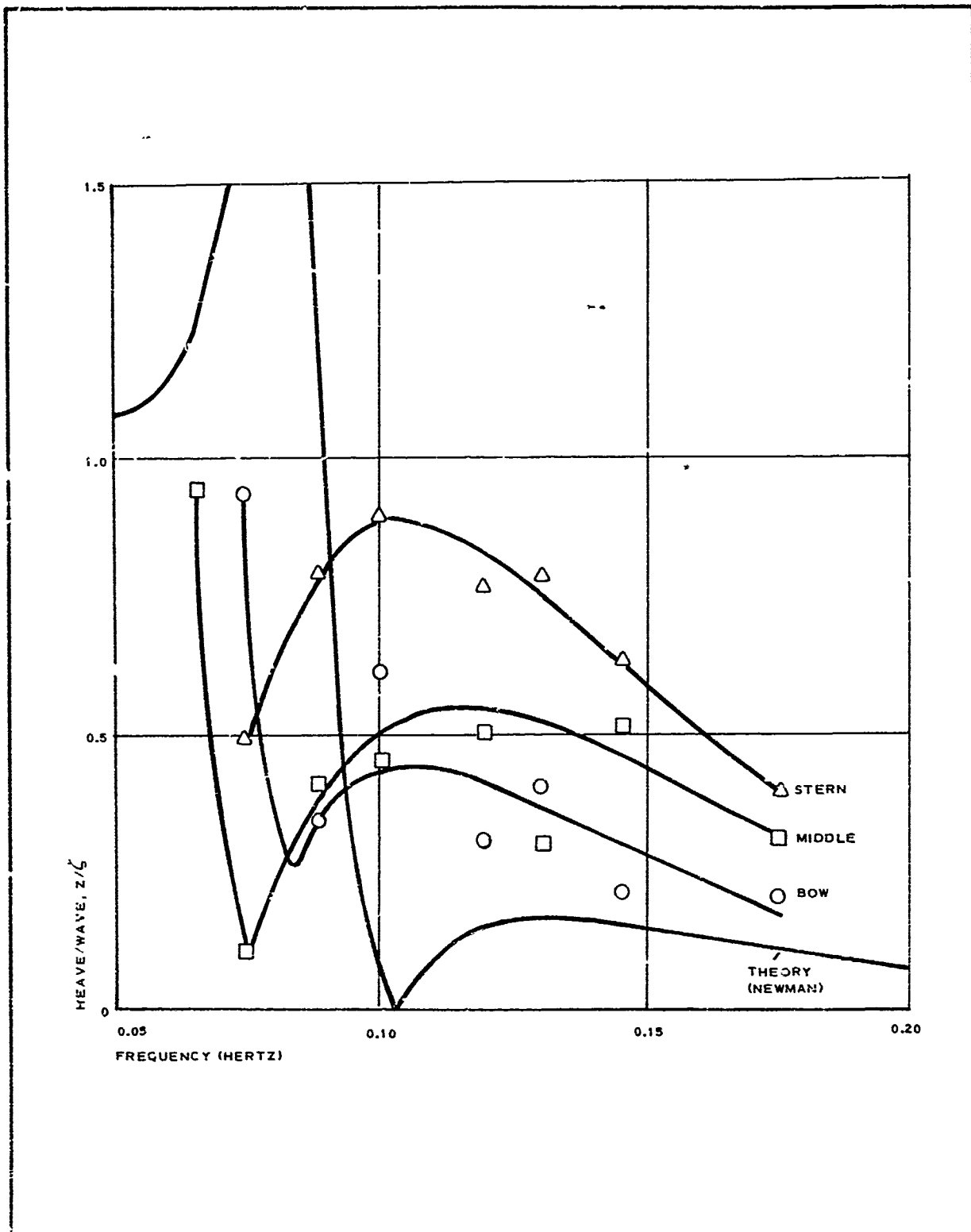


Figure 25 - Model Island Heave Motion

TABLE VIII - EXPLORATORY PROGRAM TEST SUMMARY

Test number	Model scale*		Array size	Float motion restraint		Test time [†]		Float forces	Deck motions	Wave height		Surface tension effects
	1/57.6	1/164		Array fixed	Articulated linkage	2	3			Inside array	Outside array	
1	X		6 X 35		X		X		X		X	
2	X		6 X 35	X		X		X		X	X	
3	X		6 X 35		X	X			X		X	
4		X	6 X 35	X		X		X			X	
5		X	6 X 1	X			X	X			X	X
6	X		6 X 1	X		X		X			X	

*Model geometry in full scale is that of float B previously referred to in Figure 1.

[†]Tank 2 - 75 ft by 75 ft by 4.5 ft; Tank 3 - 300 ft by 12 ft by 6 ft; CWC - Circulating water channel.

models are contained in Appendix F with photographs and drawings of the constructions (see Figures 1 to 8a of Appendix F).

Test data with faired curves for heave motion, heave force, surge force, and wave elevation are shown in Figures 9 through 33 of Appendix F.

c. Measurements

Summary plots of certain of these curves are reported in Figures 26, 27, and 28 for vertical deck motions at certain locations, heave force developed, and surge force developed. Note that the deck motion curves are faired from the previous test data presented in Figure 25 and new test data.

Wave height data are summarized in Table IX. Data in the second to seventh columns are obtained from Appendix F by normalizing the wave height values measured with no model present (Column 2) and those measured behind each of the given rows when the model is present (Columns 3 through 7). Normalizing value is that representative value measured 25 ft forward of Row 1. Column 8 is the average of all the measured rows. Average wave height within the array varies from 8 to 37 percent greater than that measured ahead of the array as shown. The last column of data is taken as the ratio of the wave height average for the rows to the height with no model present. Wave height average within the model varies from 6 to 42 percent greater than the height measured with no model present.

TABLE IX - WAVE ELEVATION SUMMARY

Wave frequency	No model	Row number 1	Normalized wave height ratios					Average/ no model
			Row number 9	Row number 17	Row number 27	Row number 35	Average of all rows	
0.49	0.76	1.36	1.11	0.89	0.84	1.20	1.08	1.42
0.80	1.19	1.41	1.38	1.05	1.46	1.08	1.28	1.03
1.00	1.29	1.29	1.24	1.17	1.58	1.57	1.37	1.06
1.30	0.93	1.02	1.06	1.11	1.36	1.28	1.17	1.26

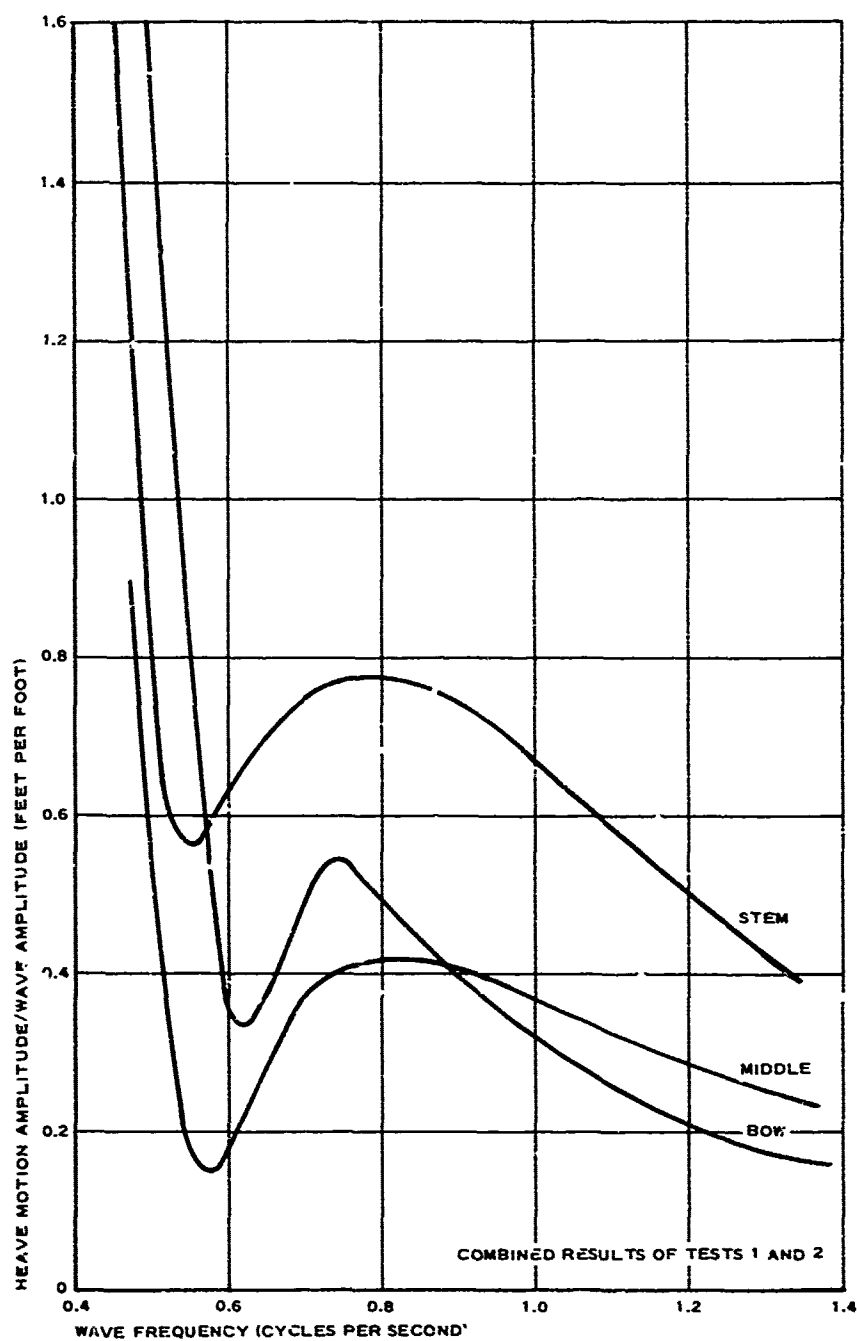


Figure 26 - Subsequent Model Island Motions

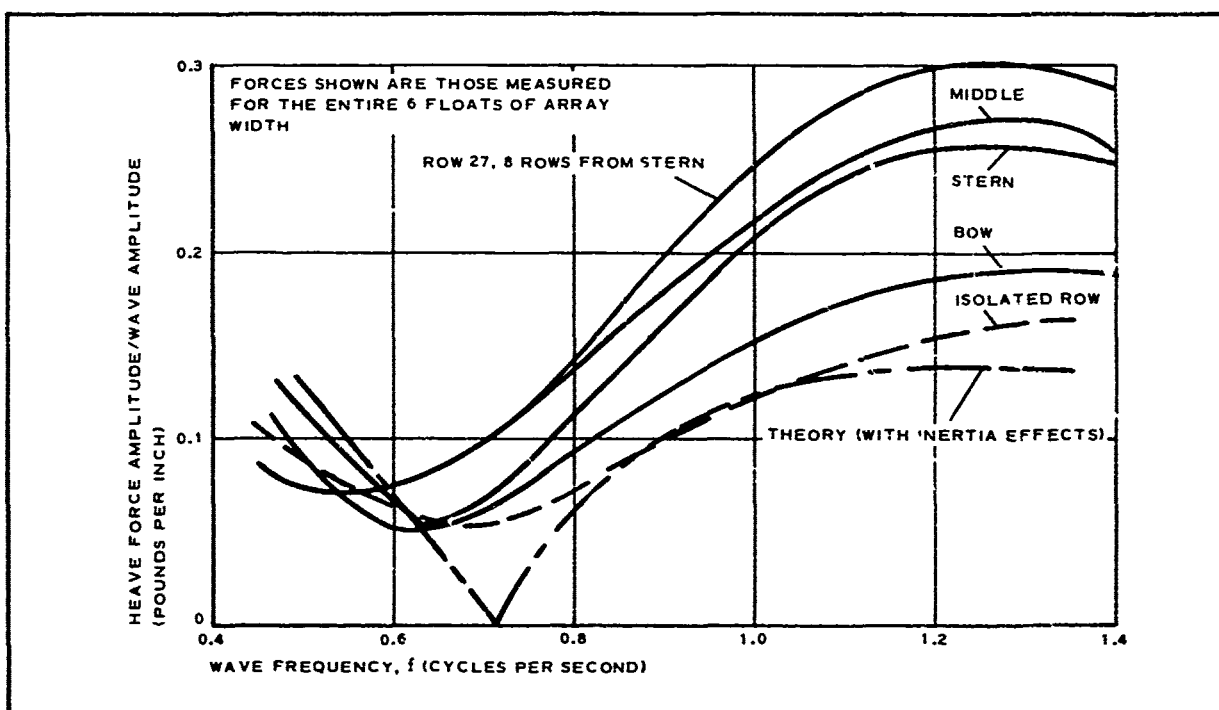


Figure 27 - Heave Force Measured on Model Island

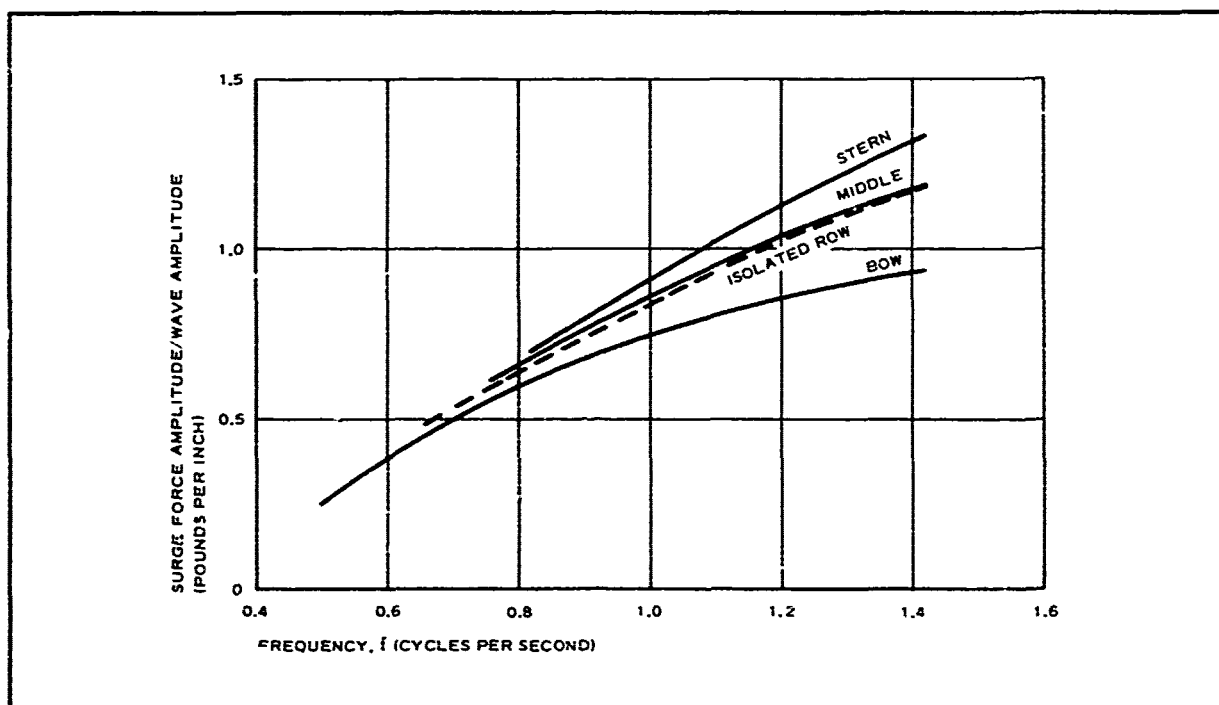


Figure 28 - Surge Force Measured on Model Island

Motions shown in Figure 26 and Appendix F indicate that deck motions over the length of the array are similar in magnitude, except at the bow and the stern. Bow motion null and resonance points shift to higher frequency than the other rows. Their effect causes bow motions to become larger than the remainder of the array at particular low frequencies. Stern motion shows increased motion at all frequencies.

Heave force amplitudes shown in Figure 27 show an increase as the stern is approached. Upon reaching the stern, the values taper off to a magnitude close to that measured at the center of the array. Forces in the array are greater than those measured for an isolated row. Theoretical predictions are adequate for the isolated row measurements.

Surge force amplitudes shown in Figure 28 show an increase from bow to stern. Forces on an isolated row are close to those measured at the middle of the array and thus represent an average for the entire array.

Figure 29 provides plots of the heave motion and heave force measured with the plots made along the length of the array. Note that for any given frequency, the motion response along the array is similar to that at any other frequency. A similar result is evident for the heave forces. As would be expected, the heave motion response decreases with wave frequency, while the heave force increases.

d. Results

An examination of Figures 26, 27, and 28 and the curves in Appendix F will aid in interpreting the following information:

1. Test tank width has little effect on the motions of the articulated array. Conclusion: Boundary or side wall channel effects of 12 ft wide tank are not significant for an island model 20.6 in. in width.)
2. Heave and surge force measurements for the small-scale models are generally lower than those for the larger scale models. (Note: These results should be further verified, because magnitudes of the forces measured on the small-scale model were on the order

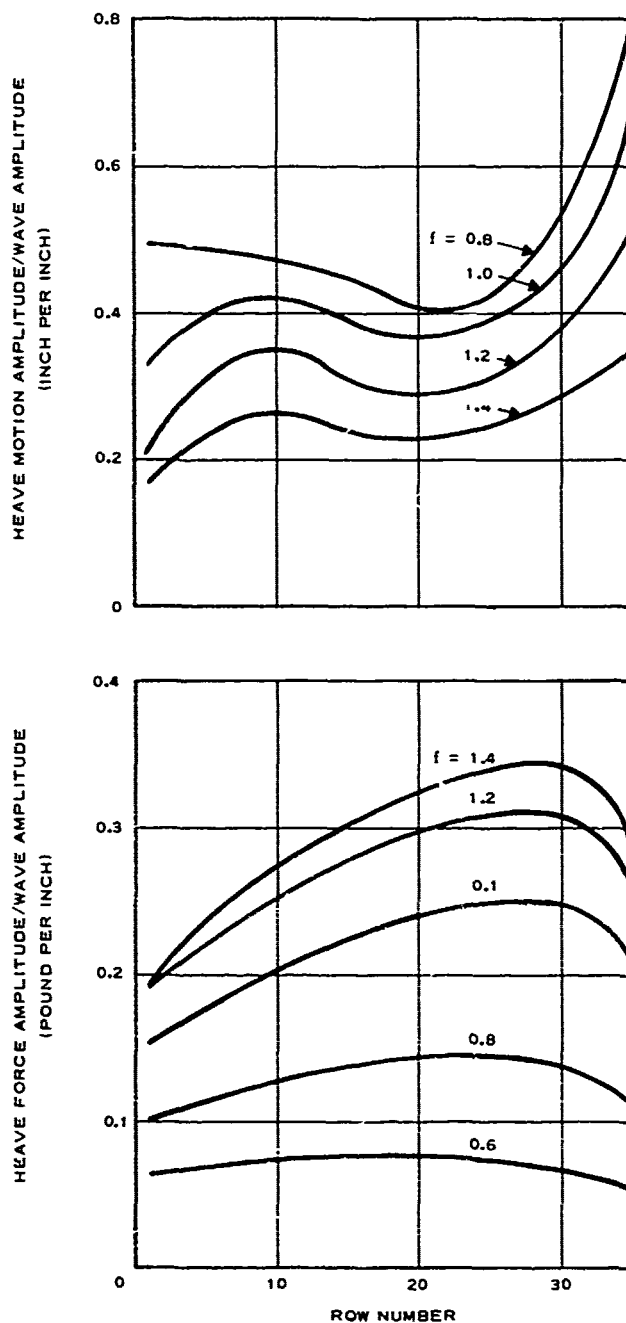


Figure 29 - Heave Motion and Heave Force Measured along Length of Array

of 0.001 lb, which may be subject to experimental error or bias.) Conclusion: If test data are valid, scale effects are important in the extrapolation of test results. Reynolds or Weber numbers can be the characterizing factor. (Efforts to isolate Weber numbers were unsuccessful.)

3. Wave elevation measurements show that in general the height of waves within the array is greater than the height outside the array. Conclusion: Hydrodynamic effects are responsible for wave elevation increases. It is suggested in Appendix F that continuity of flow within the nest of obstacles may be the cause of the increase. Porosity or float cross sectional area to total surface area is 0.906. Note that wave motion is the result of the orbital velocity of water particles; it can be reasoned that this porosity effect could cause wave heights to increase as the reciprocal of porosity or to 1.101 times the external wave height. Porosity effects at the level of the attenuators would cause an increase in wave motion at this lower level to 1.403 times the external wave height. The combined influence of these porosity effects could possibly explain the increase in wave height reported in Table IX.
4. Heave motion measurements are similar, in many respects, to the motions measured previously. Stern motion still shows significant amplification. The remainder of the deck length appears to have nearly the same motion magnitudes, which are magnified over that shown for the theoretical motion of an isolated float.
5. Heave forces show an increase in magnitude toward the stern of the island. At nearly all wave frequencies, the isolated float row results in lesser force than that

shown for any row of the array. Theory represents the force on an isolated row adequately.

6. Surge force is constant throughout the array at low frequencies, but increases as distances from the bow increases at higher frequencies. Isolated row results are similar to the forces occurring near the middle of the array and consequently represent an average of the total surge force applied to the array.
7. The amount of wave energy either dissipated or deflected by the rigidly fixed-float arrays was not significant for any of the tests conducted. This observation is independent of wave frequency.
8. Effects of varying surface tension on the small-model array yielded such scattered results that no meaningful conclusions can be drawn.
9. Magnification of heave motions of the array above the theoretical predictions for much of the array would be expected from the results of the heave force tests.
10. Heave force magnification in large measure appears related to increased wave height within the array.
11. Wave height magnification within the array appears closely related to porosity effects.
12. Stern motion amplification and bow motion frequency shift were not explained by any tests run in this program, but are intuitively thought to be associated with the peculiar articulated deck construction employed, which for small deflections has no shear transfer capability. Other suspected items include surge force interaction, pitch mast stabilizing device, and the restraint afforded by the tether. It is observed, however, that the ends of the array do not receive support from both directions as does the center of the array. Such lack of support can be expected to provide unusual end conditions including frequency changes and increased motion.

3. HYDRODYNAMIC INTERACTION EFFECTS

a. General

This task was also performed by Davidson Laboratory. Its purpose was to investigate in greater depth those hydrodynamic problems identified by the previous effort as being most influential on platform motions. At its inception, these parameters were established as warranting investigation:

1. Float spacing
2. Float configuration
3. Platform size and number of floats
4. Wave height
5. Wave frequency

As the exploratory program progressed, certain other issues arose that were added to the investigation planned for the comprehensive program. These included the effects of model tethering, of current, of hinging the floats, and varying deck stiffness. The initial comprehensive program test plan, which proved to be overly ambitious, envisioned the following motion tests in waves of new 1/48-scale models employing hinged floats:

1. Two arrays: 10 by 17 and 10 by 9
2. Two values of deck stiffness
3. Three float diameter spacings - 3 to 1, 3.75 to 1, 4.5 to 1
4. Two float slenderness ratios 1.8 to 1 and 1.5 to 1
5. Effect of tethering
6. Effect of damping collars
7. Current effects

As in the exploratory program, emphasis was placed on examination and exploration of deck motions of a multifloat array subjected to waves.

b. Model Description

Three float array models were fabricated for testing. These differed from previous models in several important aspects:

1. Floats were hinged

2. Deck structure was designed to provide for bending stiffness; two values were chosen
3. Provision was made to permit variation of float spacing

Two float configurations were selected for testing, both of which were longer and slenderer than those used in previous model arrays. The scale ratio selected was 1 to 48 with dimensions taken from the following full-scale dimensions:

	<u>Float A^a</u>	<u>Float B^a</u>
Waterplane diam	6 ft	6 ft
Attenuator diam	9 ft	10.8 ft
Slenderness ratio	1.5 to 1	1.8 to 1
Freeboard	30 ft	30 ft
Draft	96 ft	78 ft
Hinge location (below calm water line)	23 ft	23 ft

A summary of the tests conducted in this phase is given in Table X.

Additional information on geometry, test plan, and test equipment are provided in Appendix G.

c. Measurements

Frequency response plots are given in Appendix G, as shown in Table X.

Figure 30 presents data on the frequency response for the stiffest deck configuration tested (deck element 5) in a plot of the mode shape of the deck at particular frequency levels. Observing the frequency response plots, it may be noted that 3 "null" frequency exists for which deck motion is small.

These are shown in Figure 30 as 0.087, 0.144, and 0.201 cps (converted to full-scale equivalent frequencies). Note that the curves are shaped as a typical 3rd mode shape of a free-free beam. Peak motion frequencies or "resonant" frequency points appear on the response plots at frequencies of

^aThese floats bracket the dimensions of an earlier isolated float test on a previous program as shown in Reference 4, float C.

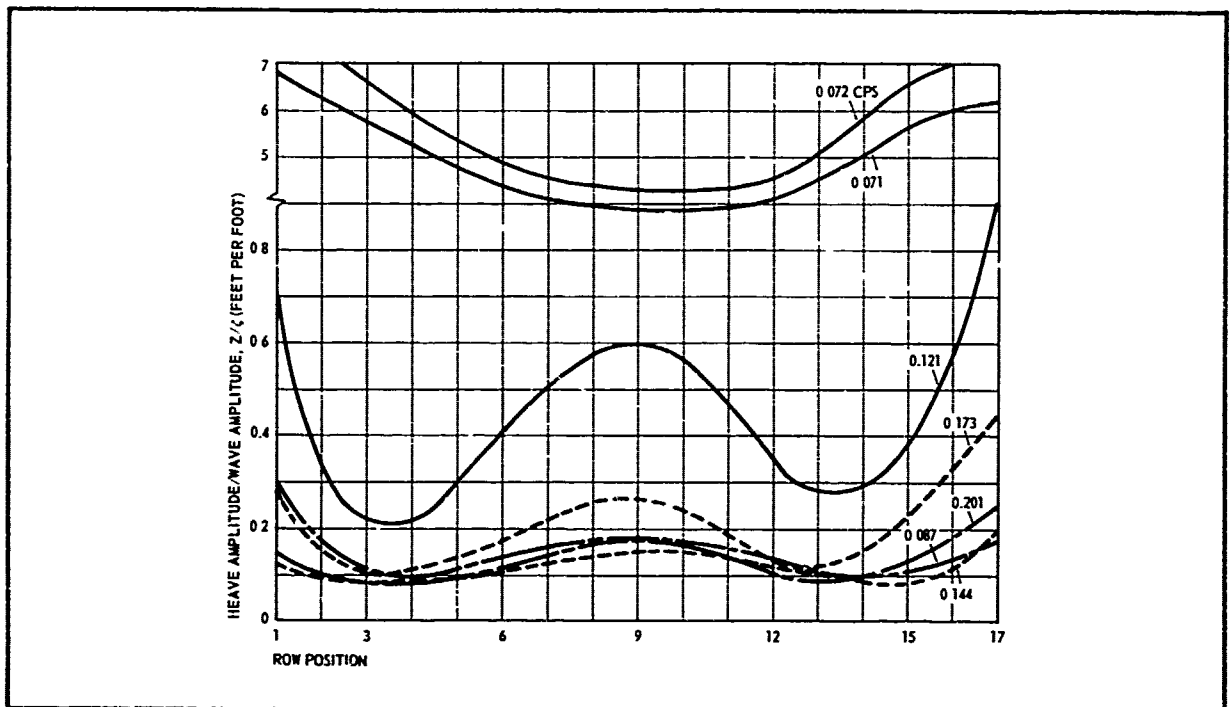


Figure 30 - Mode Shapes for Deck Stiffness 5

0.072, 0.121, and 0.173 cps. The lower frequency resonance is caused by the heaving natural frequency of the individual floats. Two curves are shown in Figure 30 for 0.071 and 0.072 cps; note the reduced scale for these extreme amplifications, which are 10 times the magnitudes shown for any of the other frequencies. Mode shape here appears to be similar to the mode of a free-free beam. Note that the stern (row 17) has less motion than the bow (row 1). Cause of the other resonance points was not established, but is related to the structural natural frequency as will be shown. Plots at these resonant frequency points of 0.121 and 0.173 cps shows the typical 3rd mode behavior noted at the null frequency points.

It is evident from the above that motion at the ends of the array are near equal and are significantly greater than that predicted for an isolated float and are generally greater than at any other point in the array. At frequencies above float heave resonance, the center of the array experiences motions nearly as large as the ends.

Figure 31 presents data for a model with a deck of significantly lower

TABLE X - COMPREHENSIVE TEST PROGRAM PLAN

Test no.	3.0 close	Spacing 3.75 medium	4.5 wide	Attenuator			Deck stiffness			Deck reinforcement			Surge lines	
				Slender 1.5 to 1	Fat 1.6 to 1	None	Narrow plastic thin normal 80 X 106 No. 1	Wide plastic 160 X 106 No. 2	Aluminum and narrow plastic No. 3	No longitudinal	Rod	Wire	On	Off
6		X			X		X			X			X	
6a		X			X		X			X				
6b												X	X	
6c		X			X		X							
6d		X			X		X			X			X	
5		X			X									
5a														
5b		X			X							X	X	
5c		X			X				X			X	X	
1		X			X		X						X	
3	X				X									
2		X		X										
2a		X												
2b														
2c														
4		X				X	X						X	

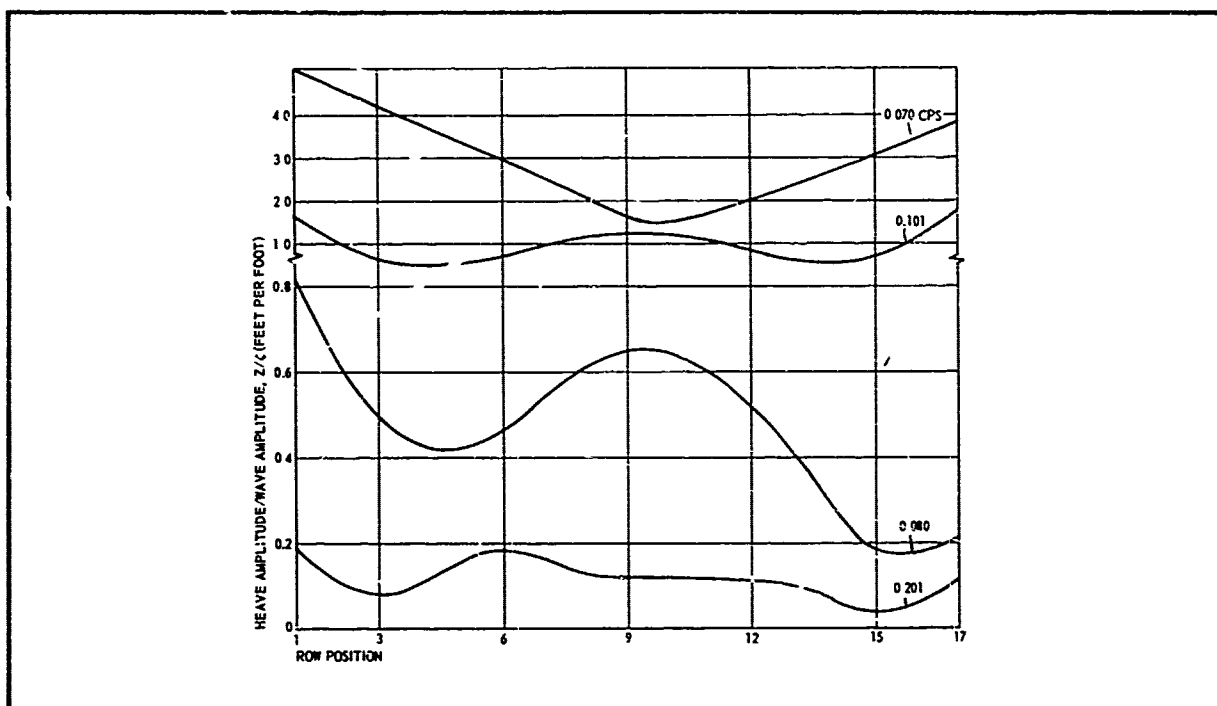


Figure 31 - Mode Shapes for Deck Stiffness 3

stiffness (deck element 3) than for the case above. Figure 32 is plotted for a model with a deck of yet lower stiffness (deck element 2) equal to half that for Figure 31.

Some observations can be made from these plots, which are similar to the stiffer deck models. Mode shapes at intermediate frequencies are essentially the same, that is, the typical third mode type. At low frequencies near resonance, the shapes are of the typical first mode type. At the highest frequency, however, the less stiff deck, Figure 31, appears to be going into a fifth mode condition. This effect is more pronounced for deck element 2 of Figure 32. Another similarity is that the mode shapes appear symmetrical, in most cases. An observation was made during one test for which it was found that some of the rows of floats had become loosened at their attachment to the deck. A reduced motion for such a row would be expected, because the entire interaction effect could not be transmitted through a loose connection.

Further observation of Figures 30, 31, and 32 indicate that a measurement of

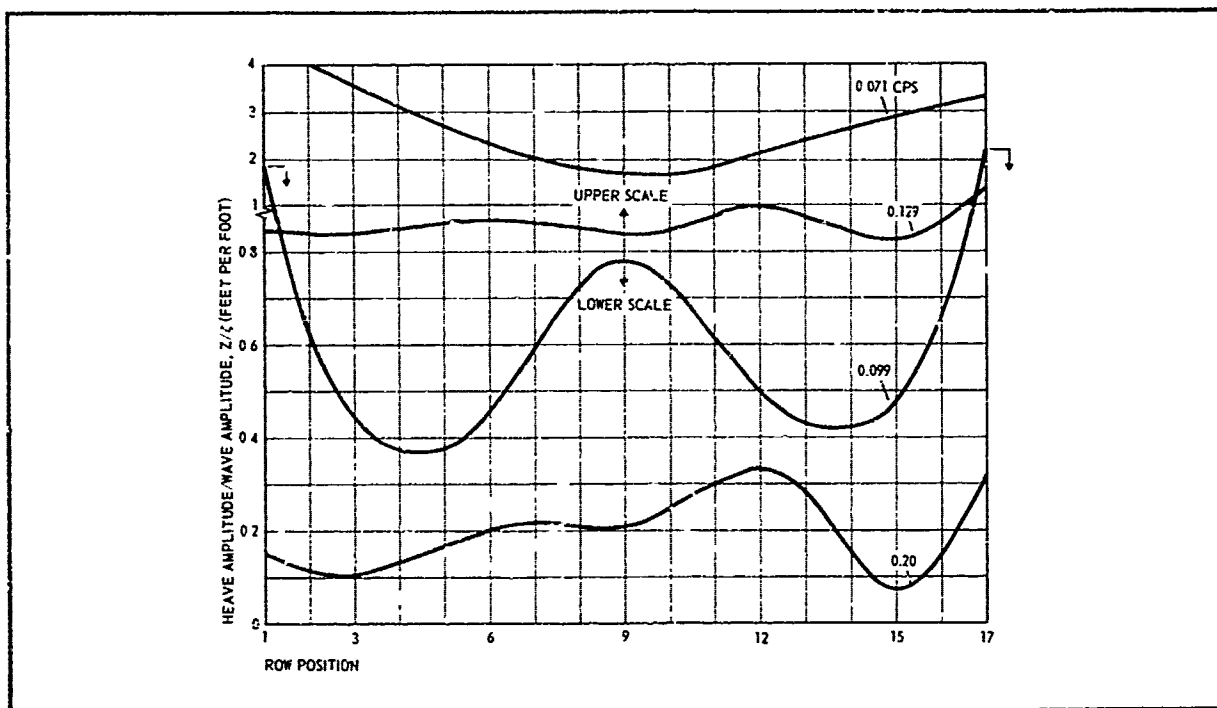


Figure 32 - Mode Shapes for Deck Stiffness 2

the occurrences at any one row could be related without difficulty to the motions at another row. Row 1 is selected for comparison purposes and is shown in Figure 33 as a frequency response plot. This plot repeats certain of the plots in Appendix G. The significant item shown in this figure is the difference in response of the various models in the range of frequencies from 0.08 to 0.14 cps immediately above the heave resonance of the float. In this region the stiffer deck has a lower response with various null and secondary resonance points occurring. The intermediate stiffness deck has a high response but still retains a null and secondary resonance point. Such points shifted to lower frequencies than for the deck of greater stiffness. The least stiff deck shows a further trend of the effect shown above, with an apparent masking of the lowest frequency null point.

A trend appears to be established from the above observations. Increasing the deck stiffness considerably above that tested might be expected to continue to lower the response and shift the secondary resonance points and null points to higher frequencies. Such a trend would tend to flatten the response curve to a low level.

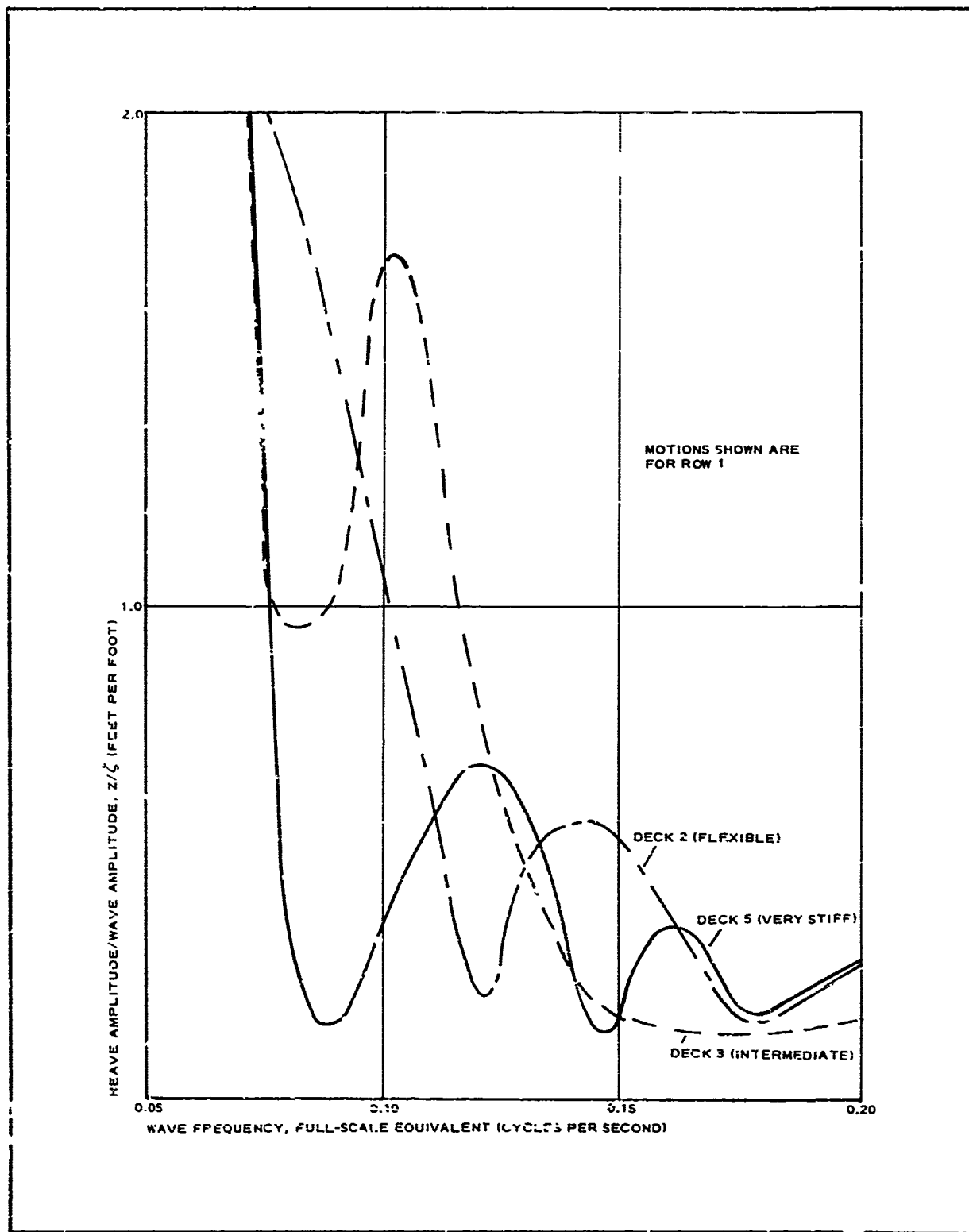


Figure 33 - Frequency Response Plot

The influence of deck stiffness on the response of the island is evident from the forced oscillation tests (test number 10). Examination of the data in the appendix will show that when row 1 is excited with the model setting in calm water, row 1 can attain motion equal to that of row 17, particularly at the intermediate frequency cases (0.073 to 0.088 cps). For this lower deck stiffness test (deck element 2), motion was not transmitted by hydrodynamic effects, but only by deck stiffness effects. This observation is opposed to an earlier hypothesis stating that deck stiffness had little effect on motion.

d. Results

Qualitative results and observations, as noted by Davidson Laboratory, are as follows:

1. Vertical motion response of the deck of these models to waves is not independent of positions along the length of the model. The motions are affected by the elastic connecting elements and exhibit beam like features.
2. Results of two tests indicate that for float slenderness ratios of 1.5 to 1 and 1.8 to 1 at a float diameter spacing ratio of 3.73, deck heaving motions are essentially the same for the wave frequencies tested.
3. Comparison of observed deck motions with theoretically calculated motions, where hydrodynamic and elastic interactions are neglected, do not show good agreement. The fundamental resonant frequency was predicted, however.
4. The magnitude of deck rigidity can have a very important influence on vertical deck motions. The fundamental heaving resonant frequency is evidently unaffected (or only slightly affected) by variations in deck rigidity. Response at other frequencies is, however, appreciably affected. In particular, additional resonant frequencies appear from Tests 11 for instance with the aluminum deck stiffener, higher mode frequencies at

about $f \approx 0.12$ and $f \approx 0.17$ Hz are detected, while for Tests 6 with 2-in. wide plexiglass deck elastic elements, $f \approx 0.10$ Hz seems to be somewhat like a resonance. This beam-like feature of the response suggests that much of the difference between theoretically calculated responses and measurements, at least for frequencies only slightly above the heave resonance, may be due to near-resonant response, where the elastic natural frequencies are only slightly separated from the pure heaving natural frequency for a resilient deck, somewhat more widely spread for a stiffer deck, and rather well defined for a very stiff deck. Additionally, the wave-induced horizontal loads on floats can couple into bending deflections of the deck.

5. Tests of a model with 1.8 float slenderness ratio and float spacing diameters of 3.00 and 3.75 show different deck motions response, but the effects of spacing cannot be discriminated from the elastic bending of the deck.
6. Tests of a model without tether restraint show no significant deck motion changes from the tethered array.
7. Tests with a dashpot attached to a single float row indicate that the amount of damping provided (about 20 percent of the critical damping for a single row) is insufficient to significantly affect the response of the total 17 float array, apparently due to the interactions occurring in adjacent rows.
8. Tests of a 9- by-10 array showed no clear indications of difference of motion response from the 17- by -10 array from which it was detached.
9. Analytical considerations, together with test observations, suggest that the elastic deck bending motion may be significantly affected by couples due to horizontal wave-induced forces acting on the floats at a great distance below the neutral axis of the deck "beam."

10. Attenuator designs selected for testing produce good reductions of wave-induced heaving motion compared with floats without attenuators, although not as good as the theory that neglects elastic and hydrodynamic interaction predicts.
11. The hinge in the attenuator performs exceptionally well, reducing the horizontal load and bending moment that would otherwise be transmitted to the deck while attenuators gently oscillate without important erratic behavior or bumping in the array.
12. Quantitative information on the specific effects of float spacing and attenuator slenderness cannot be given until the elastic character of the deck response is clarified further. This effect is presumed to be greater than the effects of variations in spacing and slenderness.

4. ANALYTIC INVESTIGATION OF ARRAY MOTIONS

a. Background

Experimental studies of array motions have established that vertical response is greater in an array than predicted for an isolated float. In particular, recent models have incorporated a deck of measurable stiffness that has shown excessive motions at the ends of the array. This phenomena, termed tail wagging, was established as a significant item of concern. Empirical explanation of this motion cannot be determined from the test data. The test data, however, provide strong evidence that deck stiffness is influencing the excessive motions. Plots of maximum motions of the array recur in a symmetrical fashion, with greater motion occurring nearly equally at the bow and stern.

Desire for an analytical explanation of this motion prompted the development of a mathematical model to evaluate parameters established as significant to the motion of an array.

b. Model Description

Basic assumptions used in the development of this model are listed below:

1. A one-dimensional array of floats is sufficient to establish structural interaction. (Width of the array is considered unimportant, because each line of floats is expected to attain motions like every other line when acted upon by a uniform frontal wave.)
2. Linear array elements are to be connected at the top by a deck maintaining shear and bending stiffness.
3. Deck element, at point of attachment to float, must remain a right angle to the float.
4. Float characteristics are to duplicate all first-order effects of a realistic hinged float.
 - a. Mass of upper portion of float and attenuator are to be located as would exist in a realistic float.
 - b. Hinge is to allow freedom of oscillation of attenuator.
5. Heave force is to be applied to attenuator at its center of buoyancy.
6. Surge force is to be applied separately to the upper portion of the float and attenuator. (Vertical location of force is assumed as a constant for the sake of simplicity).
7. Heave and surge force magnitude are to be determined by experimental or analytical techniques available for an isolated float for the particular wave frequency of interest.
8. Sinusoidal variation of surge and heave force are to be applied.
9. Positive surge force, in direction of wave, lags positive heave force, upward, by 90 deg.
10. Frequency of sinusoidal motion is to be representative of wave action.
11. Dynamic motion of the various portions of the float and deck are resisted by the float water plane spring, the deck stiffness springs, and the inertia of the components.
12. An array tether is assumed to resist drift of the array.

The following outputs were expected from the model experiments:

1. Horizontal and vertical motions of the cg of the attenuator and the float-deck intersection were to be determined at each increment of time for each float element. (A time increment of suitable length was selected to assist in avoiding errors in the solution.)
2. Forces and moments existing in various elements were to be determined at each increment of time for each float and deck element.

Variable parameters of the array are:

N - number of floats in linear array
AL - float spacing (ft)
Mu - mass of upper portion of floats and deck (slugs)
ML - mass of attenuator (slugs)
Du - center of mass of Mu measured from deck (ft)
DL - center of mass of ML measured from hinge (ft)
Iu - mass moment of inertia of MU about cg (slug ft²)
IL - mass moment of inertia of MC about cg (slug ft²)
EI - deck stiffness (lb-ft²)
Lu - float hinge location measured from deck (ft)
KF - buoyant spring constant of float (lb/ft)
KD - stiffness of tether holding array in place (lb/ft)
CU - center of buoyancy of upper portion of float
CB - center of buoyancy of attenuator

Variable parameters of wave data and wave force are:

FH - heave force amplitude (lb)
FSU - surge force on upper portion of float (lb)
FSL - surge force on attenuator (lb)
BU - location of FSU measured from deck (ft)
BL - location of FSL measured from hinge (ft)
CPS - wave frequency
PHI 1 - Solution starting position for wave (degrees)
LL - vertical center of application of heave force from hinge (ft)

The math model and the numerical methods used in computer programming the analysis are described in Item d, below.

c. Calculations

A computer program was developed for the array motion analysis. To illustrate how this program was used, a typical analysis is presented for an array of 17 floats with water plane diameter of 12 ft (see Table XI, Run No. 2).

Portions of a computer printout for time increments of 5 and 5.1 seconds for Run No. 2 are given in Table XII. Such increments are printed at 0.1-second intervals for the entire length of the run. Computations are made at 0.02-second intervals. Data outputs include horizontal deck motion of the array (XD). The motions and forces at each of the 17 floats are as follows.

- XV - vertical displacement of deck or float
- Xu - horizontal displacement of cg of upper float section
- XL - horizontal displacement of cg of attenuator section
- THu - angular displacement of upper float section
- THL - angular displacement of attenuator section
- MR - moment reaction between float and deck
- FR - vertical reaction between float and deck

A plot of the vertical motion of the first row is given in Figure 34. Note that each cycle is not an exact repeat of each other cycle because of a complex interaction of structural frequencies. Horizontal motion of the cg of the upper section of the float is shown in Figure 35. Vertical motion of the cg of the upper float section and attenuator section are considered to be equal to the deck vertical motion. Horizontal motion of the attenuator section of float 1 is shown in Figure 36. Horizontal motion of the deck is shown in Figure 37. Horizontal motion at all points on the deck are considered to follow identically.

Run No. 0 differs from Run No. 2 in regard to the number of floats (17 for Run No. 2, 4 for Run No. 0) and length of run time (22 seconds for Run No. 2, 4 seconds for Run No. 0).

TABLE XI - PARAMETERS FOR ARRAY WITH
LARGE-DIAMETER FLOATS

Parameter	Value
Array and float geometry	
N	17
AL	18 ft
Mu	635 lb sec ² /ft
ML	5800 lb sec ² /ft
Du	24.0 ft
DL	32.6 ft
Iu	0.366×10^6 slug ft ²
IL	1.22×10^6 slug ft ²
EI	1.44×10^6 lb ft ²
Lu	48 ft
KF	7060 lb/ft
KD	0 lb/ft
Cu	30.0 ft
CL	32.0 ft
Wave data	
FH	508 lb (for a 1-ft wave amplitude)
FSu	3220 lb (for a 1-ft wave amplitude)
FSL	4000 lb (for a 1-ft wave amplitude)
Bu	36.0 ft
BL	28.3 ft
CPS	0.230 cps
PHI 1	0 deg
LL	32.0 ft

TABLE XII - ARRAY MOTION AT ISOLATED TIME INCREMENT

T = 5.00 SEC		XD = 0.032 FT					
N	XV	XU	XL	THU	THL	MR	FR
1	-0.205	-0.191	-0.896	-0.53	-0.85	-3.13E 05	5.73E 02
2	-0.337	-0.095	-1.697	-0.30	-2.59	-3.68E 05	-2.07E 03
3	-0.355	0.108	-0.455	0.18	-1.12	3.66E 04	-3.07E 03
4	-0.231	0.284	1.852	0.60	2.31	4.39E 05	-1.44E 03
5	-0.034	0.300	2.754	0.64	3.84	3.40E 05	2.33E 03
6	0.125	0.187	1.414	0.37	1.88	-1.16E 05	3.76E 03
7	0.209	0.100	-0.439	0.16	-1.07	-3.77E 05	8.70E 02
8	0.270	0.129	-0.680	0.23	-1.59	-1.22E 05	-2.17E 03
9	0.367	0.193	0.822	0.38	0.82	3.58E 05	-1.15E 03
10	0.469	0.141	1.858	0.26	2.83	4.80E 05	2.38E 03
11	0.475	-0.062	0.700	-0.22	1.50	5.65E 04	3.70E 03
12	0.325	-0.271	-1.663	-0.72	-1.91	-4.42E 05	1.63E 03
13	0.075	-0.324	-2.854	-0.85	-3.82	-4.41E 05	-8.80E 02
14	-0.153	-0.218	-1.689	-0.60	-2.15	4.40E 03	-2.14E 03
15	-0.295	-0.094	0.405	-0.30	1.10	3.33E 05	-2.30E 03
16	-0.379	-0.065	0.965	-0.23	1.98	2.29E 05	-6.40E 02
17	-0.467	-0.105	-0.339	-0.33	-0.17	-1.40E 05	6.13E 02

T = 5.10 SEC		XD = 0.040 FT					
N	XV	XU	XL	THU	THL	MR	FR
1	-0.152	-0.289	-1.378	-0.75	-1.33	-4.53E 05	5.44E 02
2	-0.348	-0.152	-1.974	-0.46	-2.86	-4.33E 05	-5.69E 03
3	-0.394	0.103	-0.465	0.15	-1.11	3.75E 04	-5.01E 03
4	-0.267	0.305	1.978	0.63	2.47	4.60E 05	2.88E 03
5	-0.059	0.323	2.866	0.68	3.97	3.74E 05	7.54E 03
6	0.110	0.209	1.490	0.40	1.95	-8.23E 04	3.29E 03
7	0.206	0.130	-0.327	0.21	-0.96	-3.75E 05	-4.18E 03
8	0.289	0.171	-0.483	0.31	-1.38	-1.27E 05	-6.05E 03
9	0.413	0.231	1.019	0.46	1.05	3.50E 05	-4.81E 02
10	0.527	0.148	1.906	0.26	2.90	4.48E 05	7.15E 03
11	0.520	-0.038	0.564	-0.30	1.37	3.75E 04	9.07E 03
12	0.338	-0.311	-1.872	-0.84	-2.13	-4.35E 05	2.18E 03
13	0.057	-0.349	-2.977	-0.93	-3.94	-4.23E 05	-6.20E 03
14	-0.186	-0.216	-1.661	-0.61	-2.09	3.81E 03	-6.81E 03
15	-0.324	-0.075	0.518	-0.27	1.24	3.14E 05	-1.42E 03
16	-0.397	-0.042	1.067	-0.19	2.09	2.14E 05	1.72E 03
17	-0.474	-0.085	-0.275	-0.30	-0.11	-1.59E 05	1.46E 03

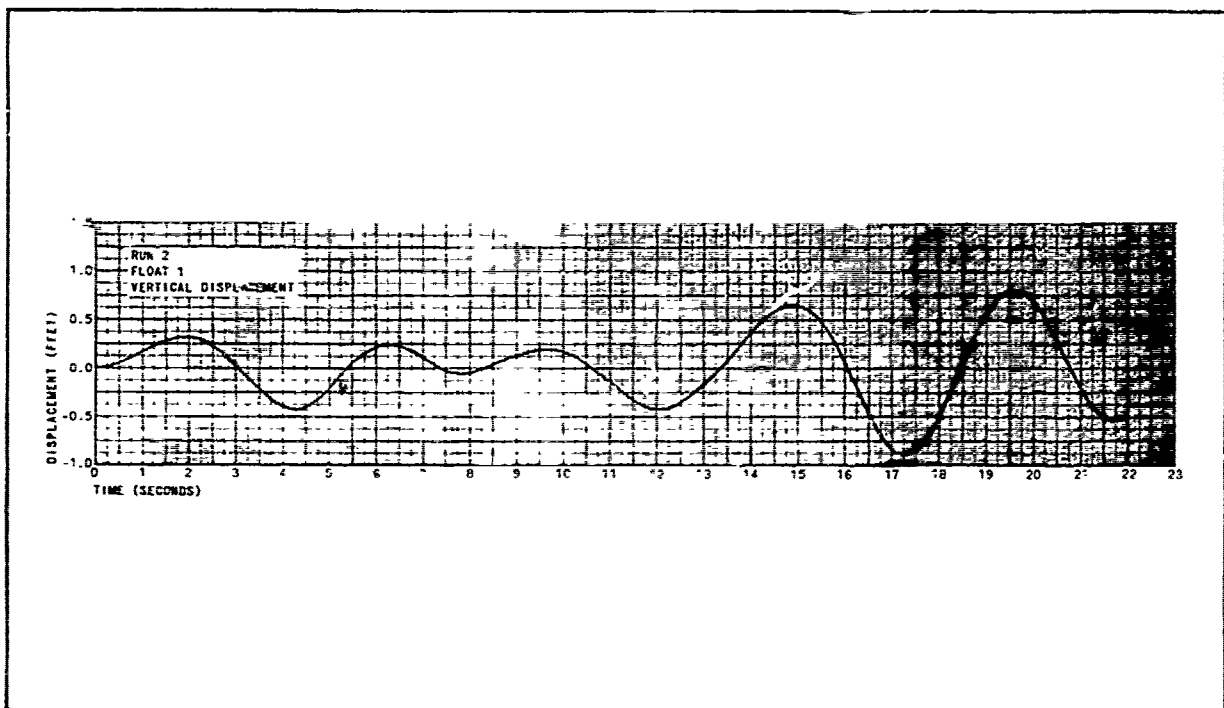


Figure 34 - Vertical Motion at Row 1

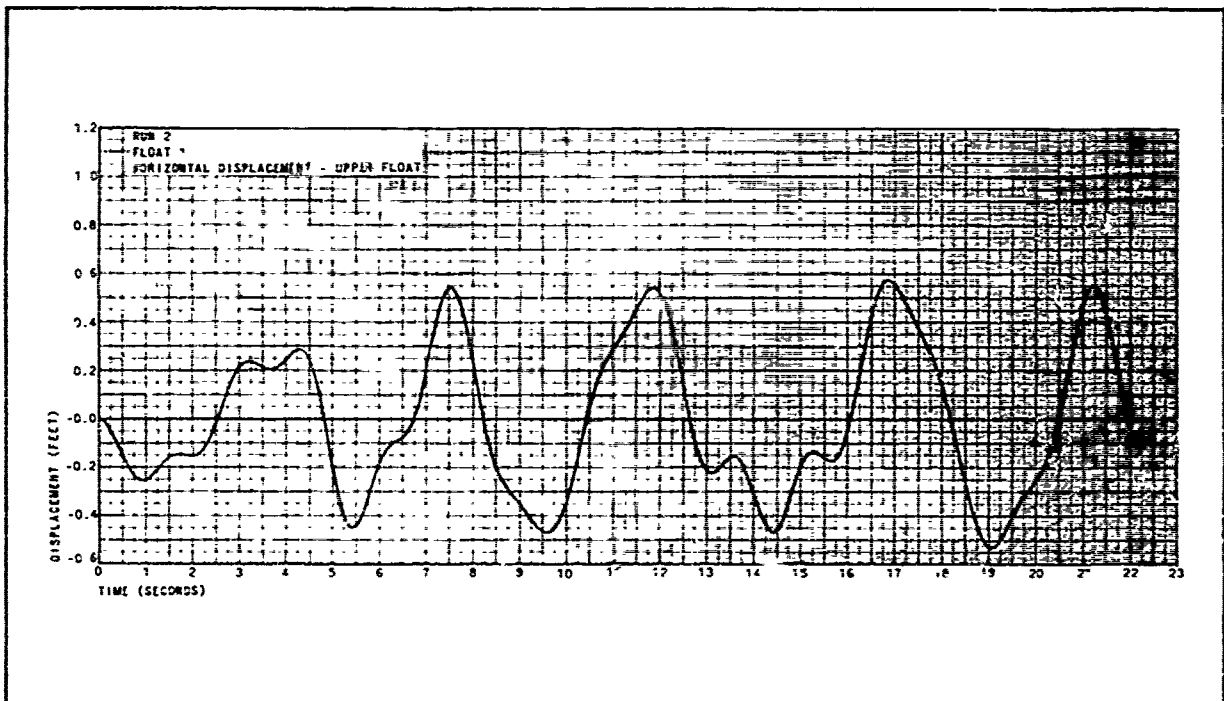


Figure 35 - Horizontal Motion of Upper Float Section

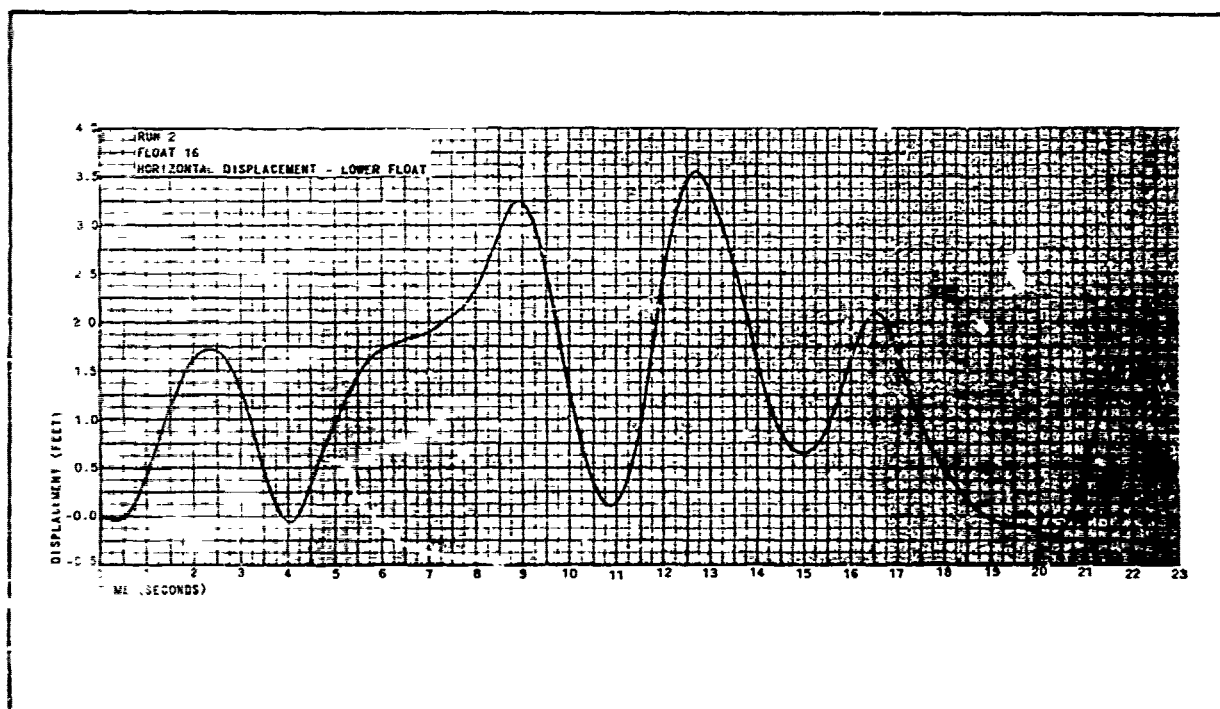


Figure 36 - Horizontal Motion of Lower Float Section

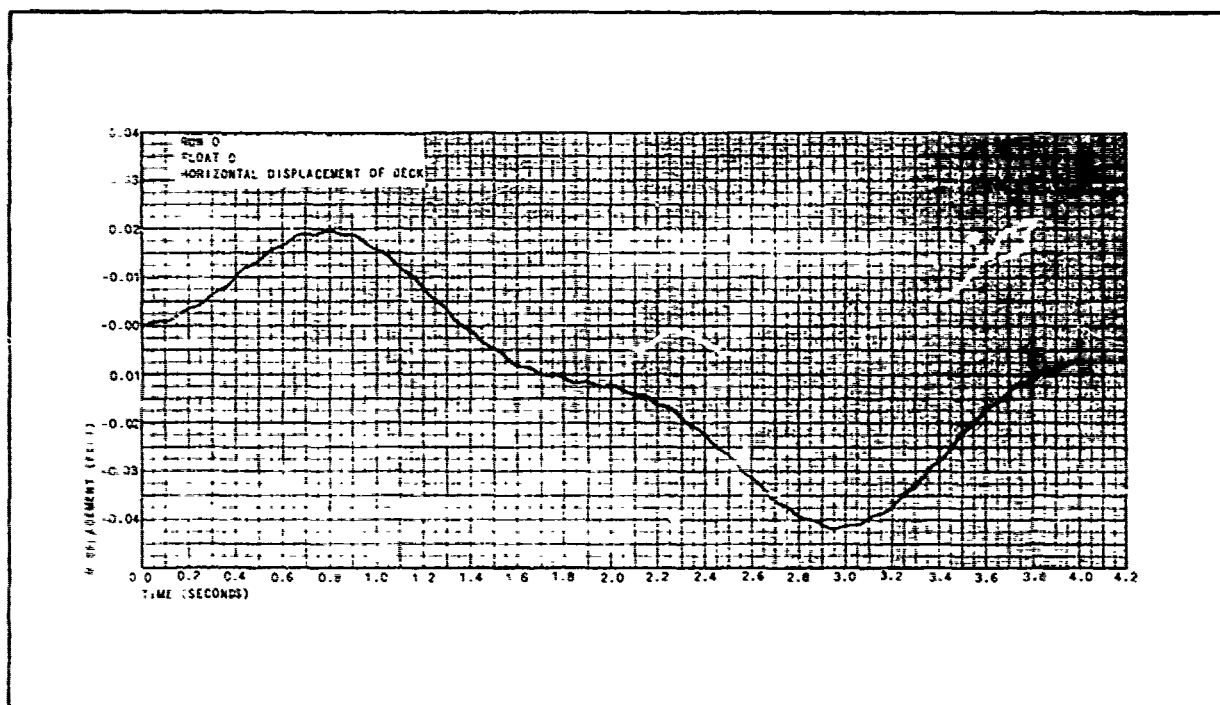


Figure 37 - Horizontal Motion at Deck

Shear force imposed on the deck by float 5 and bending moment imposed on the deck by float 14 are provided in Figures 38 and 39. Profile shapes of the deck at time increments of 17.50 and 19.60 seconds are shown in Figure 40.

Maximum excursions of motion are of interest and are summarized in Table XIII. Maximum vertical and horizontal displacements of the upper float section for each of the rows are given along with deck moment and shear values. Both the maximum positive and negative excursions are presented along with the time of occurrence of each value.

A study of an array of floats similar to that described in Table XI as Run No. 2 is discussed below. One important difference in this new array is that a more practical water plane diameter of the float was used. Diameter was set at 6 ft rather than the 12 ft used in Run No. 2. This diameter is reflected in the buoyant spring constant of $KF = 1768 \text{ lb/ft}$ rather than the 7060 lb/ft used previously.

Important characteristics of the model, not described previously, are discussed below. Float geometry, masses, and forces were taken as close approximations to those tested in an earlier program and reported in Reference 4. Wave frequency data for forces accounted for a hinge by dividing the surge force on an unhinged float into forces on the upper section and attenuator as considered reasonable in light of theory. A deck stiffness of $1440 \times 10^6 \text{ lb/ft}^2$ was utilized.

Table XIV is a summary of motions for this array due to a wave frequency of 0.23 cps. This case is designated Run No. 41. Figure 41 is a plot of the mode shape of these extremes with the positive and negative excursions averaged.

Tables XV, XVI, and XVII provide data that show the influence of changing wave frequency (and corresponding wave force magnitudes) to values of 0.20, 0.15, and 0.10 cps, respectively. Table XVIII provides the corresponding wave force amplitudes. Note that the mode shape tends to reduce as wave frequency decreases. At 0.23 cps 7 lobes appear, at 0.20 and 0.15 cps 5 lobes appear, and at 0.10 cps only 3 lobes appear. This result tends to

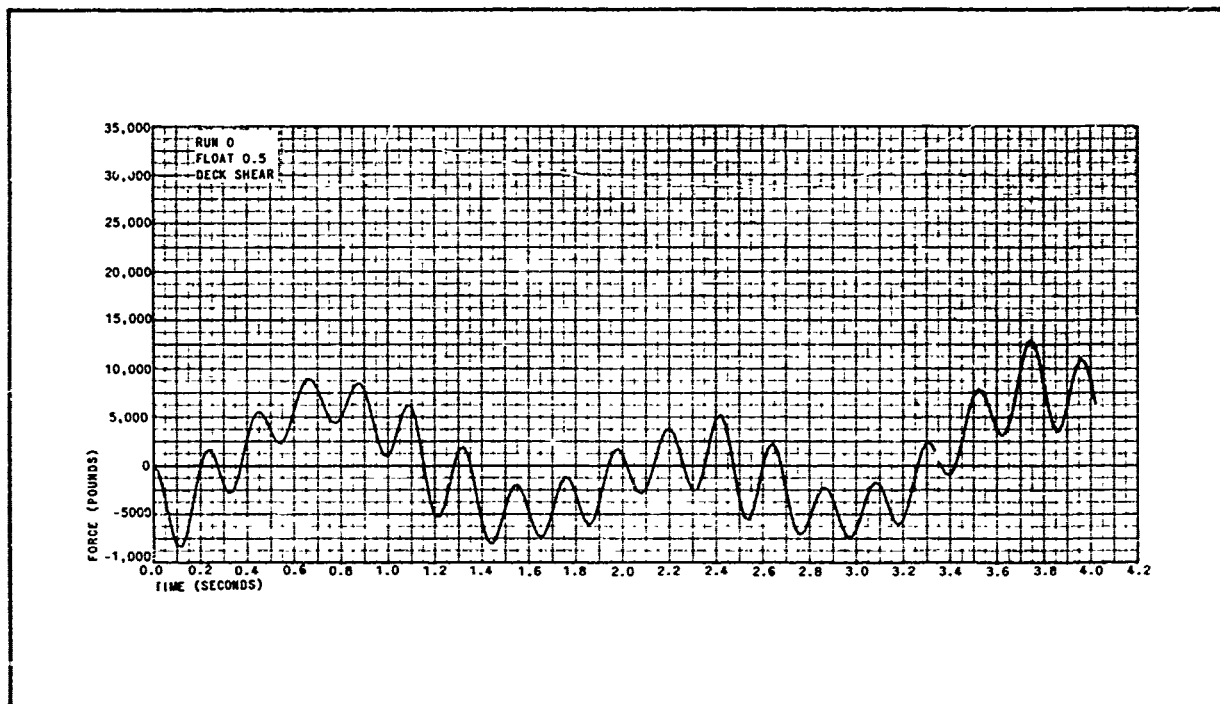


Figure 38 - Vertical Load Imposed on Deck by Float

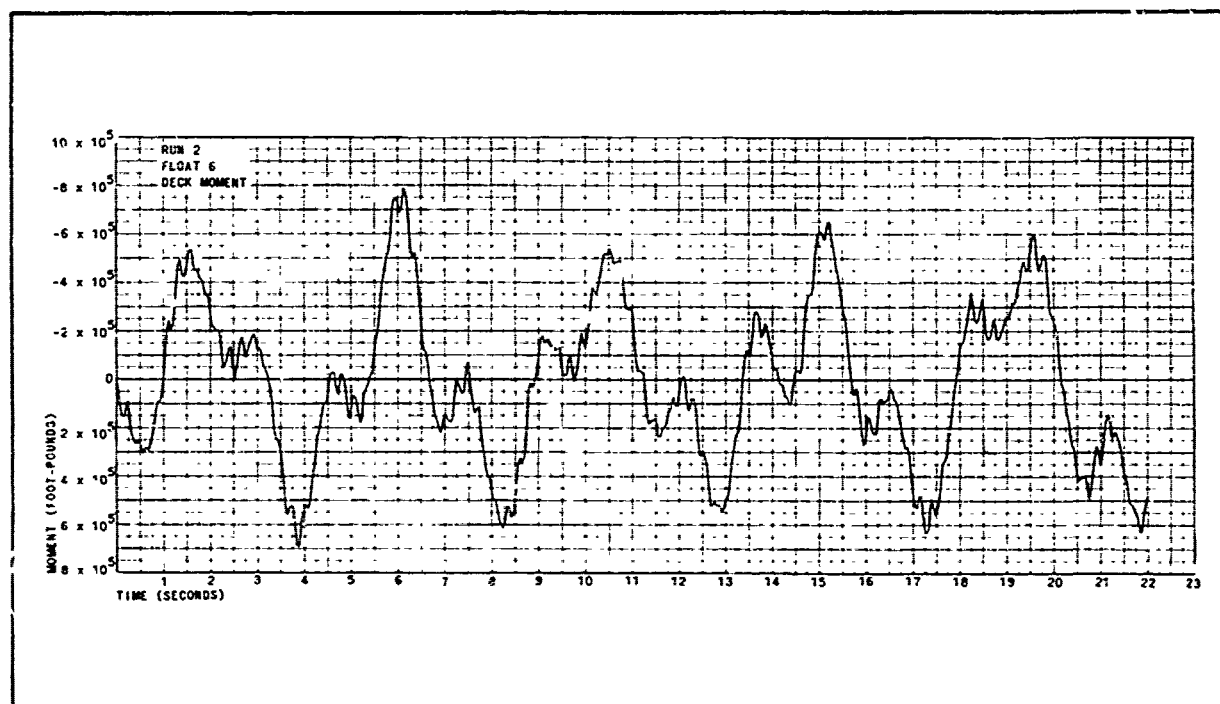


Figure 39 - Bending Moment Imposed on Deck by Float

TABLE XIII - SUMMARY OF EXTREME VALUES - RUN NO. 2

FLOAT	-- HORIZONTAL DECK MOTION --				HORIZONTAL DISPLACEMENT - UPPER FLOAT				HORIZONTAL DISPLACEMENT - LOWER FLOAT			
	* POS *	* T *	* NEG *	* T *	* POS *	* T *	* NEG *	* T *	* POS *	* T *	* NEG *	* T *
1	6.37E-01	19.16	-1.37E-01	21.46	5.74E-01	16.88	-5.31E-01	19.06	2.55E-00	16.90	-3.08E-00	19.10
2	4.56E-01	19.84	-4.65E-01	17.54	5.58E-01	17.08	-5.09E-01	19.26	2.42E-00	21.36	-3.48E-00	9.58
3	5.42E-01	7.54	-4.43E-01	5.40	5.41E-01	17.34	-5.32E-01	19.58	2.10E-00	21.92	-3.07E-00	15.10
4	5.32E-01	21.18	-5.16E-01	19.23	3.85E-01	17.56	-3.93E-01	19.70	2.04E-00	5.22	-1.79E-00	19.70
5	6.47E-01	17.30	-6.87E-01	19.44	3.03E-01	5.56	-4.36E-01	7.60	3.16E-00	5.64	-2.30E-00	20.94
6	5.95E-01	17.42	-6.25E-01	19.52	3.07E-01	5.90	-4.71E-01	20.82	2.73E-00	5.90	-2.14E-00	20.80
7	4.45E-01	17.82	-4.43E-01	20.16	5.12E-01	19.36	-5.10E-01	19.60	2.61E-00	19.34	-3.06E-00	7.56
8	4.32E-01	5.73	-5.20E-01	20.46	4.94E-01	19.18	-4.81E-01	21.40	2.41E-00	19.20	-3.53E-00	7.62
9	5.28E-01	5.56	-6.01E-01	7.52	4.51E-01	19.06	-4.23E-01	21.32	2.23E-00	19.08	-2.09E-00	21.32
10	5.04E-01	5.34	-7.00E-01	7.82	4.61E-01	14.50	-3.97E-01	16.96	3.42E-00	14.52	-2.00E-00	22.02
11	6.29E-01	13.96	-7.13E-01	21.10	4.02E-01	14.88	-4.08E-01	22.02	2.83E-00	10.72	-2.19E-00	22.02
12	5.27E-01	13.10	-5.93E-01	21.34	3.61E-01	7.54	-3.91E-01	22.02	1.77E-00	20.88	-2.10E-00	9.70
13	5.07E-01	13.52	-5.62E-01	21.90	4.27E-01	20.80	-3.70E-01	5.30	2.24E-00	20.88	-3.51E-00	9.76
14	3.36E-01	19.94	-4.59E-01	22.02	4.48E-01	8.20	-4.07E-01	10.52	1.53E-00	20.72	-2.69E-00	10.52
15	4.63E-01	20.68	-1.81E-01	5.56	4.19E-01	21.84	-5.02E-01	10.64	2.97E-00	12.82	-1.14E-00	19.60
16	5.61E-01	3.04	-4.82E-01	10.44	4.14E-01	22.02	-4.09E-01	19.94	3.55E-00	12.70	-2.07E-01	20.28
17	7.37E-01	21.46	-7.23E-01	10.56	4.17E-01	1.66	-5.08E-01	3.90	2.55E-00	22.02	-2.16E-00	3.88

FLOAT	-- DECK MOMENT --				-- DECK SHEAR --			
	* POS *	* T *	* NEG *	* T *	* POS *	* T *	* NEG *	* T *
1	6.37E-05	7.48	-7.24E-05	12.90	8.22E-03	5.50	-9.75E-03	21.22
2	5.31E-05	11.88	-4.91E-05	5.36	7.91E-03	15.06	-9.41E-03	22.02
3	6.42E-05	17.28	-7.21E-05	6.08	1.03E-04	21.22	-9.71E-03	5.50
4	6.99E-05	21.92	-6.63E-05	15.16	8.81E-03	17.16	-1.10E-04	6.00
5	4.59E-05	5.80	-5.26E-05	7.90	1.34E-04	22.00	-1.45E-04	6.04
6	7.96E-05	6.14	-7.05E-05	3.86	9.09E-03	12.76	-8.59E-03	15.28
7	5.91E-05	19.50	-6.13E-05	21.88	1.14E-04	6.04	-8.57E-03	3.76
8	4.10E-05	15.92	-4.81E-05	1.30	1.44E-04	6.04	-1.17E-04	11.22
9	5.71E-05	8.46	-5.99E-05	6.16	5.25E-03	9.50	-5.36E-03	7.24
10	5.14E-05	14.20	-5.36E-05	2.88	1.43E-04	9.90	-1.19E-04	7.60
11	5.77E-05	10.54	-5.35E-05	8.26	1.22E-04	9.90	-1.15E-04	21.02
12	6.98E-05	10.76	-6.37E-05	21.86	7.15E-03	14.66	-8.39E-03	8.14
13	5.32E-05	20.84	-5.19E-05	9.74	1.42E-04	10.66	-1.31E-04	17.38
14	7.18E-05	8.24	-6.97E-05	10.59	9.78E-03	19.02	-8.81E-03	19.02
15	5.80E-05	17.50	-6.34E-05	10.72	1.00E-04	3.96	-1.03E-04	9.12
16	4.18E-05	5.50	-4.69E-05	20.62	9.37E-03	17.38	-9.73E-03	19.68
17	6.87E-05	19.60	-7.40E-05	3.84	9.26E-03	16.84	-9.25E-03	14.32

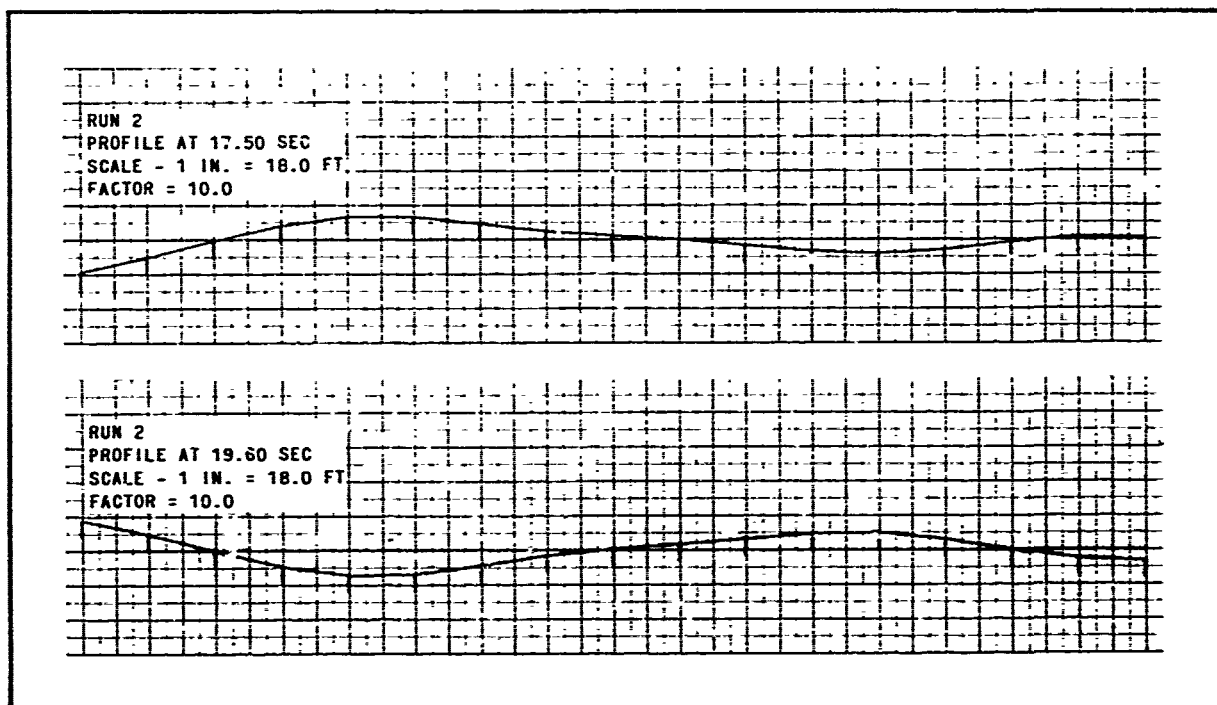


Figure 40 - Deck Profile at Isolated Time Increments

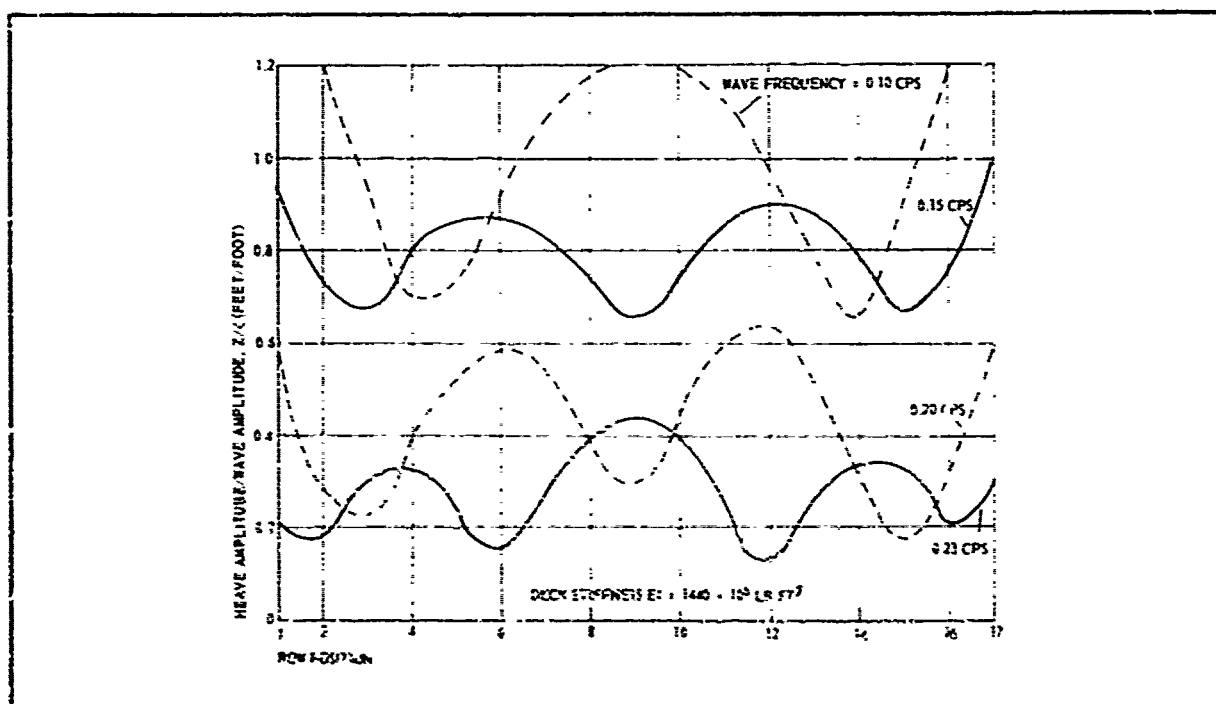


Figure 41 - Mode Shape for Analytic Studies as Wave Frequency Changes

TABLE XIV - SUMMARY OF EXTREME VALUES - RUN NO. 41

Run No. 41									
CPS = 0.023 EI = 1440									
F _H = 508 F _{SU} = 3220 F _{SL} = 4000									
-- HORIZONTAL DECK MOTION --									
* POS	* T	* NEG	* T	* POS	* T	* NEG	* T	* POS	* T
0.93E-02	4.76	-9.06E-02	1.44						
-- VERTICAL DISPLACEMENT --									
* POS	* T	* NEG	* T	* POS	* T	* NEG	* T	* POS	* T
2.75E-01	13.46	-3.34E-01	8.10	5.19E-01	7.98	-4.60E-01	13.78	2.49E-01	17.30
1.21E-01	12.27	-1.70E-01	18.74	4.27E-01	8.06	-3.44E-01	14.02	0.30	0.0
3.16E-01	12.10	-2.17E-01	9.82	3.28E-01	8.94	-2.45E-01	1.82	3.64E-02	3.78
3.78E-01	12.00	-3.19E-01	9.94	2.78E-01	8.70	-2.14E-01	2.78	6.17E-01	11.00
2.47E-01	3.42	-2.48E-01	6.26	2.95E-01	9.48	-2.29E-01	23.02	1.50E-00	11.92
1.74E-01	9.46	-1.35E-01	2.56	3.28E-01	4.74	-2.90E-01	12.02	8.14E-01	17.42
2.33E-01	9.94	-3.19E-01	12.02	2.60E-01	4.92	-1.93E-01	19.90	0.30	0.0
3.10E-01	17.93	-4.93E-01	12.00	1.89E-01	18.02	-1.61E-01	19.40	4.54E-03	0.46
3.99E-01	18.02	-4.63E-01	11.94	1.43E-01	12.10	-1.59E-01	1.64	2.16E-01	2.27
2.75E-01	14.12	-3.80E-01	11.92	2.28E-01	11.98	-1.40E-01	14.26	1.54E-00	11.00
1.24E-01	13.22	-2.45E-01	12.20	2.99E-01	11.78	-2.14E-01	14.14	1.38E-00	12.38
2.50E-01	19.06	-1.30E-01	3.84	3.50E-01	11.88	-3.02E-01	10.22	0.30	0.0
2.50E-01	15.46	-2.89E-01	13.72	3.02E-01	12.14	-2.29E-01	19.16	6.59E-02	1.00
3.33E-01	11.80	-3.26E-01	13.94	2.61E-01	12.14	-2.28E-01	19.16	1.05E-00	11.62
3.74E-01	12.00	-3.40E-01	9.84	3.05E-01	13.58	-2.59E-01	19.36	1.63E-00	12.96
2.14E-01	12.08	-1.73E-01	16.42	4.94E-01	13.82	-3.31E-01	16.06	3.68E-01	13.36
3.64E-01	13.82	-2.40E-01	7.96	5.12E-01	14.06	-3.91E-01	11.96		
-- DECK MOMENT --									
* POS	* T	* NEG	* T	* POS	* T	* NEG	* T	* POS	* T
9.03E-05	15.34	-5.06E-05	13.56	4.80E-03	10.46	-6.53E-03	8.08		
3.49E-05	15.96	-3.41E-05	13.40	5.93E-03	16.06	-5.34E-03	13.66		
3.80E-05	16.76	-4.41E-05	6.38	7.99E-03	15.82	-7.67E-03	13.44		
3.95E-05	13.54	-3.73E-05	15.94	7.55E-03	11.96	-8.75E-03	14.32		
3.07E-05	16.44	-3.28E-05	12.08	8.11E-03	3.88	-9.47E-03	6.26		
4.66E-05	6.38	-3.93E-05	4.02	4.89E-03	8.88	-3.70E-03	3.08		
3.14E-05	6.38	-3.08E-05	6.78	9.94E-03	14.24	-6.42E-03	20.02		
2.49E-05	16.70	-2.85E-05	1.36	9.93E-03	14.24	-8.07E-03	11.84		
3.42E-05	8.76	-3.89E-05	6.38	5.94E-03	14.04	-5.47E-03	11.70		
2.92E-05	1.00	-2.94E-05	2.98	9.74E-03	10.24	-6.32E-03	11.28		
3.66E-05	19.14	-2.37E-05	16.76	6.88E-03	10.24	-6.68E-03	11.28		
4.13E-05	11.38	-3.94E-05	13.52	3.98E-03	19.24	-4.30E-03	16.62		
3.31E-05	16.10	-2.96E-05	18.46	8.87E-03	19.26	-8.20E-03	13.66		
3.95E-05	3.98	-3.91E-05	19.14	7.49E-03	16.00	-7.70E-03	10.30		
3.91E-05	13.54	-4.07E-05	11.16	9.13E-03	12.08	-7.54E-03	9.68		
3.49E-05	14.34	-3.88E-05	11.96	5.57E-03	12.06	-5.31E-03	9.66		
4.11E-05	1.00	-4.63E-05	15.98	5.03E-03	14.46	-6.30E-03	11.84		

TABLE XVI - SUMMARY OF EXTREME VALUES - RUN NO. 15

Run No. 15										TAPE 43T										12-13-72																																																																																																																																																																																																																	
CPS = 0.15										EI = 1440										FSL = 3390																																																																																																																																																																																																																	
FH = 617										FSU = 2610										FSL = 3390																																																																																																																																																																																																																	
HORIZONTAL DISPLACEMENT - UPPER FLOAT										HORIZONTAL DISPLACEMENT - LOWER FLOAT										HORIZONTAL DISPLACEMENT - UPPER FLOAT																																																																																																																																																																																																																	
POS * * * T * * * NEG * * * T * *										POS * * * T * * * NEG * * * T * *										POS * * * T * * * NEG * * * T * *																																																																																																																																																																																																																	
1.23E 00	14.74	-3.79E 00	24.49	3.73E 00	27.31	-3.04E 00	17.94	4.69E-01	17.90	-4.35E 00	27.31	4.20E 00	28.01	-9.90E-01	9.20	1.42E 00	27.14	-1.18E 00	17.90	9.13E-01	29.01	-1.74E 00	9.86	6.51E-01	24.73	-6.19E-01	27.71	9.90E-02	17.90	-3.43E 00	27.23	0.0	0.0	-2.75E 00	15.94	2.44E 00	17.90	-2.00E 00	27.45	4.20E-01	17.90	-3.26E 00	19.56	2.65E 00	17.94	-2.47E 00	27.43	1.10E 00	14.80	-4.19E 00	24.53	2.29E 00	28.01	-2.04E 00	12.04	2.14E 00	17.96	-2.20E 00	27.37	3.40E 00	29.01	-1.13E 00	12.02	1.10E 00	17.92	-1.40E 00	14.72	2.32E 00	14.78	-5.40E 00	24.40	2.28E 00	27.91	-1.51E-01	12.15	3.46E-01	14.74	-6.36E-01	14.56	2.66E 00	24.38	-5.53E 00	24.38	1.33E 00	9.16	-1.49E 00	24.81	1.40E 00	27.69	-1.59E 00	24.43	2.40E 00	24.40	-4.79E 00	24.40	1.10E 00	7.66	-7.03E 00	28.01	2.34E 00	27.63	-2.55E 00	24.36	2.40E 00	24.42	7.72E-01	6.74	-5.62E 00	28.01	2.72E 00	27.59	-3.02E 00	24.32	2.90E-01	13.90	-2.74E 00	28.01	5.46E-01	25.99	-1.20E 00	9.68	1.91E 00	21.26	-1.99E 00	24.28	4.14E-01	12.80	-3.76E 00	29.01	9.59E-02	28.01	-2.00E 00	9.92	0.12E-01	14.72	-6.55E-01	24.12	4.08E-01	12.58	-3.76E 00	29.01	9.59E-02	28.01	-2.00E 00	9.92	1.66E 00	24.53	-1.42E 00	21.16	1.06E 00	12.50	-3.95E 00	29.01	4.97E-04	0.25	-1.15E 01	27.81	4.07E 00	24.63	-3.99E 00	21.22	1.83E 04	27.59	-1.95E 04	17.72	0.20E 03	14.80	-0.25E 03	24.30	4.35E 03	18.20	-4.98E 03	27.43	1.15E 04	18.24	-1.14E 04	27.29	1.59E 04	18.08	-1.59E 04	27.27	1.61E 04	24.38	-1.70E 04	27.59	1.33E 04	24.00	-1.40E 04	14.78	8.60E 03	23.92	-1.10E 04	14.84	6.05E 03	19.96	-5.82E 03	14.86	1.03E 04	27.29	-9.08E 03	18.30	1.41E 04	27.67	-1.28E 04	24.42	1.63E 04	21.08	-1.54E 04	24.04	1.67E 04	21.38	-1.51E 04	23.98	1.33E 04	21.38	-1.19E 04	24.26	5.07E 03	14.80	-5.89E 03	24.24	7.45E 03	17.82	-8.77E 03	27.69	1.81E 04	24.02	-2.07E 04	21.10

TABLE XVII - SUMMARY OF EXTREME VALUES - RUN NO. 14

Run No. 14		43P	12-12-72		
GPS = 0.10		EL = 1440			
FH = -76		FSU = 1839	FSL = 2561		
HORIZONTAL DECK MOTION		HORIZONTAL DISPLACEMENT - UPPER FLOAT		HORIZONTAL DISPLACEMENT - LOWER FLOAT	
* POS	* T	* POS	* T	* POS	* T
0.18E-03	0.62	-1.04E 01	29.05	1.87E 00	40.01
HORIZONTAL DISPLACEMENT		HORIZONTAL DISPLACEMENT		HORIZONTAL DISPLACEMENT	
* POS	* T	* POS	* T	* POS	* T
8.01E 00	33.77	-9.34E 00	39.03	1.87E 00	40.01
5.90E 00	33.77	-6.57E 00	39.03	0.0	0.0
3.15E 00	33.73	-3.76E 00	39.03	0.0	0.0
8.24E-01	22.58	-1.13E 00	39.03	0.0	0.0
1.29E 00	39.03	-1.49E 00	39.03	0.0	0.0
3.39E 00	39.03	-3.23E 00	39.03	0.0	0.0
5.09E 00	39.03	-4.51E 00	39.03	0.0	0.0
6.15E 00	39.03	-5.31E 00	39.03	0.0	0.0
6.62E 00	39.03	-5.61E 00	39.03	0.0	0.0
6.41E 00	39.03	-5.40E 00	39.03	0.0	0.0
5.93E 00	39.01	-4.68E 00	39.03	0.0	0.0
4.03E 00	39.95	-3.47E 00	39.03	0.0	0.0
2.01E 00	30.79	-1.80E 00	39.03	0.0	0.0
4.61E-01	25.31	-4.94E-01	39.03	0.0	0.0
2.77E 00	33.85	-3.28E 00	39.03	0.0	0.0
5.93E 00	33.83	-6.32E 00	39.03	0.0	0.0
8.50E 00	33.83	-9.52E 00	39.03	0.0	0.0
HORIZONTAL DISPLACEMENT		HORIZONTAL DISPLACEMENT		HORIZONTAL DISPLACEMENT	
* POS	* T	* POS	* T	* POS	* T
1.98E 05	31.77	-4.87E 05	34.43	1.87E 00	40.01
2.10E 05	37.31	-3.89E 05	33.13	0.0	0.0
2.20E 05	37.31	-2.90E 05	33.81	0.0	0.0
2.65E 05	38.47	-2.20E 05	33.45	0.0	0.0
3.00E 05	30.87	-2.23E 05	22.10	0.0	0.0
3.31E 05	39.23	-2.38E 05	22.12	0.0	0.0
3.09E 05	37.57	-2.06E 05	22.14	0.0	0.0
2.92E 05	34.23	-1.50E 05	22.14	0.0	0.0
1.26E 05	18.70	-1.39E 05	22.30	0.0	0.0
1.37E 05	18.70	-1.54E 05	22.30	0.0	0.0
1.96E 05	32.75	-1.90E 05	39.25	0.0	0.0
1.86E 05	33.07	-2.33E 05	38.85	0.0	0.0
2.17E 05	32.35	-2.43E 05	38.85	0.0	0.0
2.47E 05	32.35	-2.51E 05	38.49	0.0	0.0
2.94E 05	33.81	-2.78E 05	37.31	0.0	0.0
4.25E 05	33.79	-3.69E 05	37.69	0.0	0.0
6.08E 05	34.19	-4.91E 05	38.19	0.0	0.0
HORIZONTAL DISPLACEMENT		HORIZONTAL DISPLACEMENT		HORIZONTAL DISPLACEMENT	
* POS	* T	* POS	* T	* POS	* T
1.98E 05	31.77	-4.87E 05	34.43	1.87E 00	40.01
2.10E 05	37.31	-3.89E 05	33.13	0.0	0.0
2.20E 05	37.31	-2.90E 05	33.81	0.0	0.0
2.65E 05	38.47	-2.20E 05	33.45	0.0	0.0
3.00E 05	30.87	-2.23E 05	22.10	0.0	0.0
3.31E 05	39.23	-2.38E 05	22.12	0.0	0.0
3.09E 05	37.57	-2.06E 05	22.14	0.0	0.0
2.92E 05	34.23	-1.50E 05	22.14	0.0	0.0
1.26E 05	18.70	-1.39E 05	22.30	0.0	0.0
1.37E 05	18.70	-1.54E 05	22.30	0.0	0.0
1.96E 05	32.75	-1.90E 05	39.25	0.0	0.0
1.86E 05	33.07	-2.33E 05	38.85	0.0	0.0
2.17E 05	32.35	-2.43E 05	38.85	0.0	0.0
2.47E 05	32.35	-2.51E 05	38.49	0.0	0.0
2.94E 05	33.81	-2.78E 05	37.31	0.0	0.0
4.25E 05	33.79	-3.69E 05	37.69	0.0	0.0
6.08E 05	34.19	-4.91E 05	38.19	0.0	0.0

TABLE XVIII - WAVE FORCE DATA FOR
WAVE FREQUENCY CHANGES

Run no.	Wave frequency (cps)	FH (lb)	FSC (lb)	FSL (lb)
41	0.23	508	3220	4000
16	0.20	650	3000	3750
15	0.15	617	2610	3390
14	0.10	-76	1839	2561

support test evidence shown previously in Figures 30, 31, and 32, where the mode shape also decreased as wave frequency decreased. The least stiff deck in those cases was deck 2 shown in Figure 32. There, at 0.20 cps, 5 lobes appeared, at 0.129 and 0.090 cps 3 lobes appeared, and at 0.071 cps 1 lobe appeared.

It was also observed that as the wave frequency decreased, the tail wagging phenomena increased. This result was also noted in the tests. At higher frequencies, in Figure 41, motion at the center of the array was greater than at the ends. This effect was approached in the test results.

Figure 42 shows the changes in motion that occur as the deck stiffness is changed. Plotted in this figure are mode shapes of extreme motion values measured at a wave frequency of 0.15 cps for three deck stiffness values as listed below:

<u>Run no.</u>	<u>Deck stiffness</u>
12	$720 \times 10^6 \text{ lb-ft}^2$
41	$1440 \times 10^6 \text{ lb-ft}^2$
18	$2160 \times 10^6 \text{ lb-ft}^2$

Tables XIX and XX provide the data backup for Figure 43. A drastic reduction in motion occurs as the stiffness is increased to $2160 \times 10^6 \text{ lb-ft}^2$. It was likewise noted in the test data presented earlier in Figure 33 that an

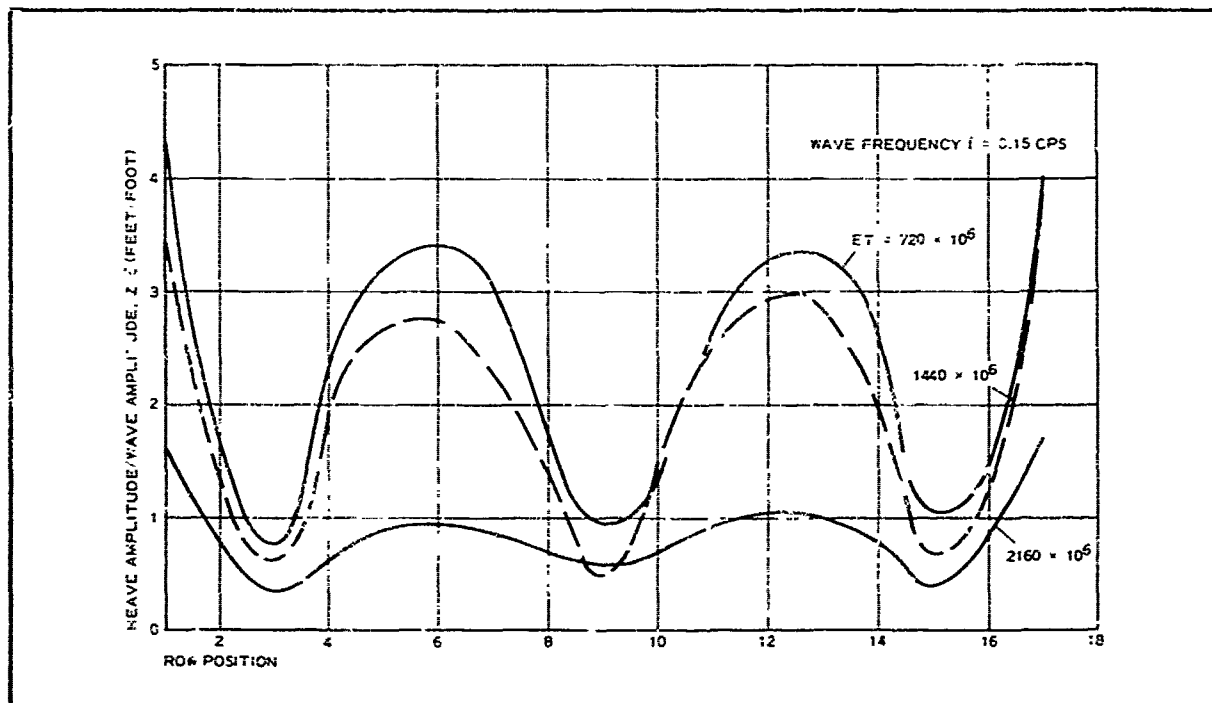


Figure 42 - Mode Shape for Analytical Studies as Deck Stiffness Changes

increase in deck stiffness generally reduced motions over a considerable portion of the frequency range.

It can be shown that both heave and surge forces contribute to vertical motion of the deck. Influence of heave force on deck motion is easily perceived. Heave forces on the float would result in bending of the deck and consequent deck deformation. Surge forces are large in magnitude and located large distances below the deck. Bending moment transmitted to the deck by the surge force is much larger than that developed by heave force (particularly because heave force is attenuated by a deep float). Accumulation of these surge force couples transmitted to the deck consequently can cause large deformation.

Two computer runs were made containing the parameters shown in Table XI with one difference. Run 3 applied only heave forces, while run 4 applied only surge forces. Tables XXI and XXII provide summary data for these cases. A comparison of Runs 3 and 4, to the previous run 2 indicated that the motions at any individual time increment were additive.

TABLE XIX - SUMMARY OF EXTREME VALUES - RUN NO. 12

RUN NO. 12		43Y		EI = 720		FSL = 3390	
CPS = 0.15		FH = 617		FSU = 2610			
HORIZONTAL DISPLACEMENT - UPPER FLUAT		HORIZONTAL DISPLACEMENT - LOWER FLUAT					
POS * * * T * * * NEG * * * T * *		POS * * * T * * * NEG * * * T * *					
1	1.54E 00	14.44	-4.63E 00	25.25	4.76E 00	29.01	-1.18E 00
2	1.40E 00	14.38	-4.35E 00	25.13	2.15E 00	24.01	-2.33E 00
3	4.06E-01	14.30	-3.83E 00	25.37	3.3	0.0	-3.29E 00
4	1.50E-01	14.04	-3.10E 00	25.09	0.0	0.0	-3.66E 00
5	2.77E-01	17.06	-4.06E 00	29.01	4.49E-03	0.74	-3.04E 00
6	1.30E 00	17.20	-4.96E 00	28.01	4.83E-01	24.01	-2.35E 00
7	2.19E 00	17.20	-5.63E 00	29.01	1.37E 00	24.67	-1.57E 00
8	2.82E 00	17.16	-6.07E 00	29.01	1.79E 00	24.30	-4.22E-01
9	3.10E 00	17.10	-6.23E 00	29.01	2.24E 00	17.18	-1.95E 00
10	2.97E 00	17.00	-6.12E 00	29.01	2.32E 00	10.30	-4.93E 00
11	2.45E 00	16.40	-5.72E 00	27.95	1.58E 00	10.12	-6.94E 00
12	1.73E 00	16.46	-5.01E 00	27.93	7.12E-01	9.90	-6.13E 00
13	9.54E-01	16.00	-4.05E 00	27.97	1.32E-01	6.32	-2.51E 00
14	4.82E-01	14.62	-2.97E 00	28.01	1.46E 00	27.33	-1.32E 00
15	1.24E 00	13.48	-3.86E 00	24.38	2.00E 00	27.71	-2.27E 00
16	2.13E 00	13.28	-4.49E 00	24.32	0.0	0.0	-5.17E 00
17	2.68E 00	13.20	-4.75E 00	24.30	3.73E-04	0.26	-1.43E 01
HORIZONTAL DISPLACEMENT - UPPER FLUAT		HORIZONTAL DISPLACEMENT - LOWER FLUAT					
POS * * * T * * * NEG * * * T * *		POS * * * T * * * NEG * * * T * *					
1	1.36E 04	17.40	-1.77E 04	20.64	1.36E 00	10.74	-1.18E 00
2	7.04E 03	24.77	-0.96E 03	21.10	2.15E 00	24.01	-2.33E 00
3	9.65E 03	14.50	-4.77E 03	12.56	3.3	0.0	-3.29E 00
4	1.14E 04	20.60	-9.78E 03	17.40	0.0	0.0	-3.66E 00
5	1.50E 04	20.64	-1.30E 04	16.94	4.49E-03	0.74	-3.04E 00
6	1.37E 04	20.66	-1.26E 04	16.96	4.83E-01	24.01	-2.35E 00
7	9.63E 03	27.33	-1.24E 04	24.32	1.37E 00	24.67	-1.57E 00
8	9.51E 03	12.64	-9.64E 03	9.48	1.79E 00	24.30	-4.22E-01
9	4.03E 03	12.14	-8.47E 03	9.46	2.24E 00	17.18	-1.95E 00
10	8.89E 03	17.38	-6.20E 03	14.92	2.32E 00	10.30	-4.93E 00
11	1.26E 04	17.44	-8.88E 03	20.14	1.58E 00	10.12	-6.94E 00
12	1.50E 04	24.42	-9.65E 03	28.01	7.12E-01	9.90	-6.13E 00
13	1.54E 04	24.38	-1.17E 04	29.01	1.32E-01	6.32	-2.51E 00
14	1.16E 04	9.94	-1.09E 04	27.63	1.46E 00	27.33	-1.32E 00
15	5.84E 03	9.36	-6.88E 03	27.25	2.00E 00	27.71	-2.27E 00
16	5.07E 03	14.28	-6.88E 03	24.40	0.0	0.0	-5.17E 00
17	1.37E 04	27.99	-1.53E 04	9.86	3.73E-04	0.26	-1.43E 01
JACK MOMENT		JACK SHEAR					
POS * * * T * * * NEG * * * T * *		POS * * * T * * * NEG * * * T * *					
1	4.39E 05	28.01	-6.18E 05	17.63	4.39E 00	29.01	-1.18E 00
2	2.48E 05	14.40	-3.46E 05	17.18	2.15E 00	24.01	-2.33E 00
3	3.00E 05	20.40	-2.43E 05	16.72	3.3	0.0	-3.29E 00
4	2.37E 05	20.86	-2.22E 05	9.72	0.0	0.0	-3.66E 00
5	2.04E 05	12.76	-2.75E 05	9.20	4.49E-03	0.74	-3.04E 00
6	3.27E 05	12.74	-3.02E 05	20.84	4.83E-01	24.01	-2.35E 00
7	2.03E 05	24.03	-4.15E 05	20.84	1.37E 00	24.67	-1.57E 00
8	3.01E 05	29.51	-3.17E 05	20.86	1.79E 00	24.30	-4.22E-01
9	3.30E 05	17.18	-3.41E 05	12.48	2.24E 00	17.18	-1.95E 00
10	4.31E 05	9.72	-4.15E 05	12.44	2.32E 00	10.30	-4.93E 00
11	5.11E 05	9.72	-3.01E 05	11.98	1.58E 00	10.12	-6.94E 00
12	4.62E 05	9.72	-2.79E 05	12.78	7.12E-01	9.90	-6.13E 00
13	2.76E 05	19.74	-2.44E 05	13.24	1.32E-01	6.32	-2.51E 00
14	2.45E 05	22.36	-2.97E 05	24.24	1.46E 00	27.33	-1.32E 00
15	2.72E 05	11.96	-3.46E 05	9.62	2.00E 00	27.71	-2.27E 00
16	4.49E 05	12.46	-4.42E 05	9.58	0.0	0.0	-5.17E 00
17	8.78E 05	27.39	-5.13E 05	16.10	3.73E-04	0.26	-1.43E 01

SECTION IV - PLATFORM MOTION INVESTIGATIONS

GER-15665

TABLE XX - SUMMARY OF EXTREME VALUES - RUN NO. 18

[illegible]

TABLE XXI - EXTREME VALUES WITH HEAVE FORCE ALONE APPLIED - RUN NO. 3

SUMMARY OF EXTREME VALUES

FLOAT	HORIZONTAL DECK MOTION				HORIZONTAL DISPLACEMENT - UPPER FLAT				HORIZONTAL DISPLACEMENT - LOWER FLAT			
	POS	T	NEG	T	POS	T	NEG	T	POS	T	NEG	T
1	1.91E-02	21.60	-1.62E-02	19.30	3.83E-02	10.62	-4.43E-02	21.42	1.81E-01	10.62	-2.16E-01	21.82
2					1.23E-02	10.56	-3.79E-02	21.72	1.52E-01	10.56	-1.74E-01	21.72
3					2.41E-02	10.34	-2.92E-02	21.40	1.13E-01	10.34	-1.40E-01	21.40
4					2.05E-02	5.24	-2.36E-02	21.10	9.62E-02	5.24	-1.15E-01	21.12
5					1.65E-02	5.25	-1.94E-02	20.54	7.70E-02	5.25	-1.06E-01	20.66
6					1.66E-02	22.02	-1.91E-02	20.24	7.34E-02	22.02	-1.06E-01	20.24
7					2.81E-02	17.02	-2.91E-02	14.70	1.24E-01	17.02	-1.41E-01	14.70
8					4.01E-02	21.78	-3.81E-02	19.44	1.74E-01	21.78	-2.10E-01	19.44
9					4.71E-02	21.72	-4.64E-02	19.44	2.17E-01	21.72	-2.10E-01	19.44
10					4.54E-02	21.58	-4.50E-02	19.44	2.15E-01	21.58	-2.10E-01	19.44
11					3.88E-02	21.38	-3.61E-02	19.16	1.78E-01	21.38	-1.66E-01	19.16
12					3.04E-02	21.18	-2.61E-02	19.16	1.35E-01	21.18	-1.20E-01	19.16
13					2.16E-02	7.62	-1.99E-02	5.60	9.89E-02	7.62	-8.55E-02	5.60
14					1.69E-02	20.24	-1.77E-02	17.92	7.98E-02	20.24	-8.15E-02	17.92
15					2.87E-02	19.38	-3.07E-02	17.14	1.33E-01	19.38	-1.46E-01	17.14
16					4.23E-02	19.46	-4.55E-02	17.20	1.97E-01	19.46	-2.17E-01	17.20
17					5.01E-02	19.52	-5.36E-02	17.24	2.41E-01	19.52	-2.44E-01	17.24

FLOAT	DECK SHEAR				DECK MOMENT			
	POS	T	NEG	T	POS	T	NEG	T
1	9.04E 02	5.38	-8.57E 02	23.00	2.13E 04	15.06	-2.42E 04	22.02
2	6.10E 02	6.38	-5.71E 02	12.38	1.80E 04	10.44	-1.82E 04	21.80
3	9.50E 02	11.66	-9.89E 02	9.34	1.77E 04	14.50	-1.34E 04	21.02
4	8.39E 02	3.88	-8.53E 02	5.86	1.64E 04	5.28	-1.74E 04	21.22
5	4.56E 02	3.86	-9.75E 02	6.16	9.50E 03	5.74	-1.27E 04	8.04
6	9.36E 02	13.96	-8.86E 02	3.08	1.39E 04	6.04	-1.37E 04	3.74
7	1.03E 03	6.16	-1.05E 03	3.86	1.38E 04	12.22	-1.44E 04	16.50
8	1.08E 03	19.56	-1.13E 03	21.88	1.75E 04	22.00	-1.81E 04	14.86
9	5.26E 02	12.09	-5.80E 02	1.10	2.73E 04	22.00	-2.41E 04	19.46
10	1.14E 03	8.46	-1.16E 03	14.98	1.88E 04	21.74	-2.06E 04	19.48
11	7.65E 02	21.88	-9.51E 02	19.58	1.74E 04	21.44	-1.76E 04	19.14
12	7.68E 02	5.72	-7.58E 02	20.36	1.89E 04	21.60	-1.72E 04	9.90
13	9.20E 02	10.78	-8.76E 02	3.86	1.05E 04	11.90	-1.10E 04	5.62
14	9.08E 02	7.52	-9.28E 02	9.50	1.35E 04	19.14	-1.43E 04	18.10
15	1.03E 03	4.02	-1.07E 03	5.50	1.55E 04	19.03	-1.35E 04	17.04
16	5.87E 02	17.26	-6.23E 02	13.76	2.00E 04	19.26	-2.00E 04	17.36
17	9.62E 02	5.50	-1.01E 03	4.02	2.62E 04	19.68	-2.61E 04	17.36

TABLE XXII - EXTREME VALUES WITH SURGE FORCE ALONE APPLIED - RUN NO. 4

SUMMARY OF EXTREME VALUES

FLUAT	HORIZONTAL DECK MOTION				HORIZONTAL DISPLACEMENT - UPPER FLOAT				HORIZONTAL DISPLACEMENT - LOWER FLOAT			
	POS	T	NEG	T	POS	T	NEG	T	POS	T	NEG	T
1.18E-01	19.16		-1.59E-01	21.54	5.96E-01	16.89	-5.61E-01	19.06	2.56E 00	16.90	-3.22E 00	19.10
					5.76E-01	17.08	-5.37E-01	19.26	2.59E 00	21.38	-3.51E 00	9.62
					5.47E-01	17.32	-5.48E-01	19.56	2.23E 00	21.90	-3.11E 00	15.10
					3.81E-01	17.56	-4.00E-01	19.68	1.94E 00	5.22	-1.78E 00	19.68
					3.47E-01	5.56	-4.19E-01	7.60	3.10E 00	9.56	-2.22E 00	20.96
					4.97E-01	5.92	-4.63E-01	20.84	2.68E 00	5.90	-2.21E 00	20.82
					5.33E-01	19.36	-5.39E-01	21.60	2.56E 00	19.34	-3.10E 00	7.96
					5.27E-01	19.20	-5.20E-01	21.42	2.52E 00	19.23	-3.59E 00	7.62
					4.89E-01	19.08	-4.68E-01	21.32	2.48E 00	19.10	-2.22E 00	21.34
					4.23E-01	14.88	-4.36E-01	16.88	3.50E 00	14.54	-2.02E 00	22.02
					3.32E-01	7.52	-4.03E-01	22.02	2.93E 00	10.70	-2.15E 00	22.02
					4.04E-01	20.80	-3.92E-01	5.30	1.71E 00	20.85	-1.98E 00	5.32
					4.39E-01	8.20	-4.03E-01	10.52	2.15E 00	20.88	-3.44E 00	9.76
					4.36E-01	21.84	-5.02E-01	10.64	1.43E 00	20.74	-2.70E 00	10.52
					4.37E-01	22.02	-4.08E-01	10.90	3.00E 00	12.60	-1.32E 00	19.50
					3.98E-01	1.66	-4.83E-01	3.90	3.67E 00	12.68	-3.00E-01	19.90
									2.77E 00	22.02	-2.04E 00	3.54
FLUAT	DECK SHEAR				HORIZONTAL DISPLACEMENT - UPPER FLOAT				HORIZONTAL DISPLACEMENT - LOWER FLOAT			
	POS	T	NEG	T	POS	T	NEG	T	POS	T	NEG	T
8.24E 03	5.50		-1.01E 04	21.22	5.96E-01	16.89	-5.61E-01	19.06	2.56E 00	16.90	-3.22E 00	19.10
7.84E 03	7.60		-9.22E 03	22.02	5.76E-01	17.08	-5.37E-01	19.26	2.59E 00	21.38	-3.51E 00	9.62
1.05E 04	21.22		-9.84E 03	12.90	5.47E-01	17.32	-5.48E-01	19.56	2.23E 00	21.90	-3.11E 00	15.10
8.69E 03	17.16		-1.04E 04	6.00	3.81E-01	17.56	-4.00E-01	19.68	1.94E 00	5.22	-1.78E 00	19.68
1.32E 04	22.00		-1.42E 04	6.04	3.47E-01	5.56	-4.19E-01	7.60	3.10E 00	9.56	-2.22E 00	20.96
9.51E 03	12.76		-8.83E 03	15.28	4.97E-01	5.92	-4.63E-01	20.84	2.68E 00	5.90	-2.21E 00	20.82
1.10E 04	6.04		-9.22E 03	14.50	5.33E-01	19.36	-5.39E-01	21.60	2.56E 00	19.34	-3.10E 00	7.96
1.43E 04	6.04		-1.23E 04	11.22	5.27E-01	19.20	-5.20E-01	21.42	2.52E 00	19.23	-3.59E 00	7.62
5.56E 03	9.50		-5.66E 03	7.24	4.89E-01	19.08	-4.68E-01	21.32	2.48E 00	19.10	-2.22E 00	21.34
1.50E 04	9.90		-1.23E 04	7.60	4.23E-01	14.88	-4.36E-01	16.88	3.50E 00	14.54	-2.02E 00	22.02
1.23E 04	9.90		-1.23E 04	7.60	3.32E-01	7.52	-4.03E-01	22.02	2.93E 00	10.70	-2.15E 00	22.02
7.16E 03	15.04		-8.19E 03	8.14	4.04E-01	20.80	-3.92E-01	5.30	1.71E 00	20.85	-1.98E 00	5.32
1.39E 04	10.66		-1.30E 04	17.38	4.39E-01	8.20	-4.03E-01	10.52	2.15E 00	20.88	-3.44E 00	9.76
9.70E 03	10.60		-8.61E 03	19.02	4.36E-01	21.84	-5.02E-01	10.64	1.43E 00	20.74	-2.70E 00	10.52
9.79E 03	3.96		-1.05E 04	9.12	4.37E-01	22.02	-4.08E-01	10.90	3.00E 00	12.60	-1.32E 00	19.50
4.11E 03	17.38		-9.57E 03	19.68	3.98E-01	1.66	-4.83E-01	3.90	3.67E 00	12.68	-3.00E-01	19.90
1.02E 04	16.84		-1.02E 04	14.32					2.77E 00	22.02	-2.04E 00	3.54
FLUAT	DECK MOMENT				HORIZONTAL DISPLACEMENT - UPPER FLOAT				HORIZONTAL DISPLACEMENT - LOWER FLOAT			
	POS	T	NEG	T	POS	T	NEG	T	POS	T	NEG	T
6.33E 05	7.48		-7.06E 05	12.88	5.96E-01	16.89	-5.61E-01	19.06	2.56E 00	16.90	-3.22E 00	19.10
5.38E 05	11.88		-4.88E 05	5.36	5.76E-01	17.08	-5.37E-01	19.26	2.59E 00	21.38	-3.51E 00	9.62
5.47E 05	17.28		-7.16E 05	6.08	5.47E-01	17.32	-5.48E-01	19.56	2.23E 00	21.90	-3.11E 00	15.10
7.00E 05	21.02		-6.65E 05	15.16	3.81E-01	17.56	-4.00E-01	19.68	1.94E 00	5.22	-1.78E 00	19.68
4.59E 05	5.98		-5.21E 05	7.90	3.47E-01	5.56	-4.19E-01	7.60	3.10E 00	9.56	-2.22E 00	20.96
7.93E 05	6.14		-7.02E 05	3.86	4.97E-01	5.92	-4.63E-01	20.84	2.68E 00	5.90	-2.21E 00	20.82
5.98E 05	19.58		-6.21E 05	21.88	5.33E-01	19.36	-5.39E-01	21.60	2.56E 00	19.34	-3.10E 00	7.96
4.08E 05	15.92		-4.78E 05	1.30	5.27E-01	19.20	-5.20E-01	21.42	2.52E 00	19.23	-3.59E 00	7.62
5.66E 05	8.46		-5.95E 05	6.16	4.89E-01	19.08	-4.68E-01	21.32	2.48E 00	19.10	-2.22E 00	21.34
5.19E 05	14.20		-5.37E 05	2.88	4.23E-01	14.88	-4.36E-01	16.88	3.50E 00	14.54	-2.02E 00	22.02
5.79E 05	10.54		-5.40E 05	8.26	3.32E-01	7.52	-4.03E-01	22.02	2.93E 00	10.70	-2.15E 00	22.02
6.97E 05	13.76		-6.41E 05	21.86	4.04E-01	20.80	-3.92E-01	5.30	1.71E 00	20.85	-1.98E 00	5.32
5.25E 05	20.84		-5.17E 05	9.74	4.39E-01	8.20	-4.03E-01	10.52	2.15E 00	20.88	-3.44E 00	9.76
7.18E 05	8.24		-6.96E 05	10.58	4.36E-01	21.84	-5.02E-01	10.64	1.43E 00	20.74	-2.70E 00	10.52
5.89E 05	17.50		-6.34E 05	19.78	4.37E-01	22.02	-4.08E-01	10.90	3.00E 00	12.60	-1.32E 00	19.50
4.17E 05	5.50		-4.68E 05	20.62	3.98E-01	1.66	-4.83E-01	3.90	3.67E 00	12.68	-3.00E-01	19.90
6.67E 05	1.54		-7.29E 05	3.84					2.77E 00	22.02	-2.04E 00	3.54

That is, heave motion of the deck due to heave and surge force applied separately gave the same result as when they were applied simultaneously.

Comparison of extreme values will show that the contribution of surge force to the motion, at the frequency tested, is on the order of 10 times that caused by the heave force.

Two conditions can aid to reduce this motion effect. Deck stiffness can be increased to reduce response. Moment transferred to the deck, as caused by surge force, can be reduced. This reduction could be accomplished by the use of a hinge located closer to the deck.

Information presented in the preceding analytical studies is for models that do not duplicate characteristics of the previously tested model arrays. Primary cause for the lack of duplication is based on deck characteristics.

The analytical model, as conceived and described earlier, incorporated a deck of conventional bending and shear stiffness properties.

Attempts to modify the analytical model to duplicate the deck of the earlier parallel linkage were made. Considering small deflections, the parallel linkage bars have no ability to transmit shear force from one float to another. In this regard, the model deck motions would follow isolated float responses. Two effects of the model, however, provide for some ability to transfer shear, and consequently can give rise to excessive deck motion.

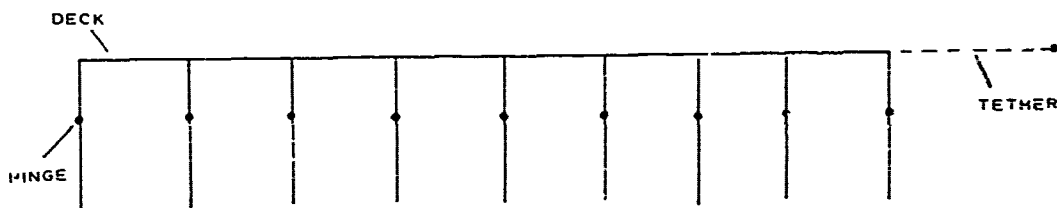
1. Plastic strips attached along the outside edges of the model provide for some bending and shear stiffness.
2. Non-linear effects of shear transmission occur as deflections between adjacent floats become large so that tension and compression forces in the upper and lower links cause vertical components of force. Because major rewriting of the program would be required, these effects were not accounted for.

The analytical model was also modified to account for the deck stiffness arrangement on the later test models. Deck configuration for these models consisted of flat plastic strips running longitudinally separated vertically by plastic blocks located at each float row. In this case, no shear web was

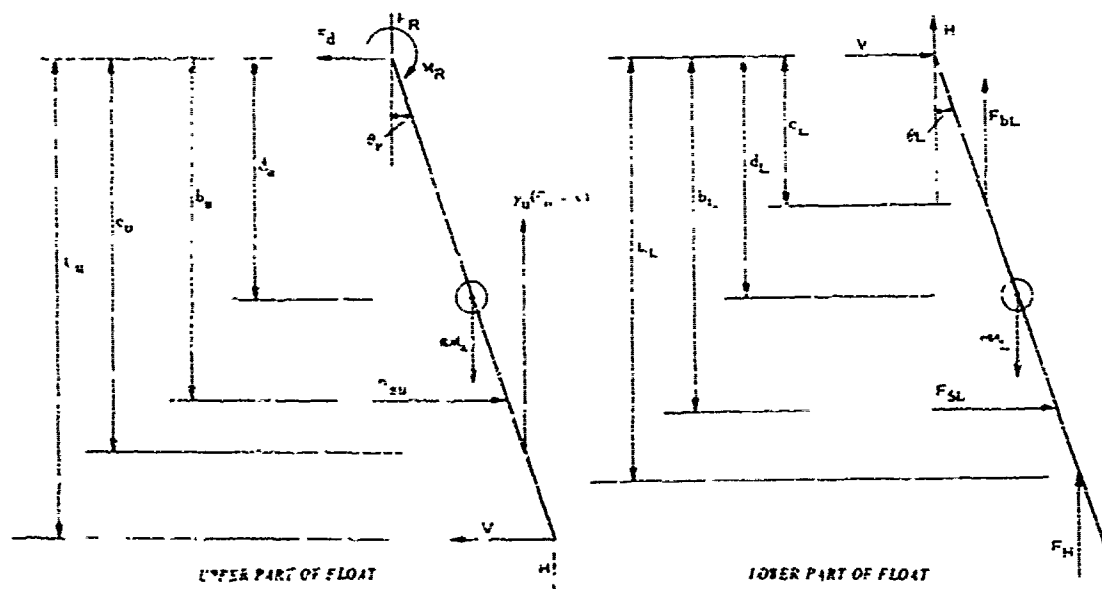
present, and consequently the bending stiffness of the deck due to vertical loads could be approximated by taking the stiffness of the strips individually. In resistance to surge force effects of moment at the deck, the strips act as tension or compression links. In this regard the effective stiffness of the arrangement can be calculated as two strips separated at a given distance (similar to the calculation for a sandwich deck). Calculation of this latter effect is shown in Appendix G. The analytic model incorporated both stiffness effects as a verendeel truss configuration. The present form of the analytic model cannot operate successfully with the stiffness conditions supplied. The manner of computing forces and moments from deflected positions requires small time increments to ensure convergence of the solution. As the deck becomes stiffer, the time increment must become shorter. Present input requires an increment too small for a practical solution within a reasonable length of computer time.

d. Analysis of Island Motion

To approximate the motion of the island, a math model was set up that accounts for the motion in one plane only, that is, a single row of floats attached to a flexible deck, as shown in the following diagram.



It is assumed in the analysis that the upper and lower portions of the floats are rigid bodies. It is also assumed that the horizontal motion of the floats (pendulum action) is quite small, so that there is no kinematic coupling between the vertical and horizontal motions. There is elastic coupling between these motions through the deck. A diagram of the forces acting on the float is given on the next page.



The terms used in the diagrams are defined below:

- y = vertical displacement of deck where float is attached
- x_d = horizontal displacement of deck - same at all floats
- x_{gu} = horizontal displacement of cg of upper part of float
- x_{gL} = horizontal displacement of cg of lower part of float
- θ_u = angular displacement of upper part of float
- θ_L = angular displacement of lower part of float
- M_u = mass of deck and upper part of float
- M_L = mass of lower part of float
- I_u = mass moment of inertia of upper part of float about its cg
- I_L = mass moment of inertia of lower part of float about its cg
- α_H = virtual mass factor for horizontal motion of float
- α_V = virtual mass factor for vertical motion of float

- α_I = virtual mass factor for rotational motion of float
- F_R = vertical reaction between float and deck
- F_D = horizontal reaction between float and deck
- M_R = moment reaction between float and deck
- V = horizontal reaction between upper and lower parts of float
- H = vertical reaction between upper and lower parts of float
- F_{SU} = surge force on upper part of float - input function of time
- F_{SL} = surge force on lower part of float - input function of time
- F_H = heave force - input function of time
- F_{bL} = buoyant force on lower part of float
- g = acceleration of gravity - 32.2 ft/sec^2
- γ_u = water plane spring constant
- $\bar{\gamma}_u = \gamma_u \bar{y}_u$ is the buoyant force on upper part of float when $y = 0$.
- d_u = distance from deck to cg of upper part of float
- b_u = distance from deck to center of surge pressure for upper part of float
- C_u = distance from deck to center of buoyancy of upper part of float
- L_u = distance from deck to hinge
- C_L = distance from hinge to center of buoyancy of lower part of float
- d_L = distance from hinge to cg of lower part of float
- b_L = distance from hinge to center of surge pressure for lower part of float
- L_L = distance from hinge to point of application of heave force
- K_d = spring constant of tether
- L = distance between floats

The following dynamic equations were used in the analysis:

1. Upper portion of float

$$F_{su} - V - F_d = \ddot{x}_u M_u \quad (1)$$

$$-F_R - gM_u - H + \gamma_u (\bar{y}_u - y) = \ddot{y} M_u \quad (2)$$

$$F_{su}(b_u - d_u) + \gamma_u(y_u - y)(C_u - d_u)\theta_u + F_R d_u \theta_u + \\ F_d d_u - H(L_u - d_u)\theta_u - V(L_u - d_u) - M_R = I_u \ddot{\theta}_u \quad (3)$$

2. Lower portion of float

$$F_{sL} + V = \ddot{x}_L \alpha_H M_L \quad (4)$$

$$F_H + H + F_{bL} - gM_L = \ddot{y} \alpha_v M_L \quad (5)$$

$$F_{sL}(b_L - d_L) + F_H(L_L - d_L)\theta_L - F_{bL}(d_L - C_L)\theta_L - \\ Hd_L \theta_L - Vd_L = I_L \alpha_I \ddot{\theta}_L \quad (6)$$

Kinematic constraints are as follows:

$$\theta_u = \frac{1}{d_u}(x_u - x_d) \quad (7)$$

$$\theta_L = \frac{1}{d_L}(x_L - x_d) - \frac{L_u}{d_L d_u}(x_u - x_d) \quad (8)$$

Eliminating V and H from Equations 1 through 6 gives the following four equations.

$$\ddot{y} = \frac{1}{M_u + \alpha_v M_L} (F_H - F_R - \gamma_u y) \quad (9)$$

$$\ddot{x}_u M_u + \ddot{x}_L \alpha_H M_L = F_{su} + F_{sL} - F_d \quad (10)$$

$$\ddot{x}_u M_u d_u + \ddot{x}_L \alpha_H M_L L_u + \ddot{\theta}_u I_u = R_u \quad (11)$$

$$\ddot{x}_L \alpha_H M_L d_L + \ddot{\theta}_L \alpha_I I_L = R_L \quad (12)$$

where

$$R_u = F_{su} b_u + F_{\varepsilon L} L_u + \theta_u \left[C_u \gamma_u \bar{\gamma}_u - C_u \gamma_u y - \right. \\ \left. L_u g M_L + L_u F_H + L_u F_{bL} - d_u g M_u - \frac{M_L \alpha_V L_u + M_u d_u}{M_u + \alpha_V M_L} \times \right. \\ \left. (F_H - F_R - \gamma_u y) \right] - M_R \quad (13)$$

$$R_L = F_{SL} b_L + \theta_L \left[F_H L_L + F_{bL} C_L - g M_L d_L - \frac{M_L d_L}{M_u + \alpha_V M_L} (F_H - F_R - \gamma_u y) \right] \quad (14)$$

Using the kinematic constraints (Equations 7 and 8), Equations 11 and 12 become:

$$A \ddot{x}_u + B \ddot{x}_L = F_1 \ddot{x}_d + R_u \quad (15)$$

$$-C \ddot{x}_u + D \ddot{x}_L = F_2 \ddot{x}_d + R_L \quad (16)$$

where

$$A' = M_u d_u + \frac{I_u}{d_u}$$

$$B = \alpha_H M_L L_u$$

$$C = \frac{\alpha_I I_L L_u}{d_L d_u}$$

$$D = \alpha_H M_L d_L + \frac{\alpha_I I_L}{d_L}$$

$$F_1 = \frac{I_u}{d_u}$$

$$F_2 = \frac{\alpha_I I_L}{d_L} \left(1 - \frac{L_u}{d_u} \right)$$

Solving Equations 14 and 15 for \ddot{x}_u and \ddot{x}_L , gives

$$\ddot{x}_u = \frac{1}{AD + BC} \left[(DF_1 - BF_2) \ddot{x}_d + DR_u - BR_L \right] \quad (17)$$

and

$$\ddot{x}_L = \frac{1}{AD + BC} \left[(CF_1 + AF_2) \ddot{x}_d + CR_u + AR_L \right] \quad (18)$$

Now

$$\Sigma F_d = k_d \ddot{x}_d \quad (19)$$

where Σ before a variable indicates a summing of that variable for all N floats.

Then, summing Equation 10 for all the floats and using Equation 18,

$$M_u \Sigma \ddot{x}_u + \alpha_H M_L \Sigma \ddot{x}_L = \Sigma F_{su} + \Sigma F_{sL} - k_d \ddot{x}_d \quad (20)$$

Summing Equations 16 and 17 for all floats and substituting for $\Sigma \ddot{x}_u$ and $\Sigma \ddot{x}_L$ in Equation 19 gives

$$\ddot{x}_d = -A_2 \Sigma R_u - A_3 \Sigma R_L + A_1 (\Sigma F_{su} + \Sigma F_{sL} - k_d \ddot{x}_d), \quad (21)$$

where

$$A_1 = \frac{1}{N(M_u B_1 + \alpha_H M_L C_1)},$$

$$A_2 = A_1 (M_u B_2 + \alpha_H M_L C_2),$$

$$A_3 = A_1 (M_u B_3 + \alpha_H M_L C_3),$$

and

$$B_1 = \frac{DF_1 - BF_2}{AD + BC}$$

$$C_1 = \frac{CF_1 + AF_2}{AD + BC}$$

$$B_2 = \frac{D}{AD + BC}$$

$$C_2 = \frac{C}{AD + BC}$$

$$B_3 = \frac{-B}{AD + BC}$$

$$C_3 = \frac{A}{AD + BC}$$

The motion of each float is now defined by Equations 9, 16, and 17, and the horizontal motion of the deck is governed by Equation 20. Therefore, for a deck with N floats, the resulting system has $3N + 1$ equations. It remains only to define M_R and F_R for each float in terms of the float displacements and the deck stiffness.

For a deck in which distortions due to either moments or transverse force are calculated using the same EI , the expressions for M_R and F_R are:

$$M_{Ri} = \frac{12EI}{L^2} \left[\frac{L}{6} (\theta_{uL-1} + 4\theta_{uL} + \theta_{uL+1}) + \frac{1}{2} (x_{uL-1} - x_{uL+1}) \right] \quad (22)$$

$$F_{Ri} = \frac{12EI}{L^3} \left[\frac{L}{2} (\theta_{uL+1} - \theta_{uL-1}) + (-x_{uL-1} + 2x_{uL} - x_{uL+1}) \right] \quad (23)$$

Here the subscript i refers to the i^{th} float. For a deck with different structural action, for instance a vierendeel truss, Equations 21 and 22 are modified somewhat. By substituting Equation 20 into Equations 16 and 17, the equations of motion are now in a form for straightforward numerical integration. A predictor-corrector method of integration is used. The system of $3N + 1$ equations for the general form:

$$\ddot{x}_L = f_L(x_1, x_2, \dots, x_{3n+1}, t) \quad L = 1, 2, \dots, 3N + 1 \quad (24)$$

The predictor recurrence formula is the parabolic differentiation formula:

$$x_{s+1} = 2x_s - x_{s-1} + h^2 f_s, \quad (25)$$

where h is the time increment and s refers to the s^{th} time step.

The corrector recurrence formula is of the Störmer type:

$$x_{s+1} = 2x_s - x_{s-1} + \frac{h^2}{12} (f_{s-1} + 10f_s + f_{s+1}). \quad (26)$$

The truncation error of this formula is of the order h^6 . Since the recurrence formula and the governing equations are both second order, no stability problems occur.

A computer program was written to carry out the integration of the equations of motion. At present, the heave and surge forcing functions can be entered

only as a sinusoidal function. However, with minor changes, any type of forcing function can be accepted.

e. Results

Analytic model array motions show trends and effects similar to test measurements. Deck stiffness is very influential on motion. As deck stiffness increases, motion decreases. Deck mode shape increases as wave frequency increases. Array mode shape at a given frequency shows that many points on the deck may have excessive motions compared with other points. Motions are nearly symmetrical in fore and aft directions. Both bow and tail wagging are observed whereby extreme motions at these points exceed the motions at the other points. At the frequency examined, surge force is responsible for the major component of deck motion.

5. SUMMARY

Increased motion within a closely packed array of floats appears related to an increase in wave height within the array. Computation of force or motion is suggested as for an isolated float with a wave height modified by float density effects.

$$\zeta_m = K \zeta_w,$$

where $K = 1/[1(A_f/S^2)]A_f$ = float cross-sectional area and S = float spacing.

Float arrays connected by decks of measurable stiffness appear to attain additional points of resonant and null behavior at frequencies higher than float resonance and null frequencies. As stiffness changes, number, magnitude, and frequency of these points change.

Deck mode shape appears to change as frequency of the wave changes. Magnitude of the motion also changes with wave frequency. Tail wagging or excessive motions of the array at the ends occurs throughout a considerable portion of the imposed wave frequency spectrum.

Analytical tools for defining interaction of deck stiffness and wave forces on the floats are presented and appear to provide results duplicating many effects observed in test. Duplication of deck properties in the analytical model was not accomplished. Comparative motions between test and the analytic model consequently was not made on a one-to-one basis.

SECTION V - COST INVESTIGATIONS

1. BACKGROUND

The ARPA review group critique of the previous program suggested that "Further work should be carried out to better define the critical restraints that limit performance and drive the costs of expandable structures and to highlight the sensitivity of costs to external design requirements. The effect of possible new developments in materials and fabricating methods on the costs of expandable platforms should also be examined."

2. DISCUSSION

During the period that GAC has studied the feasibility of developing expandable structures that could be joined together to form a floating base, two mission definitions have been considered. The earliest concept envisaged a large island (400 ft by 2000 ft) capable of landing C-130 aircraft. Subsequently an evaluation was made of a platform of more modest size (100 ft by 100 ft) capable of landing a 40,000-lb helicopter. A parametric cost study was conducted under Contract N0014-72-C-0361, reported in GER-15491¹, for platforms of these two sizes. Similar platform detail designs were considered structurally for operational sea states of 0, 5, and 7, and aircraft weights were varied from 40,000 to 100,000 to 155,000 lb. One of the results of this study is reproduced in Figure 43, which relates area unit costs for deck loads as a function of operational sea states. This analysis and the assumptions on which it was based have been re-examined and the costs appear to be reasonable approximations. It should be kept in mind, however, that a small platform has a practical maximum concentrated load-carrying capability that is smaller than a large base, and that the response of a large platform to sea states appears to be different from a small one of similar deck and float designs.

As a corollary to the current program, technical and cost proposals were prepared to design, fabricate, assemble, and test a modular 1/3-scale platform¹. Sandwich deck dimensions were 50 ft by 50 ft and float scale

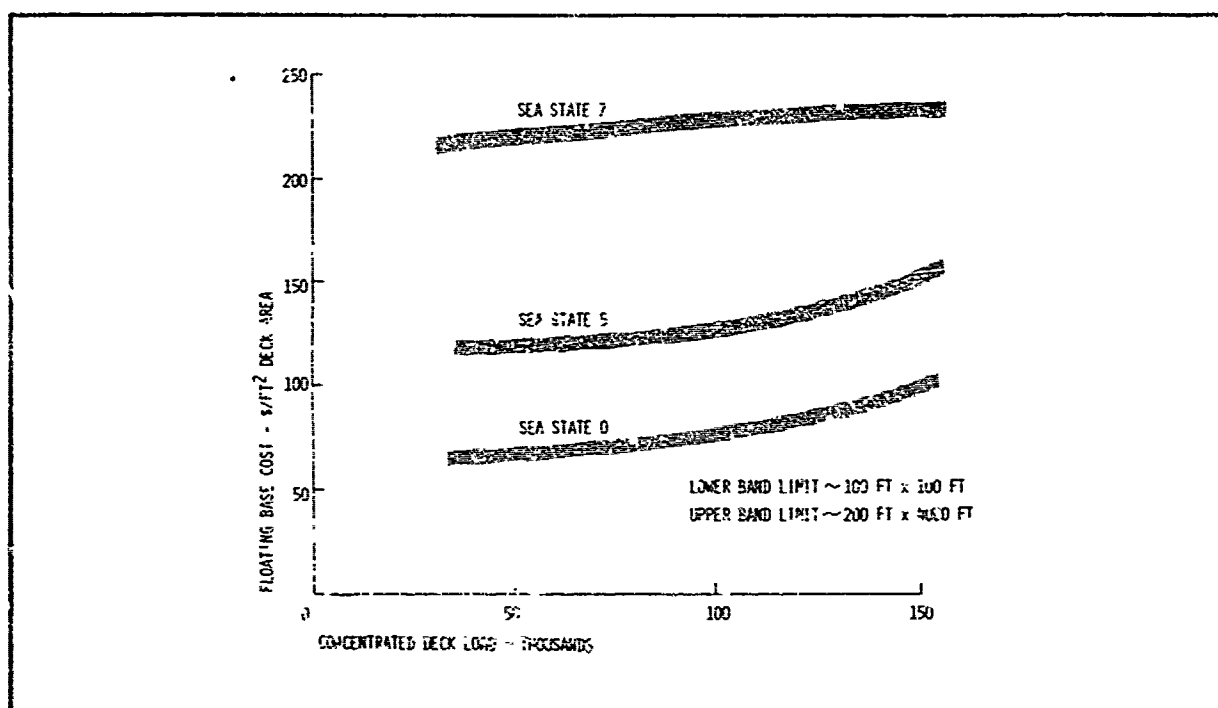


Figure 43 - Concentrated Deck Load versus Floating Base Cost

was established as 8/3 of that used in Figure 3 or 1/3 full scale. Deck load was defined as a 15,000-lb helicopter. The platform was designed for a scaled operational sea state of 5 and survival sea state (scaled) of 7. The platform was to be supported by a 7 by 7 (49) float array. Manufacturing costs, including assembly and deployment in an inland lake (Seneca), but not including detail design, development, or testing was estimated to be \$268,000 or approximately \$107 per square foot. While this may appear high in comparison with the earlier cost data for larger platforms, it should be kept in mind that the labor portion of costs does not decrease with reduction in island size as rapidly as materials do.

As will be discussed subsequently, the deck and float alternator systems represent major components of platform costs.

The effect of eliminating a modular sandwich deck on the basis of cost was determined in preparation of a budgeting estimate for a bare bones proposal (Appendix A) to fabricate a 50-ft by 50-ft platform with 1/3 scale expandable float in a 7-by-7 array with a plywood deck. Factory costs were \$62.80 per sq ft of platform area.

3. VARIABLES AFFECTING PLATFORM COSTS

Two groups of conditions directly influence cost of an expandable floating base of modular construction. These are mission definition and design alternatives. Primary among the former are:

1. Platform size and configuration
2. Deck loads: static and dynamic, concentrated, distributed, and off center
3. Operational sea state
4. Survival sea state
5. Allowable platform motion

Within the definitions established by these criteria, the following design factors may be varied to control costs:

1. Deck module size
2. Deck module material
3. Float spacing
4. Float size and configuration
5. Float materials
6. Cabling
7. Accessories

In a gross sense, the major elements of costs of a modular platform can then be associated with these components: (1) deck, (2) floats, (3) cabling, and (4) accessories. Factors affecting costs of these components are summarized below:

1. Deck costs
 - a. Module size and configuration
 - b. Panel load: distributed and concentrated
 - c. Materials of construction
 - d. Float spacing
 - e. Allowable platform motion
 - f. Survival sea state
2. Float costs
 - a. Deck weight

- b. Cargo loads
- c. Platform size and configuration
- d. Materials of construction
- e. Float size and configuration
- f. Operational sea state
- g. Allowable platform motion
- 3. Cabling costs
 - a. Float spacing
 - b. Survival sea state
 - c. Deck loads
- 4. Accessory Costs. Accessories are defined as:
 - a. Fill, drain, and vent plumbing in floats
 - b. Pressure manifold system
 - c. Pressure monitoring system
 - d. Pumps and compressors
 - e. Number of floats
 - f. Degree of sophistication in manifold and pressure surveillance systems

4. MATERIALS

a. General

In analyzing materials and fabrication processes most influential in cost of platform construction Goodyear Aerospace Corporation has examined only the deck and float systems, since cabling and accessories were believed to represent only a small portion of total platform price.

b. Deck

A criticism of platform deck design concepts has been that only aluminum-faced balsa sandwich was proposed and casted for modular panels in previous studies. This construction, which has high strength/weight and high stiffness/weight ratios is expensive in comparison with other material options. Alternatives that might be examined as potential deck constructions were costed as follows:

1. Welded steel structure - \$0.50/lb

2. Welded aluminum construction - \$2.00/lb
3. Extended aluminum - \$1.00/lb

Aluminum/balsa sandwich costs in the gage ranges (0.150 to 0.375-in. skins; 4-in. to 8-in. core) considered for platform decks would average \$4.00 per pound.

Other sandwich material options might include:

1. Cores: redwood, aluminum honeycomb
2. Skins: steel, reinforced plastics

Variation in cost as a function of gages for various materials is shown in Figures 44 and 45.

A quantitative assessment of cost of a modular deck of sandwich construction has not been undertaken in this program, since a specific design for a platform has not been evolved. Determination of costs can be derived from the foregoing information, however, when this has been accomplished.

c. Float System

The substantial reduction of bending moment achieved by articulating a long slender inflatable float supporting a deck makes feasible consideration of relatively thin-gage reinforced elastometric materials for their construction, since inflation pressure can also be grossly decreased. For the mission definition chosen for this cost study, the float shown in Figure 46 was selected. Full-scale inflation pressure was assumed to be 20 psi for the float and 11 psi for the attenuator.

Two types of material systems, both known to Goodyear and both compatible with the ocean environment, were examined for costing purposes. They are: (1) polyurethane-impregnated nylon and (2) neoprene reinforced with nylon, dacron, or Fiber B. Neither material system requires major capital equipment for fabrication of components as large as a full-scale float.

The Aviation Products Division of The Goodyear Tire & Rubber Co. has pioneered in the development of nylon fabrics impregnated with a proprietary polyurethane for use in the ocean. A large (14 ft to 10 ft diameter by 70 ft long) towed oil container for the ADEPPS program is a recent sizable

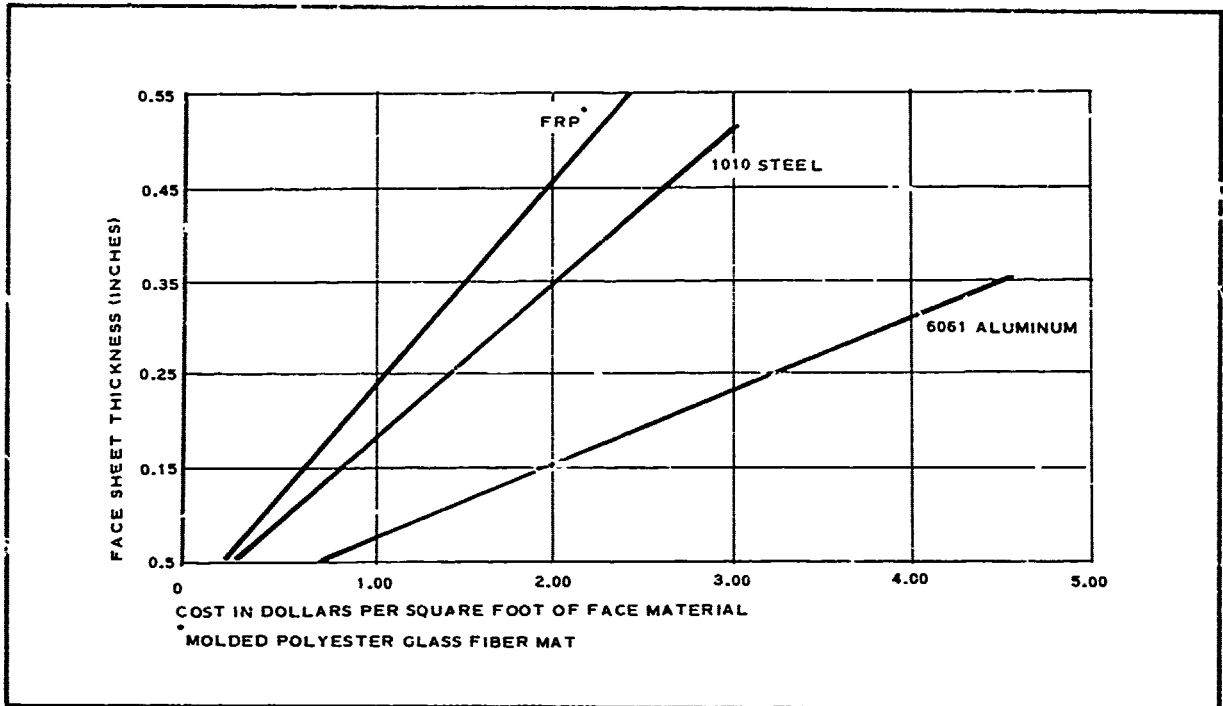


Figure 44 - Variation in Cost as Function at Face Sheet Thickness

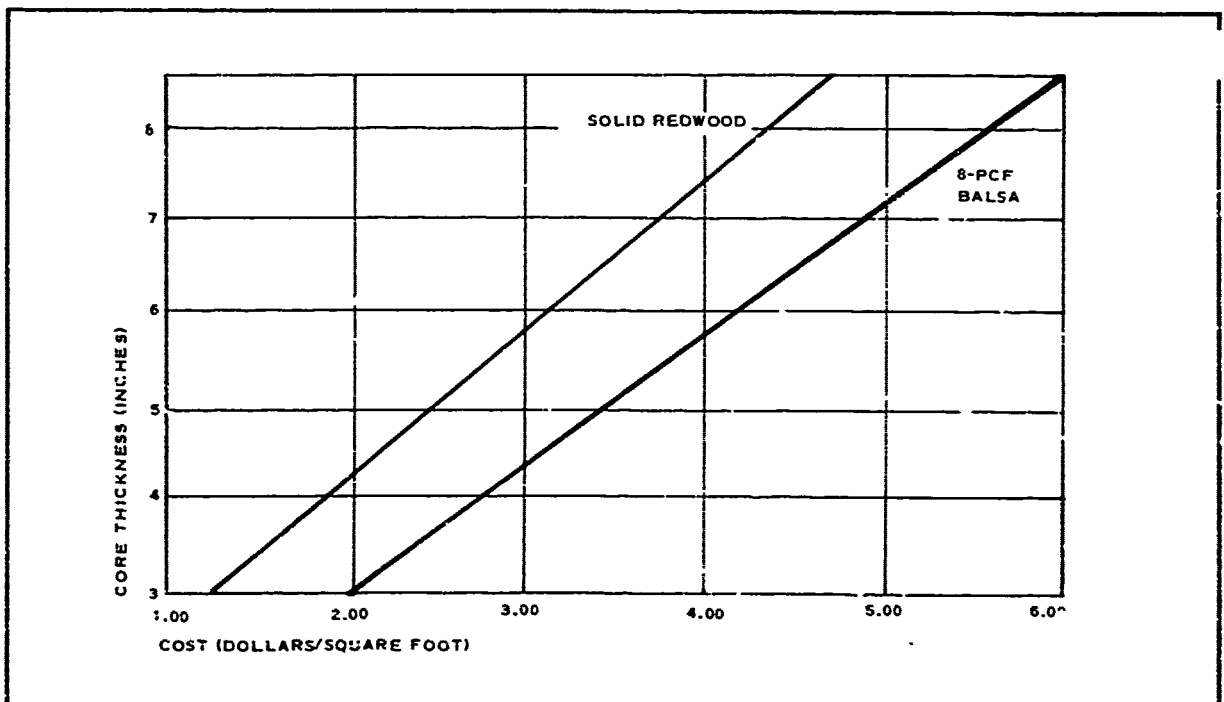


Figure 45 - Variation in Cost as Function at Core Thickness

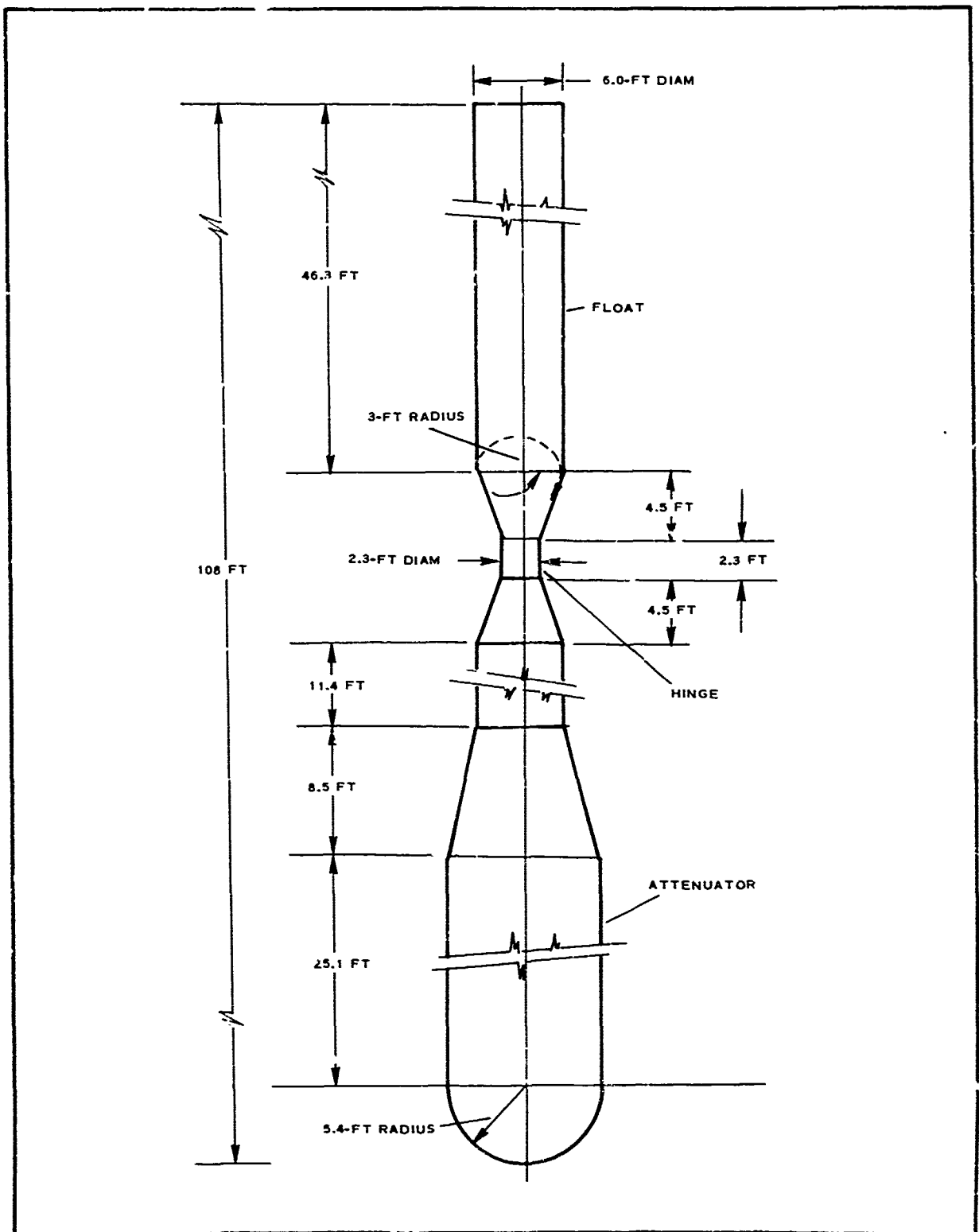


Figure 46 - Float Configuration for Cost Study

application of this technology. An item such as a float is manufactured by cutting woven nylon fabric of appropriate strength into patterns to form the various geometries that make up the part. The cloth is laid over a mandrel and lapped to create joints. These are sewn and then adhered by impregnating with liquid polyurethane. When the entire part has been assembled in this manner on a form-fitting mandrel, it is sprayed with the polyurethane at a proper viscosity and the fabric is impregnated. Cure is effected in air at ambient temperatures.

While this material process system shows considerable promise for manufacture of the type of hardware represented by the inflatable float and attenuator, it was considered to be too developmental to generate costs competitive with sewing and adhesive bonding of neoprene calendered nylon, dacron, or Fiber B. Further, these latter systems may be constructed of multiple layers, including bias orientations. The shear requirements of the float are sufficiently high to require 50 percent of principal fabric strength at 45 deg; a two-ply bias material appears mandatory and this has been accomplished with the spray polyurethane process on an experimental basis only.

Fabrication of calendered neoprene/nylon fabric stock by bonding and sewing has been employed at GAC for a large variety of applications and is believed to be applicable to manufacture of the hinged floats. In this process, cured stock of proper strength is cut into patterns to form various parts of the float. These patterns are joined by adhesive bonding of lap joints followed by sewing. The number of stitches per inch and the number of rows of stitches required are a function of fabric strength; for 2000 lb per inch material, four rows of 6 to 8 stitches per inch would be employed. Subsequent to sewing, a thin neoprene seal material would be adhesively bonded over the outer surface of the stitched area to ensure a pressure seal. All elements of the float/attenuator system could be fabricated by this process, as was demonstrated in the 1/8-scale deformable models. For these models, however, sewing was employed only at the hinge transitions.

No large autoclaves are required for this type of manufacture, although if available, uncured (rather than cured) rubberized fabric stock could be

adhered under pressure at the bonded joints without adhesive and without sewing.

5. INFLATABLE FLOAT COST EXERCISE

Estimates were made on costs to manufacture the near real-life, full-scale float/attenuator assembly (Figure 46) represented in 1/8 scale by the model tested at LUMF. Criteria established for the estimate were as follows:

1. Cured calendared neoprene to be the impregnant for all fabrics
2. Two-ply bias material to be used throughout the system
3. Float and hinge fabric break strength to be 2000 lb/in. and 1000 lb/in. at ± 45 deg
4. Attenuator fabric break strength to be 1100 lb/in. and 550 lb/in. at ± 45 deg
5. All float and hinge joints to employ four rows of stitches at 6 to 8 stitches/inch
6. All attenuator joints to employ 3 rows of stitches at 6 to 8 stitches/inch
7. All joints to be lapped: adhesively bonded and sewn
8. 100 percent inspection to be utilized on all joints
9. Estimates to be made on 1, 50, and 500 units
10. Neoprene reinforcements to be (a) nylon, (b) dacron, and (c) Fiber B
11. Costs of drain and vent lines and metal attachment to deck to be included

Factory costs are summarized in Table XXIII.

It was not possible to develop realistic pricing for Fiber B fabrics in the deniers desired, since none have yet been woven in quantity. Small amounts of 200 and 400 denier yarns have been produced by DuPont and are under evaluation by GAC at this time. Verbal prices for this material from the pilot plant in low quantity are \$20.00 and \$15.00 per pound, respectively. Weaving costs for heavier denier Fiber B fabrics purchased by Goodyear Aerospace have been \$6.00/lineal yard 60 in. wide.

TABLE XXIII - FACTORY COSTS

Construction	Quantity		
	One unit	50 units	500 units
Neoprene/nylon			
Materials cost	\$ 5,364	\$ 4,989	\$ 4,914
Labor cost	<u>41,112</u>	<u>16,390</u>	<u>9,550</u>
Total	\$46,476	\$21,379	\$14,464
Neoprene/dacron			
Materials cost	\$ 5,882	\$ 5,470	\$ 5,391
Labor cost	<u>38,104</u>	<u>15,290</u>	<u>8,975</u>
Total	\$43,986	\$20,760	\$14,366

In the future, as Fiber B production capacity increases and fibers become available in quantity for applications other than tires, the cost of filaments and fabrics will decrease substantially. Goodyear has been advised that in time Fiber B costs may drop to \$2.50 per pound. Textile suppliers that have converted large-denier Fiber B yarns for Goodyear have indicated that the fibers do not pose unusual problems in weaving.

Fiber B would be attractive as a reinforcement for rubber in fabrication of inflatable floats because of its exceptional specific strength and stiffness values in comparison with any other eligible fibers, including nylon and dacron. Even at a cost multiple of four it would be structurally competitive with either of the latter fibers. A plus factor of some minor consequence to its use in platform manufacture is the savings in weight.

A comparison of the physical properties of nylon, dacron, and Fiber B is given in Table XXIV.

TABLE XXIV - COMPARISON OF FLOAT REINFORCEMENT

FIBER PROPERTIES

Property	Nylon [*]	Dacron [*]	Fiber B
Tensile ultimate (psi)	117,000	106,000	400,000
Specific gravity	1.14	1.38	1.44
Tenacity (gpd)	8	6-8	22.0
Modulus (gpd)	55	105	480
(E)	(0.8×10^6)	(1.3×10^6)	(8.8×10^6)
Elongation, ultimate (percent)	16-28	12-16	4.0
Zero-strength temperature, deg F	473	473	850
50 percent RT strength temperature, deg F	330	350	600
Coefficient of thermal expansion	-40×10^{-6}	-20×10^{-6}	NA
Ultraviolet resistance	P	G	NA
Storage aging resistance	G	E	NA
Moisture resistance	P	G	NA
Coating adhesion	G	G	G
Impact resistance	E	G	NA
-65 deg F performance	E	E	NA
Flexing resistance	E	E	NA
Flame resistance	SE	SE	NA
Minimum yarn size available	20 denier	30 denier	1500/2
Filaments per yarn	NA	NA	2300
Filament diameter (inches)	0.001	0.001	0.0003

* Key: E = excellent; G = good; P = poor; SE = self-extinguishing; and NA = not available.

LIST OF REFERENCES

1. GER-15491: Final Technical Report - Expandable Floating Bases. Akron, Ohio, Goodyear Aerospace Corporation, 14 January 1972.
2. Wiegel, L.: Oceanographical Engineering. Englewood Cliffs, N.J., Prentice-Hall Publishing Co., International Series in Theoretical and Applied Mechanics, 1964.
3. Comstock, J.P. (editor): Principles of Naval Architecture. New York, N.Y., The Society of Naval Architects and Marine Engineers, 1967.
4. Mercier, J.A.: Hydrodynamic Analyses and Exploratory Model Tests for an Expandable Floating Base. Stevens Institute of Technology, Davidson Laboratory, Letter Report SIT-DL-72-1579, Subcontract to GAC for Expandable Floating Base Program, January 1972.
5. Newman, J.N.: The Motions of a Spar Buoy in Regular Waves. DTMB Report 1499, May 1963.

APPENDIX A - REPORT OF ARPA REVIEW GROUP ON
EXPANDABLE FLOATING BASES

FINDINGS AND RECOMMENDATIONS

The review group was briefed by Goodyear Aerospace Corporation about their study to examine the technical feasibility of expandable floating bases and their proposed program to continue the studies through prototype development. After discussing the presentation in some detail, the review group agreed that the studies to date have not established the technical feasibility of large expandable floating bases. It was further agreed that the proposed Task 2 of the Goodyear program, involving the design of a one-third scale expandable floating base, is premature at this time.

The review group recommends, however, that a technology program be carried out to develop basic understanding of the response and behavior of expandable floating structures subject to wave action. Both analytic and model studies should be carried out, including but not be limited to the following problem areas:

Expandable-Body Response. Develop basic understanding of the response of expandable bodies under wave action. This should include both analytic and model studies that examine the performance of expandable flotation components and compare that with the response of rigid components. The scaling laws of expandable structures should be investigated to assure that the prototype structure can be properly simulated and test results scaled to full-scale dimensions. It may be necessary to actually fabricate a fairly large-scale flotation unit in order to satisfy these requirements.

Hydrodynamic Problems. Because of the unusual pliable structures considered and the close packing of floats, fundamental work should be done on the following hydrodynamic problem areas:

Interaction of the viscous wake of a float with neighboring floats.
Distributed wave reflection and absorption.
Elastic response of structure to the wave induced forces.

Preceding page blank

APPENDIX A

Cost of Expandable Floating Structures. The current cost estimates on expandable floating structures appear rather high in comparison with that of other structural concepts. Further work should be carried out to better define the critical restraints that limit the performance and drive the costs of expandable structures and to highlight the sensitivity of costs to external design requirements. The effect of possible new developments in materials and fabricating methods on the cost of expandable platforms should also be examined.

The purpose of the recommended technology program is to develop basic understanding of the performance, capability, and costs of expandable floating structures in order to permit a comparison between expandable and more conventional structures. Further work beyond that, if any, should await for the results of the technology program. Although the review group was not chartered to examine potential missions for the expandable structures, it was generally agreed that the technology program should develop and feature potential unique capabilities and characteristics of such structures rather than attempting to meet certain mission-oriented design requirements. Subsequent missions, if any, for such structures are likely to emerge from a consideration of their unique features and their system costs. For example, there appears to be scientific interest in lightweight portable sparbuoys. Multiple combinations of such units may be of some military interest. In contrast, if the development work is designed to meet certain mission requirements, it has to be shown not only that an expandable base is technically feasible for the given application but also that it is the preferred system for the mission under consideration.

The above findings and recommendations are basically supported by all members of the review group. However, Mr. John Gregory of ONR has a somewhat different view on some aspects of the technology program recommended by the group. His comments are included here as an Appendix to the group's report.

INTRODUCTION

During the past 18 months, the Advanced Research Research Projects Agency has sponsored a study contract with the Goodyear Aerospace Corporation to investigate the technical feasibility of floating bases constructed of expandable

APPENDIX A

materials. Goodyear Report GAP-71-5652S6, Rev. A,^a states that the objectives of the contract were "to investigate the technical feasibility of using expandable structures and to develop the required design and material technology. Environmental operating and survival conditions, platform stability, platform mobility, requirements and capabilities of expandable structures in this application, cost, sizes of components, material life, and transportation and erection procedures were considered."

Goodyear has concluded that "no limitations have been found in these areas that would indicate that the concept is not feasible." They have submitted a proposal to ARPA to continue the program through prototype development and assembly. A detailed program plan and schedule has been prepared for Task 2 of the program, visualizing a 6-month effort through January-June in 1972. The specific effort of the proposed Task 2 is the design of a one-third scale expandable floating base.

At the request of Dr. C. J. Wang, Director of Advanced Engineering, ARPA, a group of experts was assembled to review and assess the Goodyear technical feasibility study and to assist ARPA in generating guidelines for a technology program in the area of expandable floating platforms. The review group met on 21 December 1971 at the Washington office of The Rand Corporation. The group was chaired by Drs. Laupa and Ross and included the following members:

Stanley Backer	MIT
W. Denny Freeston	Georgia Tech
John Gregory	ONR
Chester E. Grosch	Pratt Institute
Armas Laupa	Rand
Denzil C. Pauli	ONR
Charles Ravitsky	ARPA
Robert Ross	Environmental Structures
Fred N. Spiess	SIO
Alexander J. Tachmindji	IDA
Allyn C. Vine	WHOI
C. J. Wang	ARPA
Cdr. T. F. Wiener	Office, CNO

The Goodyear representatives briefed the group of their study findings and proposed follow-on studies, and answered questions of those present. After the

^aGAP-71-5652S6, Rev A: Proposal for Design of Expandable Floating Base (Task 2). Akron, Ohio, Goodyear Aerospace Corporation, 13 December 1971.

APPENDIX A

Goodyear personnel departed, the group discussed the study approach, status, and conclusions in some detail. The main topics of discussion are reported on next.

SUMMARY OF DISCUSSIONS

The review group discussed a number of technical and cost aspects of the Goodyear study. The group agreed that the studies to date have not specifically addressed certain problem areas and therefore have not clearly established the technical feasibility of expandable floating platforms. This conclusion was reached on the basis of two fundamental considerations: (1) the response and behavior of rigid versus expandable buoyant elements, and (2) the possible hydrodynamic interference between closely spaced multiple vertical floats of a large floating base. It was agreed that a technology program should be carried out to resolve these technical problems and to develop basic understanding of the response and behavior of expandable floating structures subject to wave action. The group discussions on the technical and cost problems are summarized below.

Rigid versus Expandable Floats

The Goodyear design approach has assumed that as long as the columns and attenuators, constructed of expandable material and with the attenuators filled with water, were pressurized sufficiently high to prevent buckling under wave loading, they behaved as rigid bodies. Following this assumption, scale model testing of the structure was conducted with models simulating rigid elements.

The review group believes that the above basic design assumption has to be either verified or a design model developed that represents the behavior of expandable buoyant elements. Concern was expressed about several aspects of the problem. It is possible that hydrodynamic pressures are transmitted through the expandable-fabric membrane, thus negating or modifying the theoretical response model based on rigid structures. This is especially so if the attenuators include a floating standpipe that is provided to maintain a constant pressure differential between the inside and the outside of the element. This may mean that the attenuators provide additional mass but do not reduce the vertical exciting force by their shape and depth, as now assumed in the rigid-body response model. It is also conceivable that the elastic properties of the pliable floats,

APPENDIX A

particularly the large pressurized sections on which the deck rests, are important in the motion response of the structure. For example, the modulus of elasticity of the fabric materials is some 30 times less than that of steel. This may lead to large extensions of the structure and affect its dynamic response. This elastic-body response is usually neglected in the analysis of floating structures subject to wave action. In this unusual structure, however, the elastic properties of the floats may be important.

The comparative expandable-body and rigid-body responses should be investigated by both analytic and model studies. Because of the unusual type of expandable structures visualized, this work should also include an examination of scaling laws as they may pertain to expandable structures so that the pliable structures could be properly modeled and test results scaled to prototype dimensions.

It was also brought out during the meeting that conceptually there are two basic design approaches possible with expandable structures. One approach attempts to make the expandable structure equivalent to a rigid structure so that conventional design procedures will remain applicable. In this case, the properties of expandable-fabric materials and the use of inflation pressures are considered only as far as necessary to assure the rigid-body behavior of the structure, if this can indeed be shown feasible. Of course, the use of such materials will also result in a lightweight, easily packageable and transportable structure.

The other design approach would feature expandable-body properties of a floating structure, attempting to capitalize on any desirable properties that may be established by a further study program. The purpose of the recommended technology program is thus to develop basic understanding of the behavior of expandable floating bodies, to examine whether an expandable body will behave differently from a rigid body, and whether it has any desirable properties that may make an expandable body the preferred design solution for floating platforms of certain types or sizes. It is conceivable that there is much to be learned about the unique and positive aspects of resilient structures in the sea, particularly for structures that are small enough to be deployed very rapidly.

Hydrodynamic Problem Areas

The configuration of the expandable floating structure has some rather

APPENDIX A

unusual features: the columns are closely spaced, the ratio of spacing to diameter of columns is 3, that of attenuators is 1.5; a full structure may have a regular array of hundreds to thousands of such floats; and the deck and truss structure connecting the columns is rather flexible.

A single model test of a 35 by 6 array of floats of a rather small scale (1/60) was carried out. This model test showed an unexpected amplification of heave motion from front to rear of the model. The group members were not aware of any other model tests of similar close-packed structures and none was discussed by the briefers. The Reynolds numbers are quite different, being of the order of 5×10^3 and 10^6 for the model and the full scale structure, respectively.

Because of the small spacing between floats, the interaction of the viscous wake of a float (vortex shedding, separated flow, etc.) with its neighbors may be important. If this interaction is important, the small model scale and consequent low Reynolds number may yield misleading results.

Another aspect of the problem not completely understood is that of wave reflection. In contrast to most structures, where the entire reflection takes place at a single surface, there is a distributed reflection and absorption of wave energy throughout the whole array of columns. It may be that this distributed wave-structure interaction, combined with the elastic properties of the connecting structure, is important for an understanding of the structure motion response.

The group emphasizes that the scaling of the model results may correctly predict the response of the prototype. However, we do not know any way to determine the magnitude of the scale effects involved. In view of the lack of experience with scale model tests of this unusual type of structure, the lack of a theoretical understanding of the basic hydrodynamic problems discussed above, and the small scale and small Reynolds number of the model, the group believes that there is room for reasonable doubt as to the "scaleability" of the results of the model tests.

The group recommends that further fundamental work should be done on the three basic hydrodynamic problems:

- o interaction of the viscous wake of a float with neighboring floats

APPENDIX A

- o distributed wave reflection and absorption
- o elastic response of the structure to the wave induced forces

This work should include, but not be limited to, model tests at larger scales.

Cost Aspects of Expandable Floating Platforms

The cost information presented to the review group consisted of platform unit costs expressed as a function of aircraft weight and sea states. The unit costs appear rather high in comparison with those of other structural concepts and are greatly affected by the design operational sea states.

The group discussed the available cost data and agreed that further information is of interest in two areas. Within given materials technology, an effort should be made to determine the critical restraints which limit the performance and drive the costs of an expandable floating platform in order to establish the research areas where future effort should be concentrated for maximum payoff. Closely coupled to this is a cost sensitivity analysis where the unit costs are expressed, in parametric terms, as a function of external design requirements, *i.e.*, the payload type and magnitude (including both uniform loads and concentrated loads), the operational and survival sea states, and the motion stability of the platform.

It is also of interest to examine the possible effect of new developments both in materials and fabricating methods on the cost of the proposed structures. One concept mentioned at the group meeting was the possible use of a bladder with an outside cage of fabric. Such bladder-fabric systems would drastically increase the flexibility of the material (by promoting fiber slippage during bending) and possibly reduce its weight, thereby resulting in a substantially more packageable and lighter-weight component. Since weight and cost are often commensurate, this type of material may reduce the cost of expandable platforms.

APPENDIX D - PROPOSAL FOR BARE BONES STABLE
EXPANDABLE FLOATING PLATFORM PROGRAM

1. INTRODUCTION

Goodyear Aerospace submits this unsolicited proposal for the design and fabrication of a 1/3-scale stable floating platform to be used for testing and evaluation by the Office of Naval Research and the Advanced Research Projects Agency. Specifically the proposed program will develop a 50- X 50-ft platform supported by a 5- X 5-ft inflatable float array of 1/3-scale dimensions for wave testing and observation of utility and performance in a simulated ocean environment; Seneca Lake is a tentative site for deployment.

By utilizing the technology developed on previous and current programs, Goodyear Aerospace believes that a stable platform employing an expandable structure can be fabricated and tested in a 1/3-scale size. This scale size will corroborate or modify test results and analysis generated from small scale models while permitting actual evaluation of the structure for a variety of purposes.

The program, exclusive of lake tests, can be executed in nine months. At the end of this period, the platform would be deployed in an inland lake (tentatively Seneca Lake) and be ready for wave tests or demonstration.

2. OBJECTIVES

The program objectives are to:

1. Execute a significant phase of stable expandable floating platform development by design and fabrication of a platform of appreciable scale that may be tested to substantiate dynamic and hydrodynamic math models.
2. Demonstrate the feasibility and utility of expandable structure in a platform that can be assembled and erected on site.

Preceding page blank

The technical objectives of constructing a 1/3-scale platform are to:

1. Measure vertical oscillations of a stable platform of significant scale in various sea states and compare these findings with theory.
2. Test and observe the performance of expandable float-attenuator systems.
3. Examine the packageability and deployment concepts of expandable structures.

3. SCOPE

The proposed bare bones program will encompass the design, structural analysis, and fabrication of a 50- X 50-ft platform capable of supporting a 1500-lb helicopter or other vehicle or cargo of similar weight and weight distribution characteristics in a condition of operational stability at an appropriately scaled sea state of 5. Specifically the program scope will entail the following efforts:

1. Design and fabrication of a nonmodular wood deck to a predetermined stiffness
2. Design, analysis, and fabrication of 1/3-scale expandable hinged float/attenuators
3. Evaluation of reinforced elastomer materials
4. Testing of float critical components
5. Design and fabrication of float stabilizing cable assemblies
6. Assembly and deployment on an inland lake
7. Acquisition of spectral data from inland lake
8. Recommendations for subsequent lake tests and evaluations

4. PLATFORM DESIGN

Because the major development in the expandable floating base concept is associated with the expandable multi-float arrays, it is proposed to fabricate a simple nonmodular deck of marine plywood (see Figure B-1). A

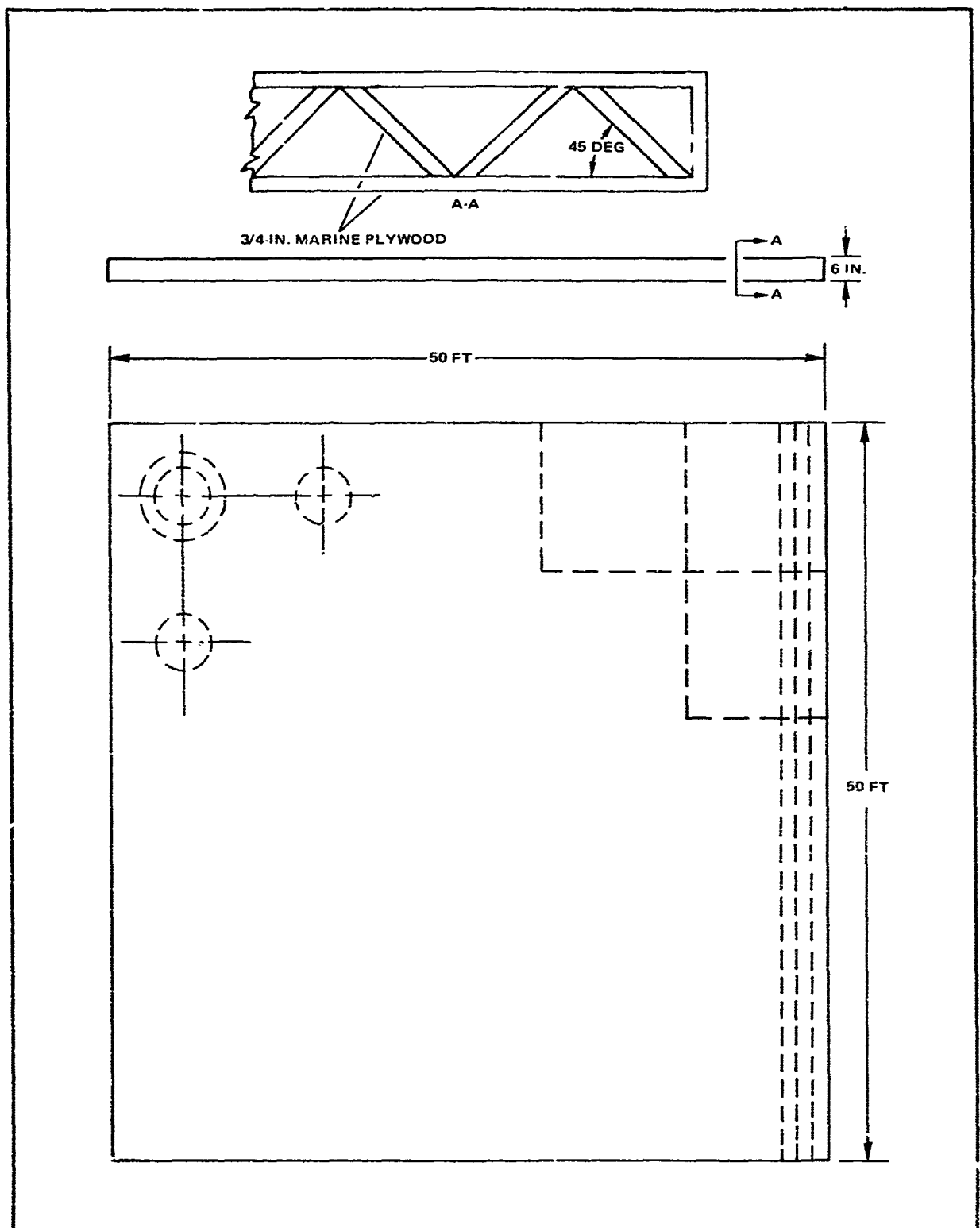


Figure B-1 - 1/3-Scale Expandable Floating Platform Deck

sandwich construction will be utilized with a V-section core to provide shear stiffness in both directions with light weight. The deck hardware will be precut and delivered to the lake site where assembly will take place. Deck stiffness characteristics will be incorporated to simulate the modular sandwich construction previously proposed.

The float/attenuator design is shown in Figure B-2. This hinged one-piece structure will be water inflated below the diaphragm and air inflated in the float above. Pressure can be maintained or varied in both float and attenuator chambers through changes in air inflation on the float. Goodyear Aerospace believes, however, that pressure in the attenuator can be maintained at a low level without disturbing its response under wave action. If this proves true, less costly and less strong fabric materials may be used in this portion of the system.

Goodyear Aerospace anticipates that a two-ply neoprene/nylon square woven fabric will be used to fabricate both float and diaphragm. Such materials were used to fabricate the floats for testing at LUMF in a current contract. The float will be fabricated by bonding most joints except at the hinge where the fabric will be sewed.

A positive pressure system will be used to inflate the float/attenuators with air and water. Internal hoses will permit both filling and draining of each. A simple manifold will be fabricated to monitor and maintain float pressures.

The floats will be joined to the deck structure through a Marmon clamp ring that will secure the upper fabric cylinder to a metal plate bolted to the underside of the deck. Platform stiffness and float column stability will be provided by tension cables except at the deck edges where compression struts will be investigated to obviate an above-deck tension load reaction terminus.

The deck will be prefabricated in 10- X 10-ft sections to which the metal attachment rings will be bolted. The floats then will be clamped to each of these modules. A row of modules will be joined by bolting transversely through bulkheads at the edges of each while they are supported on an inclined frame extending from the shore or a barge. The entire deck can be erected - under calm conditions - and deployed in the water.

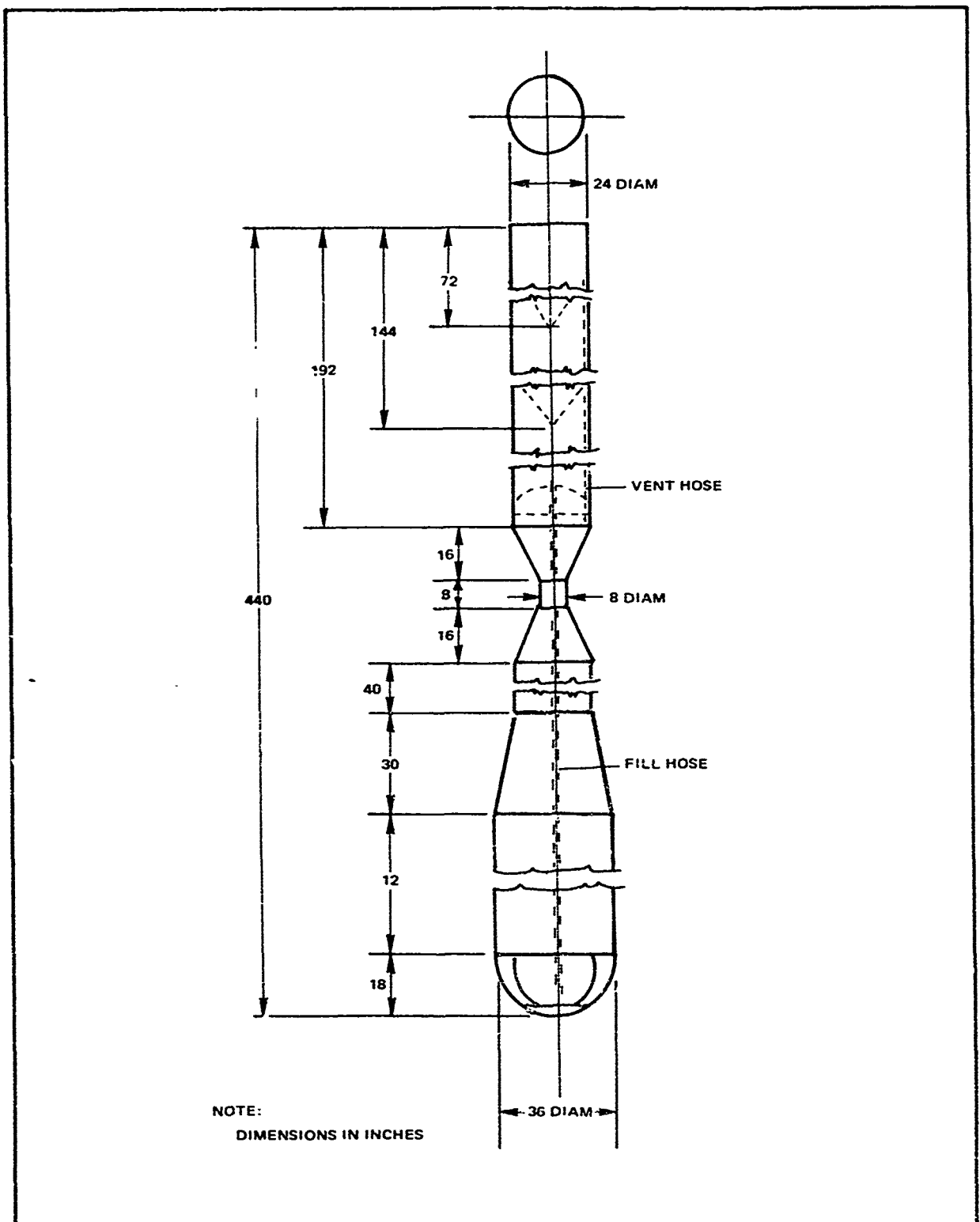


Figure B-2 - Float Attenuator for 1/3-Scale Model

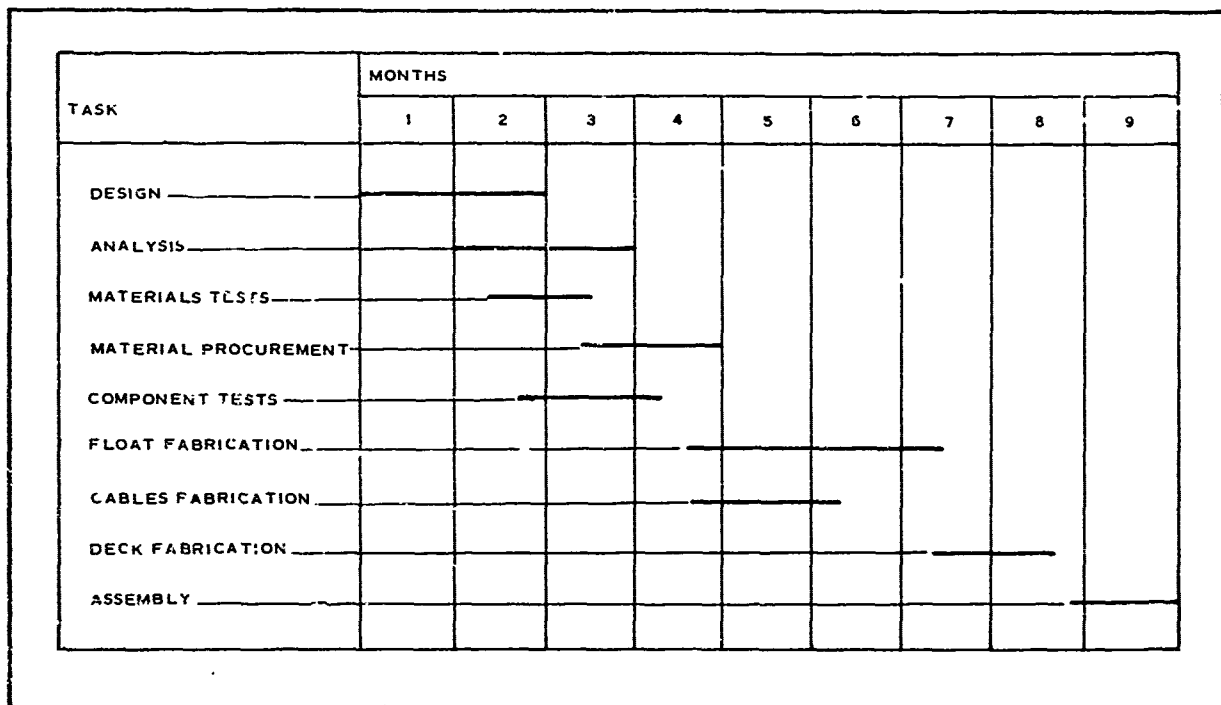


Figure B-3 - Program Schedule

APPENDIX C - SENECA LAKE SURVEY

A site suitable for hydrodynamic testing of a platform of $1/3$ scale was considered. The assumption was made that this platform would be a 7- X 7-ft float array supporting a deck that was approximately 50 X 50 ft. The site chosen ideally would offer wave conditions reproducing the Pierson-Moskowitz wave spectra for the open ocean in an appropriate scale as well as support facilities for assembly, erection, and surveillance of the platform.

The Naval Underwater Systems Center at Seneca Lake was visited and appeared to have the potential for conducting these tests. Seneca Lake is a year-round acoustics test site that is operated and managed by 12 civilians and equipped with two barges, two lighters, and various minor equipment (including a welding and repair shop) that appeared adaptable and useful to platform, erection, and testing (see Figures C-1 through C-3). Range facilities probably could be made available, long-term monitoring of instrumentation could be undertaken by knowledgeable station personnel, and local contractor support at Dresden, N. Y., could be obtained for platform assembly and deployment. Permission to use Seneca Lake for the tests resides with the Army Corps of Engineers and was not pursued.

While no quantitative spectral data for Seneca Lake were obtained, statements by NUSC station personnel indicated that wave heights (double amplitude) of four feet were observed regularly in winter and spring and that wave heights of 8 ft had been estimated. The lake is 36 mi long, 3 mi wide, and 600 ft deep at maximum depth (see Figure C-1). Most frequent high wave states occur between January and April. Wave direction is primarily north or south ($2/3$ of the time) along the long dimension of the lake.

Seneca Lake appeared to have sufficient fetch and depth to produce wave amplitudes and frequencies to reasonably simulate open ocean conditions for the scaled sea states of interest: operational sea state 5 and survival sea state 7.

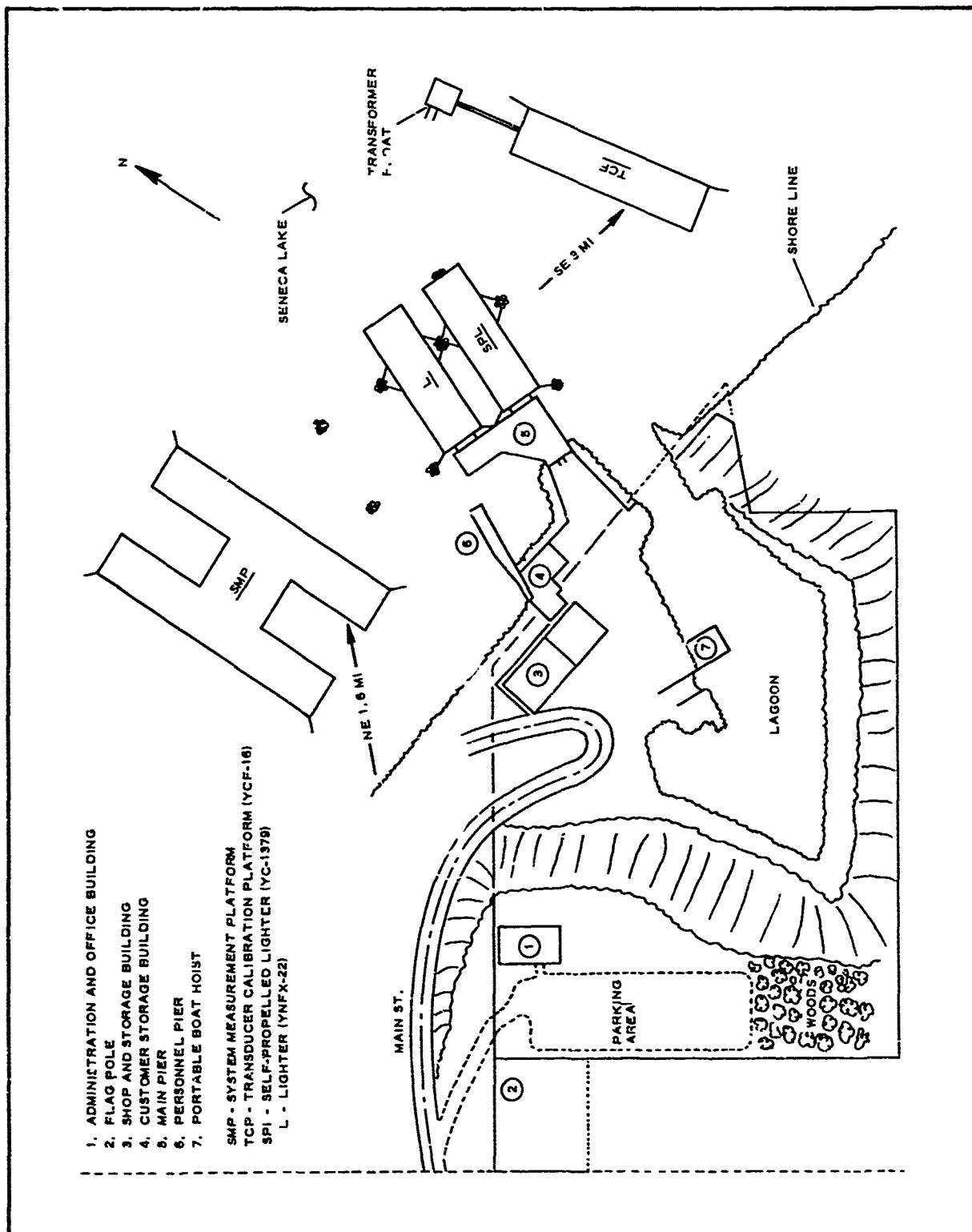


Figure C-1 - Seneca Lake Facility

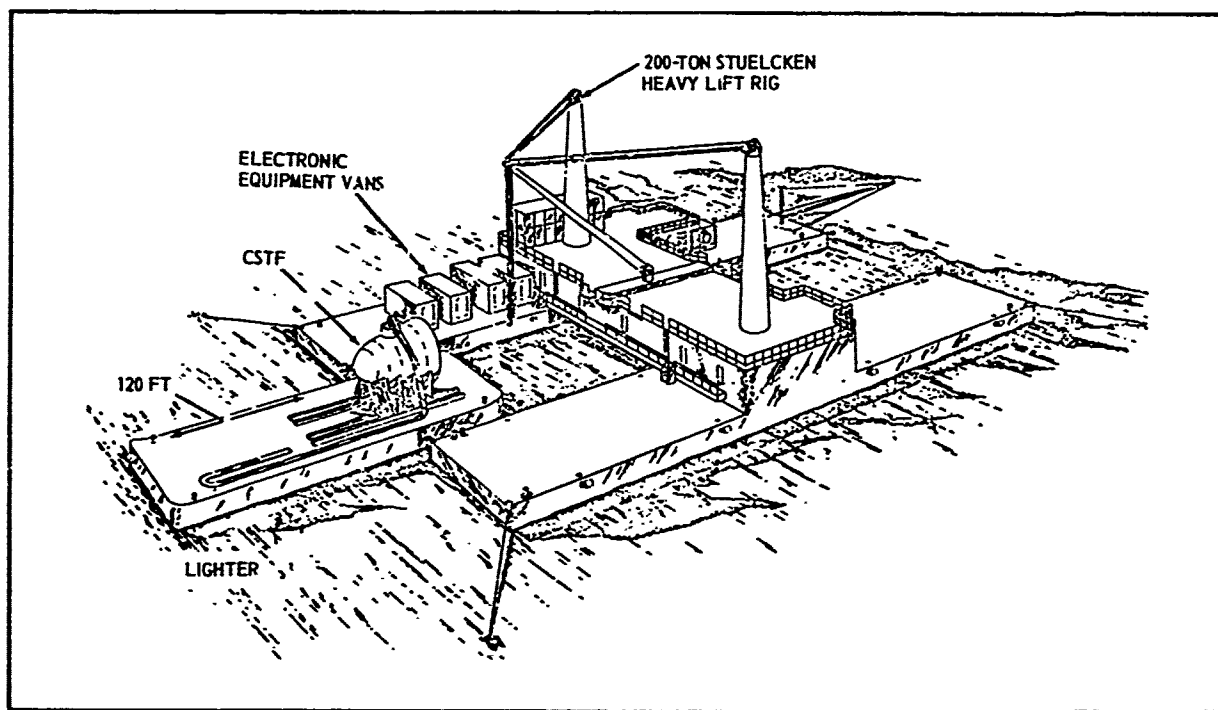


Figure C-2 - Systems Measurement Platform, Senaca Lake, N. Y.

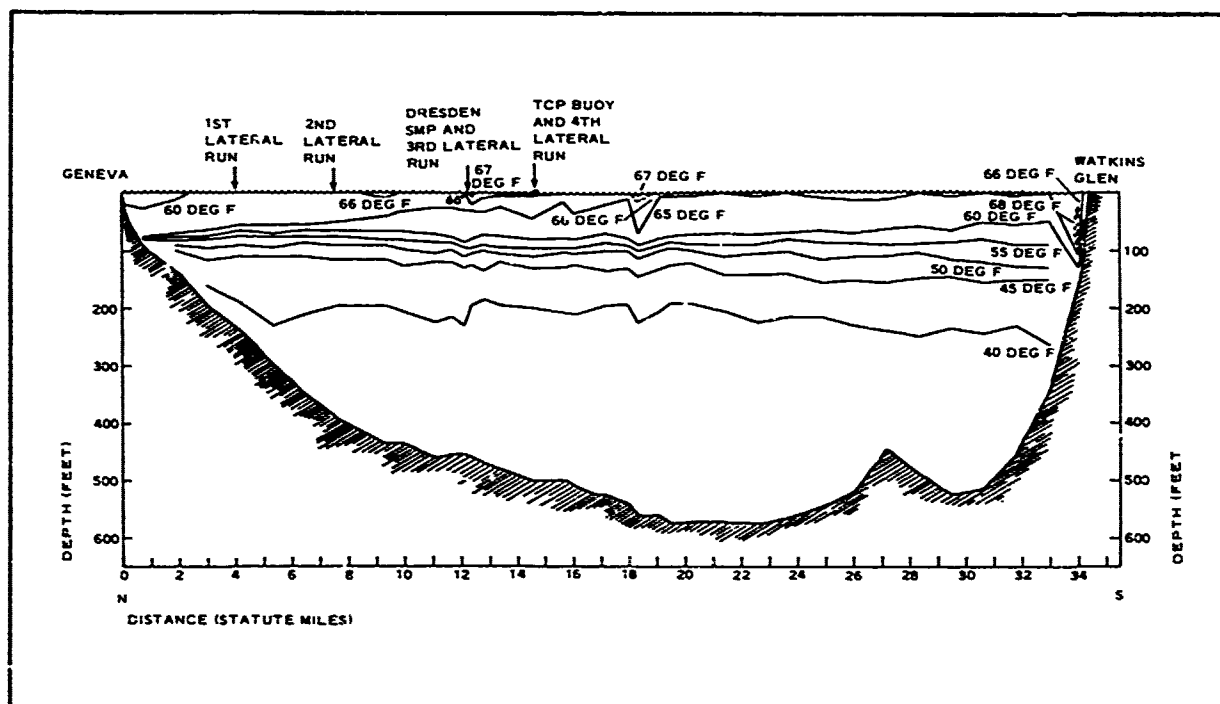


Figure C-3 - Depth Profile of Seneca Lake

APPENDIX D - PLATFORM SPIN-OFF INVESTIGATIONS

During the course of the program, a number of peripheral applications was reviewed to determine if some application of the technologies under development might be applied. These spin-offs are summarized briefly in the following paragraphs.

Personnel at Scripps Institute of Oceanography indicated that inflatable spar buoys might be useful for certain research programs because of packageability, lightweight, and probably ease of deployment. No current research contract was identified, however, with funding to cover an inflatable buoy development program.

The National Data Buoy Center, National Oceanographic and Atmospheric Agency, suggested that a discussion of flexible structure technology applicable to their requirements for free drifting buoys would be useful. Plans to pursue this discussion are underway at present.

Discussions between Goodyear Aerospace and personnel at Woods Hole Oceanographic Institute concerning the problem of mid-ocean docking of the submersible Alvin with the tender Lulu have been held. While stable platform technology does not appear relevant, heavy-walled inflatable bumpers to facilitate docking may have merit. This construction will be evaluated further.

APPENDIX E - LOCKHEED UNDERWATER MISSILE FACILITY*

1. WAVE CHANNEL AND TEST BASIN

The wave channel and test of the Lockheed Underwater Missile Facility is a rectangular, reinforced concrete tank with interior wall dimensions that are 180 ft long by 15 ft wide (see Figure E-1). With a 2-ft free board for waves, the standard water depth in the wave channel is 15 ft, resulting in 25- and 35-ft-deep water in the test basins (see Figure E-2). The 37-ft-deep basin is equipped with an elevating platform that supports missile launching or other special test equipment weighing up to 7000 lb. The 27-ft-deep basin is 40 ft long and, when used with the adjacent deep basin, provides an unobstructed basin 56 ft long with 25 ft of water. Eleven underwater optical viewing ports, 20-in. square, are flush mounted in one wall in the region of the deep basin. The wave channel is filled with fresh water.

2. WAVE GENERATOR AND BEACH

The wave channel is equipped with a 17-ft-high, piston-type wave generator that spans the tank 14 ft from the west end. Wave heights up to 2.35 ft, crest-to-trough, can be generated. Wave periods can be varied from 3.8 to 91 ft. A wave absorbing beach is provided at the opposite end of the channel. The 14-deg sloping face of the beach extends 21 ft into the tank; at this point it is truncated by a vertical face extending nearly to the floor of the channel. The beach is composed of two layers of 2-ft thick stainless steel baskets filled with stainless steel turnings on both the sloping and vertical beach face.

3. PRESSURE SHELL

The wave channel is largely enclosed in a 27-1/2-ft-diameter, horizontal, cylindrical pressure vessel. The vessel is structurally capable of withstanding complete evacuation. The walkway and work area around three sides of the tank are enclosed within the shell allowing access to the edge of

* Abstracted from Lockheed Document LMSC/DO22460).

the channel. The facility is evacuated with three, single-stage, 50-hp vacuum pumps that are installed in parallel. There are two large (10-by 10-ft) equipment hatches located in the top of the shell over the deep pits. Two smaller (36-by 36-in.) hatches in the 10-ft hatches are used for regular handling of test models and small equipment. A traveling crane is installed over the hatch area for handling of this equipment.

4. TOWING SYSTEM

The towing system is installed on the top of the walls of the wave channel. This system is composed of a rigid steel carriage that rides on fiberglass wheels on a pair of ground steel rails. The carriage, shown in Figure E-2, is 9 ft long, 17 ft wide, by 36 in. high and weighs approximately 12,000 lb. The carriage speed is adjusted and maintained by servocontrolled hydraulic motors mounted on the carriage and geared through a single-spur gear against a gear rack. A trailing system provides continuous direct connection of power, air, controls and instrumentation to the towing carriage. Test equipment weighing up to 1200 lb may be installed on the carriage. A six-component balance for measuring forces up to 1000 lb may be installed on the carriage.

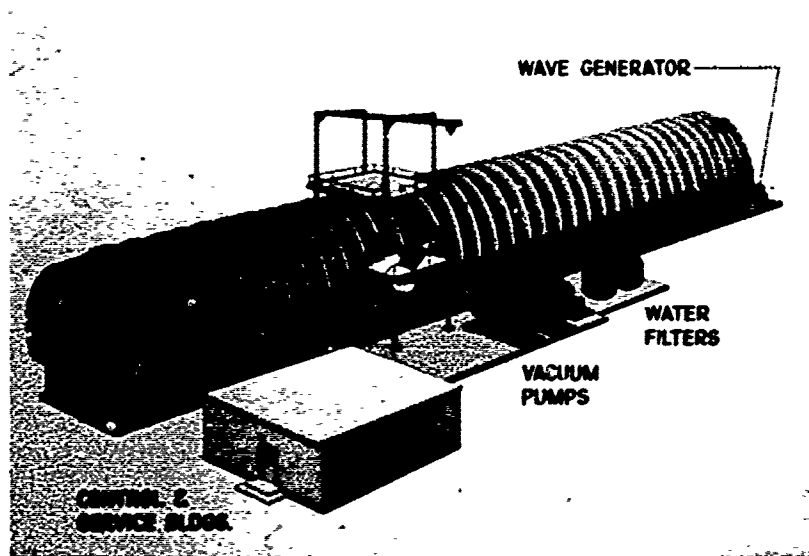


Figure E-1 - Exterior View of Underwater Missile Facility

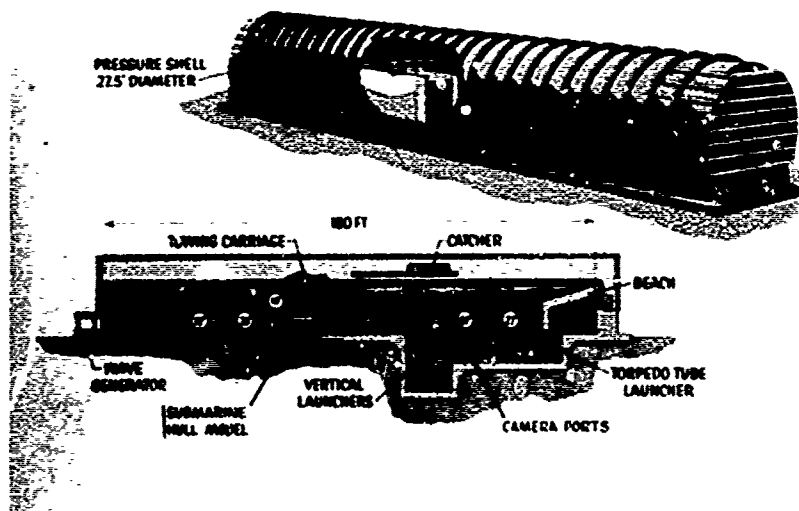


Figure E-2 - Cross Section of Underwater Missile Facility

APPENDIX F - HYDRODYNAMIC TESTS AND
ANALYSIS PROGRAM FOR EXPANDABLE FLOATING
BASES: PART 1 - EXPLORATORY INVESTIGATION OF
INTERACTION EFFECTS ON DECK MOTION

Preceding page blank

STEVENS INSTITUTE OF TECHNOLOGY
DAVIDSON LABORATORY
CASTLE POINT STATION
HOBOKEN, NEW JERSEY

Letter Report SIT-DL-72-1620

July 1972

HYDRODYNAMIC TESTS AND ANALYSIS PROGRAM
FOR AN EXPANDABLE FLICATING BASE

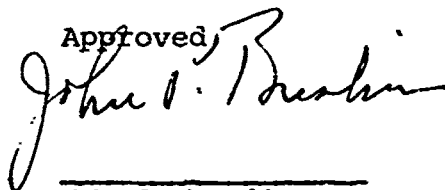
PART 1

Exploratory Investigation
of
Interaction Effects on Deck Motion

by John A. Mercier

Prepared for
Goodyear Aerospace Corporation
Akron, Ohio 44315
(DL Project 3931/745)

Approved



John P. Breslin
Director

INTRODUCTION

A particular, unexpected, result of the earlier¹ model tests program with a 35 by 6 array of floats (which have a nominal scale ratio of 1/57.6) was the "tail-wagging" phenomena where the heave motions increased from front to rear of model. This is an especially significant feature of the performance of arrays of large numbers of such floats. In this phase of work, a variety of experiments have been carried out in order to study certain aspects of the hydrodynamic interaction observed in the motions response tests of the 35 by 6 array of floats. These include wave force measurements on individual element rows of this large array to determine if the variation of wave force, with the model held fixed, is sufficient to produce the motions obtained in the previous test. The character of the response obtained suggests that a cumulative change of an added-mass type of wave force component (similar to that obtained for tests of a 5 by 5 array) may explain the phenomena.

Possible scale effects were investigated briefly because of the possibility of viscous wake interaction due to vortex shedding, separated flow, etc., being dependent on Reynolds number. Since large scale model investigations are liable to be quite expensive, smaller scale tests were undertaken. Although it is not at all clear in what way the interaction effect in this unsteady flow situation depends on Reynolds number (this dependence can only be established by extensive experimentation), it has been found that for many flow situations a modest reduction in size, or Reynolds number, can have as much effect as a substantial increase in size. A model approximately one-third of the size of the 1/57.6 scale model, resulting in about one-fifth of the Reynolds number, was employed. A brief investigation of the effect of reducing the water surface energy by introducing a chemical surfactant to minimize the possible influence of surface tension (Weber's number) was carried out.

Observations of wave reflection, absorption and transmission were made during the course of the wave force measurements on both the present

and the small scale array of models. Wave measurements at certain locations ahead of, outside of, and inside the large array were made and correlated to determine energy relations.

Review of the wave-induced force measurements with the 1/57.6 scale model indicated that the variations in forces correspond reasonably with the variations in motions over the forward and middle part of the island but do not exhibit a continuous increase toward the trailing edge, which was felt to be called for to explain the tail-wagging. Since a suitable explanation in terms of elastic interaction is still not developed, it was decided to re-test the articulated 6x35 array in the 75'x75'x4.5' deep wave test tank (No.2) in order to assure freedom from tank sidewall influences.

Results of all of these tests, wave forces and motion, including comparisons with the previously obtained motions data in Tank No.3 are presented in this report. Complete descriptions of models and measuring apparatus are also given.

An approach to an analytical description of the deck motion, taking deck elasticity into account, is discussed but an explanation of the tail-wagging does not appear to follow from this analysis.

Plans for the comprehensive test program to determine the effects of variations in parameters such as float spacing and shape, wave frequency and height, deck rigidity and number of floats on the motions of the platform.

MODELS AND APPARATUS

ARTICULATED MODEL

A preliminary design for float-attenuator shape was developed on the basis of a simplified hydrodynamic analysis and a particular limiting vertical motion criterion. The selected float had a relatively shallow draft and large diameter near the lower end. No interaction effect was anticipated in selecting the float shape. Because of this omission, and because the hydrodynamic analysis is not sufficiently accurate except for extremely slender floats, the model does not perform according to the desired specifications. This is not necessarily a crucial disadvantage since it is presently evident that interaction effects must be studied in greater detail. A scale ratio of 1/57.6 was selected; the full-size float has 6-ft diameter at the waterline while the model was fabricated with 1 $\frac{1}{4}$ -in O.D. plastic tubing.

A photograph of the articulated model of 35 rows of 6 floats each, undergoing tests in Tank No.3, is shown in Figure 1. The 210 float elements were made of plexiglas tube and sheet according to the sketch shown in Figure 2. Solvent-bonding was used to assemble the parts in a water-tight fashion.

The float elements were connected in sets of 6 to an aluminum channel, as shown in the photograph of Figure 3. The channel was lightened considerably by drilling holes and the tubes were ballasted with brass weights and lead shot so that a row floated at the correct draft and roll angle, with a small positive roll stability. This was checked by floating the sets in a fish tank while lightly restraining them against pitching (the rows are very unstable in pitch).

The rows are connected to each other by linkages consisting of 2 $\frac{3}{4}$ "x1 $\frac{1}{2}$ "x0.050" aluminum strips with 1/8" diameter reamed holes spaced 3 $\frac{1}{4}$ " center-to-center. The linkages roll on 0.1245 diameter x 1/8" long shoulder screws which are secured to light posts at the ends of the rows of floats. The vertical spacing of the linkages is 4 inches. The floats

are arranged in an equilateral triangular fashion, as indicated in the sketch of Figure 4.

Although roll stability of the articulated model is present because each row is suitably ballasted, the pitch behavior is unstable because each row is unstable and the 4-bar-linkage connections provide no restraint unless one row is held so that it can move only vertically. The center row (number 18) was restrained by a vertical tube which slides in a pair of linear-motion ball bearings, as indicated in the sketch of Figure 5.

The linear motion bearing is secured to a light weight (approximately 3 lbs) carriage which rides on low-friction wheels on a monorail about 12 inches above the water, permitting effective freedom of surge.

The vertical motions of five locations along the length of the model, at rows 1, 9, 18, 27 and 35, were measured by systems consisting of a long (approximately 8 ft) vertical string between the measurement point on the model and quadrant connected to the shaft of a rotary variable differential transformer (RVDT). These RVDT's have very low friction ball bearings and the quadrants are very slightly counterbalanced to assure that the string remains in tension.

Motions tests were carried out in November 1971 in DL Tank No.3, which is 300-ft long, 12-ft wide and 6-ft deep. Tests were conducted both in regular and irregular waves. The irregular waves have Pierson-Moskowitz type spectral-energy distributions with significant wave height (full scale) of 6.9, 10, 15 and 30 ft (corresponding to Sea States 4, 5, 6 and 7).

Additional tests were carried out in June 1972 in DL Tank No.2, which is 75-ft long, 75-ft wide and 4.5-ft deep, to check whether tank sidewall influences were appreciable. These tests were undertaken after the measurements of wave-induced forces were carried out with the same floats, secured to a different mechanism, so the floats and articulating linkages were completely disconnected and reassembled between the two sets of tests in the two tanks.

Wave elevation measurements were made at three locations during these tests: a) at a location about 10-ft forward of the "bow" of the

platform model and about 1-ft abeam of the model centerline (the bow of the model was situated 35 feet from the wavemaker; b) at a location about 1-ft abeam of the side of the model at its midlength and, c) at a location about 10-ft aft of the model's stern and about 1-ft abeam of the model's centerline. Wave measurements were made without the model in the test tank for all wavemaker settings used for the test program so that reference measurements without possible reflection effects would be available.

Spring lines were connected to the bow and stern to restrain the model against yawing or excessive drifting. The bow line was connected, through two ordinary rubber bands in series, between the deck of the model and a fixed point at the same elevation about 10-ft forward of the bow. The stern line was connected at the deck and over a pulley about 10-ft aft of the stern, to a 0.10-lb weight. The light tensions in these lines are considered to exert very little influence on the motions of the model.

WAVE-INDUCED FORCES

Large Model

In order to study the effect of interaction on wave-induced forces to correlate with motions measurements of the articulated model, the same floats used in the motions tests were adapted for use in a restrained model rig.

The sets of six floats were disconnected from the transverse channels solvent bonded to 1-inch square times 30-inch wide plexiglas bars. The bars were secured to a pair of 2"x4"x12' aluminum strongbacks which were, in turn, connected to the bridge spanning the 75-ft length of DL Tank No.2. A photograph of the setup is shown in Figure 6. The spacing and staggered array of the floats is the same as for the articulated motions model.

One row of floats is not connected to the strongbacks but is coupled to a force balance system for measuring vertical and horizontal wave forces as indicated in Figure 6. This row may be located in any desired position, while the "fixed" rows are also relocatable so that the forces acting on any one of the 35 rows of floats can be measured.

Wave elevation measurements were made at several locations during these tests: a) at a location 10-ft forward of the row of floats nearest the wavemaker and about 1-ft abeam of the model centerline (this first row was situated 35 feet from the wavemaker); b) at a location 27-in from the model centerline directly abeam of the row of floats on which measurements were being made; c) on the model centerline midway between the measurement row and the row following (or 1.5-in aft of the last row) and, d) at a location 4-ft aft of the last row of floats and about 1-ft abeam of the model centerline. As for the motions tests, wave measurements were made without the float models present for all wavemaker settings used for the test program.

Small Model

In order to study the effect of model size on hydrodynamic forces, an array of 35 rows of 6 each of smaller scale models was constructed. The scale ratio relative to the larger model was $7/20$, corresponding to the ratios of the diameters of the surface piercing tubes, $7/16:5/4$. The shape of the floats, similar to that of the large models, was produced by thin-walled wax castings. A photo of a row of small models, in company with the large models, is shown in Figure 7. The damping collars at the top of the conical part of the float are stiff mylar film glued to the tube.

The floats were attached in rows to 30-in wide bars (except for the row used for measuring forces) which were, in turn, attached to a pair of 2"x4"x5' aluminum strongbacks which were connected to the bridge in the same way as for the large model tests. The spacing ratio and staggered array are the same as for the large model.

The measurement row of floats was connected to a force balance system, shown in Figure 8, for measuring vertical and horizontal wave forces. This row of floats could be moved, as in the tests with the larger model, so that forces could be measured for any desired row of floats.

Because of the smaller size of this model, it was not possible to measure wave elevations between the rows of floats. The wave measuring

probes available were too bulky. Wave elevations were measured at three locations: a) 10-ft forward of the row of floats nearest the wavemaker and about 1-ft abeam of the model centerline (the first row was situated 35 feet from the wavemaker for the small model tests also), b) at a location 14-in from the model centerline directly abeam of the row of floats in which measurements were being made, and d) at a location 4-ft aft of the last row of floats and about 1-ft abeam of the model centerline. Again, wave tests were done at wavemaker settings for which wave measurements with the model present were available.

SURFACE TENSION EFFECT TESTS

In view of the decision to carry out scale effect tests at smaller scale ratios, to limit the expense of the investigation, it was deemed important to consider the effect of liquid surface tension on the test results. As it was considered impractical to contaminate the entire surface of the wave tank with a surfactant since this would require draining, re-filling, and extensive subsequent filtration to restore the original water quality, a program of tests was undertaken in the small circulating water channel depicted in Figure 8a. A wavemaking apparatus was installed at the nozzle end of the test section. The diverter plate at the settling chamber end of the test section acts as a partially effective wave beach. Wave frequencies were limited to the range 0.70 to 1.71 Hz.

The complete model could not be simulated in the small test section. One row of floats with the force balance used for the complete wave tank tests was installed about 4.5 feet from the wavemaker.

Surface tension was varied by adding a liquid detergent (Trend) in various quantities. A measure of surface tension was obtained by observing the height to which the water rose in a 0.047-in I.D. capillary tube. The levels of surface tension were covered: a) clear (chlorinated and filtered) tap water, b) water with 7-oz detergent added (to 380 gallons of water), and d) water with 12-oz detergent added. The corresponding capillary tube heights were: a) 0.9-in, b) 0.65-in, and c) 0.55-in.

Wave measurements were again made with resistance-type wave gauges. Calibrations and measurements without the models present were made for each water condition.

MEASUREMENTS AND DATA RECORDS

The vertical motion transducers used for the articulated model tests were described on page 4.

Force balances were of the stiff-spring-element type, with deflections sensed by linear variable differential transformers. For the large model force tests, a pair of one-component balance were connected by a right-angle bracket. The horizontal force balance had a nominal spring rate of 10-lb force for 0.005-in deflection, while the vertical force balance rate was 10-lb force for 0.050-in deflection. These balances are shown in Figure 6.

For the small model force tests, a four-post, two-component force balance was used as shown in Figure 8. The approximate force rates of this balance as used are: lift, 3-lb for 0.004-in deflection, and drag 4-lb for 0.002-in deflection.

Wave gauges were of the variable resistance type, with electronic linearizing circuits built-in.

All measurement signals were amplified and recorded with an ultra-violet light oscillograph. These oscillograms were analyzed, manually, for amplitudes of oscillatory motions, waves, and/or forces. For the case of the first sequence of tests with the articulated model only, measurements were also recorded on FM magnetic tape, to be available for later playback, analog-to-digital conversion, and more complete analysis of regular and irregular wave tests.

TEST PROGRAMS

The general procedure for carrying out these tests was to make the mechanical setup of instrumentation, calibrate equipment and test.

Wave tests were carried out with time between starting tests sufficient to permit disturbances from the previous run to die out. For regular wave tests in Tank 2 this amounts to about five minutes for all but the shortest waves, which require more time to decay while for tests in Tank 3 the necessary time is seven to ten minutes. For irregular wave tests, the required time is substantially greater.

The "standard" nominal wave height for these tests was one inch, peak-to-trough. For a few frequencies other wave amplitudes, both smaller and larger, were used to investigate the possibility of significant non-linear dependence on wave elevation.

The tests were conducted at different calendar times, as indicated in the following table.

<u>TEST</u>	<u>DATE</u>
1. Articulated model motion tests in Tank 3	Sept 20 - Oct 1, 1971
2. Large model force tests in Tank 2	May 11-18, 1972
3. Articulated model motion tests in Tank 2	June 1-6, 1972
4. Small model force tests in Tank 2	June 12-15, 1972
5. Small model force tests in circulating water channel (surface tension effects)	July 25-27, 1972

RESULTS

MOTIONS TESTS

Articulated model motions tests were carried out with regular waves in the 75-ft wide Tank No.2 to compare with results previously obtained in the 12-ft wide Tank No.3. Presumably if any effects of tank wall interference were present for the first series of tests, they will not be present in the tests in the wide tank.

Results in the form of heave amplitude divided by wave amplitude, Z/ζ (in/in) for Rows 1, 9, 18, 27 and 35 are given in Figures 9 to 13, respectively, as a function of frequency. The repeat test results of Tank 2 are given with different plotting symbols to distinguish them from the previous Tank 3 results. The differences between the results of the two tests are not great and, in particular, both sets of data show substantial "tail-wagging." The results have been cross-faired by means of "carpet-plotting" and the smoothed curves are presented in the composite Figure 14, as well as in the data Figures 9 to 13.

FORCE TESTS

Large Models

Force measurements results, in the form of oscillatory heave force amplitude divided by wave amplitude, Z/ζ (lb/in), for Rows 1, 9, 17, 27, and 35 are given in Figures 15 to 19, as a function of frequency. Surge force results are given in Figures 21 to 25. Results for force measurements on a single row of floats, without other rows present, are given in Figure 20 for heave and Figure 26 for surge force.

Cross-faired results, in the form of carpet plots, are given in Figures 27 for heave and 28 for surge, and these smoothed curves are also presented in the data Figures 15 to 24.

It is interesting to note that the heave force, shown in Figure 27, does not increase dramatically at the stern as does the heave motion, shown in Figure 14.

Small Models

The force measurements data obtained in the tests in the large tank are presented in the corresponding figures for the large models. Results have been expanded by Froude's Law so that small model data are expressed in large-model-equivalent forces and frequencies. Different plotting symbols are used to distinguish small model results from large model results. A composite carpet plot of the heave force is given in Figure 29 for these small model results.

Surface Tension Effects on Small Models

Results of wave-induced force measurements carried out in the circulating water channel are scattered to such a great extent that it is considered preferable to omit them from this presentation. The reason for the inconsistency is not clear but may be associated with wave reflections and other irregularities in the generated waves in this relatively short facility with unusual end characteristics.

WAVE MEASUREMENTS

Although wave measurements made in the tests of the restrained large model are insufficient to define the energy diffraction and transmission associated with the complete wave field, they do provide some interesting information on interaction effects.

Wave elevation measurements at several locations internal to the float array, and along its centerline, are shown in Figures 30-33 for a few of the wavemaker settings used in the tests. The "regular" waves

generated in the tank are not precisely two-dimensional, uniform waves: they vary somewhat in amplitude both in the direction of wave motion and in the direction parallel to the wave crests so that several wave sensors situated at different location will not, in general, record exactly the same wave amplitude, even if there is no model present to disturb the waves. In addition, the waves may vary slightly with time. Oscillograms are read by averaging a section of the record over several (three to eight usually) cycles of "steady-state" conditions which are reached about ten cycles after the first wave of the generated group passes. Each wave record is self-consistent but, since wavemaker mechanical settings may not have been repeated exactly for each test, the comparisons between separately conducted tests should not be expected to be exactly consistent. The results presented are representative of all the measurements made and certain trends can be noted which will be outlined in the discussion of this report.

DISCUSSION

HEAVE FORCES AND MOTIONS

Comparison of Articulated Model Tests

The results given in Figures 9 to 13 demonstrate that the previously obtained results are repeatable. Although the "scatter" of the data points even within a given test program (Tank 3 or Tank 2) is rather large, there is sufficient consistency between the tests to say with confidence that the measured motions — in particular the unexpected "tail wagging" — are characteristic of this articulated model (and its associated apparatus, viz., pitch-restraining heave mast at Row 18 and low-tension spring lines at bow and stern). The motions recorded in the tests in Tank 3 were not importantly influenced by tank sidewall effects.

The carpet plots of Figure 14 exhibits the dependency of the deck motions on position along the length of the model and frequency. The tail-wagging phenomena are shown clearly for all higher frequencies. The frequency range covered here corresponds to full-scale frequencies for which significant wave energy exists for sea states with significant wave height $H_{1/3} < 15$ feet.

Correlation Between Heave Force Measurements and Motions

Large Model Heave Force

The heave force results obtained in the large model, Figures 15-20, and carpet plot in Figure 27, show important interaction effects on the vertical wave-induced force. For instance, for $f = 1.2\text{Hz}$, the force in the middle of the model is 42% greater than that at the bow, while the force at the stern is 36% higher. Comparing Figures 15 and 20, it is found that the force at the bow is 20% higher than that for an isolated model row. These results are somewhat similar to those reported for the tests with the smaller (five rows of five) array except that the outside rows (front and back) are different from each other and different from isolated float results.

The fore-and-aft asymmetry of the wave-induced heave force suggests that the interaction may be influenced by either free-surface-type frequency dependent effects or, perhaps, some viscous wake effects. If the interaction were purely potential in character and unaffected by wave diffraction effects (as is expected for slender bodies in relatively long waves), a linearized representation of the interaction effect on the vertical force due to waves on the j^{th} float due to the presence of the other floats might be expressed, formalistically at least, as

$$\left(\frac{Z}{b}\right)_{j,K} = \left(\frac{Z}{b}\right)_{j,0} + \sum_{\substack{k=1,K \\ k \neq j}} W_{jk}(x_k - x_j, y_k - y_j; \frac{Z}{b})$$

where $\left(\frac{Z}{b}\right)_{j,0}$ is the vertical force due to waves on the j^{th} float as though it were isolated,

and W_{jk} expresses the interaction effect of the k^{th} float on the vertical force due to waves on the j^{th} float.

The interaction is expressed simply as a function of the distance between the two floats, which would be valid under the assumptions stated of negligible free surface and viscous wake effects. This representation indicates that the interaction effect should be symmetrical, fore-and-aft. It is not possible, at this time, to say whether the asymmetrical characteristic of the force is due to free-surface or viscous wake influence.

Dynamic Motions Analysis

The response of multi-degree-of-freedom dynamic systems to constant frequency exciting forces can, in general, be expressed as a sum of normal mode components (cf., Biggs²), which can be expressed for a beam in the form

$$z(x,t) = \sum_n^n A_{n,t} \cdot (DLF)_n \varphi_n(x)$$

where

$\varphi_n(x)$ = is the normalized modal shape of the n^{th} mode of oscillation of the structure

$$A_{nst} = \frac{\int p_1(x) \varphi_n(x) dx}{\omega_n^2 \int m \varphi_n^2(x) dx}$$

$p_1(x)$ = distributed exciting force

m = mass per unit length of beam

ω_n^2 = (natural frequency)² of n^{th} normal mode

$$DLF_n = \frac{1}{1 - (\omega/\omega_n)^2} ; \text{ for simple harmonic exciting force with frequency } \omega, \text{ neglecting damping}$$

Normal mode shapes, φ_n , may be characterized as symmetrical and asymmetrical about the midlength of the deck (beam).

A set of normal modes and natural frequencies for a particular assumed island structure and float-attenuator size have been calculated by J. Rice of Goodyear Aerospace.³ The first eight elastic "free-end" modes of oscillation were found to have natural frequencies corresponding within 0.23% of the pure heave natural frequency!

While these results are applicable to the particular large island which Rice considered, it seems probable that the articulated model, with its essentially negligible elastic interconnections, will also have normal modes whose frequencies correspond to the free heaving frequency of the float elements. Thus the dynamic load factors (DLF's) for all modes, symmetric and asymmetric, will be essentially the same. Then, according to the definition of the amplitude function, A_{nst} , the motion should correspond closely to a weighted sum of the distributed load. A detailed evaluation of the response would require significant numerical work but, intuitively, it does not seem reasonable to expect the modest asymmetry of the wave induced heave force (Figure 27) to produce the pronounced asymmetry of the heave motion response (Figure 14).

Surge Force Interaction

Results given in the carpet plot (Figure 28) indicated virtually no influence of position in the array on surge force due to waves at low frequencies, but as much as 43% increase (monotonic with distance from the bow) at $f = 1.4$ Hz.

There is a difference between the results of the isolated row of floats and the floats in array. Comparing Figures 21 and 26, for instance, it is seen that the isolated row of floats experienced higher forces than the floats of Row 1. Row 35 shows somewhat higher forces than the isolated row, however at least for higher frequencies.

Scale Effects

Force measurements shown in Figures 15 to 26 include the small scale model results. They are seen to be somewhat lower, in general, than the larger model results.

The scale effect exhibited may be due to either viscous effect (Reynolds Number) or surface tension effects (Weber Number). The trends of the results are, in any case, quite similar. Differences may be partly attributable to experimental error. The magnitudes of the oscillatory forces being measured on the small models are of the order of 0.001 lbs: such small measurements are not routinely executed in hydrodynamic laboratories such as Davidson Laboratory.

Wave Measurements

The results given in Figures 30-33 do not permit easy generalization, except that the amount of wave energy either dissipated or diffracted by the rigidly-fixed array of floats is not very significant for any of the tests conducted. The wave elevation at the location 4-ft astern of the model is not significantly reduced below what would be expected if the model were in place. This observation is independent of wave frequency.

The wave elevation inside the array of floats is substantially increased, probably because of the requirements of continuity of flow within the nest of obstacles.

PLANS FOR COMPREHENSIVE TEST PROGRAMS

The results of the exploratory tests have not yielded an explanation of the interaction effect, specifically the "tail-wagging" phenomena, associated with the articulated model motions tests. The force measurements reveal that a significant hydrodynamic interaction effect exists which would be expected to importantly influence the heaving response even if the tail wagging behavior were not observed. Consequently, it is necessary for design purposes to systematically investigate the effect of hydrodynamic interaction on the heave motions response of resiliently connected arrays of floats.

An experimental program to study the influence of float center-to-center spacing, expressed in terms of waterline diameter, float slenderness, deck rigidity, size of array, externally provided damping, and yaw-restraining spring-line restraint, has been developed and will be carried out during August, 1972.

Three sets of floats, having different spacing ratios (3 to 1, 3.75 to 1 and 4.5 to 1) are being built. Each set will consist of seventeen rows of ten floats each. The ten floats in each row will, in this case, provide ample roll stability: these rows consist of sufficiently stiff, yet very light weight, T-sections connected to the cylindrical floatation tubes.

The seventeen rows will be connected by two sets of plastic splines, one pair at each gunwale, which provide sufficient pitch restraint for the otherwise unstable rows of floats, and which simulate a specified deck elastic beam-like behavior. The full-size deck stiffness is assumed to be equal to a plate EI of 80×10^6 lb-ft² per ft of deck width. This stiffness scales according to the 4th power of the scale ratio, which is taken to be 1/48, with 1½-in diameter model floats corresponding to 6-ft diameter full-size (waterline diameter). For the middle-spacing set of floats, an additional simulated deck rigidity, twice as large as the nominal value, will be tested by using plastic splines of the same thickness and spacing but each twice as wide.

The float attenuators to be used are thin-walled wax castings with aluminum tubes at their upper ends. The shapes were selected so that their calculated heave responses, assuming no interaction effects, would be the same. The maximum diameters are 1.5 and 1.8 times the waterline diameter, while the corresponding full-scale drafts are 96 ft and 78 ft, respectively.

Since the full-scale floats are expected to require a hinge to alleviate the bending loads due to wave action on the upper part of the float, it has been decided to simulate these hinges for the present comprehensive test program. The hypothesis that the attenuators will oscillate in harmony under the action of waves will consequently be tested at this early stage. The hinges are made of very flexible silicone rubber.

The attenuators are to be ballasted so that when flooded with water, they have effectively neutral buoyancy and the center-of-gravity slightly below the center-of-volume so that a small positive pendular restoring moment exists. The attenuators and hinges can be interchanged from one row of floats to another.

Tests in regular waves to determine the heaving motions will be carried out with all possible combinations of floats and attenuators, plus the increased deck stiffness for the intermediate-spacing floats with one of the sets of attenuators.

An auxiliary investigation will be made of the motions of a smaller array of floats, 10 rows of 10 each, to explore the effect of extent of the array on the interactions.

Other auxiliary investigations will include a brief study of the effect of externally applied (not from appendages immersed in the test tank) viscous damping for a range of frequencies, including as nearly as possible the heaving natural frequency. Some tests will also be carried out without the yaw restraining spring lines in place.

Results will be compared with theoretical calculations and, it is expected, sets of interaction coefficients derived.

REFERENCES

1. Mercier, J. A., "Hydrodynamic Analyses and Exploratory Model Tests for an Expandable Floating Base," Stevens Institute of Technology, Davidson Laboratory Letter Report SIT-DL-72-1579, January 1972.
2. Biggs, J. M., Introduction to Structural Dynamics, McGraw Hill Book Company, New York, 1964.
3. Goodyear Aerospace Corporation, "Phase I Technical Report - Expandable Floating Bases," GER-15048, 15 November 1970, pp.206 et.seq.

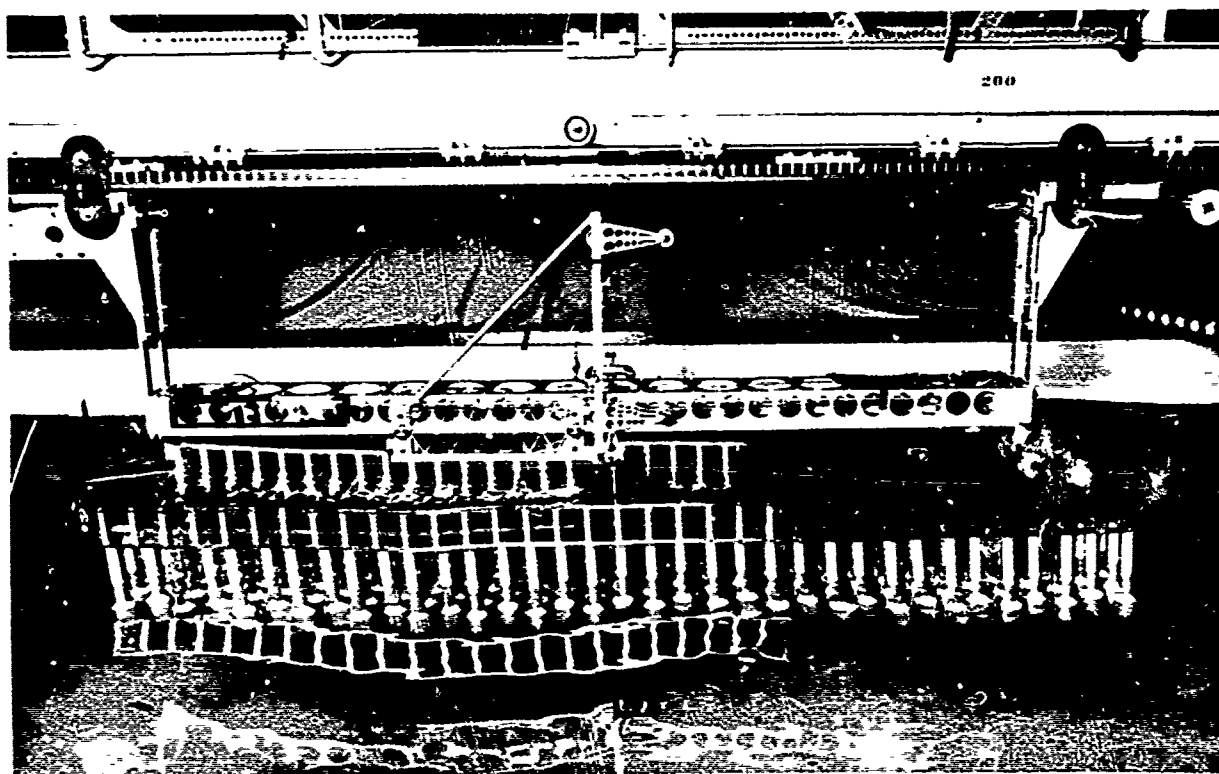


FIGURE 1. ARTICULATED MODEL, 35 ROWS OF 6 FLOATS EACH,
BEING TESTED IN TANK 3

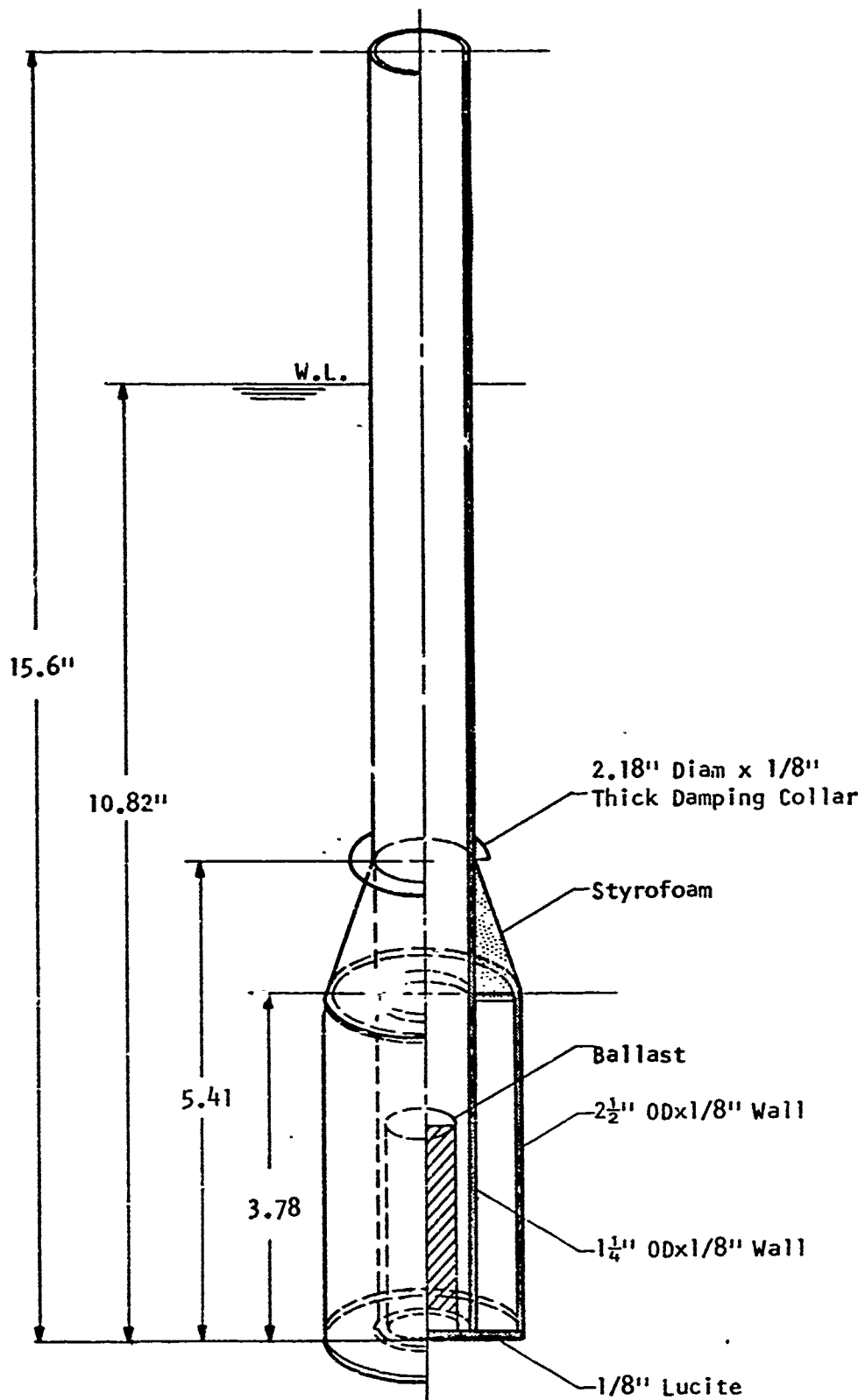


FIGURE 2. SKETCH OF FLOAT FABRICATION METHOD

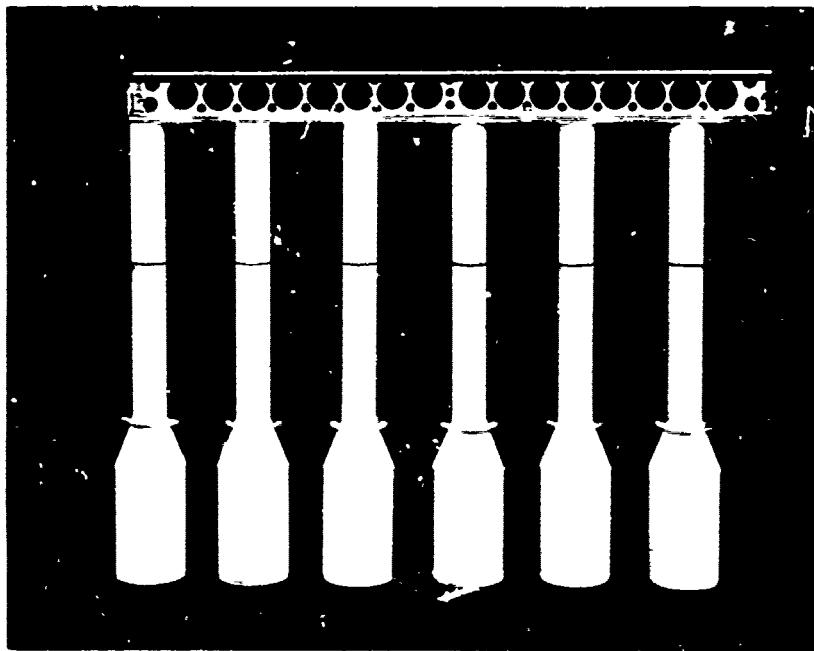


FIGURE 3. PHOTOGRAPH OF SET OF 6 FLOATS CONNECTED TO TRANSVERSE BEAM
(Lightened Channel)

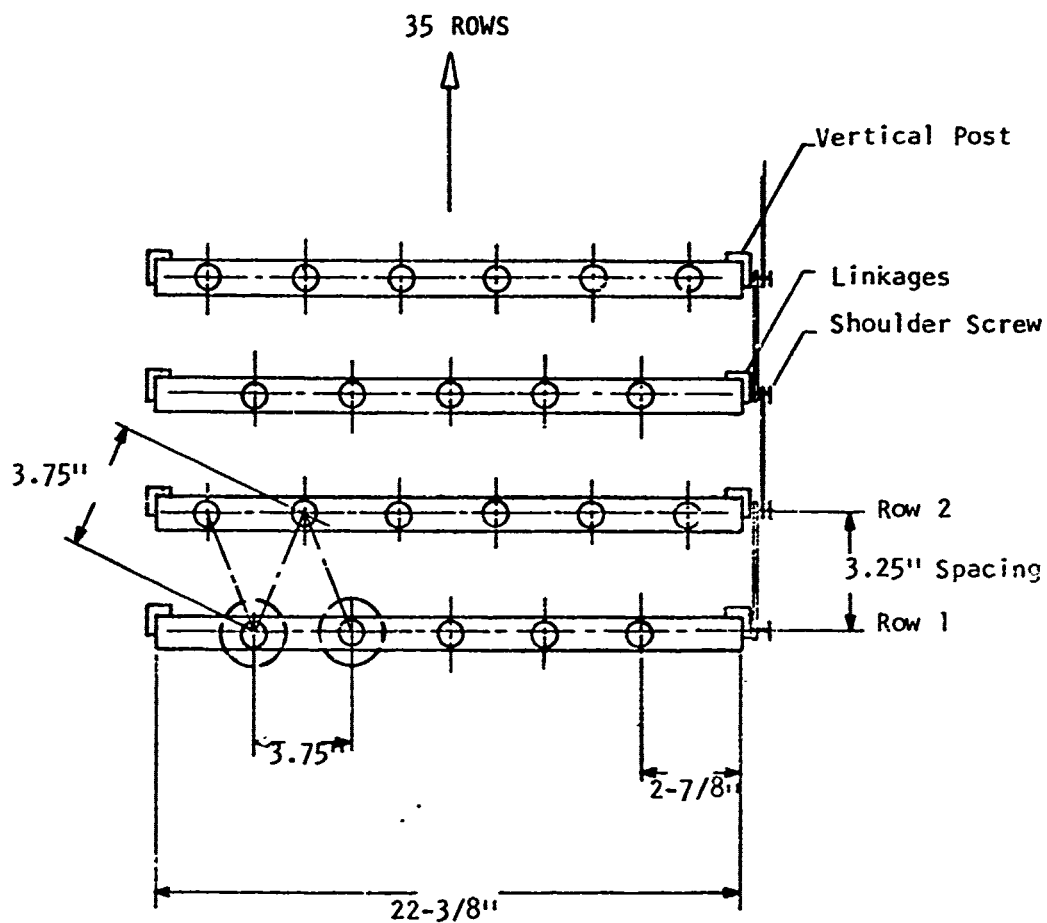
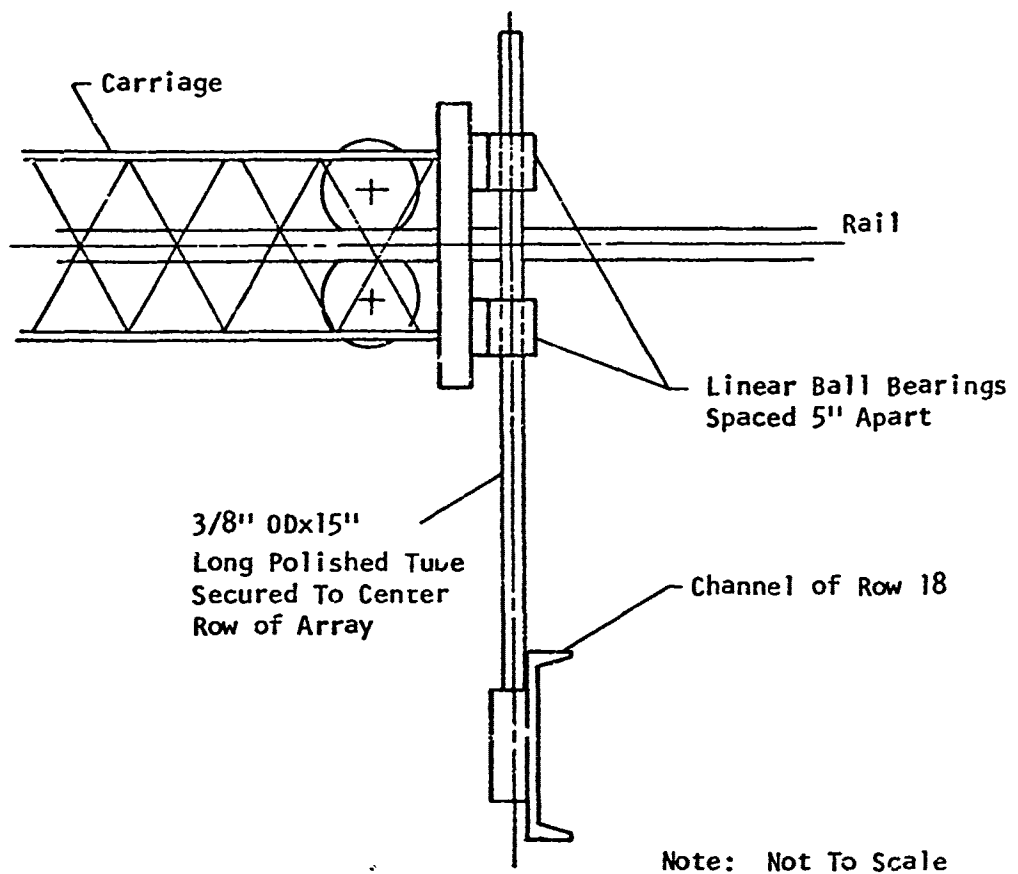


FIGURE 4. ARRANGEMENT AND SPACING OF FLOATS



Note: Not To Scale

FIGURE 5. SKETCH OF HEAVE MAST-PITCH RESTRAINING DEVICE

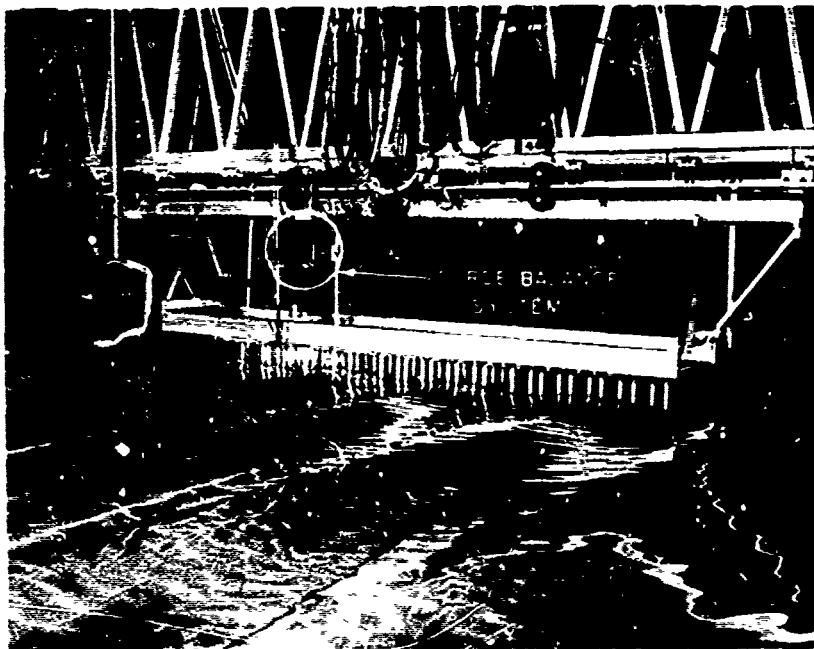


FIGURE 6. PHOTOGRAPH OF TEST SET-UP
FOR WAVE-INDUCED FORCES ON LARGE MODEL

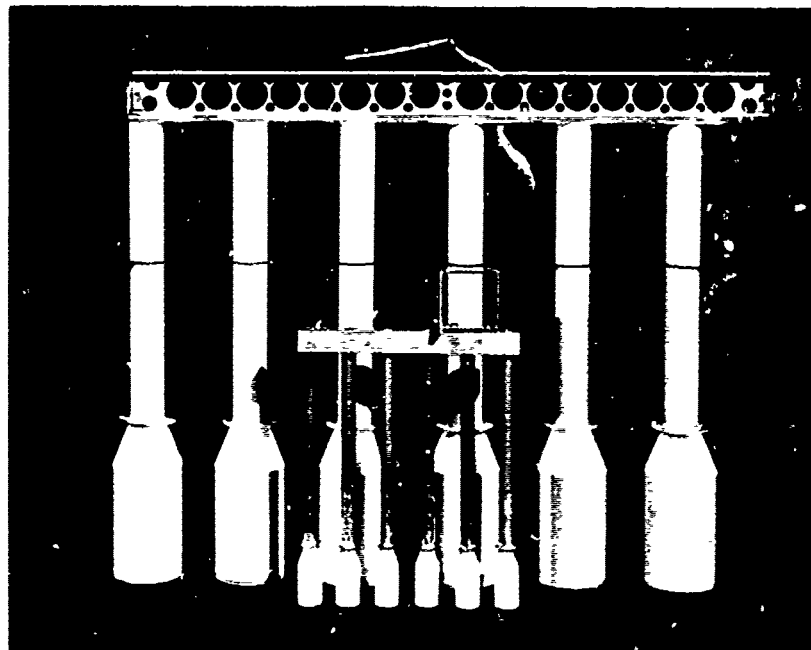


FIGURE 7. PHOTOGRAPH SHOWING ROW OF 6 SMALL-SCALE FLOATS
WITH THE LARGER FLOATS

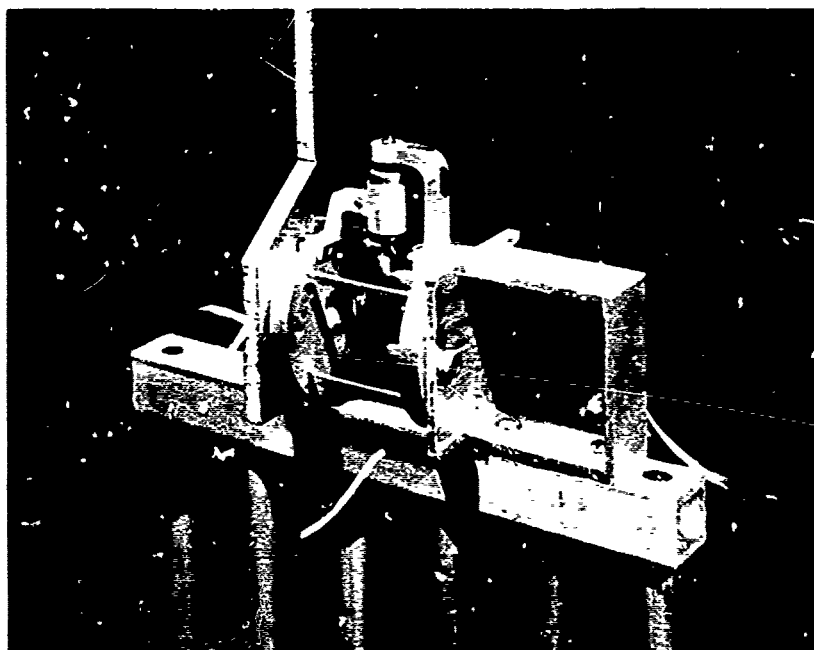


FIGURE 8. PHOTOGRAPH SHOWING LIFT-DRAG BALANCE
USED FOR FORCE MEASUREMENTS WITH SMALL-SCALE MODELS

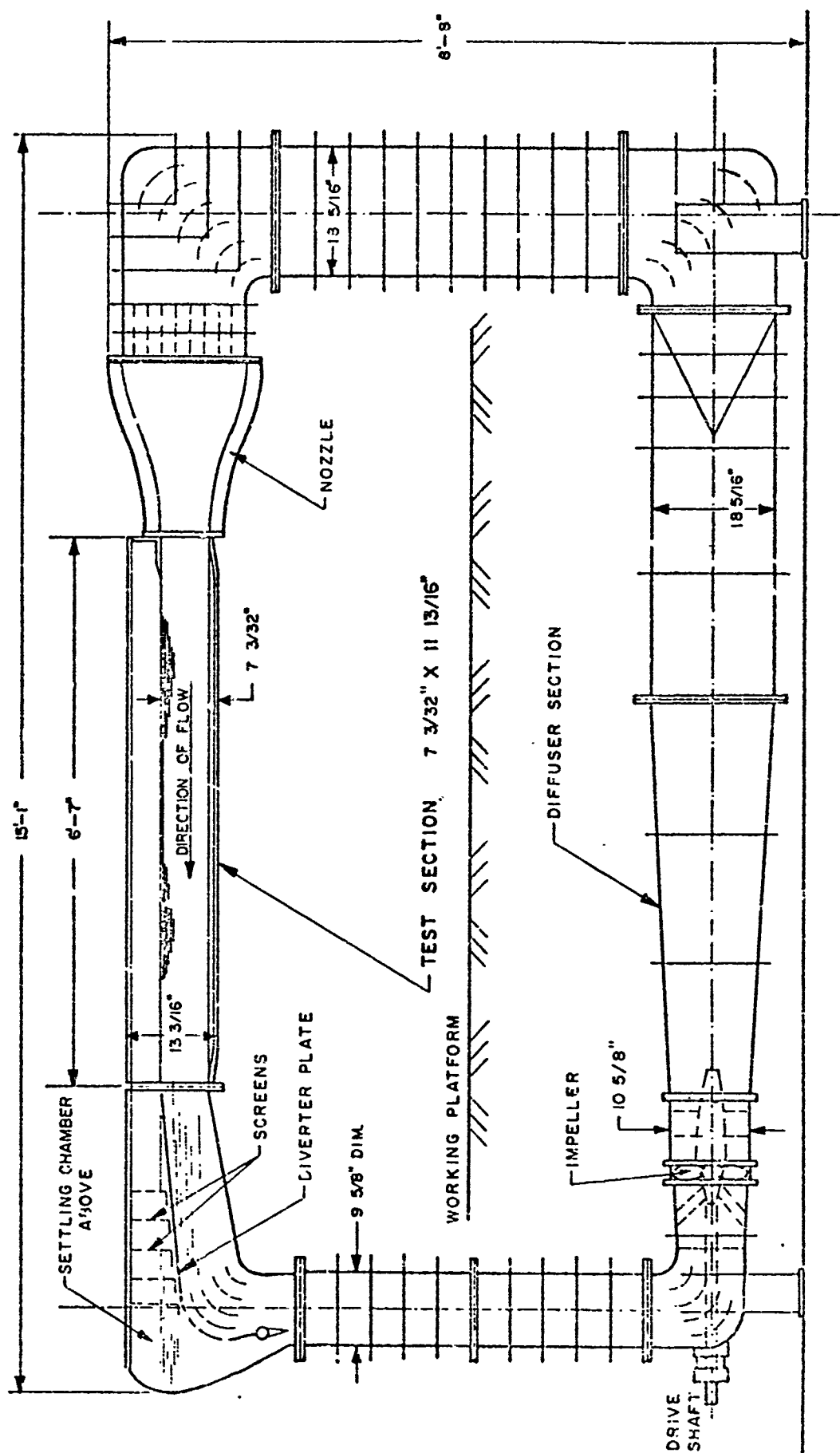


FIG. 8a. DAVIDSON LABORATORY VARIABLE PRESSURE CIRCULATING WATER CHANNEL

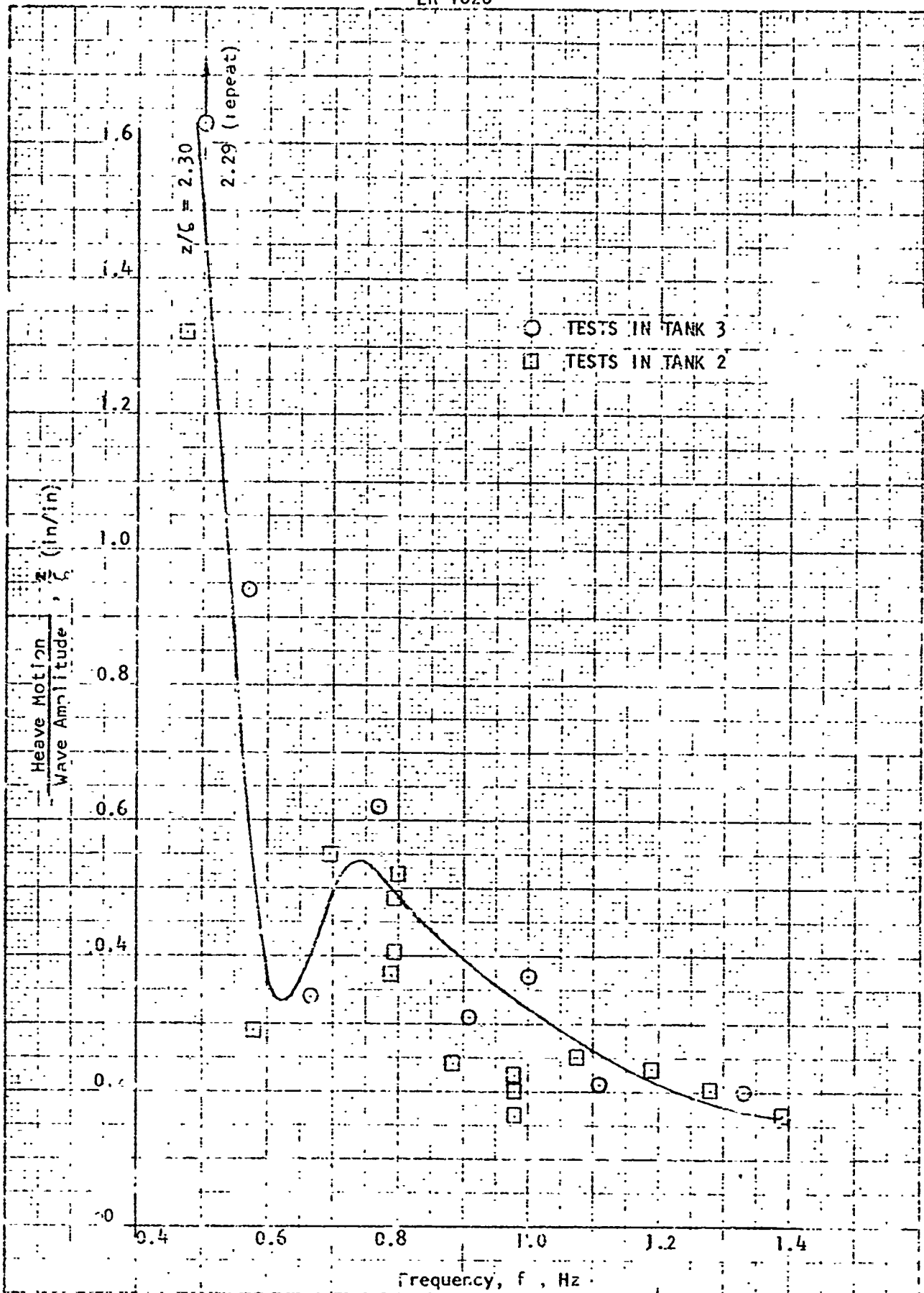


FIGURE 9. HEAVE MOTIONS DUE TO WAVES ON ROW 1 OF MODEL ISLAND

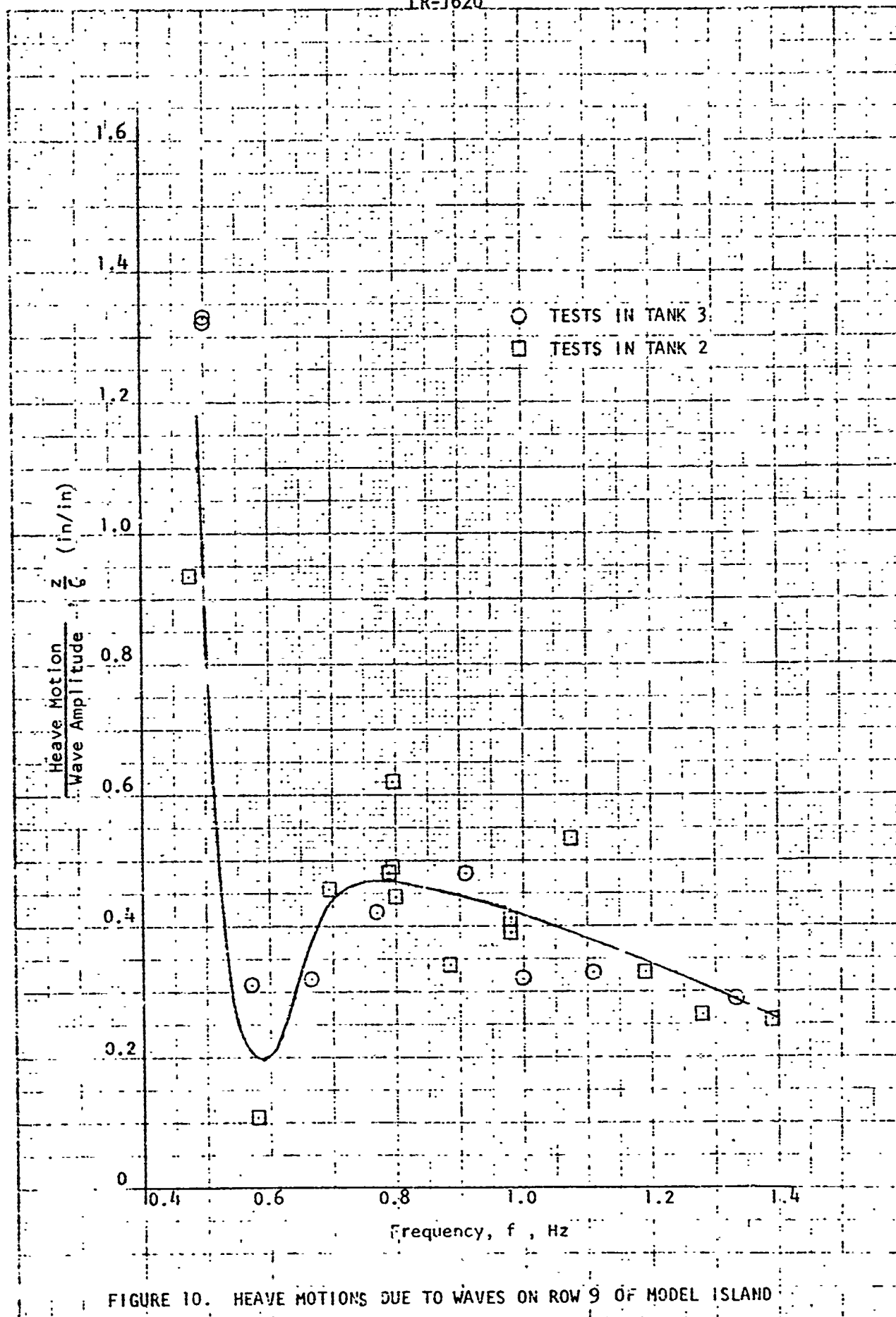


FIGURE 10. HEAVE MOTIONS DUE TO WAVES ON ROW 9 OF MODEL ISLAND

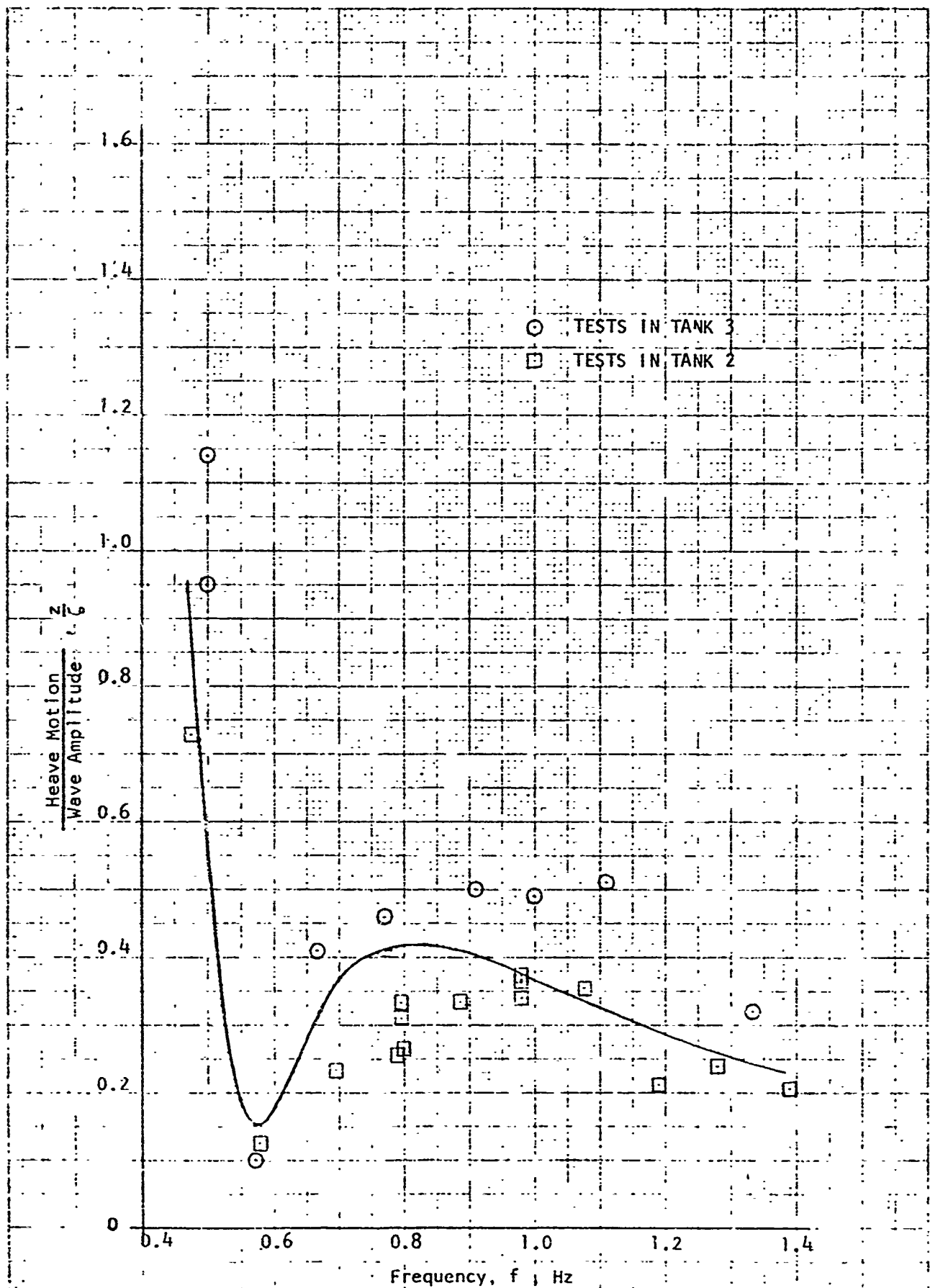


FIGURE 11. HEAVE MOTIONS DUE TO WAVES ON ROW 18 OF MODEL ISLAND

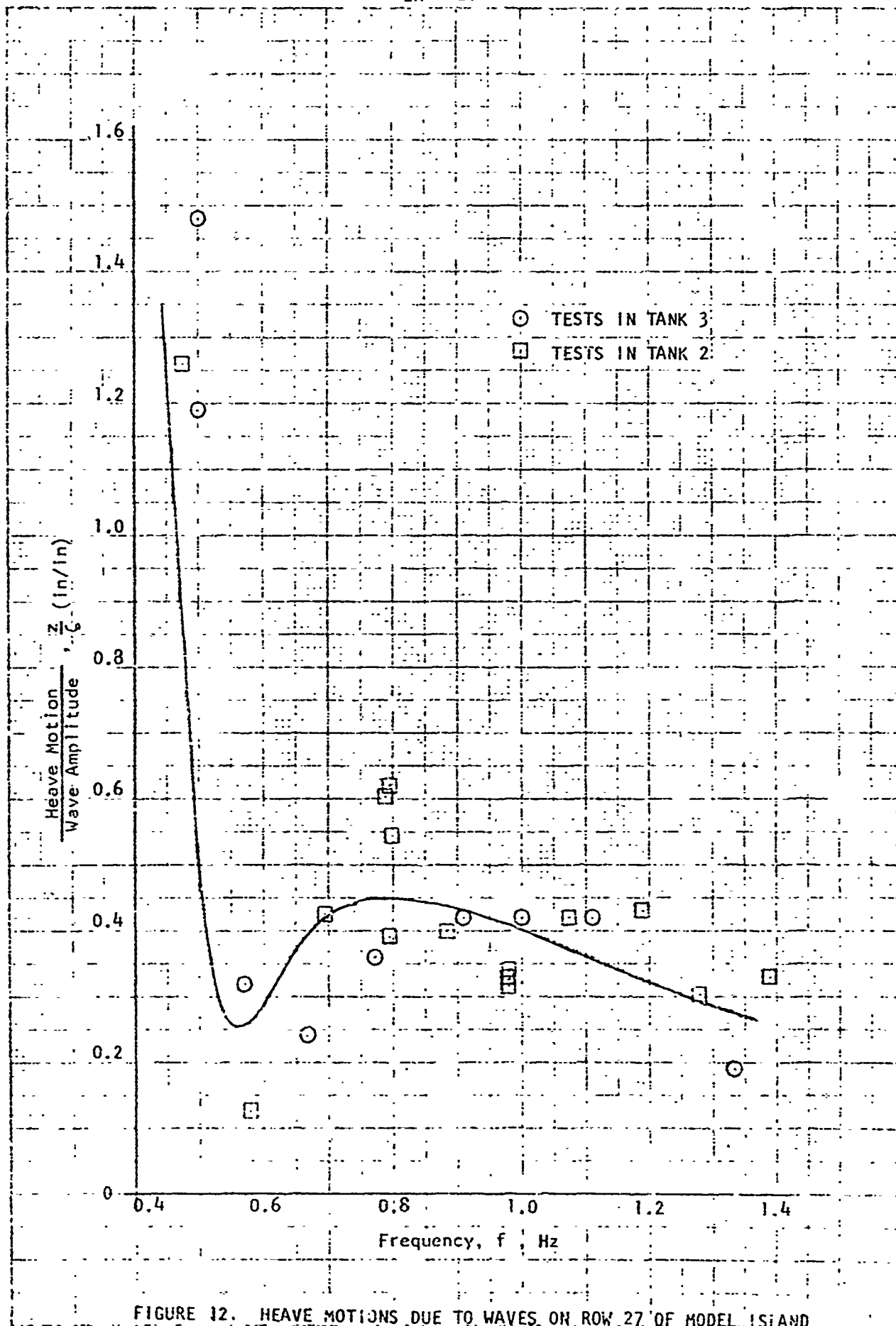


FIGURE 12. HEAVE MOTIONS DUE TO WAVES ON ROW 27 OF MODEL ISLAND

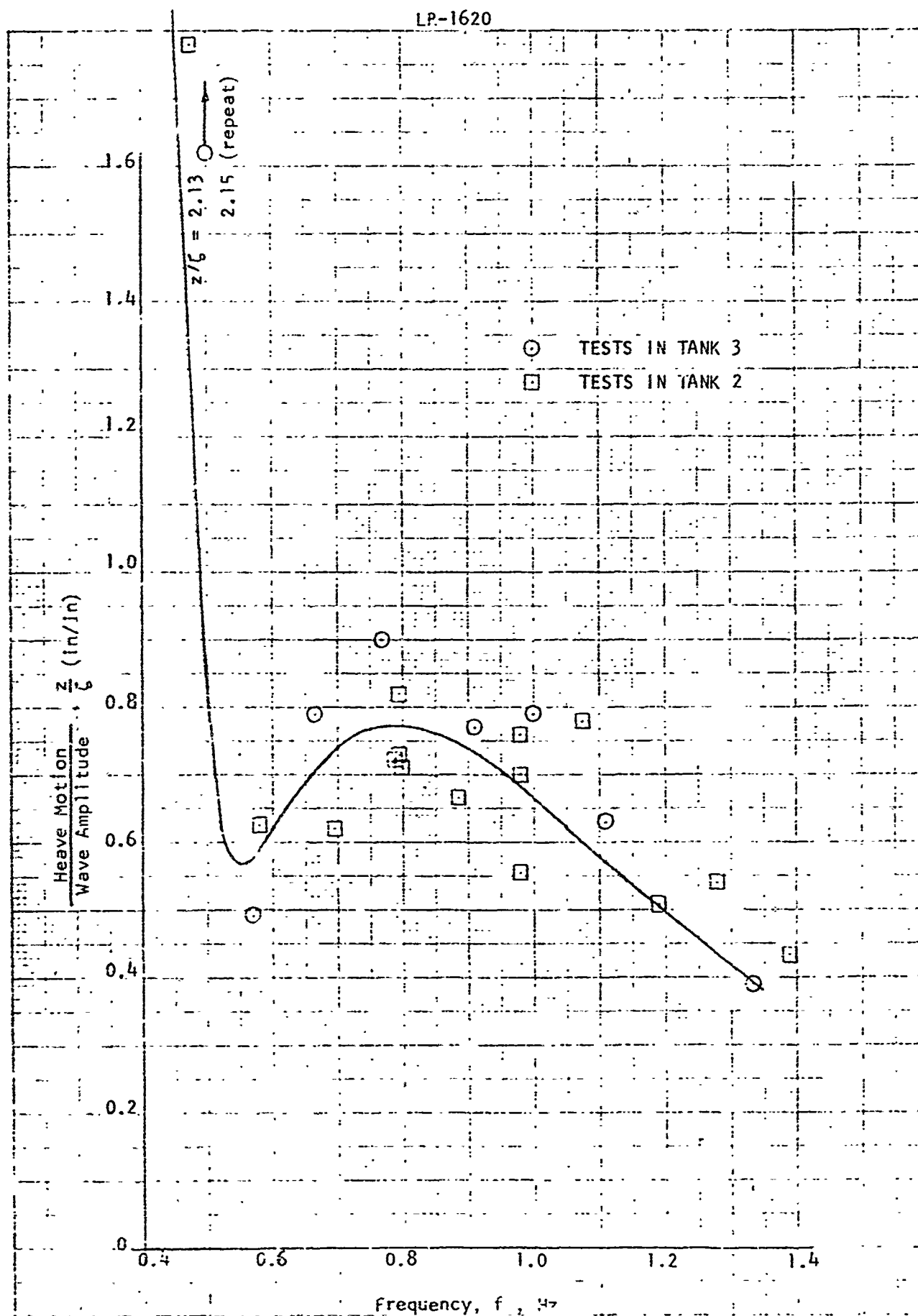


FIGURE 13. HEAVE MOTIONS DUE TO WAVES ON ROW 35 OF MODEL ISLAND

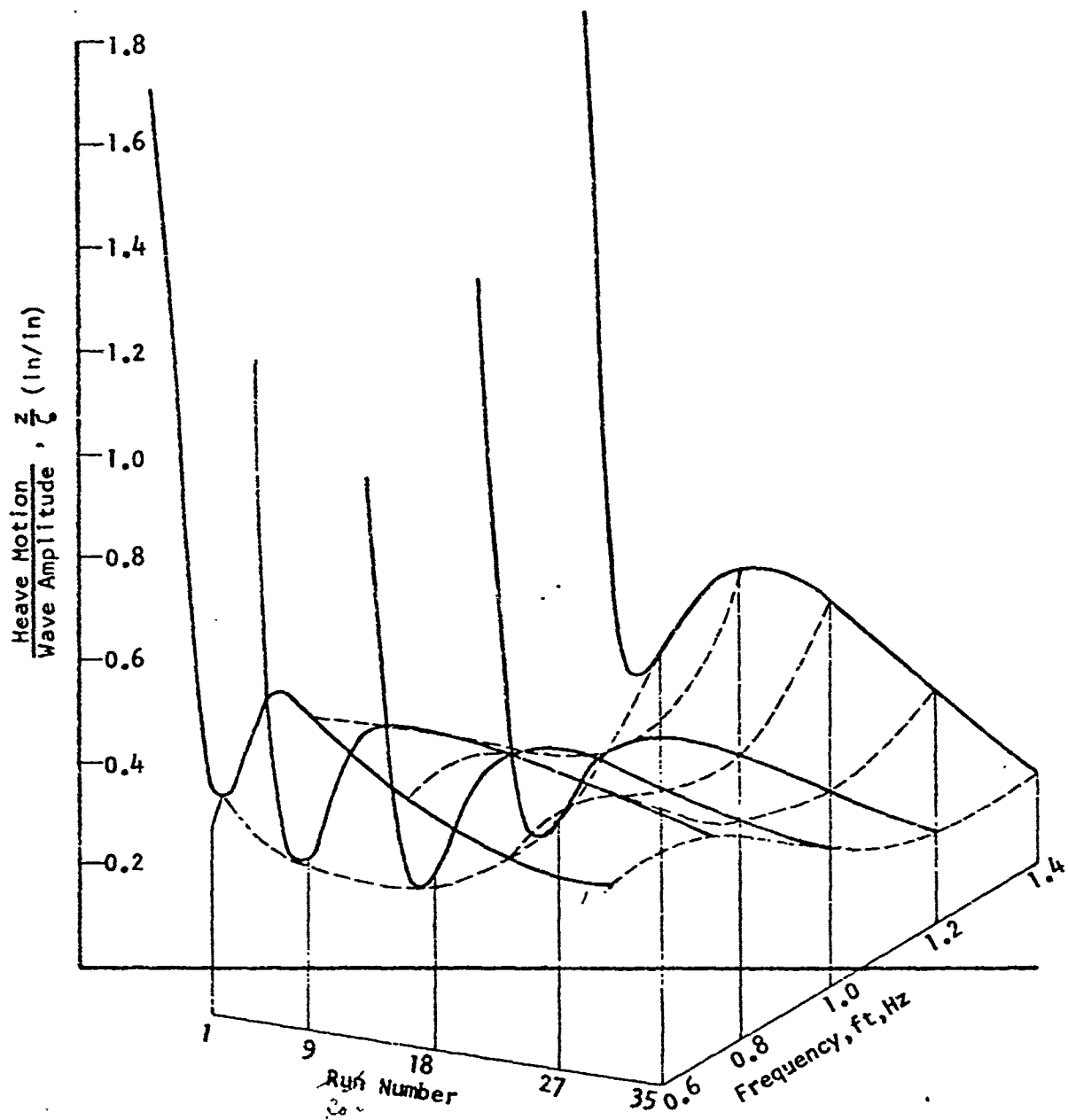


FIGURE 14. CARPET PLOT OF HEAVE MOTION DUE TO WAVES
FOR ARTICULATED MODEL

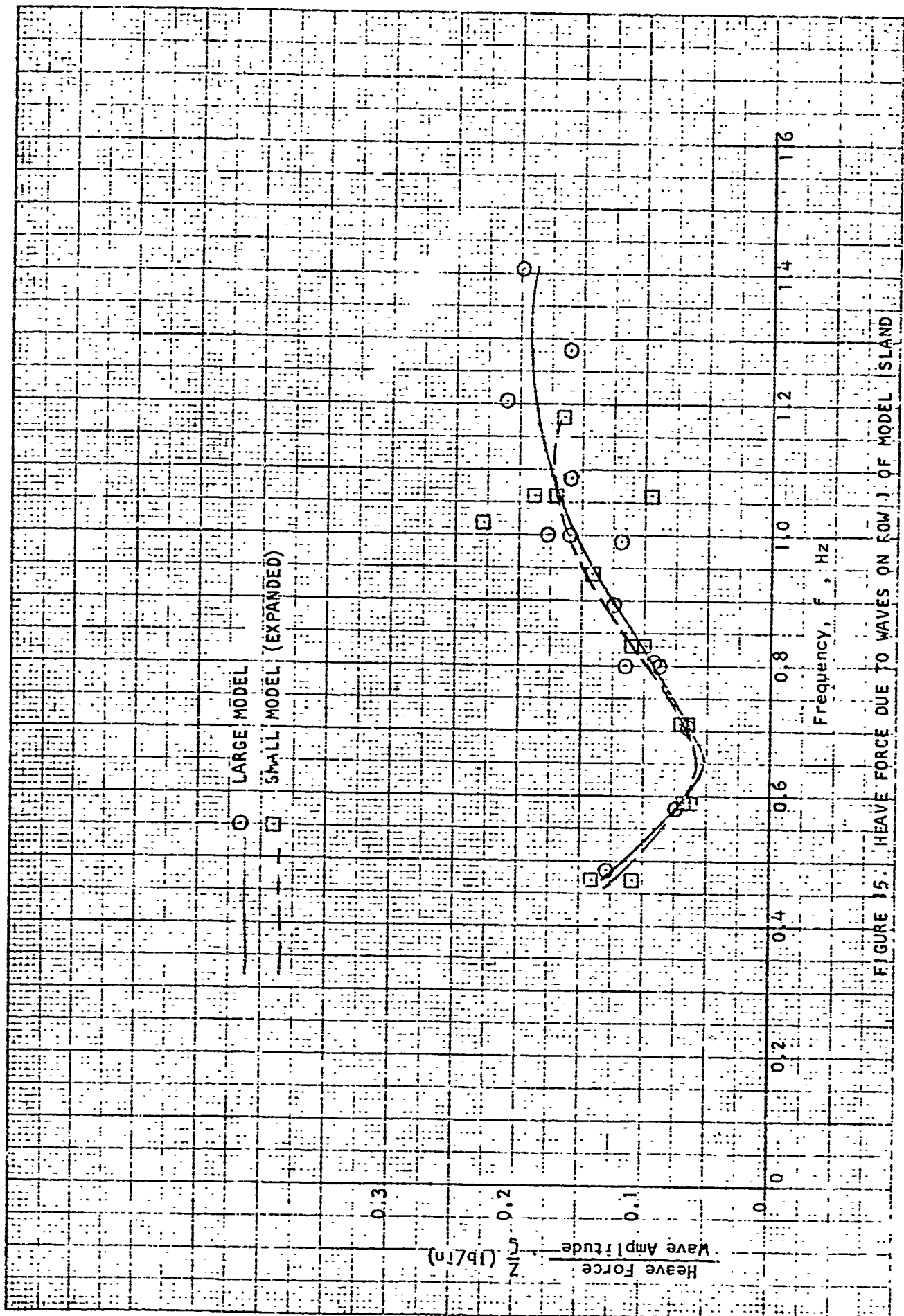


FIGURE 15: HEAVE FORCE DUE TO WAVES ON ROW J OF MODEL ISLAND

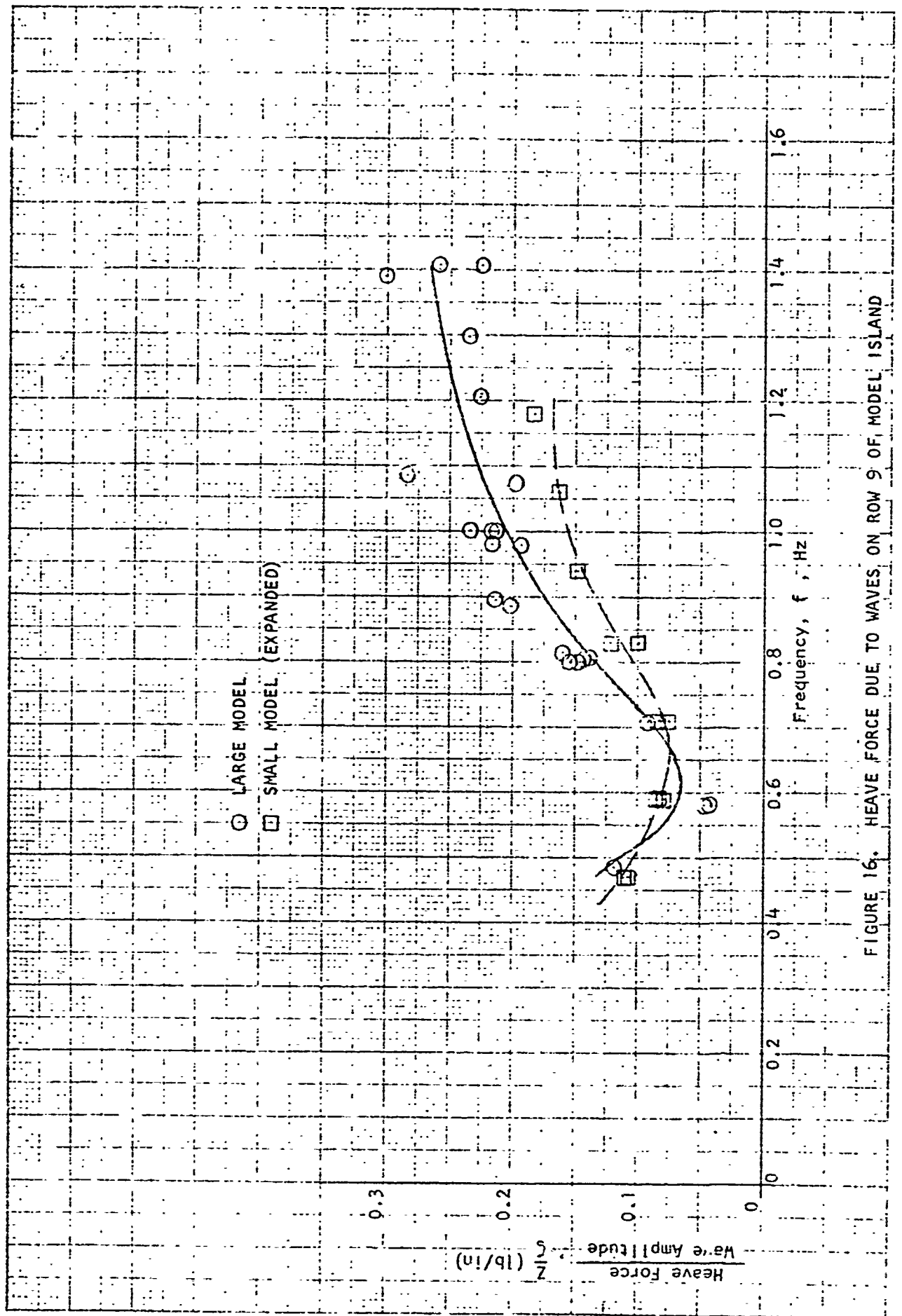


FIGURE 16. HEAVE FORCE DUE TO WAVES, ON ROW 9 OF MODEL ISLAND

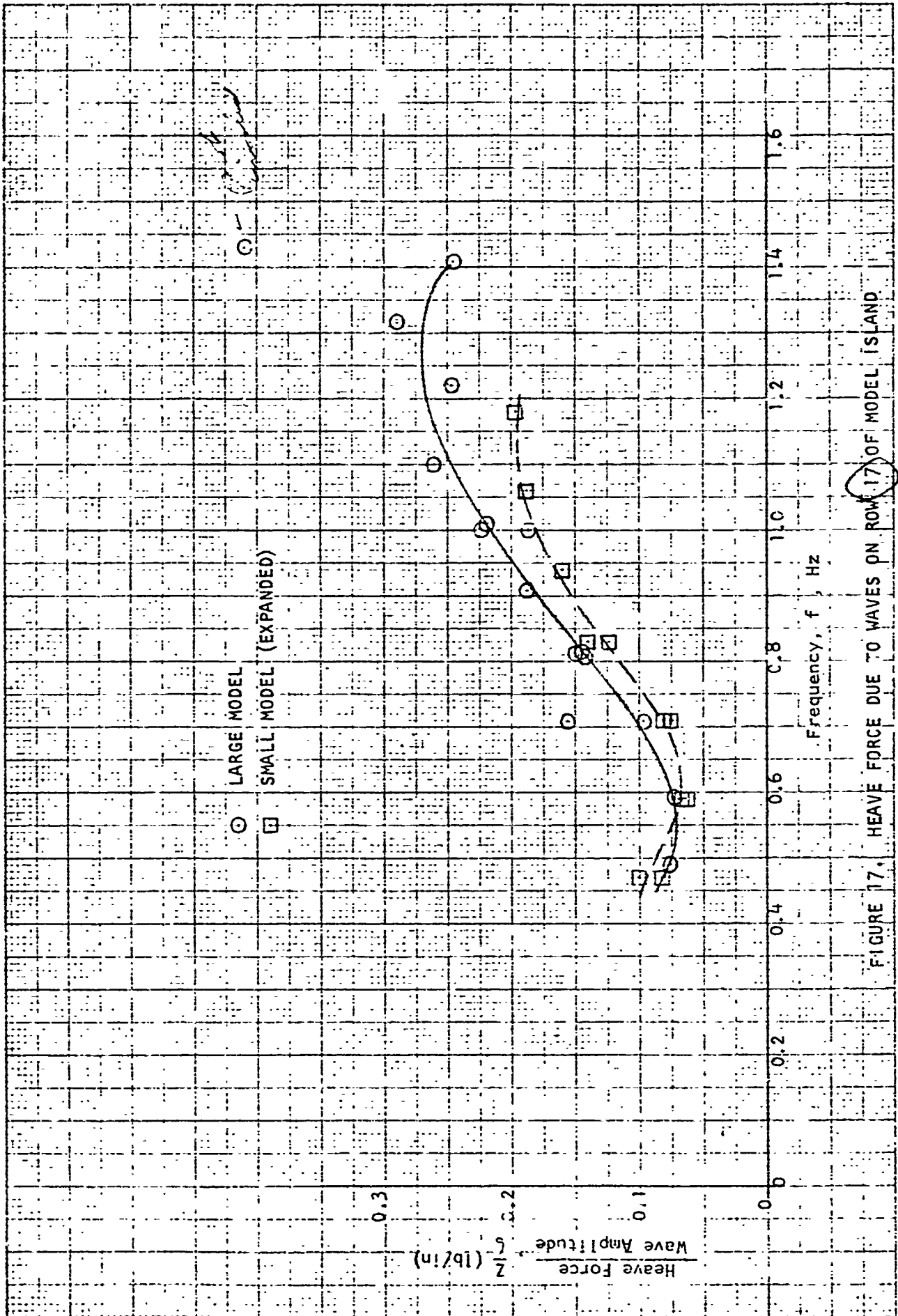


FIGURE 17. HEAVE FORCE DUE TO WAVES ON ROW 17 OF MODEL ISLAND

18

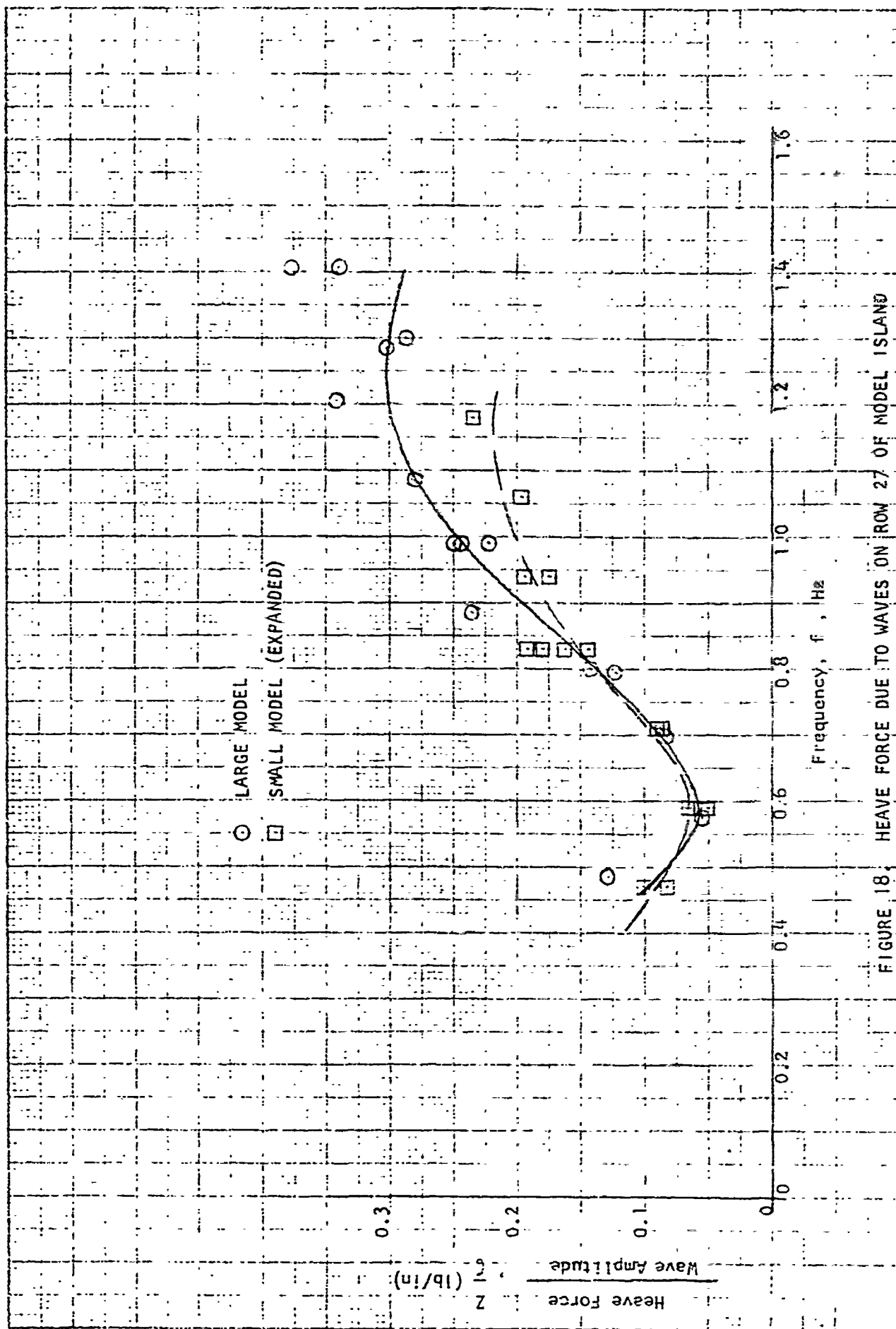


FIGURE 18. HEAVE FORCE DUE TO WAVES ON ROW 27 OF MODEL ISLAND

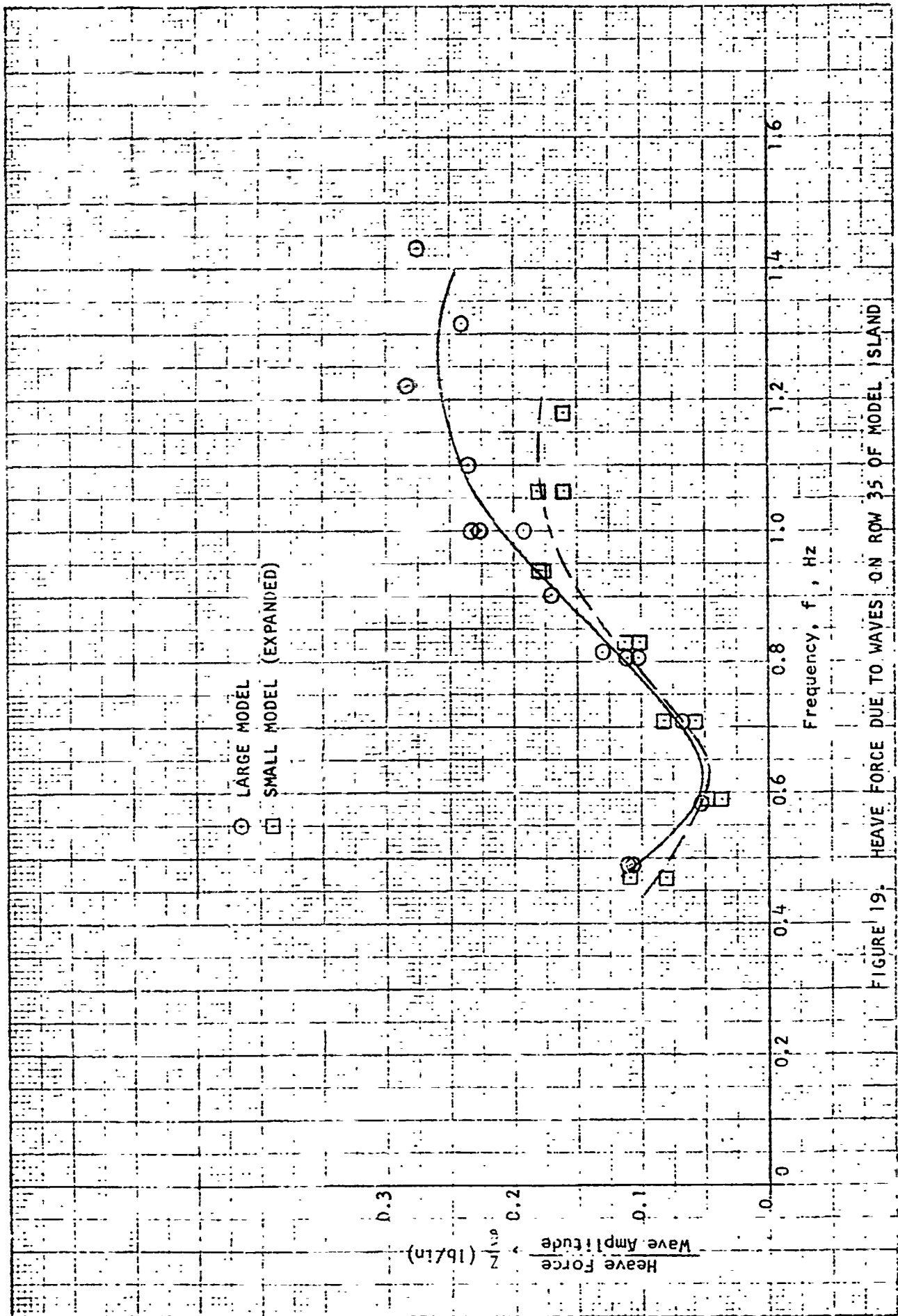


FIGURE 19. HEAVE FORCE DUE TO WAVES ON ROW 35 OF MODEL ISLAND

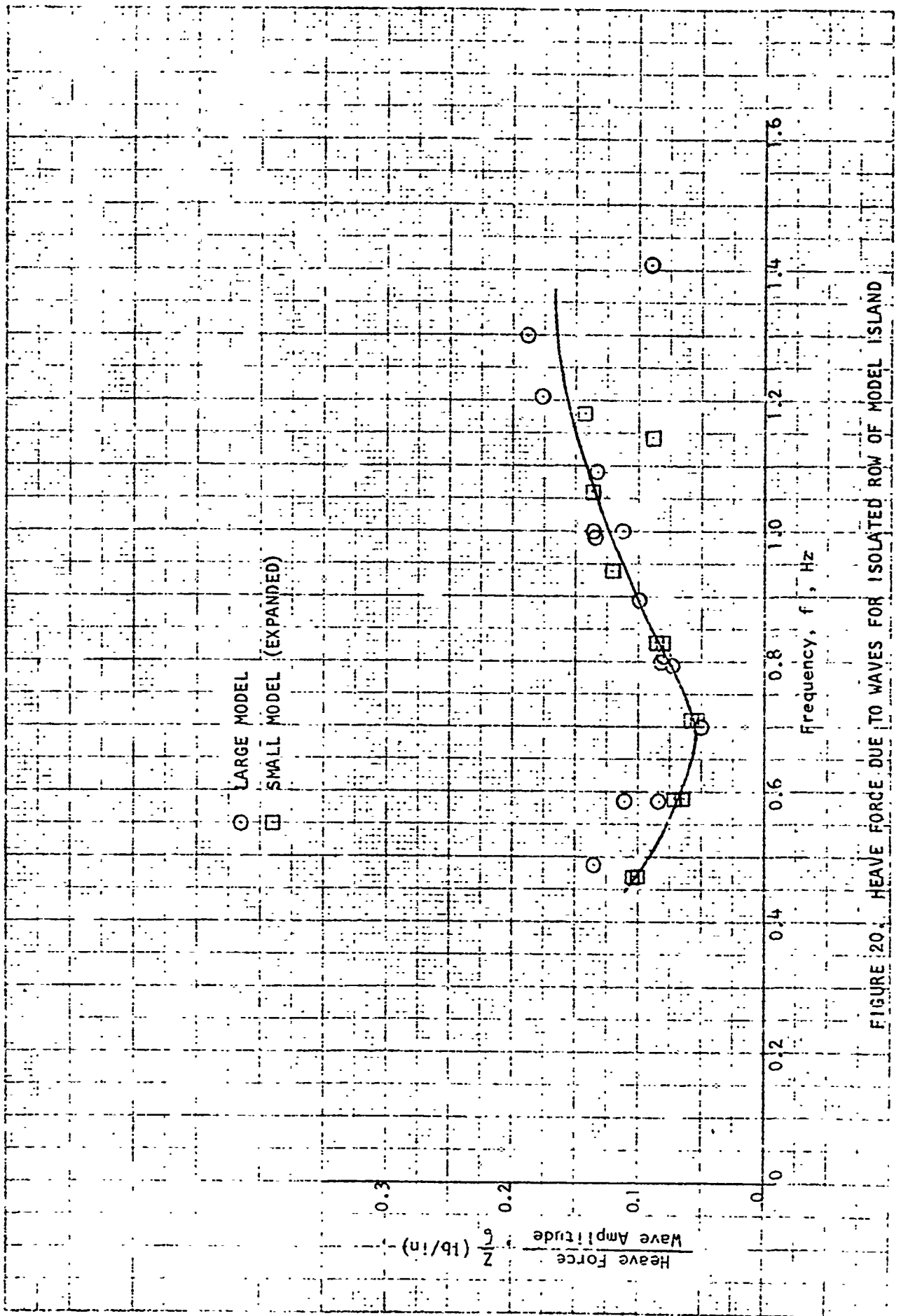


FIGURE 20. HEAVE FORCE DUE TO WAVES FOR ISOLATED ROW OF MODEL ISLAND

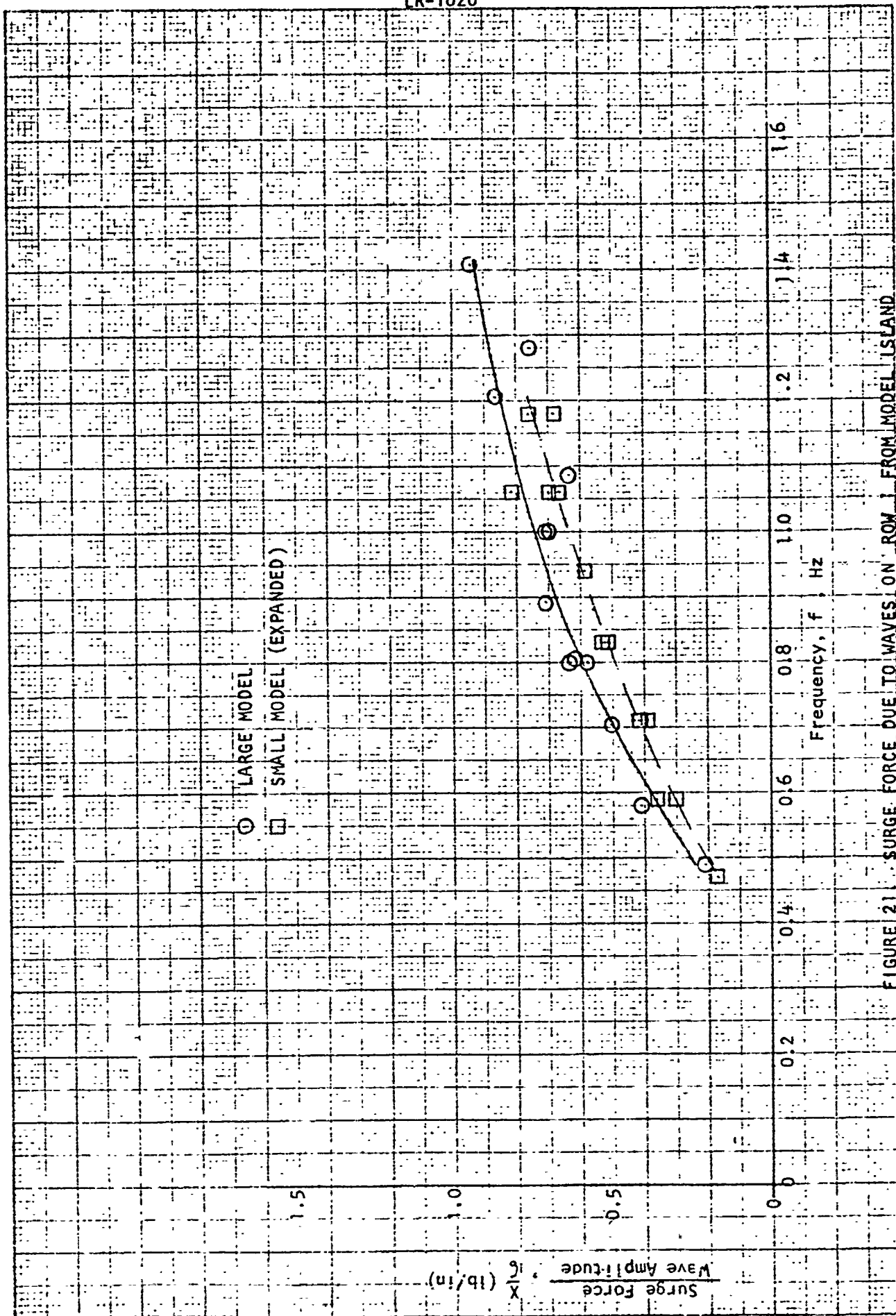


FIGURE 21 SURGE FORCE DUE TO WAVES ON ROW 1 FROM MODEL ISLAND

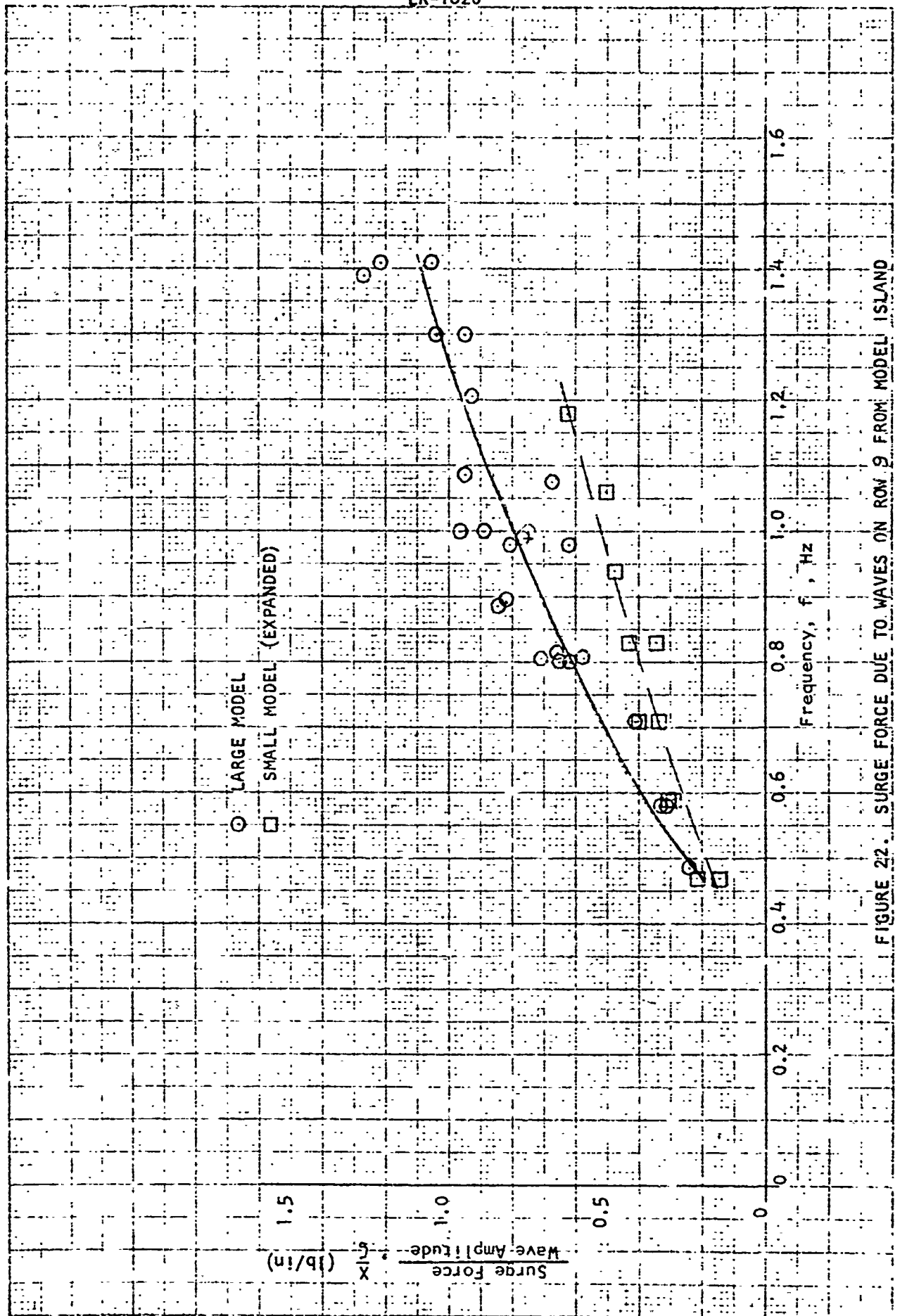


FIGURE 22. SURGE FORCE DUE TO WAVES ON ROW 9 FROM MODEL ISLAND

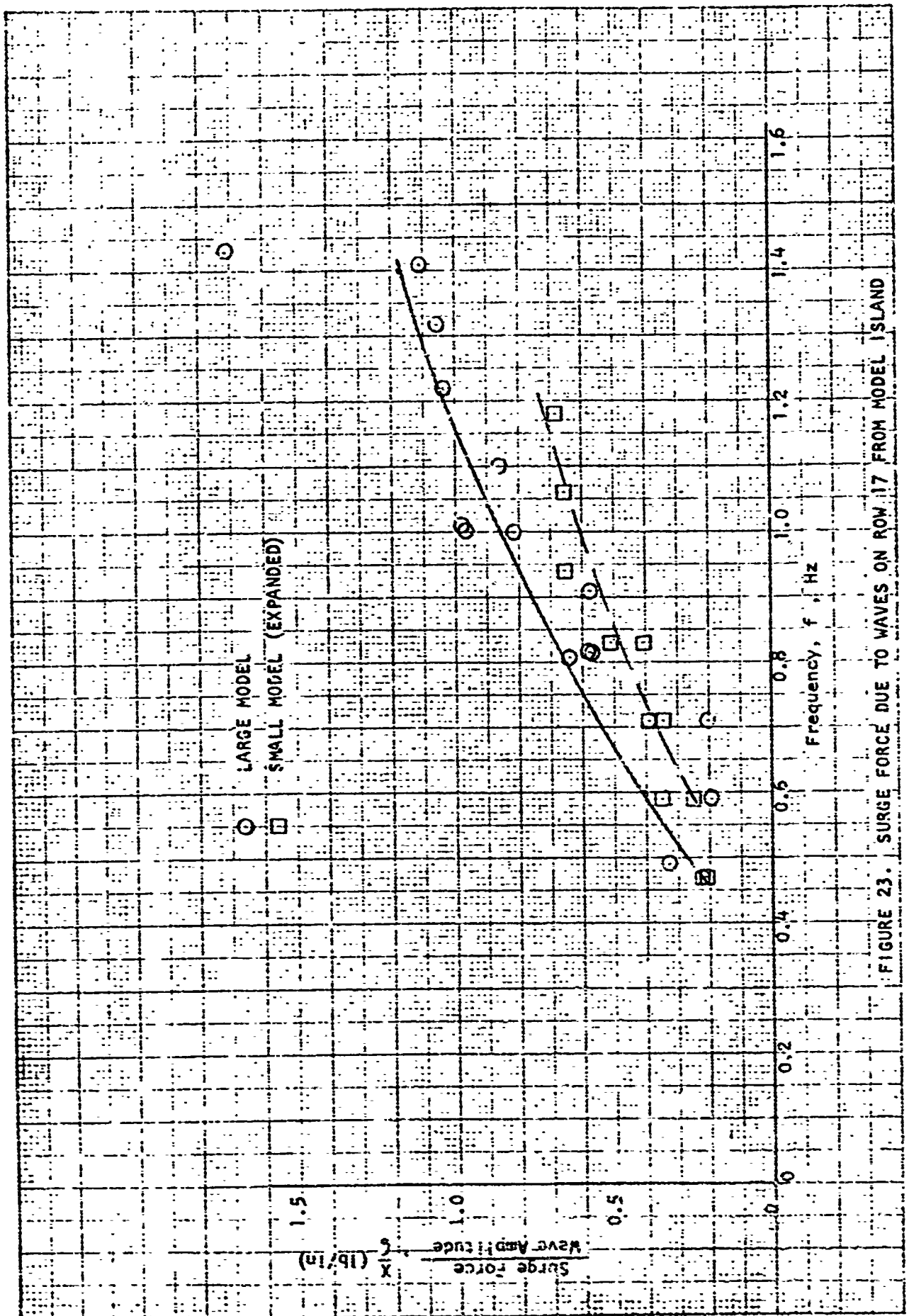


FIGURE 23. SURGE FORCE DUE TO WAVES ON ROW 17 FROM MODEL 1 ISLAND

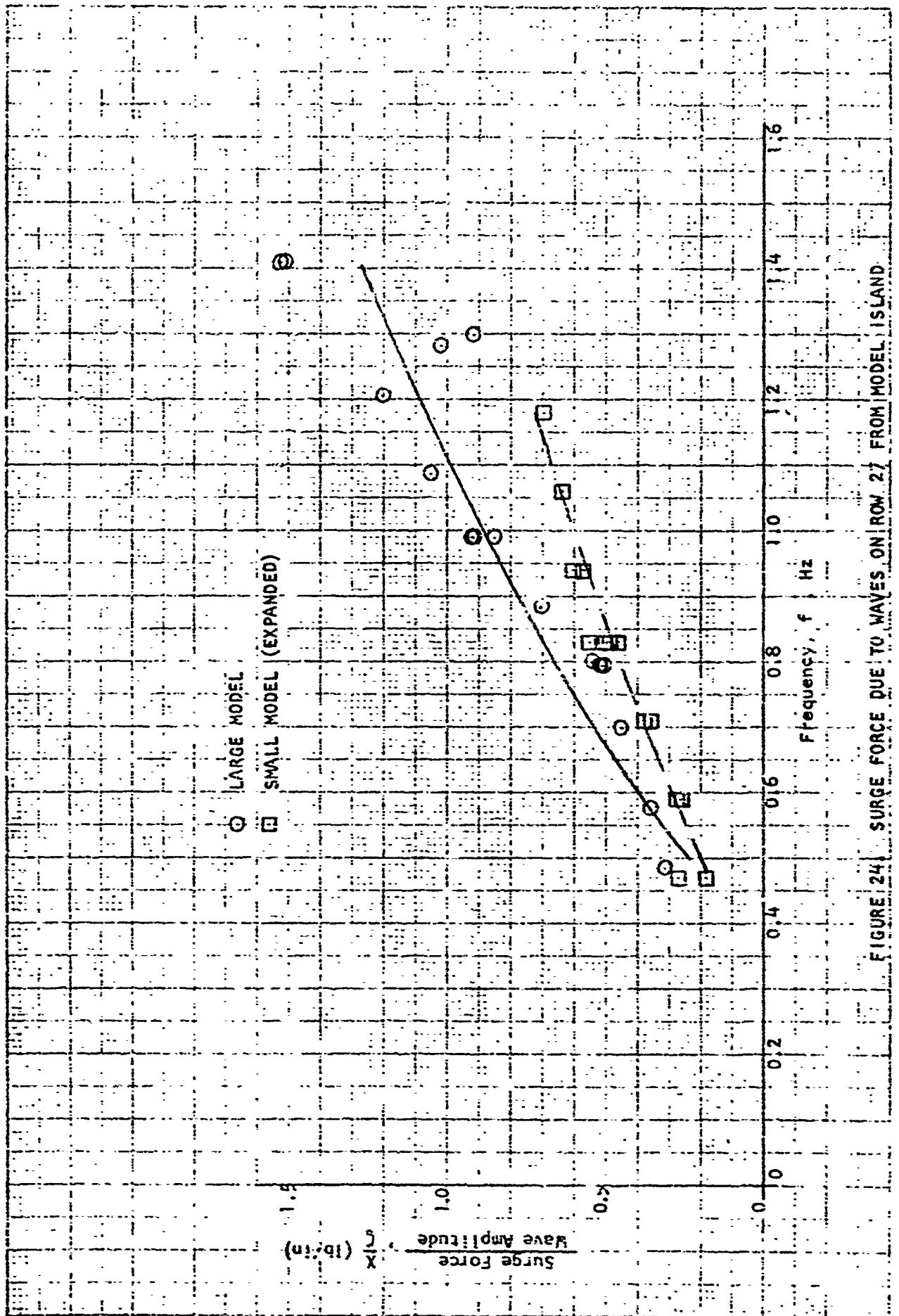


FIGURE 24 SURGE FORCE DUE TO WAVES ON ROW 27 FROM MODEL ISLAND

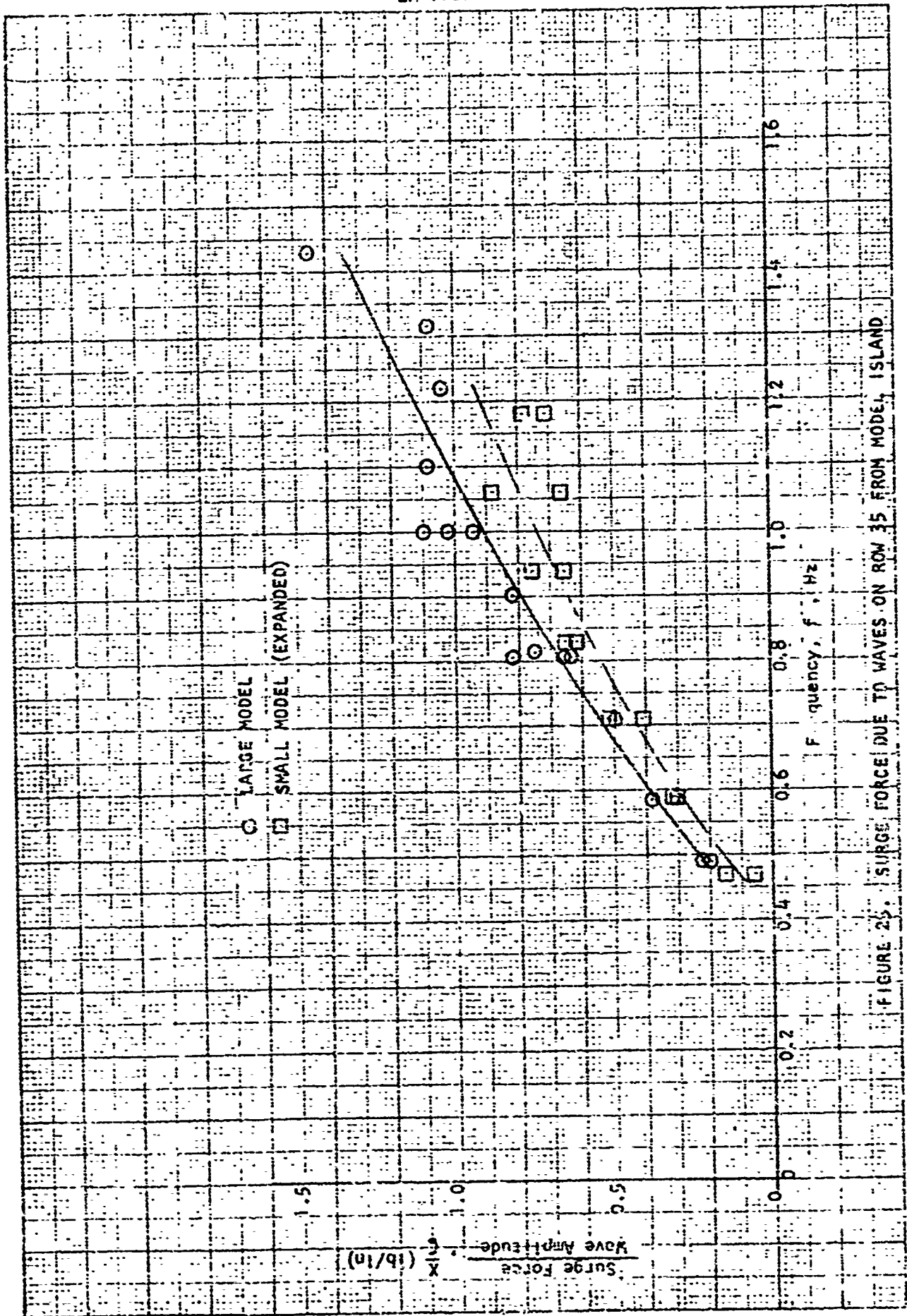


FIGURE 25. SURGE FORCE DUE TO WAVES ON ROW 35 FROM MODEL 4 ISLAND

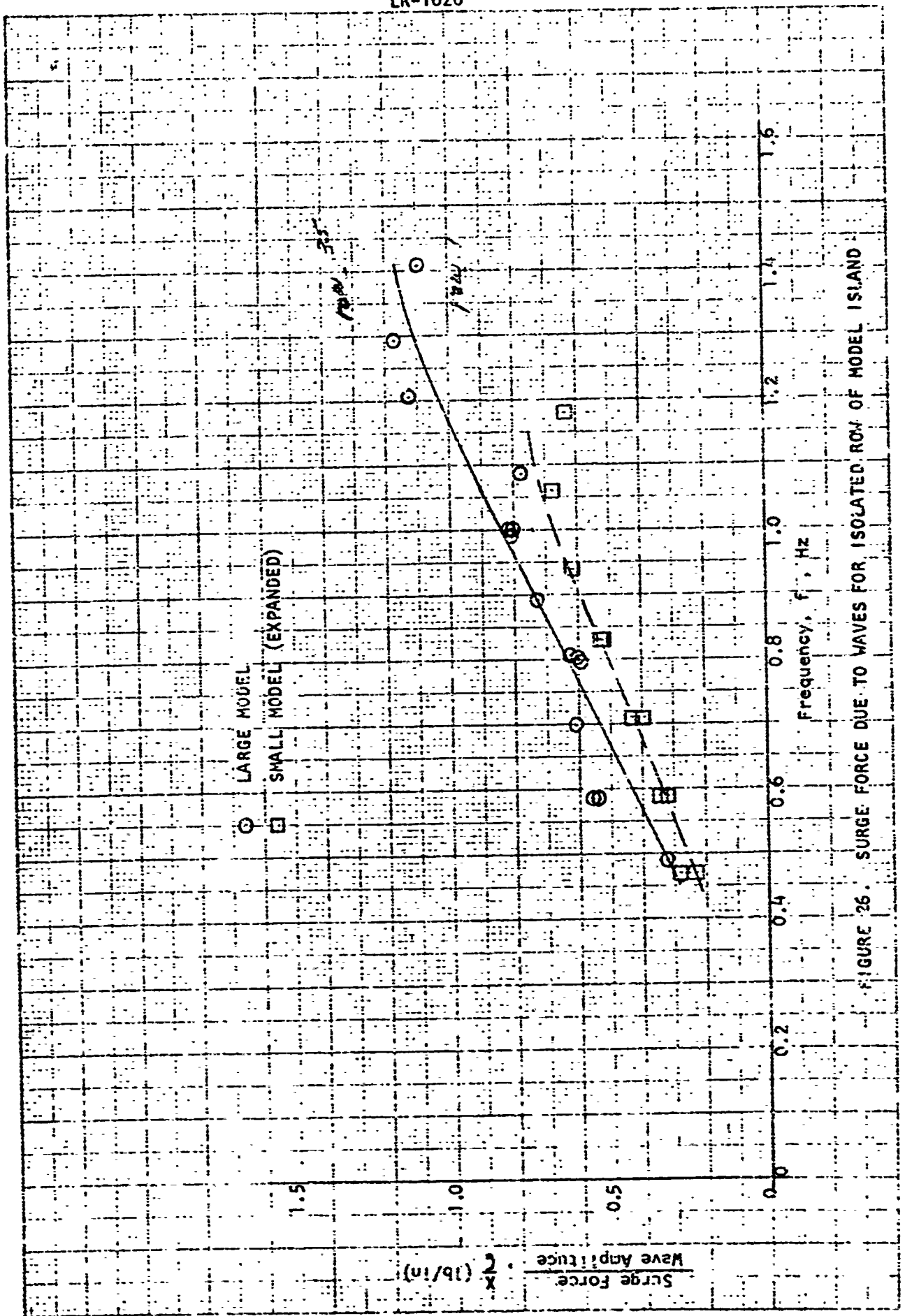


FIGURE 26. SURGE FORCE DUE TO WAVES FOR ISOLATED ROW OF MODEL ISLAND

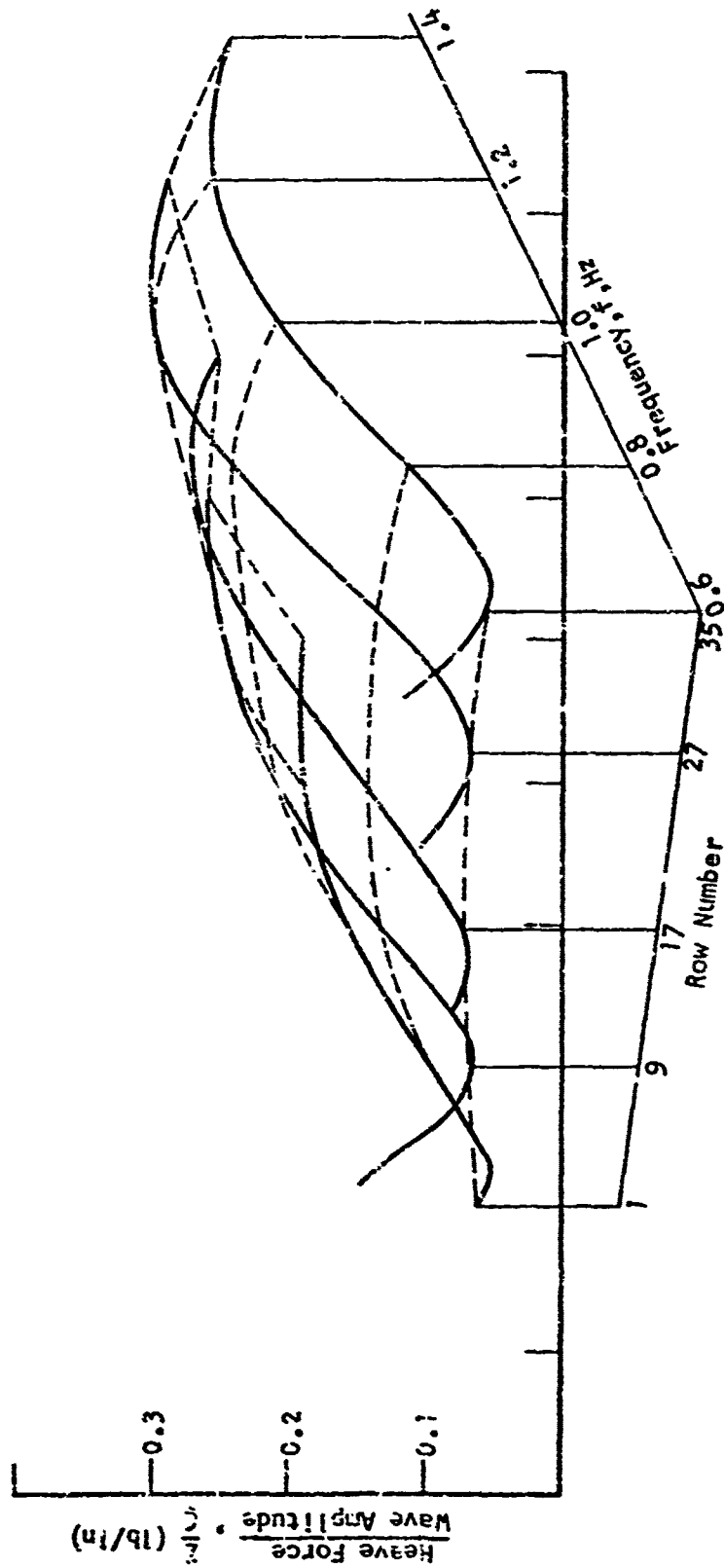


FIGURE 27. CARPET PLOT OF WAVE-INDUCED VERTICAL FORCE ON RESTRAINED 6x35 ARRAY OF FLOATS

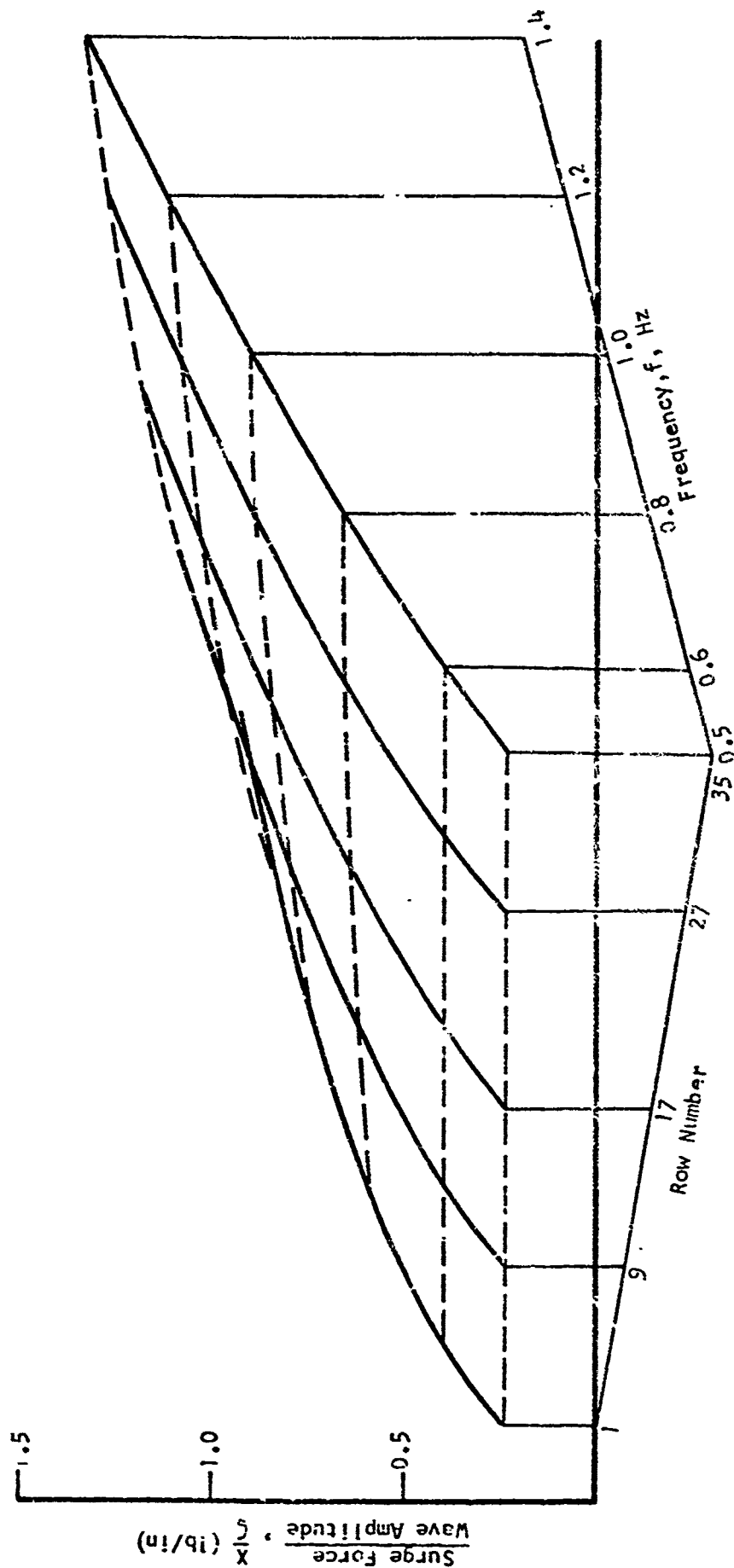


FIGURE 28. CARPET PLOT OF SURGE FORCE DUE TO WAVES

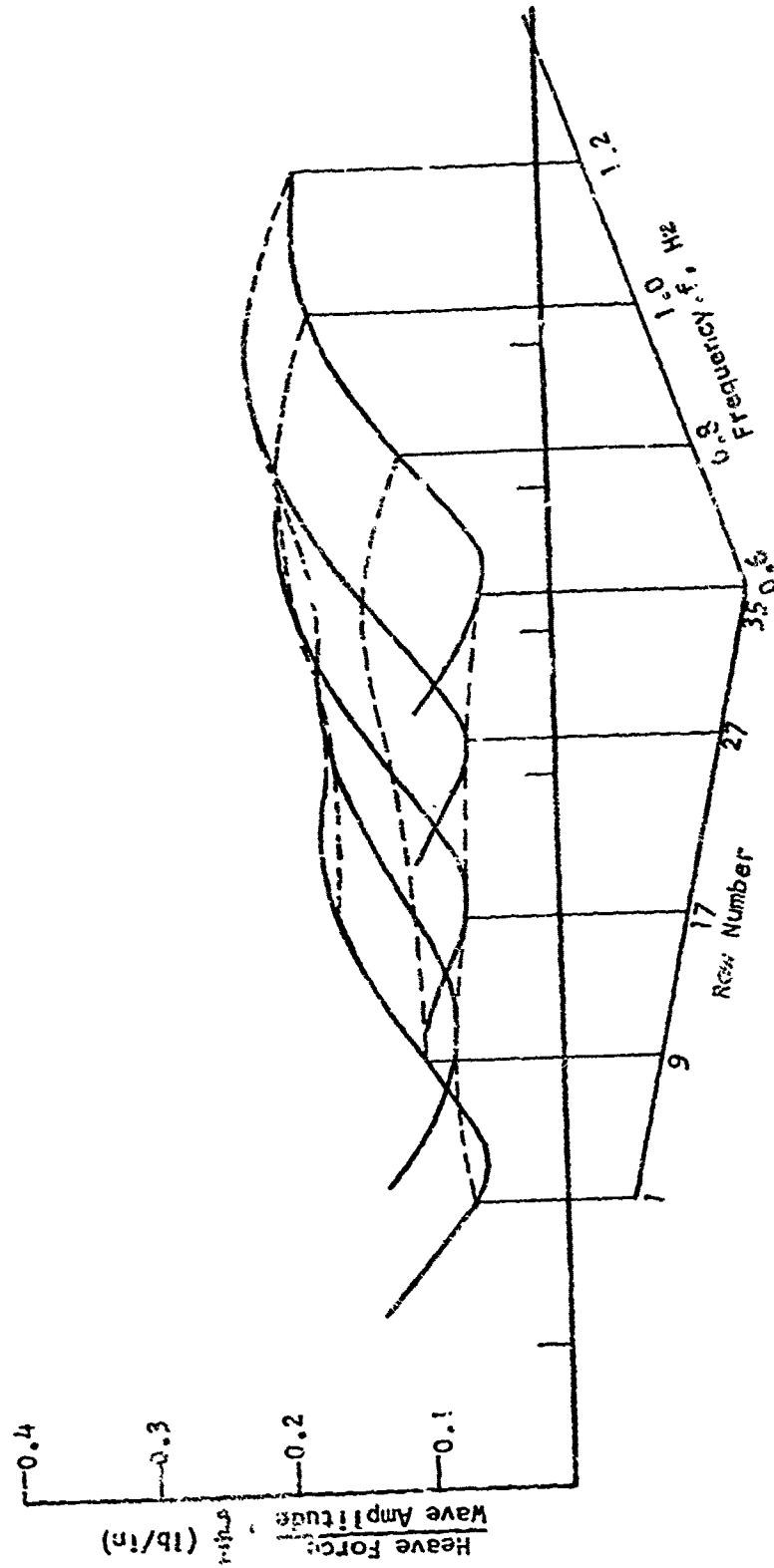
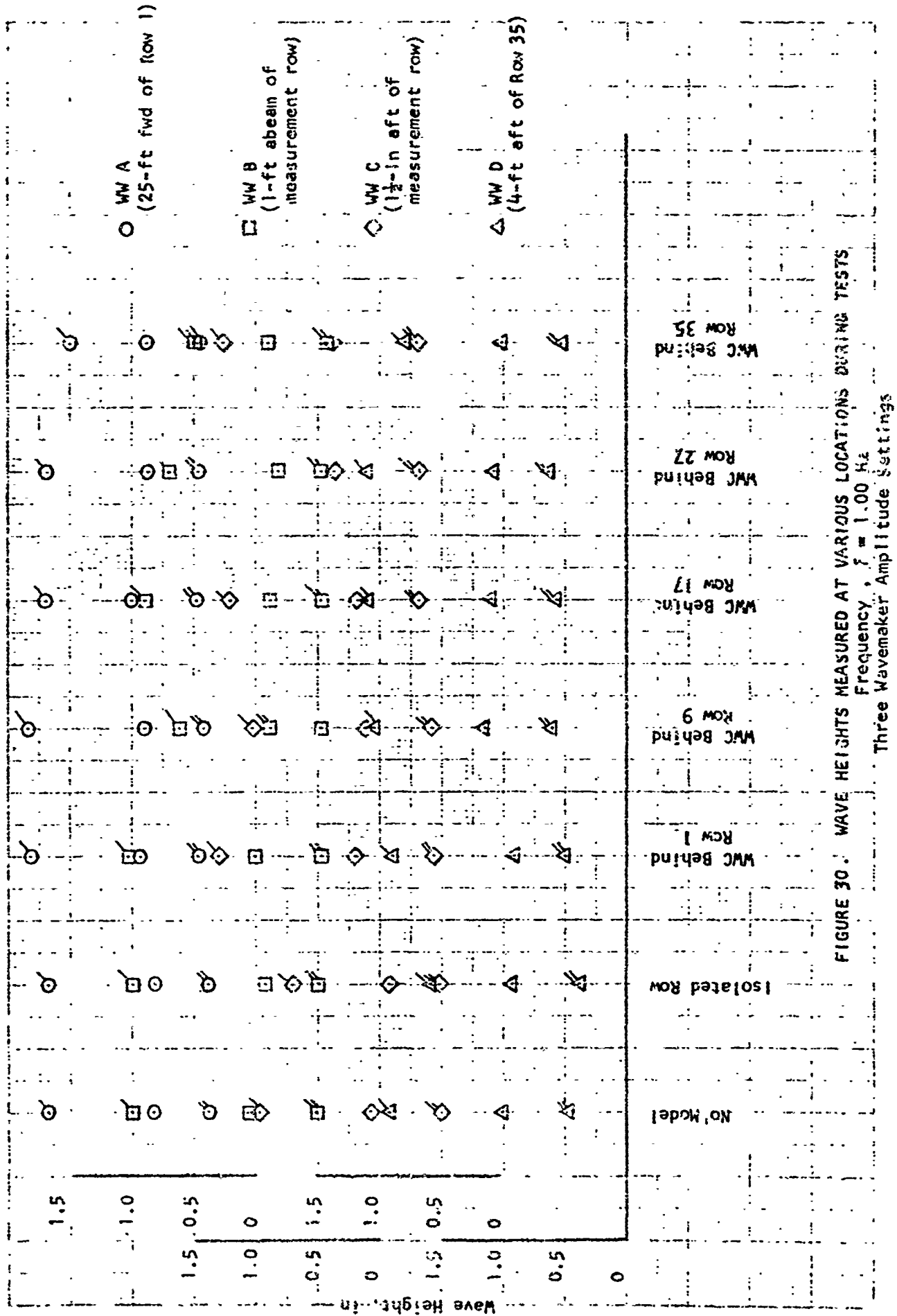
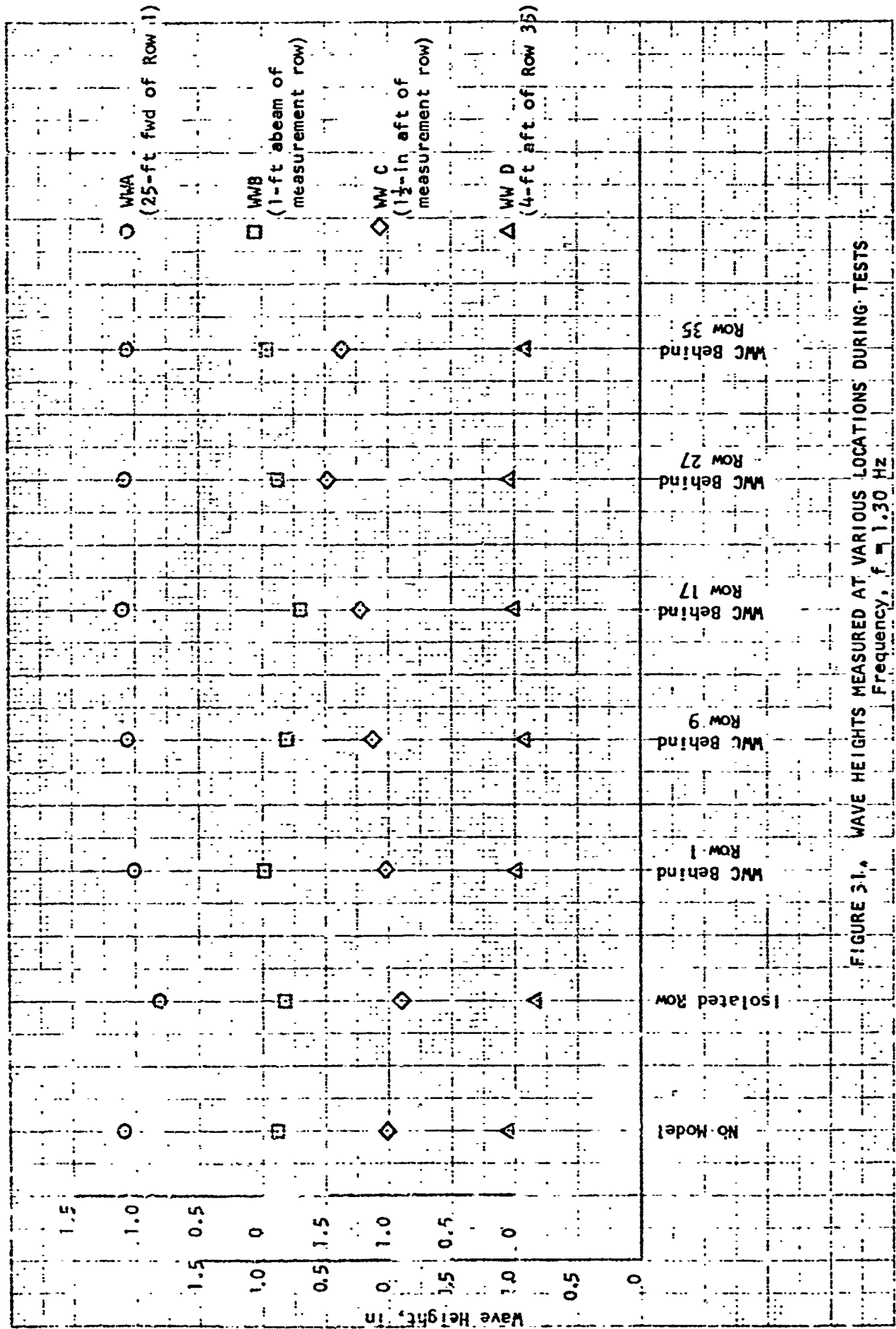


FIGURE 29. CARPET PLOT OF HEAVE FORCE DUE TO WAVES FOR SMALL MODEL
(Results Expanded to Correspond With Large Model)





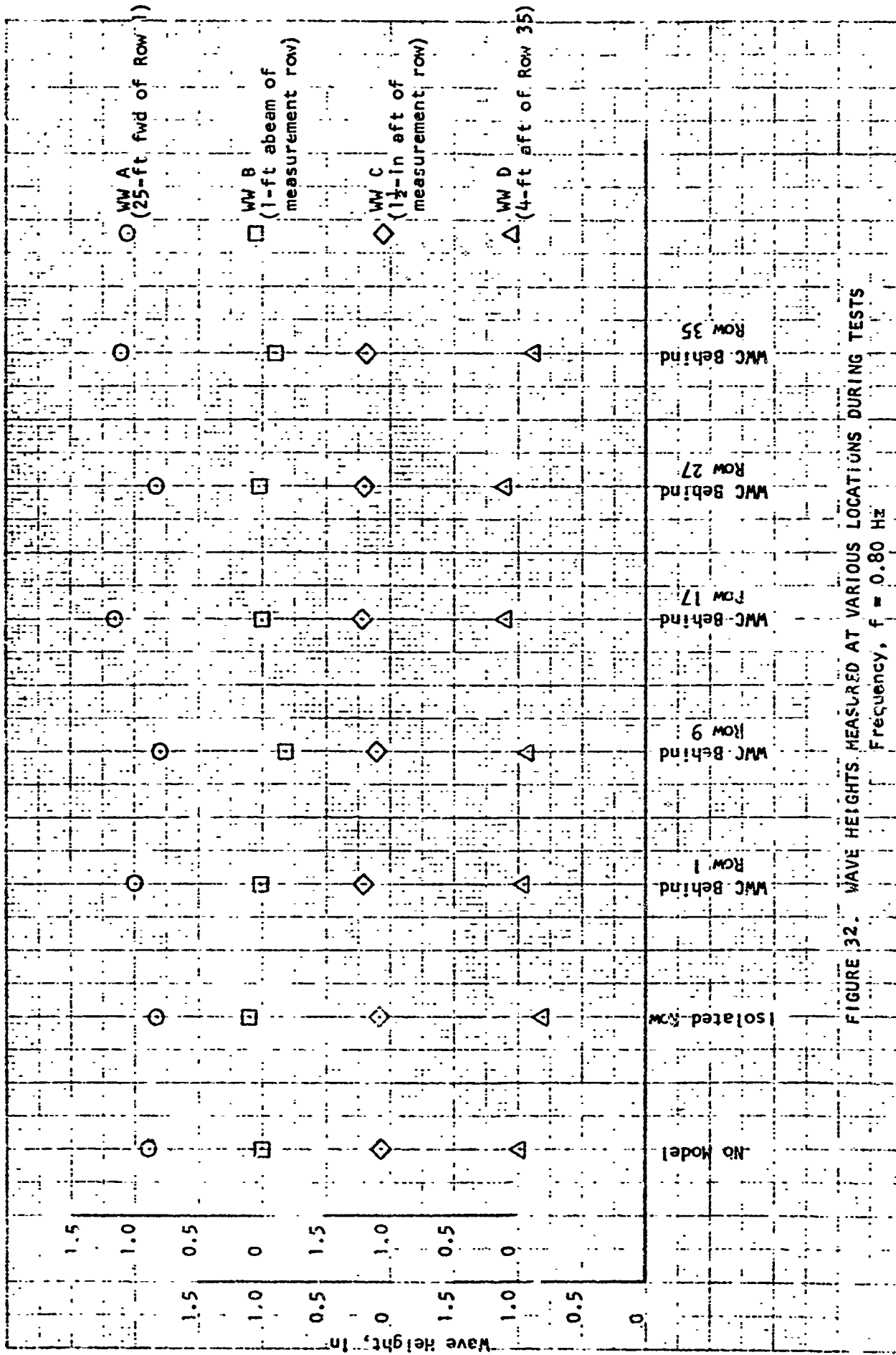


FIGURE 32. WAVE HEIGHTS MEASURED AT VARIOUS LOCATIONS DURING TESTS

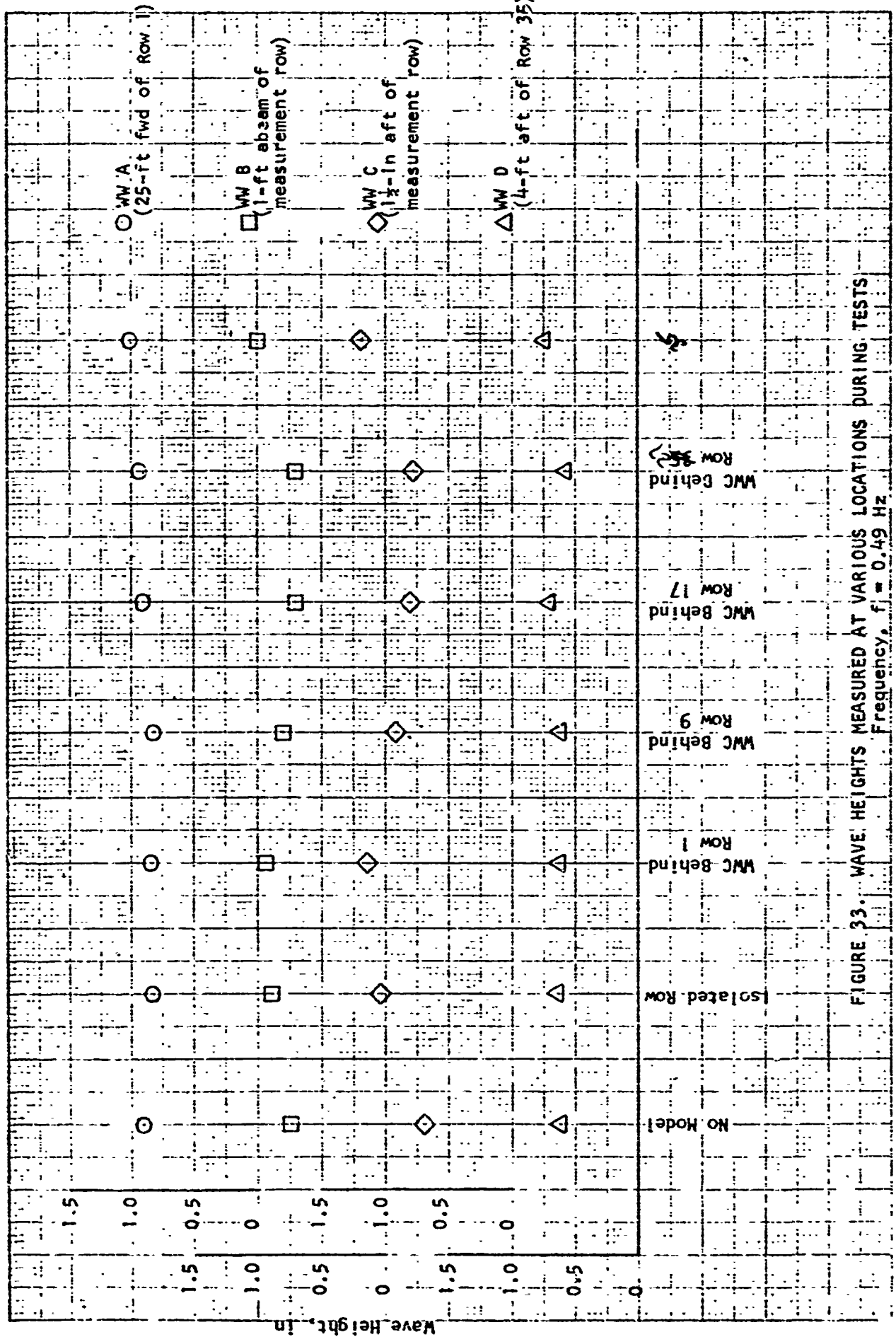


FIGURE 33. WAVE HEIGHTS MEASURED AT VARIOUS LOCATIONS DURING TESTS
Frequency, $f = 0.49$ Hz

APPENDIX G - HYDRODYNAMIC TESTS AND
ANALYSIS PROGRAM FOR EXPANDABLE FLOATING
BASES: PART 2 - COMPREHENSIVE PROGRAM ON
HYDRODYNAMIC INTERACTION EFFECTS

STEVENS INSTITUTE OF TECHNOLOGY
DAVIDSON LABORATORY
CASTLE POINT STATION
HOBOKEN, NEW JERSEY

Letter Report SIT-DL-72-1635

November 1972

HYDRODYNAMIC TESTS AND ANALYSIS PROGRAM
FOR AN EXPANDABLE FLOATING BASE

PART 2

Comprehensive Program on
Hydrodynamic Interaction Effects

by John A. Mercier

Prepared for
Goodyear Aerospace Corporation
Akron, Ohio 44315
GAC P.O. 2B1115YX
(DL Project 3948/754)

APPROVED

S. Tsakonas

S. Tsakonas
Head
Fluid Dynamics Division

Preceding page blank

INTRODUCTION

The Comprehensive Program on Hydrodynamic Interaction Effects for An Expandable Floating Base was formulated after the completion of an Exploratory Program, which has been reported by Mercier.¹ Unfortunately while the results of the Exploratory Program elucidated the effects of float proximity and scale on wave forces and the influence of tank walls, a specific explanation of the phenomena which has been called "tail-wagging" was not developed. The articulated model experienced dynamic motions response which cannot be explained except as due to mechanical interactions through the linkages. A detailed dynamic analysis for the articulated model has not been undertaken as it is believed that the interaction must be either nonlinear or due to unobserved elastic deformations or mechanical "slop" (imperfect fit of shoulder screws and bearings).

An experimental program to study the effect of hydrodynamic interaction on vertical motions response of resiliently connected arrays of floats was carried out in Davidson Laboratory's Tank No.2 during August and September 1972. The influence of float center-to-center spacing, expressed in terms of waterline diameter, float slenderness, deck rigidity, size of array, externally provided damping, and yaw-restraining spring-line restraint, have been investigated.

The heave response characteristics of isolated slender vertical floats have also been investigated in greater detail than previously,² making use of more complete and accurate hydrodynamic analysis. These results which include a rather complete discussion on the importance of damping, were presented by Mercier and Kim³ at the recent 9th Symposium on Naval Hydrodynamics. This material is reproduced here, with changes in paginations and numbering of equations and references only.

¹ Superior numbers in text matter refer to similarly numbered references listed at the end of this report.

Comprehensive results of the model test program are presented and discussed. The response is cleanly strongly influenced by the elastic characteristics of the simulated deck. Observations of the behavior of the hinged attenuators in regular and irregular waves are reported.

This work constitutes PART 2 of Phase a "Comprehensive Program on Hydrodynamic Interaction Effects" performed by Davidson Laboratory (DL) for Goodyear Aerospace Corporation (GAC) under Purchase Order 2B1115YX.

ISOLATED FLOAT HEAVE RESPONSE

(The following material is taken directly from Reference 3, with changes made only in pagination and numbering of equations and references.)

Elementary Equation of Motion

In the configuration depicted in Figure 1, the net buoyancy comes from the portion of the float above the hinge, which is located some distance below the stillwater level. The float shape, which is enlarged below the waterline, is intended to minimize the wave-induced vertical forces transmitted to the deck and structure, and thus minimize deck motions over a "sufficient" range of wave frequencies. The hinge is introduced to alleviate lateral loads in the float and in the structure: the wave-induced forces produce pendular motions of the lower part of the float (which is called an "attenuator") which relieve the elastic stresses and transmitted loads which would develop without the hinge.

Since the deck structure is assumed to be quite flexible, the (linearized) equation for the heave (z) motion, neglecting elastic restoring forces, can be expressed simply as

$$\rho \nabla \ddot{z} = -m'' \ddot{z} - Z_d \dot{z} - Z_r z + Z_\zeta \zeta \quad (1)$$

where

∇ = total displaced volume of float and attenuator

m'' = added mass

Z_d = damping force rate

Z_r = buoyant restoring-force rate = $\rho g A_w$

A_w = waterplane area

Z_ζ = wave-induced vertical force per unit wave elevation

ζ = wave elevation

If the deck's elastic restoring-force is to be taken into account, a term such as $EI \frac{\partial^4 z}{\partial x^4}$ must be incorporated to describe motion in regular long-crested waves, such that the deck structure behaves like a beam (the more general case would have to represent the deck's elasticity as plate-like, or describe the details of the deck-truss structural behavior). These partial differential equations are considerably more complicated than the simpler equation (1). The deformation of the deck of a

rectangular array of floats in regular "head" seas, assuming that no hydrodynamic interaction effects occur on the vertical forces on float elements, will be (at least in the case of linear response) a traveling wave with the same frequency and celerity as the incident water wave:

$$z_b = z_c \sin \left(\frac{2\pi x}{\lambda} - \omega t \right) \quad (2)$$

then

$$\frac{\partial^4 z_b}{\partial x^4} = \left(\frac{2\pi}{\lambda} \right)^4 z_b \quad (3)$$

or, since for water waves $2\pi/\lambda = \omega^2/g$,

$$\frac{\partial^4 z_b}{\partial x^4} = \frac{\omega^4}{g^2} z_b \quad (4)$$

The importance of a restoring force term like $EI \frac{\partial^4 z}{\partial x^4}$, compared to $\rho g A_{up} z$, increases as the frequency increases, or the wave length decreases. The design of the float-attenuator geometry is intended to produce vanishingly small wave-induced vertical force as frequency is increased. GAC structural analysts decided that the simple Equation (1) is appropriate for analyses of the motions of the deck supported by a resiliently-connected array of floats, such as is shown in Figure 1.

Coefficients of the Equation and Forces for Regular Waves

Elementary hydrodynamic theory can be applied to the estimation of the hydrodynamic coefficients and the wave-exciting forces for the equations of motion of slender vertical floats without external appendages. In the present instance, it is anticipated that external appendages will be required to assure sufficient heave damping and analyses of the hydrodynamic effects of the appendages must be approximate and empirical.

The buoyant force rate has already been expressed as $\dot{z}_z = \rho g A_{v1} \cdot$

The vertical wave-exciting force can be expressed as

$$F_z = \underbrace{\rho g \zeta S(0)}_{\text{Hydrostatic}} + \underbrace{\rho g \zeta \int_{-T}^0 (1 - e^{kz}) \frac{dS}{dz} dz}_{\text{"Smith" Correction}} - \underbrace{Z_\zeta \frac{\partial \zeta_e}{\partial t}}_{\text{Damping}} - \underbrace{\sum m' \omega^2 \zeta_e e^{kz_e}}_{\text{Added Mass}} \quad (5)$$

Froude-Krylov

where S = sectional area of body

k = wave number = $\omega^2/g = 2\pi/\lambda$

λ = wave length

Z_ζ = damping coefficient

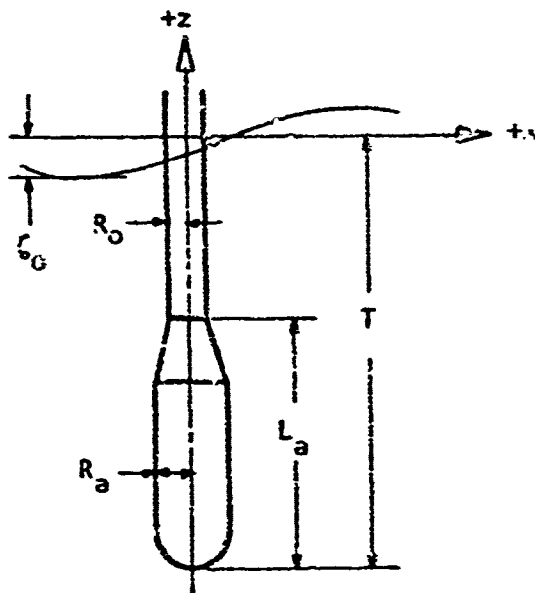
ζ = wave elevation

ζ_0 = wave amplitude

ζ_e = wave motion evaluated at depth corresponding to assumed damping source

m' = element of effective added mass in vertical direction

z_e = effective depth for evaluating wave acceleration for element of added mass



The Froude-Krylov force corresponds to that predicted by slender body theory and is the same as predicted by assuming that the presence of the body does not influence the wave's pressure field. For finite draft, T , the Froude-Krylov force decreases with increasing wave frequency (because of more rapid attenuation of wave pressure with depth) and, if the attenuator is shaped as in the sketch, may become opposed in sense to the wave elevation for sufficiently high frequencies.

The response of slender spar buoys to waves has been studied by Newman,⁴ who performed a detailed slender-body analysis and by Rudnick,⁵ who derived equations similar to Newman's⁴ on the basis of a more elemen-

tary analysis, and who compared results of calculations with field measurements of the motions of the Flip platform. Newman notes that the slender-body theory applied to floats in waves loses its applicability at higher values of slenderness ratio than is the experience for aerodynamic analyses. Adey and Bai⁵ have conducted experiments with cylindrical models having either flat or conical bottom ends and various draft-to-diameter ratios. They find that it is important to account for added mass effects even for quite slender floats. However, while they include added mass effects on the inertial force (proportional to \ddot{z}), they appear to have neglected its effect on the vertical wave-induced force. For non-cylindrical floats, such as shown in the sketch, the inclusion of added mass effects is still more significant.

The added mass wave force results because the flow is unsteady and the presence of the body does modify the fluid acceleration patterns (contrary to the Froude-Krylov assumption) resulting in a pressure force in phase with the vertical wave acceleration. The added mass may be associated with two principal sources, the primary one being the enlarged attenuator at the lower end of the float. Externally-attached damping devices will also have associated added masses. The effective added mass from the primary source, the enlarge attenuator, may be estimated by assuming that the attenuator is similar to a prolate spheroid with a ratio of semi-major to semi-minor diameter, a/b equal to $L_a/2R_a$. Lamb⁷ gives theoretical added mass coefficients for translation "end-on" that can be expressed as

$$m'_a = \frac{1}{3} \rho \pi R_a^3 k'_1 \quad (6)$$

where k'_1 can be taken from the following table

TABLE 1 VERTICAL ADDED MASS COEFFICIENT

$L_a/2R_a$	k'_1
1.0	0.5
1.5	0.458
2.0	0.418
2.51	0.392
2.99	0.365
3.99	0.327
4.99	0.294

It has been found, of course, that the ideal fluid theory added mass is insufficient for slender craft such as airships and surface ships in monotonic rectilinear motion, presumably because of boundary layer influences (cf. Thompson and Kirschbaum⁸ and Smith⁹). The reasons for the differences between theory and experience for these craft may not be relevant to the float-attenuator in the wave flow field so the tabulated theoretical values are recommended for use pending more complete experimental results. The wave acceleration can be evaluated at an effective depth, $z_e = T - L_a/2$.

The added mass associated with the damping devices, which probably would be attached to the float at the upper end of the conical transition above the attenuator (see sketch), is not derivable from familiar simplified cases. The interaction of the flow about the damping "collar" with the flow about the cylinder may be important and ought to be studied experimentally. For the purposes of the present analysis, the added mass of damping devices will be assumed to be a fraction of the added mass of the attenuator

$$m_d' = c m_a' \quad (7)$$

where appropriate values of c should be obtained experimentally or simply assumed. The value of z_e to be used for evaluating the wave acceleration for this component of force should be the depth corresponding to the damping source.

The total added mass, m'' , is the sum of that associated with the attenuator shape plus that due to damping devices.

The heave damping force rate, Z_z , is partly due to generation of radiated surface waves and partly to viscous influence associated with turbulent eddies around the float and damping plates and skin friction drag. It will be shown in the following section that the damping due to wave generation, which is strongly dependent on frequency, is quite small for slender vertical floats and, therefore, it is advantageous to provide additional viscous damping, which is likely to be independent of frequency. The damping coefficient will be expressed in terms of the ratio of the

damping coefficient, (c/c_c) , in the form

$$Z_z = \left(\frac{c}{c_c}\right) \times (2\rho \nabla + m'') \omega_n \quad (8a)$$

$$= \left(\frac{c}{c_c}\right) \times 2\rho A_w \sqrt{gTC_{vp}(1+C_{HH})} \quad (8b)$$

where

$$C_{vp} = \text{vertical prismatic coefficient, } \frac{\nabla}{A_w \bar{T}}$$

$$C_{HH} = \text{added mass coefficient, } \frac{m''}{\rho \nabla}$$

The viscous drag due to external damping devices will not, in general, be simply linearly proportional to velocity (although for small waves and motions it will be approximately so). The use of a linear coefficient may be justified on the bases that calculations based on such a simplification are instructive and that "equivalent" linearized coefficients may be derived for drag which is proportional to some other power of velocity in the way that Blagoveshchensky¹⁰ and others have dealt with square-law damping.

Particular values of drag coefficients may be estimated for plates oscillating in a direction normal to their surfaces from results of significant investigations by Keulegan and Carpenter,¹¹ McNown,¹² McNown and Keulegan,¹³ Paape and Breusers,¹⁴ Martin,¹⁵ Ridjanovic,¹⁶ Brown,¹⁷ Henry,¹⁸ Woolam¹⁹ and Tseng and Altman.²⁰ Additional investigations of the oscillating drag of ring-type damping collars around bodies of revolution will be needed to provide information on the type of configuration being considered for these floats, as shown in Figure 1, where damping plate-body interaction effects may be significant.

The wave-exciting force associated with the damping devices, $Z_z \frac{\partial \zeta_e}{\partial t}$, may be estimated by taking $Z_z = Z_z$, and $\frac{\partial \zeta_e}{\partial t}$ is the wave motion evaluated at the depth corresponding to the damping plate. Of course, since the oscillatory drag force on the damping devices is, in general, nonlinearly related to the relative velocity between the fluid and the plate,

the detailed analysis of the motions would be rather more complicated than the simplified treatment given here. The effects of the nonlinearity of the drag may be expected to be important only for frequencies near the resonant frequency.

Responses

Although analyses have been presented by Newman⁴ and others for wave-induced forces and motions of isolated spar-type floats, no results of systematic evaluations of the dependence of the forces and motions on geometric characteristics of floats are known to be available in published literature. Some results for the special case of floats like that shown in the sketch accompanying Eq.(5) will be presented here.

The influence of the ratio of the diameters of the lower and upper cylindrical parts R_a/R_o , the ratio of the length of the lower cylinder to the overall draft, L_a/T , and the ratio of the draft to waterplane radius (slenderness ratio), T/R_o , will be shown. Wave forces and motions due to regular waves will be presented as a function of frequency, and spectral response information will be given as a function of significant wave height. The influence of the degree of damping on the responses will be described in a subsequent section.

Wave-Induced Force

The wave-induced vertical force, $Z_c \zeta$, expressed as a function of the buoyant force, $\rho g S(o) \zeta$, is exhibited in Figure 2 as a function of the dimensionless frequency parameter $\omega^2 T/g$, showing the influence of R_a/R_o . Other geometric parameters were held fixed for these results, viz., $L_a/T = 0.5$, $T/R_o = 30$; the assumed damping coefficient corresponds to a value of $c/c_c = 0.07$. Figure 3 shows the influence of L_a/T for $R_a/R_o = 1.8$, $T/R_o = 30$; again, $c/c_c = 0.07$. The influence of T/R_o is presented in Figure 4 for $R_a/R_o = 1.8$, $L_a/T = 0.5$ and $c/c_c = 0.07$. For all cases presented the damping plate added mass, m'_d , is assumed to be $0.3 m'_a$ and its effective depth $z_e = T - L_a$.

The results presented are typical: as frequency increases, the

vertical force decreases at first until it reaches a minimum value (which corresponds very closely to the "damping" component of the wave-induced force, Eq. (5), and then increases again when the components of force which are out-of-phase with wave elevation (due to pressure gradient and added mass) become important, followed by asymptotic attenuation to zero force for very short waves. Both R_a/R_o and L_a/T are seen to have important effects on the wave-induced force, T/R_o is less important; in fact, the simplified theory (Kewman⁴) neglecting added mass and damping indicates no dependence on T/R_o .

Transfer Functions

The ratio of heave motion to wave elevation can be derived from the solution of Eq. (1). This may be re-written in a form similar to that for the familiar simple harmonic oscillator

$$\frac{z}{\zeta} = - \frac{z_e \zeta / \rho g S(o) \zeta}{\sqrt{\left(1 - \frac{\omega^2}{\omega_n^2}\right)^2 + \left(2 \left(\frac{c}{c_c}\right) \frac{\omega}{\omega_n}\right)^2}} \quad (9)$$

where

$$\frac{\omega_n^2 T}{S} = \left[c_{vp} (1 + c_{HH}) \right]^{-1} \quad (10)$$

Only one set of transfer functions, exhibiting the dependence on R_a/R_o for $L_a/T = 0.5$, $T/R_o = 30$, $c/c_c = 0.07$, $m'_d = 0.3m'_a$ and $z_e = 0.5$ (for damping plates), will be given in Figure 5. These results are, again, typical: the trends of the variation of motions with frequency follow the wave forces modified by the dynamic amplification factor. Note that the damping coefficient assumed, $c/c_c = 0.07$, results in values of the transfer function around 2.0 at resonance, and that the maximum value depends on the float shape as well as the relative damping.

Spectral Response

The statistics of the heave motion response may be derived for

slender vertical floats using the transfer functions and the (dimensionless form of the) Pierson-Moskowitz wave spectrum, as was done in the first part of the paper³ for three- and four-float platforms. The significant dimension for use in non-dimensionalizing will be the draft for this case, instead of $\nabla^{1/3}$.

Some results showing the effect on "significant heave motion," $z_{1/3}/T$, of R_a/R_o , are given in Figure 6 with other particulars, the same as for Figure 2. The influence of L_a/T on the significant heave is shown in Figure 7 for the same cases as are considered in Figure 3. The effect of T/R_o on the statistical responses is small, as might be expected from the results for forces shown in Figure 4 — at least for floats which are sufficiently slender.

According to Figures 6 and 7, the "best" float shape is evidently a function of the design sea state or significant height: slender floats with displacement relatively uniformly distributed being better for mild sea conditions while higher values of R_a/R_o with the displacement concentrated near the bottom are better for more severe seas. An irregularity, or "bump," is discernible in some of the curves for values of $H_{1/3}/T$ at which an increase of sea state introduces a large increment of wave energy at the resonant frequency of the float.

It is interesting to note that the dependence on significant wave height of other heave-related spectral response characteristics may differ from that of heave. Figure 8 shows significant values of heave motion, vertical acceleration, and deck curvature, $\frac{\partial^2 z}{\partial x^2}$, for a particular float having $R_a/R_o = 1.8$, $L_a/T = 0.5$, and $T/R_o = 30$. Since the transfer functions for acceleration and deck curvature depend on frequency in a different way than does heave, weighing high frequency more heavily, while attenuating low-frequency input, higher sea states do not produce as much increase of response as for heave. This is because an increase of sea state (according to the Pierson-Moskowitz spectra) adds significant energy in the low frequency range but not much at higher frequencies. For the case presented, the deck curvature (and therefore the deck stresses) are very nearly proportional to the significant wave height, since

$\left(T \frac{\partial^2 z}{\partial x^2}\right) / \left(H_{1/3}/T\right) \approx 0.3$ over the range of $H_{1/3}/T$ values presented.

The Importance of Damping

The primary effect of an increase in the damping coefficient on the heave transfer functions is to reduce the maximum heave response, which occurs at a frequency slightly lesser than the resonant frequency, and to increase the minimum value which occurs for the frequency when the wave-induced force is due to the damping devices alone.

For design-analyses, the spectral response is most useful.

Figure 9 shows effect on significant heave motion of damping coefficient, c/c_c , for a particular float geometry. It is evident that damping is very useful to control motions in high sea states where some wave energy exists at frequencies corresponding to heave natural frequencies.

The damping which is available due to wave radiation can be obtained from the Haskind-Newman relations,²¹ which gives the same result as Newman's slender-body analysis for the forces at resonance.⁴ These give

$$Z_{z_w} = \frac{k^2}{2\rho g w} |Z_{\zeta}|^2 \quad (11)$$

thus, at resonance $\omega = \omega_n$, the ratio of wave-damping to critical damping can be obtained as

$$\begin{aligned} \left(\frac{c}{c_c}\right) &= \frac{Z_{z_w}}{2\rho\gamma(1+C_{HH})\omega_n} \\ &= \left|\frac{Z_{\zeta w}}{\rho g A_w}\right|^2 \frac{1}{4} \left(\frac{\omega_n^2 T}{g}\right)^2 \frac{A_w}{T^2} \end{aligned} \quad (12)$$

and the corresponding transfer function

$$\begin{aligned} \frac{z}{\zeta} &= \frac{|Z_{\zeta w}/\rho g A_w|}{2(c/c_c)_w} \\ &= \frac{2T^2/A_w}{|Z_{\zeta w}/\rho g A_w| \left(\frac{\omega_n^2 T}{g}\right)^2} \end{aligned} \quad (13)$$

where Z_{Gw} is the wave-induced vertical force evaluated without taking into account the damping term.

Since, at resonance, $|Z_{Gw}/\rho g A_w| < 1$, and for slender vertical floats $T^2/A_w \gg 1$ and $\frac{\omega^2 T}{\zeta} < 1$, then $c/c_c \ll 1$ and $z/\zeta \gg 1$. For example, for $T/R_o = 30$, $R_a/R_o = 1.8$ and $L_a/T = 0.5$, the calculated 'wave-damped' resonant heave motion z/ζ would be almost 8000! Wave-associated damping is inadequate for slender floats and viscous damping controls the resonant motion.

Results of tests on a 1/13th-scale model of a Manned Open Sea Experimentation Station (MOSES) reported by the Oceanic Institute, Waimanalo, Hawaii,²² showed that a ratio of damping to critical damping of 0.075 could be achieved. This was discovered in tests of the model with about 18 external rings attached to a slender shaft. The rings, which are intended to provide structural stiffening, have outside diameter about 15% larger than the shaft. Complementary tests were carried out with acetate sheet wrapped tightly around the rings to present a smooth, unbroken surface. With this shroud the damping was about 1% of critical.

Damping coefficients will, in general, be obtained most effectively by experiments, or will be estimated on the basis of empirical results. It has been known since Froude's investigations in 1874,²³ that the drag coefficient for an oscillating bluff body can be very different from that for the same body in steady flow. As in all model experimental work, it is important to be sure that the model conditions correspond to the full scale: thus, for dynamic similarity to exist, the model should be geometrically similar and the flow kinematically similar to the full size.

Certain experience from investigations of roll damping of ships with appendages can give insight into questions relevant to damping of platforms oscillating in waves. It is important to recognize that a small ambient current, due to oceanic circulation or induced by wind, can have an appreciable effect on energy dissipation, as has been found by many investigators into the rolling of ships.²³⁻²⁹ This is because the model, in the course of its cyclical motion, must impart motion to fresh, previously unentrained water. Consider that for a current speed of only

one knot past a moored platform, the fluid which is "entrained" by the motion of a platform may convect about 17 feet during a 10-sec period; such a period is common for ocean waves, and the distance is about half of a typical column diameter for a large semi-submersible drill rig. Entrained fluid energy can be convected away at an appreciable rate by modest currents producing important effects on damping and, hence, resonant response.

Indeed, when the damping force is non-linear and, hence, superposition cannot be applied, it may be inappropriate to apply an oscillatory drag coefficient obtained for a particular structural element from tests with rectilinear oscillatory motion^{11-13,15-19} to the somewhat different kinematic conditions of the orbital velocity pattern of waves. The differences may be modest but the question should be posed and, hopefully, investigated.

The question of scale effects is persistently present and model experimenters must be alert (and somewhat intuitive) to recognize when it may be appreciable. When phenomena are recognized to be predominantly viscous in origin, we are likely to suspect the possibility of scale effect. This is, of course, due in large part to the history and experience of testing ship models for resistance. Very little is known about scale effects on oscillatory hydrodynamic forces which may be relevant to platform motions testing and analysis. Some years ago, however, a program of experiments to study scale effects on roll damping of circular cylinders with and without appendages was undertaken by the Naval Ship Research and Development Center and Davidson Laboratory. While these studies were not directed to platform motions, the results are relevant to the phenomena of oscillatory damping in general and since they are the only results with which we are familiar showing the effect of model size, it may be useful to discuss them. Three cylinders with diameters of 6-in, 12-in and 24-in were suspended vertically in water by torsion springs. Three kinds of appendages were symmetrically attached to the models, as shown in Figure 10 for the smallest (6-in-diam) cylinder. Curves of decaying oscillation from various initial angular displacements were recorded and

analyzed to obtain "square-law" damping moment coefficients of the form

$$C_m = \frac{\text{damping moment}}{(\rho/2) A R_{c.a.}^3 \dot{\theta} |\dot{\theta}|} \quad (14)$$

where A is the frontal area of both appendages and $R_{c.a.}$ is the radius from the axis of rotation to the center of area of the appendage. The results are tabulated in Table 2.

TABLE 2. EFFECT OF MODEL SIZE ON ROLL DAMPING MOMENTS FOR CYLINDERS WITH APPENDAGES. (C_m values Eq.14)

<u>Cyl. Diameter</u>	<u>Bilge Keels</u>	<u>Sharp-Edged Fins</u>	<u>Streamlined Fins</u>
6 in	17	16	4.2
12 in	16	17	3.1
24 in	15	Not Tested	2.9

The 6-in and 12-in diameter models were tested at Davidson Laboratory by Mercier,²⁸ while the largest model was tested at the Naval Ship Research and Development Center by Gersten.²⁹

The lessons of these test results are not entirely unexpected: sharp-edged geometric details produce high drag and little scale effect while well-rounded geometries produce lesser drag and are susceptible to perceptible scale effect. These results may provide qualitative guidance for other applications and configurations, such as for choosing a suitable scale ratio for a wave test of a floating platform with buoyant caisson- and -footing floatation elements.

Damping effects, while of principal importance for a fairly narrow band of frequencies near resonance, can have an appreciable effect on spectral response when there is appreciable wave energy at the resonant frequency. The nature of the damping and its dependence on geometric and flow features is as yet only imperfectly understood and needs to be studied more vigorously.

DECK ELASTIC RESPONSE

Some very simplified discussions of elastic models of the deck and flotation system for the Expandable Floating Base will be presented which indicate that the horizontal forces acting on float-attenuators can produce important deck deformations for the model and, perhaps, the prototype base. It may be that elastic response to the rather large horizontal forces (large compared to vertical forces) accounts for the observed so-called "tail-wagging" of the articulated model and the "beam-like" behavior of the elastically-scaled models which will be described below.

The correspondence (and difference) between features of the elastically scaled model of a segment of the Expandable Floating Base will be discussed later.

More detailed and comprehensive studies of the dynamics of the structure may be expected to produce a more complete explanation and understanding of the reactions to waves of large arrays of elastically-connected floats in waves.

Static Response to Vertical and Horizontal Float Forces

The behavior of an infinite beam on an elastic foundation subjected to normal loads and couples, distributed sinusoidally along the length of the beam may be considered to be analogous to that of the Expandable Floating Base (of large length compared to wave length) acted on by wave-induced vertical and horizontal forces on the flotation elements. The relationship between the horizontal forces on the floats and the distributed couples is due to these forces being applied to the floats below the waterline which is well below the neutral axis of the deck structure. (Actually, this truss structure may behave only approximately as a beam, but the simplification permits the application of the well developed analysis of beams on elastic foundations.)

The wave-induced loads and buoyant resistance to vertical motions are associated with the individual float elements (or rows of floats) but, in

the spirit of railroad track analysis, where closely-spaced cross-ties are assumed to act as uniformly distributed foundations, both buoyant stiffness and wave-induced loads will be assumed to be uniformly distributed. The differential equation for bending of a beam with rigidity EI is

$$EI \frac{d^2 z}{dx^2} = M \quad (\text{moment}) \quad (15)$$

which can be differentiated to give

$$EI \frac{d^4 z}{dx^4} = \frac{d^2 M}{dx^2} = w \quad (\text{distributed load}) \quad (16)$$

For the beam on an elastic foundation, part of the distributed load w is due to externally applied loads while part is due to the foundation reaction.

The foundation reaction, due to buoyancy, for the elastic deck is, approximately,

$$q = -kz = - \frac{npgA_w}{S} z \quad (17)$$

where n is the number of floats in one row (transverse to the "length" direction of the beam, which is assumed to be the direction of wave motion) and S is the row-to-row spacing of floats; pg is the specific weight of water and A_w is the waterplane area.

The equivalent wave forces are distributed sinusoidally. The distributed vertical force may be expressed as:

$$p_w = \frac{nZ_\zeta \cdot \zeta \cdot pgA_w}{S} \sin \frac{2\pi x}{\lambda} \cdot (\cos \omega t \mp \epsilon_z) \quad (18)$$

where the wave elevation is

$$\zeta \sin \frac{2\pi x}{\lambda} \cos \omega t \quad (19)$$

and

$$Z_\zeta = \frac{\text{Amplitude of Heave Force Due To Waves}}{\text{Amplitude of Wave}} \cdot \frac{1}{pgA_w} \quad (20)$$

ω = wave frequency (rad/sec)

ϵ_z = phase lag of heave force after wave

A distributed wave-induced couple due to horizontal loads may be expressed as

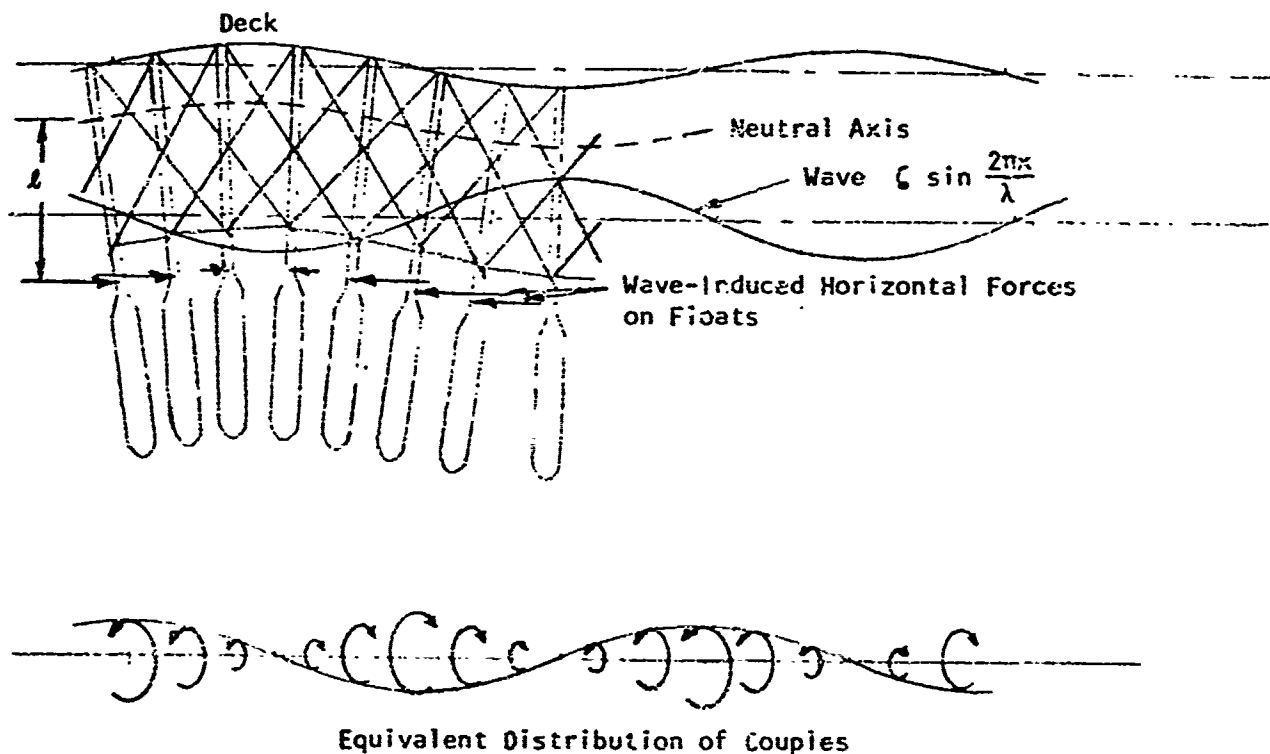
$$M_w = \frac{n l x_s \cdot \zeta \rho g A_w}{S} \sin \frac{2\pi x}{\lambda} \cos(\omega t - \epsilon_x) \quad (21)$$

where

$$x_s = \frac{\text{Amplitude of Surge Force Due to Waves}}{\text{Amplitude of Wave} \times \rho g A_w}$$

ϵ_x = phase lag of surge force after wave

l = distance from center of surge force to neutral axis of beam (see sketch)



SKETCH OF
DECK AND FLOAT SYSTEM SUBJECTED TO HORIZONTAL WAVE-INDUCED LOADS
AT DISTANCE l FROM THE NEUTRAL AXIS
OF THE BEAM, AND THE EQUIVALENT DISTRIBUTED COUPLES

This distributed couple can be introduced on the equation for the beam on an elastic foundation in terms of its derivative

$$p_w = \frac{dM_w}{dx} = \frac{2\pi n \ell \chi_c}{\lambda S} \zeta \rho g A_w \sin \frac{2\pi x}{\lambda} \cos(\omega t - \epsilon_x + \frac{\pi}{2}) \quad (22)$$

Dynamic effects, transverse inertia, rotatory inertia and, perhaps, elastic shear rigidity effects, should be accounted for but will be omitted to simplify the analysis and discussion.

The quasi-static response of the assumed infinite beam may be obtained from the equation

$$\frac{d^4 z}{dx^4} + \frac{k}{EI} z = C_i \sin \frac{2\pi x}{\lambda} \cos(\omega t - \epsilon_i) \quad (23)$$

whose (steady-state) solution may be written

$$z = \frac{C_i \sin \frac{2\pi x}{\lambda} \cos(\omega t - \epsilon_i)}{\left(\frac{2\pi}{\lambda}\right)^4 + \frac{k}{EI}} \quad (24)$$

Since the differential equation is linear, we may consider the response to have exciting forces ($i=z$), where

$$C_z = \frac{n Z_c \cdot \zeta \rho g A_w m}{EI S} \quad (25)$$

and $\epsilon_i = \epsilon_z$ separately from response to moments due to surge force ($i=x$), where

$$C_x = \frac{-2\pi n \ell \chi_c}{EI \lambda S} \cdot \zeta \rho g A_w \quad (26)$$

and $\epsilon_i = \epsilon_x - \pi/2$.

The importance of the different kinds of excitation, in terms of the deflections they may be expected to produce depends on the ratio C_x/C_z , that is

$$\frac{C_x}{C_z} = \frac{-2\pi \ell \chi_c}{\lambda Z_c} \quad (27)$$

Since χ_c is of the order of ten times Z_c , it may be expected that deck deflections due to horizontal float forces will be of equal or greater importance than those due to vertical forces if $\lambda \leq 20\pi l$. Since l , the distance from the center of the horizontal forces to the neutral axis of the deck may, for example, be greater than half the freeboard, which is about 30 feet, the horizontal forces may be more important for waves less than about 900 feet in length, with a corresponding period of 13 seconds. This influence of horizontal forces may be even more important if certain kinds of dynamic effects are appreciable, as is suspected to be the case for the present elastic models.

The importance of deck bending elasticity compared to buoyant restoring forces may be judged from the ratio

$$\frac{\text{Elastic}}{\text{Buoyant}} = \frac{16\pi^4 EI}{k\lambda^4} = \frac{16\pi EI \cdot S}{npg A_w \lambda^4} \quad (28)$$

This may be evaluated for values of the parameters which have been considered in some of the preliminary design-analyses for the Expandable Floating Base, and for the model tests described in the present report, viz.:

$$n = 10 \text{ floats in a row}$$

$$A_w = \pi \cdot 3^2 = 28.3 \text{ ft}^2$$

$$\rho g = 64 \text{ lb/ft}^3 \text{ (sea water)}$$

$$S = 3.75 \cdot 6 \text{ ft} \times \cos 60^\circ = 19.5 \text{ ft}$$

$$EI = 80 \times 10^6 \text{ lb ft}^2/\text{ft} \times 225 \text{ ft breadth} = 18 \times 10^9$$

so that

$$\frac{\text{Elastic}}{\text{Buoyant}} = \frac{302 \times 10^8}{\lambda^4} \quad (29)$$

It appears then that the buoyant restoring forces are more important than the beam-like elastic forces for wave lengths, λ , greater than about 400 ft, where the wave period is about 9 sec.

These (over-) simplified considerations suggest both that deck elasticity ought to be taken into account in evaluating motions response

and that moments due to wave-induced surge forces on floats and attenuators can produce significant vertical deck deflections. These investigations ought to be pursued further, including important inertia effects and considering finite-length decks and with elastic connections of float elements for both the tested models and the proposed prototypes carefully accounted for.

A Rudimentary Dynamic Model

Studies of the dynamic response to vertical wave-induced forces of a very large island, with very large float-attenuators, having relatively resilient decks, were reported by GAC in the Phase I Technical Report on Expandable Floating Bases,³⁰ dated 15 November 1970. The scale models which have been tested are not of correspondingly large extent, being limited to 35 rows (articulated model) or 17 rows (elastic models) and having rather smaller floats and attenuators than those considered in the early GAC investigation.

The present, admittedly qualitative and elementary analysis was undertaken to check whether a shorter array of smaller floats might exhibit dynamic amplification effects, especially at the fore and aft ends, suggestive of those observed with the articulated and, later, the elastic arrays. The most rudimentary elastic model is like a string, where a large initial tension (large compared to perturbations) produces elastic restoring forces. The differential equation, without excitation, of a string with uniformly distributed mass is

$$T \frac{\partial^2 z}{\partial x^2} = \mu \frac{\partial^2 z}{\partial t^2} \quad (30)$$

where

T = string tension

μ = mass per unit length of string

The normal modes are

$$\varphi_i(x) = \sin \frac{i\pi x}{l} \quad i = 1, 2, \dots, n \quad (31)$$

where

l = a characteristic length, the length between ends of the string.

For a uniform beam the corresponding equation is:

$$EI \frac{\partial^4 z}{\partial x^4} = -\mu \frac{\partial^2 z}{\partial t^2} \quad (32)$$

The normal modes for simply supported end conditions are

$$\varphi_i(x) = \sin \frac{i\pi x}{l} \quad i = 1, 2, \dots, n \quad (33)$$

The correspondence between response of a model with string-like elasticity elements and one with beam-like elasticity elements is imperfect, to be sure, but the evaluation is quite simple and may be of interest.

The model is discretized, and the finite-difference equation is written:

$$K(z_{j+2} - 2z_{j+1} + z_j) + (-\omega^2 M + B)z_j = F_j \quad m=1, \dots, N \quad (34)$$

where

z_j = heave amplitude of j^{th} float

M = mass of one float

B = heave restoring force due to buoyancy

K = spring constant = $\frac{\text{string tension}}{\text{float spacing distance}}$

F_j = heave exciting force on j^{th} float

A few calculations have been carried out for an array having 35 rows of floats with mass and buoyancy characteristics like the articulated model which has been tested.^{1,2} The amplitudes of wave-exciting force F_j used were obtained from the tests of the rigidly-held array reported in Ref.1, which show a variation with position in the array and a small fore and aft

asymmetry. The phasing of the exciting forces was assumed to be described as

$$F_j = |F_j| \sin \left(\frac{2\pi x_j}{\lambda} + \epsilon \right) \quad (35)$$

where ϵ is assumed to be independent of j . Several values of spring constant, K , were taken, viz., $K/B = 0.002, 0.02, 0.1$ and 0.2 . Results for a model scale frequency, $f = 1$ Hz, are shown in Figure 11, compared with the observed experimental results. The spring stiffness is seen to have no discernible influence over the range of values covered. The distribution of calculated motion amplitudes follow very closely the measured wave-induced forces, and are appreciably different from the measured motions of the articulated model.

These results suggest that the anomalous feature ("tail-wagging") measured heave response of the articulated model is not due to a coupling between elastic characteristics of the float connections and the particular distributed pattern of heave exciting forces. The relationship of these observations to the anomalous feature of the elastic model behavior, which (as will be described below) is a more nearly fore-and-aft symmetric beam-like response, is not clear. Various experimental observations suggest an alternate explanation of this behavior.

MODELS

Since the exploratory tests did not yield a full explanation of the dynamic response to waves observed with the articulated model, it was decided to investigate hydrodynamic interaction effects on heave motion responses of arrays of floats connected by an elastic deck-like structure of known characteristics which approximately represents a prototype structure. This program of motions measurements constitutes an alternative approach to that which was originally anticipated, where wave-induced forces would be measured.

It was necessary to choose a size of array which was sufficiently large to assure adequate statical stability in roll and pitch, and also to

provide data for a representatively extensive island: an array 17 rows long having 10 floats per row was selected, roughly corresponding to a 200'x300' helicopter platform. Some tests were carried out with a configuration having only 9 rows of 10 floats each.

An important feature of the GAC proposal float-attenuator system is the hinge introduced to alleviate the transference of lateral wave-induced loads through the pressurized, water-filled fabric floats to the deck and truss structure. Since the dynamic response to wave action of the hinged attenuators, all in close proximity to one another, is important for applications of this concept, it was decided to model these hinges for this program of tests.

Floats and Transverse Structure

Rows of floats, which are parallel to wave crests during experiments, were assembled in units as depicted in the sketch of Figure 12. The floats are 1.5" O.D. x 0.035" wall thickness anodized aluminum tubes, each 12.5-in long. The tubes are interconnected by a built-up T-section having 1½-in wide top flange and 2-in deep web, of 1/16-in thick anodized aluminum with lightening holes milled in them. The outboard webs of the T-section incorporate small tabs with drilled holes to match the elastic interconnecting elements. The parts of the row (tubes, top flange, webs) are all bonded together with epoxy cement. The equilibrium draft is approximately 4.75 inches giving a freeboard to the bottom of the web of the T of about 5.75 inches.

Float structure components were made for three ratios of float spacing to waterline diameter, $S/D = 3.0, 3.75$ and 4.5 . Only two of these structures having $S/D = 3.0$ and 3.75 were actually assembled and tested however.

Modifications of the interconnections between the structures were introduced because it was noticed that the T-sections were rotating and twisting. Much of the rotation occurred due to twisting of the relatively weak tabs which were connected to the deck elastic elements (described in the following section), but there was also a large amount of twisting along

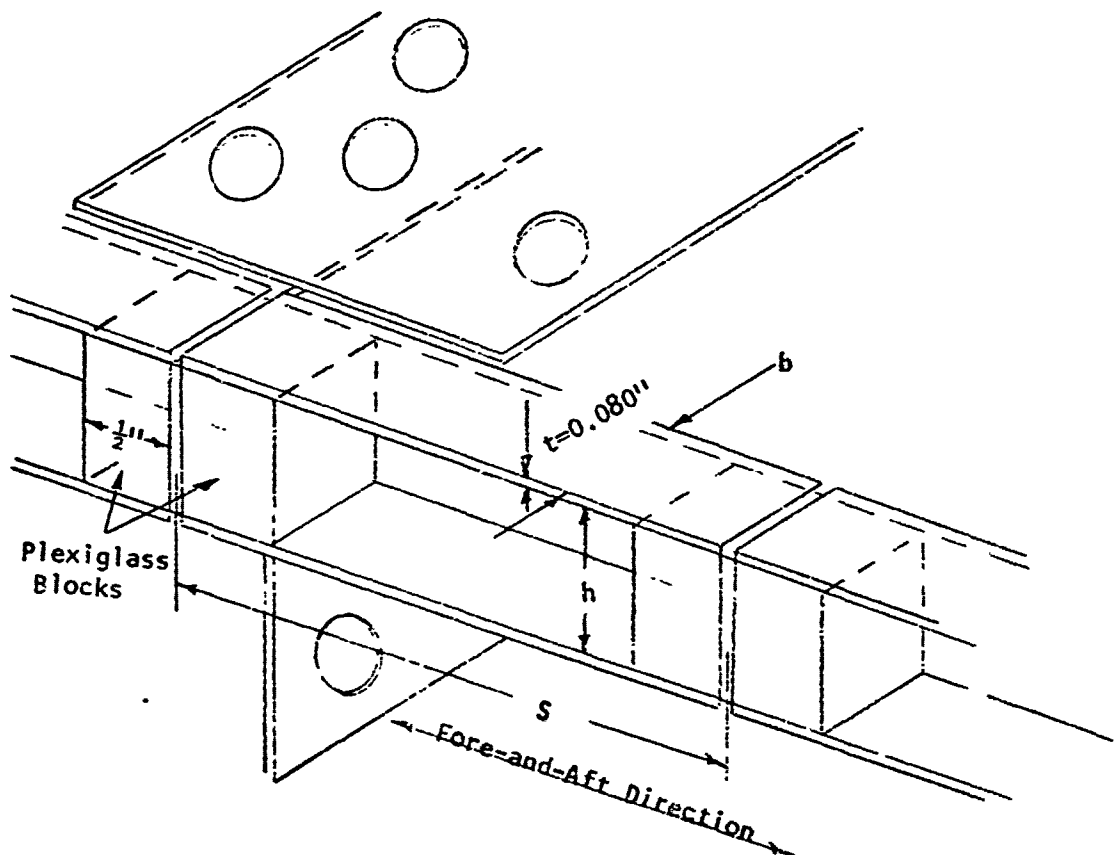
the span of the row, so that the middle floats rotated appreciably more than the floats at the ends of the rows. The rows of floats were tied together with lightly-tensioned wire, alternate rows, with floats in line with one another, being connected by fore-and-aft wires at two float positions in the middle of the row. Since end rows appeared to twist more than interior rows, a further modification was made so that rows 1 and 3, 2 and 4, 14 and 16 and 15 and 17 were connected by 1/8-in diameter aluminum rods, capable of withstanding compression, also at two float positions in the middle of the row. The bracing was connected to the float tubes, just below the web of the T-section, as depicted in the view of the deck structure looking athwartships in Figure 12. The effects of these ad-hoc improvements, which significantly reduce the twisting of the T-sections, on the equivalent deck rigidity (EI) is not known. Based on comparisons of test results (heave motions of deck in waves) with and without the stiffening, it is felt that the influence is not great.

Simulated Elastic Deck

GAC's studies of deck-truss behavior under wave action (Ref. 31, Table 12, p. 65) show a number of alternative effective deck-truss bending stiffnesses, evaluated for various assumptions concerning extreme wave loads and deck construction, on the assumption that the lower chord is in tension. If the wave position is such as to produce a "hogging" attitude, the lower chord would be put in compression. If it is a cable unable to withstand compression, the effective bending stiffness is dramatically different. Selection of a model-scale bending stiffness was based on correspondence between GAC and DL. dated 4 Jan 1971,³² where an equivalent plate EI of $80 \times 10^6 \text{ lb-ft}^2$ per foot is indicated to be suitable. In any case, it has been hypothesized that deck elastic reactions have small influence on heaving motions (compared to changes in float buoyancy). This is essentially the

reason for having selected the articulated interconnecting mechanism for the first series of large-array motions tests.

The equivalent plate rigidity of the model, according to Froude-Cauchy scaling laws, must be proportional to the fourth power of the scale ratio. Plexiglass deck flexural elements were designed to simulate on a scale of 1/48 the prototype EI of $80 \times 10^6 \text{ lb-ft}^2$ per foot. The design is in accordance with the sketch and Table 3 given below where the vertical spacing of the "flanges" of the beam depends on the total deck width, which depends on the float spacing ratio.



SKETCH OF
PLEXIGLASS DECK ELASTIC ELEMENTS

TABLE 3
CHARACTERISTICS OF DECK ELASTIC ELEMENTS
 $E \approx 450,000 \text{ lb/in}^2$ for plexiglass

BEAM	FLOAT SPACING S/D	WIDTH OF 10 ROWS in	EI MODEL lb-in ²	b in	h in
<u>plexiglass</u>					
1	3.00	57.0	8,000	1.0	0.391
2	3.75	67.6	10,000	1.0	0.447
3	3.75	67.6	20,000	2.0	0.447
4	4.50	78.3	12,000	1.0	0.497
<u>alum.</u>					
5	3.75	67.6	520,000 (3/4"x1/4"x1/16" Alum. L)		

Actually, a wider float spacing would probably call for increased deck rigidity, to accomodate local deck loads. Provision was made for studying the influence of variations in deck rigidity for one case (S/D = 3.75) where a beam with double-width "flanges" was prepared. A further, extemporaneous, variation in deck rigidity was investigated in which a light-weight, unequal leg angle (described in Table 3, as beam 5) was bonded to the ends of the T-section of the S/D = 3.75 model in addition to the standard width beam.

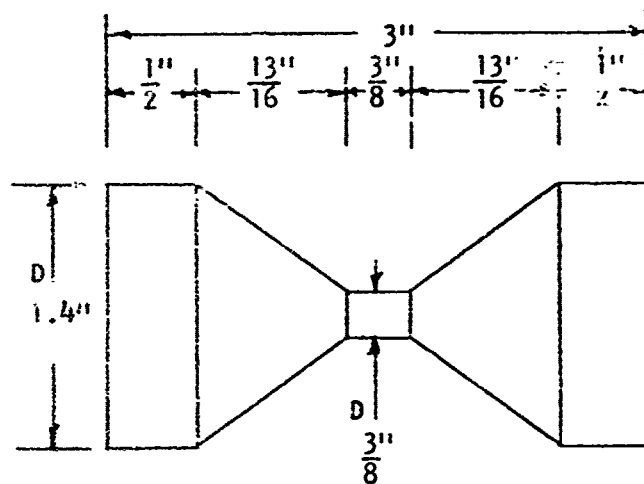
The design of the plexiglass flexural elements, without a "web" connecting the "flanges," permits appreciable deflection in response to shear forces while the deflections due to bending moments may be considered to be properly in accord with the scaled EI. The scaled value of shear rigidity (AG/k in Timoshenko's³³ notation) for the deck-truss structure is not known in any case.

The elastic elements are bolted to the tabs of the T sections as separate elements. Originally, it was planned that the elastic elements would be continous, but difficulties in aligning the rows and assembling them made it preferable to separate the flexures into individual segments.

Attenuators and Hinges

Inasmuch as alternative attenuator shapes were to be tested, it was necessary that they be interchangeable. It was decided to make the connection between the attenuators and the floats simulate the hinge of the planned prototype. Although it had previously been found¹ (at least for isolated floats) that the vertical wave-induced forces are unaffected by the presence of the hinge, it was felt that by introducing the hinge in the present tests some important information concerning the dynamic performance of large arrays of attenuators in close proximity would be developed.

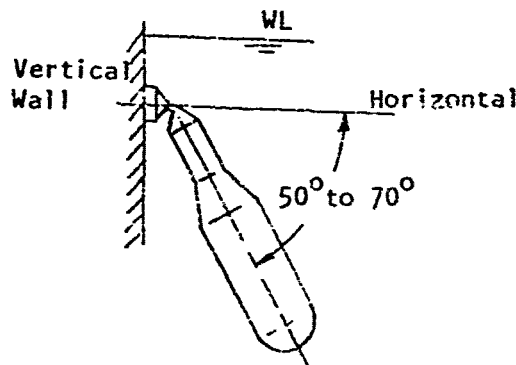
The hinges were supplied by GAC, made of silicone rubber in accordance with the sketch below. The hinges are quite flexible.



SKETCH OF SILICONE RUBBER HINGE

Attenuator shapes were chosen to satisfy a theoretical heave response criteria, as isolated spar buoys, of 1.75-ft extreme heave motion (calculated according to the motions response theory given in the ISOLATED FLOAT HEAVE RESPONSE ANALYSIS section of this report, with the extreme response statistical procedures of Ref.1) in Pierson-Moskowitz wave spectra having $H_{1/3} = 10$ ft. Two maximum diameters were chosen to be built and tested. Model scale dimensions are shown in Figure 13.

The upper parts of the floats are lengths of anodized aluminum tubes. The shaped portion is a thin-walled (approx. 1/8") wax casting. These attenuators were free-flooding and were ballasted to be very nearly neutrally buoyant and to have a vertical center-of-gravity slightly below the vertical center-of-buoyancy. Flooding with water and venting of air were accomplished through 1/8-in diameter holes in the bottom and near the top of the tube (below the hinge insert). The upper part of the tube was stuffed with styro-foam for buoyancy (approx. 1" of 4 lb/ft³ foam) and lead shot was added internally near the bottom of the float. Heated lead shot added to the casting became imbedded in the wax and, hence, would not fall out the fill hole. Proper balance of weight and buoyancy was noted by observing the free-floating attitude where the upper end of the hinge was made to float with a perceptible meniscus keeping it from sinking. Proper center-of-gravity was noted by assuring that, when the top of the hinge was held flush against a vertical wall in a tank of water, the attenuator ought to assume an equilibrium angle between 50 and 70 degrees from the horizontal, as shown in the sketch below:



CHECKING FOR PROPER VERTICAL CENTER OF GRAVITY OF ATTENUATOR

This rather tedious trial and error process was repeated for each of 340 attenuators. Occasionally, the equilibrium conditions changed slightly during tests due, perhaps, to loss of lead ballast or absorption of water.

Dash Pot

A series of tests were undertaken in which it was desired to investigate the effect of external-damping of one row (the aft row, number 17) of the array. In this case the damping device (such as damping collars on each float) could not extend into the water, where it would be acted upon by wave forces as well as provide damping. A special dash-pot system was developed.

The critical damping, $2\sqrt{km}$, for a row of floats is approximately 4.7 lb-sec/ft. A series of auxiliary tests were carried out for the cases of decaying oscillations of a spring-suspended vertical sheet-metal plate immersed in a narrow plastic tank ($\frac{1}{2}$ -in wide, $3\frac{1}{4}$ -in deep and $4\frac{1}{4}$ -in long) filled with Dow-Corning "200" Dimethyl Silicone Fluid. Damping rates for this type of dash pot with fluid viscosities of 100 centistokes and 1000 centistokes were obtained. Based on the calibration tests, a dash pot was configured consisting of a vertical sheet-metal plate, whose surface is parallel to the longitudinal centerplane of the model, attached near the center of Row 17 (aft) and suspended in the same narrow plastic tank filled with 1000 centistoke viscosity fluid to give a damping rate of 0.86 lb-sec/ft, about 20 percent of the critical value for one row.

APPARATUS

Measurements

The free-floating models were tethered in DL Tank 2, which is 75'x75' x4.5' deep, by lightweight bow and stern spring lines connected by yokes to restrain the model in yaw and against excessive drift. The bow line passed under a pulley and upward to a very soft (0.043 lb/in) spring, while the stern line passed over a pulley and had a 0.1-lb weight attached to it. This system of restraint is expected, because of previous experience with ships and platforms, to have very little influence on vertical heave response: a few tests were carried out to check this hypothesis. The models were situated with their bows approximately 38 ft from the paddle-type generator and 15 ft from starboard sidewall of the tank. There is an effective wave absorbing beach along the tank wall opposite the wave generator (astern of the model).

Wave measuring probes, having ± 5.0 -in range, were situated at three positions: (a) on the model centerline, 13-ft forward of the bow, (b) about 1-ft abeam of the middle row of the model, and (c) on the model centerline, 5-ft aft of the stern. Heave measurements are normalized by dividing by the wave measurement from Probe (b), abeam of the middle of the model.

Vertical deck motions were measured at seven fore-and-aft locations on the model, at Rows 1 (bow), 3, 6, 9, 12, 15 and 17 (stern), all at the starboard gunwale. An eighth heave measurement was made at Row 9 (the middle row) at the port gunwale. The measurements were made with a long (approximately 8 ft) vertical string between the measurement point on the model and a quadrant connected to the shaft of a rotary variable differential transformer (RVDT). These RVDT's have very low friction ball bearings and the quadrants are very slightly counterbalanced to assure that the string remains in tension.

An attempt was made to monitor surge motions by recording the motions of the bow spring line pulley, which rotates as the spring line surges.

The surge motions being quite small (of the order of a few tenths of an inch), and the spring line rather long (about 13 ft), transverse oscillations of the string might be suspected of significantly modifying the measurement. It was decided, in view of this uncertainty, not to present the results of these measurements and merely to note that surge motions were typically small compared to wave elevation.

Signals from the transducers were amplified by Sanborn 350 Series conditioning unit and recorded simultaneously on Visicorder chart paper and by the PDP-8E Digital computer and A-to-D converter.

A program of oscillation tests, where Row 17 (aft) of the model was forced to heave while the motions of the deck were measured, was also undertaken. The apparatus used for these tests was an improved version of the equipment described by Mercier in published references.^{34,35} A sine-cosine potentiometer coupled to the shaft of the oscillator was used as a motion-phase reference indicator.

Data Reduction

The Visicorder oscillographic records were read by hand during the course of testing to obtain preliminary results. The digitized computer records were processed with a Fourier analysis program to obtain the amplitude of the fundamental component of motion and wave records and phase lags of motions relative to wave (or relative to the motion of Row 17, for oscillation tests).

TEST PROGRAMS

The schedule of tests conducted with various configurations are delineated in Table 4 in the chronological order in which the tests were carried out. The numbers of the figures in which the data are presented are listed in this table.

RESULTS

Wave tests data, including amplitude and phase information, are given in Figures 14 to 18 and 20 to 22 as a function of frequency, f (scaled according to Froude's Law, $f_{\text{full size}} = f_{\text{model}} \times \frac{1}{\sqrt{\lambda}}$, where the scale ratio $\lambda = 48$). These results are also tabulated in Table 5. A curve showing the theoretical heave response of an isolated spar buoy (assuming neither hydrodynamic nor structural interaction between nearby floats) having the shape and proportions of the float and attenuator is included in Figures 14d and 16d only, for reference. Amplitude ratios, $1z/\zeta_1$, and phase information relating vertical deck motion to wave elevation measured abreast of Row 9 are given in separate charts for each heave measurement position on the deck.

Results of forced heaving oscillation tests, where an end row (No.17) of the model is forced to oscillate vertically in otherwise calm water, are given in Figures 19a-d, where the vertical motions of the deck are plotted as a function of position along the length of the model for several frequencies. Motions in-phase and out-of-phase with the motion of Row 17 are presented.

The results of wave tests 6, with the spacing ratio of 3.75, the full attenuators and the 2-in wide deck elasticity elements, are shown plotted as a function of fore-and-aft position for several frequencies in Figures 23a-k. In-phase and out-of-phase components of motion are arbitrarily referred to the motion of the middle Row 9, which is taken to have zero phase angle.

Some underwater still photographs of the action of the hinged attenuators taken during tests 5, with the spacing ratio of 3.75, the full attenuators and the 2-in wide deck elasticity elements, are shown in Figures 24a-d. These photos show a "fish-eye" view of the model in waves with full-scale-equivalent length of about 330 ft, close to the model length. Four phases of the motion are shown corresponding approximately to maximum hogging, maximum sagging and the two motion positions midway between hogging and sagging. In general, for regular and irregular wave tests with wave heights of the order of 1" = 4' full scale (the greatest values were about 2" = 8' full scale), the attenuator motions were quite

gentle, with adjacent attenuators usually oscillating in harmony with one another. It appeared that much of the attenuator motion might be effected by the rotation of the deck-float structure as it undergoes a beam-like motion, induces large fore-and-aft oscillations at the level of the hinges. Occasional non-harmonious behavior was noted, in which apparently soft bumping of attenuators in adjacent rows occurred. This was observed only for attenuators in Rows 1 and 2 and Rows 16 and 17. There was some visual indication of the low frequency oscillations of the attenuators which had been observed in the tests with a 1/8-scale isolated model during tests at the Lockheed Underwater Missile Facility,³⁶ but this occurred only occasionally, not during each test run.

DISCUSSION

The results have been presented in tabular form so that alternative methods of plotting and interpretation can readily be investigated.

Certain general observations can be given on the basis of the results presented, reinforced by the impressions obtained during the conduct of the tests. Specific comments will be given concerning comparisons of results of related tests.

The vertical motions response to waves of the deck of this model is not independent of position along the length of the model. The motions are affected by the elastic connecting elements and exhibit beam-like features. (This point will be elaborated later when considering a comparison of response with different deck stiffnesses.) While the rotation of the floats, due to resiliency in twist of the T sections, is not representative of prototype structure or in any other way desirable, it is felt that this aspect of the modeling, leading to a sort of double pendulum behavior of the floats and hinged attenuators, does not result in an important modification of the harmonic vertical force. However, it can have a dynamic effect on the couple due to horizontal force transmitted to the deck beam which would modify the magnitude, but not the nature, of beam-like response to these loads. The natural frequency of the twist of the T-section with floats and attenuators is somewhat higher than frequencies used for wave tests (however, this was not measured precisely).

Comparisons of Experimental Results

Effect of Float Slenderness

Results of Tests 1 and 3, for the medium spacing given in Table 5, Figures 14 and 16, indicate that the two shapes of floats are approximately equivalent over the range of frequencies covered in regard to deck heaving motions.

Comparison with results of Tests 2, Table 5 and Figures 15, where

no attenuators or hinges were attached, indicates the very large and effective job that the hinged attenuators do in reducing the motions of float-supported platforms.

Comparison with the theoretically-calculated motions, where hydrodynamic and elastic interaction are neglected, does not, however, show good agreement with deck motions obtained at any of the measurement locations. The fundamental resonant heaving frequency is well predicted.

Effect of Reinforcing

Comparison of results of Tests 4, 5 and 6 and of Tests 3 and 7, tabulated in Table 5 and presented in Figures 17 for deck elastic elements of type 3 (2-in wide plexiglass), do not permit a concise statement of the effects of reinforcing of the deck structure because of significant scatter of results plotted as a function of frequency. It is apparent, in any case, that the effect is small except around a frequency $f \approx 0.080$ Hz, where the amplitudes of the fore-and-aft ends of the deck are apparently somewhat reduced by the introduction of the finally-adapted reinforcing scheme.

Effect of Deck Stiffness

Results of Tests 6, 7 and 11, Table 5 and Figures 17, 18 and 20, show that the magnitude of the deck rigidity can have a very important influence on vertical deck motions. The fundamental heaving resonant frequency is evidently unaffected (or only slightly affected) by variations in deck rigidity. Response at other frequencies is, however, appreciably affected. In particular, additional resonant frequencies appear from Tests 11 for instance with the aluminum deck stiffener, higher mode frequencies at about $f \approx 0.12$ and $f \approx 0.17$ Hz are detected, while for Tests 6 with 2-in wide plexiglass deck elastic elements, $f \approx 0.10$ Hz seems to be somewhat like a resonance.

This beam-like feature of the response suggests that much of the difference between theoretically-calculated responses and measurements, at least for frequencies only slightly above the heave resonance, may be

due to near-resonant response, where the elastic natural frequencies are only slightly separated from the pure heaving natural frequency for the resilient deck (1-in wide plexiglass), somewhat more widely spread for the stiffer deck (2-in wide plexiglass), and rather well defined for the aluminum-beam-stiffened deck. Additionally, the wave-induced horizontal loads on floats can couple into bending deflections of the deck, as discussed in the section on DECK ELASTIC RESPONSE, may produce significant effects at higher frequencies.

The results of Tests 6, plotted as a function of fore-and-aft position along the deck for each of the tested frequencies in Figures 23a-k exhibit certain beam-like features. At $f = 0.101$ Hz, for instance, a two-moded bending mode of deck motion occurs where all parts of the deck apparently move in phase with one another. Other wave responses, plotted in this fashion, are suggestive of beam-like behavior, as are the responses to forced heaving of Row 17, presented in Figure 19a-l.

It is important to note that while this study has focussed on arrays of floats which are "softly" connected structurally, any large array of floats will have structural resonant frequencies which can, in principle, be excited by wave forces. The resonant responses should be carefully studied, accounting for effects of damping. The present test models did not incorporate any specially-designed dampers which would surely attenuate heave resonances somewhat; unfortunately, it is not clear how much reduction is possible.

Effect of Float Spacing

There are differences between the responses measured in Tests 3, where float spacing is 3.75-diam, and in Test 12, where float spacing is 3.00-diam, but the effects of spacing cannot be discriminated from the effects of elastic bending behavior. Perhaps the effects could be separated if a complete analytical method for accounting for deck elasticity were available. There is no clear advantage of one spacing over the other in this comparison.

Effect of Surge-Spring Lines

Only a few tests at relatively low frequencies were carried out with no fore-and-aft spring lines because the model drifts away from the wavemaker at excessive rates to permit collecting data at higher frequencies. Results, given in Figures 18a-h (Tests 8) do not indicate any effect of the spring lines on the vertical deck motions.

Effect of Dash Pot

Results of these tests are also included in Figures 18a-h (Tests 9) and indicate that the amount of external damping provided (about 20 percent of the critical damping for a single row) is insufficient to importantly effect the response of the 17-row-array, presumably because of the important interactions of adjacent float rows.

Effect of Size of Array

The array with 3-diam float spacing was tested with just 9 rows of floats, Tests 13, and results are presented in Figures 22a-e. Beam-like features of response were noted in this case also and no clear indications of important advantages of smaller or larger arrays appear.

SUMMARY

1. Deck motions appear to be importantly affected by elastic characteristics of the deck. This observation is based on model test results and is considered to be applicable to full-scale arrays.
2. Analytical considerations, together with test observations, suggest that the elastic deck bending motion may be significantly affected by couples due to horizontal wave-induced forces acting on the floats at a great distance below the neutral axis of the deck "beam."
3. Attenuator designs selected for testing produce good reductions of wave-induced heaving motion compared to floats without attenuators, although not as good as the theory which neglects elastic and hydrodynamic interaction predicts.
4. The hinge in the attenuator performs exceptionally well, reducing the horizontal load and bending moment which would otherwise be transmitted to the deck while attenuators gently oscillate without important erratic behavior or bumping in the array.
5. Yaw-restraining spring lines and small amounts of externally supplied damping have little effect on the measured response to waves.
6. Small arrays (9 rows) exhibit beam-like responses similarly to those shown by 17-row-arrays. No statement can be made about preferability of small or large arrays.
7. Quantitative information on the specific effects of float spacing and attenuator slenderness cannot be given until the elastic character of the deck response is clarified further. This effect is presumed to be greater than the effects of variations in spacing and slenderness.
8. Results of a rather detailed theoretical investigation of heave response of slender vertical floats to waves, including consideration of added mass and damping, are presented.

REFERENCES

1. Mercier, J.A., "Hydrodynamic Tests and Analysis Program for an Expandable Floating Base, PART 1, Exploratory Investigation of Interaction Effects on Deck Motions." Stevens Institute of Technology, Davidson Laboratory Letter Report SIT-DL-72-1620, July 1972.
2. Mercier, J.A., "Hydrodynamic Analyses and Exploratory Model Tests for an Expandable Floating Base." Stevens Institute of Technology, Davidson Laboratory Letter Report SIT-DL-72-1579, January 1972.
3. Kim, C.H. and Mercier, J.A., "Analyses of Multiple-Float-Supported Platforms in Waves." Stevens Institute of Technology, Davidson Laboratory Technical Memorandum SIT-DL-72-164, August 1972. (Presented at 9th Symposium on Naval Hydrodynamics, Paris, August 20-26, 1972.)
4. Newman, J.N., "The Motions of a Spar Buoy in Regular Waves." David Taylor Model Basin Report 1499, May 1963.
5. Rudnick, P., "Motions of a Large Spar Buoy in Sea Waves." Journal of Ship Research, December 1967.
6. Adee, B. and Bai, K.J., "Experimental Studies of the Behavior of Spar Type Stable Platforms in Waves." Report No. NA-70-4, College of Engineering, University of California, Berkeley, July 1970.
7. Lamb, H., Hydrodynamics. Cambridge University Press, 1932, republished by Dover Publications, New York 1945.
8. Thompson, F.L. and Kirschbaum, H.W., "The Drag Characteristics of Several Air Ships Determined by Deceleration Tests." NACA Report No. 397, 1931.
9. Smith, S.L., "BSRA Resistance Experiments on the LUCY ASHTON Part IV, Miscellaneous Investigations and General Appraisal." Transactions, Institution of Naval Architects, Vol.97, 1955. See especially Fig.12, page 542.
10. Blagoveshchensky, S.N., Theory of Ship Motions. Dover Publications, New York, Vol.1, pp.141-143, 1962.
11. Keulegan, G.H. and Carpenter, L.H., "Forces on Cylinders and Plates in an Oscillating Fluid." National Bureau of Standards Report 4821, September 1956.
12. McNown, J.S., "Drag in Unsteady Flow." Proceedings of IX International Congress of Applied Mechanics, Brussels, 1957.
13. McNown, J.S. and Keulegan, G.H., "Vortex Formation and Resistance in Periodic Motions." Proceedings of the American Society of Civil Engineers, Engineering Mechanics Division, January 1959.

14. Paape, A. and Breusers, H.N.C., "The Influence of Pile Dimensions on Forces Exerted by Waves." Proceedings of the Xth Conference on Coastal Engineering, Tokyo, 1966.
15. Martin, M., "Roll Damping Due to Bilge Keels." Ph.D. Dissertation, State University of Iowa, June 1959.
16. Ridjanovic, M., "Drag Coefficients of Flat Plates Oscillating Normally to Their Planes." Schiffstechnik, Bd 9-Helf 45, 1962.
17. Brown, P.W., "The Effect of Configuration on the Drag of Oscillating Damping Plates." Davidson Laboratory Report 1021, May 1964.
18. Henry, C.J., "Linear Damping Characteristics of Oscillating Rectangular Flat Plates and Their Effect on a Cylindrical Float in Waves." Davidson Laboratory Report 1183, June 1967.
19. Woolam, W., "Drag Coefficients for Flat Plates Oscillating Normal to Their Planes - in Air." Southwest Research Institute Final Report 02-1973 (NASA CR-66544), March 1968.
20. Tseng, M. and Altmann, R., "The hydrodynamic Design of Float-Supported Aircraft. I - Float Hydrodynamics." Hydronautics, Inc., Technical Report 513-5, October 1968.
21. Newman, J.N., "The Exciting Forces on Fixed Bodies in Waves." Journal of Ship Research, Vol.6, No.3, December 1962.
22. Norris, K.S. and Hanson, J.A., "Manned Open Sea Experimentation Station (MOSES) A Feasibility Study." Oceanic Institute, Waimanalo, Hawaii, June 1971.
23. Froude, W., "On Resistance in Rolling of Ships." Naval Science, 1874.
24. Hishida, T., "A Study on the Wavemaking Resistance for the Rolling of Ships, Part VI, Effect of Motion Ahead on Wave Resistance to Rolling." Journal of Zosen Kiokai (Society of Naval Architects of Japan), Vol.87, 1955.
25. Baker, G.S., "Rolling of Ships Underway. The Decrement of Roll Due to Hull and Bilge Keels." Transactions North-East institution of Engineers and Shipbuilders, Vol.56, pp.25-42, 1939-1940.
26. Gerritsma, J., "The Effect of a Keel on the Rolling Characteristics of a Ship." International Shipbuilding Progress, Vol.6, pp.295-304, 1959.
27. Gersten, A., "Effect of Forward Speed on Roll Damping Due to Viscosity and Eddy Generation." Naval Ship Research and Development Center, Report 2725, June 1968.
28. Mercier, J.A., "Scale Effect on Roll-Damping Forces at Zero Forward Speed." Davidson Laboratory Report 1057, February 1965.
29. Gersten, A., "Roll Damping of Circular Cylinders with and without Appendages." Naval Ship Research & Development Center Report 2621, Oct. 1969.

30. Goodyear Aerospace Corporation: "Phase I Technical Report Expandable Floating Bases." GER-15048, 15 November 1970, pp.206-265.
31. Goodyear Aerospace Corporation: "Quarterly Technical Report Expandable Floating Bases Report No.3." GER 14978 S2, 31 March 1971.
32. Ltr., Request for Quotation, GAC to DL, RFQ 64402 (Inquiry No.B21613), 4 January 1971.
33. Timoshenko, S.P. and McCullough, G.H., Elements of Strength of Materials. D. van Nostrand Co., Princeton, N.J., 1949.
34. Mercier, J., "A Method for Computing Float-Platform Motions in Waves." Journal of Hydronautics, Vol.4, No.3, July 1970, pp.98-104.
35. Mercier, J., "Hydrodynamic Forces on Some Float Forms." Journal of Hydronautics, Vol.5, No.4, October 1971, pp.109-117.
36. Numata, E., "Hydrodynamic Tests and Analysis Program for Expandable Floating Bases, Part 4, Large Scale Model Tests of Response of Deformable Floats." Stevens Institute of Technology, Davidson Laboratory Letter Report SIT-DL-72-i631, October 1972.

ACKNOWLEDGMENTS

Mr. Michael Chiocco was responsible for accomplishing the considerable task of testing of the elastic model. The assistance and advice of Mr. Edward Numata, Dr. Stavros Tsakonas and Mr. John Adams, was very helpful. Dr. C. H. Kim undertook the calculations of the rudimentary dynamic model of the elastically-connected arrays of floats.

TABLE 4

TEST CONFIGURATIONS

Designation	Date Aug 72	Float Spacing diam	Attenu- ators	Deck Elastic Elements Table 3	Comments	Tests	Run Numbers	Data in Figures
1	25	3.75	Slender	2	-	Waves	2-12	14a-h
2	28	3.75	None	2	-	Waves	13-22	15a-h
3	29	3.75	Full	2	-	Waves	23-30	16a-h
4	30	3.75	Full	3	-	Waves	31-38	17a-h
5	31	3.75	Full	3	with reinforcing "A"	Waves	40-51	17a-h
Sept								
6	7	3.75	Full	3	with reinforcing "B"	Waves	60-72	17a-h
7	8	3.75	Full	2	with reinforcing "B"	Waves	73-83	14a-h, & 18a-h
8	8	3.75	Full	2	with reinforcing "B" and no surge lines	Waves	84-87	18a-h
9	11	3.75	Full	2	with reinforcing "B" dash pot at leg 17	Waves	88-96	18a-h
10	12	3.75	Full	2	with reinforcing "B"	Forced heaving oscillation of Row 17	97-108	19a-h
11	13-14	3.75	Full	5	with reinforcing "B"	Waves	113-132	20a-h
12	15	3.00	Full	1	-	Waves	135-151	21a-h
13	15	3.00	Full	1	9 rows only (rows 9 to 17)	Waves	152-164	22a-e

TABLE 5. LISTINGS OF TEST DATA

RUN	$f_{fullsize}$	$\zeta_{fullsize}$	ft	ROW 17	ROW 15	ROW 12	ROW 9	ROW 9 P	ROW 6	ROW 3	ROW 1
Hz		$\frac{z}{\zeta}$	ϕ°	$\frac{z}{\zeta}$	ϕ°	$\frac{z}{\zeta}$	ϕ°	$\frac{z}{\zeta}$	ϕ°	$\frac{z}{\zeta}$	ϕ°
TEST 1 (for details of test conditions, see Table 3)											
3	0.101	2.47	1.350	186	0.384	198	0.608	3	0.644	17	0.672
4	0.101	3.06	1.317	187	0.363	198	0.624	4	0.662	16	0.671
5	0.088	2.47	1.471	176	0.571	183	0.478	344	0.679	355	0.727
6	0.088	2.46	1.460	177	0.562	185	0.490	347	0.701	357	0.749
7	0.131	1.84	1.232	251	0.336	189	0.784	80	0.490	31	0.719
8	0.162	2.69	0.553	287	0.214	239	0.335	110	0.245	43	0.286
9	0.147	2.58	0.635	262	0.261	203	0.424	89	0.358	25	0.444
10	0.123	2.08	1.307	223	0.331	167	0.812	56	0.523	13	0.586
11	0.201	2.63	0.041	306	0.021	255	0.070	112	0.051	338	0.056
12	0.088	2.31	1.626	165	0.629	169	0.516	340	0.743	346	0.776
TEST 2											
13	0.203	2.54	0.110	28	0.060	26	0.031	165	0.084	195	0.054
14	0.161	2.09	1.495	88	1.094	99	0.355	133	0.546	229	0.383
16	0.146	2.24	0.868	269	0.673	270	0.568	258	0.732	240	0.328
17	0.132	1.99	1.405	163	0.713	153	0.160	47	0.297	337	0.183
18	0.122	2.21	2.102	138	1.254	134	0.207	105	0.297	313	0.419
19	0.103	2.22	2.170	95	1.480	89	0.656	57	0.535	352	0.391
20	0.088	2.15	1.708	81	1.261	73	0.733	44	0.676	358	0.763
21	0.156	2.30	1.325	52	1.004	59	0.369	61	0.246	232	0.588
22	0.175	2.16	0.373	108	0.192	155	0.247	236	0.428	253	0.518
TEST 3											
23	0.202	1.84	0.061	305	0.032	210	0.082	115	0.063	316	0.080
24	0.175	1.39	0.384	290	0.091	219	0.254	86	0.163	343	0.211
25	0.160	2.52	0.550	281	0.183	214	0.407	96	0.264	21	0.292
26	0.146	2.37	0.710	256	0.306	188	0.517	83	0.391	10	0.455
27	0.131	1.81	1.072	239	0.382	157	0.807	71	0.442	2	0.673
28	0.123	2.10	1.220	214	0.362	141	0.873	51	0.468	359	0.566
29	0.102	2.16	1.284	174	0.299	182	0.700	359	0.708	13	0.691
30	0.088	2.08	1.330	164	0.425	168	0.659	345	0.900	350	0.931

Note: Phases are referred to wave elevation measured abeam of Row 9
(for details of test conditions, see Table 3)

[cont'd]

TABLE 5 (Cont'd)

RUN	$f_{fullsize}$ Hz	$\zeta_{fullsize}$ ft	ROW 17 $\frac{\zeta}{\zeta}$	ϕ°	ROW 15 $\frac{\zeta}{\zeta}$	ϕ°	ROW 12 $\frac{\zeta}{\zeta}$	ϕ°	ROW 9 $\frac{\zeta}{\zeta}$	ϕ°	ROW 9P $\frac{\zeta}{\zeta}$	ϕ°	ROW 6 $\frac{\zeta}{\zeta}$	ϕ°	ROW 3 $\frac{\zeta}{\zeta}$	ϕ°	ROW 1 $\frac{\zeta}{\zeta}$	ϕ°
TEST 4																		
31	0.087	2.29	1.616	140	0.504	146	0.855	313	1.227	315	1.114	313	0.514	314	0.838	137	1.826	136
32	0.102	2.21	1.416	171	0.445	169	0.705	358	0.970	2	0.850	1	0.406	6	0.523	191	1.134	193
33	0.122	2.16	0.977	192	0.290	132	0.670	34	0.425	9	0.340	353	0.191	248	0.367	213	0.333	215
34	0.130	1.87	0.961	214	0.275	154	0.638	51	0.403	14	0.355	349	0.244	257	0.342	214	0.236	209
35	0.161	2.53	0.414	247	0.178	204	0.252	73	0.261	23	0.271	343	0.126	283	0.155	198	0.108	158
36	0.147	2.45	0.568	228	0.232	175	0.353	63	0.320	7	0.248	344	0.234	276	0.244	203	0.210	157
37	0.175	2.64	0.123	240	0.070	198	0.100	53	0.106	359	0.186	340	0.090	206	0.085	153	0.060	22
38	0.203	2.73	0.113	210	0.002	327	0.079	39	0.034	249	0.020	310	0.156	216	0.036	69	0.160	31
TEST 5																		
40	0.174	2.35	0.007	173	0.113	103	0.774	29	0.185	258	0.255	253	0.080	200	0.127	51	0.142	34
41	0.160	2.53	0.311	190	0.143	119	0.293	360	0.257	294	0.257	262	0.198	201	0.160	121	0.197	62
42	0.145	2.29	0.436	182	0.098	48	0.343	357	0.112	238	0.128	219	0.311	171	0.070	141	0.198	331
43	0.131	2.14	0.682	185	0.140	216	0.383	356	0.282	36	0.247	35	0.231	111	0.209	208	0.458	247
44	0.123	2.45	0.818	173	0.249	180	0.389	357	0.482	14	0.425	15	0.203	46	0.294	204	0.640	218
45	0.102	2.34	1.636	164	0.610	161	0.734	352	1.185	352	1.065	350	0.580	350	0.583	180	1.385	178
46	0.087	2.19	0.812	45	0.229	32	0.508	236	0.703	228	0.679	228	0.283	205	0.592	68	1.207	59
47	0.088	2.21	0.927	54	0.260	45	0.575	242	0.815	236	0.780	234	0.351	217	0.613	75	1.278	66
48	0.102	2.40	1.505	168	0.547	165	0.697	356	1.110	356	0.983	354	0.537	356	0.548	182	1.290	181
49	0.123	2.37	0.891	175	0.270	182	0.422	357	0.515	14	0.456	13	0.208	44	0.318	205	0.682	218
50	0.161	2.36	0.342	190	0.200	104	0.323	16	0.275	285	0.301	260	0.292	209	0.149	121	0.218	55
51	0.201	2.13	0.134	136	0.065	63	0.104	306	0.114	261	0.169	249	0.136	131	0.153	62	0.011	242
TEST 6																		
60	0.085	2.11	0.513	68	0.269	96	0.456	212	0.639	219	0.582	217	0.303	211	0.412	57	0.956	49
61	0.101	2.07	not working		0.734	162	0.870	347	1.431	348	1.196	346	0.728	349	0.692	172	1.702	171
62	0.101	2.19	1.852	163	0.690	163	0.840	346	1.372	347	1.144	346	0.697	348	0.655	171	1.615	170
63	0.121	2.23	1.086	173	0.369	176	0.491	357	0.634	6	0.505	6	0.235	25	0.358	200	0.736	207
64	0.129	2.00	0.986	182	0.279	194	0.488	358	0.459	16	0.344	13	0.169	85	0.298	200	0.532	225
65	0.146	2.20	0.639	201	0.060	182	0.406	17	0.085	11	0.063	308	0.267	177	0.139	197	0.171	297
66	0.160	2.31	0.535	194	0.195	129	0.400	22	0.264	312	0.314	283	0.290	215	0.162	150	0.190	64
67	0.174	2.34	0.293	191	0.159	160	0.216	3	0.255	323	0.240	289	0.036	218	0.129	134	0.130	140
68	0.201	2.38	0.114	217	0.037	2	0.117	25	0.111	283	0.127	292	0.186	214	0.083	55	0.198	43
69	0.080	2.30	0.209	66	0.180	175	0.521	199	0.621	195	0.675	190	0.460	168	0.498	99	1.829	75
70	0.070	1.31	3.740	165	3.015	156	1.958	130	1.907	84	1.286	62	2.939	54	4.112	42	5.187	37
71	0.077	1.86	0.505	227	0.589	211	0.690	192	0.725	174	0.766	174	0.720	147	0.786	114	0.981	96
72	0.129	2.66	1.040	190	0.276	198	0.533	8	0.485	22	0.330	20	0.141	95	0.326	207	0.542	228

[Cont'd]

TABLE 5 (Cont'd)

RUN	$f_{full\ size}$ Hz	$\zeta_{full\ size}$ ft	ROW 17 $\frac{\zeta}{\zeta}$	φ°	ROW 15 $\frac{\zeta}{\zeta}$	φ°	ROW 12 $\frac{\zeta}{\zeta}$	φ°	ROW 9 $\frac{\zeta}{\zeta}$	φ°	ROW 9P $\frac{\zeta}{\zeta}$	φ°	ROW 6 $\frac{\zeta}{\zeta}$	φ°	ROW 3 $\frac{\zeta}{\zeta}$	φ°	ROW 1 $\frac{\zeta}{\zeta}$	φ°
TEST 7																		
73	0.129	2.51	1.494	233	0.254	190	1.017	63	0.436	22	0.345	50	0.653	270	0.432	228	0.461	132
74	0.086	1.91	1.501	169	0.638	173	0.515	348	0.981	351	0.853	351	0.473	1	0.785	171	1.650	172
75	0.099	2.13	1.237	167	0.490	178	0.498	347	0.839	5	0.725	0	0.453	23	0.442	190	0.980	202
76	0.121	2.12	1.549	206	0.284	185	0.984	35	0.504	15	0.622	39	0.512	235	0.479	213	0.219	92
77	0.144	2.17	1.154	258	0.362	155	0.902	90	0.404	350	0.398	319	0.678	292	0.279	200	0.567	144
78	0.159	2.63	0.672	279	0.282	184	0.468	90	0.451	5	0.421	351	0.303	305	0.257	192	0.395	159
79	0.172	2.22	0.441	259	0.249	184	0.405	58	0.327	353	0.250	337	0.148	247	0.158	189	0.166	192
80	0.200	2.34	0.332	343	0.075	286	0.334	144	0.182	3	0.237	347	0.203	291	0.105	94	0.150	137
81	0.079	2.50	2.204	165	1.195	172	0.366	291	0.923	327	0.826	323	0.424	339	1.063	145	2.231	146
82	0.071	1.56	3.411	145	2.936	140	2.152	126	1.721	95	1.718	84	2.335	61	3.571	44	4.670	39
83	0.129	1.80	1.640	228	0.247	184	1.129	58	0.426	23	0.382	43	0.738	257	0.462	224	0.474	112
TEST 8																		
84	0.100	1.80	1.212	162	0.460	171	0.497	348	0.820	3	0.712	359	0.429	22	0.445	191	0.977	203
85	0.086	2.08	1.653	164	0.724	164	0.518	352	1.030	352	0.877	349	0.503	351	0.814	177	1.726	175
86	0.079	2.16	1.902	142	0.852	150	0.579	300	1.142	310	1.029	305	0.515	302	1.203	143	2.515	138
87	0.072	1.40	3.440	153	3.124	156	2.515	157	2.036	144	2.179	135	2.467	110	4.095	87	5.631	79
TEST 9																		
88	0.086	1.14	1.893	165	0.889	176	0.578	320	1.163	338	0.959	337	0.598	354	0.945	145	2.015	151
89	0.100	1.24	1.189	157	0.468	169	0.489	337	0.855	357	0.696	354	0.480	18	0.447	178	1.052	193
90	0.080	1.30	2.782	106	1.608	108	0.115	255	1.067	280	0.752	282	0.725	270	0.932	123	2.226	113
91	0.080	1.05	2.871	119	.574	121	0.281	277	1.244	293	0.976	293	0.760	287	1.077	139	2.530	122
92	0.129	0.91	1.754	199	0.216	152	1.240	27	0.420	355	0.414	26	0.822	224	0.384	196	0.614	60
93	0.130	0.97	1.695	197	0.230	147	1.201	26	0.429	350	0.374	33	0.801	225	0.461	191	0.635	65
94	0.087	1.11	1.683	159	0.787	160	0.439	340	0.992	343	0.821	343	0.517	346	0.738	159	1.656	160
95	0.101	1.22	1.144	150	0.424	160	0.491	336	1.010	355	0.524	353	0.425	16	0.435	182	1.066	198
96	0.080	0.80	2.550	121	1.251	129	0.580	270	1.680	287	0.854	288	0.698	282	1.209	120	2.718	116

TABLE 5. (Cont'd)

RUN	$f_{fullsize}$ Hz	ROW 17	ROW 15	ROW 12	ROW 9	ROW 9 P	ROW 6	ROW 3	ROW 1								
		$\frac{z}{z_{17}}$	ϕ°	$\frac{z}{z_{17}}$	ϕ°	$\frac{z}{z_{17}}$	ϕ°	$\frac{z}{z_{17}}$	ϕ°								
TEST 10 (Forced heaving oscillations of Row 17, ± 0.5 in. Phase is referred to motion of Row 17 in this case only)																	
97	0.077	1.0	0	0.96	24	0.97	55	0.94	74	1.03	80	0.52	78	0.32	288	0.95	279
98	0.088	1.0	0	0.75	7	0.17	47	0.39	170	0.41	156	0.37	179	0.23	4	0.77	4
99	0.102	1.0	0	1.11	15	0.76	27	0.06	52	0.47	175	0.39	206	0.23	177	0.34	91
100	0.054	1.0	0	0.75	0	0.37	0	0.13	1	0.10	2	0.02	182	0.12	183	0.18	178
101	0.041	1.0	0	0.70	0	0.29	358	0.07	355	0.04	345	0.03	191	0.07	187	0.11	183
102	0.057	1.0	0	0.78	0	0.41	0	0.15	0	0.12	1	0.02	180	0.14	180	0.23	182
103	0.064	1.0	0	0.85	1	0.52	3	0.24	5	0.23	6	0.02	215	0.28	193	0.46	191
104	0.073	1.0	0	1.08	24	1.21	49	1.20	63	1.24	68	0.69	66	0.30	271	1.08	260
105	0.088	1.0	0	0.77	7	0.18	32	0.35	177	0.42	147	0.35	180	0.25	23	0.74	13
106	0.138	1.0	0	0.68	40	0.53	115	0.29	153	0.52	263	0.14	355	0.16	359	0.09	235
107	0.120	1.0	0	0.84	47	0.77	100	0.26	163	0.49	213	0.46	277	0.26	301	0.16	119
108	0.102	1.0	0	1.11	16	0.77	30	0.06	63	0.47	173	0.40	209	0.24	175	0.35	91

TEST 11

	$f_{fullsize}$ ft	ROW 17		ROW 15		ROW 12		ROW 9		ROW 9 P		ROW 6		ROW 3		ROW 1	
		$\frac{z}{z_{17}}$	ϕ°	$\frac{z}{z_{17}}$	ϕ°	$\frac{z}{z_{17}}$	ϕ°	$\frac{z}{z_{17}}$	ϕ°	$\frac{z}{z_{17}}$	ϕ°	$\frac{z}{z_{17}}$	ϕ°	$\frac{z}{z_{17}}$	ϕ°	$\frac{z}{z_{17}}$	ϕ°
113	0.072	1.14	194	3.853	188	2.003	165	1.531	99	1.687	47	2.985	60	4.744	48	5.978	94
114	0.080	1.01	183	0.542	181	0.496	173	0.436	163	0.479	166	0.360	143	0.320	108	0.374	90
115	0.076	1.00	220	0.429	200	0.568	180	0.733	169	0.827	174	0.888	160	0.989	152	1.104	146
116	0.072	0.46	208	6.542	200	4.545	179	3.924	145	4.684	140	4.844	112	6.586	93	8.035	86
117	0.066	1.35	59	4.209	55	3.274	55	2.711	41	2.426	9	2.361	20	2.374	357	2.583	343
118	0.071	0.76	176	5.652	168	4.078	147	3.638	116	4.235	109	4.336	86	5.713	68	6.825	60
119	0.087	1.71	65	0.108	99	0.132	161	0.174	174	0.178	166	0.139	164	0.083	98	0.149	51
120	0.100	1.32	41	0.243	41	0.075	203	0.203	211	0.166	210	0.095	211	0.182	27	0.401	23
121	0.121	1.28	84	0.373	81	0.357	259	0.641	258	0.542	256	0.400	256	0.216	73	0.707	71
122	0.109	0.98	59	0.425	60	0.121	205	0.336	225	0.303	225	0.201	233	0.222	19	0.552	27
123	0.111	0.81	49	0.115	62	0.150	209	0.379	225	0.341	225	0.248	230	0.174	18	0.507	28
124	0.144	1.26	105	0.082	75	0.120	274	0.168	254	0.128	258	0.109	219	0.090	127	0.122	104
125	0.133	1.27	108	0.266	98	0.251	286	0.423	281	0.372	279	0.238	272	0.189	113	0.515	103
126	0.160	1.32	41	0.186	38	0.161	253	0.300	230	0.234	228	0.194	206	0.164	82	0.365	47
127	0.173	1.41	53	0.226	62	0.130	241	0.285	235	0.238	236	0.170	224	0.109	69	0.282	61
128	0.201	1.55	45	0.134	32	0.101	233	0.195	225	0.163	219	0.114	210	0.115	44	0.294	36
129	0.230	1.97	149	0.040	141	0.033	330	0.067	327	0.048	157	0.048	346	0.037	223	0.078	120
130	0.120	1.32	87	0.341	84	0.309	259	0.588	259	0.496	258	0.355	259	0.190	75	0.656	73

[Cont'd]

RUN f_fullsize 6_fullsize

-253-

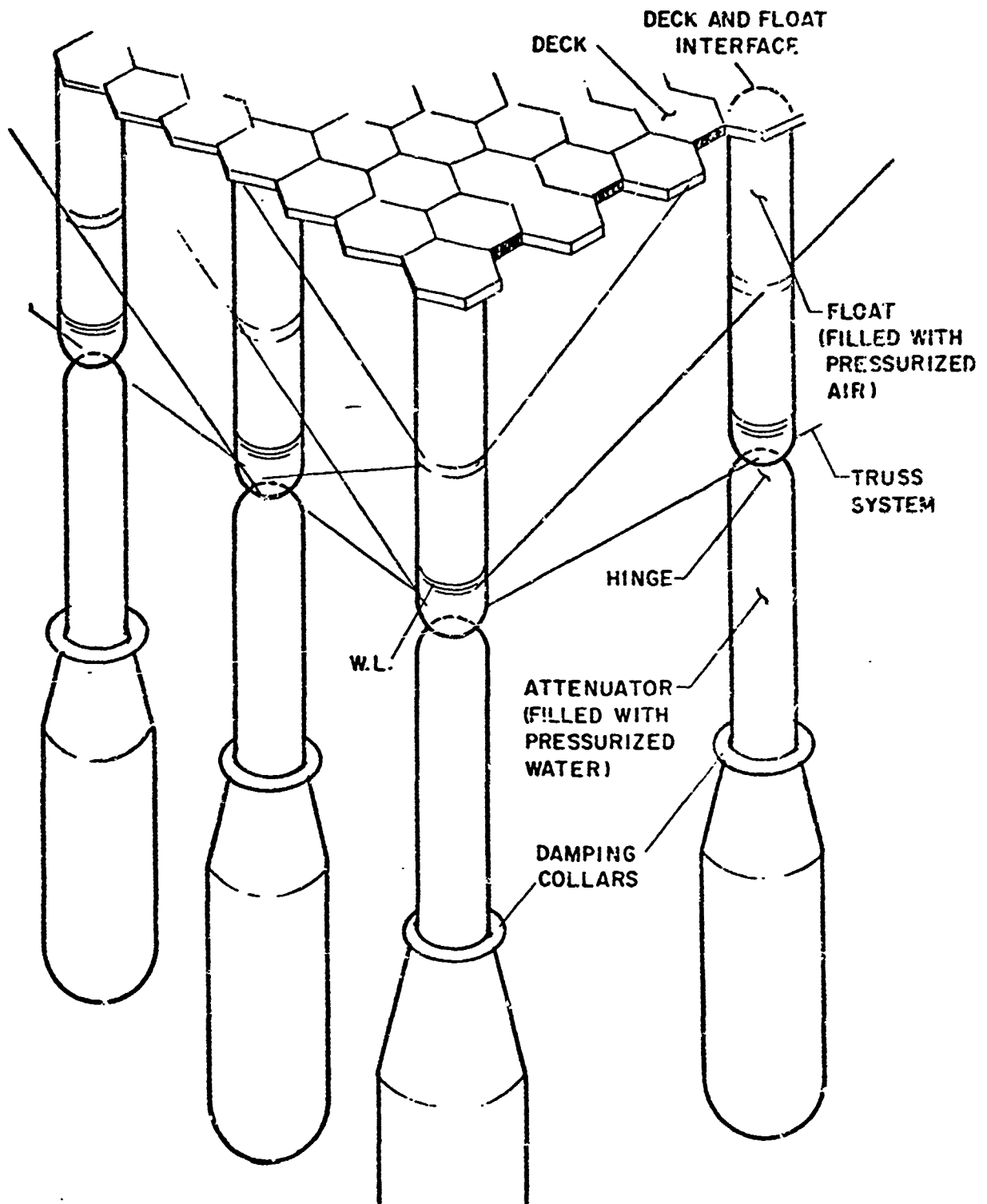
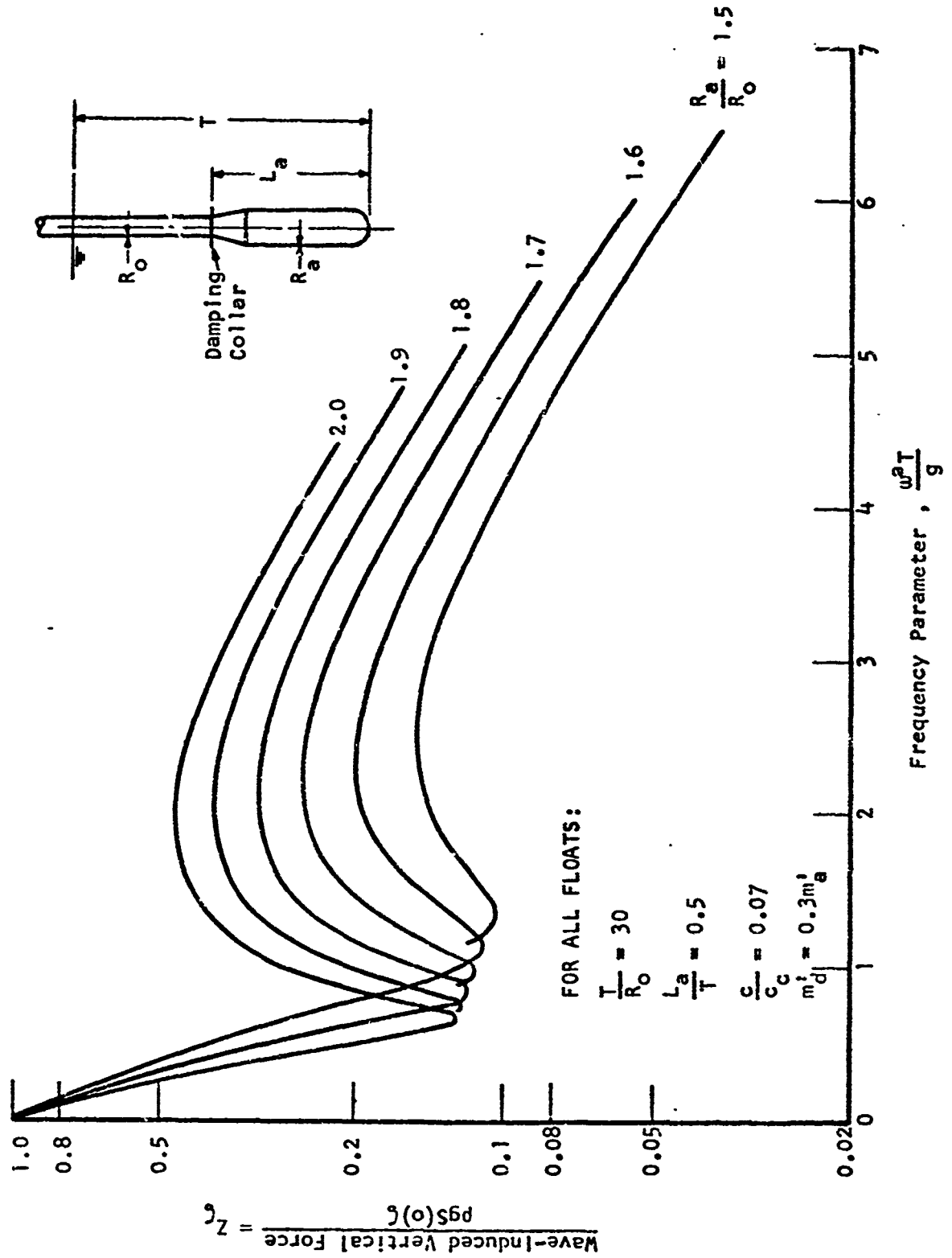
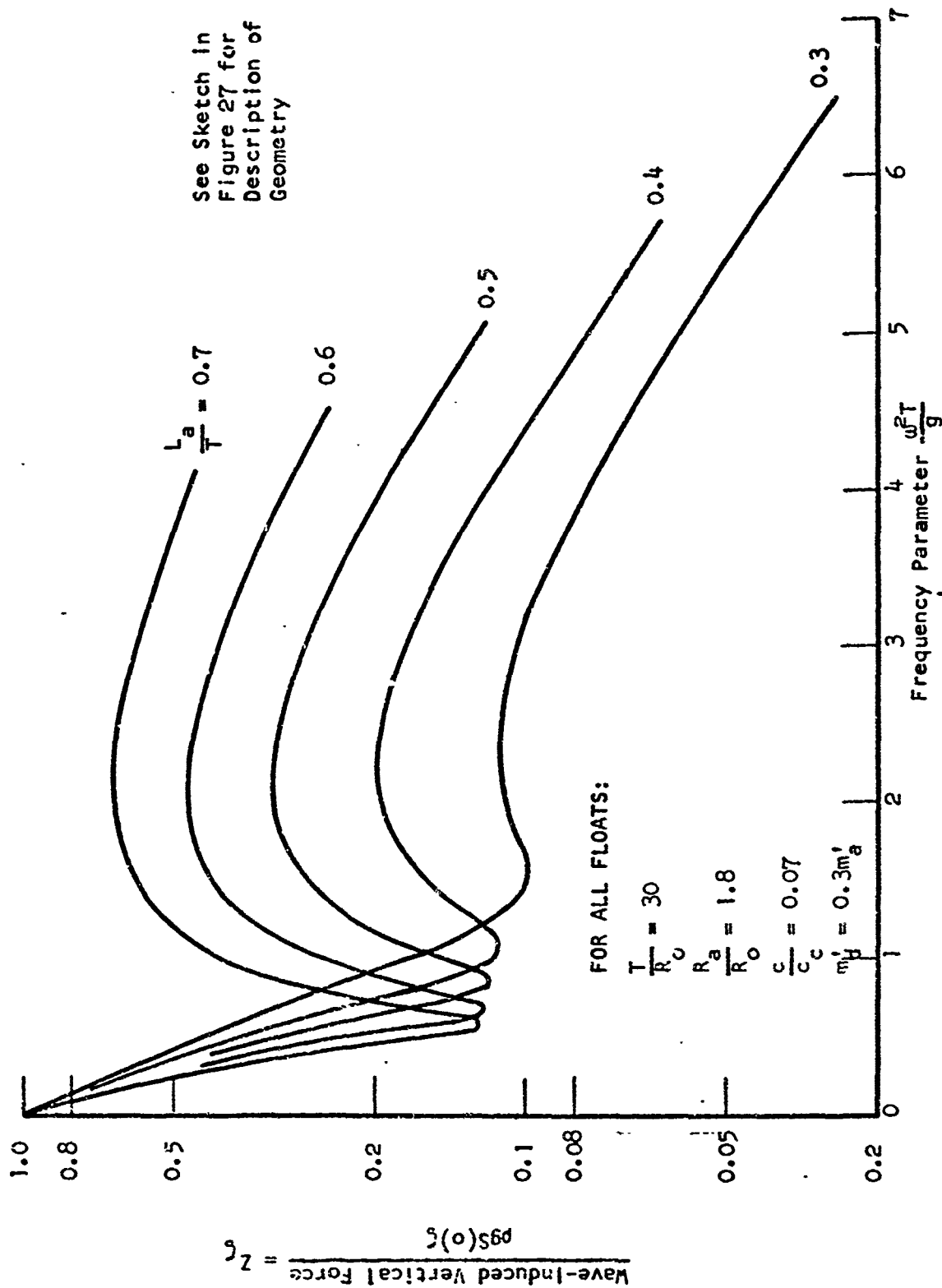


FIG. 1. ILLUSTRATION OF FLOAT CONFIGURATION

FIGURE 3 THE INFLUENCE OF $\frac{R_a}{R_0}$ ON WAVE-INDUCED VERTICAL FORCE

FIGURE 3. THE INFLUENCE OF $\frac{L_a}{T}$ ON WAVE-INDUCED VERTICAL FORCE

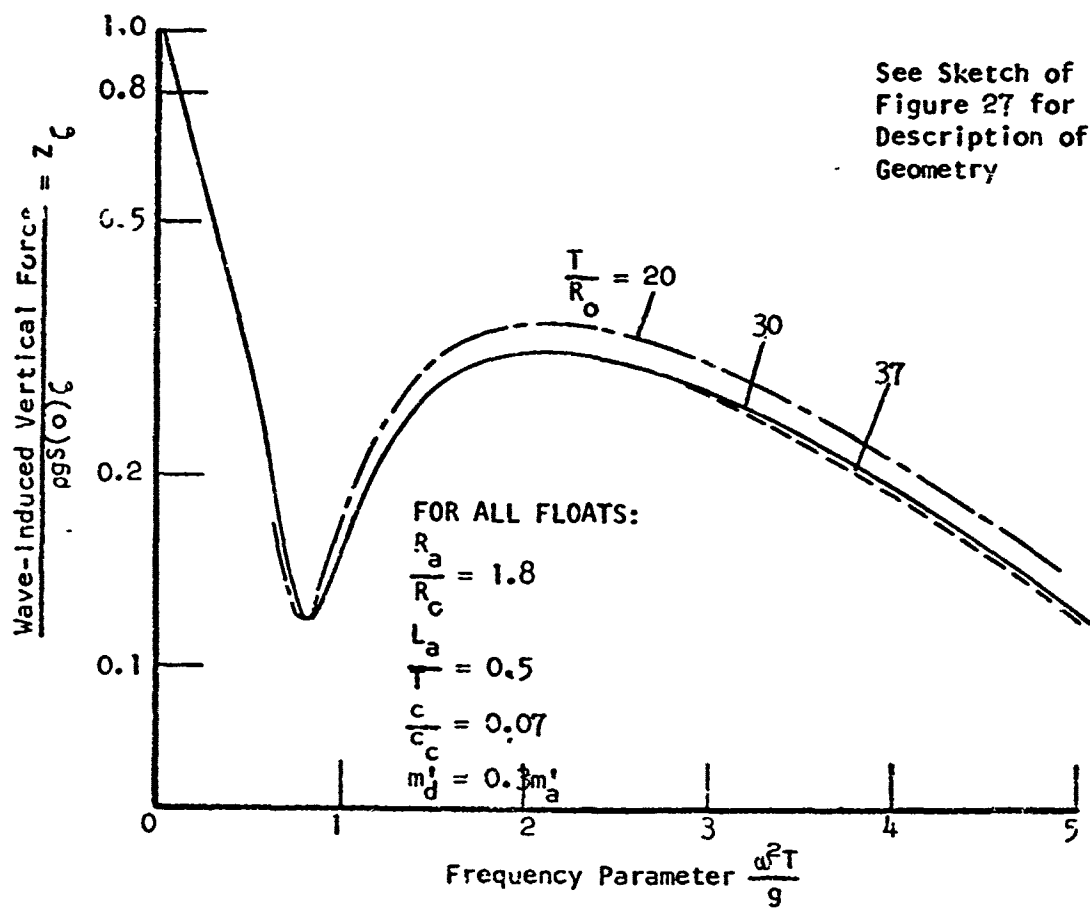


FIGURE 4. THE INFLUENCE OF $\frac{T}{R_0}$ ON
WAVE-INDUCED VERTICAL FORCE

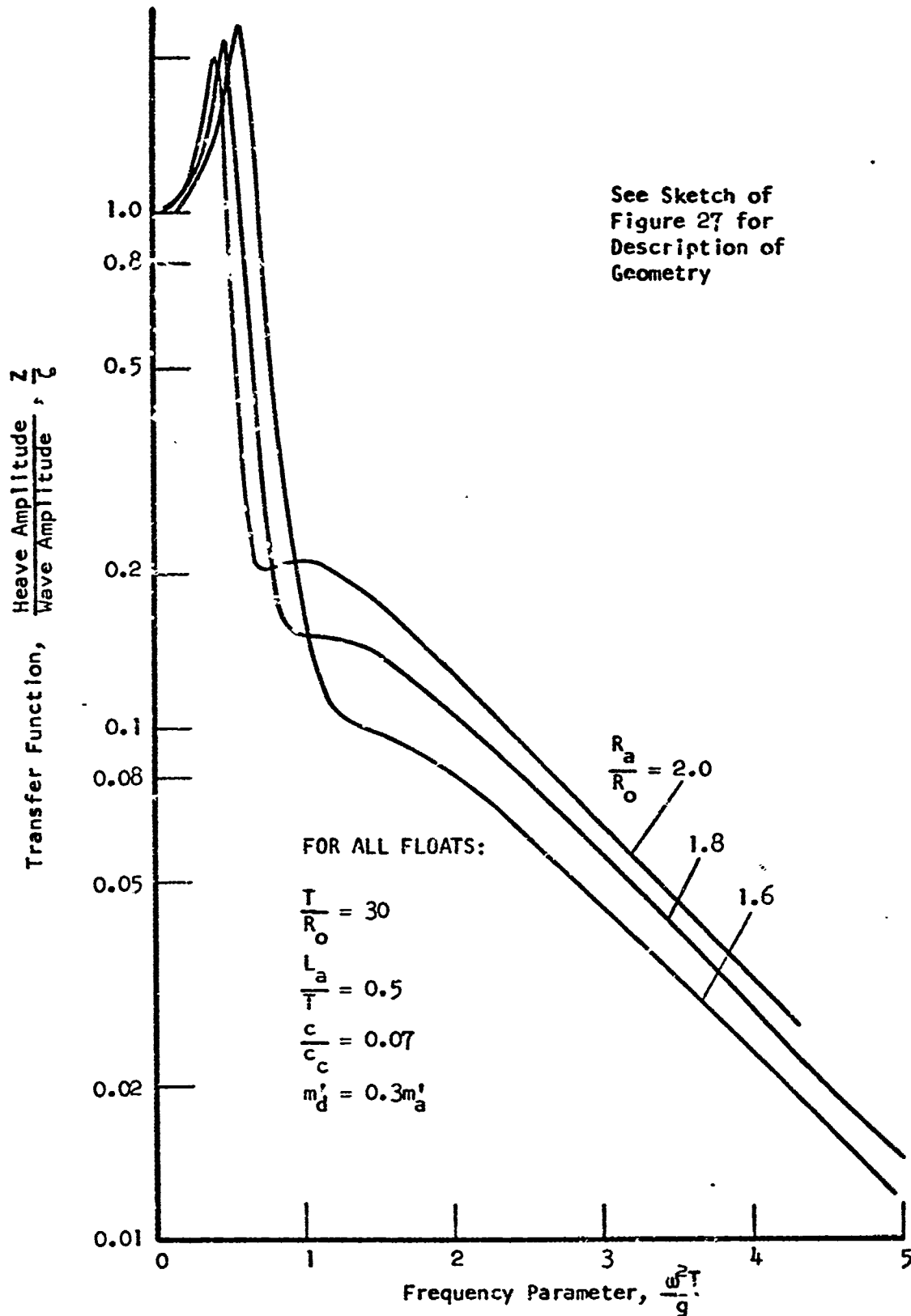


FIGURE 5. THE INFLUENCE OF $\frac{R_a}{R_o}$ ON THE
HEAVE TRANSFER FUNCTION

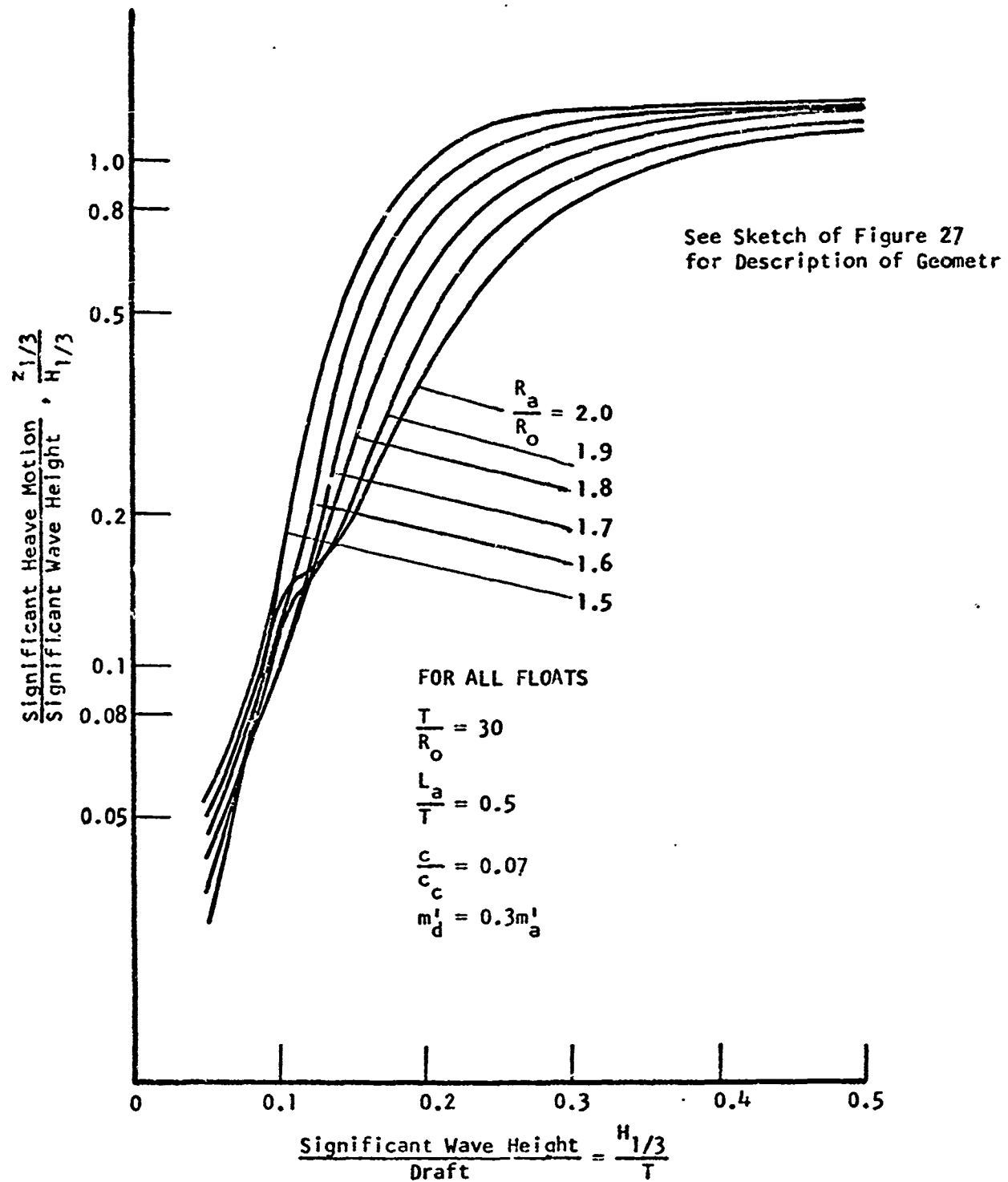


FIGURE 6. THE INFLUENCE OF $\frac{R_a}{R_o}$ ON HEAVE SPECTRAL RESPONSE

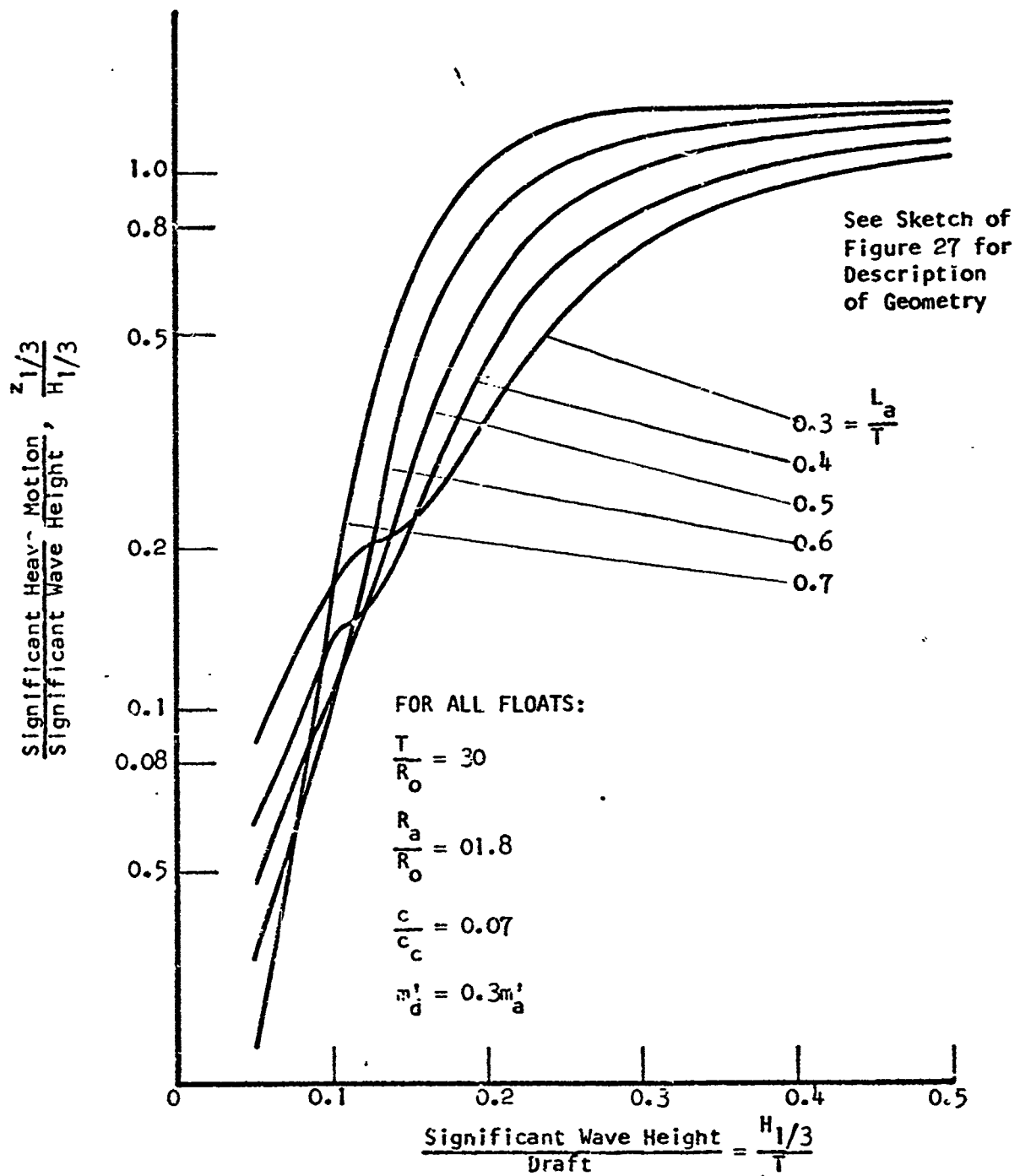


FIGURE 7. THE INFLUENCES OF $\frac{L_a}{T}$
ON HEAVE SPECTRAL RESPONSE

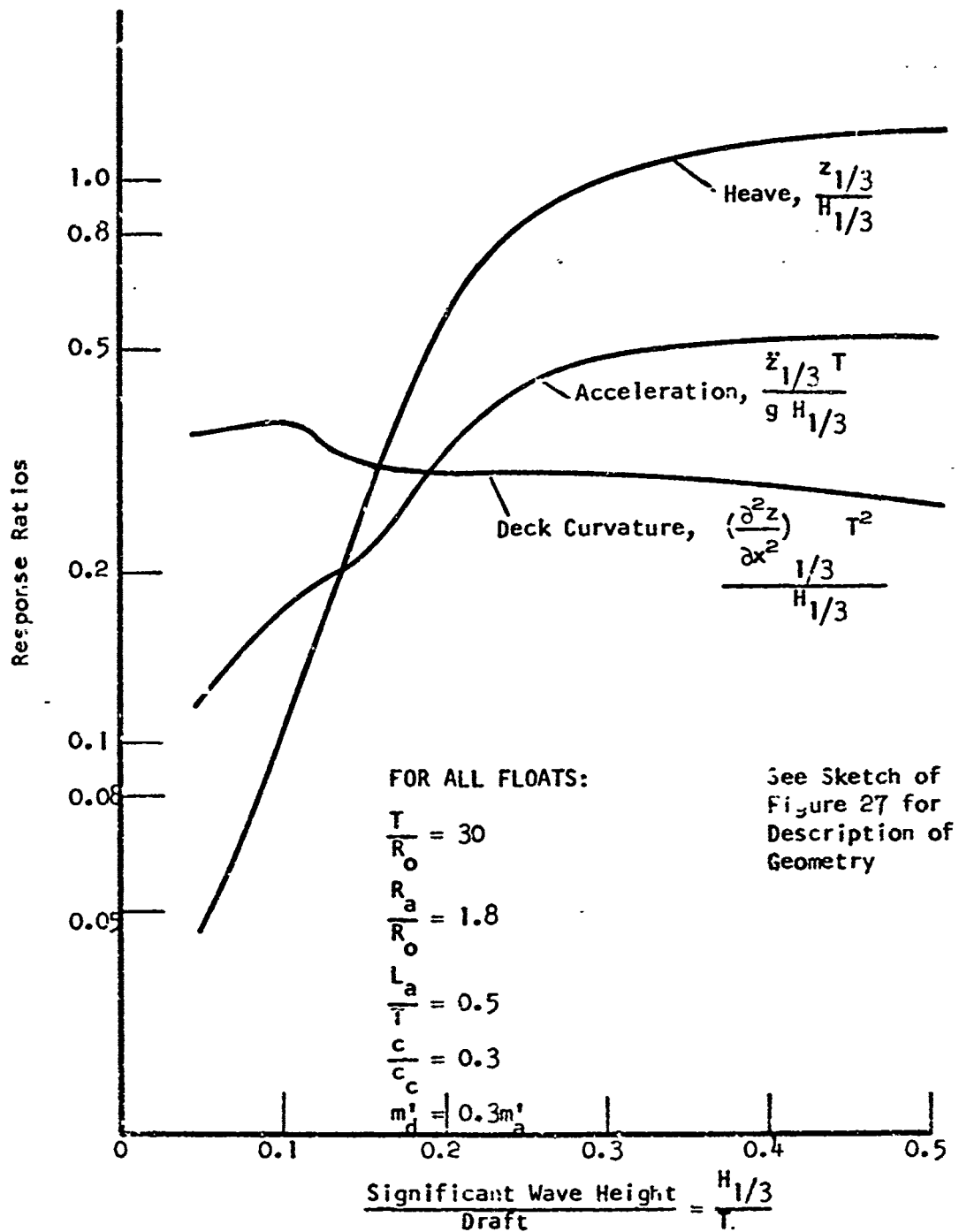


FIGURE 8. THE EFFECT OF SEA STATE (SIGNIFICANT WAVE HEIGHT) ON THREE HEAVE-RELATED SPECTRAL RESPONSES

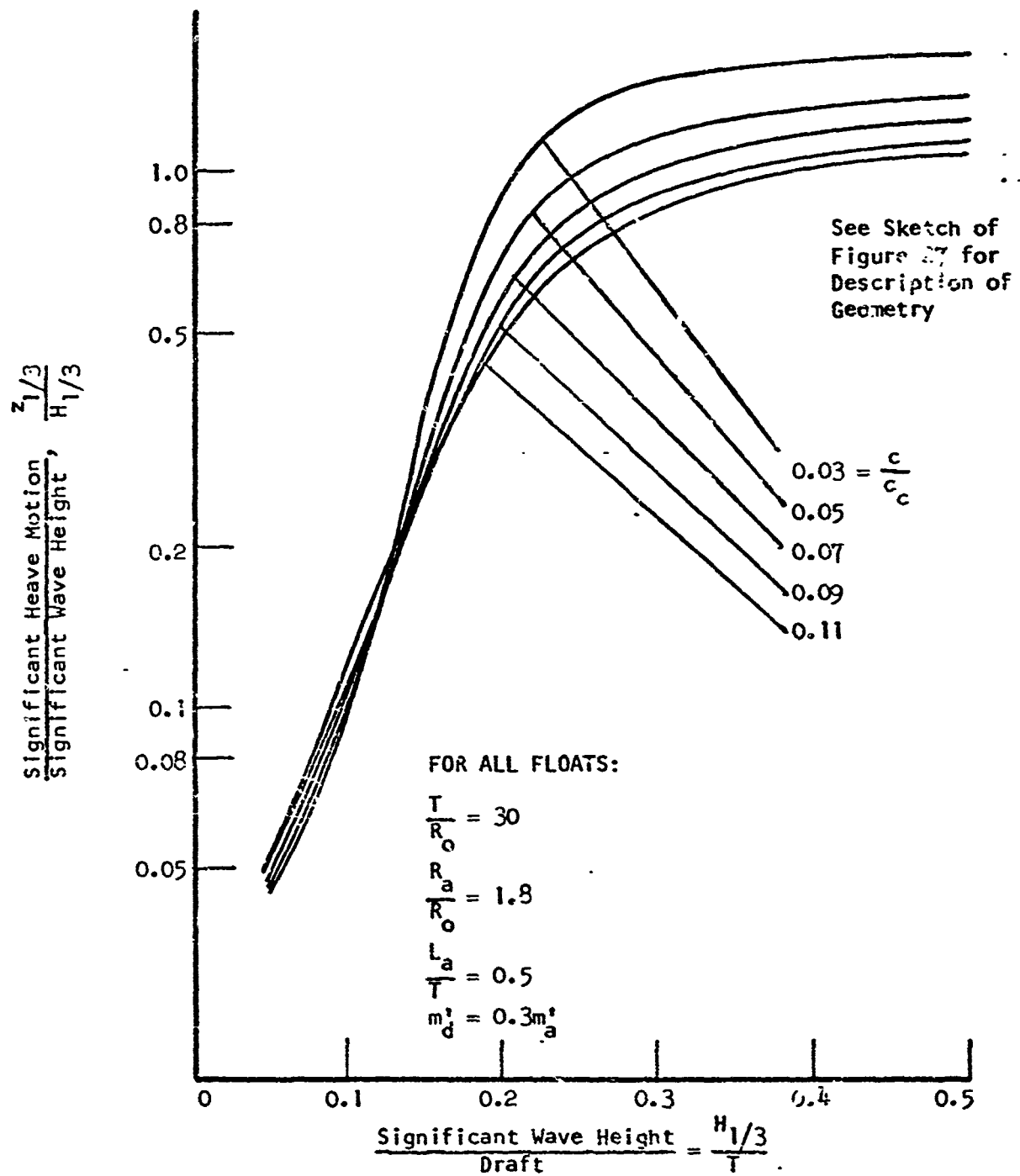


FIGURE 9. THE INFLUENCE OF DAMPING
COEFFICIENT ($\frac{c}{c_c}$) ON HEAVE SPECTRAL RESPONSE

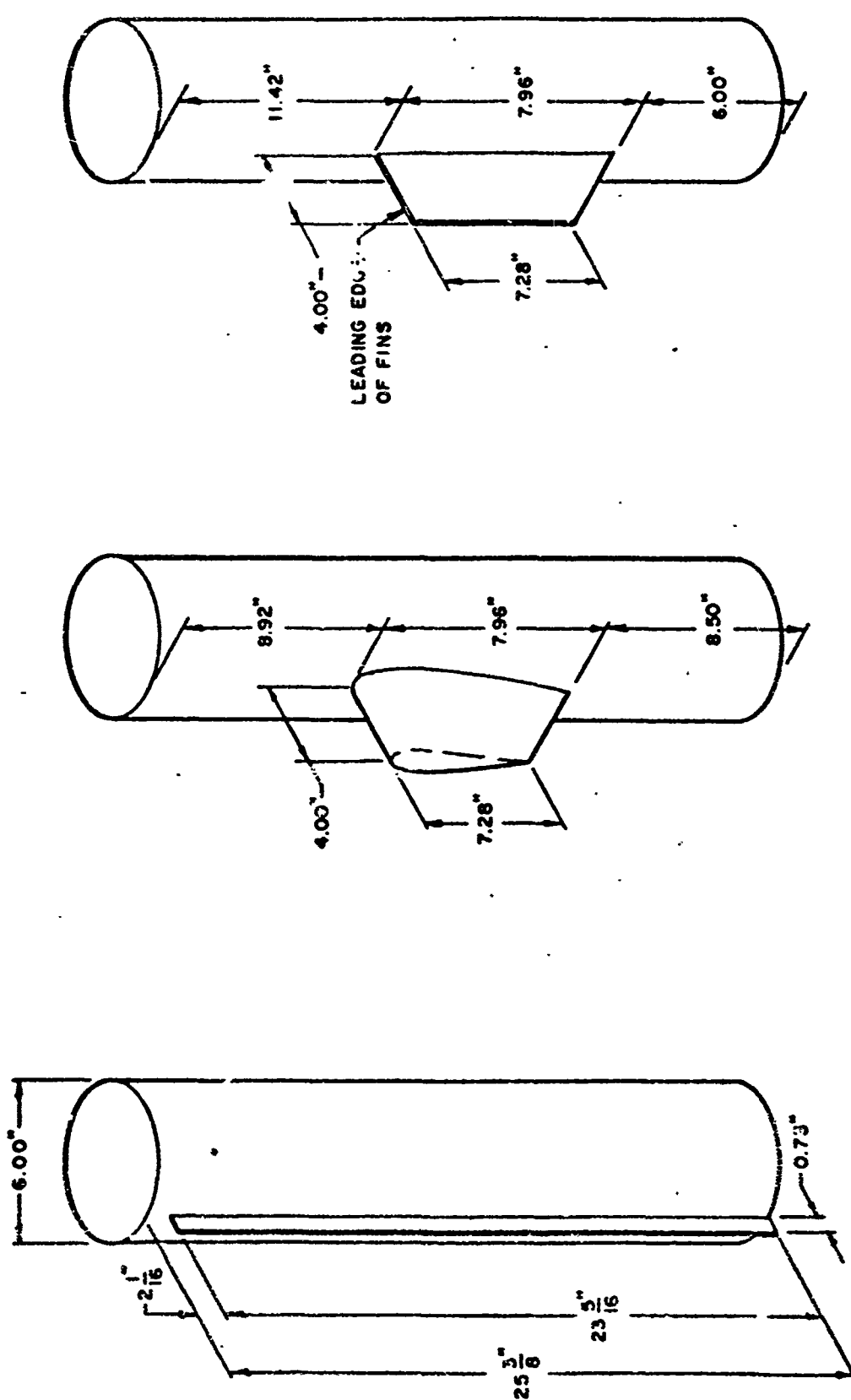


FIGURE 10. SKETCH OF 6" DIAMETER CYLINDER WITH VARIOUS APPENDAGES

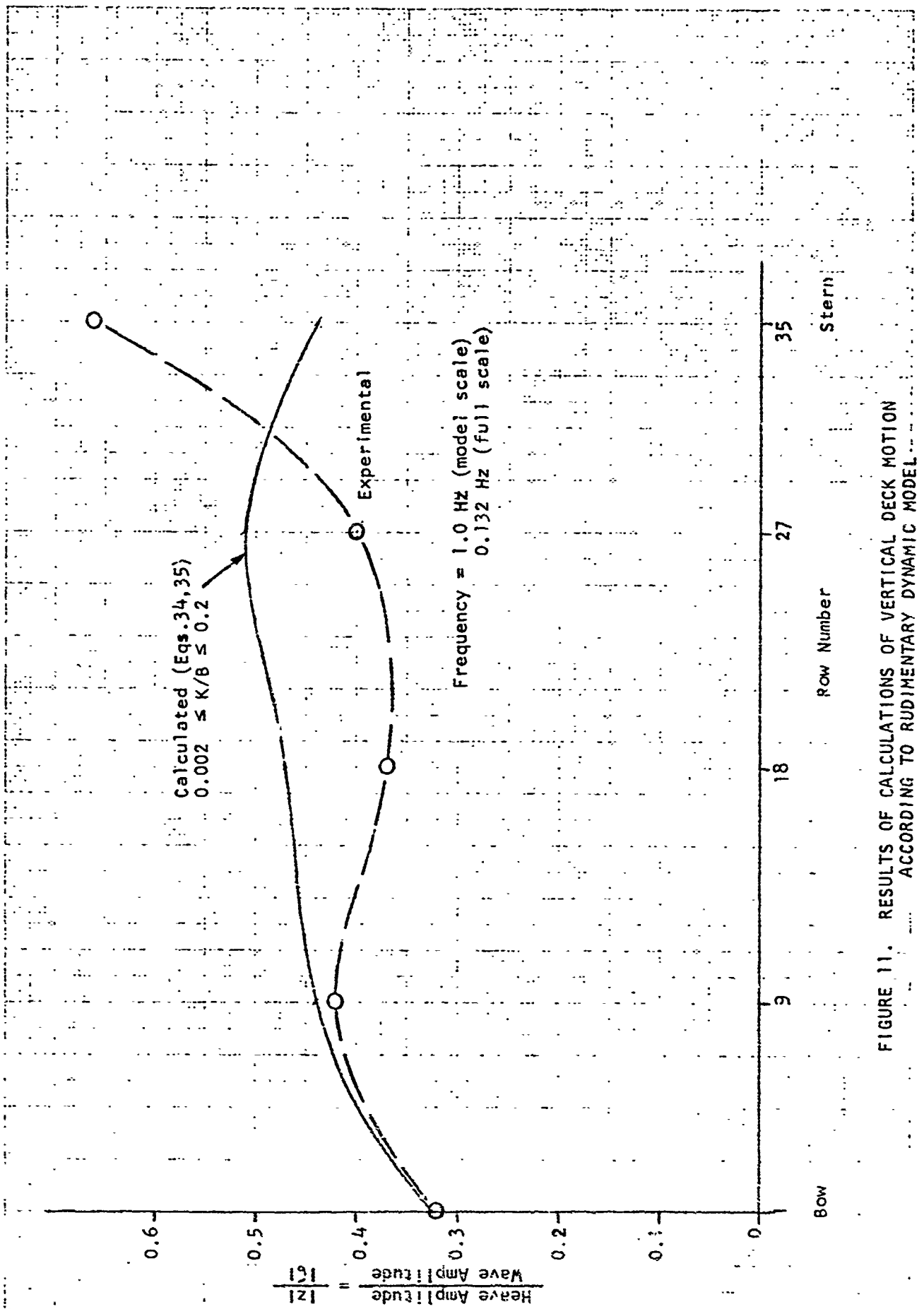


FIGURE 11. RESULTS OF CALCULATIONS OF VERTICAL DECK MOTION
ACCORDING TO RUDIMENTARY DYNAMIC MODEL

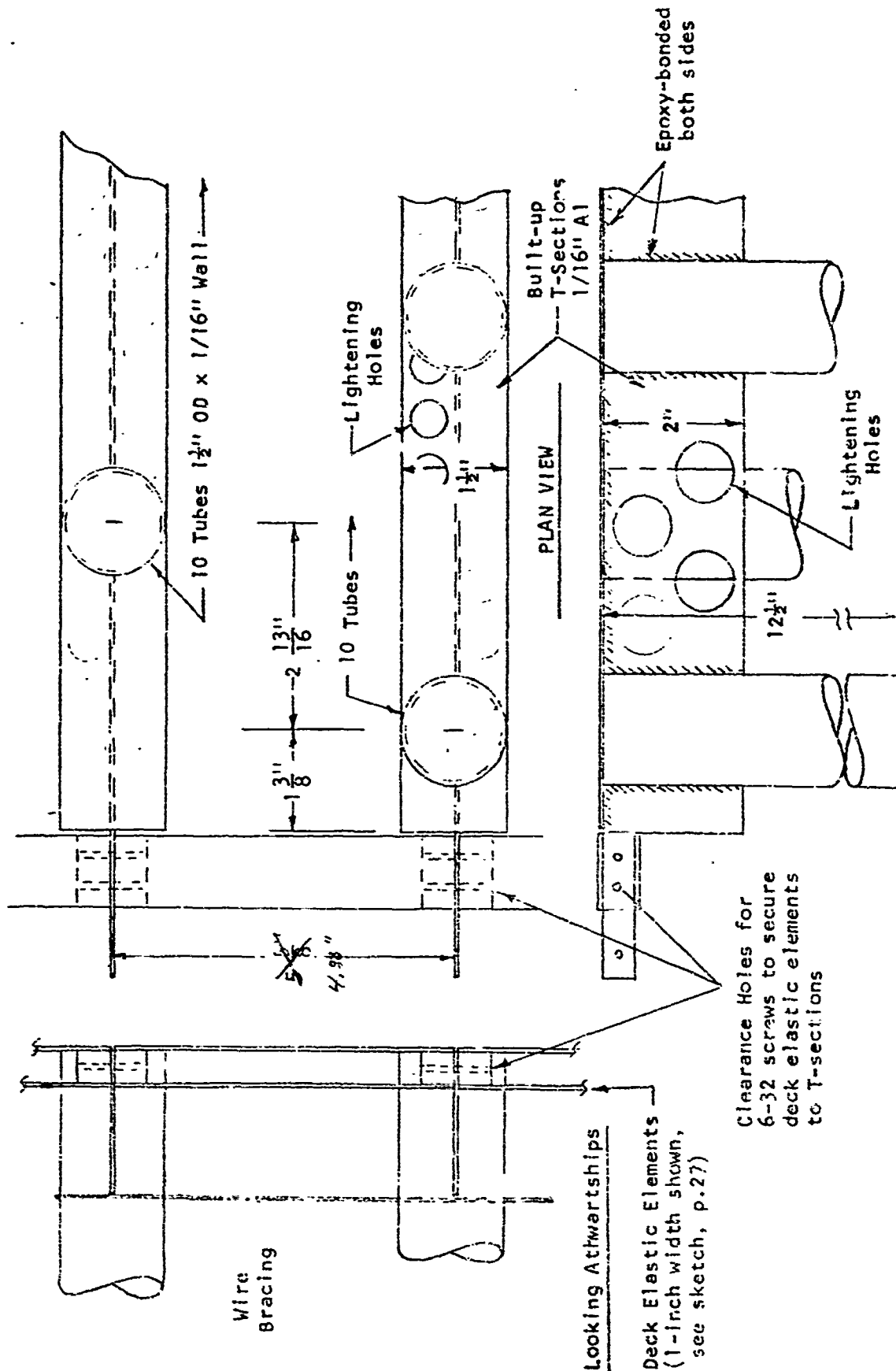


FIGURE 12. SKETCH OF ASSEMBLY OF ROWS OF FLOATS (MEDIUM SPACING ARRAY SHOWN)

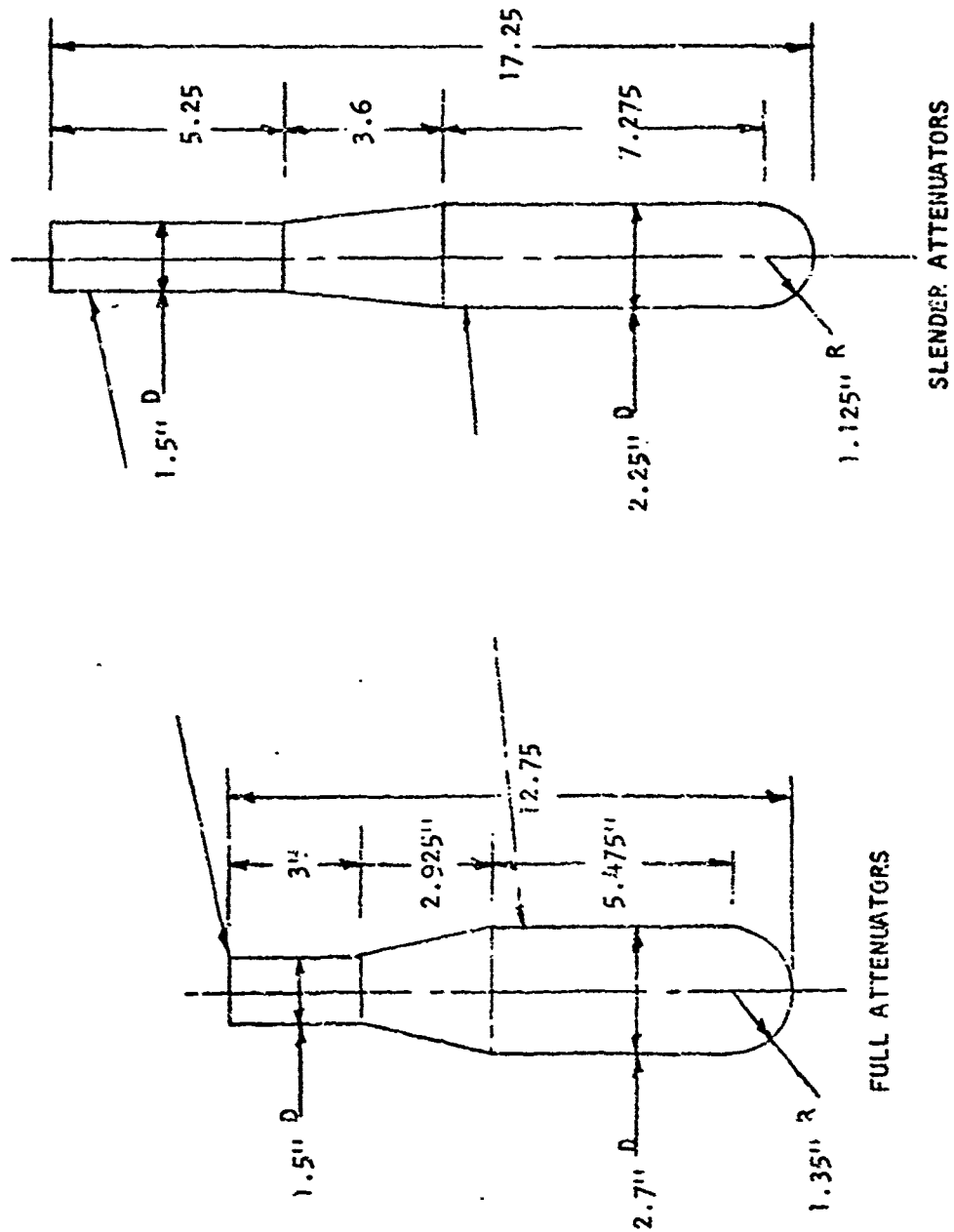


FIGURE 13. GEOMETRY OF ATTENUATORS (Scale Ratio 1:48)

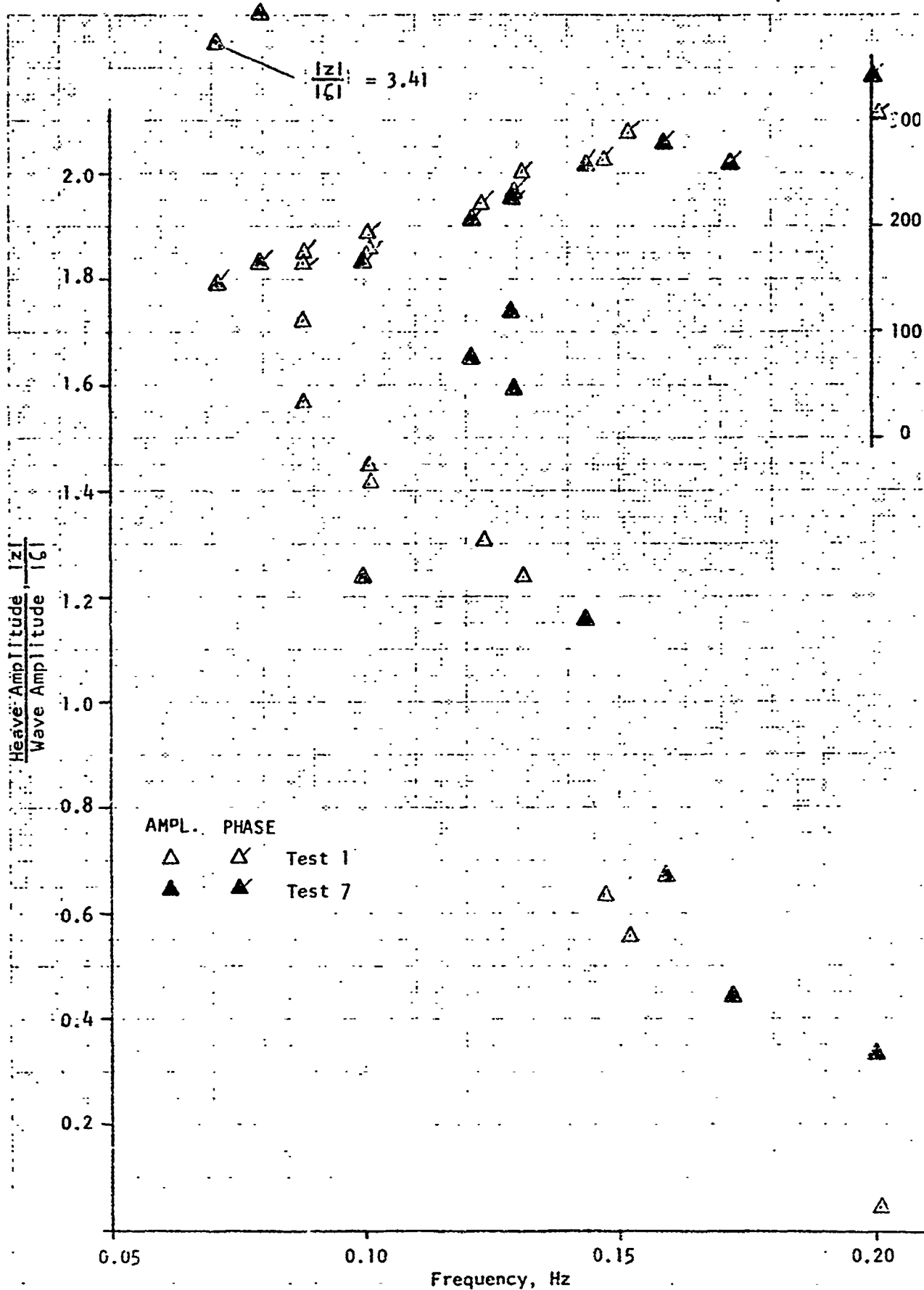


FIGURE 14a. WAVE TEST RESULTS FOR TESTS 1 AND 7, ROW 17

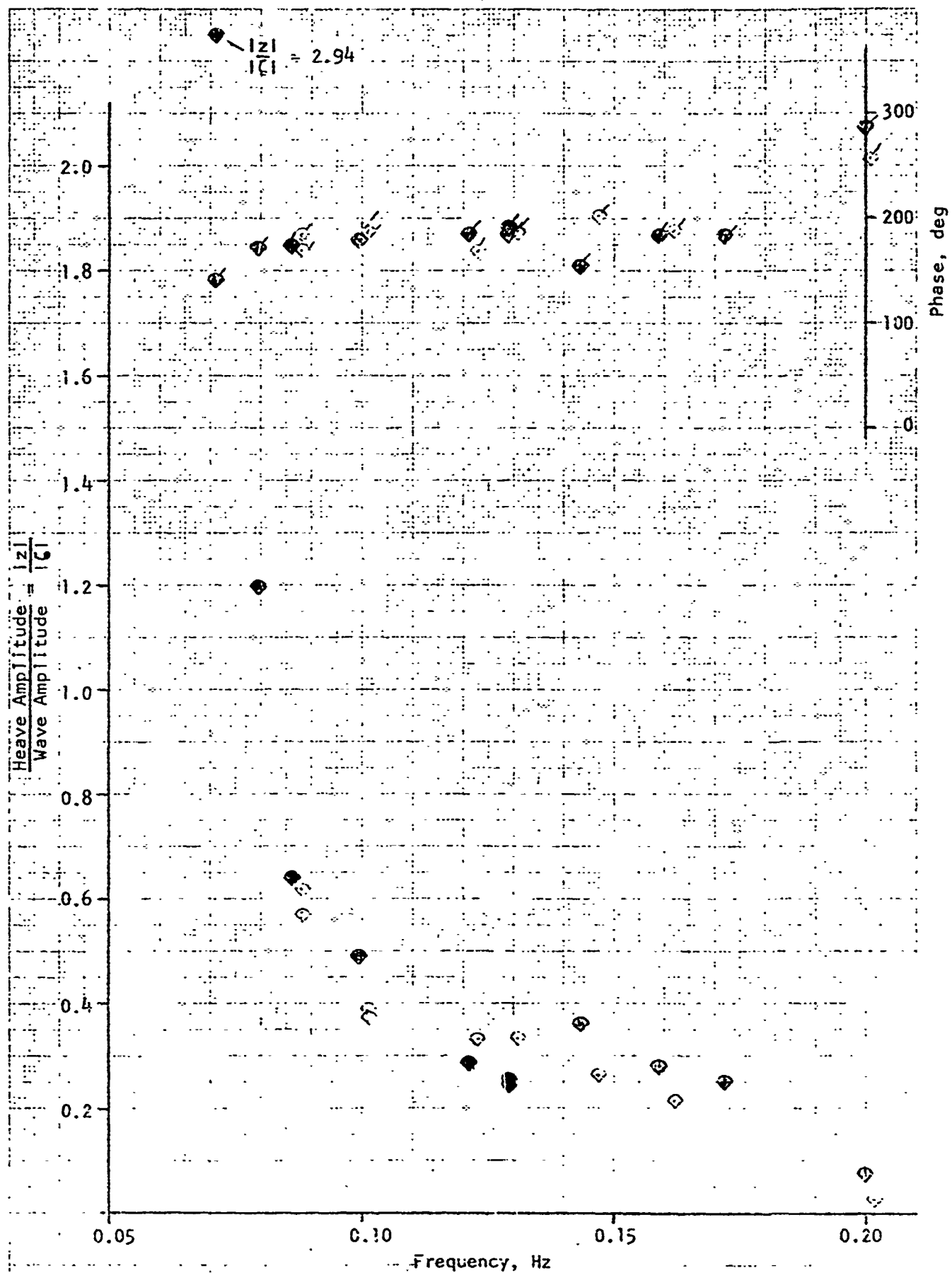


FIGURE 14b. WAVE TEST RESULTS FOR TESTS 1 AND 7, ROW 15.

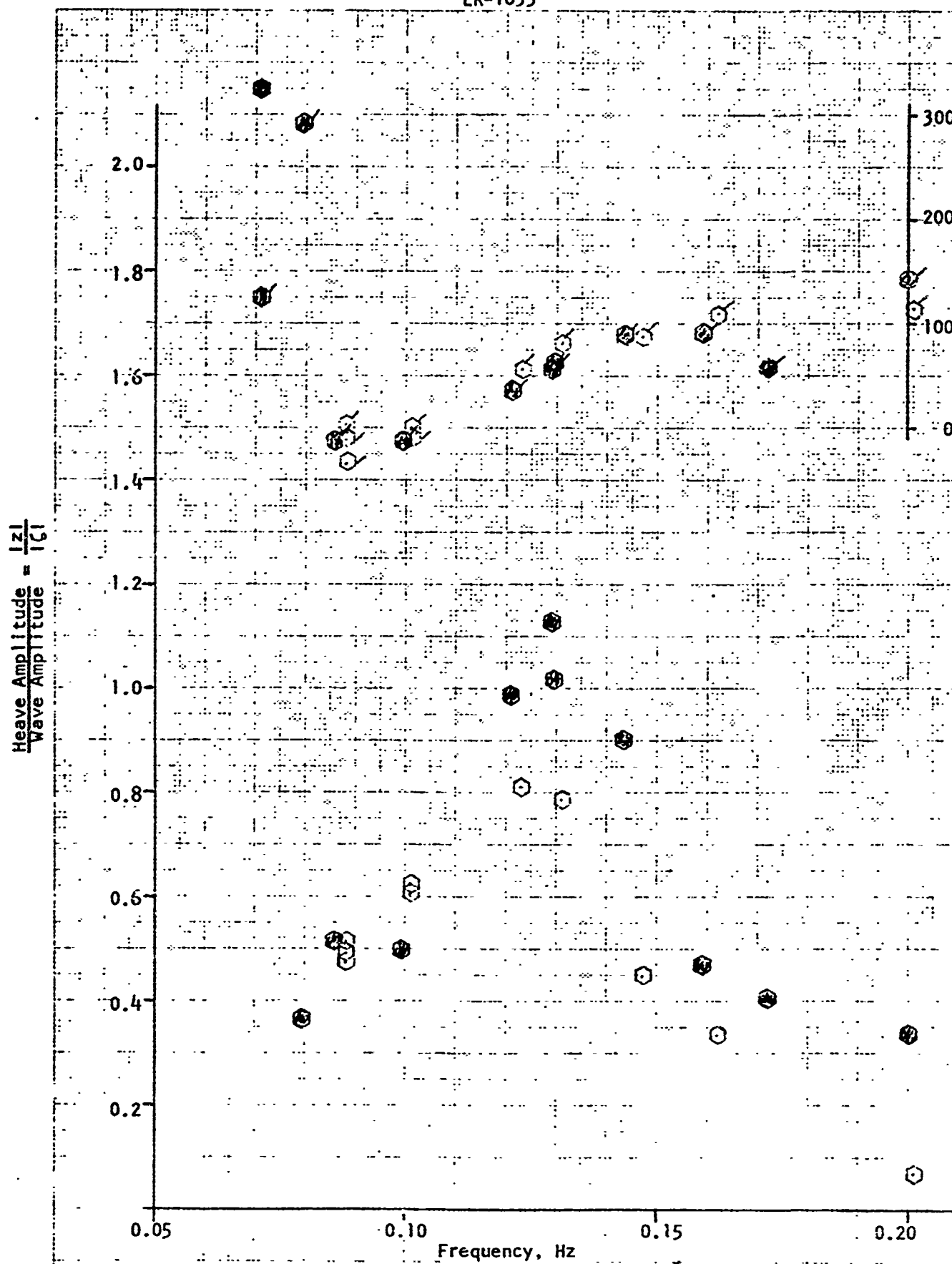


FIGURE 14c. WAVE TEST RESULTS FOR TESTS 1 AND 7, ROW 12

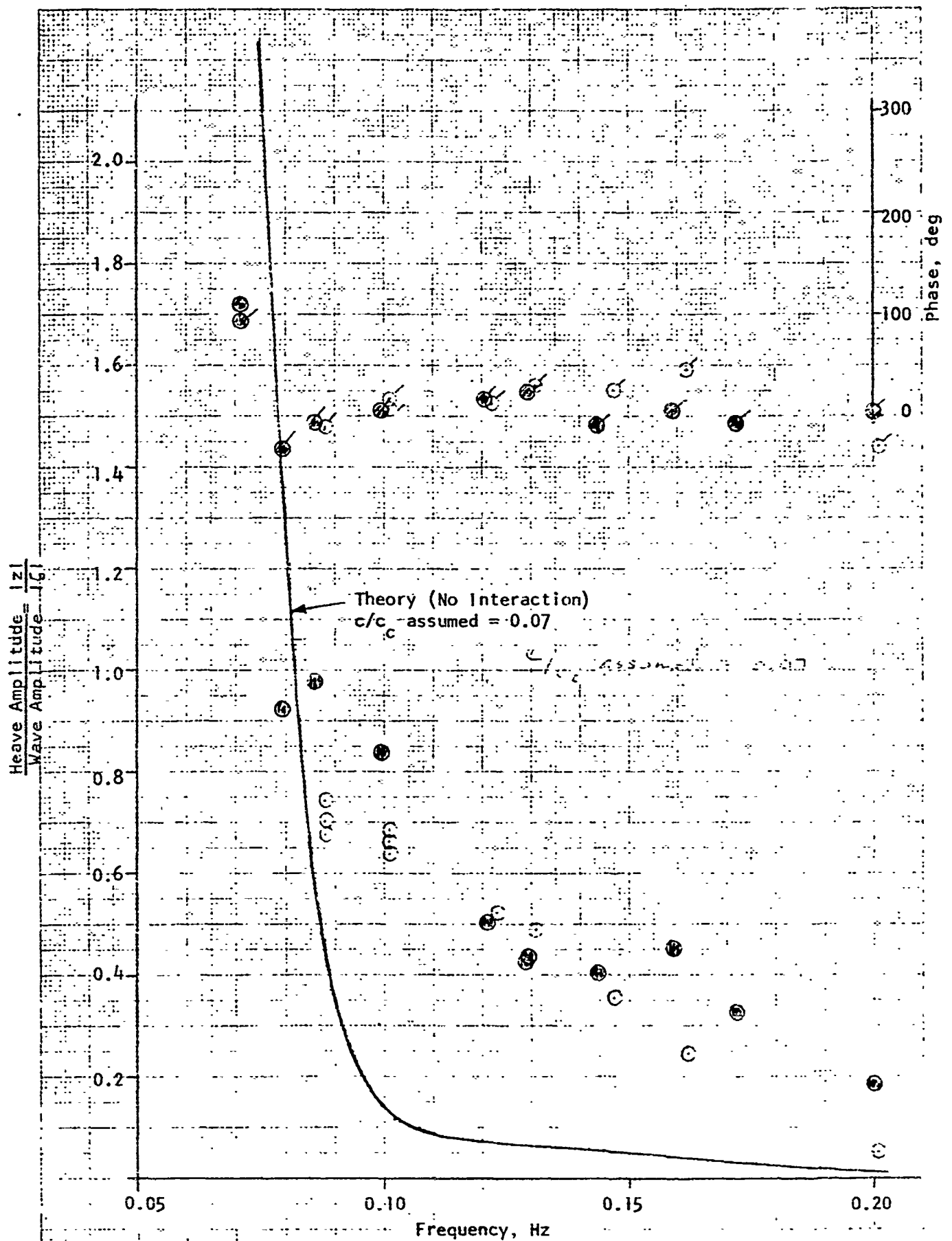


FIGURE 14d. WAVE TEST RESULTS FOR TESTS 1 AND 7, ROW 9

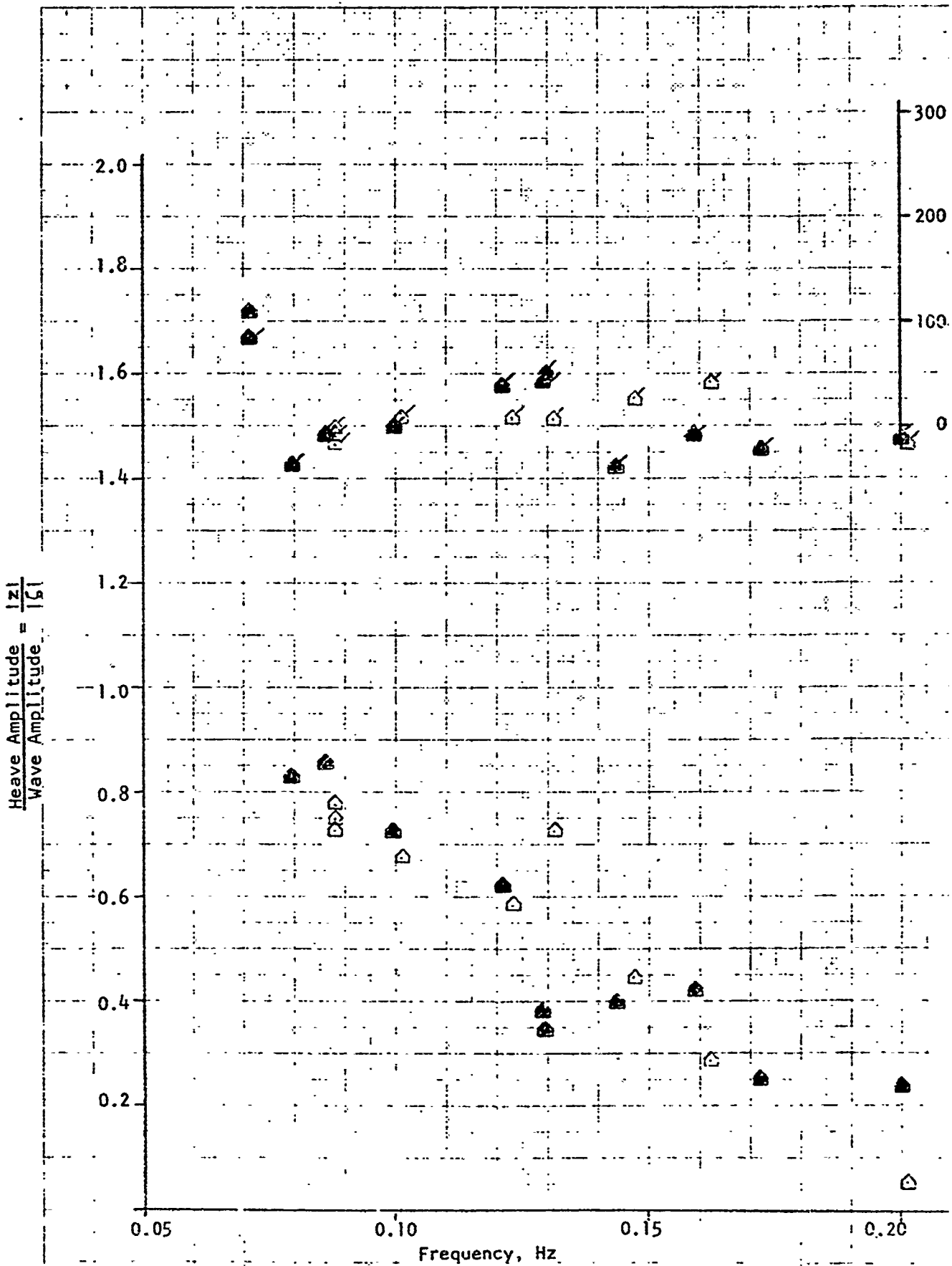


FIGURE 14e. WAVE TEST RESULTS FOR TESTS 1 AND 7. ROW 9 (Port)

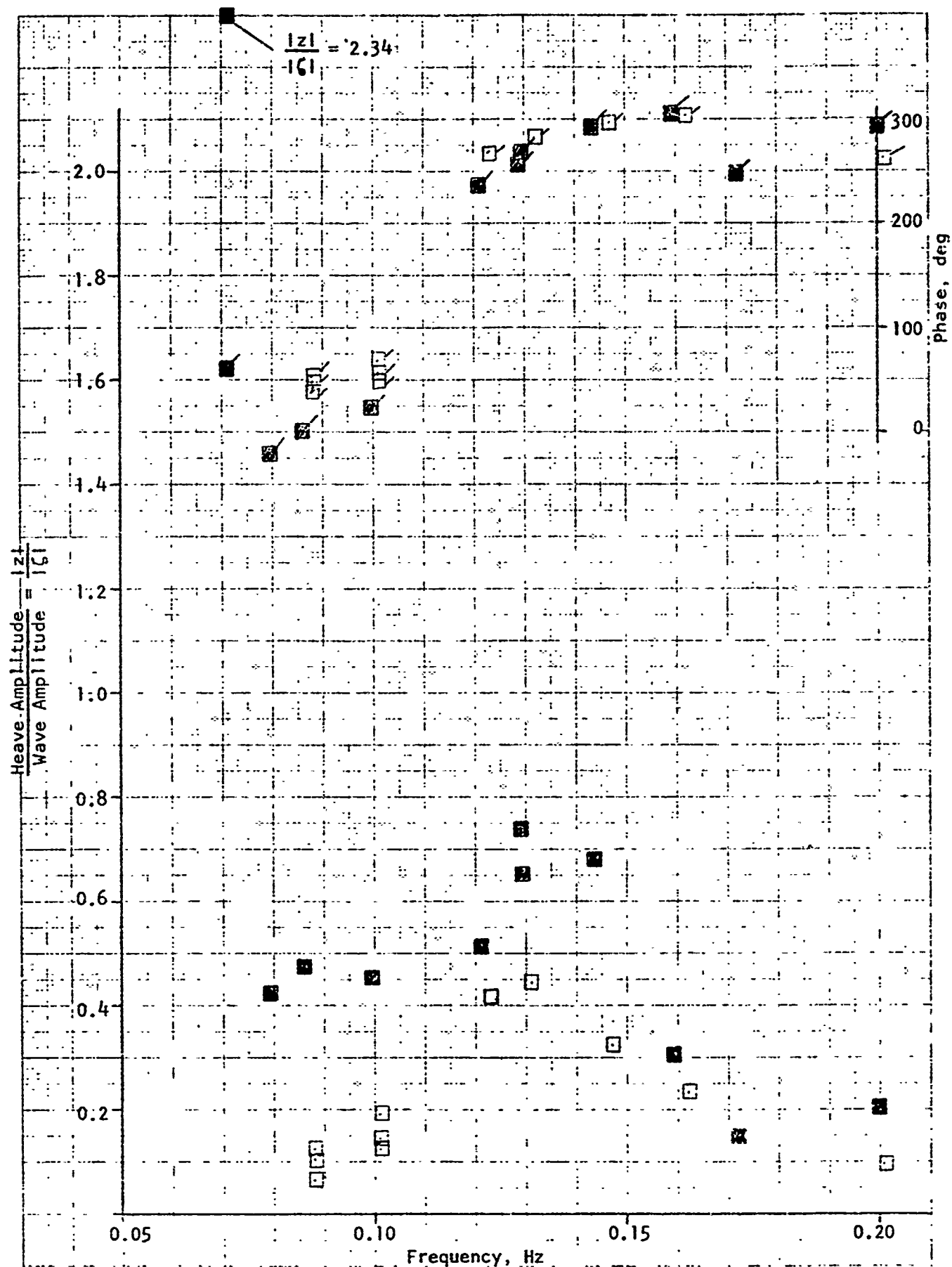


FIGURE 14f. WAVE TEST RESULTS FOR TESTS 1 AND 7, ROW 6

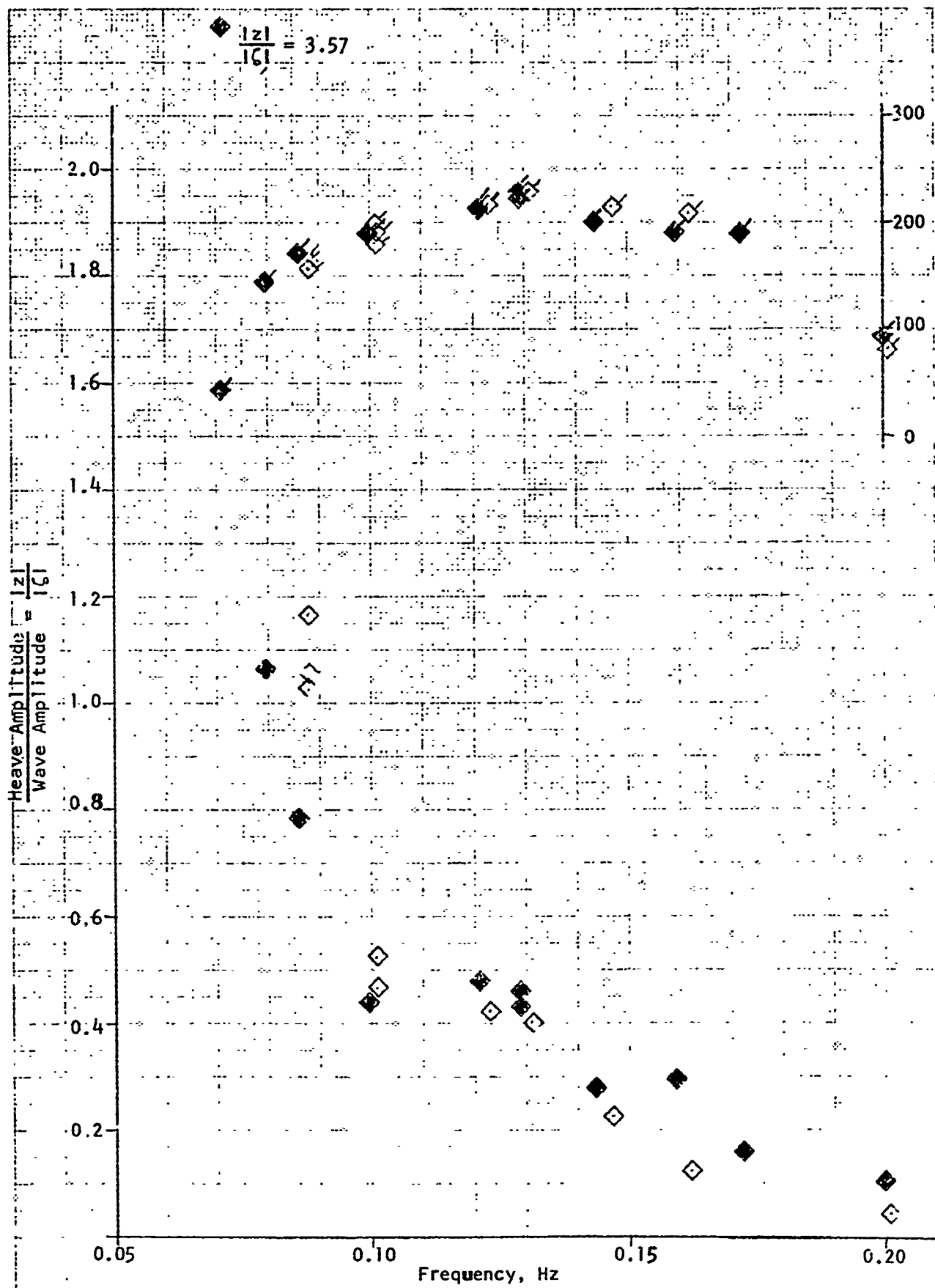


FIGURE 14g. WAVE TEST RESULTS FOR TESTS 1 AND 7, ROW 3

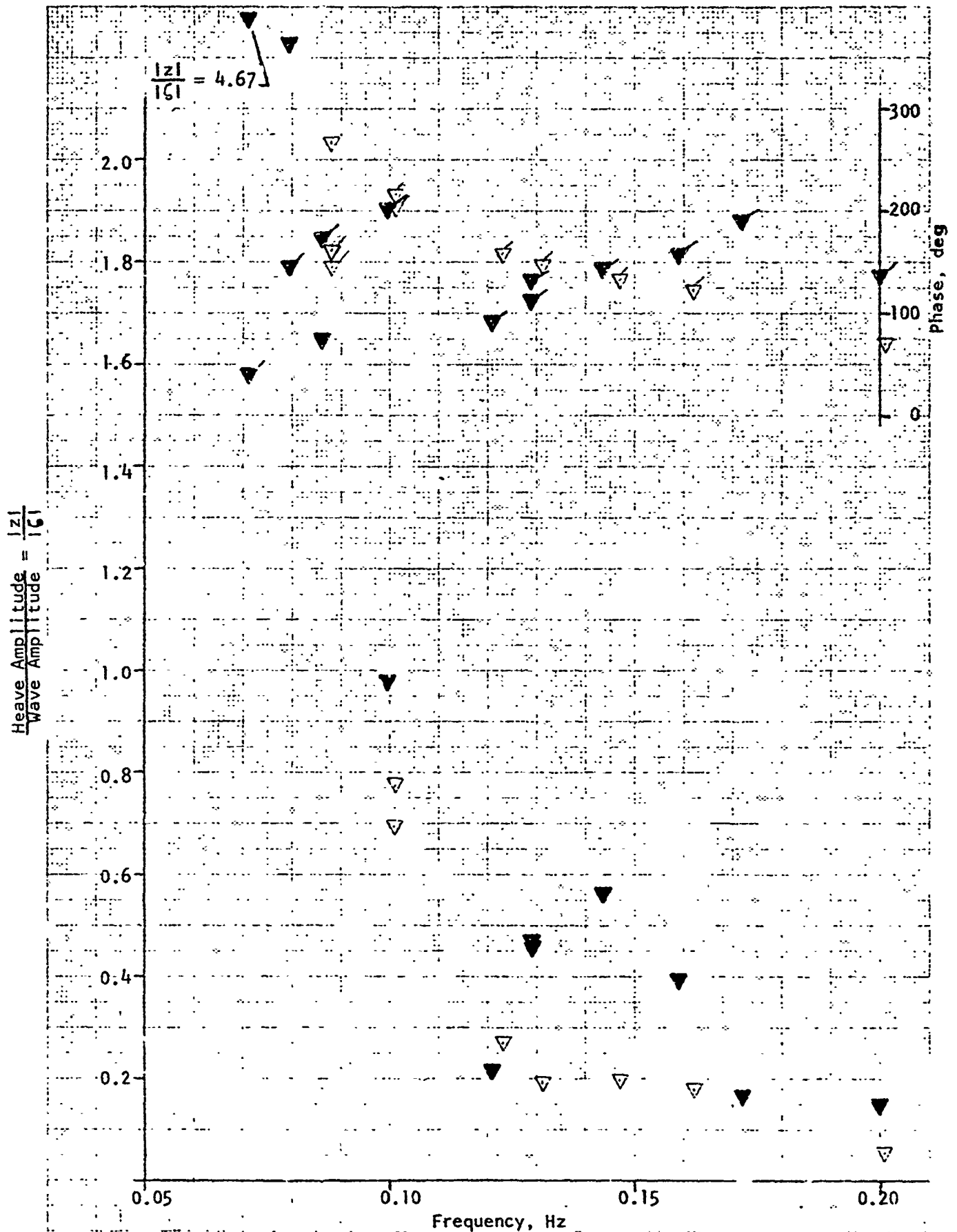


FIGURE 14h. WAVE TEST RESULTS FOR TESTS 3 AND 7, ROW 1

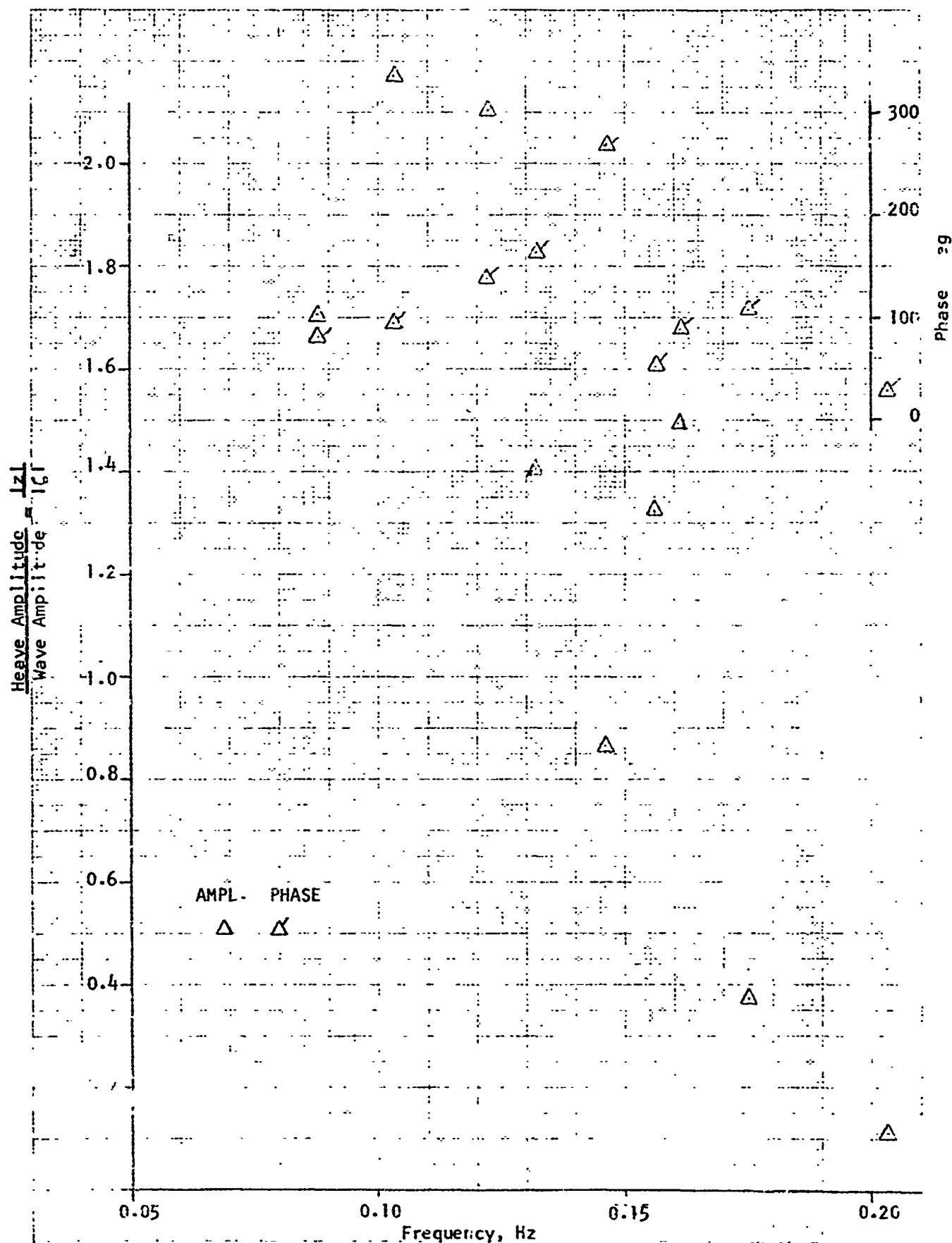


FIGURE 15a. WAVE TEST RESULTS FOR TESTS 2, ROW 17

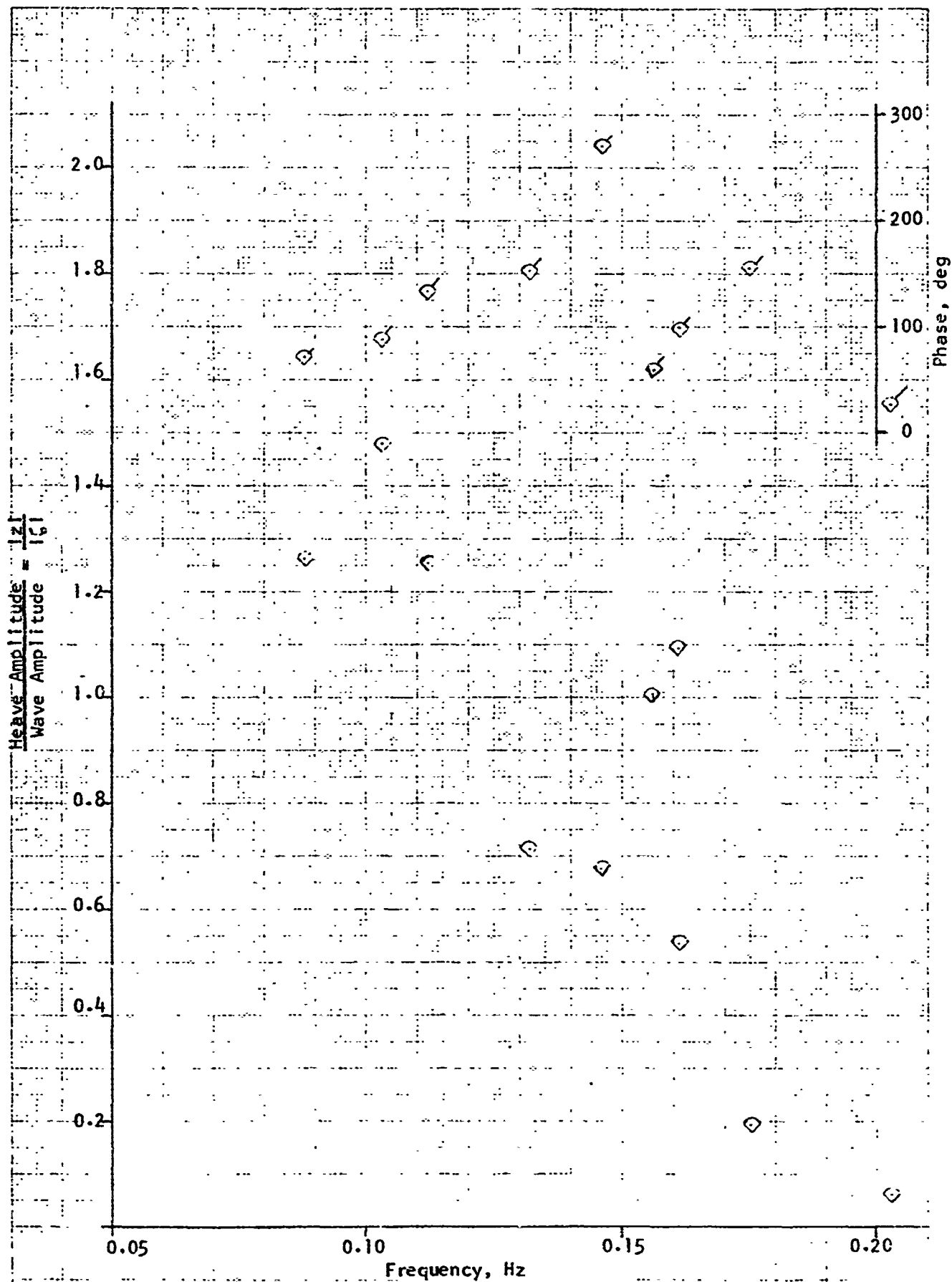


FIGURE 15b. WAVE TEST RESULTS FOR TESTS 2, ROW 15.

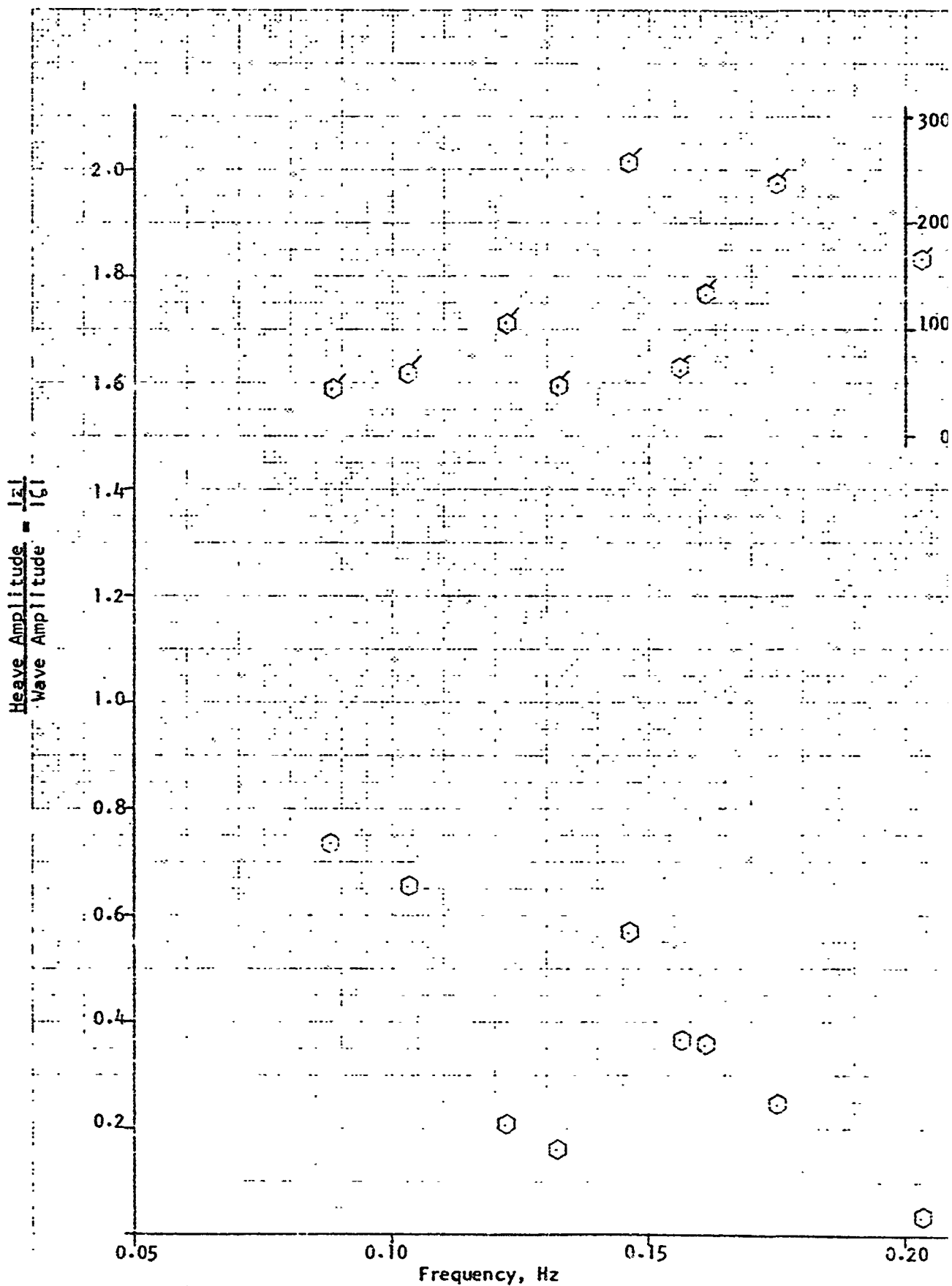


FIGURE 15c. WAVE TEST RESULTS FOR TEST 2, ROW 12

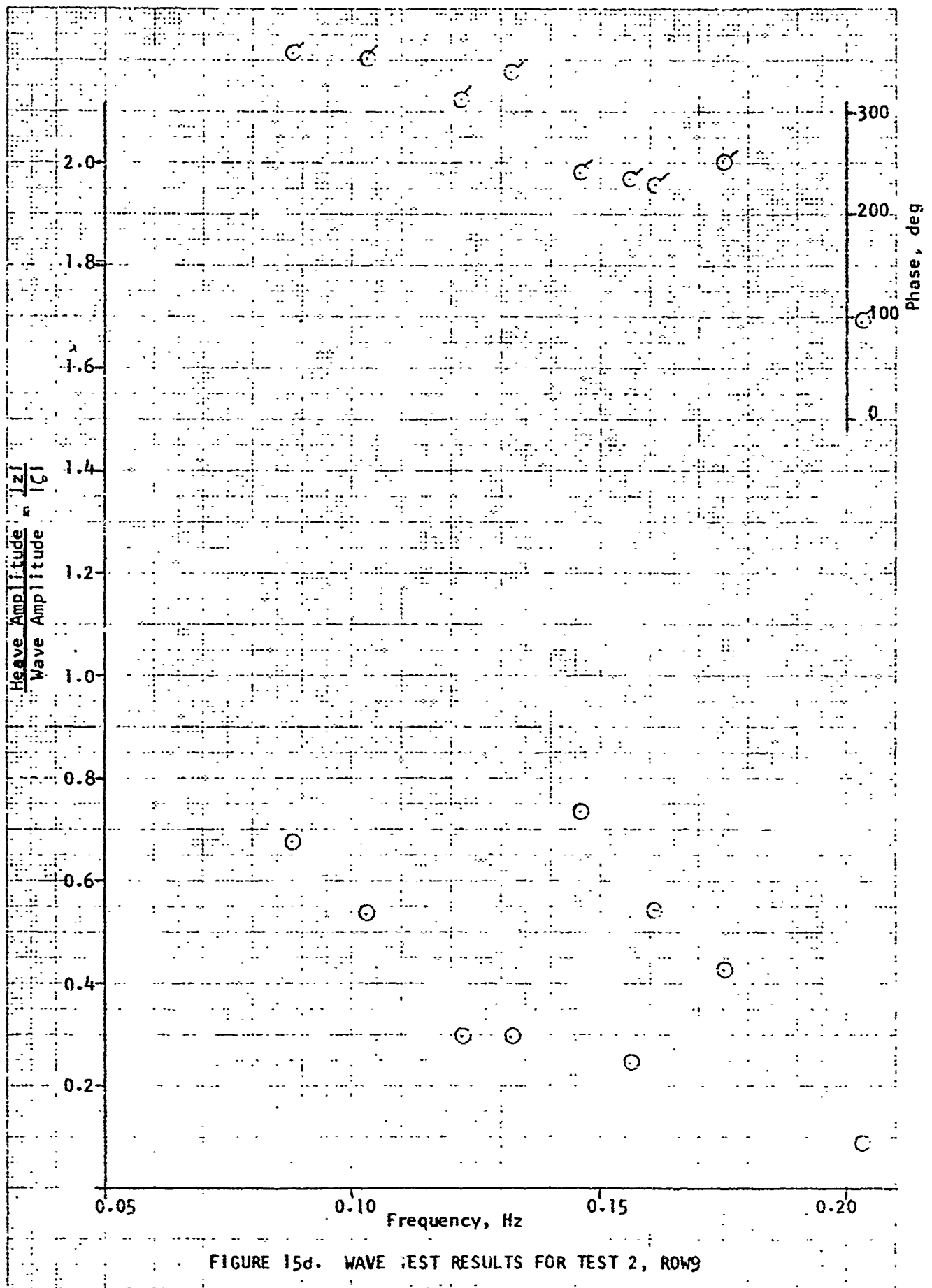


FIGURE 15d. WAVE TEST RESULTS FOR TEST 2, ROW9

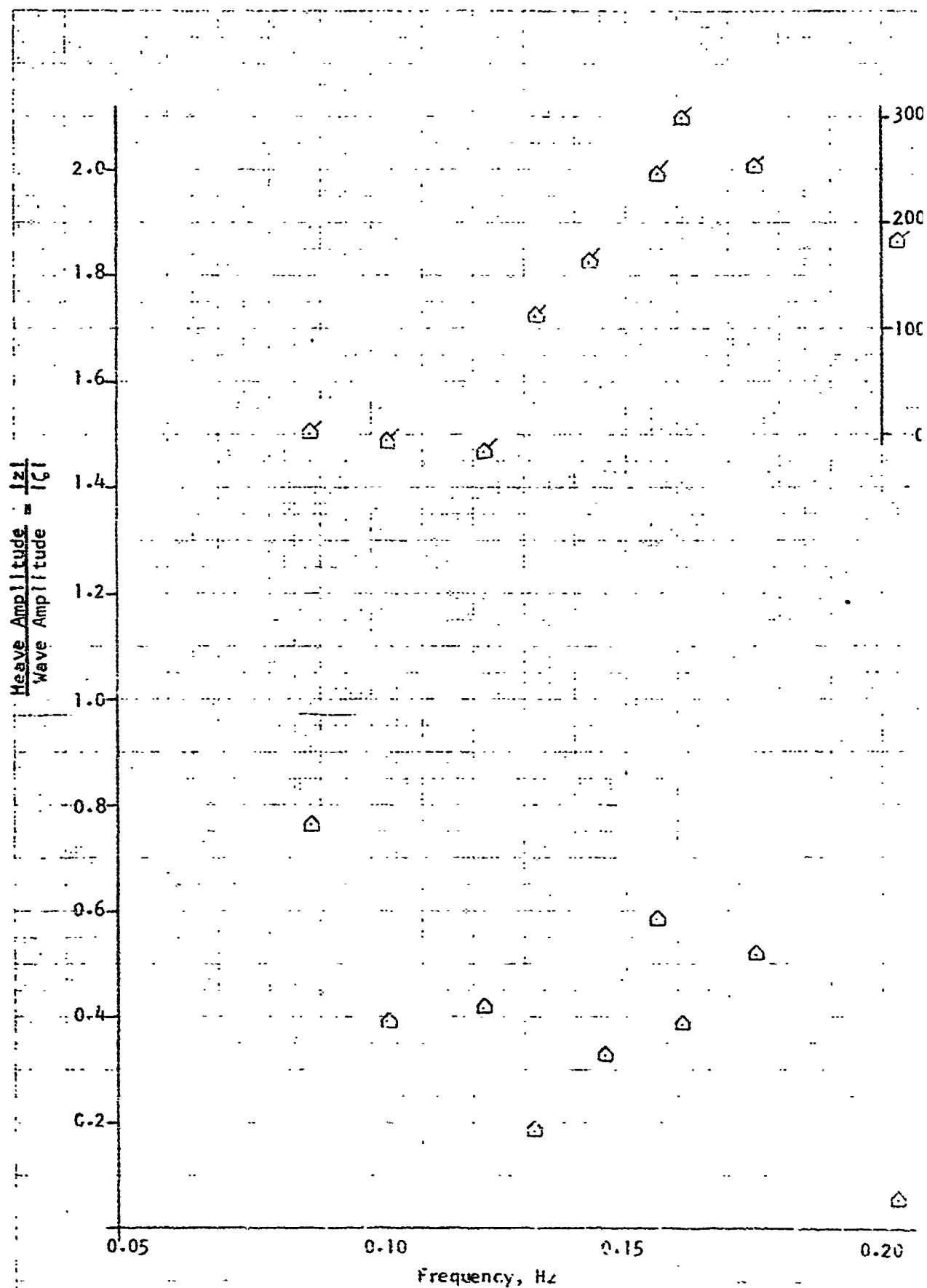


FIGURE 15e. WAVE TEST RESULTS FOR TEST 2, ROW 9P

LR-1635

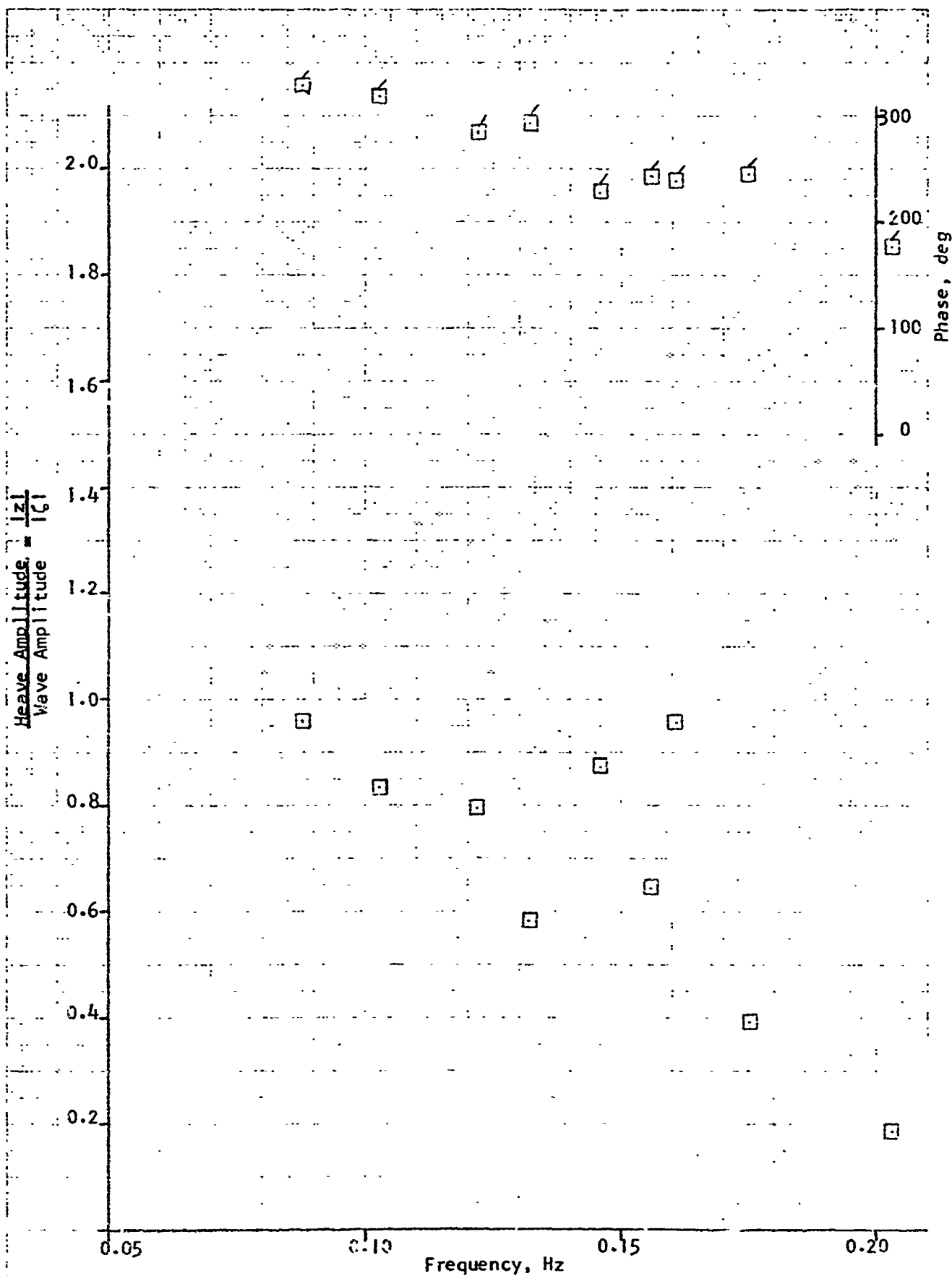


FIGURE 15f. WAVE TEST RESULTS FOR TEST 2, ROW 6

LR-1635

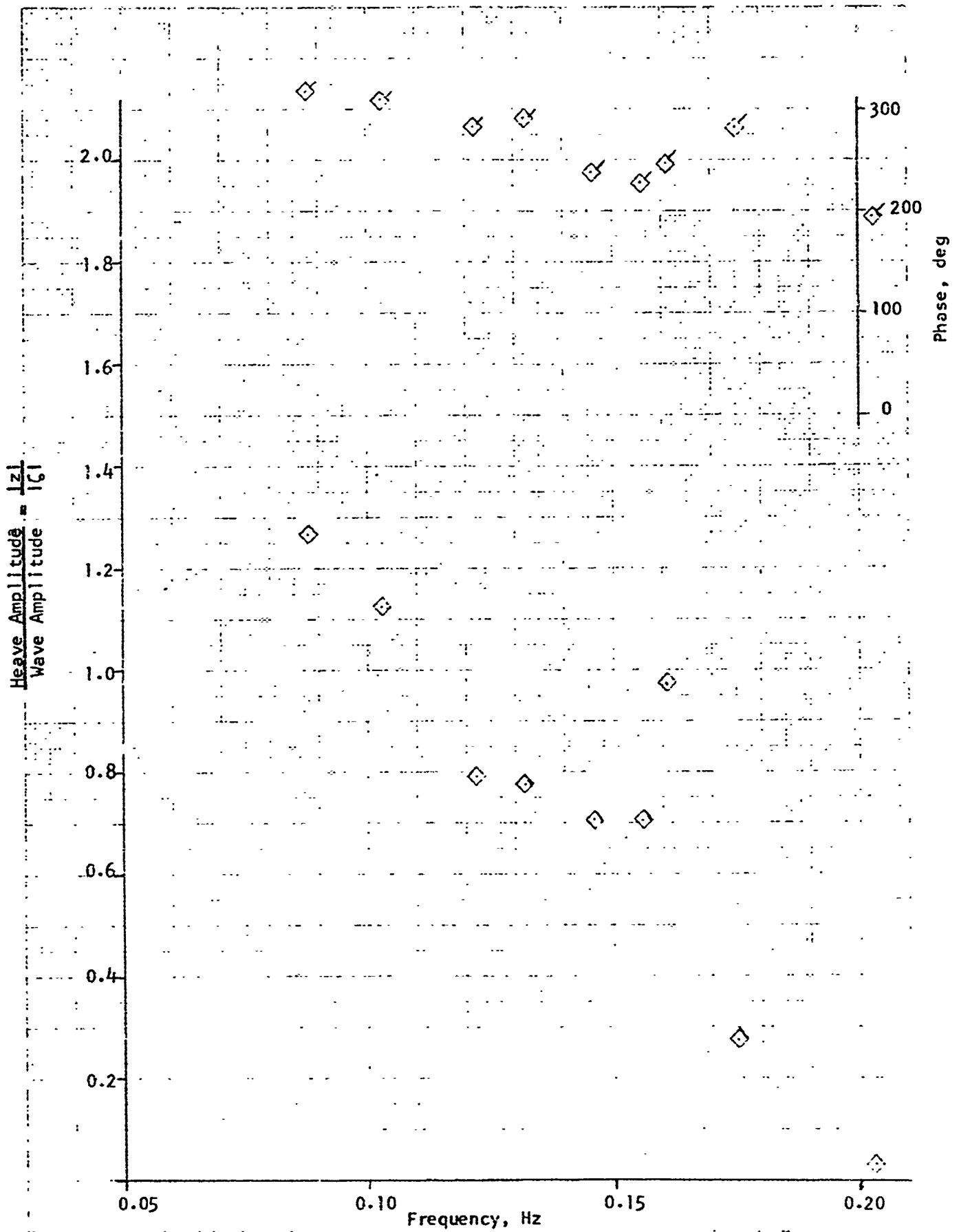


FIGURE 15g. WAVE TEST RESULTS FOR TEST 2, ROW 3

LR-1635

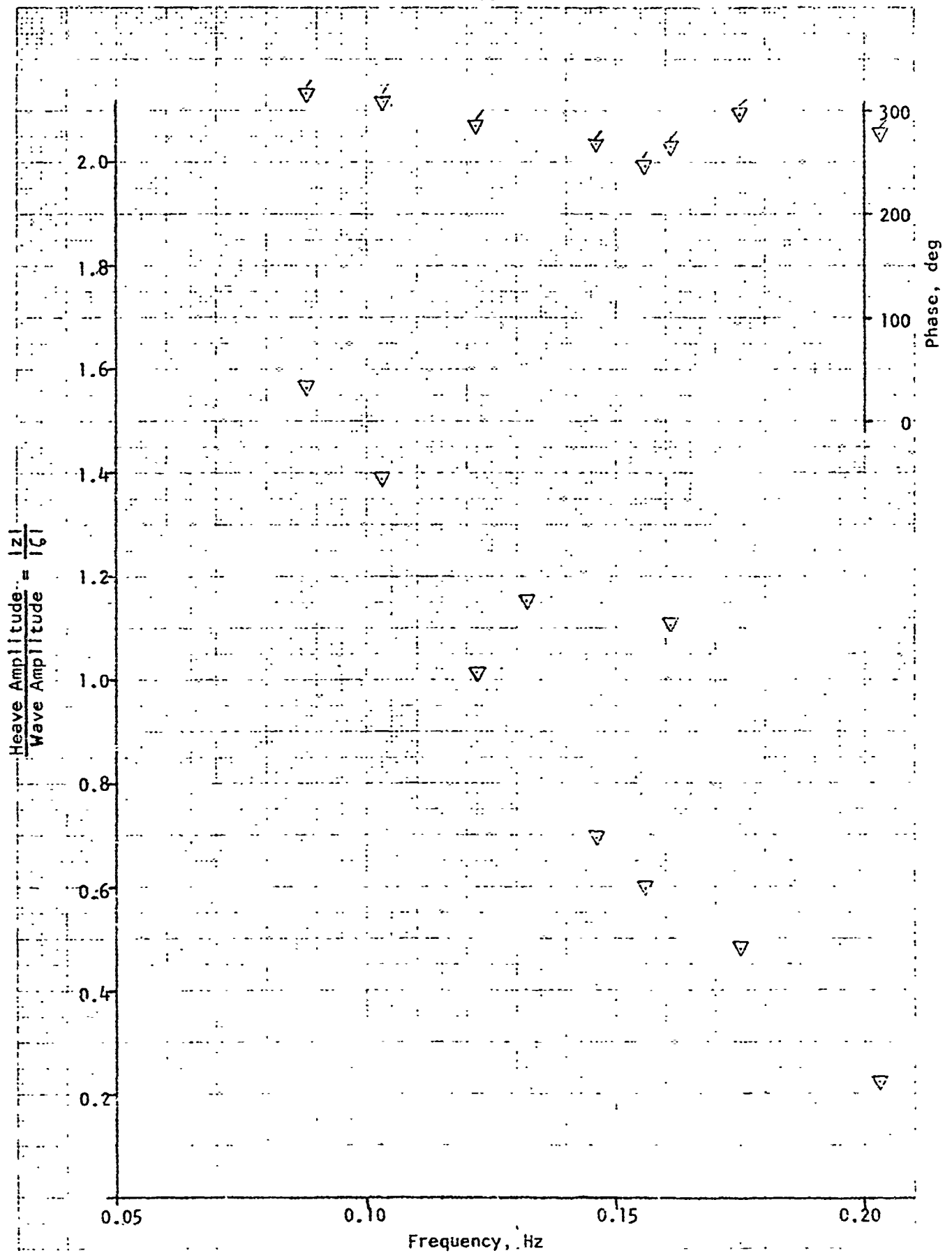


FIGURE 15h. WAVE TEST RESULTS FOR TESTS 2, ROW 1

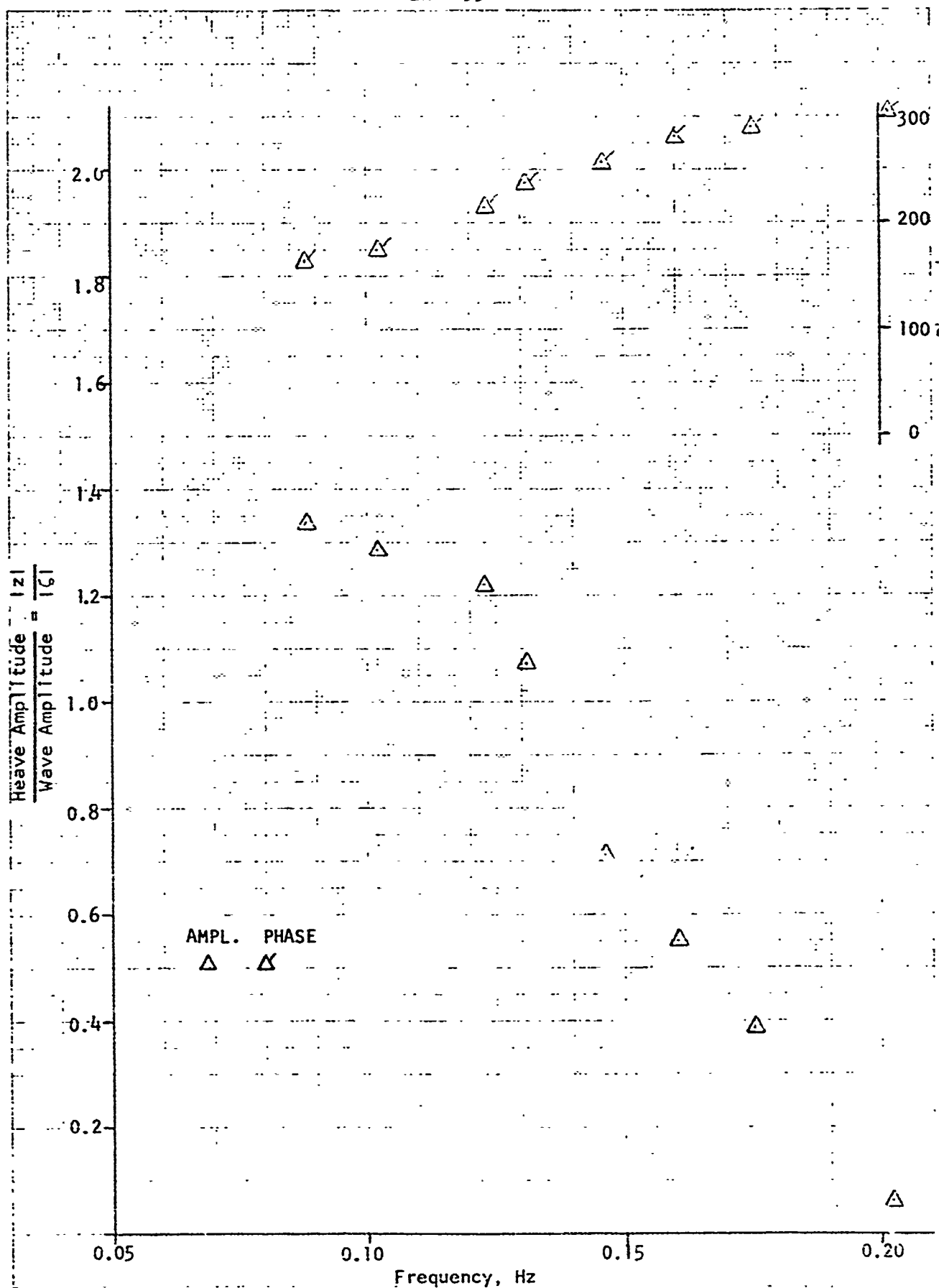


FIGURE 16a. WAVE TEST RESULTS FOR TEST 3, ROW 17

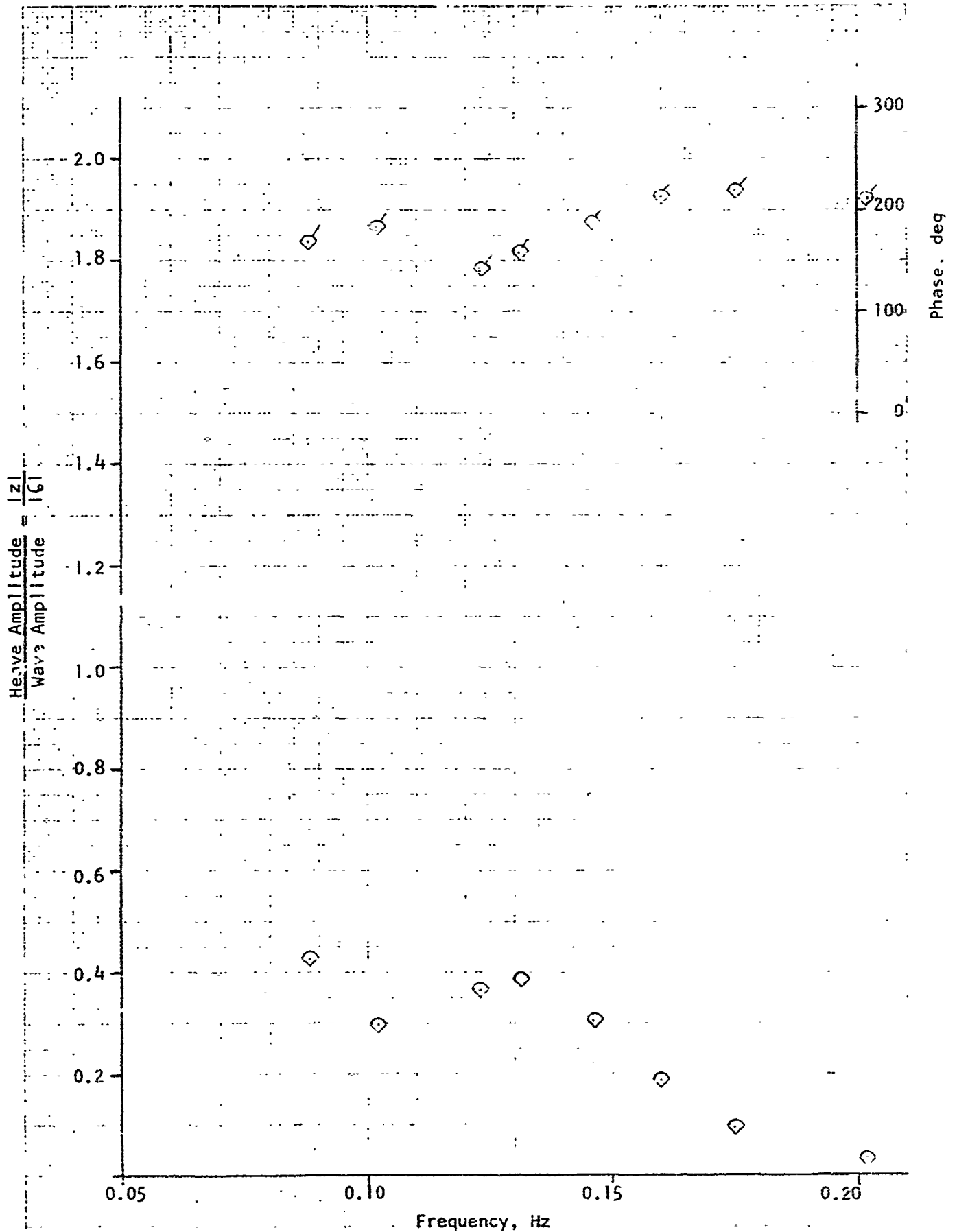


FIGURE 16b. WAVE TEST RESULTS FOR TEST 3, ROW 15

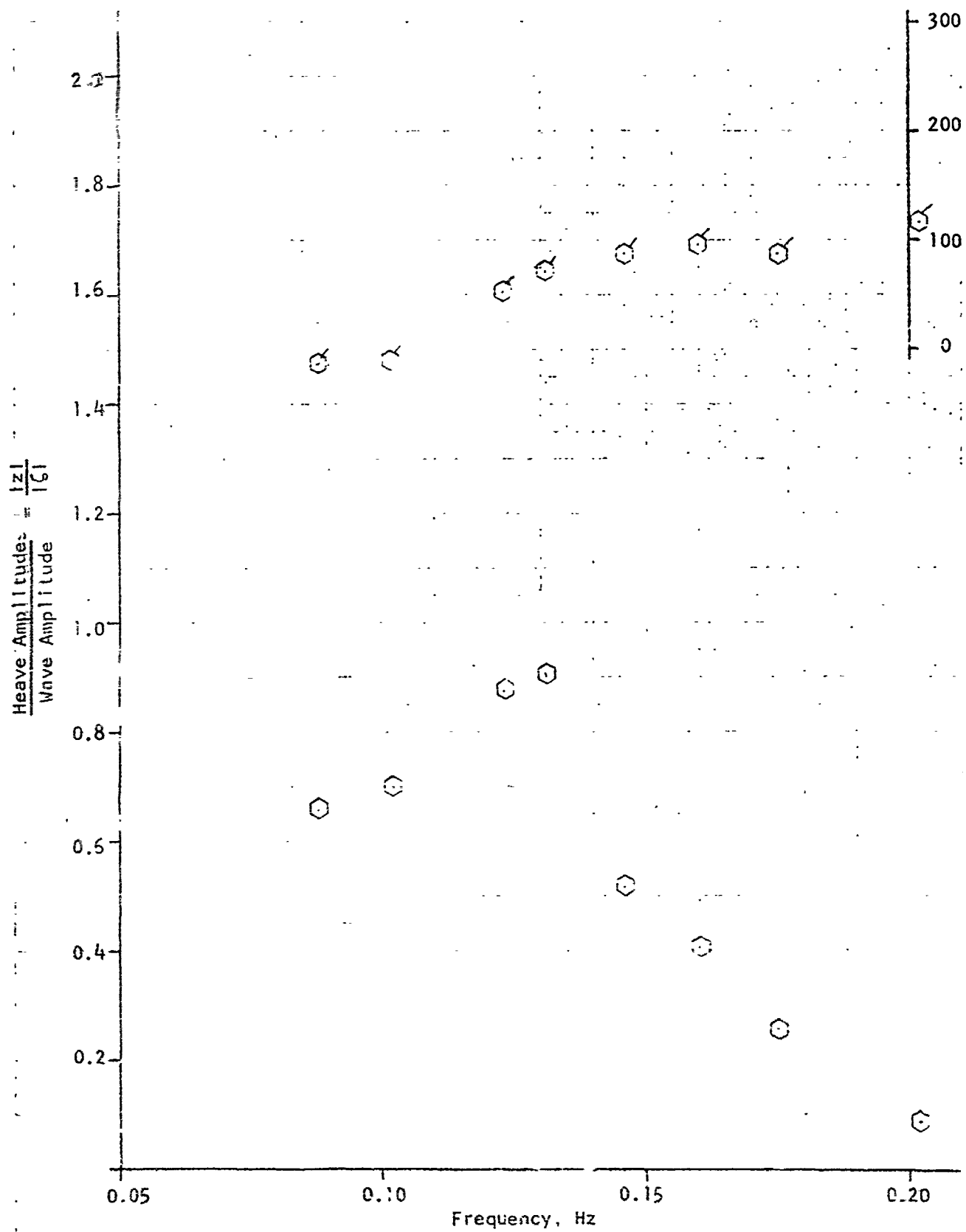


FIGURE 16c. WAVE TEST RESULTS FOR TEST 3, ROW 12

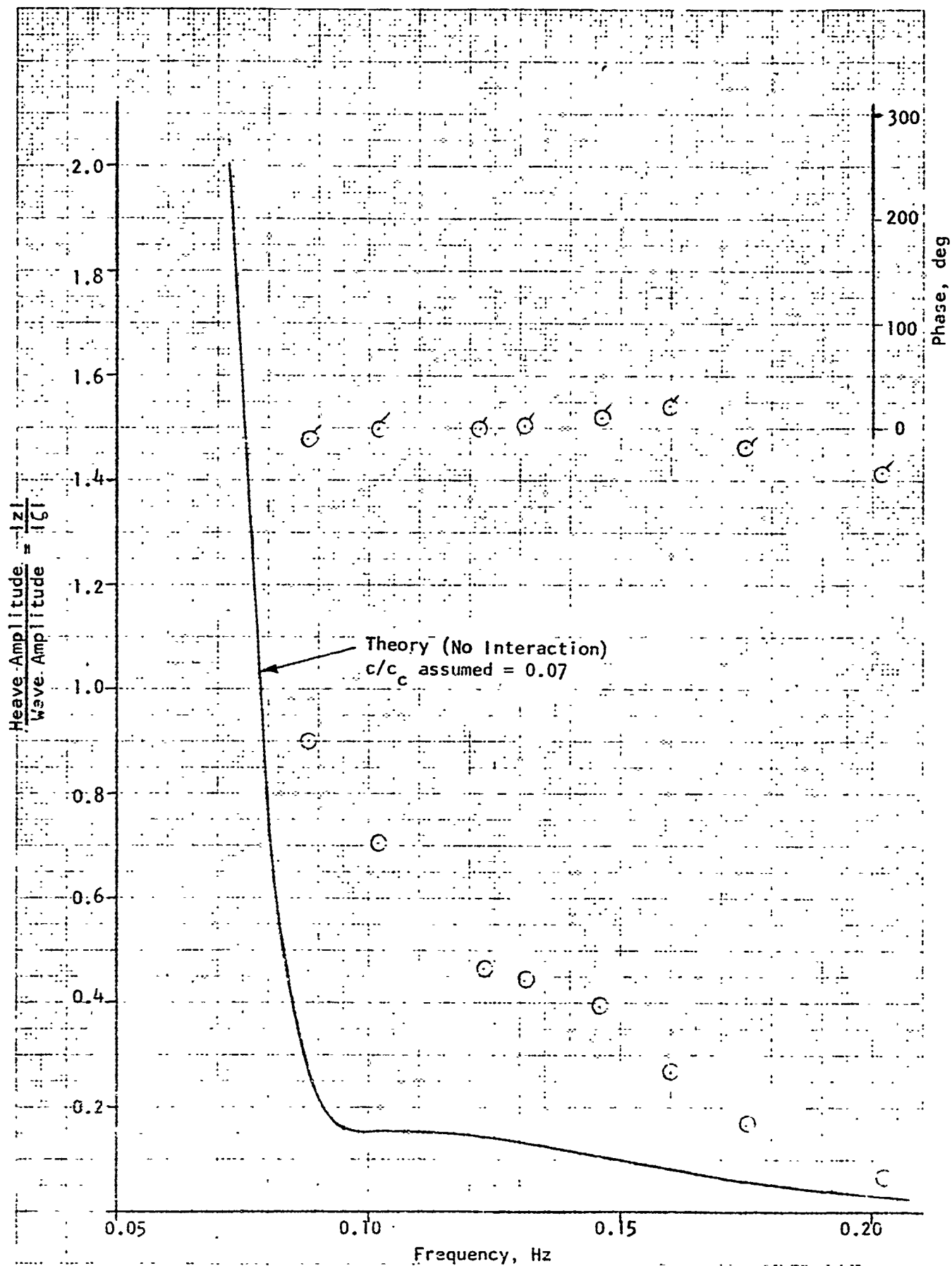


FIGURE 16d. WAVE TEST RESULTS FOR TEST 3, ROW 9

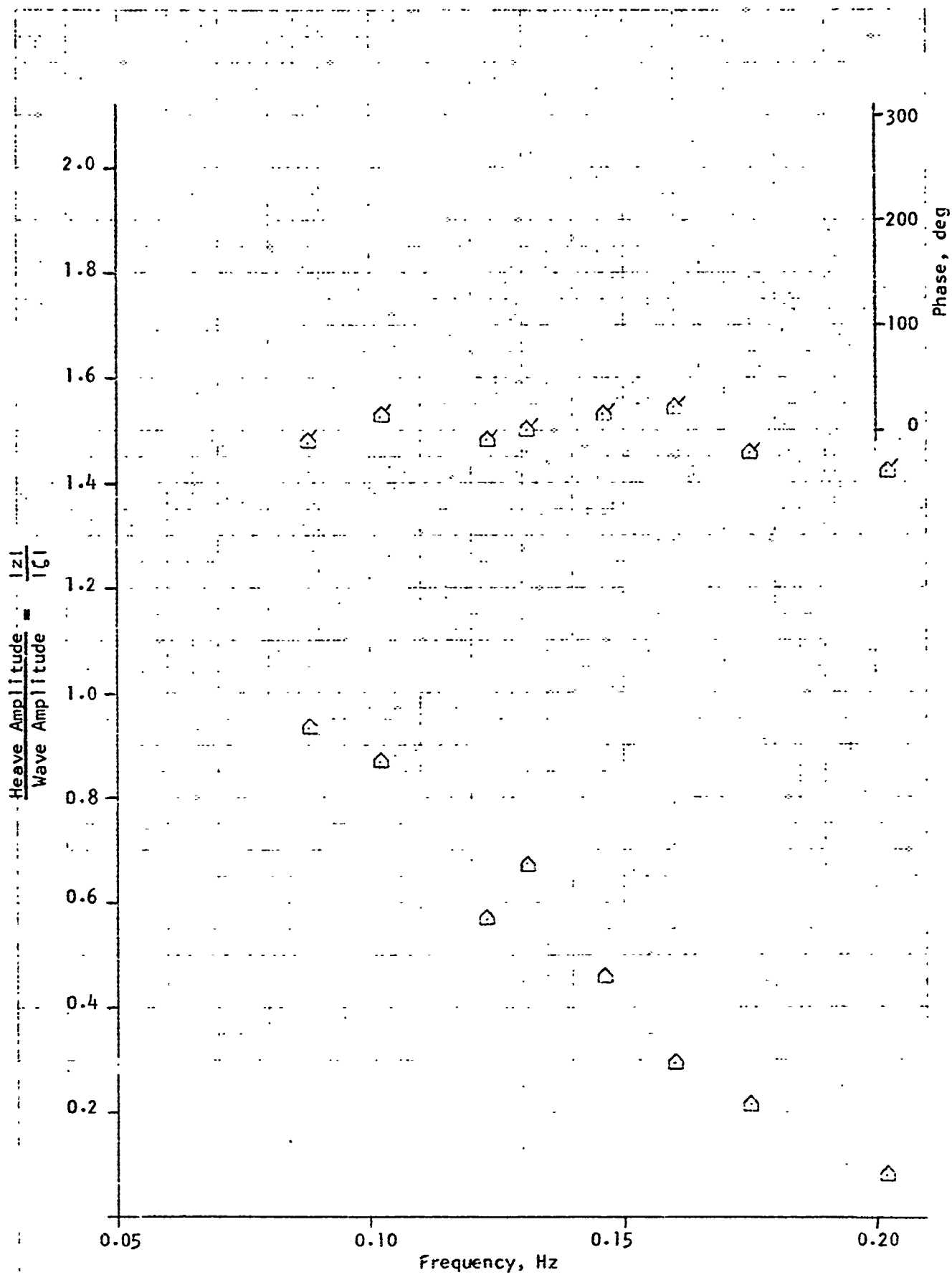


FIGURE 16e. WAVE TEST RESULTS FOR TEST 3, ROW 9P

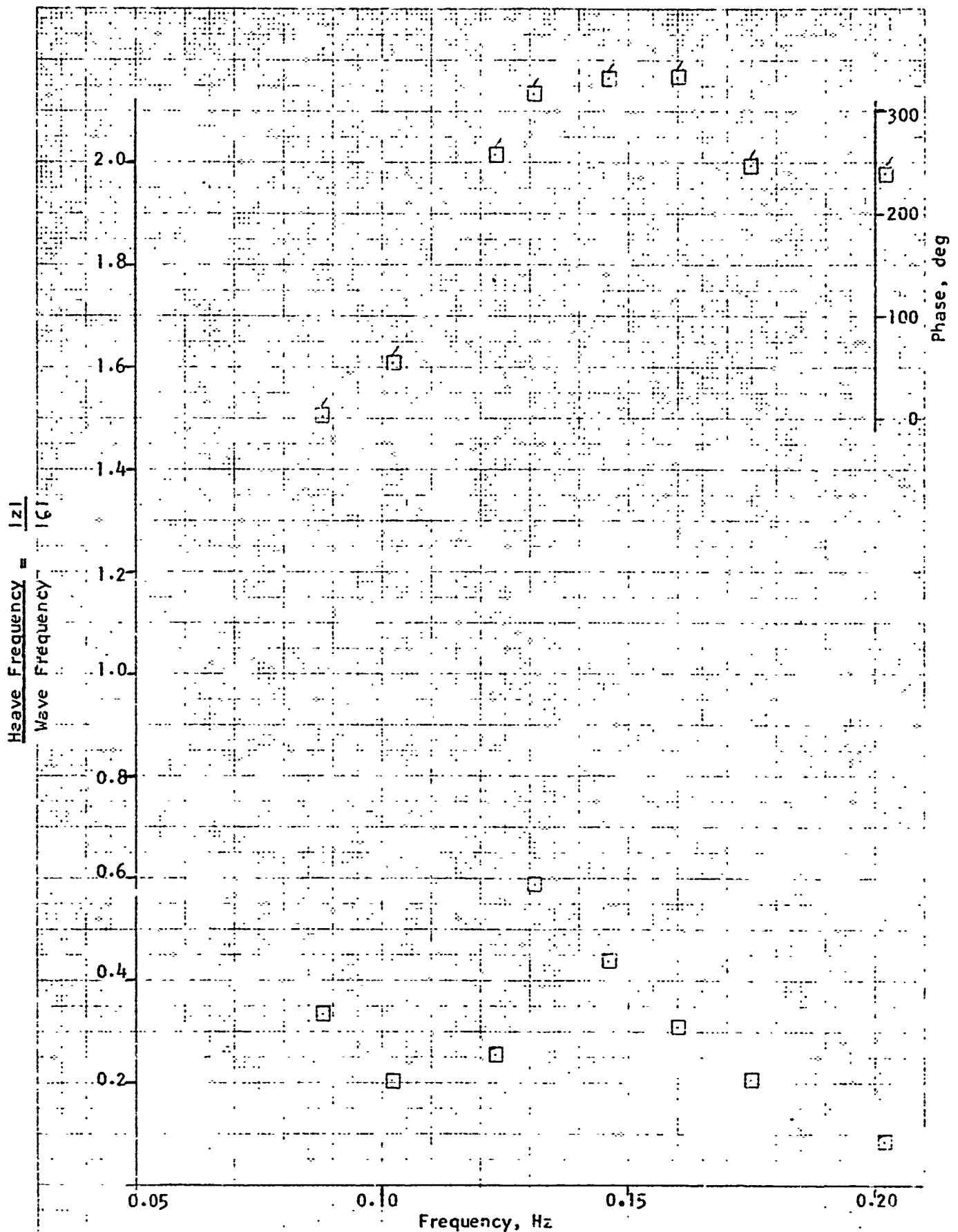


FIGURE 16f. WAVE TEST RESULTS FOR TEST 3, ROW 6

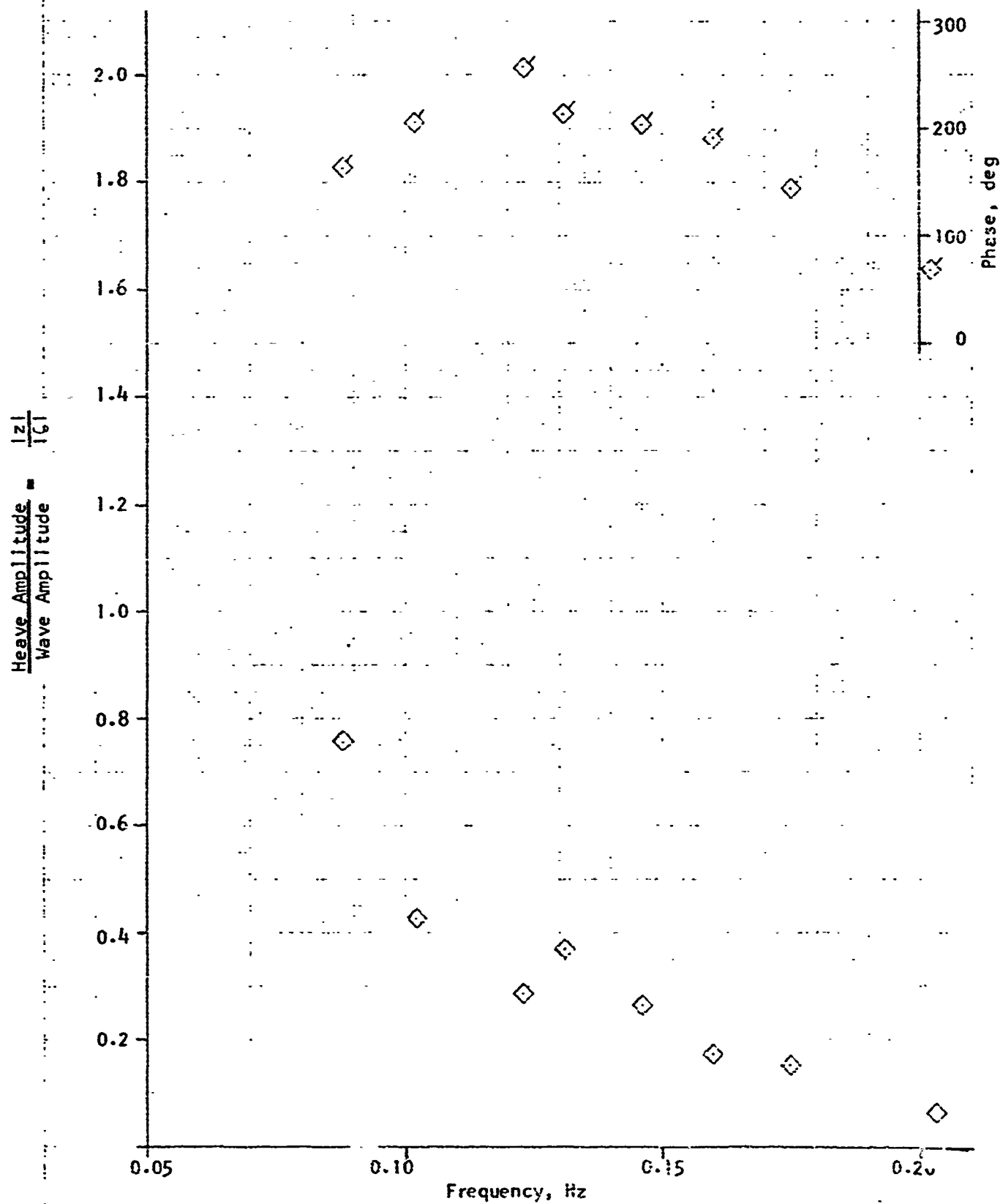


FIGURE 16g. WAVE TEST RESULTS FOR TEST 3, ROW 3

LR-1635

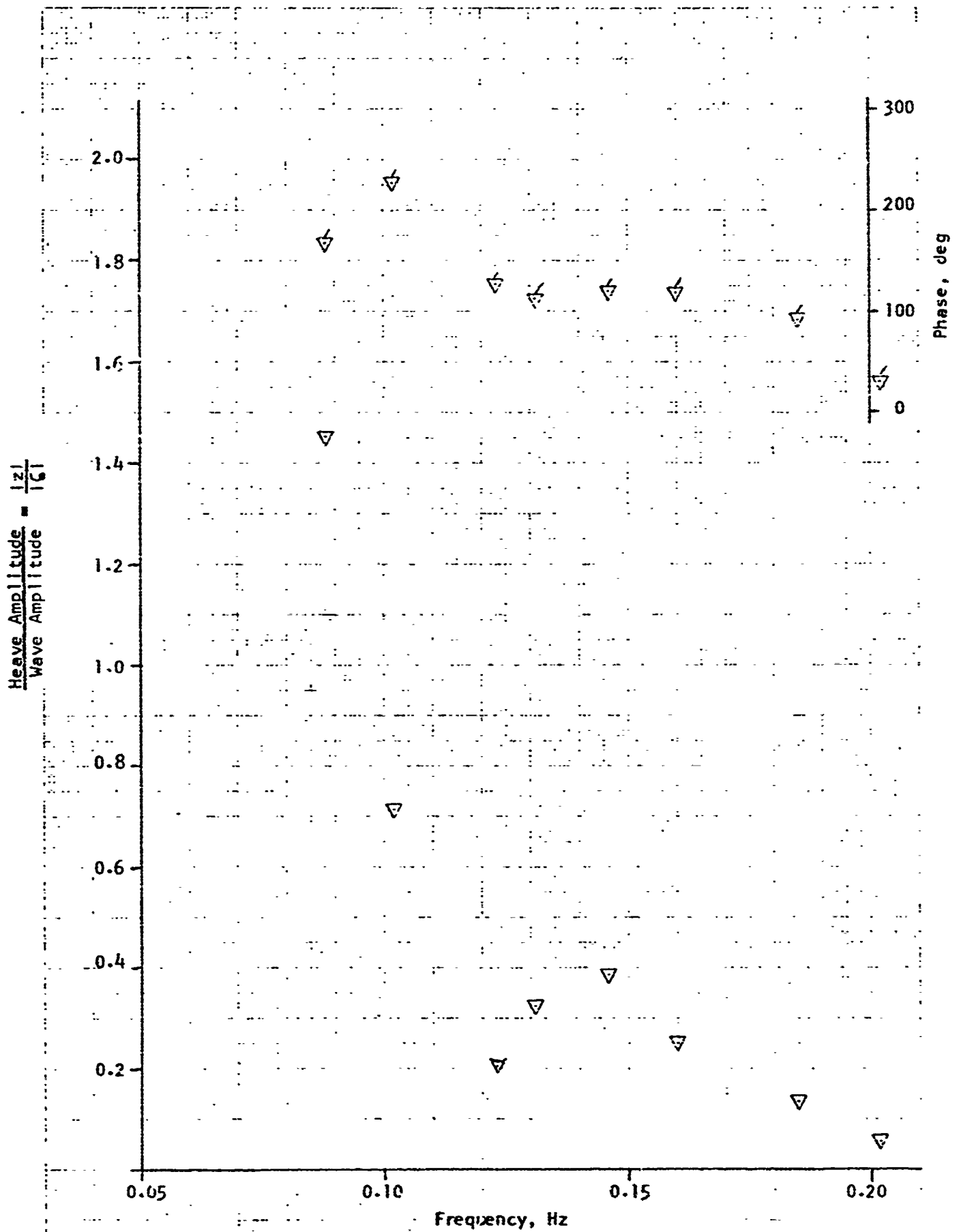


FIGURE 16h. WAVE TEST RESULTS FOR TEST 3, ROW 1

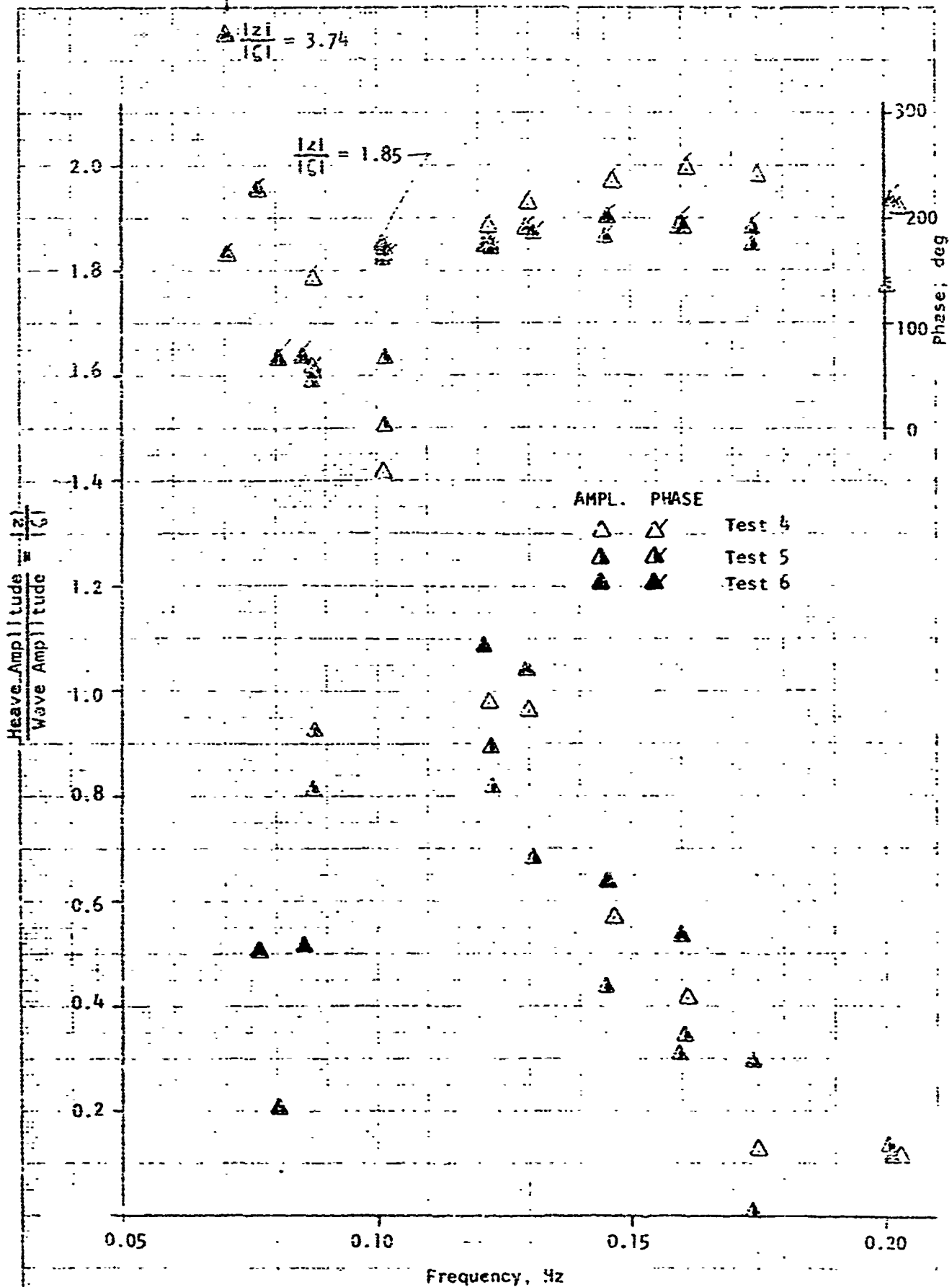


FIGURE 17a. WAVE TEST RESULTS FOR TESTS 4,5,6, ROW 17

LR-1635

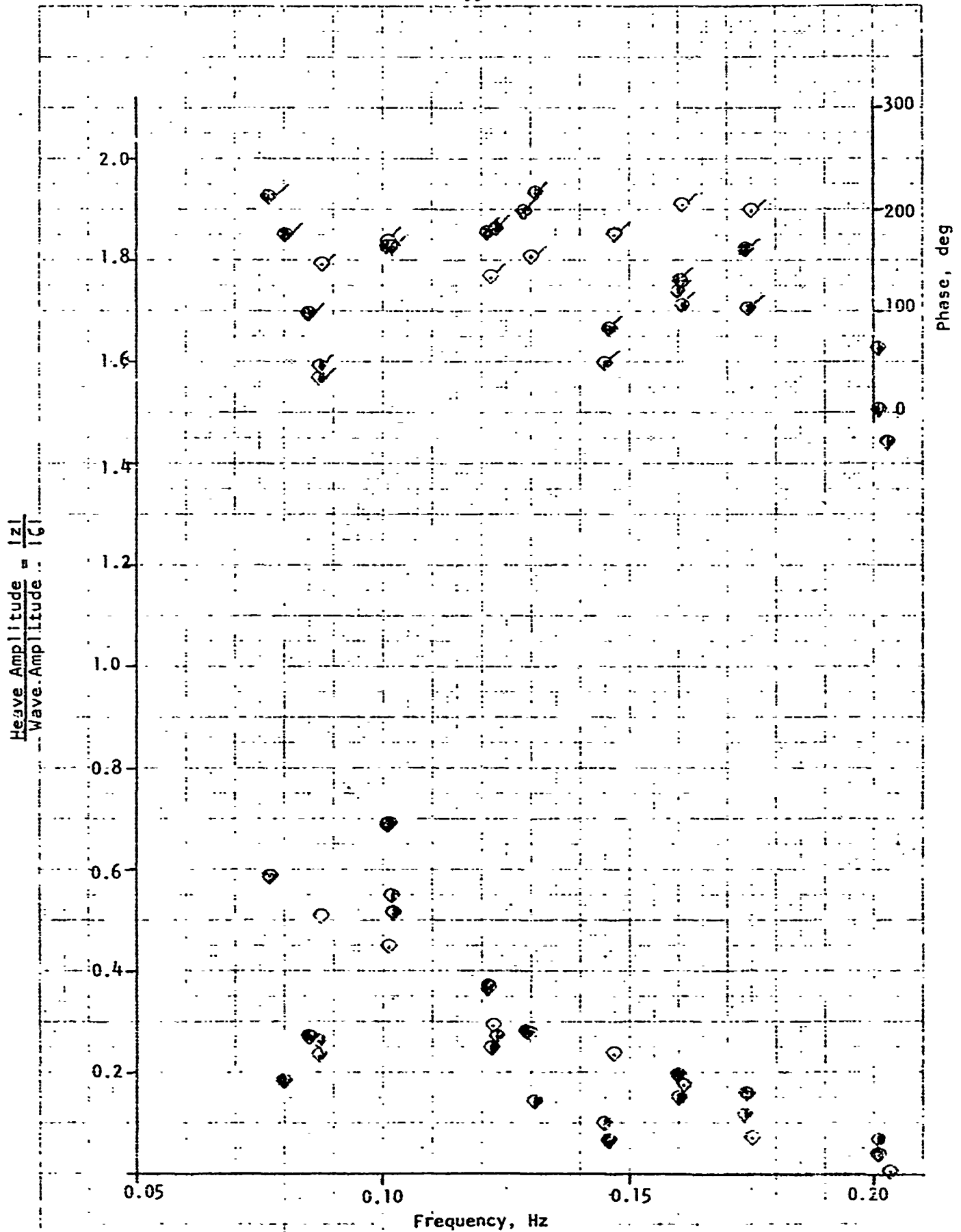


FIGURE 17b. WAVE TEST RESULTS FOR TESTS 4,5,6, ROW 15

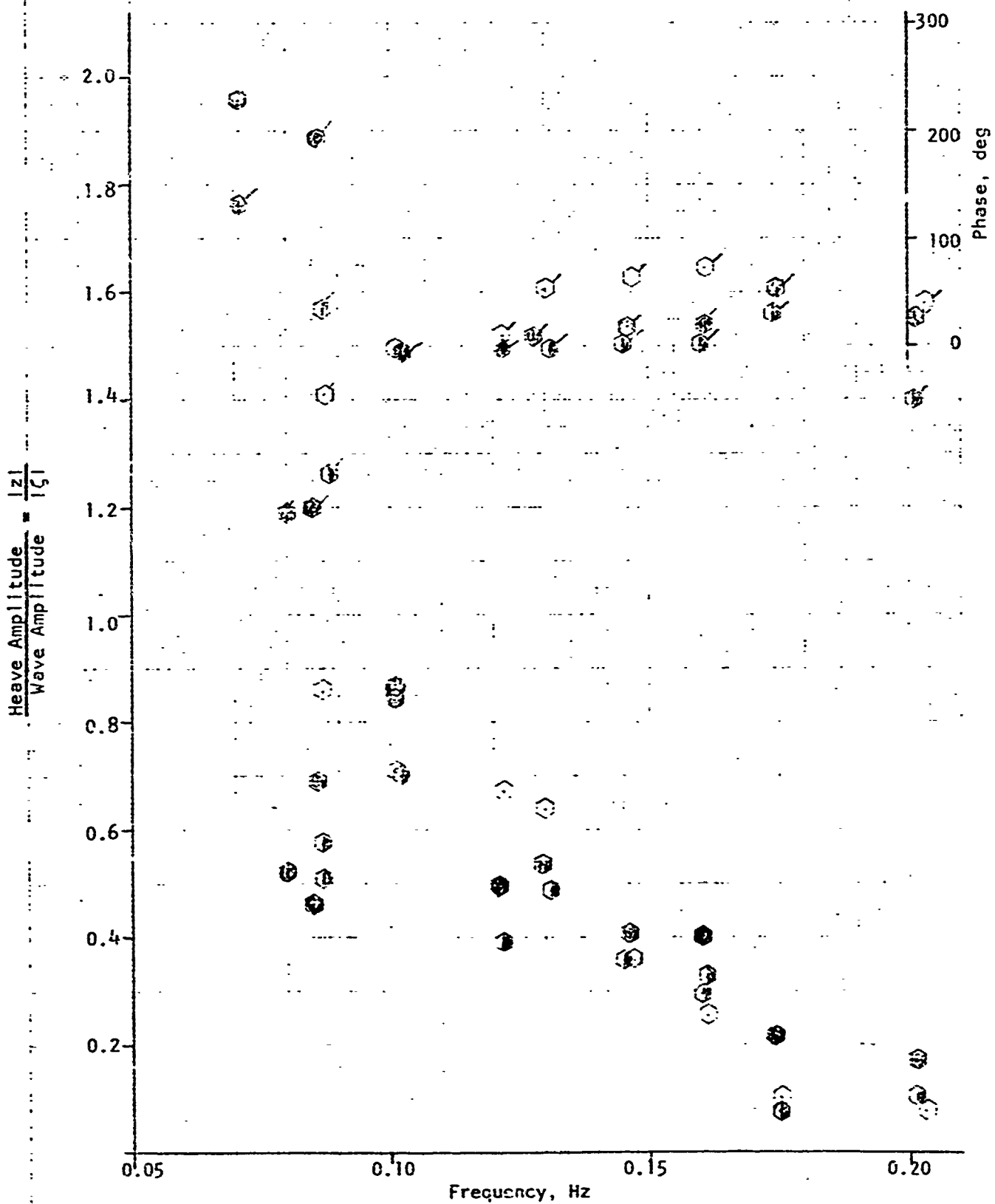


FIGURE 17c. WAVE TEST RESULTS FOR TESTS 4,5,6, ROW 12

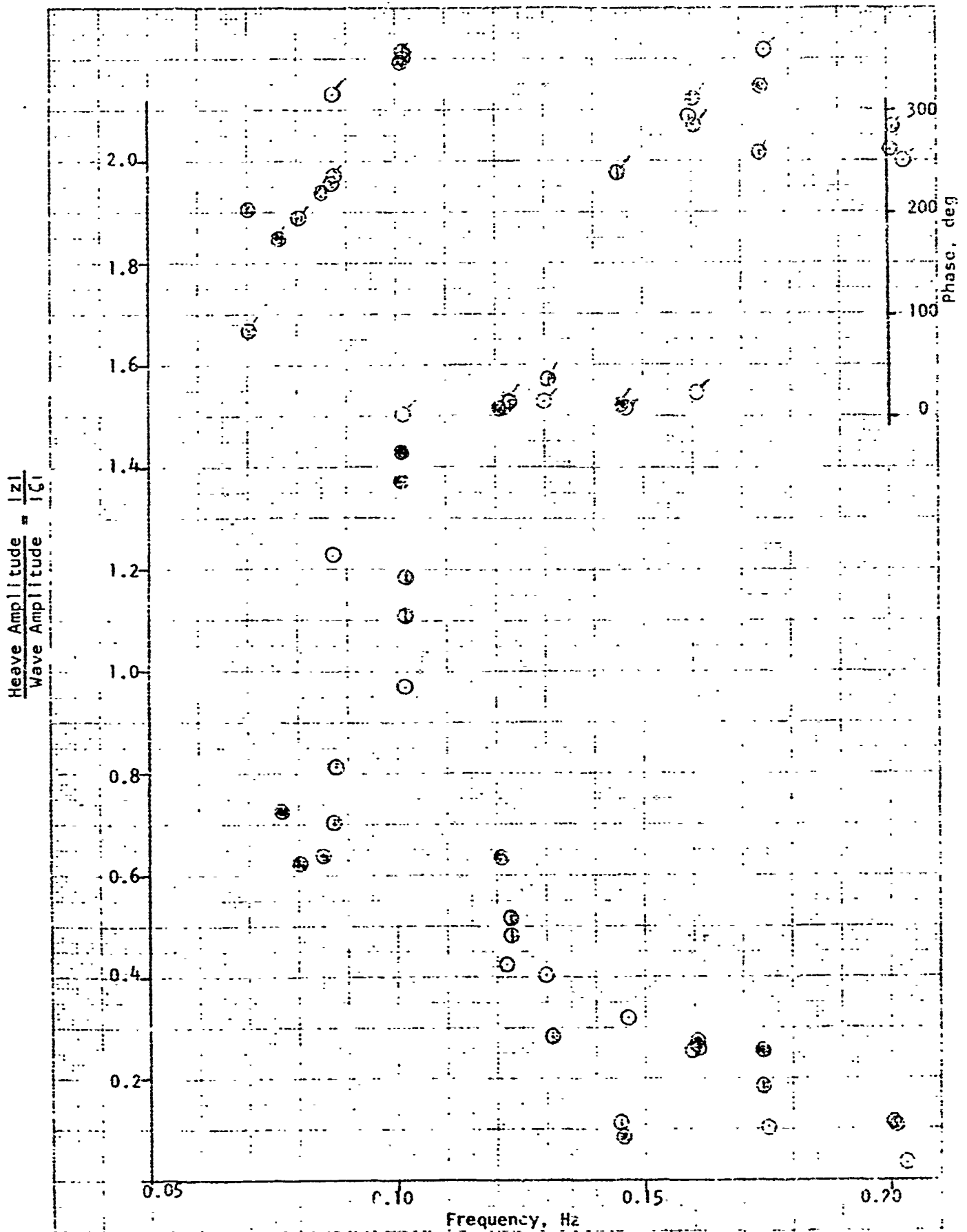


FIGURE 17d. WAVE TEST RESULTS FOR TESTS 4,5,6. ROW 9

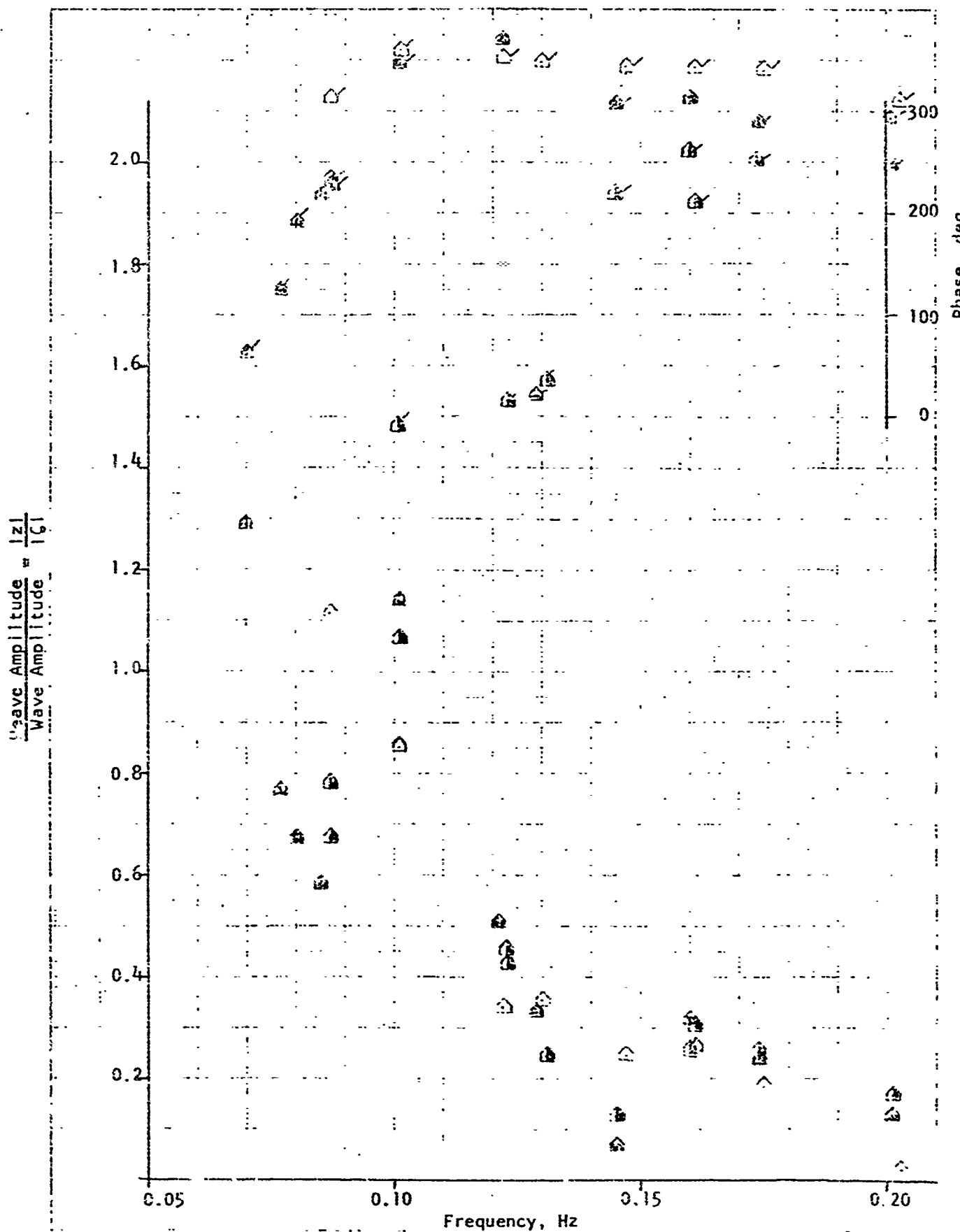


FIGURE 17e. WAVE TEST RESULTS FOR TESTS 4,5,6, ROW 9P

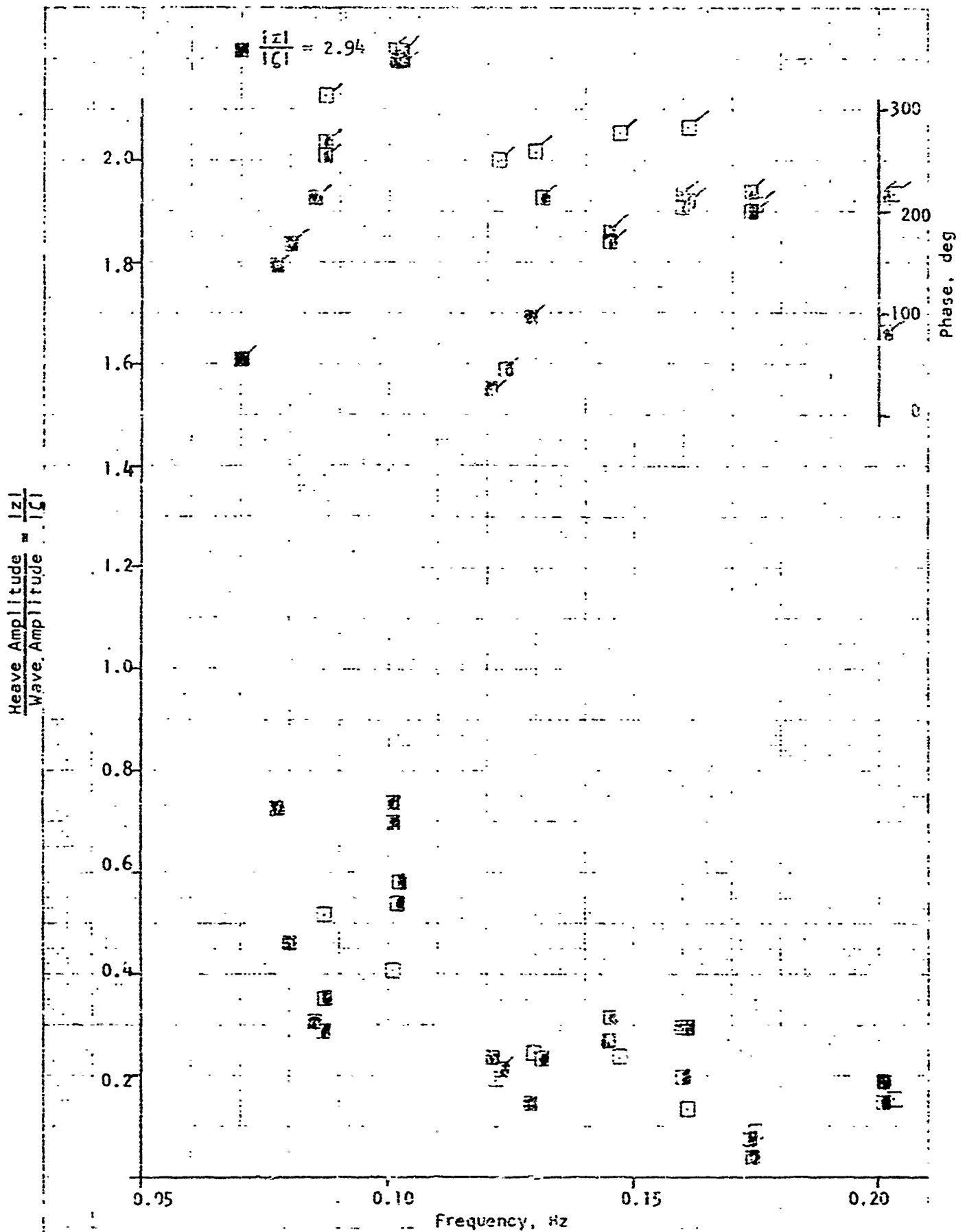


FIGURE 17F. WAVE TEST RESULTS FOR TESTS 4,5,6. ROW 6

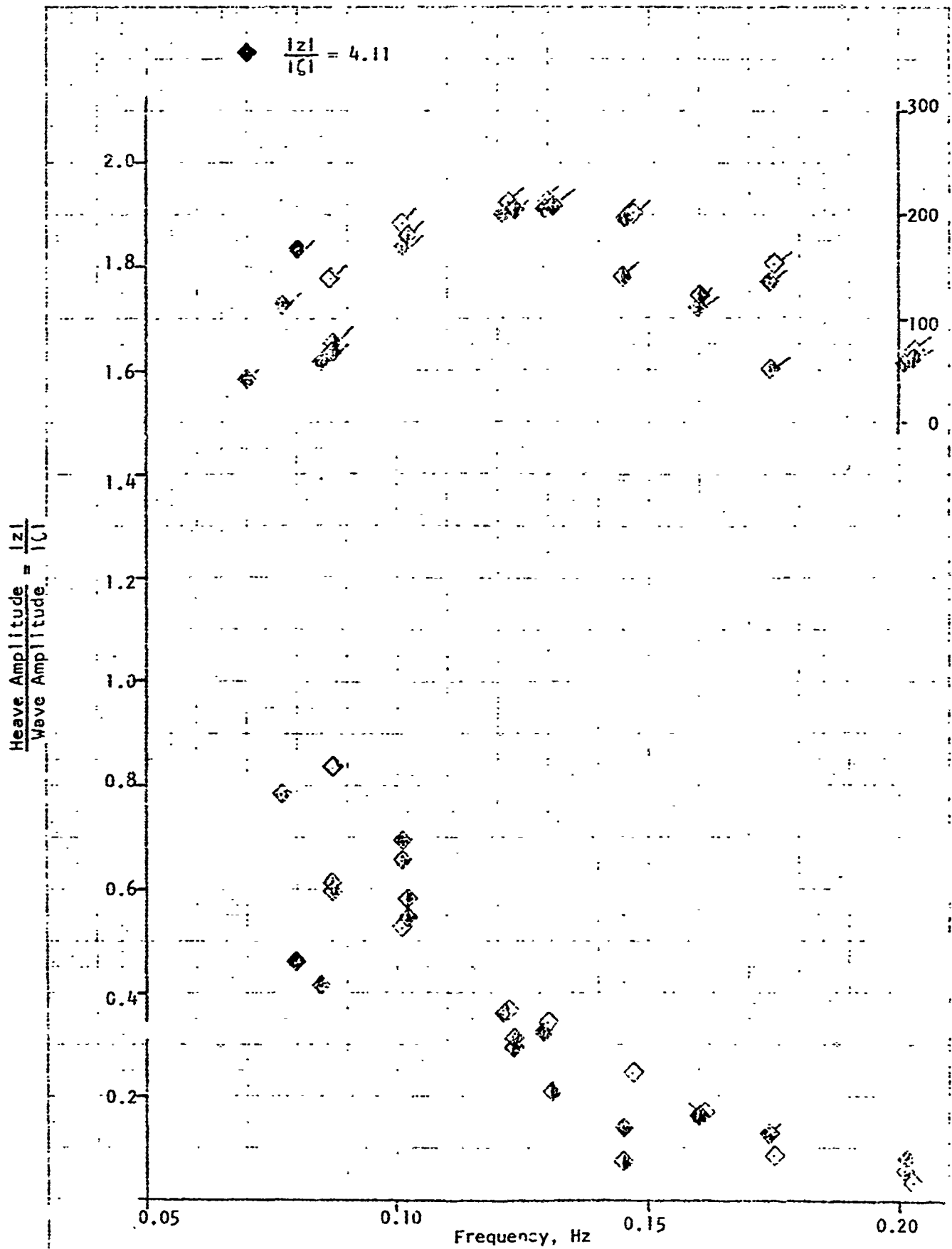


FIGURE 17g. WAVE TEST RESULTS FOR TESTS 4,5,6, ROW 3

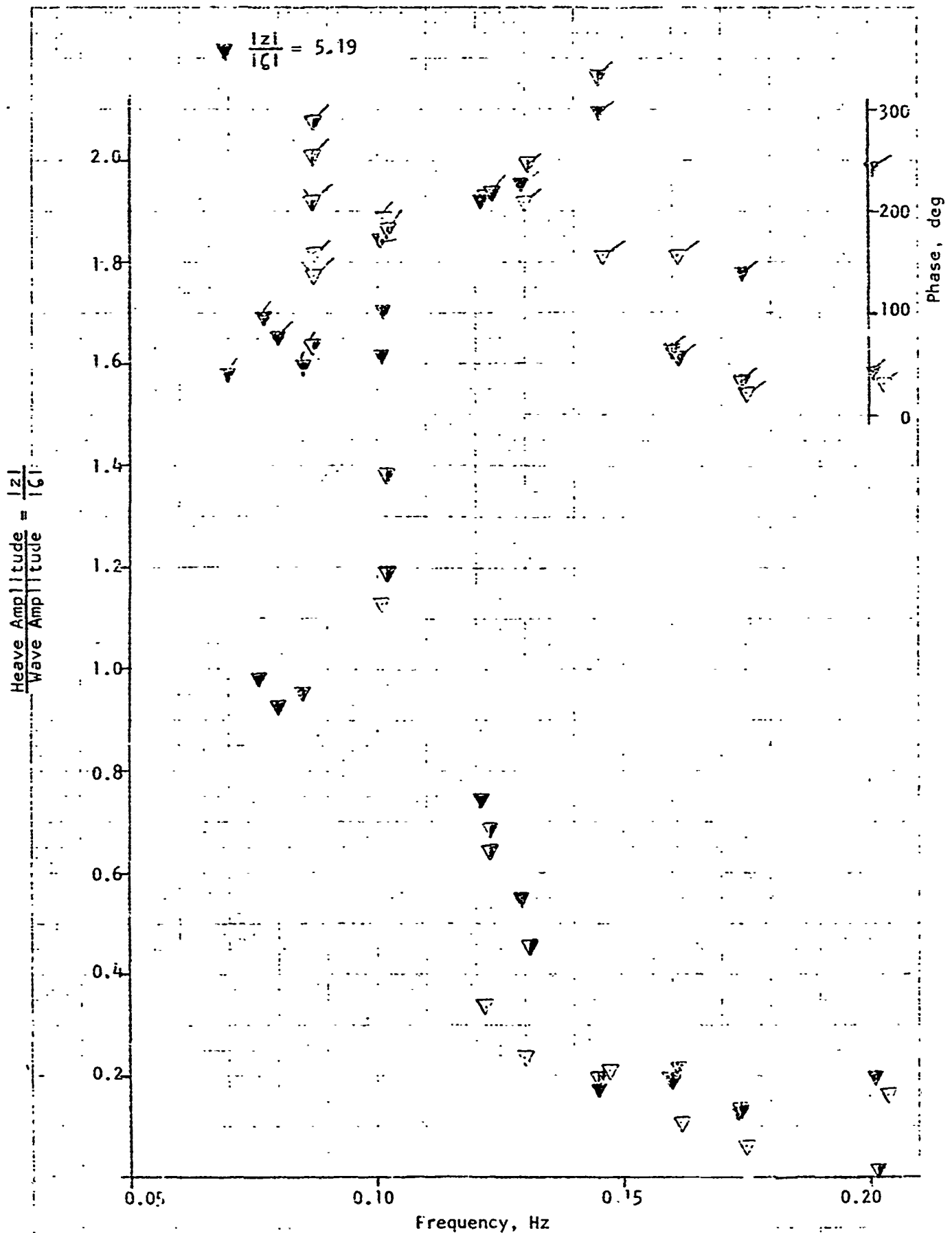


FIGURE 17h. WAVE TEST RESULTS FOR TESTS 5, 6, ROW 1

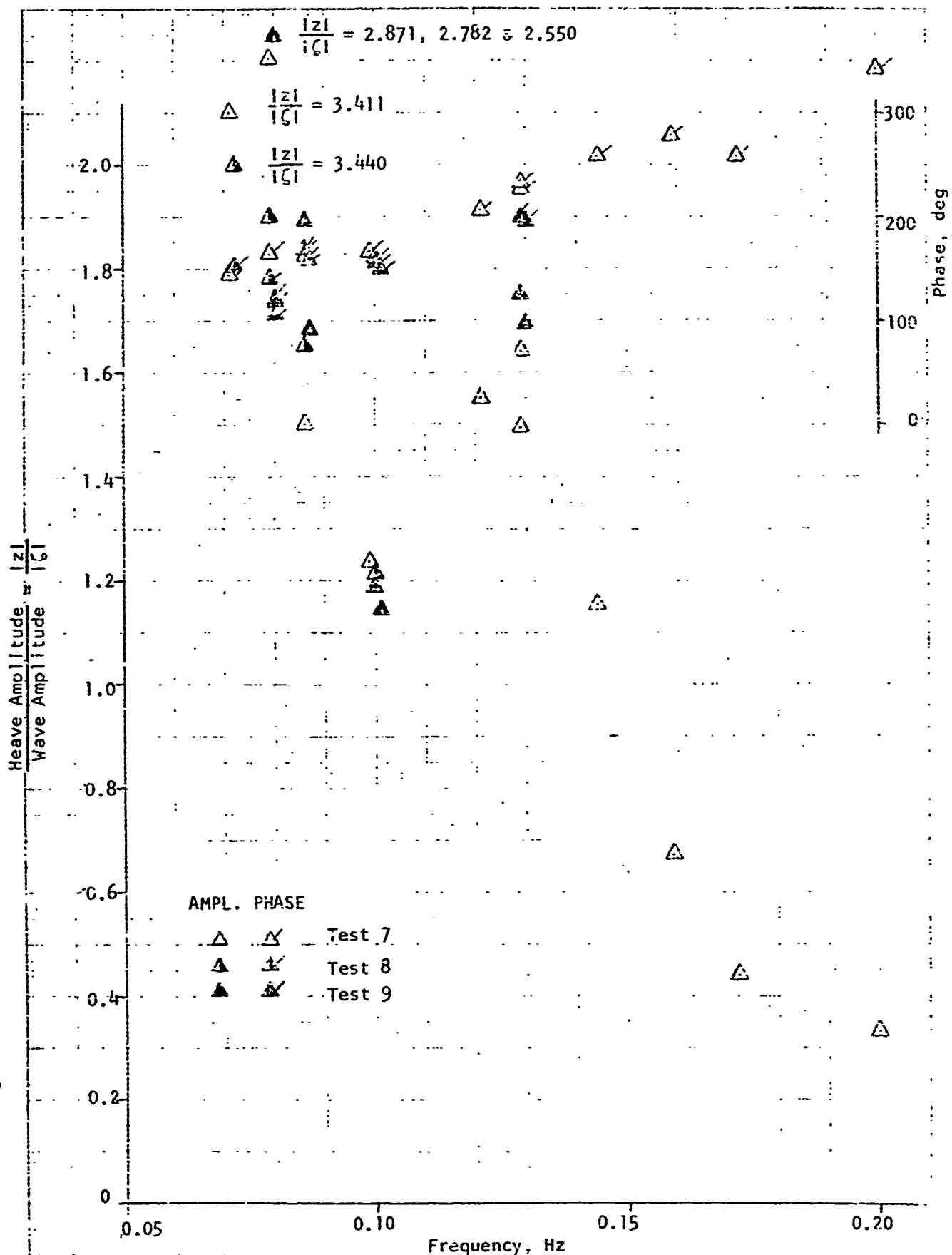


FIGURE 18a. WAVE TEST RESULTS FOR TESTS 7, 8, and 9, ROW 17

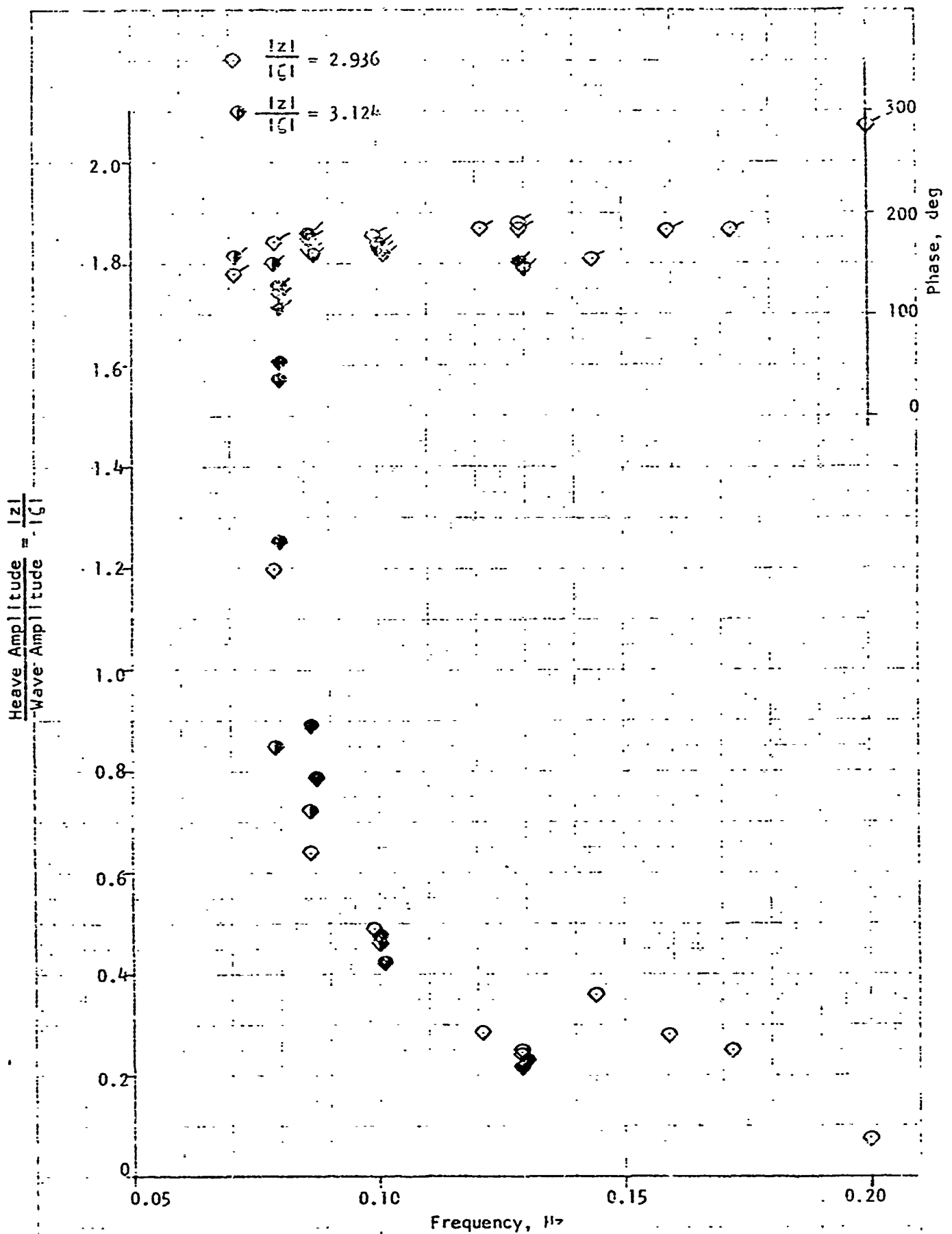


FIGURE 18b. WAVE TEST RESULTS FOR TESTS 7, 8, and 9, ROW 15

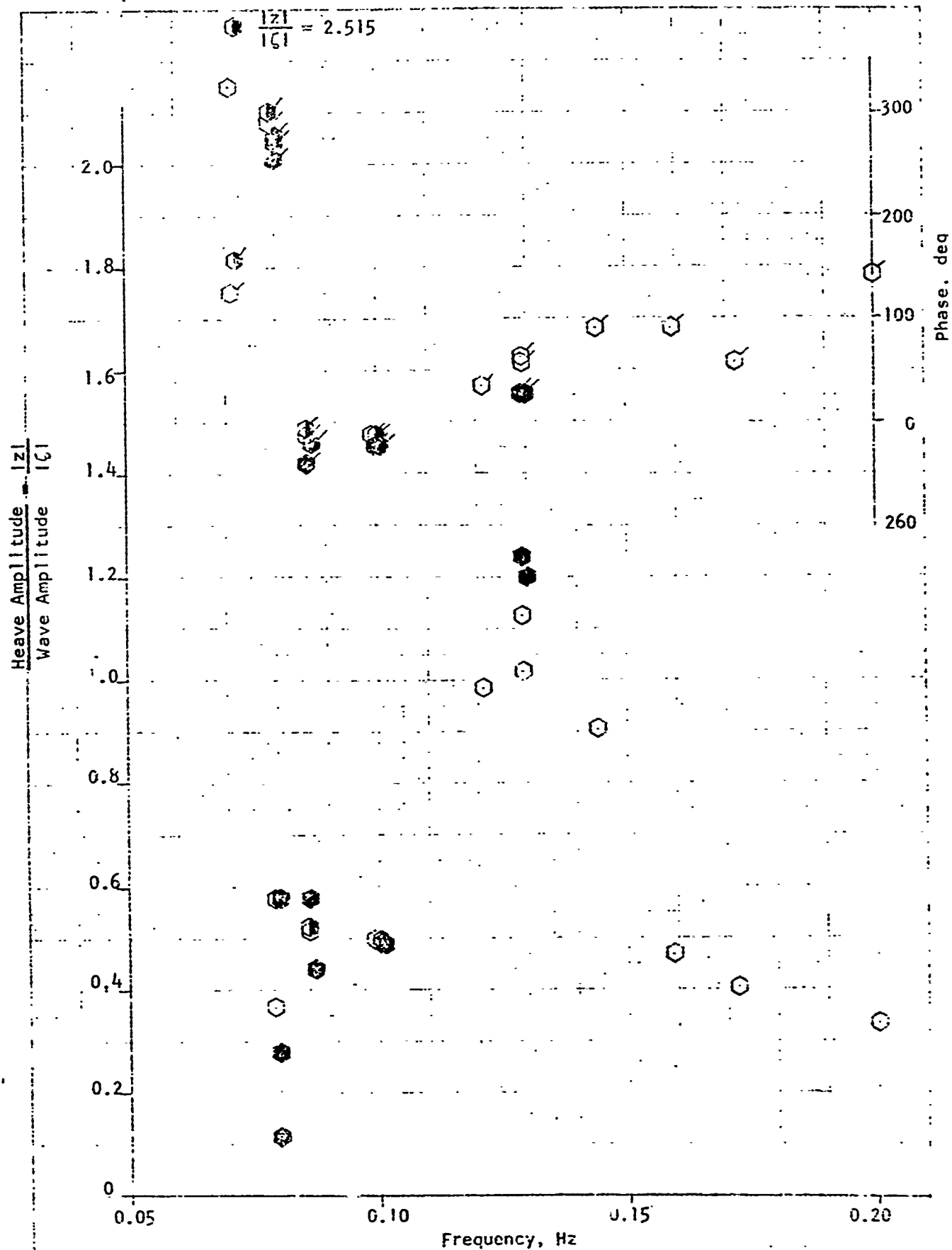


FIGURE 18c. WAVE TEST RESULTS FOR TESTS 7, 8 and 9, ROW 12.

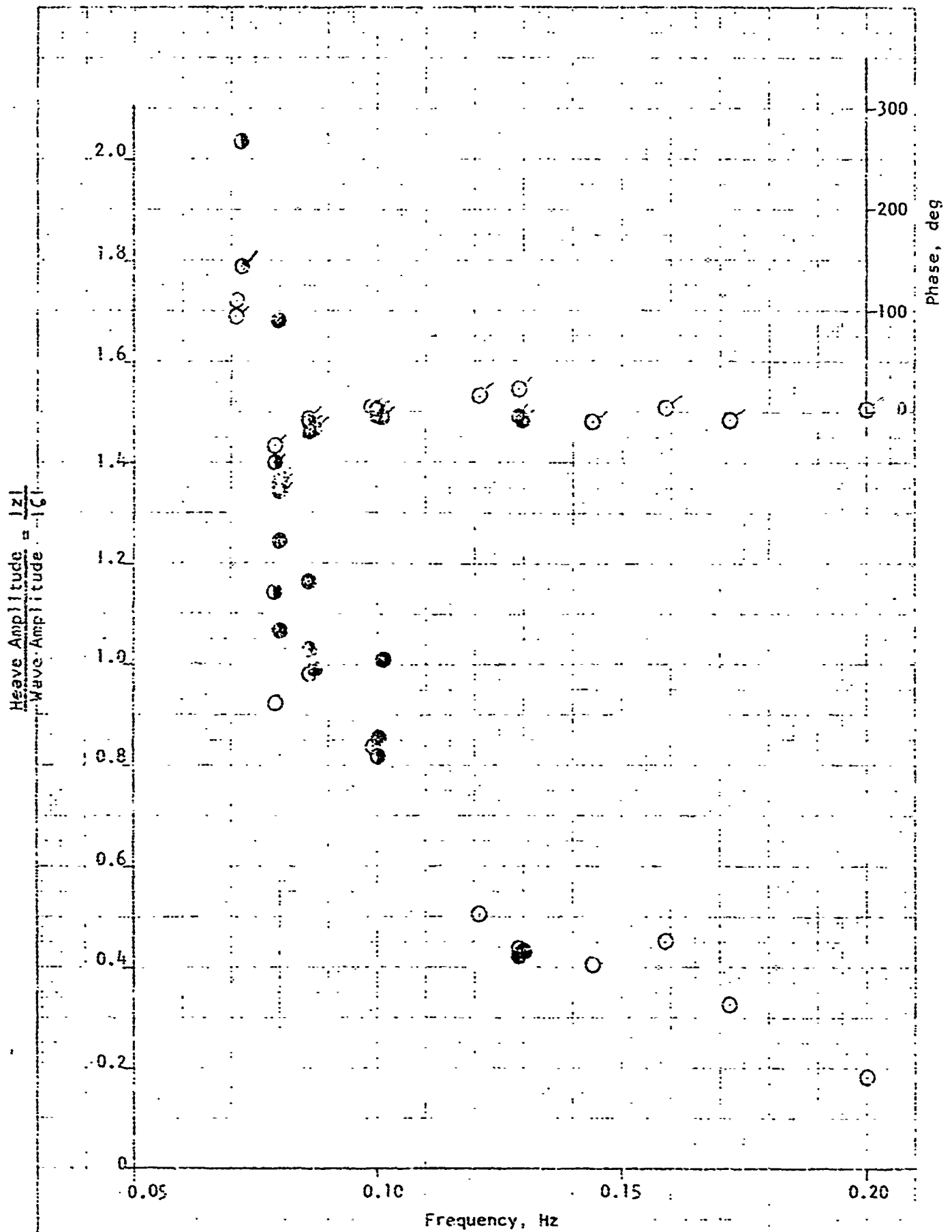


FIGURE 18d. WAVE TEST RESULTS FOR TESTS 7, 8 and 9, ROW 9

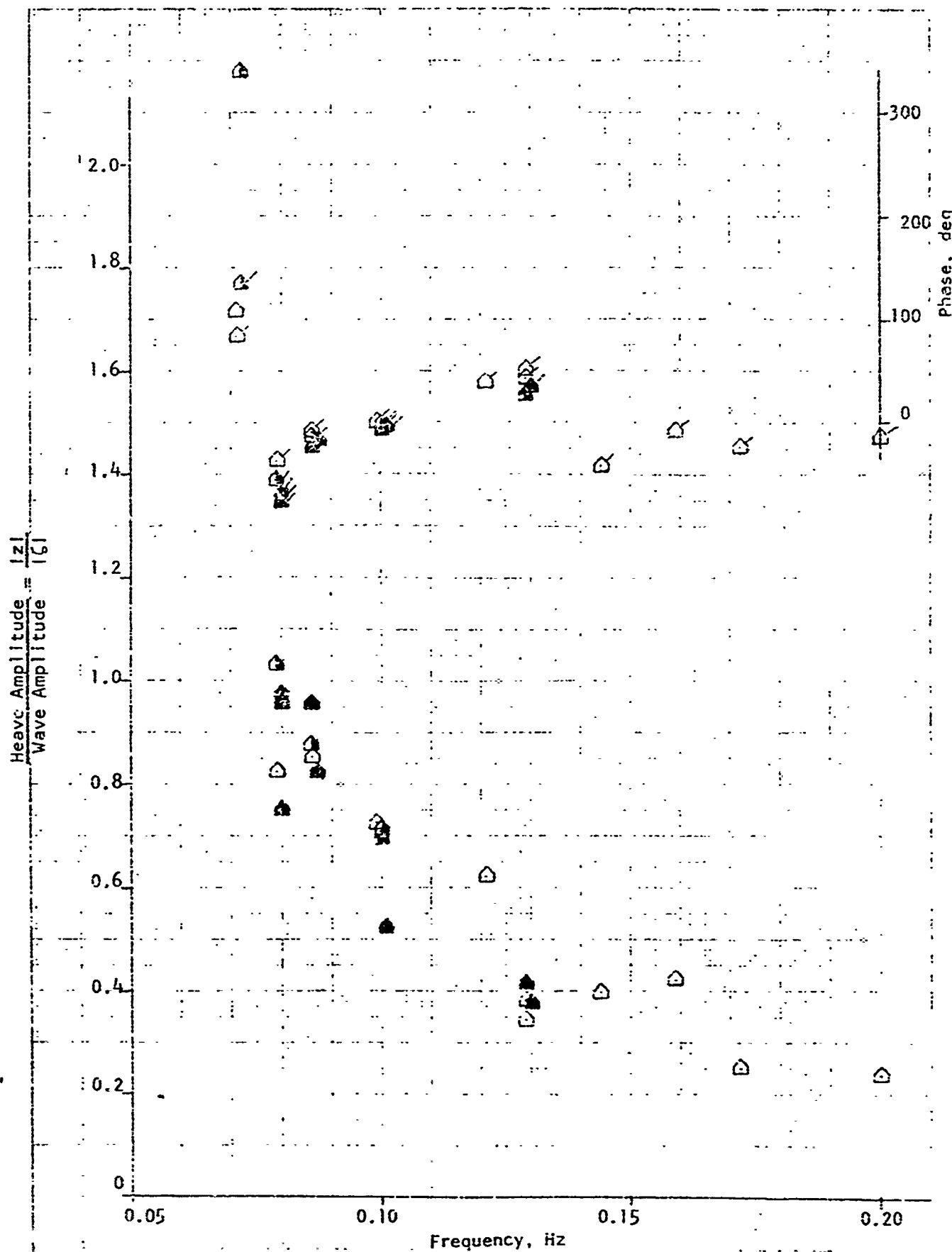
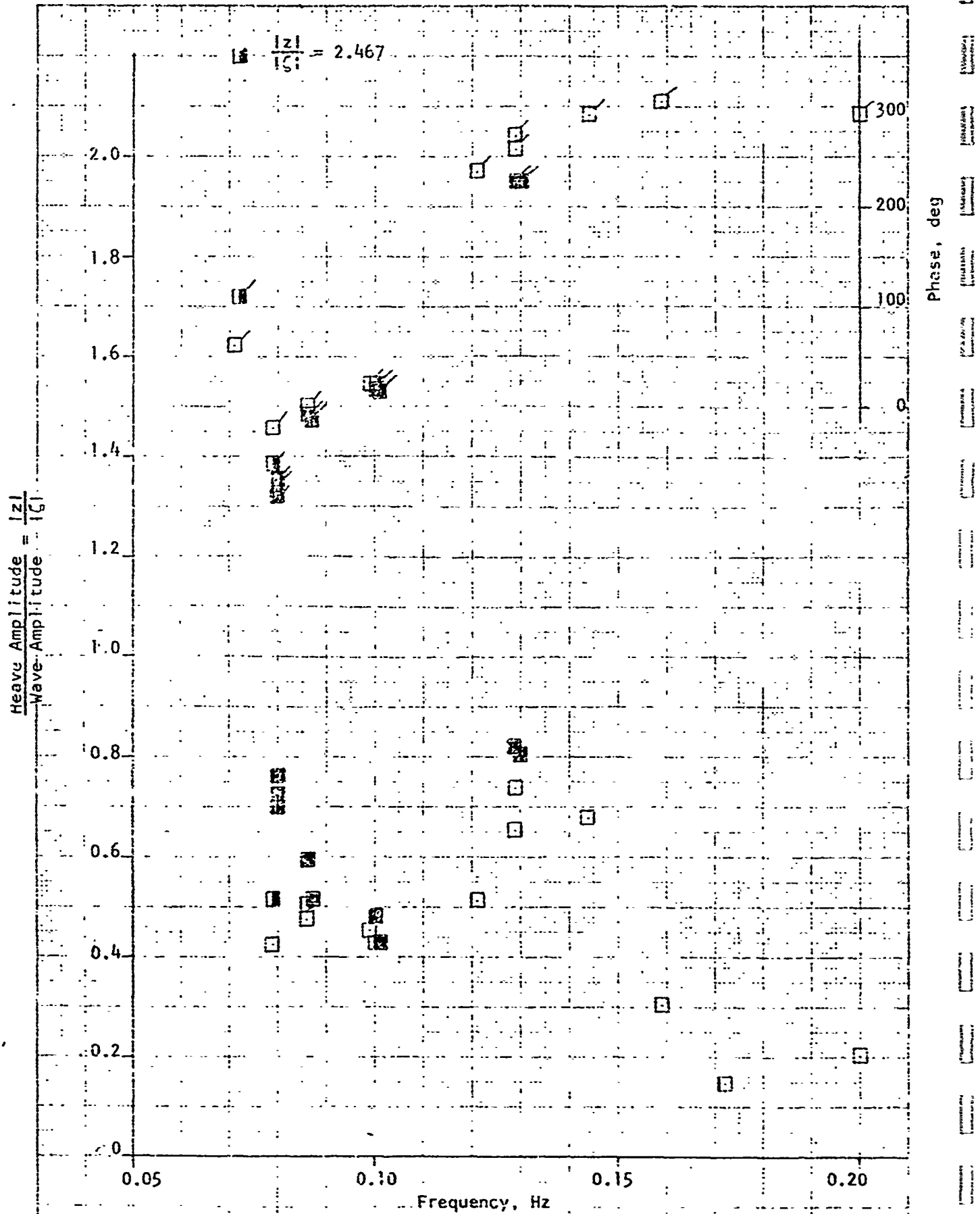


FIGURE 18e. WAVE TEST RESULTS FOR TESTS 7, 8 and 9, ROW 9P



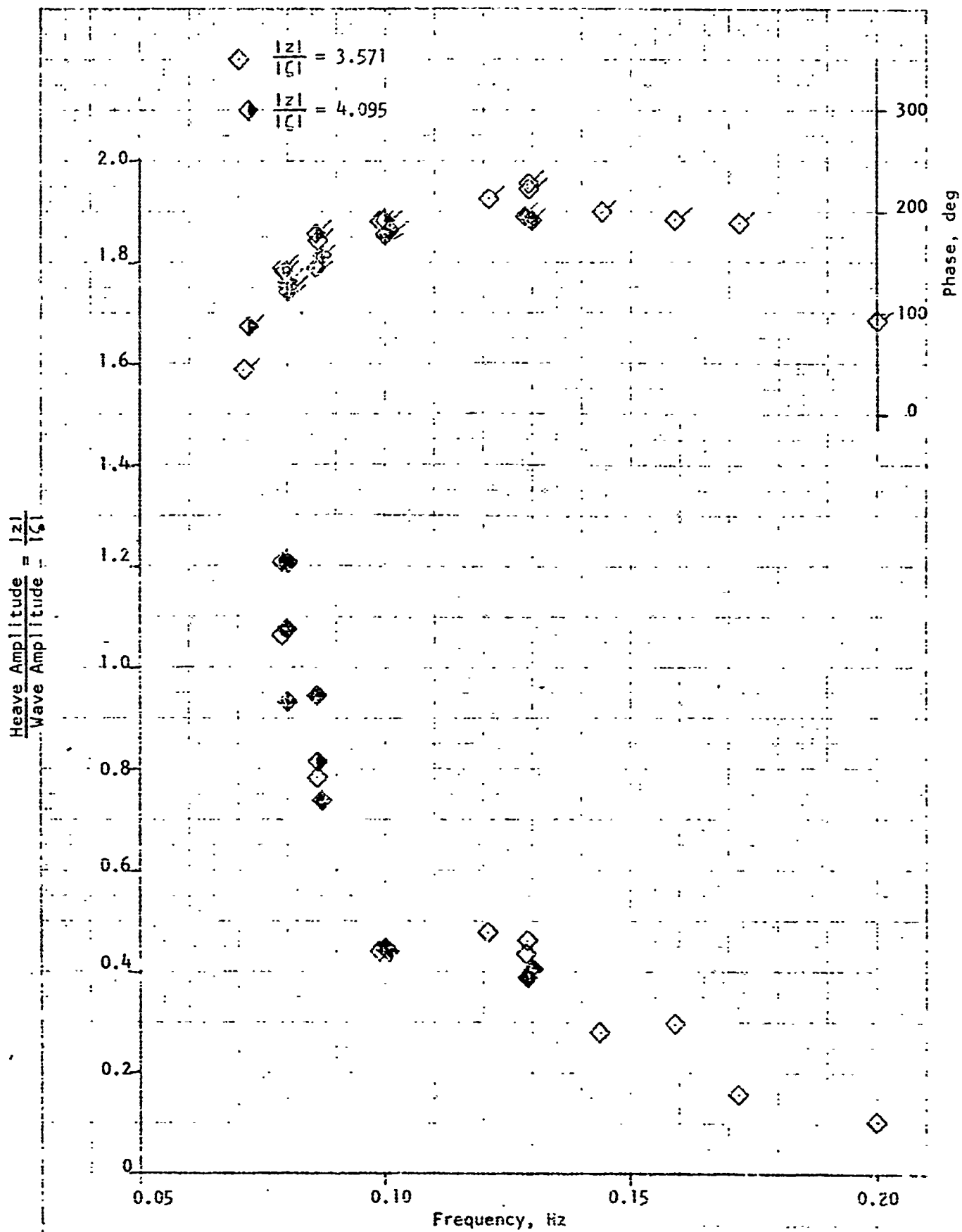


FIGURE 18g. WAVE-TEST RESULTS FOR TESTS 7, 8 and 9, ROW 3

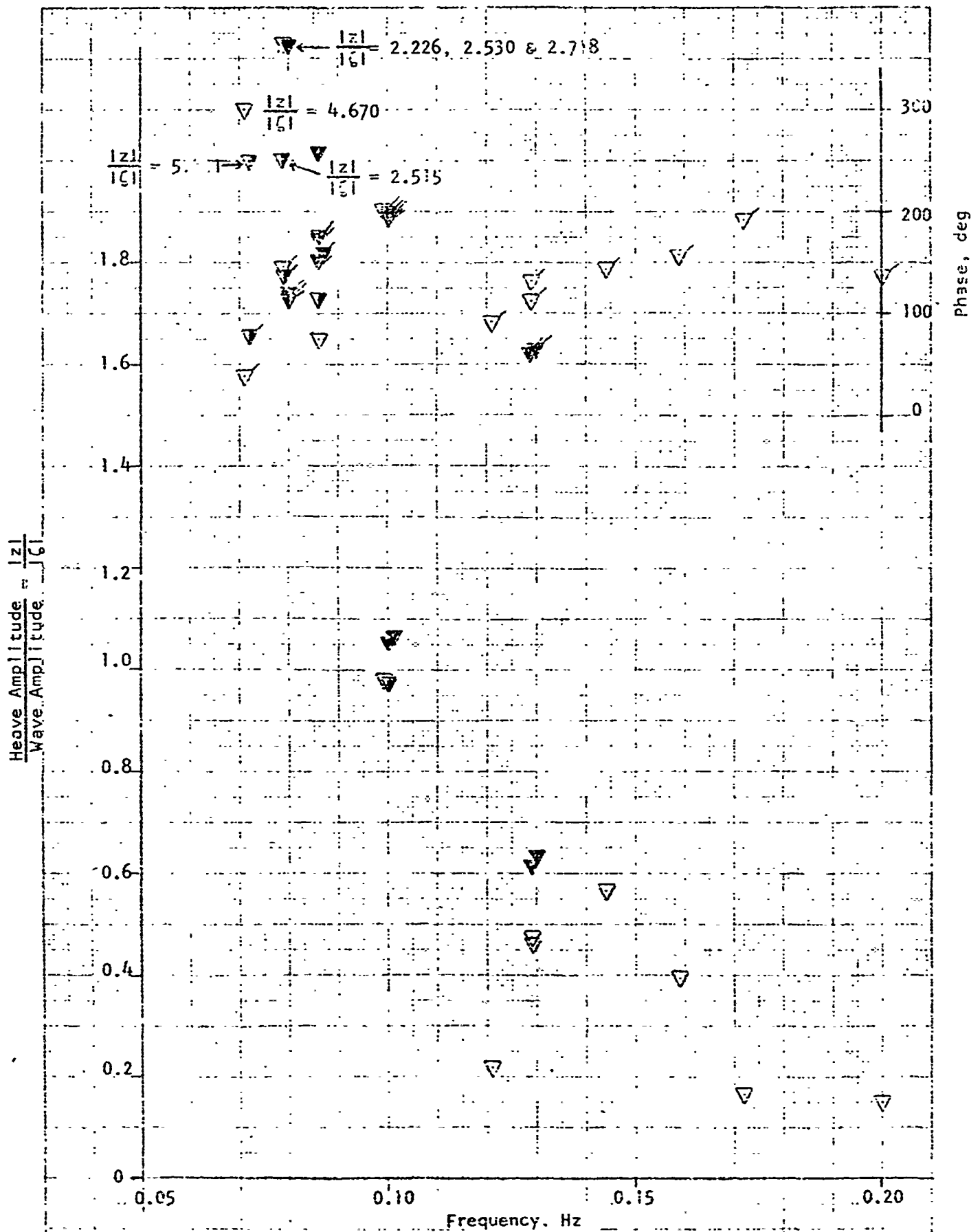


FIGURE 18n. WAVE TEST RESULTS FOR TESTS 7, 8 and 9, ROW 1

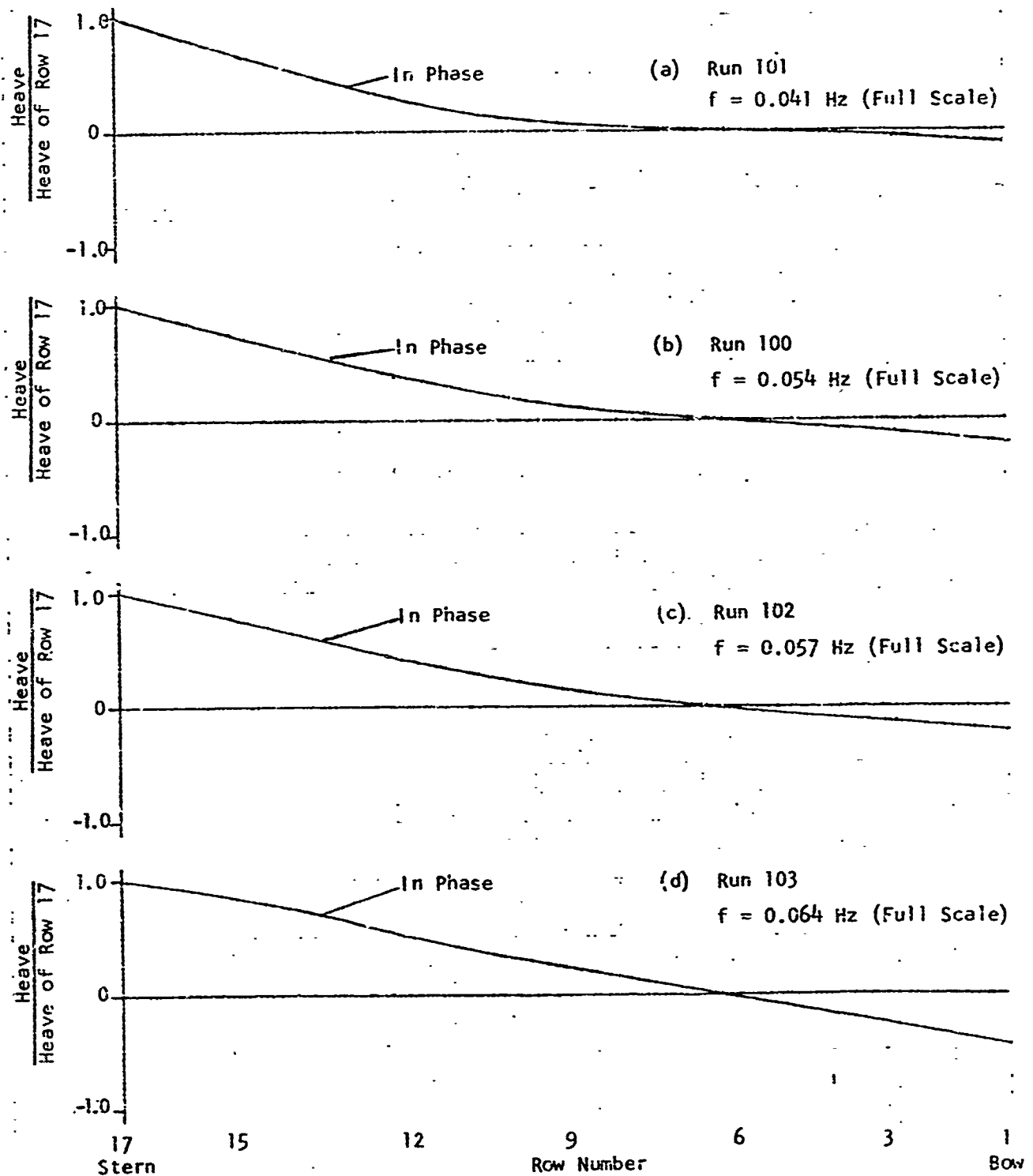


FIGURE 19(a-d). RESULTS OF FORCED HEAVE OSCILLATION OF ROW 17, TESTS 10, NARROW DECK ELASTIC ELEMENTS, FULL ATTENUATORS

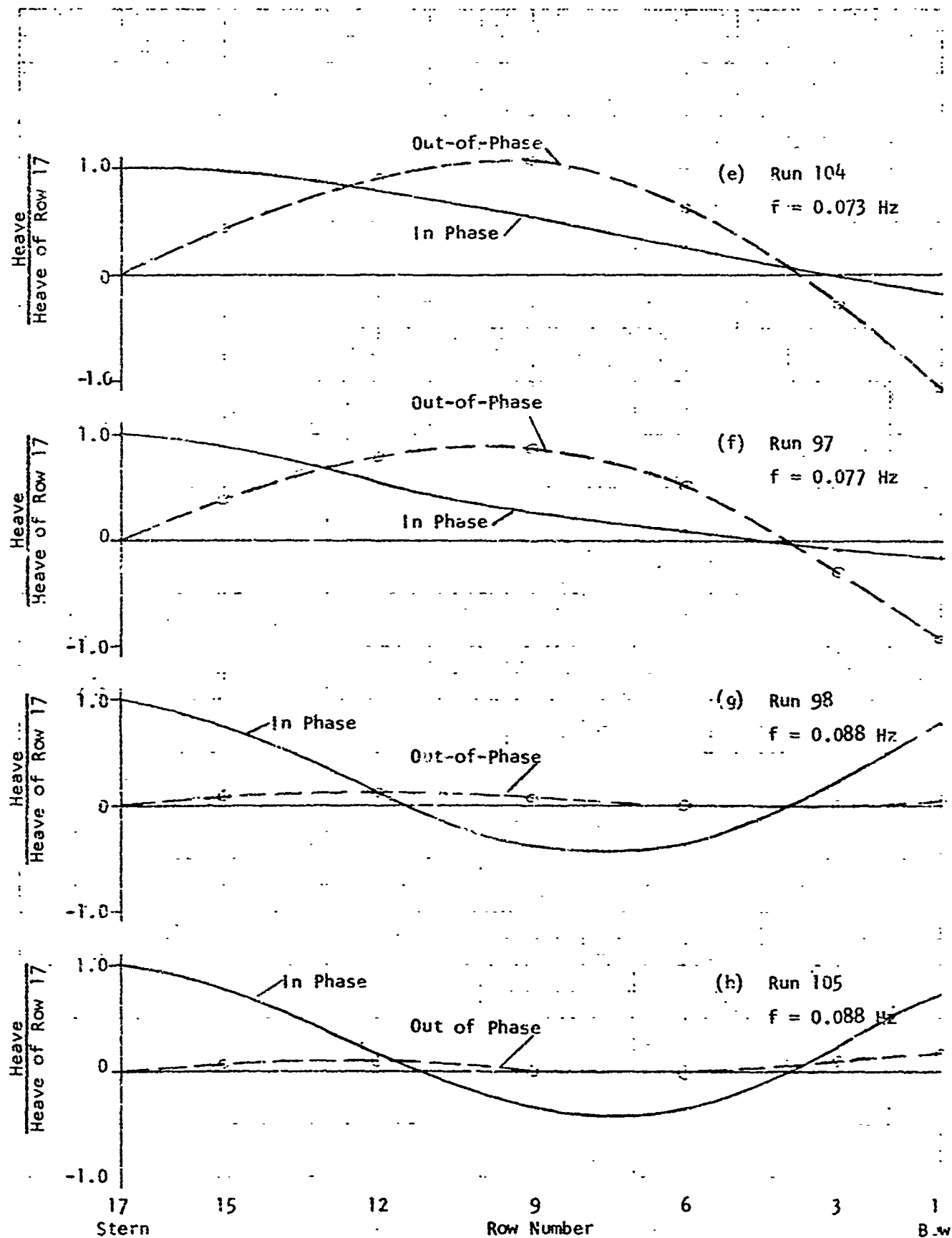


FIGURE 19(e-h). RESULTS OF FORCED HEAVE OSCILLATION OF ROW 17, TESTS 10, NARROW DECK ELASTIC ELEMENTS, FULL ATTENUATORS

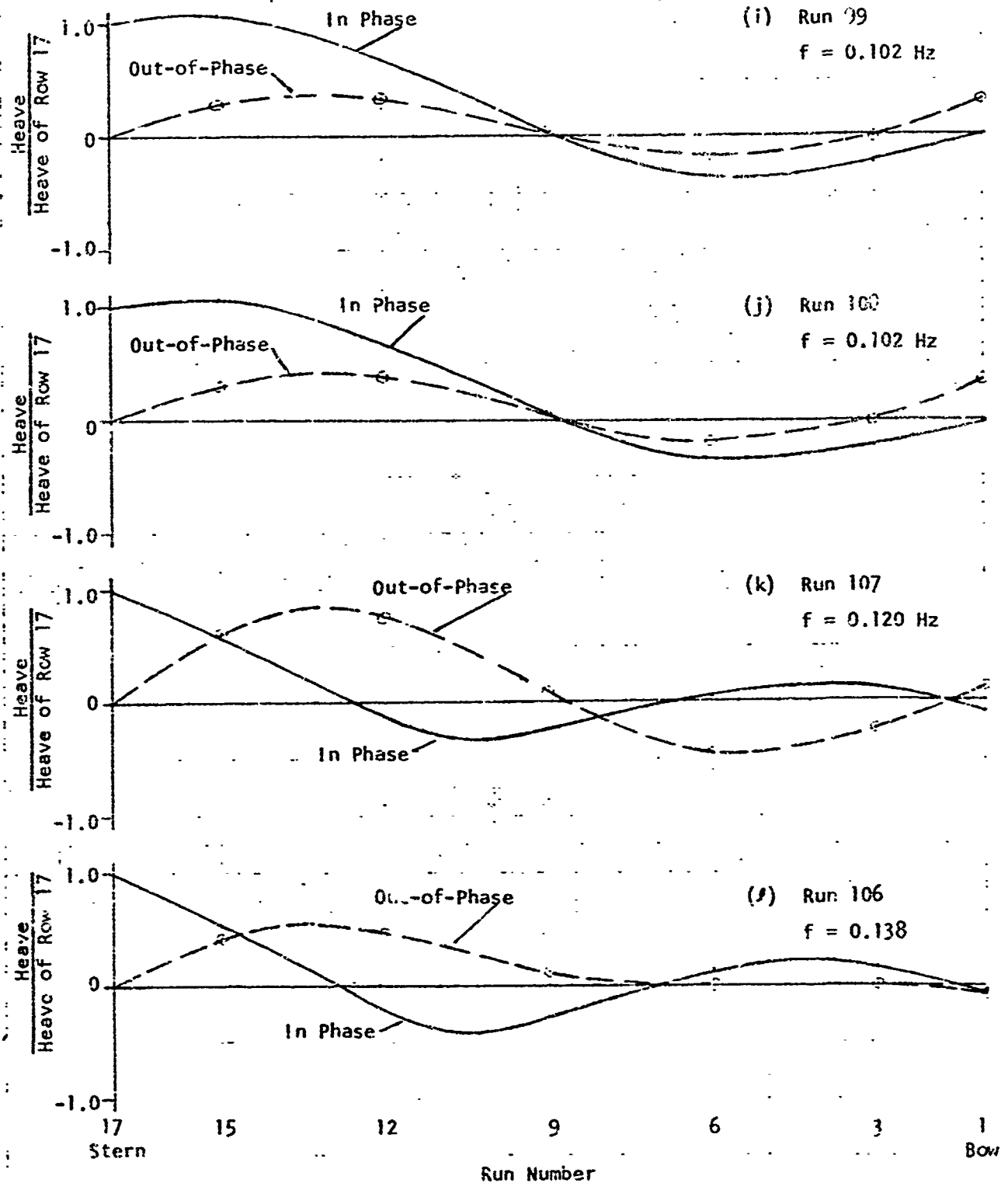


FIGURE 19(i-l). RESULTS OF FORCED HEAVE OSCILLATION OF ROW 17, TESTS 10, NARROW DECK ELASTIC ELEMENTS, FULL ATTENUATORS

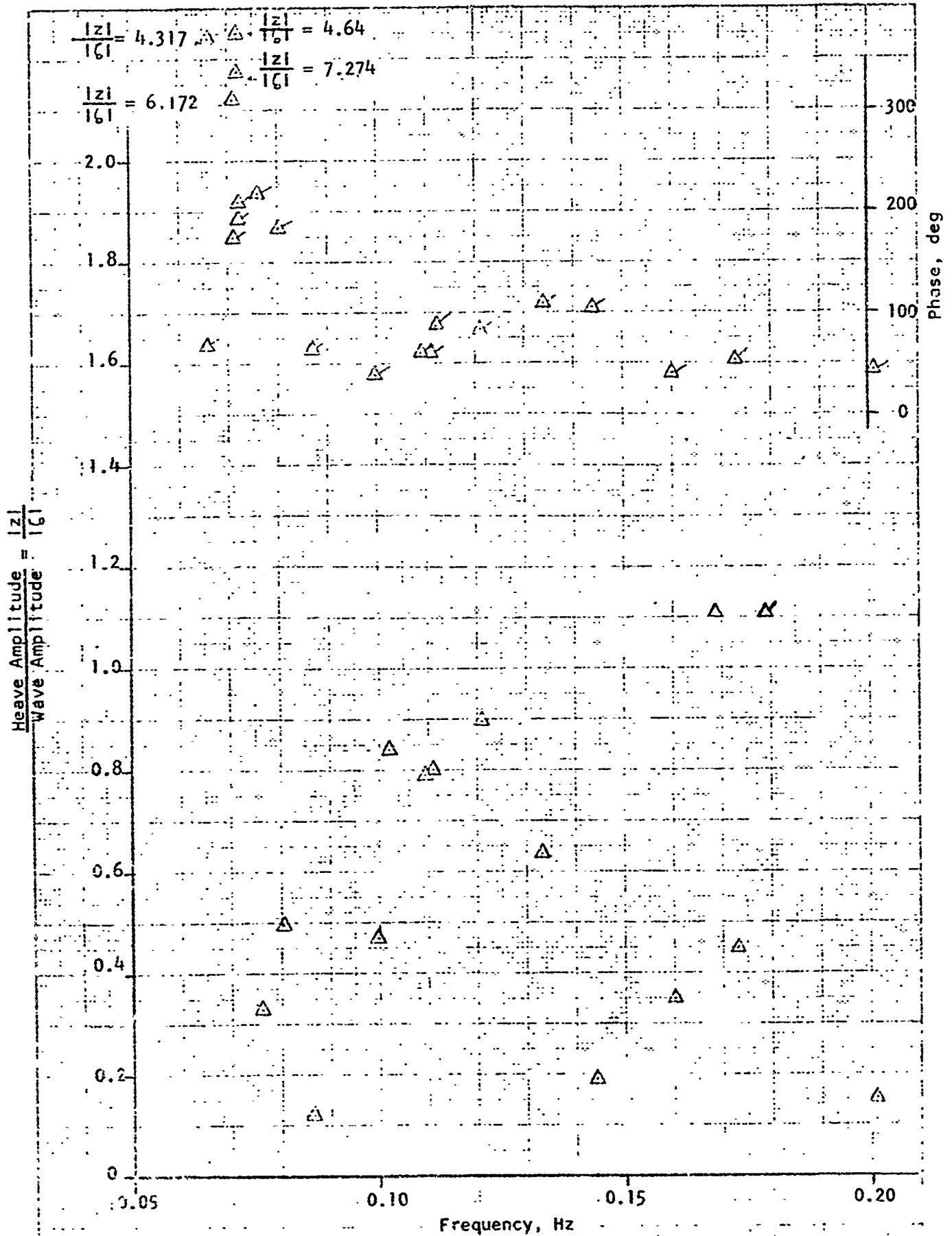


FIGURE 20a. WAVE TEST RESULTS FOR TESTS 11, ROW 17

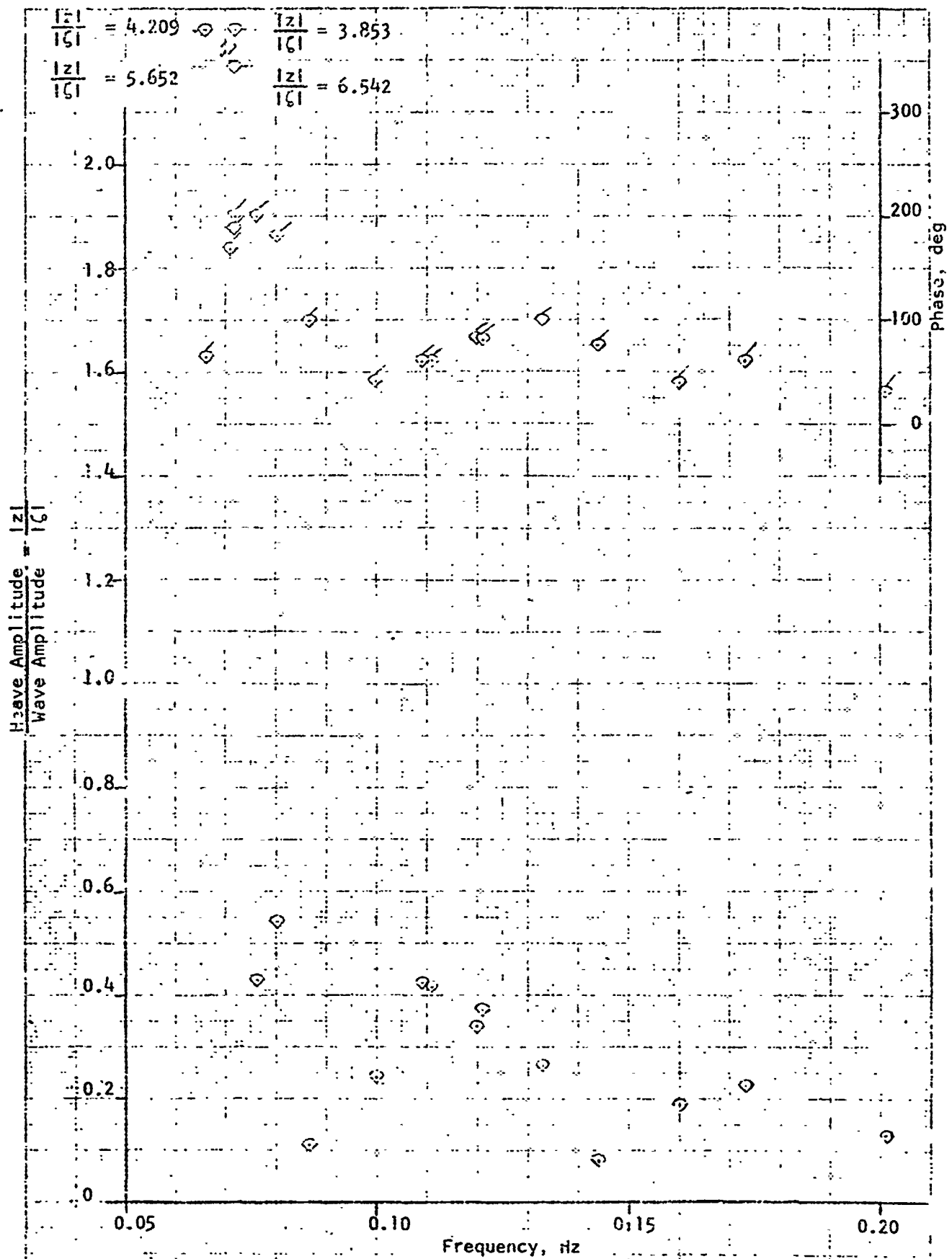


FIGURE 20b. WAVE TEST RESULTS FOR TESTS 11, ROW 15

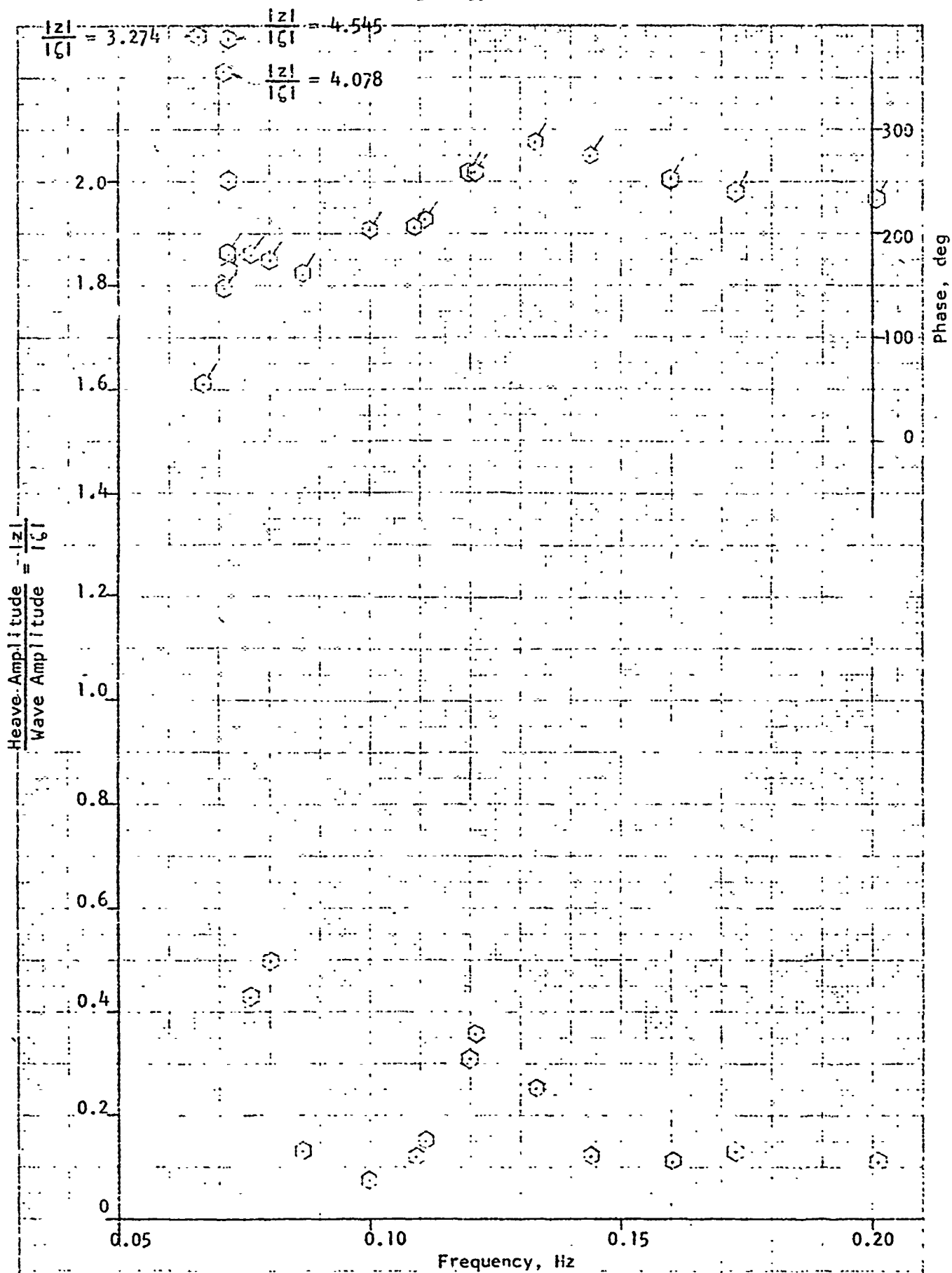


FIGURE 20c. WAVE TEST RESULTS FOR TESTS 11, ROW 12

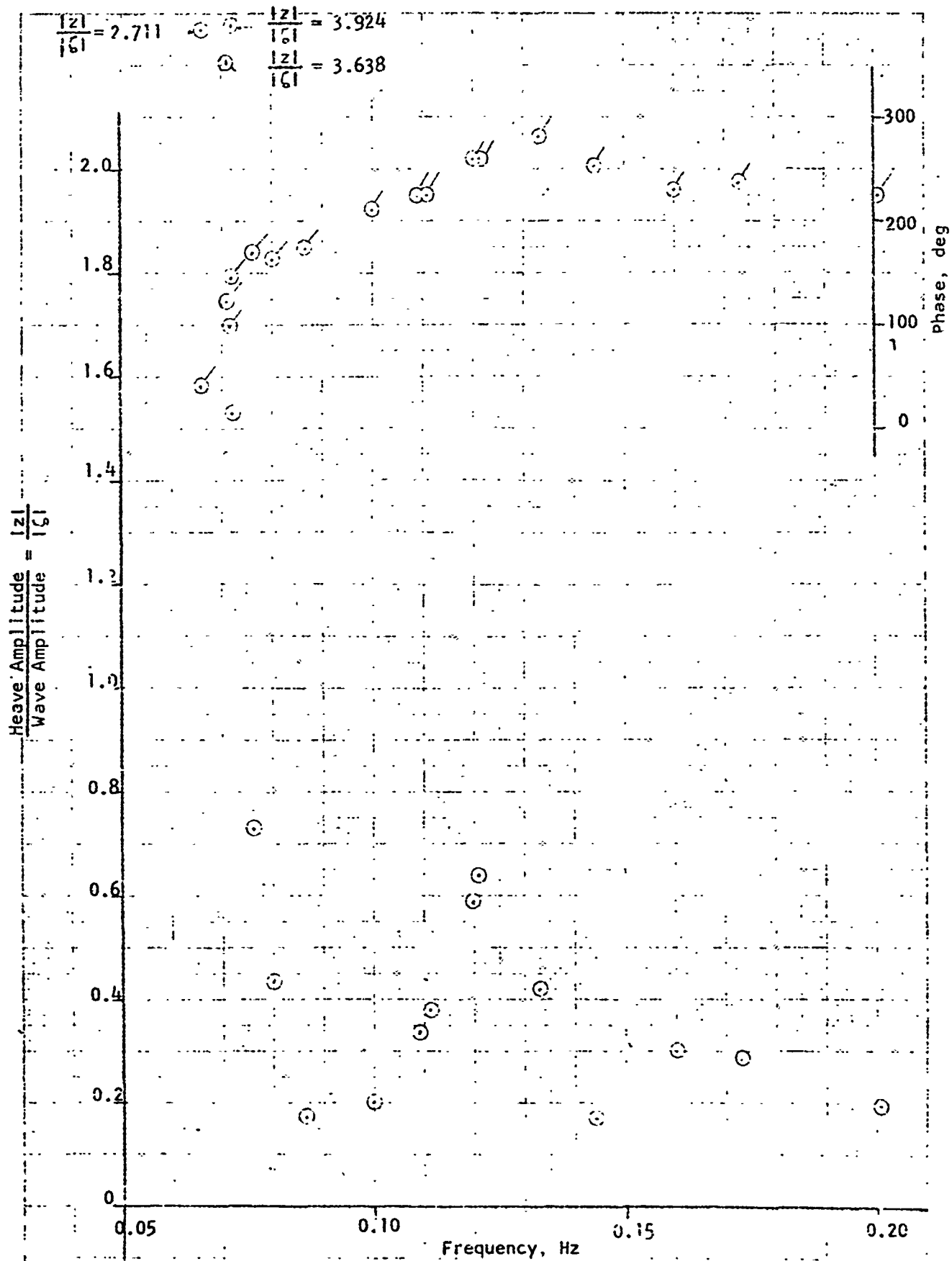


FIGURE 20d. WAVE TEST RESULTS FOR TESTS 11, ROW 9

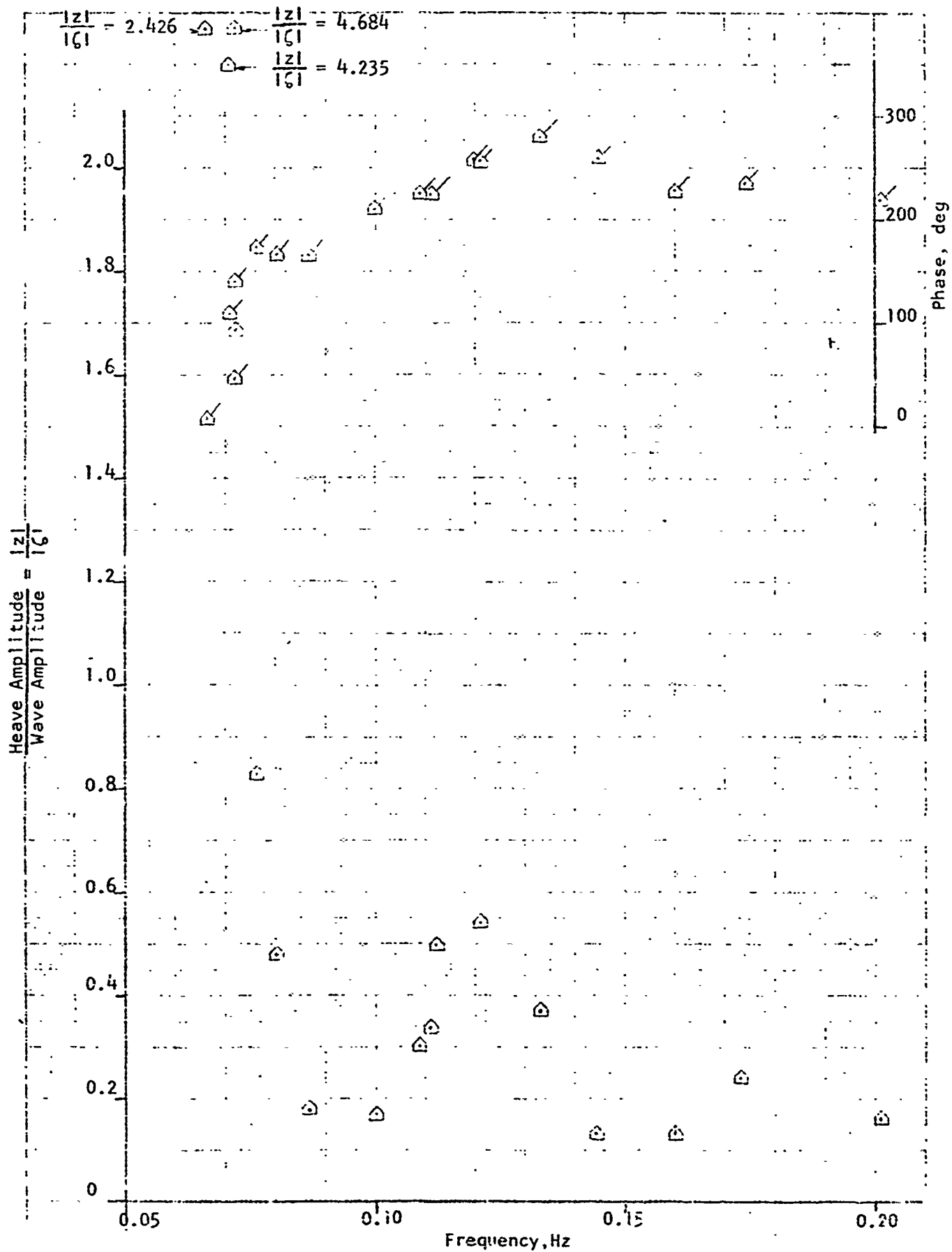


FIGURE 20e. WAVE TEST RESULTS FOR TESTS 11, ROW 9P

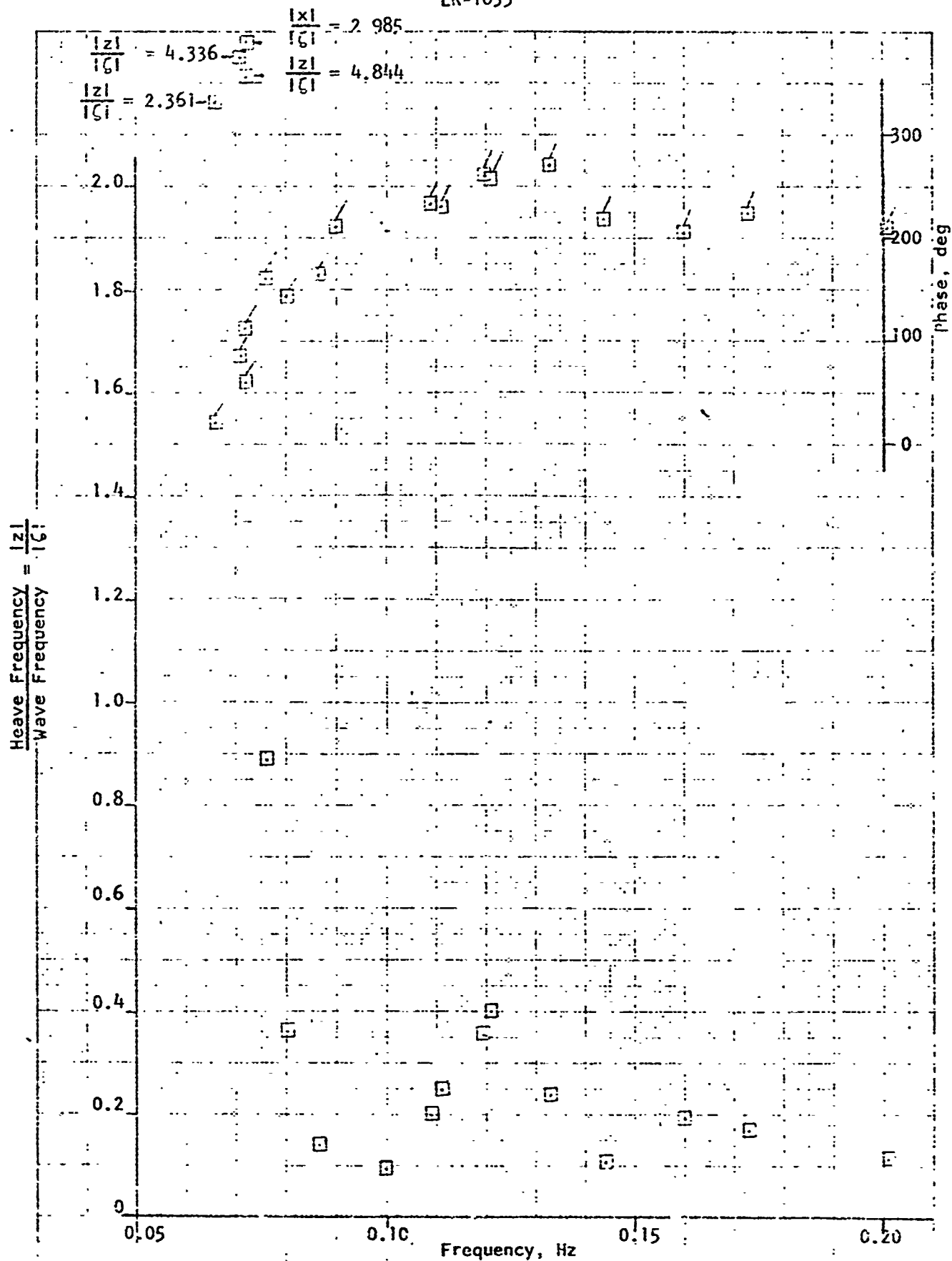


FIGURE 200. WAVE TEST RESULTS FOR TESTS 11, ROW 6

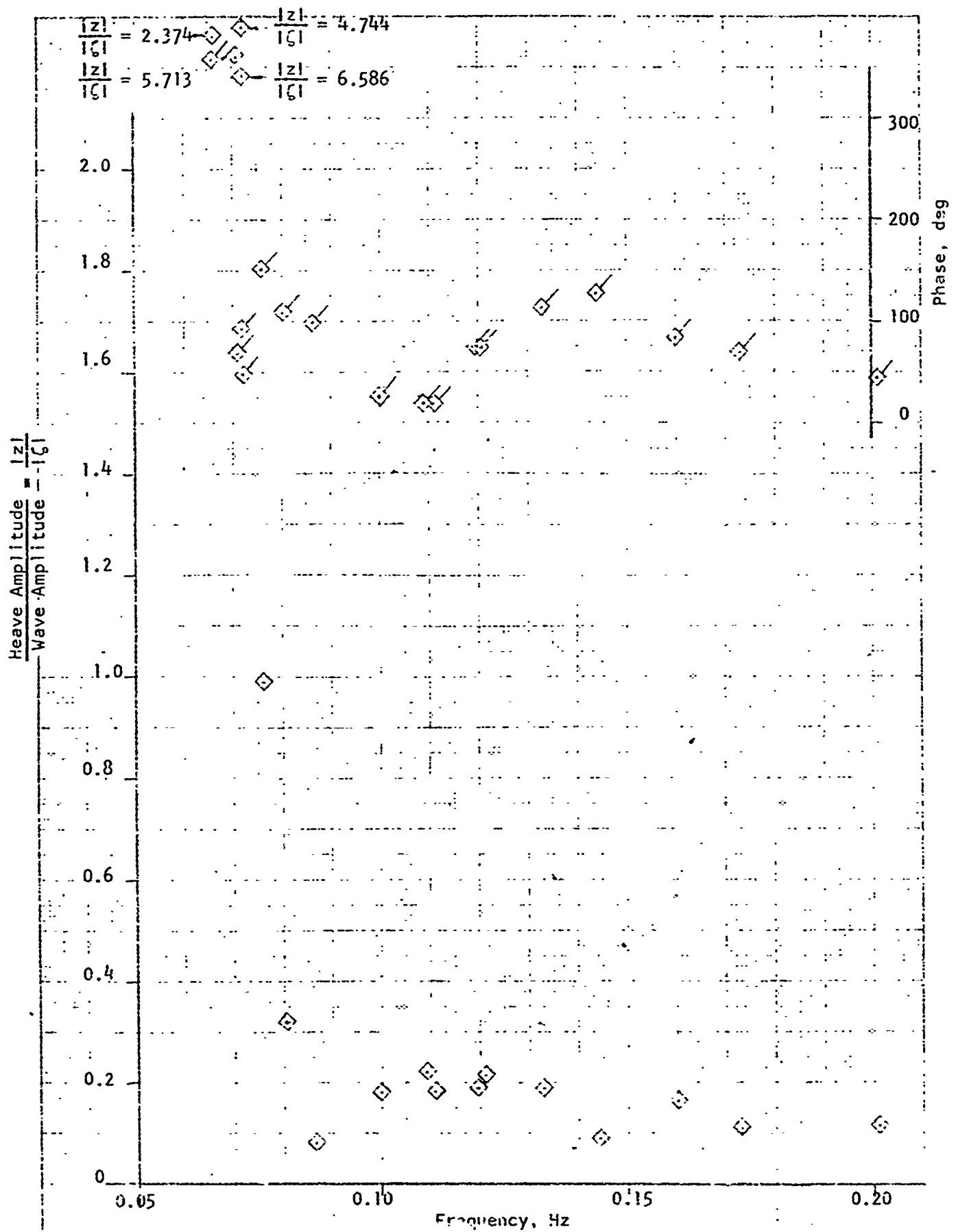


FIGURE 10. WAVE TEST RESULTS FOR TESTS 11, ROW 3

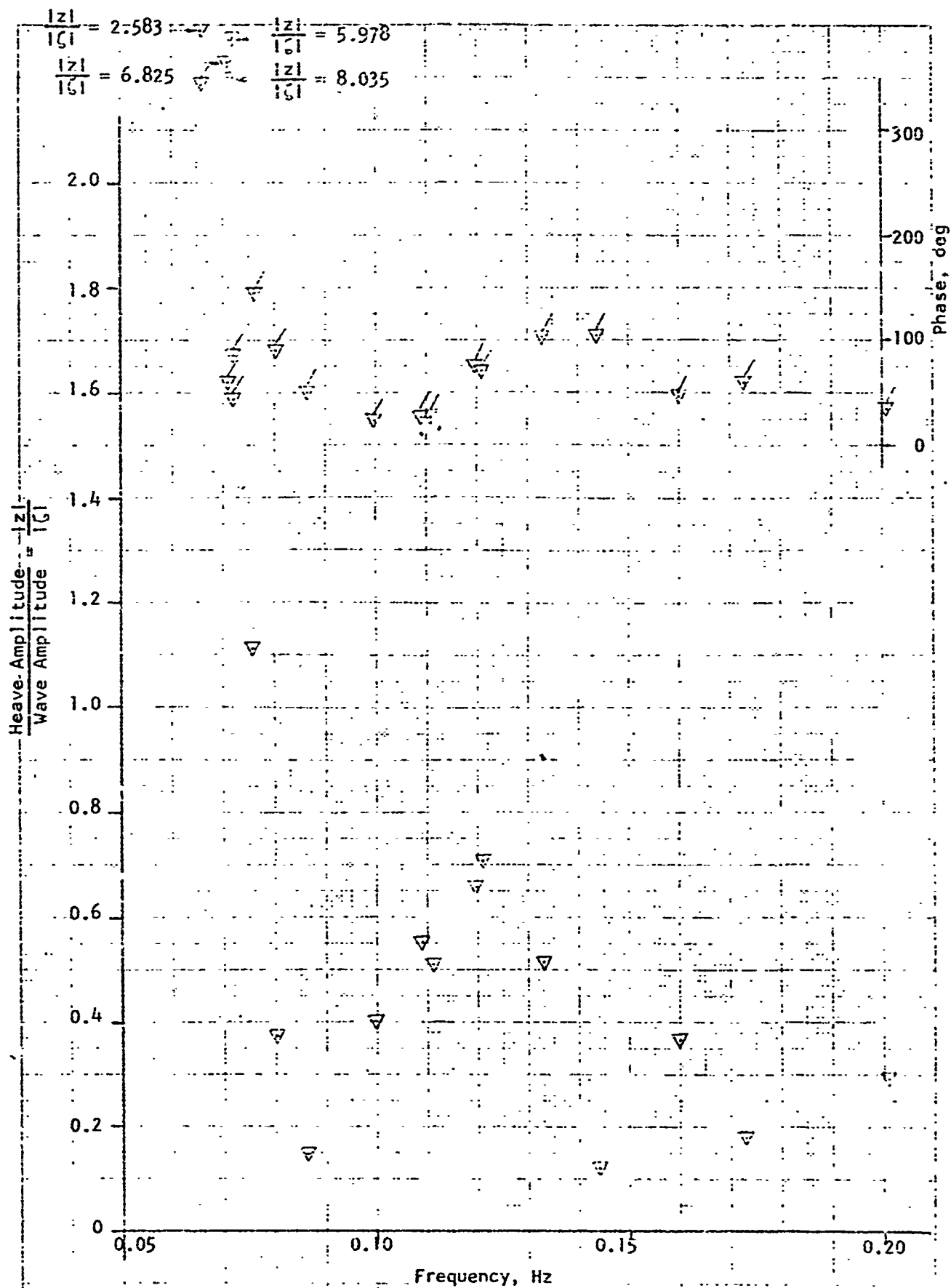


FIGURE 20h. WAVE TEST RESULTS FOR TESTS 11, ROW 1

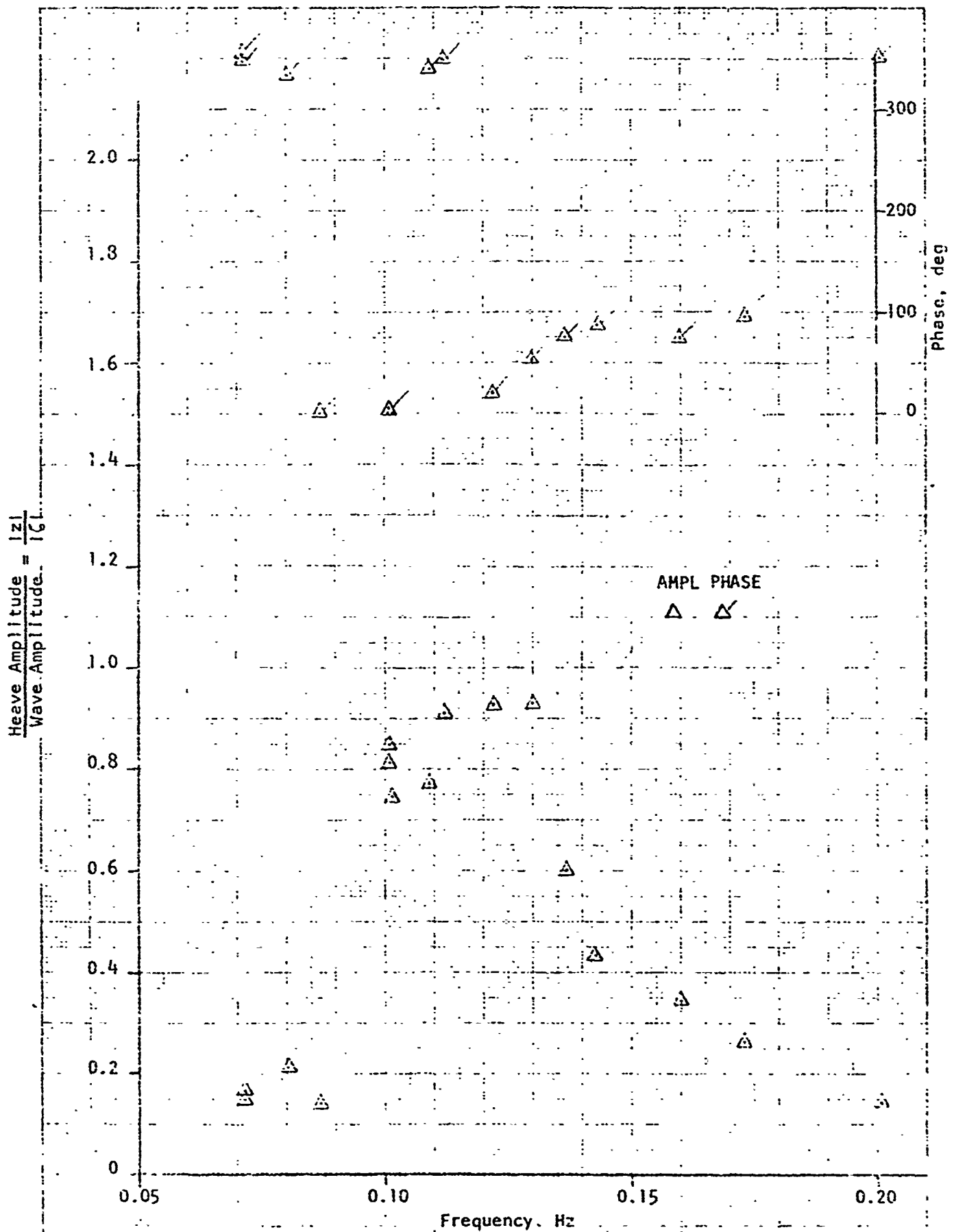


FIGURE 21a. WAVE TEST RESULTS FOR TESTS 12, ROW 17

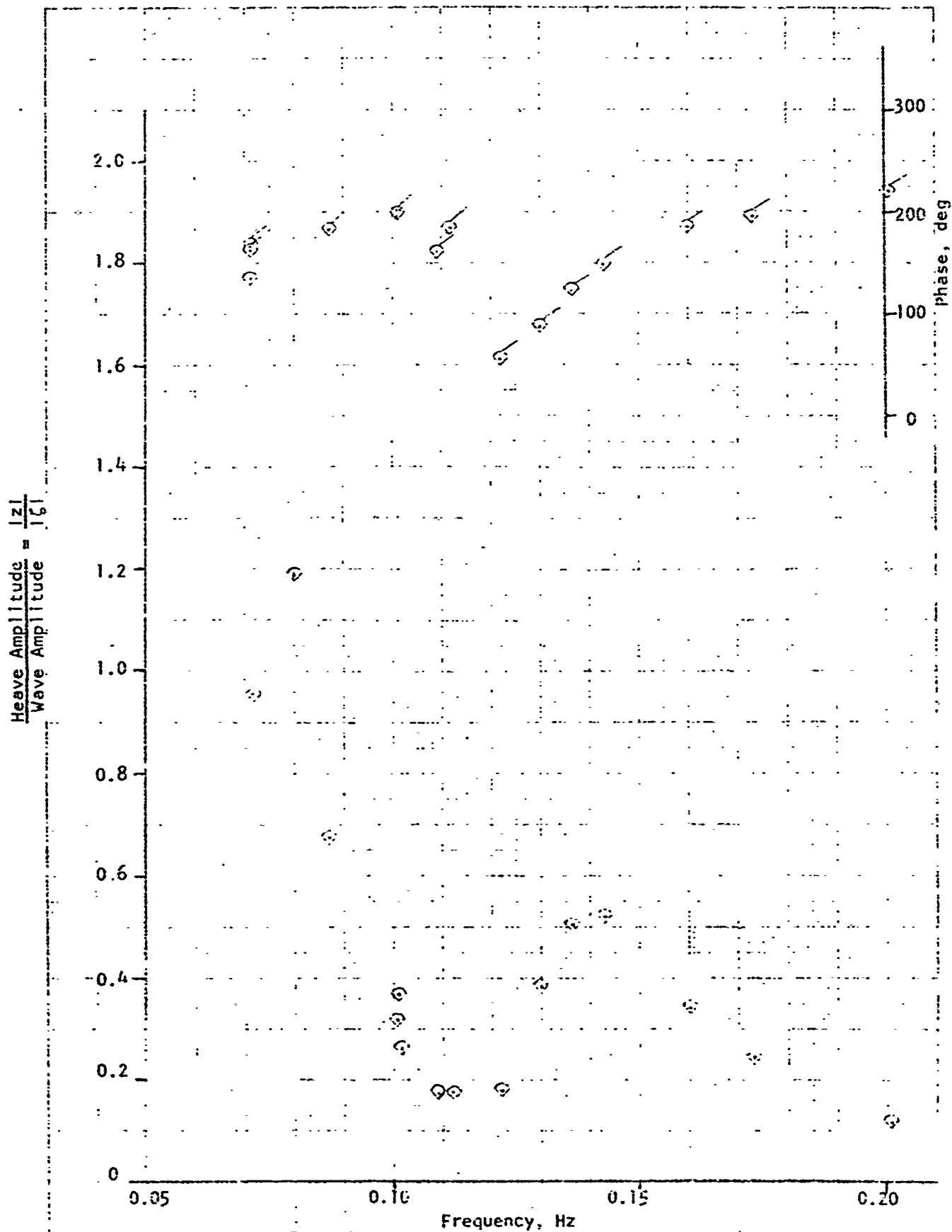


FIGURE 21b. WAVE TEST RESULTS FOR TESTS 12, ROW 15

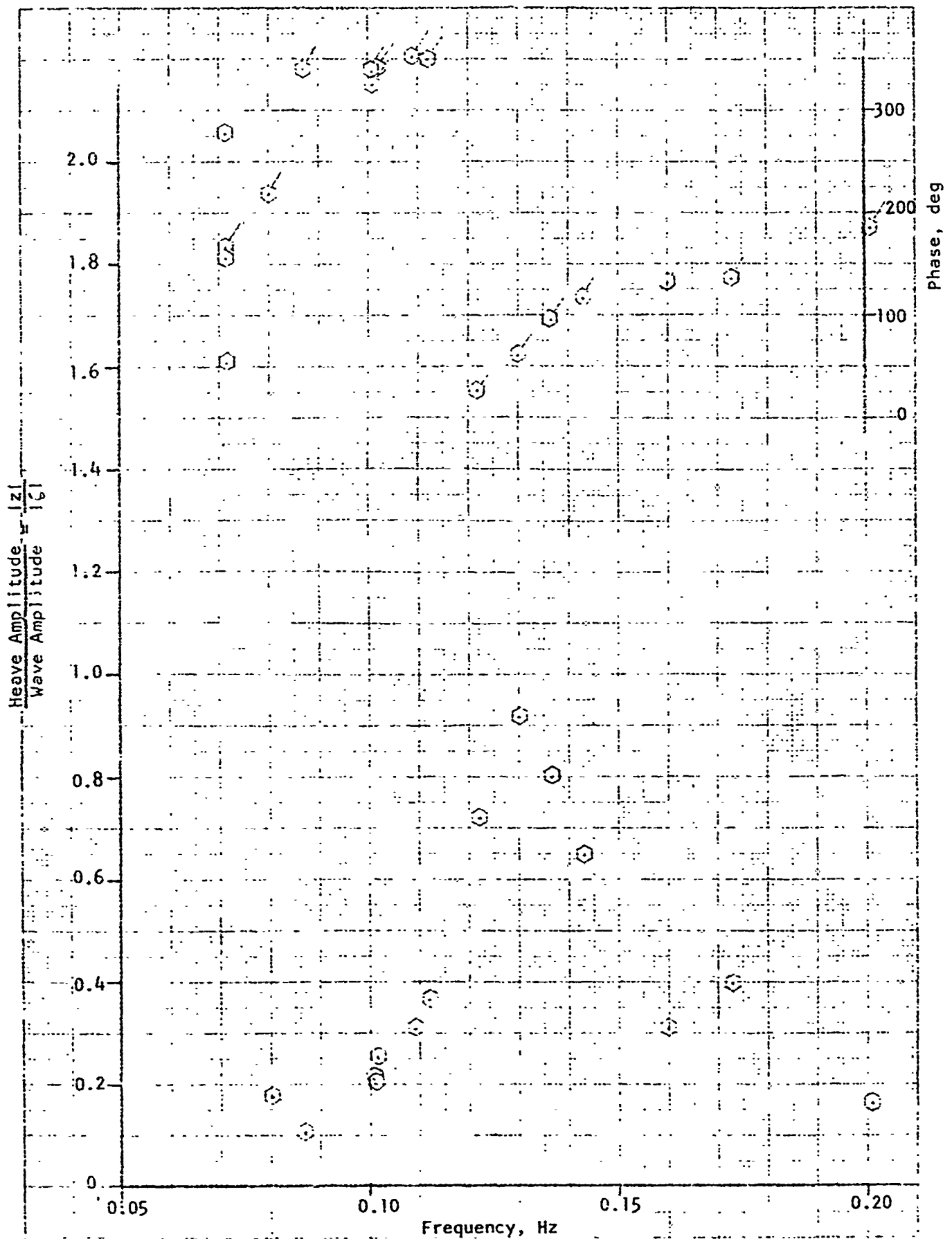


FIGURE 21c. WAVE TEST RESULTS FOR TESTS 12, ROW 12

LR-1635

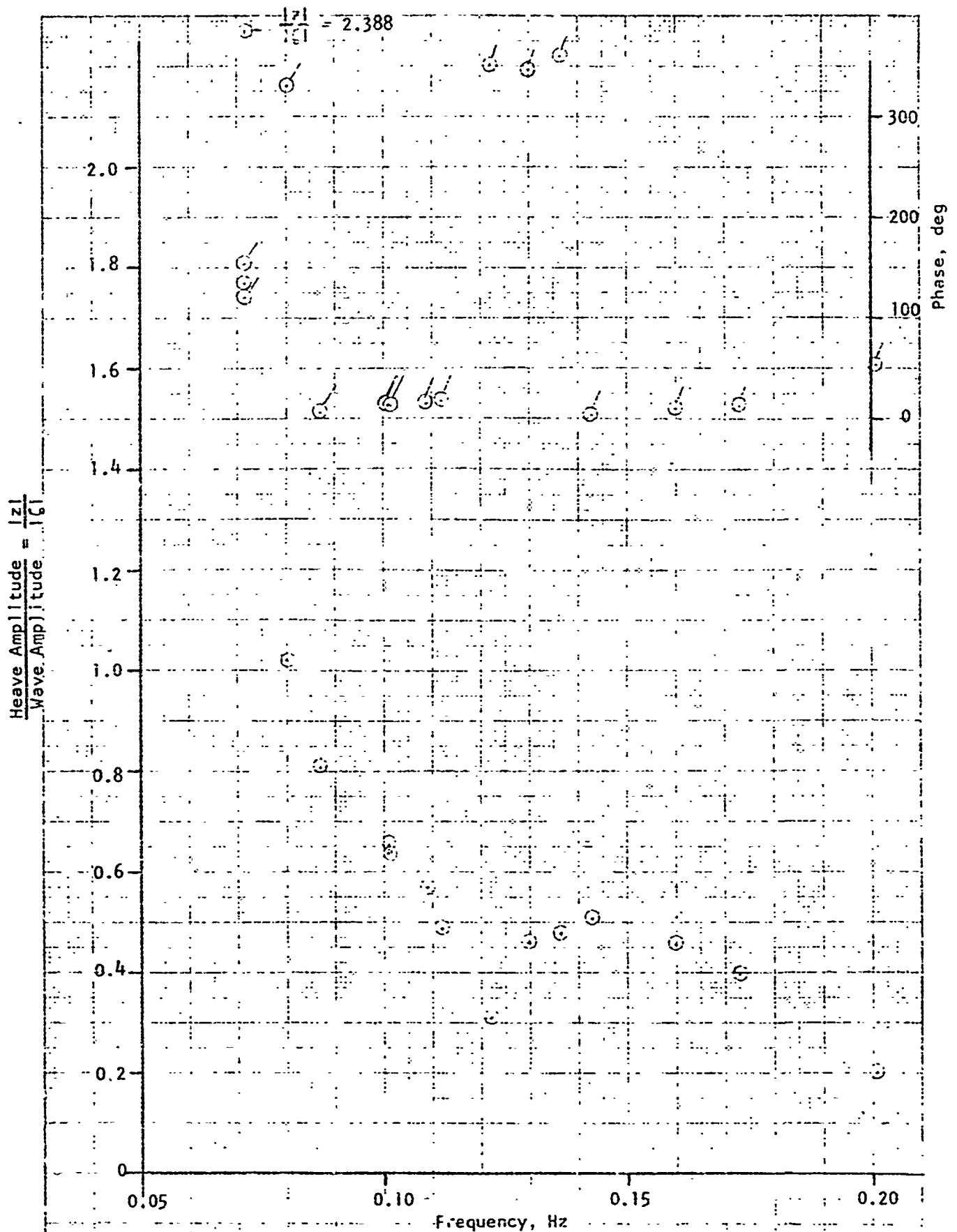


FIGURE 21d. WAVE TEST RESULTS FOR TESTS 12, ROW 9

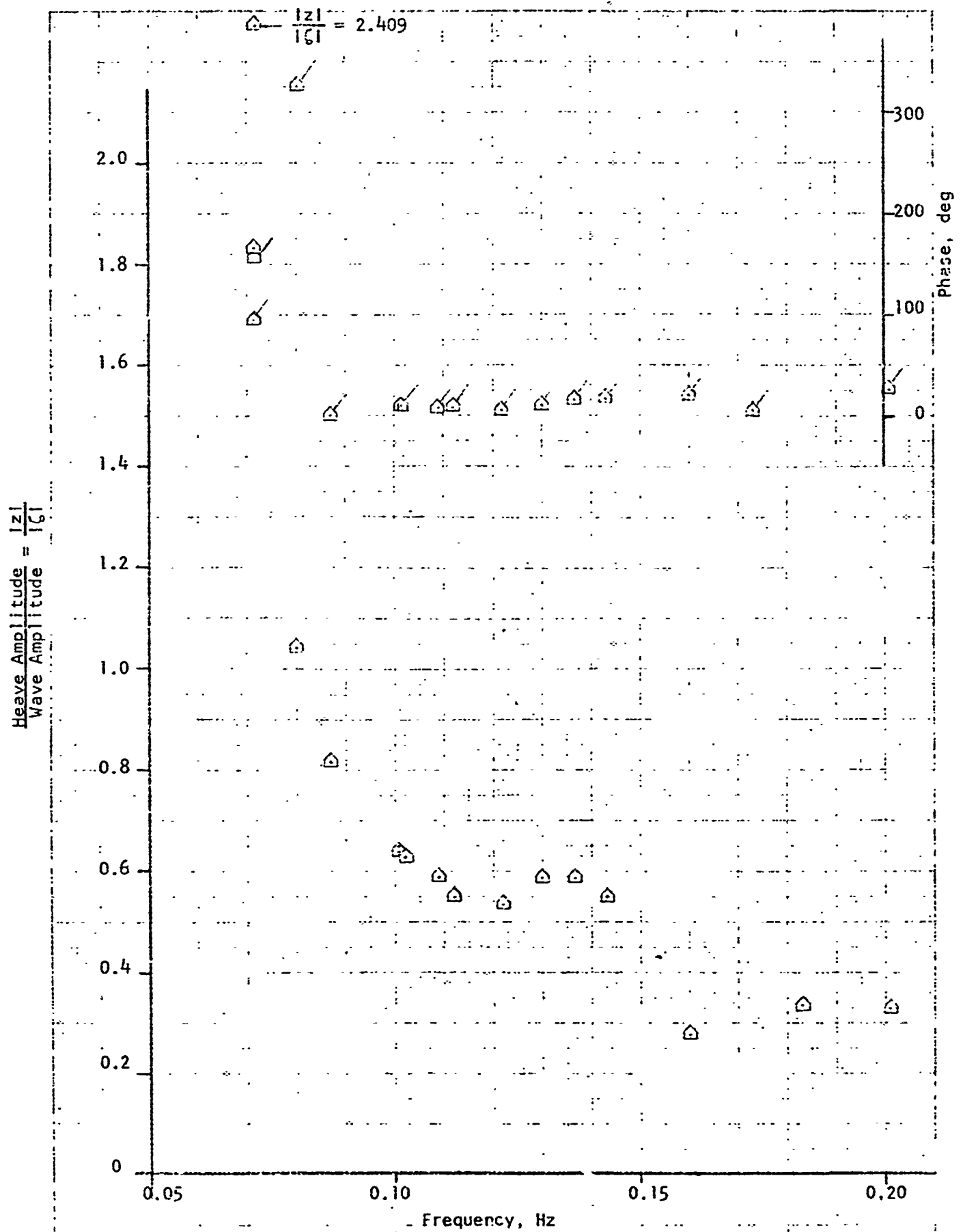


FIGURE 21e. WAVE TEST RESULTS FOR TESTS 12, ROW 9P

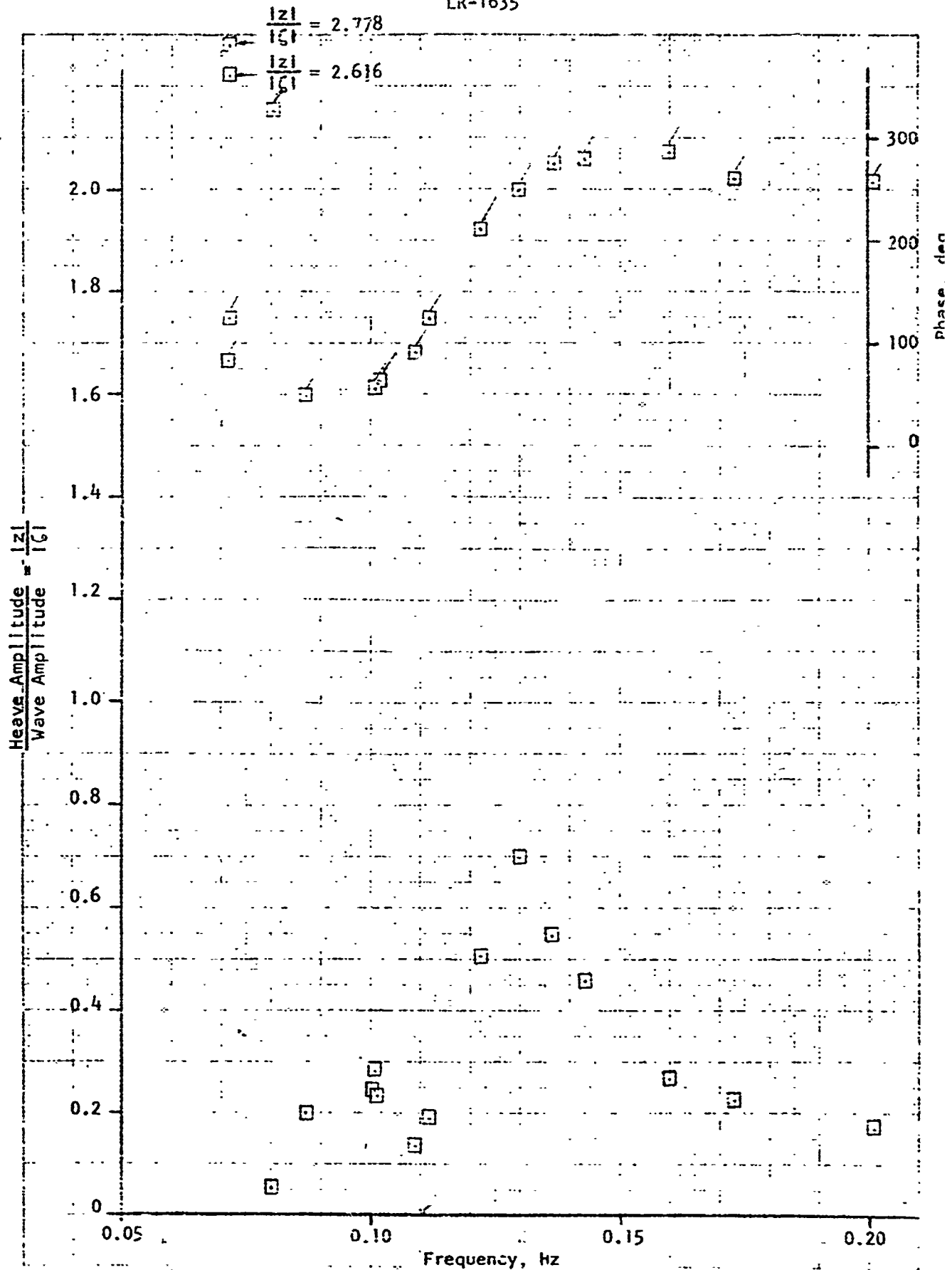


FIGURE 21f. WAVE TEST RESULTS FOR TESTS 12, ROW 6

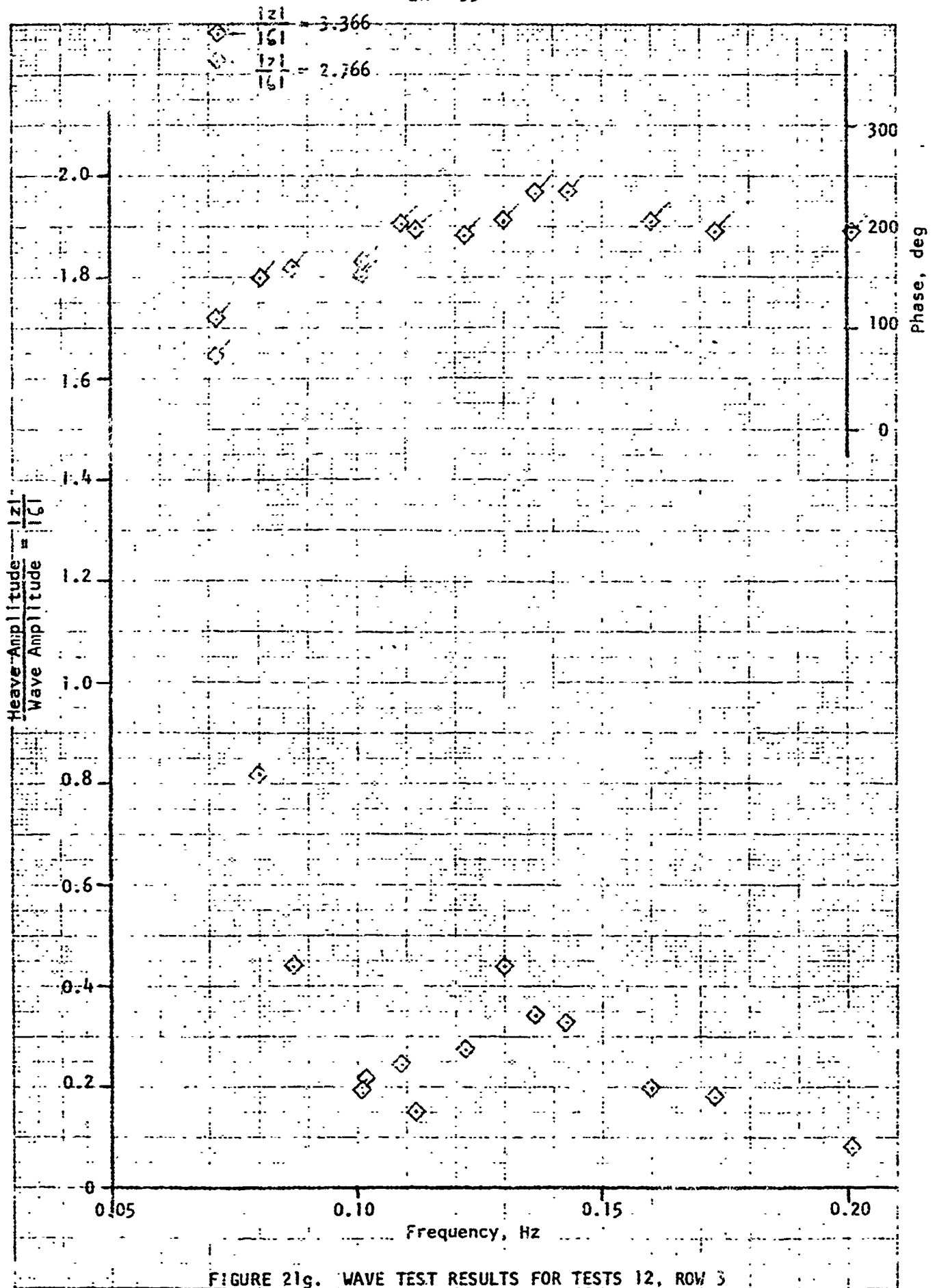


FIGURE 21g. WAVE TEST RESULTS FOR TESTS 12, ROW 3

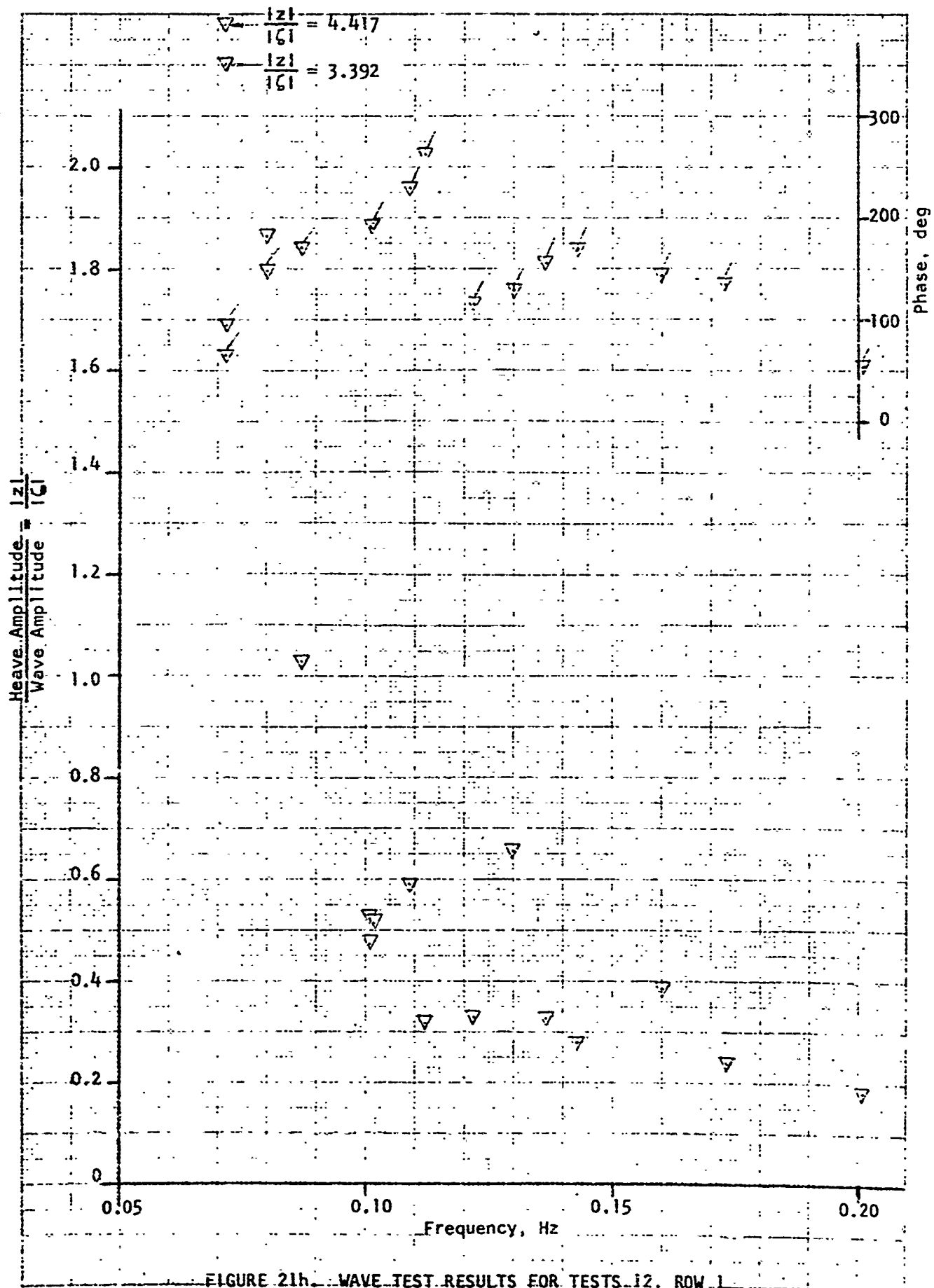


FIGURE 21h. WAVE TEST RESULTS FOR TESTS 12, ROW 1

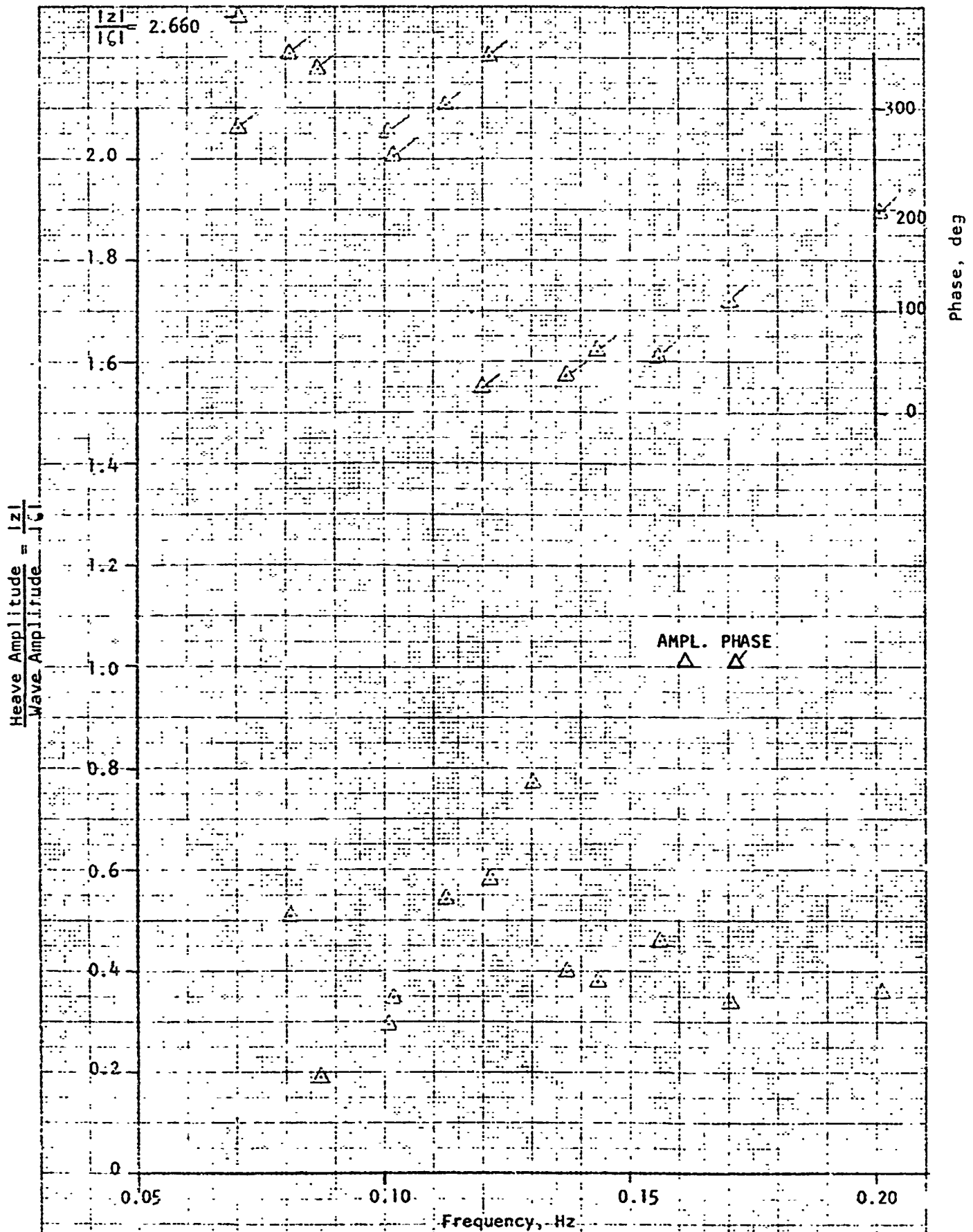


FIGURE 22a. WAVE TEST RESULTS FOR TESTS 13, ROW 17

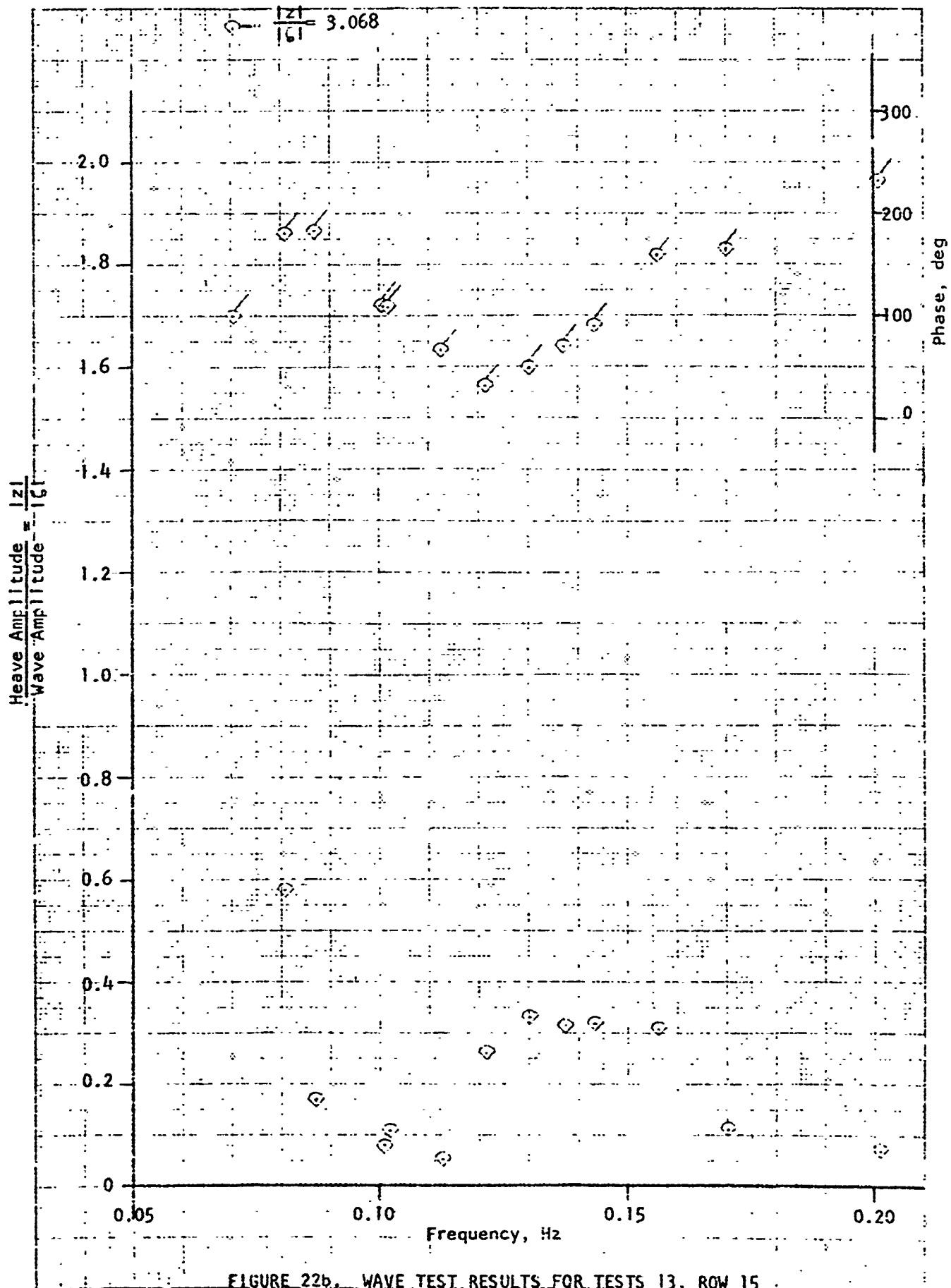


FIGURE 22b, WAVE TEST RESULTS FOR TESTS 13, ROW 15.

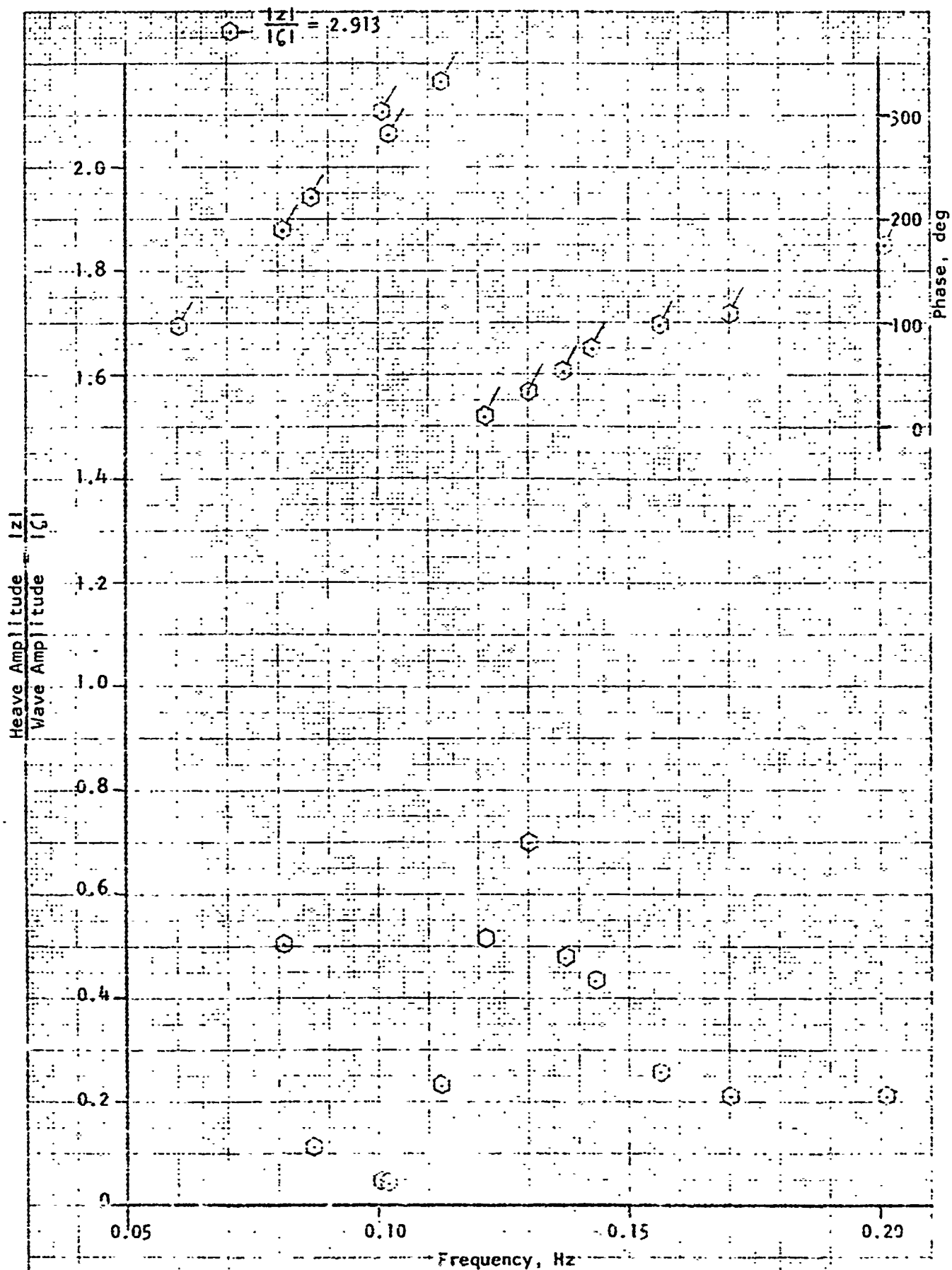


FIGURE 22c. WAVE TEST RESULTS FOR TESTS 13, ROW 12

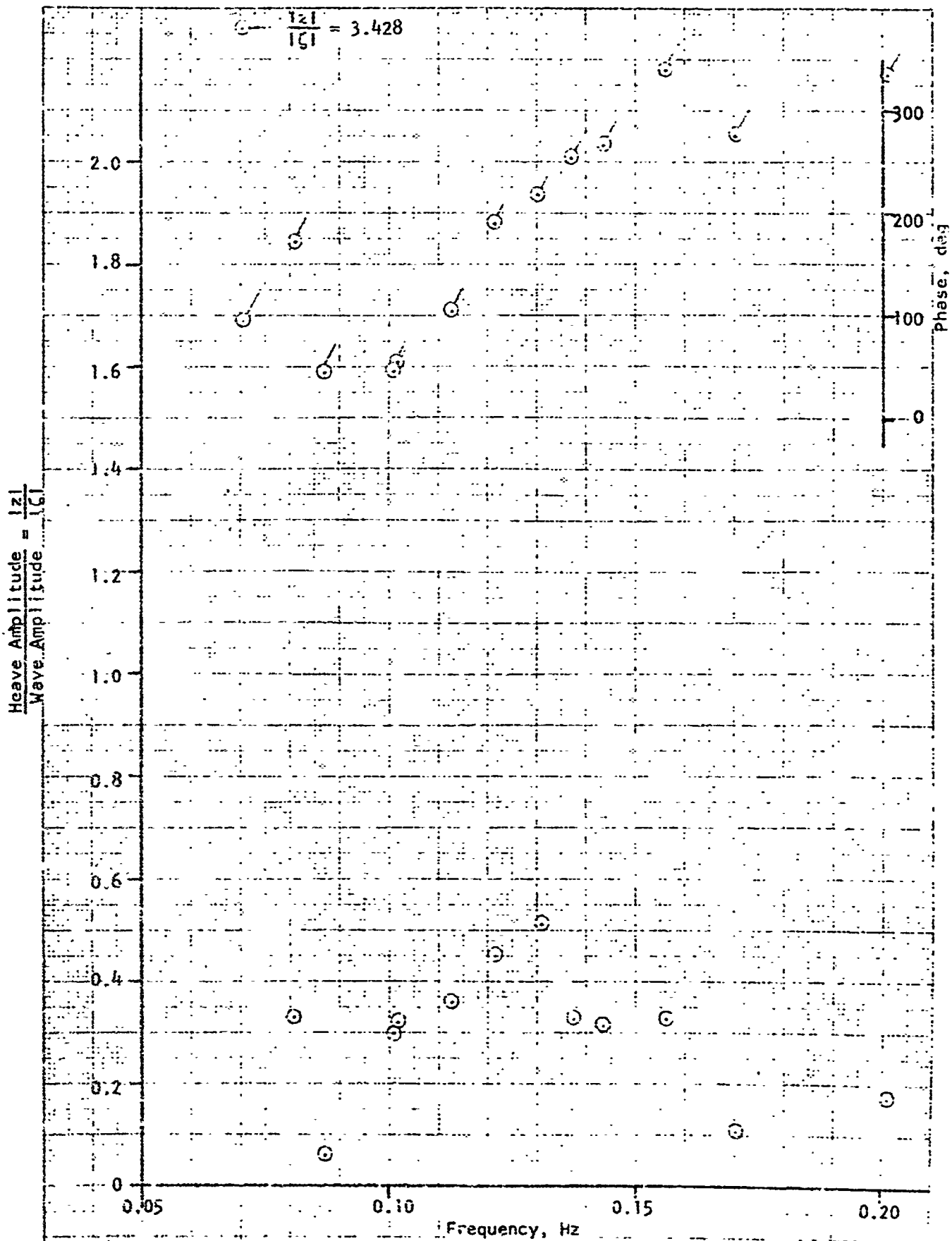


FIGURE 22d. WAVE TEST RESULTS FOR TESTS 13, ROW 9.

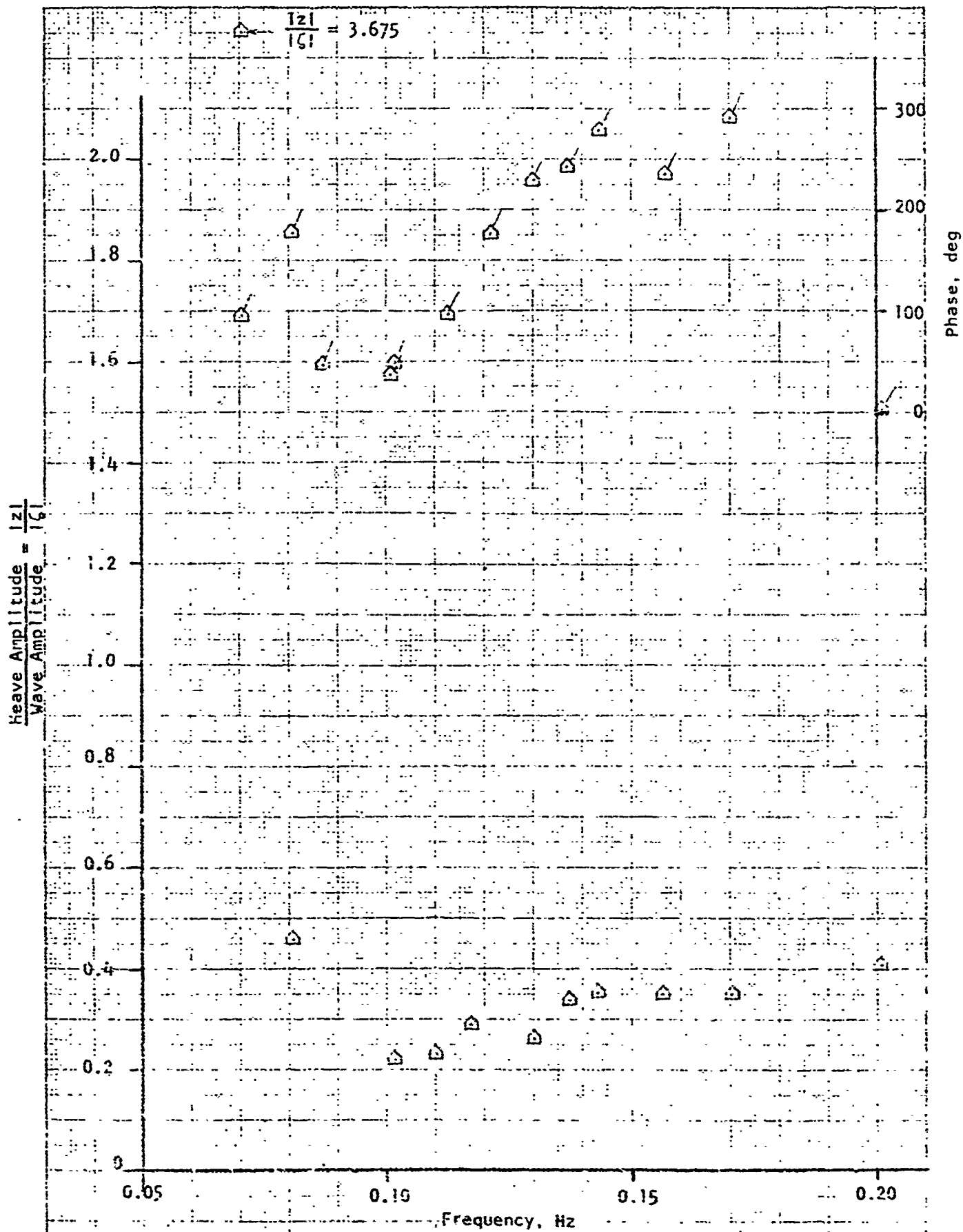


FIGURE 22e. WAVE TEST RESULTS FOR TESTS 13, ROW 9P

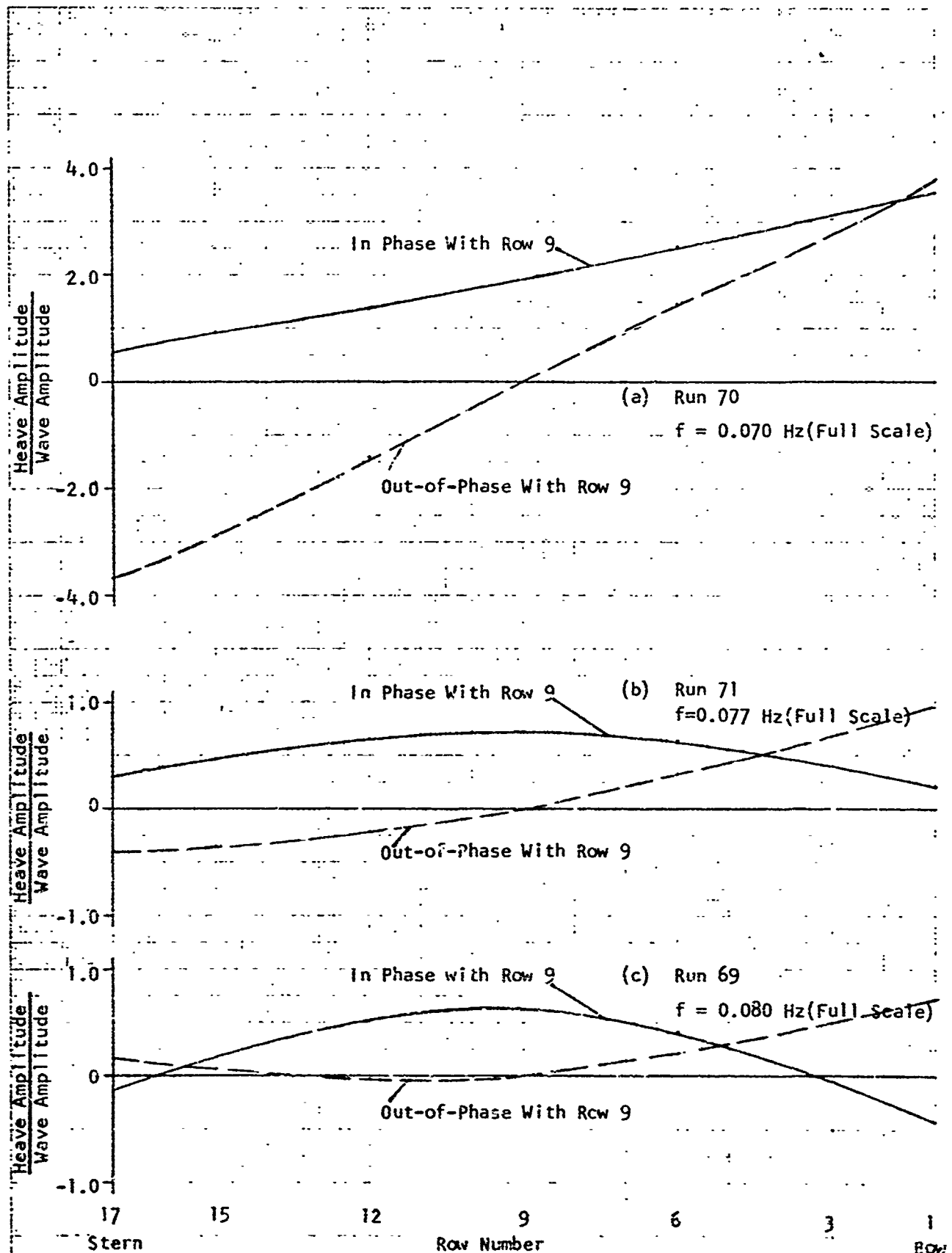


FIGURE 23(a-c). WAVE TEST RESULTS PLOTTED AS FUNCTION OF FORE-AND-AFT POSITION ON DECK, TESTS 6, WIDE DECK ELASTIC ELEMENTS FULL ATTENUATORS

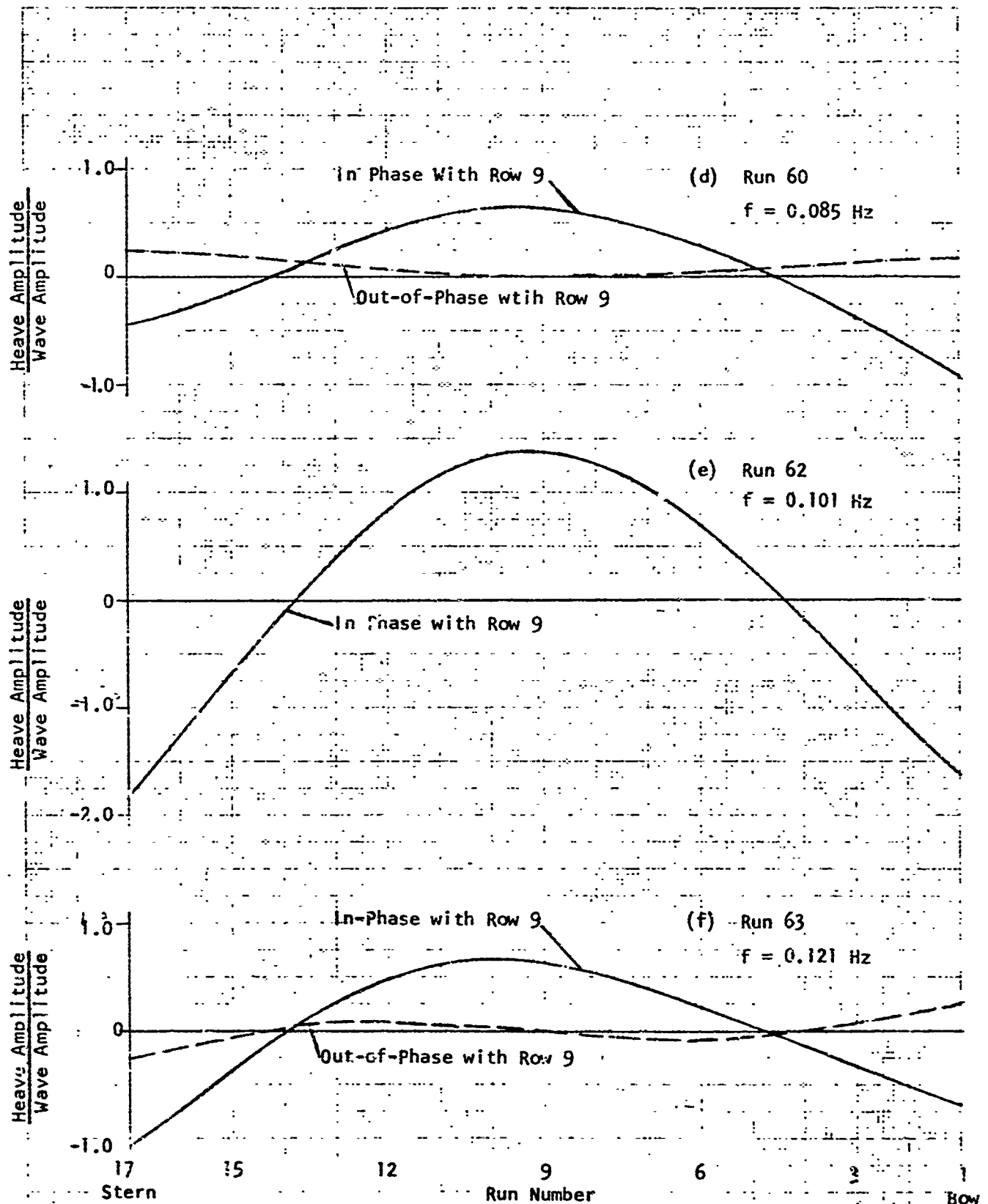


FIGURE 23(d-f). WAVE TEST RESULTS PLOTTED AS FUNCTION OF FORE-AND-AFT POSITION ON DECK, TESTS 6, WIDE DECK ELASTIC ELEMENTS FULL ATTENUATORS

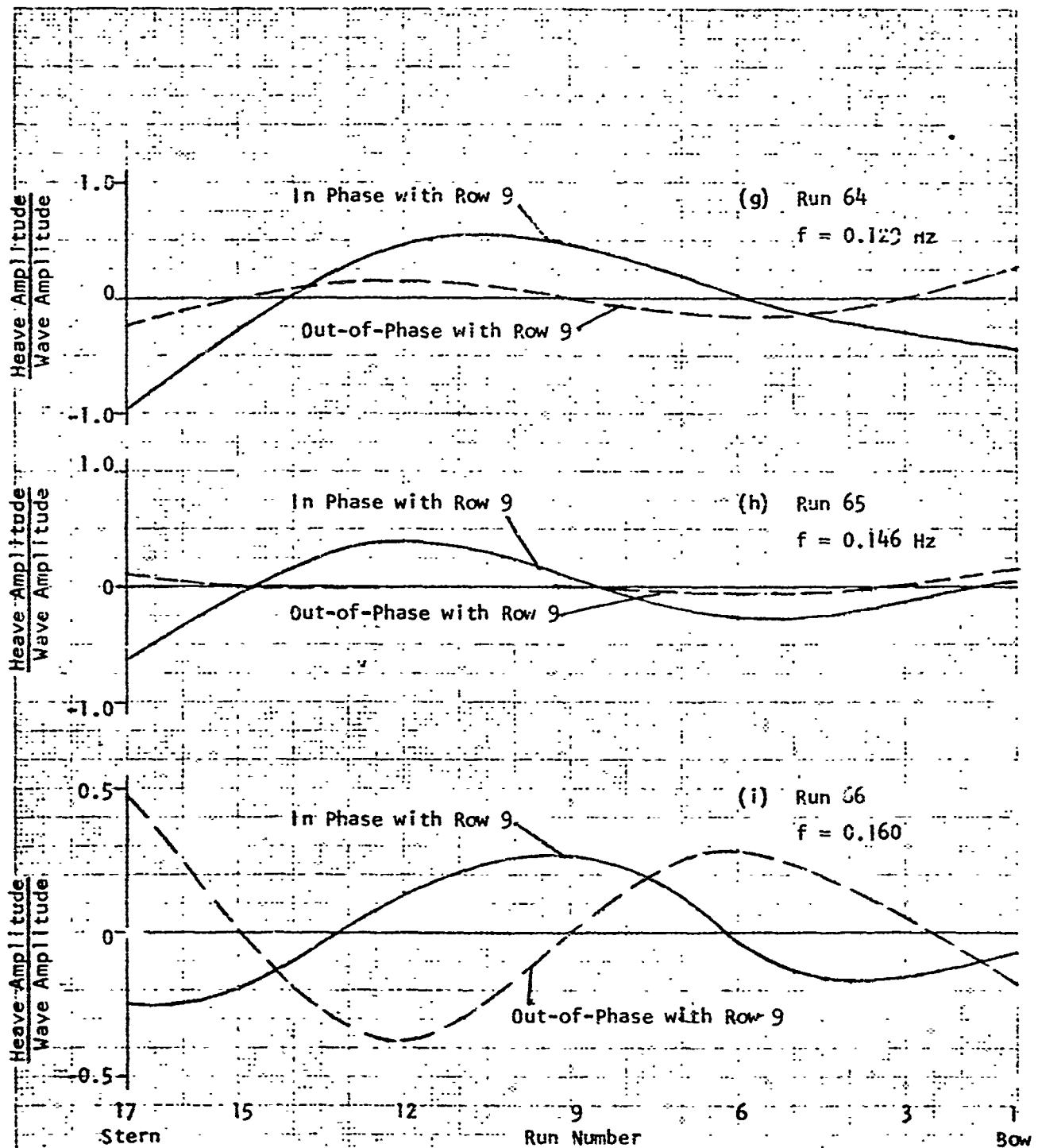


FIGURE 23 (g-i). WAVE TEST RESULTS PLOTTED AS FUNCTION OF FORE-AND-AFT POSITION ON DECK, TESTS 6, WIDE DECK ELASTIC ELEMENTS FULL ATTENUATORS

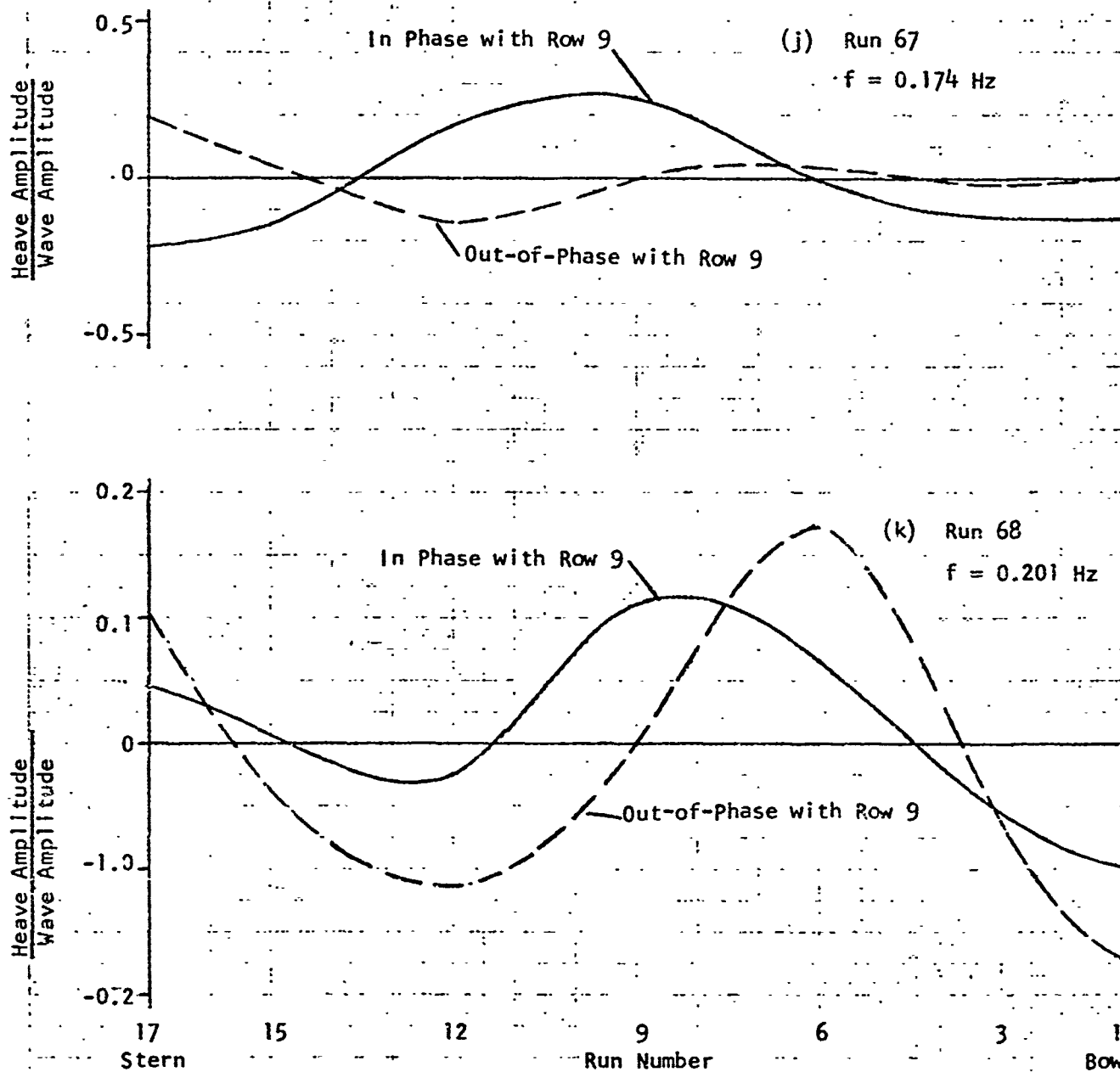


FIGURE 23(j-k). WAVE TEST RESULTS PLOTTED AS FUNCTION OF FORE-AND-AFT POSITION ON DECK, TESTS 6, WIDE DECK ELASTIC ELEMENTS FULL ATTENUATORS



FIGURE 24a. UNDERWATER PHOTO SHOWING ATTITUDE OF ATTENUATORS
IN RESPONSE TO REGULAR WAVES WITH (FULL SCALE) LENGTH OF 330 FT
HOGGING



FIGURE 24b. UNDERWATER PHOTO SHOWING ATTITUDE OF ATTENUATORS
IN RESPONSE TO REGULAR WAVES WITH (FULL SCALE) LENGTH OF 330 FT
NULL AFTER HOGGING



FIGURE 24c. UNDERWATER PHOTO SHOWING ATTITUDE OF ATTENUATORS
IN RESPONSE TO REGULAR WAVES WITH (FULL SCALE) LENGTH OF 330 FT
SAGGING



FIGURE 24d. UNDERWATER PHOTO SHOWING ATTITUDE OF ATTENUATORS
IN RESPONSE TO REGULAR WAVES WITH (FULL SCALE) LENGTH OF 330 FT
HULL AFTER SAGGING

APPENDIX H - HYDRODYNAMIC TESTS AND
ANALYSIS PROGRAM FOR EXPANDABLE FLOATING
BASES: PART 3 - ANALYSIS AND SUPPORTING TEST
WORK OF STUDY OF RESPONSE OF DEFORMABLE FLOATS

1. MODEL FABRICATION BY GAC

Considerations for float construction, as accomplished by GAC, are presented here with the test results and analysis provided in the following report prepared by Stevens Institute, Item 2 of this appendix.

The selection of model shape and size for use in the small-scale testing program was based on several considerations. The depth of water in the available Davidson Laboratory test facility limited the model draft. The combination of Froude-Cauchy scaling and suitable elastomeric deformable materials constrained the model diameter and, hence, draft-to-diameter ratio. Since these limitations prevented the selection of a slender model similar to the anticipated prototype float-attenuator shape, an alternate shape having a relatively simple geometry of which a rigid model had previously been studied, was chosen. The geometry and dimensions of the models selected are shown in Figure 2 of the Davidson Laboratory report, Item 2, below.

The model scale ratio chosen was 1/12 based on a full-scale water plane diameter of 6 ft. Full-scale Et values of 13,000 lb per inch and 6900 lb per inch were established as ranges for rubberized fabric construction to be simulated in scale by the test model. Evaluation of readily available materials showed that no fabric-reinforced elastomers in suitable gages could be obtained in a suitable time frame; further, the techniques of fabricating rubberized fabrics necessitated lap splicing, which would not permit a uniform skin thickness to be achieved.

Polyvinylchloride film was available in a range of gages and moduli at Good-year Aerospace. It was readily thermoformable and could be easily joined by adhesive bonding. Two PVC films were chosen for model fabricating with these characteristics:

	<u>Et (lb/in.)</u>	<u>Thickness (in.)</u>
Thick skin	90	0.030
Thin skin	40	0.020

The models were fabricated by vacuum forming the spherical segments and adhesively bonding them to joining cylindrical sections. It proved necessary to reinforce this juncture with a number of narrow strips of film to reduce the high stress condition that would occur otherwise at the transition during pressurization.

2. DAVIDSON LABORATORY TEST AND ANALYSIS

Part 3 of the Davidson Laboratory subcontract program is given on the following pages of this appendix.

STEVENS INSTITUTE OF TECHNOLOGY
DAVIDSON LABORATORY
CASTLE POINT STATION
HOBOKEN, NEW JERSEY

Letter Report SIT-DL-72--1632

October 1972

HYDRODYNAMIC TESTS AND ANALYSIS PROGRAM
FOR EXPANDABLE FLOATING BASES

PART 3

Analysis and Supporting Test Work
of Study of Response of Deformable Floats

by John A. Mercier

Prepared for

Goodyear Aerospace Corporation
Akron, Ohio 44315
GAC P.O. 2B1115YX
(DL Project 3949/755)

APPROVED

S. Tsakonas

ii+34 pp.
+ 6 figures

S. Tsakonas
Head, Fluid Dynamics Divi.

INTRODUCTION

The response to wave action of expandable fabric, deformable membrane, liquid-filled structures like the float-attenuators planned for use in the multi-float Expandable Floating Base may differ from that for rigid, non-deforming, bodies.

This report describes analytical investigations of certain hypothetical models of the non-rigid response of the float-attenuators, with special interest in the vertical response, particularly wave-induced forces transmitted to the deck and resulting heaving motions. Shell-like responses are considered, as well as beam-like behavior which is relevant to the horizontal response. The most interesting and, perhaps, important observations come from a treatment of the float-attenuator system as lumped masses connected by springs (the hinge connection between float and attenuator, especially) under the action of wave forces.

Complementary small-scale model tests in waves and with forced heaving oscillations were carried out with two deformable models of a float having elementary geometrical characteristics. Hydro-elastic scaling laws (Froude-Cauchy) used to relate model-scale material resiliency and other quantities to comparable full-size quantities are described. A "rigid" version of this model had previously been tested at Davidson Laboratory (DL) as well as by others (Motoya,¹ Ochi²).

The experimental part of this program had been considered to be useful for comparison with the analyses as well as for a preliminary learning exercise prior to carrying out large scale (1/8th full size) tests of the elastically-scaled version of a slender float and attenuator, representative of the kind of float to be adapted for the prototype Expandable Floating Base. These large scale tests were actually carried out, under Part 2, Phase b, of the present project, very shortly after the present small scale

¹Superior numbers in text matter refer to similarly numbered references listed at the end of this report.

experiments were completed and before they were fully analyzed. The small scale testing clearly indicated that certain auxiliary tests, such as natural frequency measurements for various modes of oscillation, are of substantial usefulness in addition to the primary testing for wave response measurements.

This report describes work done under Part 1 of Phase b, "Response of Deformable Floats; Analysis and Supporting Test Work" for Goodyear Aerospace Corporation (GAC) under Purchase Order 2B1115YX.

ANALYTICAL CONSIDERATIONS

Several models for certain kinds of dynamic response of closed liquid-filled membrane structures are hypothesized and examined. Shell-like responses are considered first, followed by a brief description of lateral beam-like behavior which was described previously in DL Letter Report 1579, "Hydrodynamic Analyses and Exploratory Model Tests For An Expandable Floating Base."³ Finally, the behavior of a lumped-mass system composed of the attenuator and float and certain axial springs, responding to vertical wave-induced forces, is discussed. Because of difficulties in assessing effective spring stiffnesses, firm conclusions concerning the importance of deformability cannot be made without confirming evidence from scale model tests such as those conducted by DL and GAC on a representative slender water-filled float-attenuator at the Lockheed Underwater Missile Facility under Part 2, Phase b, of the present Purchase Order, as reported by Numata.⁴ The analysis can, however, be used as a sort of interpolation formula for evaluating the influences of variations in certain parameters from the values for a tested model.

SHELL-LIKE VIBRATIONS

Spherical And Spheroidal Shells

An interesting discussion of the frequency equations and mode shapes for the axisymmetric extensional, non-torsional vibrations of fluid-filled spherical and spheroidal shells has been presented by Rand and DiMaggio.⁵ The effect of external fluid is not included.

A particular kind of shell-like response is of greatest interest in view of questions posed by the ARPA review group⁶; viz., can the hydrodynamic pressures due to waves produce motions of the internal liquid in such a way that the wave-exciting force is not attenuated as it would be with a non-deformable float-attenuator? This situation can occur for the attenuator, for instance, if the center-of-mass of the enclosed liquid oscillates periodically in the axial direction. The work of Rand and DiMaggio permits us to make some rough approximations of the natural frequency of liquid-filled shells in such a mode of vibration. This frequency estimate can be compared to the frequencies of ocean waves to see if a possibility of resonance exists, in which case, dynamic amplification may produce important effects (it being tentatively assumed that non-resonant response will not produce important variations from rigid-envelope behavior).

The frequency equations for a fluid filled elastic spherical shell of radius R have been obtained as

$$\left\{ \left[\left(\frac{1-\nu}{1+\nu} \right) \lambda z^2 - 2 \right] + n(n+1) \left(1 - \frac{\lambda z^2}{1+\nu} \right) \right\} \left[n - z \frac{J_{n+\frac{1}{2}}(z)}{J_{n+\frac{1}{2}}(z)} \right] + \kappa_0 \lambda z^2 \left[\left(\frac{1-\nu}{1+\nu} \right) (1 + \lambda z^2) - \frac{n(n+1)}{1+\nu} \right] = 0 \quad (1)$$

where the dimensionless characteristic frequency

$$z = \frac{\omega R}{c} \quad (2)$$

depends on mode number n and parameters

$$\begin{aligned} \lambda &= \text{acoustical parameter} \\ &= \frac{1}{2} \left(\frac{\text{velocity of sound in water}}{\text{shear wave velocity of in shell}} \right) \end{aligned} \quad (3)$$

and

$$\kappa_0 = (\rho/\rho_s) R/h \quad (4)$$

in addition to Poisson's ratio, ν . In the above equations

ω = frequency, rad/sec

c = velocity of sound in water

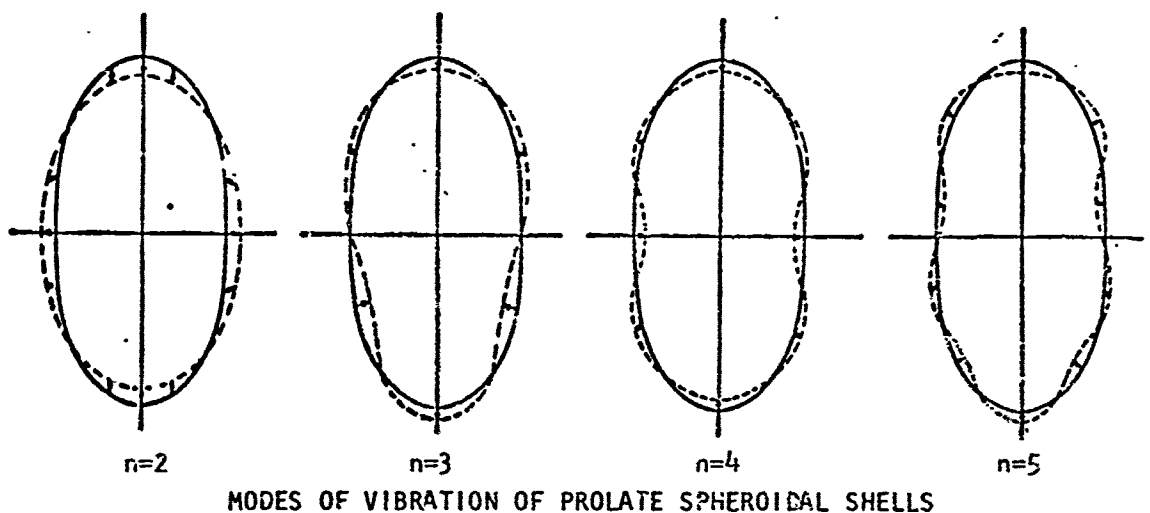
h = minimum shell thickness

ρ = density of fluid

ρ_s = density of shell material

$J_k(z)$ = Bessel function of the first kind of order k

For applications in which water is enclosed in rubberized fabric, both λ and κ_0 are large. In addition, the lowest axially oscillating mode corresponds to $n=3$ (see sketch, adapted from Nemergut and Brand⁷):



Evaluations of Eq.(1) have been given by Rand and DiMaggio⁵ only for a few cases of ν_1 and κ_0 . In addition, some numerical evaluations have been carried out for prolate spheroidal shells with a ratio of major to minor axis, $\tau = 10$. For each model pattern of shell displacement, n , there are many roots of the frequency equation, z , only the lowest of which is of interest.

Table 1 compares the dimensionless frequency derived from the analysis of Rand and DiMaggio,⁵ expressed in a form which is useful for our present scale model test program, $\omega \sqrt{\frac{R}{g}}$, which is related to Rand's⁵ parameter

$z = \frac{\omega R}{c}$ by the relation

$$\omega \sqrt{\frac{R}{g}} = \frac{c}{\sqrt{Rg}} z \quad (5)$$

For the presently described model tests, R is about 0.5 ft, $c \approx 4700$ ft/sec and $g = 32.2$ ft/sec², so that $\omega \sqrt{\frac{R}{g}} \approx 1200z$.

TABLE 1

LOWEST NATURAL FREQUENCY FOR $n=3$ MODE

	ν	λ	κ_0	z	$\omega \sqrt{\frac{R}{g}}$
Spheres	0.33	0.103	17.60	1.2	1440
	0.33	6.00	17.60	≈ 0.02	24
Spheroid ($\tau=10$)					
	0.33	0.103	17.60	0.12(eq.)	144

For the spheroid, an equivalent value of $z = \frac{\omega R_{eq}}{c}$ is taken where R_{eq} is assumed to be the radius of the sphere having the same volume as the spheroid having $\tau=10$.

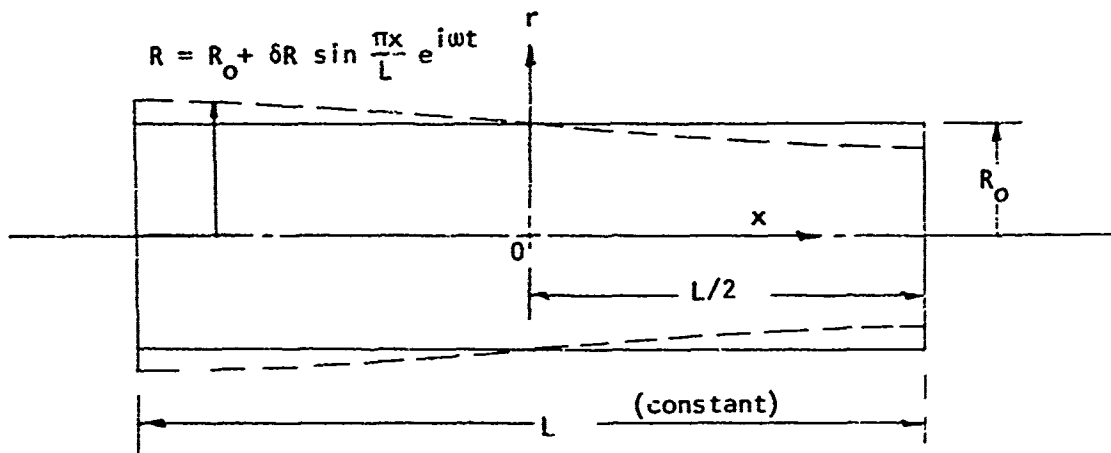
The range of values of $\omega \sqrt{\frac{R}{g}}$ covered in the present experimental program is about 0.3 to 1.5, well below any of the values found in Table 1. Higher values of λ , κ_0 and τ lead to lower resonant frequencies. Attenuator slendernesses of interest, however, have $\tau < 10$. It must be noted, also, that the presence of liquid external to the shell, in addition to inside, must reduce the natural frequency by an amount which cannot readily be evaluated.

The results given in Table 1 can be interpreted only very roughly: shell-like vibrations of liquid-filled membrane structures typically have high natural frequencies compared to wave frequencies. Difficulties in assigning values to parameters λ and κ_0 for fabric-reinforced elastomeric

membranes filled with water and further complications of evaluating roots of equations like Eq.(1) prevent drawing stronger conclusions on the basis of the analysis of Rand and DiMaggio.⁵ An alternative elementary analysis, described in the appendix, leads to other approximate expressions for the natural frequency of interest from which numerical estimates can readily be made.

Tubular Membrane

The appendix contains a development of a simple formula, based on Rayleigh's energy method, for estimating the natural frequency of a fluid-filled tubular membrane depicted in the sketch below:



DEFINITION SKETCH FOR FLUID-FILLED TUBULAR MEMBRANE

The principle assumptions, besides the approximation of the mode of motion are:

1. incompressible liquid-filled tube (consequently, $c = \infty$, which would give $\lambda = \infty$)
2. All of the kinetic energy of the motion is due to liquid motion, with no contribution from the tube material (this might be interpreted as $\rho_s \ll \rho$, or $\kappa_0 \gg 1$)

3. All of the strain energy is due to deformation of the tubular part of the membrane. The end bulkheads deform (in their plane) but do not contribute strain energy.

The estimate of the natural frequency may be expressed as

$$\frac{\omega^2 R_o}{g} = \frac{\pi E t \left(\frac{\pi R_o}{L} \right)}{\frac{\rho g V}{L} (1+\nu) (1-\nu)} \frac{i_1 (\pi R_o / L)}{i_0 (\pi R_o / L)} \quad (6)$$

where

$E t$ = "membrane modulus" of elasticity

R_o = tube radius

ρ = fluid mass density

g = acceleration of gravity

∇ = displaced volume

ν = Poisson's ratio

i_k = modified Bessel function of first kind of order k

Representative values for certain parameters may be adopted for calculations:

$E t$ = 1500 lb/in

R_o = 54 in

$\rho g \nabla$ = 339L lb, with L in inches

$\nu \cong 0.3$

Results of calculations with these values of parameters for $f = \frac{\omega}{2\pi}$, Hz, are exhibited in Table 2:

TABLE 2
NATURAL FREQUENCIES ESTIMATED FROM EQ. (6)

L/R_o	$\omega^2 R_o / g$	f
12	5.20	0.98
10	7.45	1.15
8	11.50	1.44
6	20.30	1.91
4	44.00	2.80

Since attenuators envisioned for the projected Expandable Floating Base would be likely to have $L/R_0 < 10$ and be situated at depths of over 20 feet below the water surface, it is unlikely that they would encounter resonance problems due to ocean wave excitation. Even accounting for the crudeness of the assumed model and the neglect of "added mass" due to external fluid motion, the natural frequencies for an axial surging mode of vibration of a "representative" attenuator must be fairly high. If, for instance, it were as low as $f_n = 0.5$ Hz, which corresponds to a 20-ft long gravity wave, it may be noted that the energy contained in ocean waves around this length is usually not large and that effects of attenuation with depth and the small ratio of wave length to attenuator diameter must severely ameliorate excitation near resonance.

On the basis of the foregoing discussions of shell-like vibrations, either spherical, spheroidal or tubular membranes, it may be inferred that resonant axial surging oscillations, which could give rise to significant effects on wave-induced vertical force or response, are not likely to occur. The analyses which could be treated under this task are not, unfortunately, close analogs of the float-attenuator-structure immersed in water, so that the influence is not as conclusive as one might wish: confirmation must depend on results of tests of large scale elastically-scaled models, such as reported by Numata.⁴ These tests did not reveal the existence of any shell-like axial oscillations.

BEAM-LIKE VIBRATIONS

A discussion of the lateral natural frequencies of deformable inflated attenuators according to Rayleigh's method was given in an appendix to the first DL report on Expandable Floating Bases.³ Results were given for estimates of the bending natural frequencies of hinged-free beams (attenuators) with $EI = 180,000\pi R^3 \text{ lb-ft}^2$, where R is the local float radius in feet, for coated fabric having tensile strength of 3000 lb/in. The distributed mass included the effects of entrained external water. These results will be repeated here for completeness.

Calculations have been made to show the effect of variations in length (Table 3) and slenderness (Table 4) on the natural frequency for floats similar to the one shown in the sketch below:

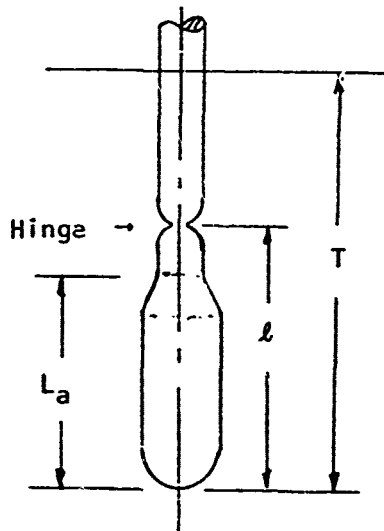


TABLE 3

EFFECT OF LENGTH ON BENDING NATURAL FREQUENCIES
 $R_a = 1.6$ times waterplane radius

l	L_a/l	f_n , Hz
38	≈ 0.80	0.72
48	≈ 0.75	0.44
58	≈ 0.70	0.29

TABLE 4

EFFECT OF SLENDERNESS ON BENDING NATURAL FREQUENCIES
 $l = 48$ ft $L_a/l \approx 0.75$

R_a /waterplane radius	f_n , Hz
1.6	0.44
1.8	0.46
2.0	0.48

There is an important dependence of natural frequency on attenuator length but slenderness does not have much influence.

In view of the attenuation of wave orbital motion with depth, and consequent decay of exciting force, it would appear that attenuators made of this type of coated fabric could be rather long, say 65-75 feet or more without expecting significant resonant response effects. For greater lengths, this mode of response ought to be considered in greater detail in the course of design, selection of hinge location, fabrics, etc.

SIMPLIFIED LUMPED-MASS-ELASTIC SYSTEMS

Some parts of the float-hinge-attenuator structure may, for certain conditions of design and construction, be quite resilient compared to other parts of the structure and, thus, lumped-mass dynamic models may be hypothesized for analyzing the response to wave-exciting forces. Two models will be considered for investigating the vertical force and motion responses.

Resilient Column

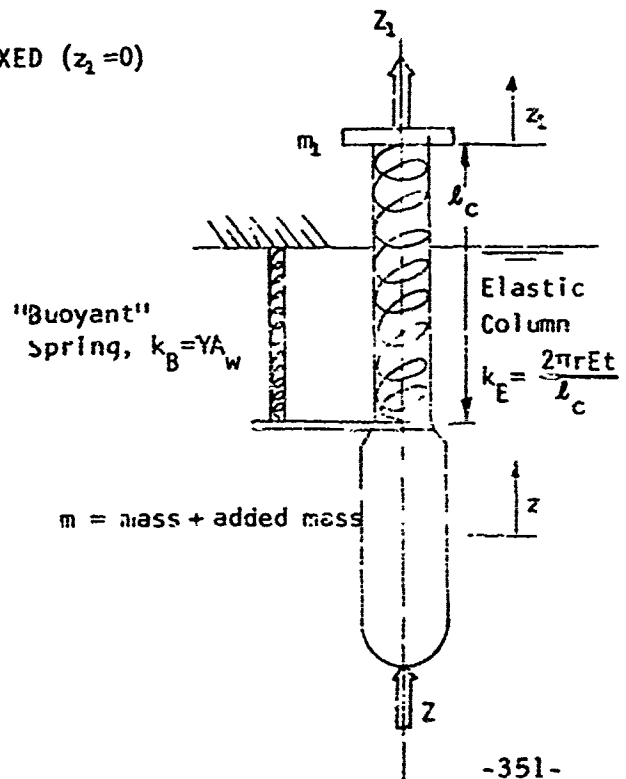
The model is depicted in the sketches below. Two cases will be considered: 1) upper end fixed (as for wave-induced force measurement tests) and, 2) upper end free (as for free span buoy).

1) UPPER END FIXED ($z_1 = 0$)

$$z_1 = k_E z$$

(7)

$$m\ddot{z} = -(k_B + k_E)z + Z$$



With the assumption of harmonic exciting force F , the solution may be expressed as

$$\frac{Z_1}{Z} = \frac{1}{1 + \frac{k_B}{k_E} \left[1 - \left(\frac{\omega}{\omega_n} \right)^2 \right]} \quad (8)$$

where

$$\omega_n = \sqrt{\frac{k_B}{m}} \quad (9)$$

is the heave natural frequency of the float, if it is rigid.

The result of Eq.(8) is plotted in Figure 1 for several values of k_B/k_E . An important effect due to elasticity is evident for higher frequencies, where exciting forces are quite small. Damping plates, which are needed to control rigid-body heave resonances, should also minimize the effect of any elastic heave resonance.

If the column resiliency is due to the float fabric alone (it may also be affected by guy wires), the ratio may be expressed as

$$\frac{k_B}{k_E} = \frac{\gamma \pi r^2 l_c}{2 \pi r (Et)} \quad (10)$$

Assuming representative (perhaps exaggerated since guy wire stiffness is neglected) values, viz.,

$$\gamma = 64 \text{ lb/ft}^3$$

$$r = 3 \text{ ft}$$

$$l_c = 50 \text{ ft}$$

$$Et = 15000 \text{ lb/in} = 180,000 \text{ lb/ft}$$

k_B/k_E is found to be 0.027, for which value a fairly small effect on transmitted force is found over the important (low-frequency) part of frequency range.

2) UPPER END FREE ($z_1=0$)

$$\begin{aligned} m_1 \ddot{z}_1 &= -k_E(z - z_1) \\ m \ddot{z} &= -k_B z - k_E(z - z_1) + Z \end{aligned} \quad (11)$$

With the same assumption as before, the solution may be expressed in the form

$$\begin{aligned} \frac{z_1}{z} &= \frac{1}{1 - \frac{m_1 \omega^2}{k_E}} \\ &= \frac{1}{1 - \frac{m_1}{m} \frac{k_B}{k_E} \left(\frac{\omega}{\omega_n} \right)^2} \end{aligned} \quad (12)$$

since both k_B/k_E and m_1/m (ratio of deck and payload mass to attenuator mass) are much less than unity $z_1/z \approx 1$ for all frequencies of interest.

Resilient Hinge

In this model it is assumed that the float-column, as well as the attenuator, is rigid but that the hinge, which might be constructed as hemispherical fabric "caps" on the attenuator and float, can deform axially. In this case, we must recognize that wave pressures produce vertical forces acting on the "caps" above and below the hinge which are assumed to cancel if the hinge is rigid. This wave force may be estimated as

$$Z_h = \gamma A_w \zeta \cdot S \cdot e^{\frac{-\omega^2 d_h}{g}} \quad (13)$$

where

ζ = wave elevation

S = a solidity factor

$$= 1 - \frac{\text{cross section area of hinge}}{A_{wp}}$$

d_h = depth of hinge below waterline

The model is shown in the adjoining sketch. Again, two cases will be treated.

1) UPPER END FIXED ($z_1=0$)

$$z_1 = z_h + k_h z \quad (14)$$

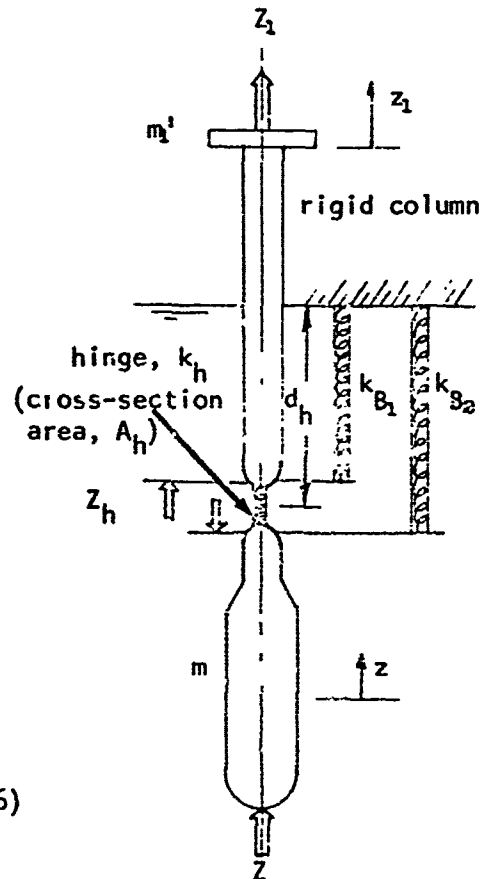
$$m\ddot{z} = -(k_h + k_{B2})z + F - F_h$$

where

$$\begin{aligned} k_{B1} &= \gamma(A_w - A_h) \\ k_{B2} &= \gamma A_h \\ k_{B1} + k_{B2} &= \gamma A_w = k_B \end{aligned} \quad (15)$$

are buoyant spring rates. Again assuming harmonic motion, a solution may be given

$$\frac{z_1}{z} = \frac{1 + \frac{k_{B2}}{k_h} \left[1 - \frac{k_B}{k_{B2}} \left(\frac{\omega}{\omega_n} \right)^2 \right] \frac{z_h}{z}}{1 + \frac{k_{B2}}{k_h} \left[1 - \frac{k_B}{k_{B2}} \left(\frac{\omega}{\omega_n} \right)^2 \right]} \quad (16)$$



The behavior of this expression depends importantly on the ratio k_{B2}/k_h , which must be quite small, but which cannot easily be evaluated, unless k_h is known (experimentally, for instance).

2) UPPER END FREE ($F_1=0$)

$$\begin{aligned} m_1 \ddot{z}_1 &= -k_{B1} z_1 - k_h (z_1 - z) + F_h \\ m \ddot{z} &= -k_{B2} z - k_h (z - z_1) + F - F_h \end{aligned} \quad (17)$$

The solution may be given as

$$\frac{z_1}{z} = \frac{1 + \frac{F_h}{F} \frac{k_{B_2}}{k_h} \left[1 - \frac{k_B}{k_{B_2}} \left(\frac{\omega}{\omega_n} \right)^2 \right]}{1 + \left(1 - \frac{F_h}{F} \right) \frac{k_{B_1}}{k_h} \left[1 - \frac{m_1}{m} \frac{k_B}{k_{B_1}} \left(\frac{\omega}{\omega_n} \right)^2 \right]} \quad (18)$$

These solutions (Eqs. 16 and 18) should be evaluated for a range of values of the parameters and compared with test results such as those reported by Numata.⁴ Equation (16) can be rewritten in terms of a natural frequency, ω_n^1 , related to the attenuator oscillating with the hinge as a spring,

$$\omega_n^1 = \sqrt{\frac{k_h}{m}} \quad (19)$$

so that

$$\frac{F_1}{F} = \frac{1 + \frac{F_h}{F} \left[\frac{k_{B_1}}{k_h} - \left(\frac{\omega}{\omega_n^1} \right)^2 \right]}{1 + \frac{k_{B_2}}{k_h} - \left(\frac{\omega}{\omega_n^1} \right)^2} \quad (20)$$

Since $k_{B_2}/k_h \ll 1$ (almost surely), it should be sufficient to assure $(\omega/\omega_n^1)^2 \ll 1$ to have small dynamic effect on response.

Tests carried out at Lockheed Underwater Missile Facility with a 10-ft draft, elastically-scaled float-attenuator model⁴ showed $\omega_n^1 \approx 15.7$ rad/sec and, for the highest wave test frequency $(\omega/\omega_n^1)^2 \approx 0.07$. The dynamic effect must be considered to have been small.

This lumped mass system may be the most significant as far as exhibiting dynamic effects of all of those considered. It appears that no problems are likely to arise due to these effects for typical designs and that certain dynamic characteristics can readily be considered in the course of design.

MODELS AND APPARATUS

MODEL SHAPE AND SIZE

The selection of model shape and size for use in the experimental program was based on several considerations. The depth of water in the available DL test facility limited the model draft while the combination of Froude-Cauchy scaling and suitable elastomeric deformable materials constrained the model diameter and, hence, draft-to-diameter ratio. Since these limitations prevent the selection of a slender model similar to the anticipated prototype float-attenuator shape, an alternate shape having a relatively simple geometry of which a rigid model had previously been studied, was chosen. The geometry of the models selected is shown in Figures 2a-c.

SCALING LAWS

The rules of modeling similitude which must be satisfied in dynamic testing of elastically-deforming structures are the so-called Froude-Cauchy laws which entail geometric, dynamic and kinematic requirements.

1. Geometric similarity is satisfied by scaling all dimensions by a common factor, λ , where λ is less than one when the model is smaller than the prototype. (Wall thickness of the fabric-reinforced rubber is not critically important for the present tests.)
2. Dynamic similarity requires Froude number to be satisfied (ratio of inertial to gravitational force), $v/\sqrt{gL} = \text{constant}$, or $\omega\sqrt{L/g} = \text{constant}$, where L is a characteristic length of the model. Thus velocity, v , is proportional to $\sqrt{\lambda}$, frequency, ω , is proportional to $\sqrt{1/\lambda}$, and forces vary as λ^3 .
3. Kinematic similarity calls for identical elastic strain of the structure, or stress/Young's modulus equals a constant. For

hydrodynamic loading, the stress is proportional to the fluid dynamic pressure $\rho v^2/2$. Thus Young's modulus, E , must be proportional to $\rho v^2/2$ which, according to Froude's Law (for tests of model and prototype in water), is proportional to λ . For the fabric strain modulus, which is expressed in units of (lb/in) rather than lb/in² — for Young's modulus, an additional factor of λ is required so that fabric modulus, E_t , must be scaled in proportion to λ^2 .

Two resilient models were supplied by Goodyear Aerospace Corporation, fabricated of polyvinylchloride (PVC) film having different fabric moduli and thicknesses as follows:

	E_t (lb/in)	Thickness (in)
"Thick" Model	90	0.030
"Thin" Model	40	0.020

If the scale ratio is taken to be 1/12th (6-in diam waterline model corresponds to 6-ft diam waterline prototype), the "full-size" E_t values for the "thick" and "thin" versions are about 13000 and 6000 lb/in, respectively.

MODEL FABRICATION DETAILS

The circular junctions of the spherical and cylindrical segments of these models were reinforced by multiple heavy bands of PVC since at this juncture the radii of curvature are discontinuous, a condition which would impose severe stress concentrations on an unreinforced membrane structure. These reinforcements are illustrated in the sketches of Figures 2b and 2c.

PRESSURIZATION AND SUSPENSION OF PVC MODELS

The deformable models were pressurized by filling with water through a "stand-pipe" system composed of flexible 1/4-in I.D. PVC tubing. Separate fill- and vent-tubes were provided, the fill-tube incorporating a wide-mouth

(approximately $1\frac{1}{2}$ " diam) upper section. Both tubes incorporate valves to hold the pressure set by adjusting the head of water in the tubes. The PVC models are secured to a 5.94-in diam x 0.95-in thick plexiglass plate by a hose clamp. The stand-pipe tubes connect to the plexiglass plate and it is readily evident whether air is trapped in the model.

The plexiglass plate has two $\frac{1}{4}$ "-20 TPI tapped blind holes to permit connecting to a force balance through a mounting bracket. The rigid (expoxy-coated urethane foam) model of Figure 2a was attached to the force balance system by the same bracket.

Two kinds of behavior of the deformable models in waves deserve comment in this description of the setups used. The models must be pressurized to a sufficient level to assure that the membrane skin remains in tension under the action of external loads. The thick model was tested with a pressurization of 35.25 ± 1.0 -in head of water while the thin model was tested with a head of 24.5 ± 1.0 -in of water. Under these pressurization conditions the PVC models creep and water must be added regularly to maintain constant head, and consequently satisfactory membrane tension. An alternative test procedure in which the model could be de-pressurized between test runs only being fully pressurized for the fairly brief (about 0.5 to 1 min) duration of a wave test, was considered. Because of the substantial increase in testing time due to the slowness of the filling process and recognizing that significant creep would occur during the pressurized intervals, this procedure was not followed during the bulk of the testing.

A second feature of the model behavior in which the spherical lower end of the model oscillated horizontally at rather large amplitudes was observed. Additional tests were conducted with the models constrained by guy wires of low-stretch dial-cord connected from a horizontal fore-and-aft boom to the reinforcing bands around the junction of sphere and cylinder of the models. The arrangement is depicted in the sketch of Figure 3 which also shows the pressurization system and the attachment to the force balance system. The thick PVC model was tested both with and without the guys but the thin PVC model was tested only with the guys.

MEASUREMENTS

For regular wave tests, the models were connected to a pair of force balances, as shown in Figure 3, for measuring vertical and horizontal forces. Rated capacities of the balances were:

Vertical force: ± 10 lb

Horizontal force: ± 20 lb

The water-filled models had an excess of weight over displacement which exceeded the vertical force balance capacity. A weight (about 10 lb) connected by a string over a pulley to the vertical force balance unloaded this bias and put the force transducer in the middle of its range.

Wave elevation abreast of the model was measured with a resistance-type probe having ± 5 -in range.

Signals from the transducers were amplified by Sanborn 350 Series conditioning unit and recorded simultaneously on FM analog magnetic tape and Visicorder chart paper.

A program of heave oscillation tests for deriving added mass and damping characteristics of the floats was also undertaken. The apparatus used for these tests was an improved version of the equipment described by Mercier in published references.^{8,9} An existing force balance was adapted (range ± 25 lbs) for these tests. A sine-cosine potentiometer coupled to the shaft of the oscillator was used as a motion-phase reference indicator.

TEST PROGRAMS

The sequence of testing in regular waves covered five phases:

1. Rigid model
2. Thick PVC model, no bracing
3. Thick PVC model, with bracing
4. Thin PVC model, with bracing

Wave periods covered the range from about 0.7 to 2.0 sec while heights

(double amplitudes) of around 1 inch were used, with a few tests with higher and lower waves.

5. In addition the thick PVC model, with bracing, was tested with forced heaving oscillations of ± 1 inch.

Attempts were made to record natural frequencies of various modes of model and force balance vibration for some of the inflated PVC models. The results are summarized in Table 5.

TABLE 5
MODEL NATURAL FREQUENCIES

MODEL	MODE	FREQ., Hz	REMARKS
Thick PVC	Heave	3.1	Model oscillates with vertical balance as spring
Thick P.V.C (no bracing)	Surge	1.02	Bending of model
Thick PVC (no bracing)	Surge	8.3	Model oscillates with horizontal balance as spring
Thick PVC (with bracing)	Surge	1.22	Bending of model
Thin PVC (no bracing)	Heave	2.6	Model oscillates with vertical balance as spring
Thin PVC (no bracing)	Surge	0.56	Bending of model
Thin PVC (with bracing)	Surge	0.83	Bending of model

No wave tests were carried out with the thin PVC without bracing. Two surge frequencies were found: one by striking the spherical end of the model a horizontal blow appears to be due to the spherical end of the model oscillating with the cylindrical part acting as a spring (beam). The other, found by ringing the drag balance, appeared on the oscillograph superimposed on the much lower bending mode frequency. Attempts to separate a mode of heave resonance where the spherical end oscillates with the cylindrical part as a spring from that mode for which the whole model oscillates with the balance as a spring were unsuccessful.

DATA REDUCTION AND RESULTS

The Visicorder oscillographic records were read by hand during the course of testing to obtain preliminary results. The FM magnetic tape records were processed using the PDP-8E digital computer and A-to-D converter with a Fourier analysis program to obtain the amplitude of the fundamental component of force and wave (or motion, for oscillation tests) records and phase lags of forces relative to wave (or motion, for oscillation tests).

Tables 6 to 9 contain the results of the computer data-analysis of the wave tests including amplitudes, phases and nondimensionalized coefficients:

$$\begin{aligned} Z_w &= \frac{Z}{\zeta} \cdot \frac{1}{YA_w} \\ X_w &= \frac{X}{\zeta} \cdot \frac{1}{YA_w} \end{aligned} \quad (21)$$

where

- Z = heave force amplitude
- ζ = wave amplitude
- Y = specific weight of water (ρg)
- A_w = waterplane area
- Z = surge force amplitude

A dimensionless frequency parameter is used, $\omega \sqrt{T/g}$, where ω = circular frequency, rad/sec, T = draft, ft, and g = acceleration of gravity. The vertical wave force coefficient Z_w should be 1.0 for $\omega=0$ (static conditions). The horizontal force is expressed in the same fashion in order to permit quantitative comparisons. The sign conventions used for phase evaluations are:

- + wave crest
- + heave force upward
- + surge force toward wavemaker

Nominal values of A_w and T are used for the PVC models, corresponding to the "design" cylinder diameter and draft. Actual values were

somewhat different and varied during the tests due to creep. They were not accurately measured and, hence, are not suitable for use in data presentation.

Heave force results are plotted in Figure 4, where results which had been obtained previously for the rigid cylinder, using a somewhat different measuring system (Mercier¹⁰) are also shown. Results of the present and previous tests of the rigid model agree well but the flexible models perform dramatically differently from the rigid model and from each other. No satisfactory explanation of these differences can be suggested. It may be noted that when wave tests were done with the fill tube open to the atmosphere, only very small (less than $\pm \frac{1}{4}$ ") oscillations of the head of water in the stand-pipe were observed. No differences of response were found between tests with the fill tube open and closed.

Horizontal force results are exhibited in Figure 5. Again, there are appreciable differences between the rigid and water-filled PVC models. It is noted that the differences appear to be "tuned" to the natural frequencies (see Table 5). The theory of vibration isolation (cf., Thomson¹¹) shows that the ratio of transmitted force to periodic excitation force for a spring-mass system may be written as

$$TR = \frac{F_T}{F_E} = \frac{\sqrt{1 + \left(2 \frac{c}{c_c} \frac{\omega}{\omega_n}\right)^2}}{\sqrt{\left[1 - \left(\frac{\omega}{\omega_n}\right)^2\right]^2 + \left(2 \frac{c}{c_c} \frac{\omega}{\omega_n}\right)^2}} \quad (22)$$

where $\frac{c}{c_c}$ is the ratio of damping to critical damping. The curves fitting the data in Figure 5 roughly follow the pattern described by Equation (22), if it is assumed that c/c_c is in the range of 0.13 to 0.20. The phase change, also shown in Figure 5, agrees qualitatively with the results of the theory of vibration isolation, too. This theory does not, however, describe the differences between "rigid" and PVC models with accuracy, probably because some of the wave excitation force is applied to the system "spring" (the cylindrical part of the float) while the rest acts on the system "mass" (the spherical end of the float).

Results of the vertical oscillation tests are presented as added mass coefficients in Table 10 and Figure 6. These results have been corrected for the effect of model and apparatus weight, and are considered to be due to (a) external hydrodynamics, and (b) dynamic effects due to distortions of the model and its contained fluid. Results for the rigid model, from Ref.10, are also shown in Figure 6. The differences between rigid and PVC models may be considered small compared to the differences for wave-induced heave forces. The added mass coefficients of the PVC model show greater difference from the rigid model at high frequencies.

SUMMARY

Several analytical models for dynamical response of float attenuator systems have been considered.

1. Shell-like modes of vibration of the water-filled attenuator which could give rise to appreciable modifications of the vertical force appear to be unlikely to occur since estimates of resonant frequencies are well above frequencies for significant wave energy.
2. A beam-like bending mode of vibration of the attenuators may be important for rather long attenuators where the resonant frequency may fall in the range where significant ocean wave excitation could occur. This mode of response can readily be taken into account in the selection of shape, size and materials for attenuators. Dynamic effects on guy-wire supported floats, with attenuators at the lower end, may also be significant although this behavior has not been investigated in this report (it may be inferred from the tests carried out with the 1/8-scale model at the Lockheed Underwater Missile Facility⁴).
3. Consideration of lumped mass models of vertical response of float-attenuators indicates that the hinge connecting the float and attenuator is probably the weakest "spring" for vertical motions. The characteristics of this spring should be considered in the course of detail design. However, tests of the 1/8-scale model indicate that it is unlikely that problems would occur from this source.

Experimental studies of simple models of floats, having geometric shapes substantially different from realistic slender float-attenuators, show that membrane material characteristics can affect hydrodynamic response.

Significant differences were found between measured wave-induced forces for water-filled PVC models and a rigid (epoxy-coated polyurethane foam) model. The differences in the horizontal forces could be explained in terms of elementary vibration isolation theory, but no explanation has been found for the differences in vertical forces.

ACKNOWLEDGMENTS

Mr. Michael Chiocco carried out the bulk of the experimental program. Dr. C. H. Kim and Dr. S. Tsakonas contributed to the discussions of dynamical effects, especially the analyses of spherical and spheroidal shell-like vibrations.

REFERENCES

1. Motora, S. and Koyama, T., "Wave Excitationless Ship Forms." Sixth Symposium on Naval Hydrodynamic, Report ACR-136, 1966.
2. Ochi, M.K. and Vuolo, R.M., "Seakeeping Characteristics of A Multi-Unit Ocean Platform." Society of Naval Architects and Marine Engineers, Spring Meeting, 1971.
3. Mercier, J.A., "Hydrodynamic Analyses and Exploratory Model Tests for An Expandable Floating Base." Davidson Laboratory, Stevens Institute of Technology, Letter Report SIT-DL-72-1579, January 1972.
4. Numata, E., "Hydrodynamic Tests and Analysis Programs for Expandable Floating Bases, Part 4, Large Scale Model Tests of Response of Deformable Floats." Davidson Laboratory, Stevens Institute of Technology, Letter Report SIT-DL-72-1631, October 1972.

5. Rand, R. and DiMaggio, F., "Vibrations of Fluid-Filled Spherical and Spheroidal Shells." Journal of the Acoustical Society of America, Vol.42, No.6, pp.1278-1286, 1967.
6. Anon., "Report of ARPA Review Group on Expandable Floating Bases." Office of Naval Research, Ocean Technology Program, Memo dated 17 January 1972.
7. Nemergut, P.J. and Grand, R.S., "Axisymmetric Vibrations of Prolate Spheroidal Shells." Journal of the Acoustical Society of America, Vol.37, pp.262-265, 1965.
8. Mercier, J., "A Method for Computing Float-Platform Motions in Waves." Journal of Hydronautics, Vol.4, No.3, July 1970, pp.98-104.
9. Mercier, J., "Hydrodynamic Forces on Some Float Forms." Journal of Hydronautics, Vol.5, No.4, October 1971, pp.109-117.
10. Mercier, J., "Hydrodynamic Characteristics of Several Vertical Floats in Waves." Davidson Laboratory, Stevens Institute of Technology, Letter Report SIT-DL-70-1481, October 1970.
11. Thomson, W.T., Vibration Theory and Applications. Prentice-Hall, Inc. Englewood Cliffs, N.J., 1965.

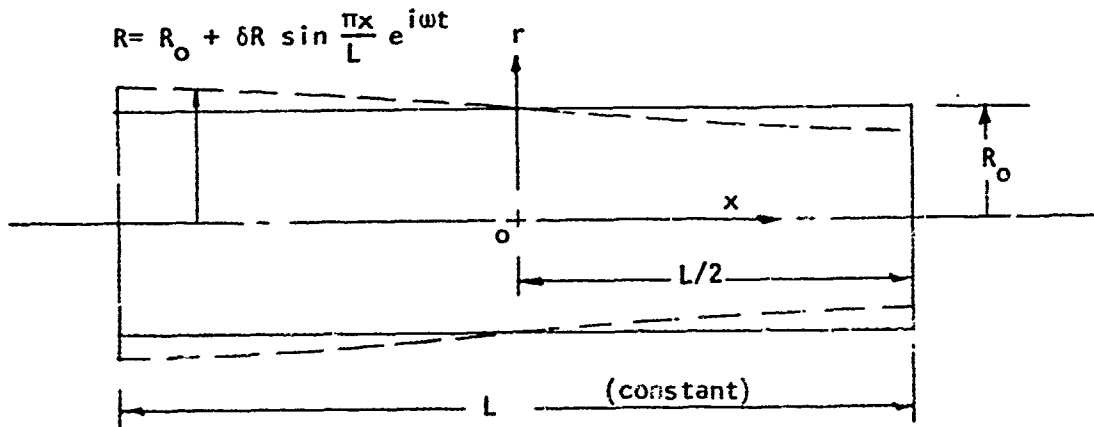
APPENDIX

ESTIMATION OF THE NATURAL FREQUENCY
OF A
FLUID-FILLED TUBULAR MEMBRANE

The lowest (fundamental) frequency of a dynamical system with distributed mass may be estimated with good accuracy by the energy method due to Rayleigh provided a reasonable approximation of the mode or pattern of displacements of the system can be made. Such an estimate will be somewhat greater than the true fundamental frequency.

An elementary model will be postulated which approximates the case of a slender tube filled with an incompressible fluid which is assumed to surge to-and-fro axially, in such a way that a periodic axial (inertial) force acts on the tube-fluid system. An analogy is intended with the slender water-filled float-attenuator system distorting under the action of an externally applied pressure distribution due to waves (having, in particular, an axial gradient) and thus experiencing a modification of the vertical wave-induced force transmitted to the deck. For the present analysis, only an estimate of the lowest natural frequency will be made so that by comparing with ocean wave frequencies, the possibility of unfavorable dynamic amplification can be discerned; it may be assumed that the distortion of the fluid filled tube due to pressure gradients will be unimportant unless magnified by resonant response.

Assume a circular cylindrical tube with length L and radius R_0 to be connected to end bulkheads having the special characteristic that they can stretch in their own plane but not deform normal to their plane. Water contained in the tube is assumed to surge periodically in the axial direction so that the tube bulges alternately over one half while contracting over the other half and vice-versa. The situation is depicted in the sketch



The flow of fluid within the tube can be assumed to be described by a velocity potential function which satisfies Laplace's equation, which can be expressed in cylindrical coordinates for axi-symmetric flow, as

$$\nabla^2 \varphi = \frac{\partial^2 \varphi}{\partial r^2} + \frac{1}{r} \frac{\partial \varphi}{\partial r} + \frac{\partial^2 \varphi}{\partial x^2} = 0 \quad (\text{A-1})$$

Assuming that the velocity potential has the form

$$\varphi = A \sin \frac{\pi x}{L} f(r) e^{i\omega t} \quad (\text{A-2})$$

fixes the mode of oscillation of the fluid and its containing membrane. The axial and radial velocities are obtained as

$$u_x = - \frac{\partial \varphi}{\partial x} = -A \cos \frac{\pi x}{L} f(r) e^{i\omega t} \quad (\text{A-3})$$

$$u_r = - \frac{\partial \varphi}{\partial r} = -A \sin \frac{\pi x}{L} f'(r) e^{i\omega t}$$

The boundary conditions which are to be satisfied are

$$u_x = 0 \quad \text{at } x = \pm L/2 \text{ (satisfied by assumed form of } \varphi) \quad (\text{A-4a})$$

$$u_r = 0 \quad \text{at } r = 0$$

$$u_r = \frac{dR}{dt} \quad \text{at } r = R_0 \quad (\text{A-4b})$$

The function $\bar{r}(r)$ is obtained as the solution of Eq. (A-1), subject to

the boundary conditions (A-4b). After separation of variables, the Laplacian reduces to

$$\frac{d^2 f}{dr^2} + \frac{1}{r} \frac{df}{dr} - \left(\frac{\pi}{L}\right)^2 f = 0 \quad (\text{A-5})$$

whose solutions are modified Bessel functions of order zero. For the boundary conditions (A-4b), of zero radial velocity at the axis, the modified Bessel functions of the first kind must be taken,

$$f(r) = C I_0 \left(\frac{\pi r}{L} \right) \quad (\text{A-6})$$

and the constant C is found from the boundary condition at the outer radius

$$u_r = \frac{dR}{dt} = -A \sin \frac{\pi x}{L} C \frac{\pi}{L} I_1 \left(\frac{\pi R_0}{L} \right) e^{i\omega t} \quad (\text{A-7})$$

Expressing the membrane deformation as

$$R = R_0 + \delta R \sin \frac{\pi x}{L} e^{i\omega t} \quad (\text{A-8})$$

$$\frac{dR}{dt} = i\omega \delta R \sin \frac{\pi x}{L} e^{i\omega t}$$

we obtain

$$C = \frac{i\omega \delta R L}{\pi A I_1 \left(\frac{\pi R_0}{L} \right)} \quad (\text{A-9})$$

or

$$\varphi = \frac{i\omega \delta R L}{\pi} \sin \frac{\pi x}{L} \frac{I_0 \left(\frac{\pi r}{L} \right)}{I_1 \left(\frac{\pi R_0}{L} \right)} e^{i\omega t} \quad (\text{A-10})$$

The kinetic energy of the internal flow can be obtained (cf. Lamb, Hydrodynamics, 6th Ed., 1932, reprinted by Dover Press 1945) as

$$T = -\frac{\rho}{2} \int \varphi \frac{\partial \varphi}{\partial n} dS \quad (\text{A-11})$$

where the integration extends over the moving surface. The result of this

operation is found as

$$\begin{aligned}
 T_{int} &= \frac{\rho}{2} (\omega \delta R)^2 \frac{L}{\pi} \frac{I_0 (\pi R_0 / L)}{I_1 (\pi R_0 / L)} \cdot \frac{L}{\pi} \int_{-\pi/2}^{\pi/2} \sin^2 \frac{\pi x}{L} \cdot 2\pi R_0 \cdot d\left(\frac{\pi x}{L}\right) \\
 &= \rho \frac{L^2 R_0}{2} (\omega \delta R)^2 \frac{I_0 (\pi R_0 / L)}{I_1 (\pi R_0 / L)} \quad (A-12)
 \end{aligned}$$

The kinetic energy of the membrane material itself is ignored since it is small compared to that of the fluid.

The elastic strain energy of the membrane can be readily evaluated, assuming axial strains are negligible compared to hoop strains, and ignoring strain energy in the end bulkheads, as

$$\begin{aligned}
 U &= \frac{Et}{2(1+\nu)(1-\nu)} \int_{-\pi/2}^{\pi/2} \left(\frac{\delta R}{R_0}\right)^2 \sin^2 \frac{\pi x}{L} \cdot 2\pi R_0 \cdot \frac{L}{\pi} d\left(\frac{\pi x}{L}\right) \\
 &= \frac{Et}{2(1+\nu)(1-\nu)} \cdot (\delta R)^2 \cdot \frac{\pi L}{R_0} \quad (A-13)
 \end{aligned}$$

where Et is the "membrane modulus" and ν is Poisson's ratio.

An estimate of the lowest natural frequency of a slender fluid-filled elastic tube of finite length may be obtained by equating the two kinds of energy (whose maximum values occur periodically out-of-phase with one another).

$$\omega^2 = \frac{\pi^2 Et}{\rho(1+\nu)(1-\nu)\nabla} \frac{I_1 (\pi R_0 / L)}{I_0 (\pi R_0 / L)} \quad (A-14)$$

where ∇ = enclosed volume = $\pi R_0^2 L$.

If external kinetic energy, due to a surrounding fluid, is to be taken into account, the analysis becomes somewhat more complicated. The assumption of a velocity potential $\phi \sim \sin \frac{\pi x}{L}$ to describe the external flow does not allow a suitable three-dimensional axial diffusion of the induced flow associated with finite-length effects unless some rather laborious analysis is pursued;

consequently, the participating fluid kinetic energy would be substantially overestimated. This analysis will not be carried out here. The natural frequency of a fluid-surrounded membrane is, of course, less than that of the membrane in vacuum.

TABLE 6

WAVE AND RESPONSE RESULTS
 RIGID MODEL
 (Epoxy-Coated Urethane Foam)
 Draft, T=12" 25 June 1972

RUN	PERIOD sec	FREQ 1/sec	WAVE AMPL ζ , in	HEAVE FORCE Z, lb	SURGE FORCE X, lb	HEAVE PHASE ϕ_z , deg ¹	SURGE PHASE ϕ_x , deg ²	DIMENSIONLESS RESPONSE		
								Z_w^3	X_w^4	$\omega \sqrt{\frac{T}{g}}^5$
1	0.785	1.274	0.445	0.156	0.671	192	111	0.775	3.33	1.411
2	0.718	1.393	0.491	0.162	0.766	192	117	0.728	3.44	1.543
3	0.843	1.186	0.552	0.165	0.720	184	103	0.684	2.99	1.314
4	0.930	1.075	0.516	0.157	0.616	198	106	0.671	2.64	1.187
5	1.014	0.986	0.521	0.133	0.564	194	100	0.563	2.39	1.093
6	1.133	0.883	0.550	0.116	0.540	193	101	0.466	2.17	0.978
7	1.258	0.795	0.454	0.056	0.459	192	103	0.320	2.23	0.881
8	1.441	0.694	0.599	0.034	0.408	205	97	0.148	1.50	0.769
9	1.736	0.576	0.504	0.038	0.302	350	84	0.166	1.32	0.638
10	2.083	0.480	0.465	0.082	0.134	356	116	0.389	0.64	0.532
11	0.780	1.282	0.472	0.152	0.667	191	110	0.711	3.12	1.420
12	0.716	1.397	0.499	0.163	0.774	192	117	0.722	3.42	1.547

Footnotes:

¹ Upward force lags wave crest² Surge force toward wavemaker lags wave crest³ $Z_w = \frac{Z}{\zeta} \cdot \frac{1}{\sqrt{A_w}}$, where γ = specific weight of water (0.0361 lb/in³), A_w = waterplane area⁴ $X_w = \frac{X}{\zeta} \cdot \frac{1}{\sqrt{A_w}}$ ⁵ $\omega \sqrt{\frac{T}{g}}$, $\omega = 2\pi \text{ Freq}$, T = draft, g = acceleration of gravity

TABLE 7
 WAVE AND RESPONSE RESULTS
 THICK PVC MODEL
 (No Bracing)
 Draft (Nominal), T=18" -- 6 July 1972

RUN	PERIOD	FREQ.	WAVE AMPL	HEAVE FORCE	SURGE FORCE	HEAVE PHASE	SURGE PHASE	DIMENSIONLESS RESPONSE		
	sec	1/sec	ζ , in	Z, lb	X, lb	ϕ_z , deg ²	ϕ_x , deg ²	Z_w^3	X_w^4	$w\sqrt{\frac{T}{g}}^5$
1	2.070	0.483	0.567	0.006	1.106	58	123	0.011	1.91	0.654
3	1.740	0.575	0.799	0.308	2.041	180	107	0.378	2.50	0.777
4	1.467	0.682	0.930	0.640	3.780	176	99	0.674	3.99	0.922
5	1.029	0.972	0.943	1.134	5.035	183	185	1.180	5.24	1.315
6	1.282	0.780	0.362	0.507	2.831	168	111	1.372	7.67	1.054
7	1.133	0.883	0.514	0.720	3.490	190	146	1.374	8.56	1.200
8	1.020	0.980	0.494	0.608	4.404	175	171	1.207	8.74	1.330
9	0.928	1.078	0.421	0.678	3.888	183	202	1.578	9.05	1.462
10	0.830	1.193	0.499	0.574	2.490	184	231	1.127	4.89	1.619
11	1.257	0.796	0.243	0.355	1.993	171	111	1.448	8.04	1.079
12	0.776	1.289	0.452	0.444	1.403	184	241	0.964	3.05	1.749
14	1.014	0.986	0.249	0.348	2.616	174	177	1.370	10.30	1.338

Footnotes: See Table 6

TABLE 8

WAVE AND RESPONSE RESULTS

THICK PVC MODEL
(With Bracing)

Draft (Nominal), T=18" - 7 July 1972

RUN	PERIOD	FREQ	WAVE AMPL	HEAVE FORCE	SURGE FORCE	HEAVE PHASE	SURGE PHASE	DIMENSIONLESS RESPONSE		
	sec	1/sec	ζ , in	Z, lb	X, lb	ϕ_z , deg ¹	ϕ_x , deg ²	Z_w^3	X_w^4	$\omega \sqrt{\frac{T}{g}}^5$
15	1.014	0.986	0.209	0.223	1.155	175	108	1.046	5.42	1.338
16	1.258	0.795	0.243	0.249	0.955	179	93	1.006	3.85	1.079
18	0.712	1.404	0.436	0.386	2.574	190	227	0.868	5.79	1.906
19	1.014	0.986	0.443	0.542	2.978	171	115	1.200	6.59	1.338
20	0.924	1.082	0.459	0.626	4.157	171	131	1.340	8.86	1.469
21	0.832	1.202	0.525	0.735	4.750	179	179	1.373	8.87	1.631
22	1.248	0.801	0.451	0.494	2.2	175	96	1.074	4.81	1.087
23	1.122	0.891	0.524	0.657	3.314	182	110	1.228	6.20	1.209
24	1.011	0.989	0.878	1.343	5.143	172	145	1.500	5.74	1.342
25	1.437	0.696	0.769	0.704	3.088	176	97	0.897	3.94	0.944
26	1.738	0.575	0.677	0.329	1.579	177	99	0.476	2.29	0.781
27	1.734	0.577	0.791	0.404	1.896	176	100	0.501	2.85	0.783
28	2.072	0.483	0.575	0.079	1.172	167	123	0.135	2.00	0.655
29	1.253	0.798	1.498	1.896	5.236	173	114	1.240	3.43	1.083

Footnotes: See Table 6

TABLE 9

WAVE AND RESPONSE RESULTS

THIN PVC MODEL
(With Bracing)Draft (Nominal), $T=18''$ - 7-11 July 1972

RUN	PERIOD	FREQ	WAVE AMPL	HEAVE FORCE	SURGE FORCE	HEAVE PHASE	SURGE PHASE	DIMENSIONLESS RESPONSE		
	sec	1/sec	ζ , in	Z, lb	X, lb	ϕ_z , deg ²	ϕ_x , deg ²	Z_w^3	X_w^4	$\omega \sqrt{\frac{T}{g}}^5$
31	1.789	0.559	0.633	0.390	2.613	171	111	0.605	4.05	0.759
33	1.448	0.691	0.773	1.578	5.100	190	195	2.000	6.47	0.937
34	1.023	0.978	0.896	1.780	3.716	191	234	1.920	4.07	1.326
35	1.268	0.789	0.434	1.103	4.496	190	196	2.590	10.16	1.070
36	1.135	0.881	0.531	1.245	3.688	197	225	2.300	6.81	1.196
37	1.017	0.983	0.462	0.926	2.248	189	234	1.970	4.77	1.334
38	0.920	1.087	0.461	0.906	1.581	185	239	1.930	3.36	1.475
39	0.830	1.205	0.473	0.869	0.813	177	240	1.800	1.68	1.634
40	1.261	0.793	0.288	0.711	2.583	193	212	2.420	8.79	1.076
41	0.775	1.290	0.453	0.823	0.393	180	238	1.780	0.85	1.751
42	0.710	1.408	0.503	0.768	0.326	176	189	1.500	0.64	1.911
43	0.716	1.397	0.308	0.499	0.126	179	188	1.590	0.40	1.895
44	1.006	0.994	0.241	0.523	0.833	1.86	239	2.130	3.39	1.349
45	1.432	0.698	0.406	0.862	2.518	189	214	2.080	6.08	0.948

Footnotes: See Table 6

TABLE 10

FORCED HEAVE OSCILLATION TESTS

THICK PVC MODEL

(With Bracing)

Draft (Nominal), T=18"

$\omega \sqrt{\frac{T}{g}}$	$\frac{\text{Added Weight}}{\text{Displaced Weight}}$
0.645	0.396
0.552	0.376
1.180	0.517
1.336	0.546
1.554	0.541
1.574	0.511
1.851	0.588
2.104	0.562
2.372	0.632
2.570	0.661

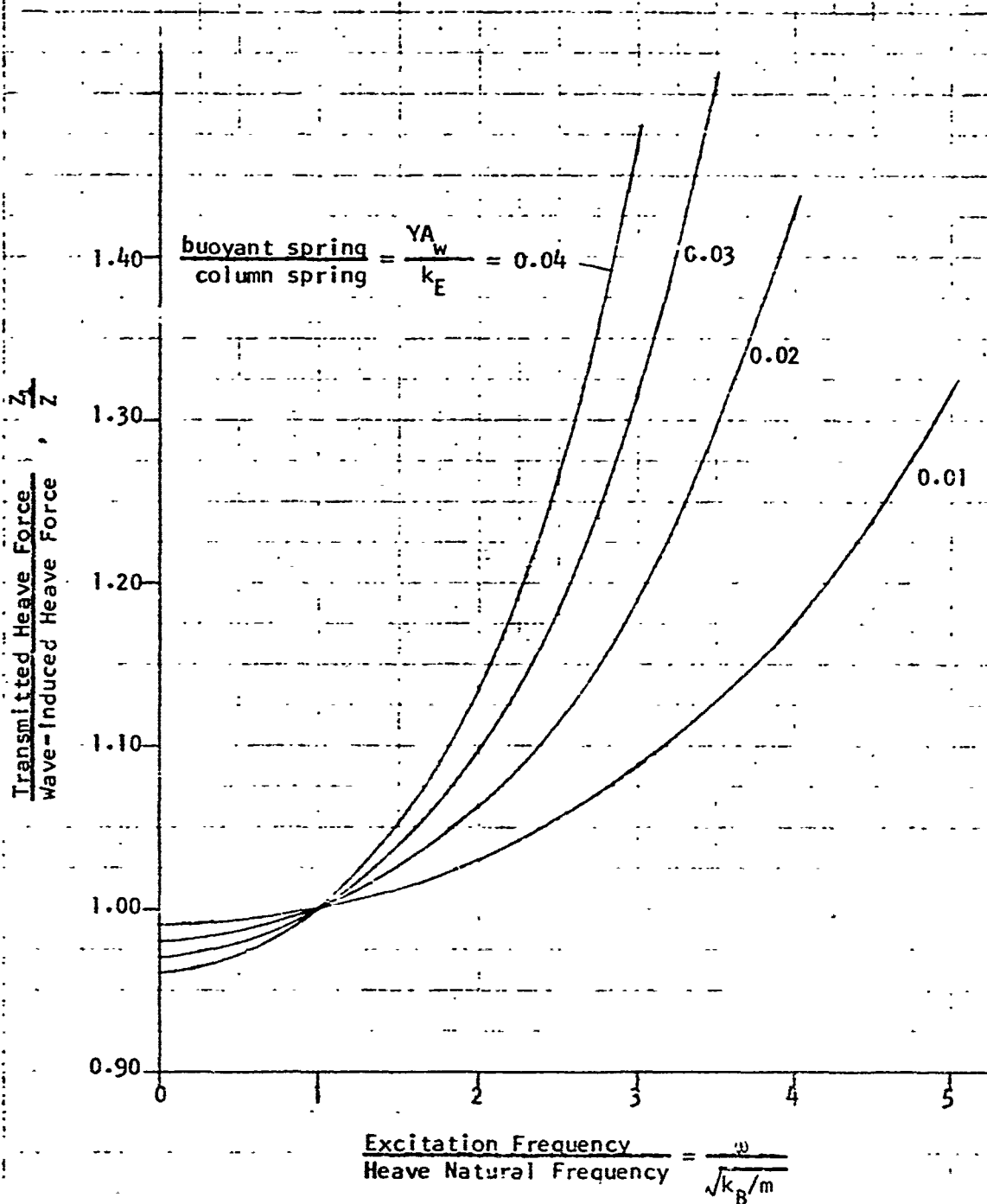


FIGURE 1. EFFECT OF COLUMN ELASTICITY ON HEAVE FORCE
MEASURED BY FIXED FORCE BALANCE

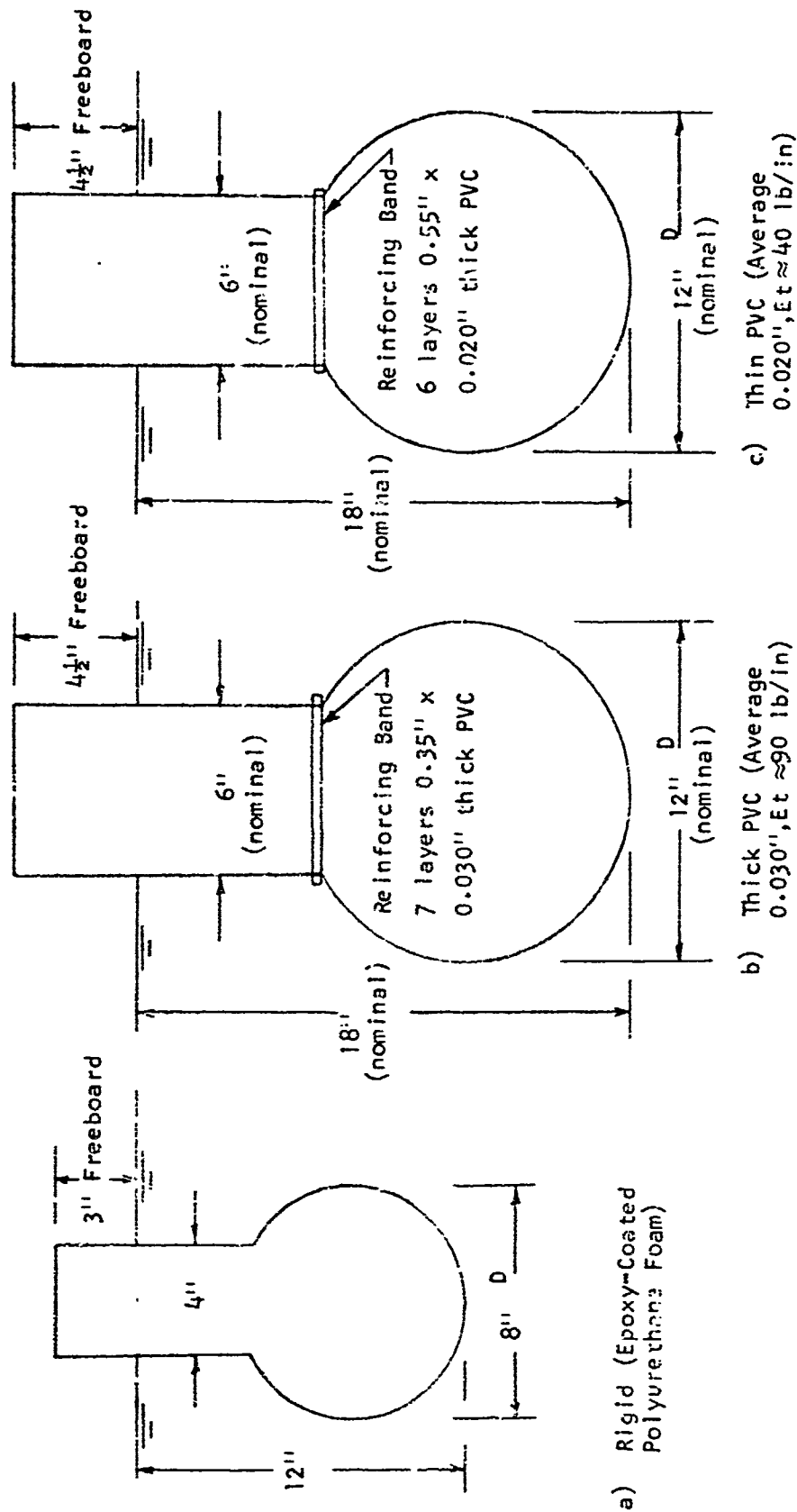


FIGURE 2. GEOMETRY OF MODELS

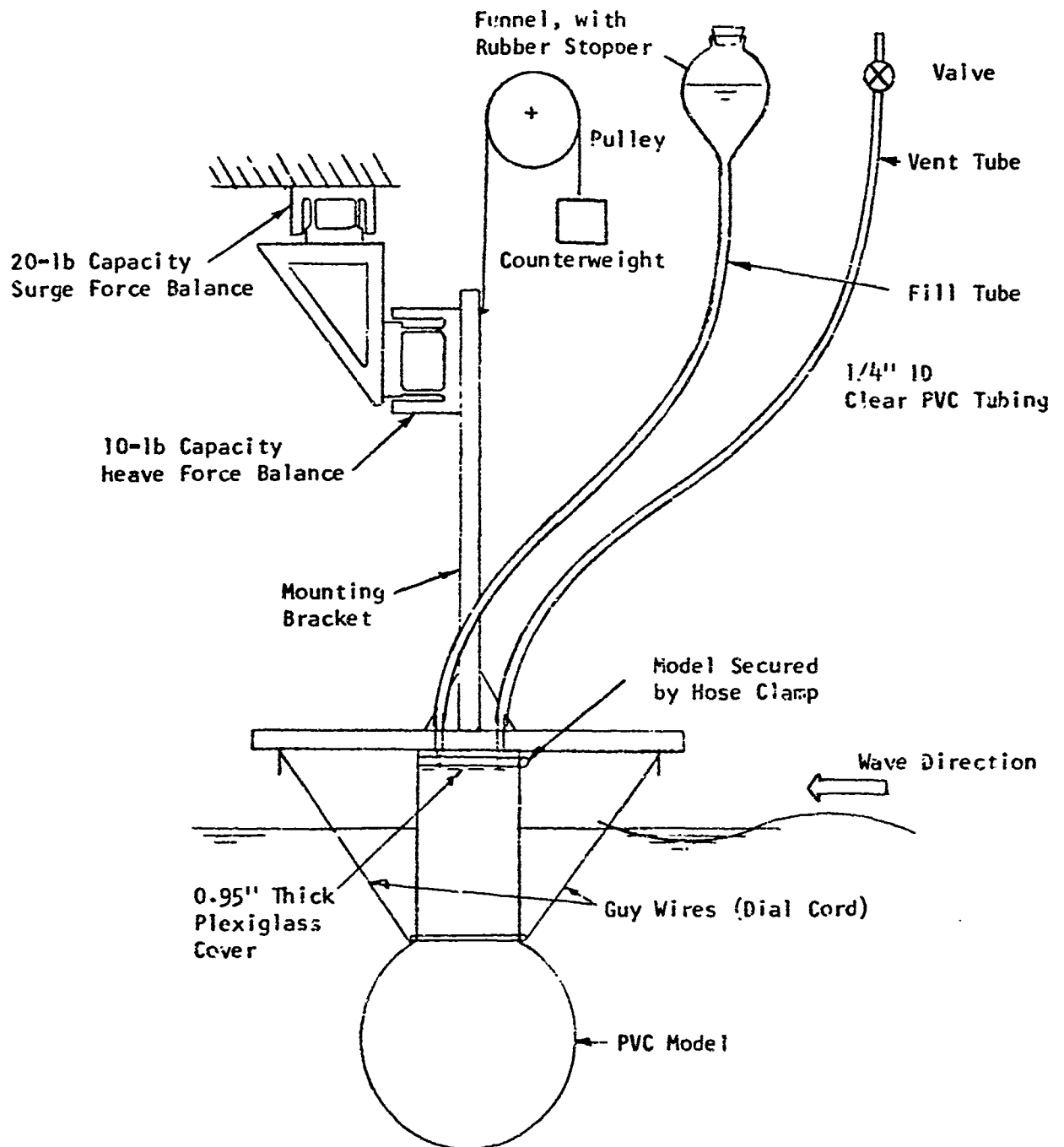


FIGURE 3. TEST SETUP, SHOWING FORCE BALANCES, MODEL SUSPENSION AND PRESSURIZATION

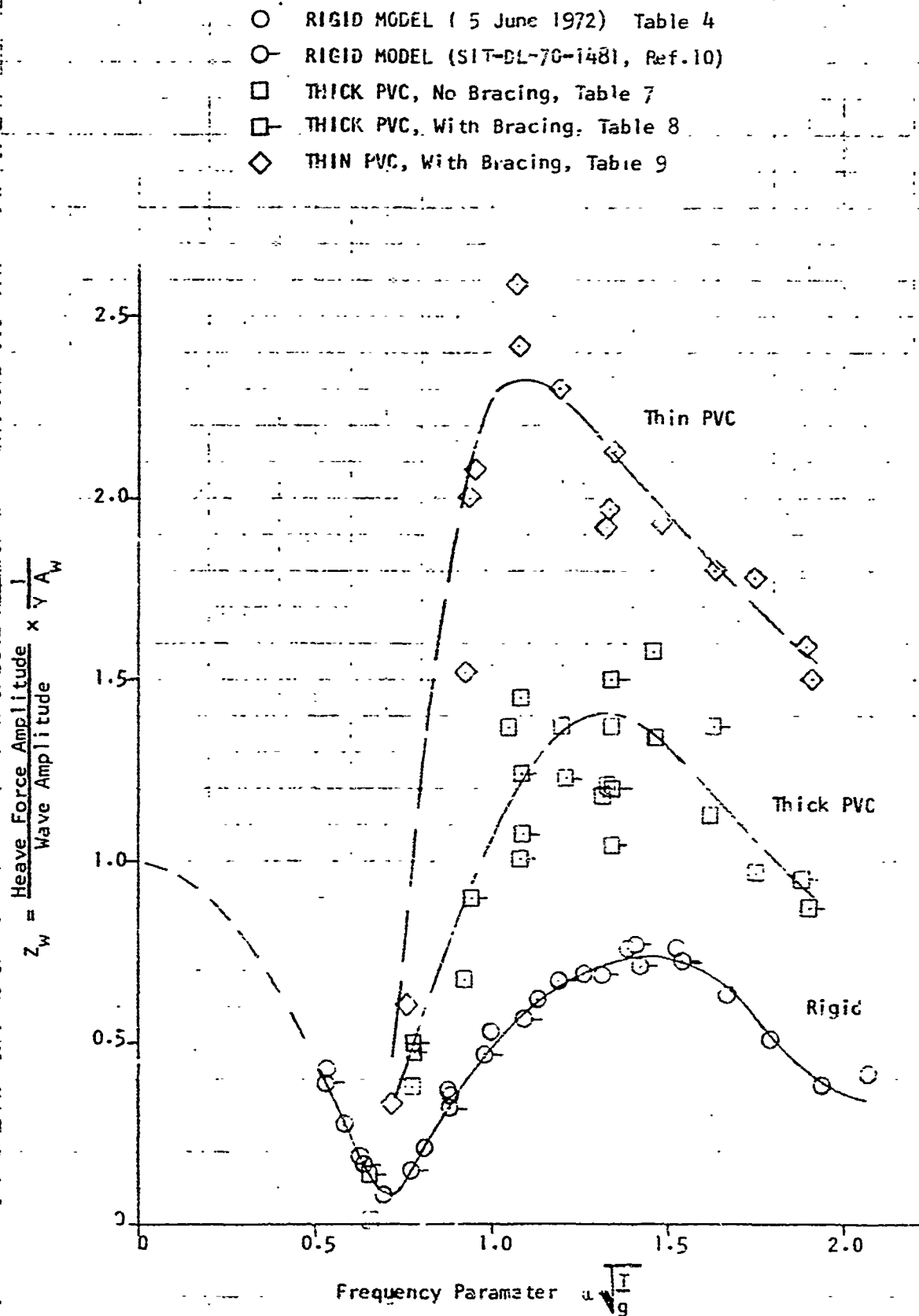


FIGURE 4. HEAVE FORCE DUE TO WAVES FOR CYLINDER-AND -SPHERE MODELS

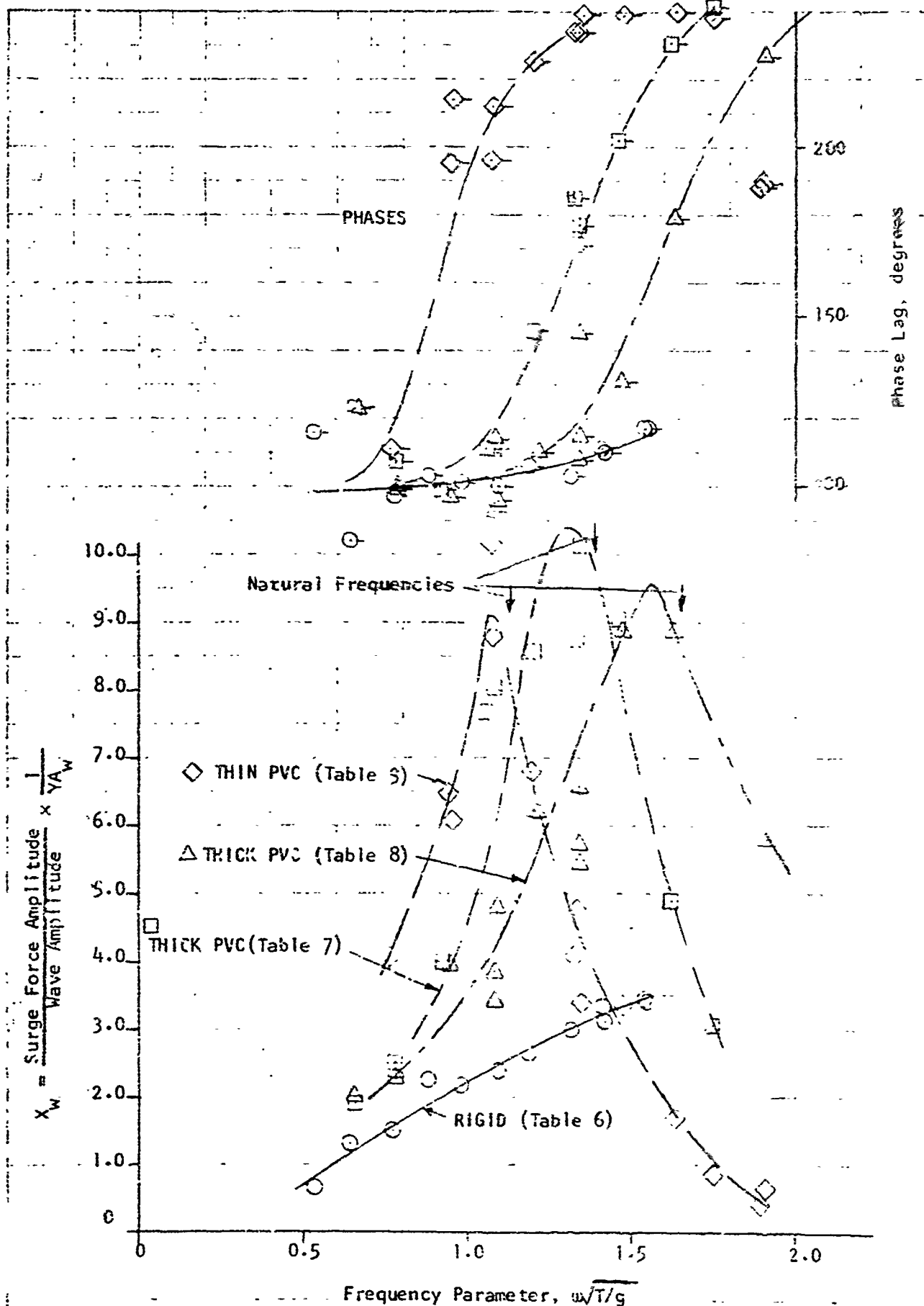


FIGURE 5. SURGE FORCE DUE TO WAVES FOR CYLINDER AND SPHERE MODEL

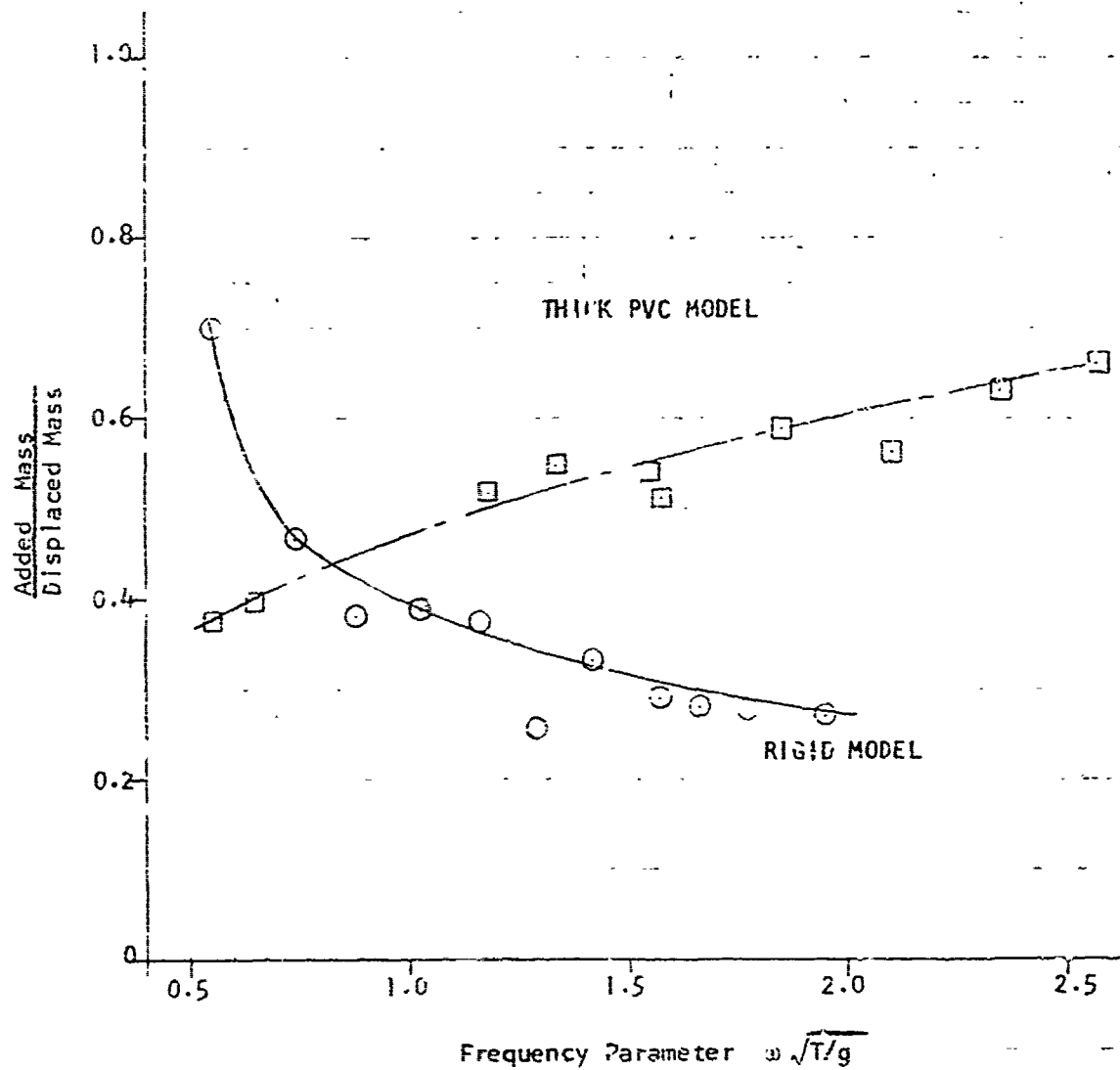


FIGURE 6. HEAVE ADDED MASS FOR CYLINDER AND SPHERE MODELS

APPENDIX I - HYDRODYNAMIC TESTS AND
ANALYSIS PROGRAM FOR EXPANDABLE FLOATING
BASES: PART 4 - LARGE SCALE MODEL TESTS OF
RESPONSE OF DEFORMABLE FLOATS

1. MODEL FABRICATION BY GAC

a. General

Float construction is discussed below prior to the test procedure and results provided in the Davidson Laboratory report, Item 2, below. Four significant items had to be determined before fabrication of the rigid and expandable test floats could be undertaken. These were:

1. Full-scale float dimensions and configuration
2. Float design basis: cantilever versus hinged
3. Model test scale
4. Materials of construction

b. Full-Scale Dimensions and Configuration

Based on data generated in the previous program - which did not, however, take into account the effects of interaction - an overall full-scale float length of 110 ft was chosen with float water plane diameter of 6 ft, slenderness ratio of 1.5 to 1, and the configuration described in Section III of this report.

c. Float Design Basis: Cantilever versus Hinged

Despite the preponderance of hydrodynamic data previously generated by this program and in the literature on cantilevered floats, a decision was made to hinge the test models, since reduction of the bending moment by this device so dramatically reduced pressurization requirements in an inflatable float construction with potentially commensurate reduction of cost. It had earlier been calculated that the heave forces acting on a hinged or cantilevered float of similar configuration would be the same, whereas surge forces could be grossly diminished by an articulated design.

d. Model Test Scale

A survey of tank test sites indicated that the Lockneed Underwater Missile Facility^a was best adapted to accomplishing wave tests in the time frame established by the program. Based on a full-scale overall float length of 110 ft, a test scale model of 1/8 appeared to be maximum for the tank dimensions and wave-making capabilities.

e. Materials of Construction

Selection of materials for the test units is related in the following description of the models.

Configuration and dimensions of the rigid float/attenuator assembly are shown in Section III. After evaluation of the characteristics of the water and air-inflatable model, which required duplication in the rigid unit - equivalent buoyancy, similar center of gravity, and center of percussion - it was apparent that a wood construction could more readily be fabricated and properly ballasted than metal. Pattern pine was selected because of availability and uniformity. Ballasting of the attenuator was accomplished by insertion of a steel cylinder and a lead-filled pipe at appropriate positions along the axis. To provide free hinge movement in any direction of the attenuator relative to the float, a ball and socket-type automotive universal joint was employed. Weight of the assembly, including all fittings was 355.2 lb in air and 15.0 lb in water.

A common mounting platform was fabricated to join either rigid or flexible float assemblies to the Davidson Laboratory instrumentation package. The platform comprised an interface hub that joined three equally spaced booms to which were attached cable trusses to stabilize the upper floats, both rigid and inflatable.

The fundamental design problems associated with the inflatable floats were determination of inflation pressure and fabric strength. These were resolved by evaluation of the data given below:

The bending moment was calculated at a point located six feet below the water

^a A description of this facility is provided in Appendix E.

line where the cable truss is to be attached. Bending moment is considered most severe here because of the cantilever effect of the stub extending below this point.

Maximum strength required is 111 lb/in. quick break, occurring circumferentially in the attenuator. Calculations supporting this strength are shown in the main body of the report. This value is considered conservative in regard to a full-scale design. Full-scale design would optimize the hinge and truss location to provide for a reduced stress on the float fabric. Note, however, that the geometry of the float considered here does not identically match the model float from which the test data were taken. Differences in the float are judged unimportant in regard to the forces of interest on the basis of extrapolation of other test data.

It was decided to fabricate two inflatable floats for test purposes in the event that one might be damaged at the test site, which was so remote from the fabrication shop. Each of these was manufactured by cutting patterns to evolve a specific geometric area and then adhesively bonding in lap joints. Sewing was additionally employed in fabricating the necked down "hinge" section between the float and attenuator.

Two different rubberized fabrics were used for each model. The unit tested was fabricated of N313A40, a calendered neoprene/nylon airship fabric with quick break strength of 165×180 lb/inch. The backup model employed N313A140, also a neoprene impregnated nylon fabric with quick break strength of 225×240 lb/inch.

The float and attenuator are individually compartmented; a hemispherical diaphragm above the hinge separates the water-filled attenuator from the air- and water-inflated float. Volume of water in the float is determined by degree of buoyancy required. Whereas earlier float concepts had envisaged a water-filled stand pipe connected to the attenuator to vary its pressure with wave passage, it was decided to pressurize positively both float and attenuator of the test mode by application of pneumatic pressure in the float, which could be transmitted through the domed diaphragm to the water-filled attenuator. Pressure level in both was read out through gages connected to water- and air-fill lines. Drain tubing was also provided for

both chambers. Fill and drain tubing in the models was vinyl water hose. Both terminated in female fittings connected to the float upper plate - an aluminum disk, which was bonded and clamped to the end of the float cylinder. Structural connection to the test mounting platform was made through this plate.

2. DAVIDSON LABORATORY TEST RESULTS

Part 4 of the Davidson Laboratory test program is presented on the following pages.

STEVENS INSTITUTE OF TECHNOLOGY
DAVIDSON LABORATORY
CASTLE POINT STATION
HOBOKEN, NEW JERSEY

Letter Report SIT-DL-72-1631

October 1972

HYDRODYNAMIC TESTS AND ANALYSIS PROGRAM
FOR EXPANDABLE FLOATING BASES


PART 4

Large Scale Model Tests
of Response of Deformable Floats

by Edward Numata

Prepared for
Goodyear Aerospace Corporation
Akron, Ohio 44315
GAC P.O.2B 1115YK
(DL Project 3950/756)

Approved


Daniel Savitsky
Assistant Director

INTRODUCTION

The objective of this experimental investigation was to measure the wave forces acting on two 1/8-scale captive models of a float configuration proposed for use in a multi-float array forming an Expandable Floating Base. The basic unit consists of a surface-piercing vertical cylinder called a "float," to which is hinged at its lower end a cylindrical "attenuator" which has a slight excess of weight over buoyancy.

One model was made of fabric and designed to provide scaled simulation of prototype fabric thickness, strength, and stiffness. The float portion was pressurized with air and the attenuator was filled with water under pressure.

The second model was constructed of wood with the attenuator being ballasted to simulate the mass and inertia characteristics of the fabric attenuator. This model was representative of the type of construction used for 1/48 and 1/57.6-scale models of float arrays for parallel investigations conducted at Davidson Laboratory (DL). Thus, a comparison between the measured forces on the two 1/8-scale models should reveal whether or not a rigid-walled model is a satisfactory representation, hydrodynamically, of a fabric model. Results can also be compared to analytical predictions of wave forces, and can provide needed information for design of prototype structures.

This work constituted Part 2 of Phase b "Response of Deformable Floats; Large Scale Model Tests," performed by Davidson Laboratory (DL) for Goodyear Aerospace Company (GAC) under Purchase Order 281115YX as amended in September 1972. The testing was performed at the Lockheed Underwater Missile Test Facility (LUMF), Sunnyvale, California, during the period July 17-22, 1972.

MODELS AND APPARATUS

The 1/8-scale models were constructed by GAC; their dimensions and configuration are shown in Figures 1 and 2 from GAC publication GAP-72-5652S8. Each model could be bolted to a mounting flange fitted with three horizontal outrigger booms for attaching the guy wire cables to the float.

The mounting flange was bolted to a DL three-component balance mounted on the LUMF carriage. Rated capacities of the balance were

Vertical force	± 50 lb
Horizontal force	± 500 lb
Pitch moment	± 250 ft-lb

The axis for moments was located 1.15 inches above the top surface of the aluminum cap of each model (see Figures 1 and 2).

Each model together with the mounting flange and outriggers had a weight in excess of its displacement, thus causing a downward bias force on the balance system. Since this static force exceeded the vertical force capacity of the balance, a simple 5:1 lever was fitted to provide unloading of the bias force. Figure 3 shows the general setup in the LUMF basin.

In addition to the two forces and one moment, the following measurements were made:

4. Wave elevation abreast of model: resistance-type probe, ± 7.5 inches range.
- 5,6 Tension in forward (0°) and one aft (120°) guy cable: load cells, 500-lb range.
- 7a. Horizontal force at hinge of wood model: strain gage link, 100-lb range.
- 7b. Pressure variation in water in fabric attenuator: strain gage pressure gage, 5psi range.

Signals from the transducers were amplified by a Sanborn 350 Series signal conditioning unit and recorded simultaneously in analog form on magnetic tape and Visicorder chart paper. These instruments were furnished by the DL instrument pool.

Pressures in the upper and lower sections of the fabric model were adjusted and monitored through a filling system equipped with dial-type pressure gages.

The model was positioned on the centerline of the LUMF basin about 100 feet from the bulkhead-type wave generator and about 60 feet from the wave-absorbing beach. The tank cross-section was 15'x15'. Two 16mm movie cameras supplied by LUMF were mounted behind underwater viewing windows directly abreast of the model. Above-water lighting was used. A synchronizing signal for the start of each data run appeared as a voltage pulse on both the magnetic tape and chart paper records and as a small light source in the movie background. The upper camera viewed the hinge area of each model; the lower camera viewed the middle 2/3 length of the attenuator.

TEST PROCEDURE

The test crew consisted of the following:

<u>Name</u>	<u>Organization</u>	<u>Responsibility</u>
John Burkley	GAC	Models
Bill Conley	GAC	Models
Ed Numata	DL	Test Program
Jim Starrett	DL	Instrumentation
John Bard	LUMF	Test Operations Supervisor
Bob Smith	LUMF	Photographer
Lee Guilford	LUMF	Test Technician

The sequence of testing in regular waves covered these four phases:

1. Wood model, hinged
2. Wood float without attenuator
3. Wood model cantilevered
4. Fabric model

Wave periods covered the range from 1.5 to 4.0 seconds and heights ranged from 6 to 12 inches. Run lengths for recording purposes were regulated to

give at least 4 wave encounters for the 4 second wave, and 8 encounters for the 1.5 second wave. At a wave period of 2.3 seconds, several wave heights were used to check linearity of responses.

Attempts were made to record natural frequencies of various modes of model vibration. The results are summarized as follows:

Model	Mode	Freq. 1/sec	Remarks
Wood	Heave	4.3	Model plus balance system
	Surge	1.7	Model plus balance system
Fabric	Heave	7.7	Float plus balance system
	Heave	2.5	Attenuator-hinge
	Surge	1.0	Model plus balance system

The fabric model has a fabric hinge which allows relative vertical motion between the float and the attenuator. Thus there are two distinct heave frequencies, as listed. The first higher frequency is for the float plus balance system without the attenuator, i.e., the attenuator mass is isolated due to the hinge. This frequency was isolated by striking the mounting flange above the float. The second frequency is associated with a spring-mass system consisting of the hinge as a spring, and the attenuator mass. The upper end of the attenuator was struck a vertical blow and the resulting vertical oscillation record showed the two frequencies superimposed.

DATA REDUCTION AND RESULTS

The Visicorder chart records were read by hand during the course of testing to obtain preliminary trends of test results. Upon returning to DL, the magnetic tape records were processed on the in-house PDP-8E digital computer. An existing computer program made use of the analog-to-digital conversion capability of the machine and performed a Fourier analysis of the regular waves and the six responses to produce an output consisting of the amplitude of the fundamental of each of the seven quantities, as well as the phase lag of each response referred to the wave.

The motion pictures were analyzed on a film reader to obtain amplitudes of angular motion. It was observed that the attenuator of each model tended to oscillate both at wave frequency and at its own natural frequency, the latter oscillation becoming quite large in the longer waves.

Table 1a lists the amplitudes of the fundamental harmonics for the wood model; Table 1b lists phase lags for these results. Table 2a shows amplitudes and Table 2b lists phases for the fabric model. All amplitudes are model scale. Table 3 lists angular motion amplitudes. The sign conventions used for phase evaluations are:

+ wave	crest
+ heave force	upward
+ surge force	toward wavemaker
+ pitch moment	tends to pitch float bottom toward wave-maker
+ tensions	increases in cable tension
+ hinge force	toward wavemaker
+ attenuator pressure	increase in pressure

Figure 4 shows a comparison of vertical or heave force for the hinged wood and fabric models on a base of wave frequency; also shown is an analytical prediction. Figure 5 is a similar plot of horizontal or surge force vs. wave frequency. Both force amplitudes have been divided by wave amplitude in Figures 4 and 5. Results are presented in non-dimensional form, with force amplitude per unit wave amplitude divided by $\rho g \times \text{waterplane area}$ ($\rho g \times A_p = \text{static heave force rate}$) given as functions of the frequency parameter $\omega/\text{draft}/g$, where $\omega = 2\pi$ frequency.

In the course of testing the cantilevered wood model, it was found that surge forces were extremely large, causing appreciable deflection of the model-plus-balance system. Even when wave heights were reduced to about 2 inches (1-inch amplitude), significantly larger deflections than for the hinged model were observed. We are reasonably certain that dynamic coupling occurred between the various component force balance units, giving unreliable results. Heave forces, which in principle should have been the

same as for the hinged model, were over twice as large. Surge forces were characterized by unpredictable trends also. Thus, we believe that these data are meaningless and we have not reported them.

The difference between the surge force response of the fabric and the wood models may be at least partly due to dynamic effects. The discrepancy is greatest at higher frequencies which are noted to be fairly close to the recorded natural frequency in surge of the fabric model plus balance system, namely $f_n \approx 1.0$ Hz. The details of the mode of response are not known. From the elementary theory of vibration isolation (cf., Thomson, Vibration Theory and Applications, Prentice Hall Inc., Englewood Cliffs, N.J., pp.64-66), the ratio of transmitted force to periodic excitation force for a sprung mass system may be written approximately (neglecting damping) as

$$TR = \frac{F_T}{F_E} = \frac{1}{1 - \left(\frac{\omega}{\omega_n}\right)^2}$$

Since the wood model also has a fairly low natural frequency ($f_n \approx 1.7$ Hz), dynamic effects on its response should not be neglected. Assuming the excitation forces are similar for both models, the fabric model response may be estimated from the wood model response:

$$\frac{x_{\text{fabric}}}{x_{\text{wood}}} = \frac{1 - \left(\frac{f}{1.7}\right)^2}{1 - \left(\frac{f}{1.0}\right)^2}$$

The following table compares the measured surge force (per unit wave height) for fabric model with calculated values obtained from the wood model results and the foregoing approximate dynamic response formula:

Freq	$\frac{x}{(G)}_{\text{wood}}$	$\frac{x}{(G)}_{\text{fabric}}$ calculated	$\frac{x}{(G)}_{\text{fabric}}$ measured
0.4	2.86	3.22	4.00
0.55	3.92	5.03	5.90
0.65	5.20	7.68	7.50

Although the agreement is not perfect, it is much improved and it must be considered that dynamic effects account for most of the difference between the surge force responses of the wood and the fabric models. An explanation of the lower resonant frequency of the fabric model may be found in the lower bending rigidity of the fabric "beam," which may be importantly affected by the details of the guy-wire bracing system used for any particular application.

Dynamic effects also partially account for the discrepancy between the measured surge force phase and the anticipated value, around 90 degrees.

ACKNOWLEDGMENT

The very helpful cooperation and assistance of the staff of the LUMF Facility as well as members of the GAC staff made it possible to accomplish this arduous test program expeditiously and effectively. The discussion of the dynamic effects on surge force response was prepared by J. Mercier.

TABLE 1a

WAVE AND RESPONSE AMPLITUDES
WOOD MODEL

RUN	PERIOD sec	FREQ 1/sec	WAVE ζ , in	HEAVE FORCE z, lb	SURGE FORCE x, lb	PITCH MOMENT ft-lb	0° TENSION lb	HINGE FORCE lb	DIMENSIONLESS Z_w^1	X_w^2	RESPONSE $\omega \sqrt{\frac{T}{g}}^3$
<u>FLOAT AND HINGED ATTENUATOR</u>											
1	1.48	0.675	2.12	1.22	11.90	44.4	1.37	1.75	0.250	2.43	2.36
2	1.49	0.670	2.20	1.17	11.93	44.4	0.51	1.84	0.230	2.35	2.35
3	2.00	0.500	5.54	2.04	18.84	73.4	2.35	0.08	0.161	1.48	1.75
4	2.32	0.430	5.50	2.21	19.70	77.2	1.21	4.80	0.174	1.56	1.51
9	2.32	0.430	4.24	1.86	17.16	67.1	0.79	4.10	0.191	1.76	1.51
10	2.34	0.430	7.17	3.19	27.96	108.4	2.99	6.70	0.193	1.70	1.51
5	2.57	0.390	6.80	1.86	17.28	69.8	2.30	4.39	0.117	1.11	1.37
6	2.98	0.335	6.99	1.13	13.09	51.8	2.20	3.62	0.070	0.80	1.17
7	3.62	0.275	5.64	2.62	10.85	44.9	5.08	2.94	0.202	0.83	0.96
8	4.08	0.245	5.92	4.42	7.25	29.0	5.19	1.88	0.324	0.52	0.86

FLOAT ONLY

11	2.33	0.430	5.62	7.02	14.82	54.6	1.22	-	0.543	1.15	1.51
12	2.96	0.340	7.55	11.50	9.80	37.7	1.01	-	0.660	0.57	1.19
13	3.99	0.250	6.75	12.34	6.44	25.0	2.71	-	0.795	0.41	0.89
14	1.52	0.660	3.75	2.47	16.14	59.1	0.99	-	0.287	1.87	2.34

Footnotes:

$$^1 Z_w = \frac{Z}{\zeta} \cdot \frac{1}{YA_w}, \text{ where } Y = \text{specific weight of water (0.0361 lb/in}^3\text{)} \\ A_w = \text{waterplane area}$$

$$^2 X_w = \frac{X}{\zeta} \cdot \frac{1}{YA_w}$$

$$^3 \omega \sqrt{\frac{T}{g}}, \text{ where } \omega = 2\pi \text{ Freq, } T = \text{draft (10 ft), } g = \text{acceleration of gravity}$$

TABLE 1b
 RESPONSE PHASE LAGS RELATIVE TO WAVES
 WOOD MODEL

RUN	PERIOD sec	FREQ 1/sec	HEAVE deg	SURGE deg	PITCH MOMENT deg	0° TENSION deg	HINGE FORCE deg
<u>FLOAT AND HINGED ATTENUATOR</u>							
1	1.48	0.675	90	346	84	164	22
2	1.49	0.670	95	350	87	172	23
3	2.00	0.500	134	31	102	183	183
4	2.32	0.431	122	28	89	189	37
9	2.32	0.421	125	28	89	203	32
10	2.34	0.427	129	35	95	227	30
5	2.57	0.390	128	42	96	203	45
6	2.98	0.335	60	39	88	253	45
7	3.62	0.275	25	51	93	261	55
8	4.08	0.245	13	61	98	177	83
<u>FLOAT ONLY</u>							
11	2.33	0.429	7	31	94	237	312
12	2.96	0.340	2	41	95	323	82
13	3.99	0.251	1	64	107	140	130
14	1.52	0.660	39	354	89	167	243

TABLE 2a

WAVE AND RESPONSE AMPLITUDES
FABRIC MODEL

RUN	PERIOD sec	FREQ 1/sec	WAVE C, in	HEAVE FORCE z, lb	SURGE FORCE x, lb	PITCH MOMENT ft-lb	0° TENS. lb	120° TENS. lb	ATTEN. PRESS. psi	DIMENSIONLESS Z_w^1	RESPONSE X_w^2	$\omega \sqrt{\frac{T}{g}}^3$
<u>AIR AND WATER PRESSURES 4.11 psi</u>												
21	1.51	0.660	2.81	1.24	28.1	99.8	20.4	13.2	0.05	0.181	4.10	2.31
35	1.51	0.660	4.25	2.47	32.9	124.9	25.6	19.3	-	0.238	3.17	2.31
22	2.00	0.500	4.52	1.74	23.7	84.3	17.4	9.2	0.03	0.158	2.15	1.75
23	2.30	0.435	4.14	2.09	21.2	75.7	16.1	9.9	0.04	0.207	2.10	1.52
29	2.27	0.440	6.24	4.06	30.6	111.1	22.6	15.4	0.05	0.267	2.01	1.54
24	2.61	0.385	4.80	1.22	16.4	60.0	13.6	7.2	0.05	0.104	1.40	1.35
25	2.99	0.335	4.64	0.49	9.4	32.0	6.1	3.8	0.06	0.043	0.83	1.17
26	3.64	0.275	3.91	1.93	7.9	26.1	6.1	2.9	0.07	0.202	0.83	0.96
34	3.65	0.275	4.01	1.86	8.6	29.2	2.8	3.6	-	0.190	0.88	0.96
28	4.03	0.250	3.80	2.64	5.0	17.6	9.5	1.8	0.08	0.270	0.54	0.88
<u>WATER PRESSURE 2.25 psi, AIR PRESSURE 4.11 psi</u>												
30	2.24	0.445	4.66	2.98	23.4	84.0	17.4	10.8	0.02	0.262	2.06	1.56
31	2.92	0.340	4.43	0.60	10.8	38.6	8.8	4.5	0.03	0.560	1.00	1.19
32	3.87	0.260	5.64	3.46	9.7	34.5	8.6	4.4	0.05	0.614	0.71	0.91
<u>AIR AND WATER PRESSURES 2.25 psi</u>												
33	3.90	0.255	5.70	3.46	9.3	33.0	10.2	4.0	0.11	0.249	0.674	0.89

Footnotes ^{1,2,3}: See Table 1a

TABLE 2b

RESPONSE PHASE LAGS RFLATIVE TO WAVES

FABRIC MODEL

RUN	PERIOD sec	FREQ 1/sec	HEAVE deg	SURGE deg	PITCH MOMENT deg	0° TENSION deg	120° TENSION deg	ATTEN. PRESSURE deg
<u>AIR AND WATER PRESSURES 4.11 psi</u>								
21	1.51	0.660	91	356	90	178	90	191
35	1.51	0.660	115	352	86	174	94	355
22	2.00	0.500	145	34	104	210	95	248
23	2.30	0.435	135	34	96	217	99	272
29	2.27	0.440	135	40	102	214	108	288
24	2.61	0.385	129	45	99	224	96	284
25	2.99	0.335	52	42	89	222	91	299
26	3.64	0.275	8	55	93	179	100	305
34	3.65	0.275	13	50	87	230	91	107
28	4.03	0.250	12	55	90	237	79	318
<u>WATER PRESSURE 2.25 psi, AIR PRESSURE 4.11 psi</u>								
30	2.24	0.445	135	37	99	216	109	265
31	2.92	0.340	77	35	82	213	81	287
32	3.87	0.260	11	53	92	269	94	307
<u>AIR AND WATER PRESSURES 2.25 psi</u>								
33	3.90	0.255	9	51	91	251	91	314

TABLE 3

ANGULAR MOTION OF ATTENUATOR

WOOD MODEL					FABRIC MODEL				
RUN	WAVE PERIOD sec	WAVE AMPL in	AMPL A deg	AMPL B deg	RUN	WAVE PERIOD sec	WAVE AMPL in	AMPL A deg	AMPL B deg
2	1.49	2.20	0.2	2.0	21	1.51	2.81	1.8	3.0
3	2.09	5.54	1.2	4.5	22	2.00	4.52	1.7	4.0
4	2.32	5.50	1.2	4.2	23	2.30	4.14	2.0	3.5
9	2.32	4.24	1.3	4.5	29	2.27	6.24	3.0	*
10	2.34	7.17	2.0	3.2	24	2.61	4.80	*	4.7
5	2.57	6.80	2.1	5.0	25	2.99	4.64	2.0	3.0
6	2.98	6.99	2.2	5.0	26	3.64	3.91	2.4	4.2
7	3.62	5.64	4.0	6.0	28	4.03	3.80	2.7	5.0
8	4.08	5.92	4.0	4.0					

Amplitude A refers to motion at wave period.

Amplitude B refers to motion at natural period of attenuator.

Natural Periods: Wood Model 15.5 sec

Fabric Model 15.0 sec

* Could not be determined due to insufficient data

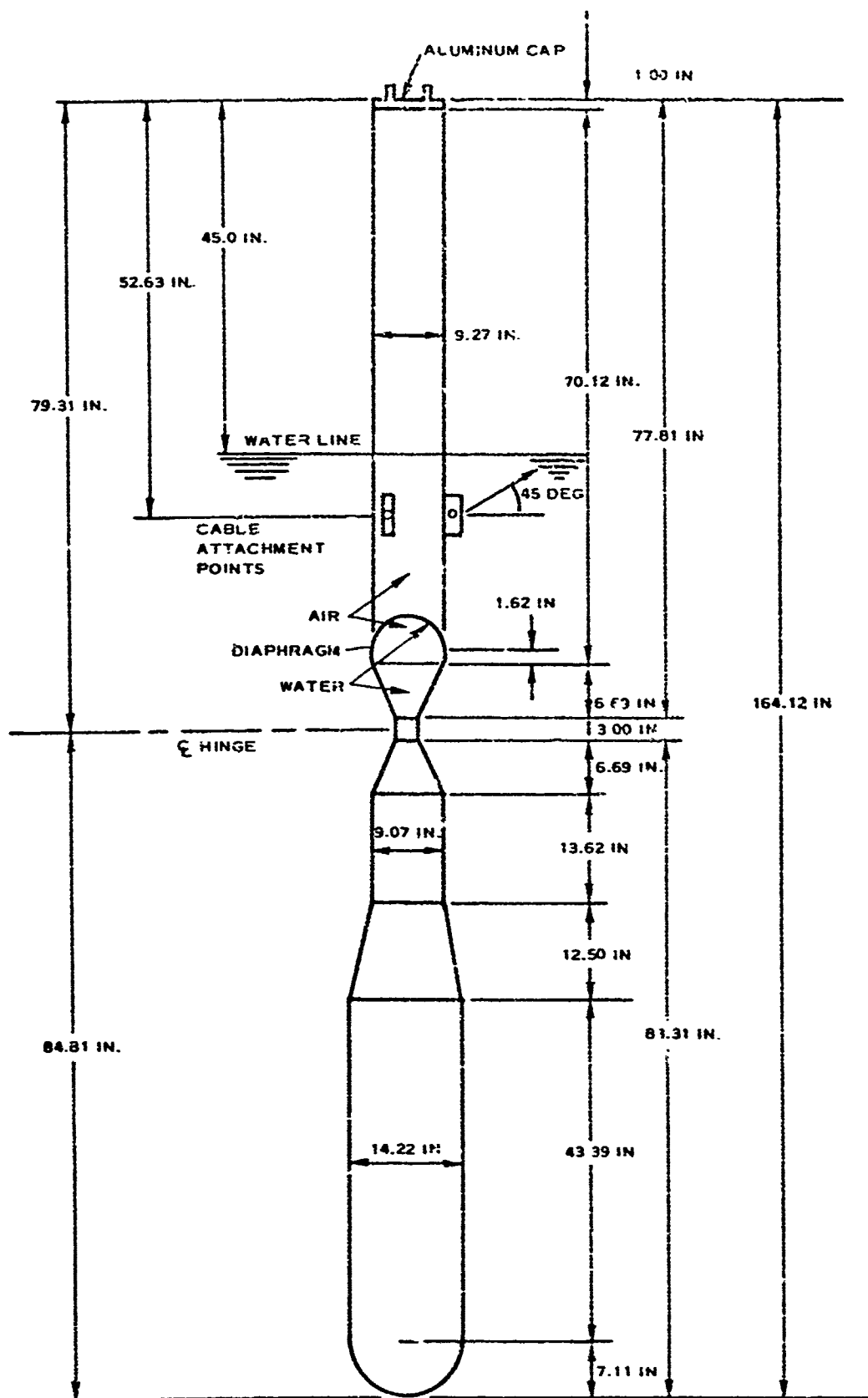


FIGURE 1. FABRIC MODEL DIMENSIONS (1/8 Scale)
(From GAP-72-5652S8)

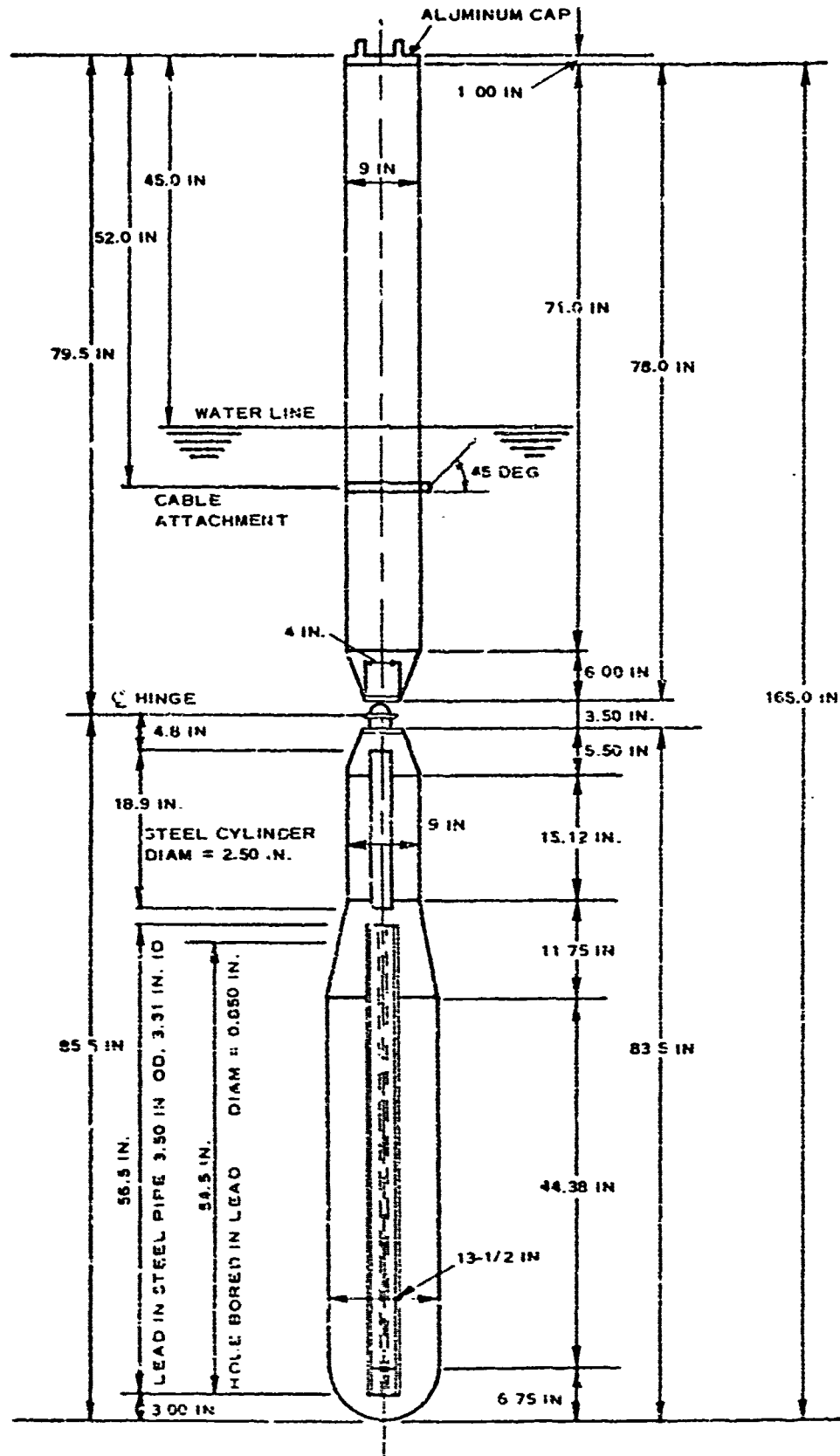


FIGURE 2. WOOD MODEL DIMENSIONS (1/8 Scale)
(From GAP-72-5652SS)

LR-1631

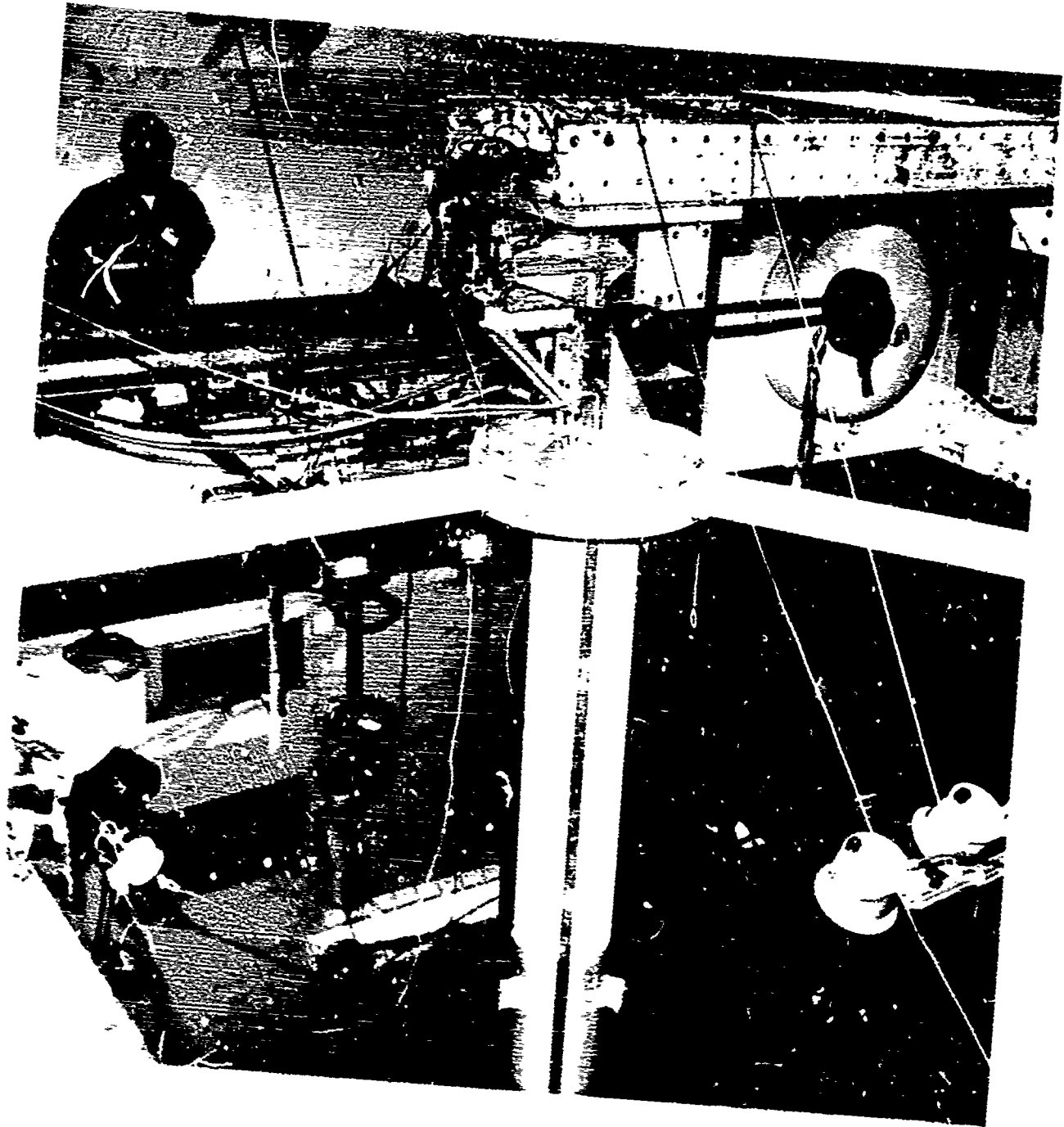
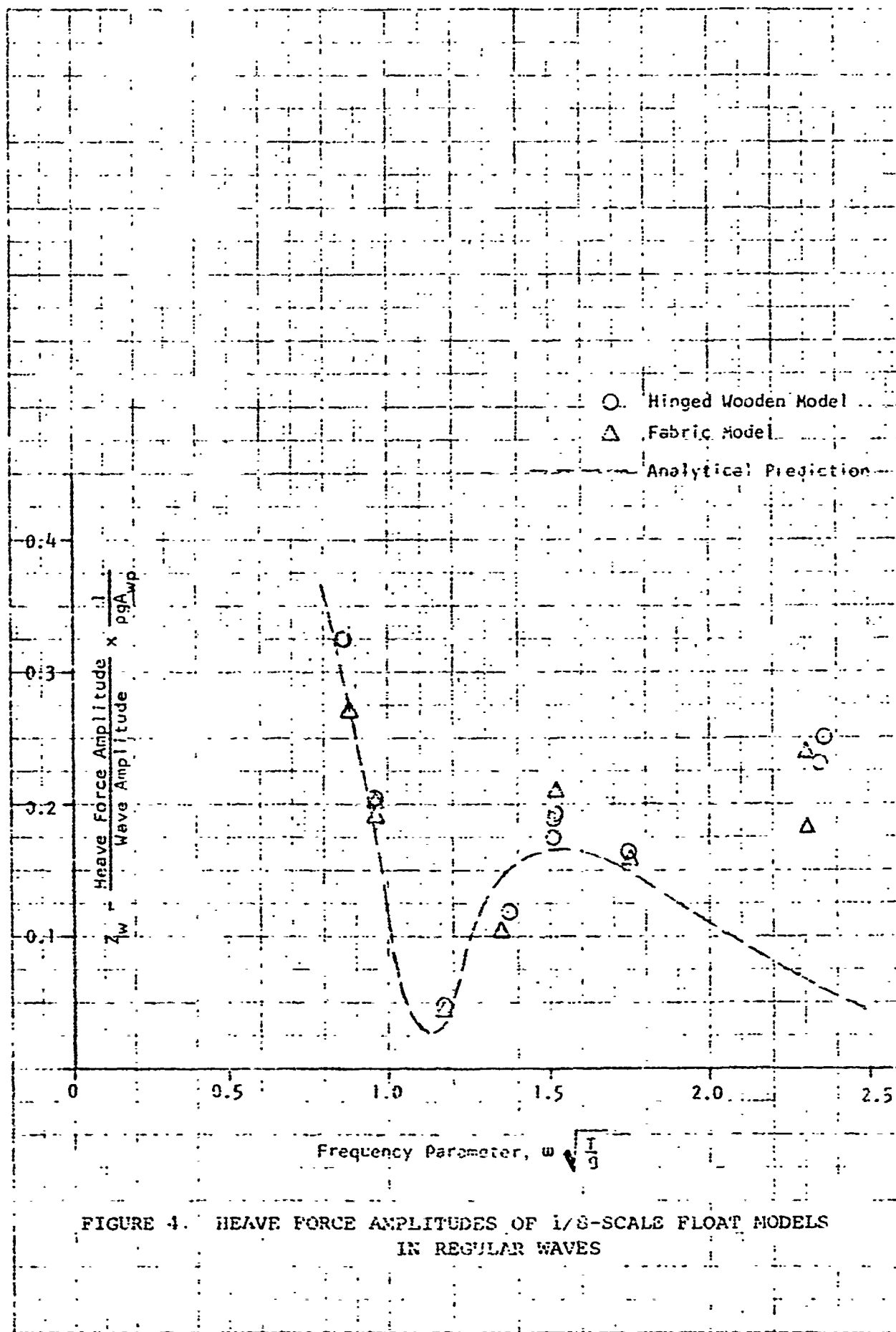


Figure 3 Test Setup in LUMF 33sin



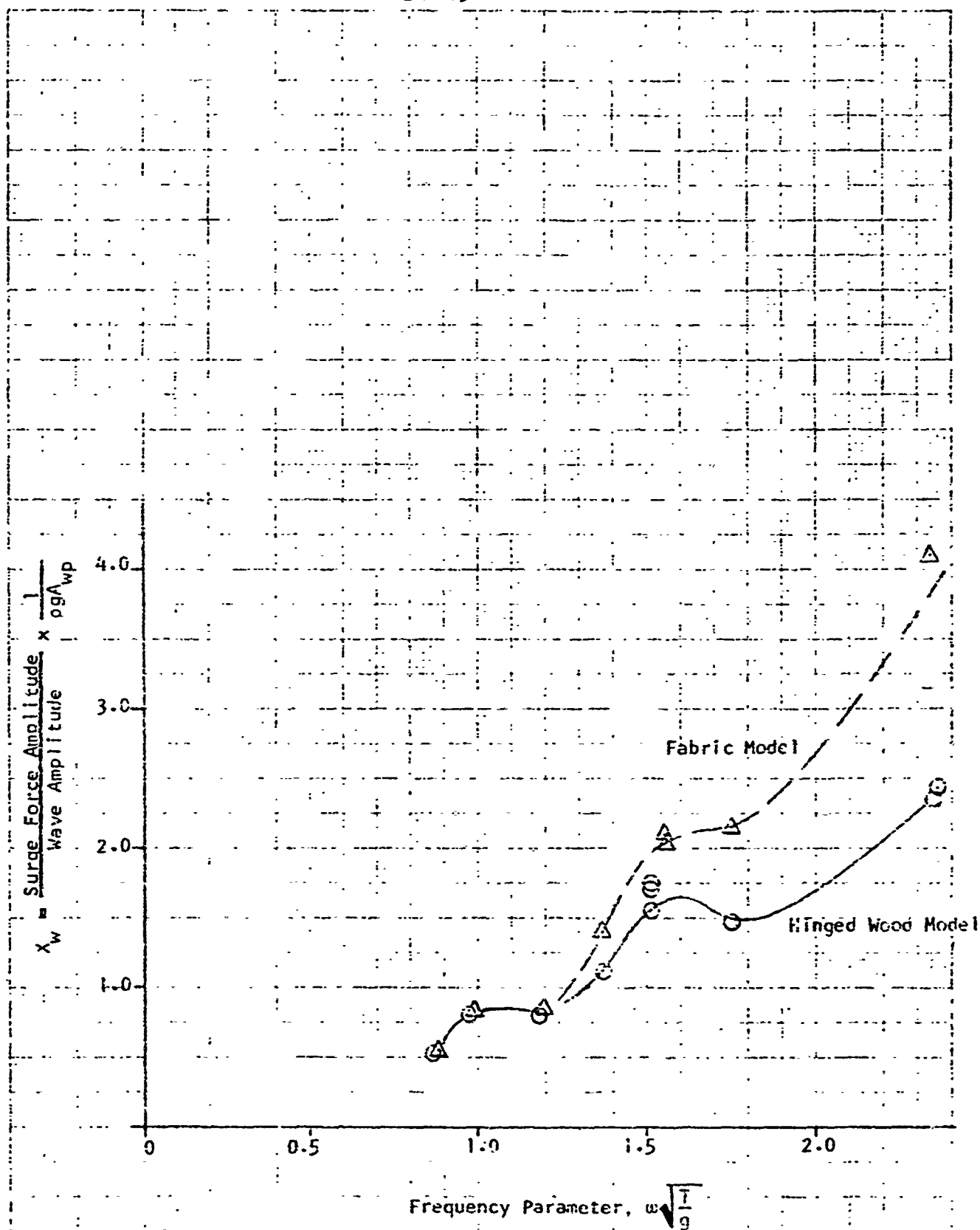


FIGURE 5. SURGE FORCE AMPLITUDES OF 1/8-SCALE FLOAT MODELS IN REGULAR WAVES